

Biogeography, diversity and risk potential of toxigenic Amphidomataceae (Dinophyceae) in the North Sea and adjacent areas

Dissertation zur Erlangung des akademischen Grades

- Dr. rer. nat. -

im Fachbereich 2 (Biologie/Chemie) der



vorgelegt von

Stephan Wietkamp

2020

Versicherung an Eides Statt

Ich, Stephan G. Wietkamp,

versichere an Eides Statt durch meine Unterschrift, dass ich die vorstehende Arbeit selbständig und ohne fremde Hilfe angefertigt und alle Stellen, die ich wörtlich dem Sinne nach aus Veröffentlichungen entnommen habe, als solche kenntlich gemacht habe, mich auch keiner anderen als der angegebenen Literatur oder sonstiger Hilfsmittel bedient habe.

Ich versichere an Eides Statt, dass ich die vorgenannten Angaben nach bestem Wissen und Gewissen gemacht habe und dass die Angaben der Wahrheit entsprechen und ich nichts verschwiegen habe.

Die Strafbarkeit einer falschen eidesstattlichen Versicherung ist mir bekannt, namentlich die Strafandrohung gemäß § 156 StGB bis zu drei Jahren Freiheitsstrafe oder Geldstrafe bei vorsätzlicher Begehung der Tat bzw. gemäß § 161 Abs. 1 StGB bis zu einem Jahr Freiheitsstrafe oder Geldstrafe bei fahrlässiger Begehung.

Bremen, den 27. August 2020

Stephan G. Wietkamp

Beginn der Doktorarbeit:	01.08.2017
Dissertation beim Prüfungsausschuss eingereicht:	27.08.2020
1. Gutachter:	Prof. (em.) Dr. Allan Cembella
2. Gutachter:	Prof. Dr. Haifeng Gu
Datum des Kolloquiums:	14.10.2020

Acknowledgements

I have many people to thank for supporting my work and me during the time of this PhD.

First, I cordially thank Prof. Dr. Tilmann Harder for the opportunity to work on this project and for being a very helpful advisor and supporter for any kind of request. I owe very special thanks to Dr. Urban Tillmann, who guided me throughout this intense time on a daily base and who was literally available at any time. You taught me “the good scientific practice” and how to focus on the substantial things, which will be of use for my entire life. Likewise, I will always remember your enthusiasm, surrender and professionalism with respect to our research, which was very inspiring. Especially concerning (but not restricted to) the chemical part of this work, I was lucky to have Dr. Bernd Krock by my side, being a great and experienced expert in the field. I will never forget your happy face when Pricilla finally woke up on Heincke to support us with excellent data. I thank all members of my PhD committee, i.e. Prof. Dr. Tilmann Harder, Dr. Urban Tillmann, Dr. Bernd Krock, Dr. Katja Metfies and Dave Clarke for your time, interest and our constructive discussions. Katja, special thanks go to you, because you paved the way, which led me starting this adventure. I deeply appreciate the advices by Prof. Dr. Allan Cembella, which significantly improved the composition of this thesis. Many thanks to Dr. Kerstin Klemm for our fruitful discussions and your support in several ways, piloting me through windy times. Dave and Rafael, I want to thank you very much for your cooperation. You brought in great ideas, helpful hands and last, but not least, a lot of great fun. I am glad about the experience that a PhD can actually mean making new friends - I enjoyed this!

Special thanks go to Dr. Johannes Rick and Tatyana Romanova (Sylt samples), Dr. Jens Floeter (HE534 samples), Dr. Justus van Beusekom (HE541 samples), Dr. Katja Metfies, Johanna Hessel, Swantje Rogge and Kerstin Oetjen (PS92 samples), Dr. Rüdiger Röttgers (HE517 samples), Laura Käse, Kristine Carstens and Robin Klenk (Helgoland samples), Pim Sprong (Cuxhaven samples), Dennis Gowland (Orkney samples), Michaela Gerriets (Wilhelmshaven samples), as well as everyone else who was somehow involved in providing field samples. Many thanks go to Annegret Müller, Thomas Max and Nancy Kühne for helping me out and being always available. Without you, the progress of this work would never have been that smooth. Special thanks to Joyce, who made my day with interesting intercultural exchange, mental motivation and last, but definitively not least, the very tasty Filipino food. The best PhD combatant I can imagine – Maráming salámat!

I want to express my deepest gratitude to my family, friends and to the affectionate girl by my side for continuous motivation, encouragement, understanding and backing me up at any time. Even when most violent storms were ravaging, you all were and are my safe harbor.

„The Sea, once it casts its spell, holds one in its net of wonder forever.”

Jacques-Yves Cousteau

Table of Contents

Acronyms and key symbols	9
List of peer-review publications	11
Abstract	13
Zusammenfassung	17
1. Introduction	23
1.1 Harmful microalgae: Role in marine ecosystems, human health and economy	23
1.2 Azaspiracids - a group of marine biotoxins	26
1.3 Amphidomataceae - the source of azaspiracids	29
1.4 AZA and Amphidomataceae in the North Sea area	37
2. Objectives	39
3. Results and Discussion	41
3.1 Diversity of Amphidomataceae	41
3.1.1 Taxonomic diversity	41
3.1.2 AZA diversity	48
3.2 Molecular detection and quantification of toxigenic Amphidomataceae	52
3.2.1 Assay specificity and ribotypes	53
3.2.2 Quantification ability	56
3.2.3 Comparative method analysis	59
3.3 Biogeography of toxigenic Amphidomataceae in the North Sea	65
3.3.1 qPCR-based spatial distribution and cell abundance	65
3.3.2 Vertical distribution	68
3.3.3 Seasonal occurrence	68
3.4 Toxigenic Amphidomataceae and environmental parameters	74
3.4.1 Salinity	74
3.4.2 Temperature	75
4. Conclusions and future perspectives	80
Funding	86
Publications	87
Publication I: New real-time PCR assay for toxigenic <i>Amphidoma languida</i>	88
Publication II: Toxigenic Amphidomataceae in Danish coastal waters	102
Publication III: Amphidomataceae in Greenland and <i>Az. perforatum</i> sp. nov.	118
Publication IV: AZA producers in North Atlantic waters in 2018	146
Publication V: qPCR assay for Amphidomataceae	174
Publication VI: Description of three new <i>Azadinium</i> species	182
Publication VII: New amphidomatacean strains from the North Atlantic	238
Publication VIII: Temperature effect on toxigenic Amphidomataceae	298
References	334
Supplementary material	352

Acronyms and key symbols

ANOVA	Analysis of Variance
AZA	Azaspiracid
AZP	Azaspiracid Shellfish Poisoning
CARD-FISH	Catalyzed Reporter Deposition - Fluorescence <i>In Situ</i> Hybridization
CBC	Compensatory Base Change
C _T	Threshold Cycle
CTD	Conductivity-Temperature-Depth Profiler
DNA	Deoxyribonucleic Acid
DSP	Diarrhetic Shellfish Poisoning
HAB	Harmful Algal Bloom
ITS	Internal Transcribed Spacer (of rDNA)
LC-MS/MS	Liquid Chromatography - Mass Spectrometry
LOD	Limit of Detection
LOQ	Limit of Quantification
LSU	Large Subunit (of rDNA)
MGB	Minor Groove Binding
<i>m/z</i>	mass-to-charge ratio
NGS	Next-Generation-Sequencing
PCR	Polymerase Chain Reaction
PSP	Paralytic Shellfish Poisoning
qPCR	quantitative Polymerase Chain Reaction
rDNA	ribosomal Deoxyribonucleic Acid
RNA	Ribonucleic Acid
rRNA	ribosomal Ribonucleic Acid
SEM	Scanning Electron Microscopy
SPATT	Solid Phase Adsorption Toxin Tracking
SST	Sea Surface Temperature
SSU	Small Subunit (of rDNA)
T _m	Melt Temperature
μ	Growth rate

List of peer-review publications

- Publication I*:** Wietkamp, S., Tillmann, U., Clarke, D. & Toebe, K. (2019). Molecular detection and quantification of the azaspiracid-producing dinoflagellate *Amphidoma languida* (Amphidomataceae, Dinophyceae). *Journal of Plankton Research*, 41 (2), 101-113.
- Publication II:** Wietkamp, S., Krock, B., Gu, H., Voß, D., Klemm, K. & Tillmann, U. (2019). Occurrence and distribution of Amphidomataceae (Dinophyceae) in Danish coastal waters of the North Sea, the Limfjord and the Kattegat/Belt area. *Harmful Algae*, 88, 101637.
- Publication III:** Tillmann, U., Wietkamp, S., Krock, B., Tillmann, A., Voss, D. & Gu, H. (2020). Amphidomataceae (Dinophyceae) in the western Greenland area, including description of *Azadinium perforatum* sp. nov. *Phycologia*, 59(1), 63-88.
- Publication IV:** Wietkamp, S., Krock, B., Clarke, D., Voss, D., Salas, R., Kilcoyne, J. & Tillmann, U. (2020). Distribution and abundance of azaspiracid-producing dinophyte species and their toxins in North Atlantic and North Sea waters in summer 2018. *PLoS ONE*, 15(6).
- Publication V:** Tillmann, U., Wietkamp, S., Gu, H., Clarke, D. & Smith, K. (in press). qPCR assay for Amphidomataceae: State of the art and new challenges. In: *ICHA 2018 Proceedings* (ISBN - n°. 978-87-990827-7-3), Copenhagen DK (IOC & ISSHA). In press.
- Publication VI:** Salas, R., Tillmann, U., Gu, H., Wietkamp, S., Krock, B. & Clarke, D. (submitted). Morphological and molecular characterization of three new *Azadinium* species revealed a high diversity of non-toxicogenic species of Amphidomataceae (Dinophyceae) in Irish waters, North East Atlantic. *Phycological Research*. Submitted.
- Publication VII:** Tillmann, U., Wietkamp, S., Gu, H., Krock, B., Salas, R. & Clarke, D. (submitted). Multiple new strains of Amphidomataceae (Dinophyceae) from the North Atlantic revealed a high toxin profile variability of *Azadinium spinosum* and a new non-toxicogenic *Az. cf. spinosum*. *Microorganisms*. Submitted.
- Publication VIII:** Wietkamp, S., Bantle, A., Krock, B. & Tillmann, U. (to be submitted). The effect of temperature on growth and toxin production in three toxicogenic amphidomatacean species. To be submitted.

* Awarded the David-Cushing Prize 2019 by the Journal of Plankton Research for “the best paper by an early career stage scientist published in the journal during the previous year, where the first author is aged 30 or younger”.

Other contributions:

- Publication IX:** Wang, N., Mertens, K. N., Krock, B., Luo, Z., Derrien, A., Pospelova, V., Liang, Y., Bilien, G., Smith, K., De Schepper, S., **Wietkamp, S.**, Tillmann, U. & Gu, H. (2019). Cryptic speciation in *Protoceratium reticulatum* (Dinophyceae): Evidence from morphological, molecular and ecophysiological data. *Harmful Algae*, 88, p. 101610. doi:<https://doi.org/10.1016/j.hal.2019.05.003>
- Publication X:** Sunesen, I., Rodríguez, F., Tardivo Kubis, J.A., Aguiar Juárez, D., Risso, A., Lavigne, A.S., **Wietkamp, S.**, Tillmann, U. & Sar, E.A. (2020) Morphological and molecular characterization of *Heterocapsa claromecoensis* sp. nov. (Peridiniales, Dinophyceae) from Buenos Aires coastal waters (Argentina). *Eur. J. Phycol.*, 1-17.
- Publication XI:** Tillmann, U., Krock, B., **Wietkamp, S.** & Beran, A. (2020) A Mediterranean *Alexandrium taylorii* (Dinophyceae) strain produces goniiodomin A and lytic compounds but not paralytic shellfish toxins. *Toxins*, 12(9), 564.

Abstract

Azaspiracids (AZAs) are a group of lipophilic biotoxins responsible for the azaspiracid shellfish poisoning syndrome (AZP) in humans after consumption of contaminated shellfish. AZAs are produced by four representatives of the marine nanoplanktonic family Amphidomataceae (Dinophyceae), i.e. *Azadinium spinosum*, *Az. poporum*, *Az. dexteroporum* and *Amphidoma languida*. Among those species, *Az. spinosum* producing AZA-1, -2 and -33 (as known in 2017) and, to lesser extent, *Az. poporum* producing AZA-37, are known from the North Atlantic. These toxigenic species pose a major concern, especially for the coastal shellfish production in Ireland, and are thus frequently monitored along with AZA toxins by the regulatory authorities of the Irish government. A third North Atlantic AZA producer, *Amphidoma languida*, has been described based on an isolate obtained from Irish coastal waters, but the actual threat by this species and the respective AZA variants (AZA-38, -39) is unknown. In contrast to AZAs produced by *Az. spinosum* and *Az. poporum*, these AZA congeners are currently not regulated within the EU. The three AZA producers have been confirmed in the North Sea as well, but current knowledge on the biogeography of toxigenic Amphidomataceae relies on a limited number of observations and studies. The lack of data impedes an assessment of the actual risk of AZP in the North Sea and adjacent waters at present. However, shellfish farming in European coastal waters including the North Sea is of increasing importance for seafood supply, and enhanced production capacities are heavily advocated by the European Commission (EC).

The goal of this thesis study was to increase knowledge about the current biogeography of toxigenic Amphidomataceae in the eastern North Atlantic, and to evaluate the risk potential of AZP in the area under the perspective of global change. Interpretations of the results should help to improve safety and sustainable use of coastal seafood production sites in the North Sea and adjacent areas. Major difficulties for reliable species detection and identification are the small cell size and inconspicuousness of nanoplanktonic Amphidomataceae, as well as the sympatric occurrence of toxigenic and non-toxigenic representatives. Multiple methods, i.e. light microscopy (LM) and scanning electron microscopy (SEM) for morphological inspection, liquid chromatography coupled with tandem mass spectrometry (LC-MS/MS) for AZA analysis, and quantitative polymerase chain reaction (qPCR) for DNA-based cell detection, were applied to respond to these challenges and to gain a broad spectrum of new insights into (toxigenic) Amphidomataceae.

The isolation and characterization of (in total) 102 new *Az. spinosum* and *Am. languida* strains from the North Atlantic in 2016 and 2018 yielded increased knowledge on variation in AZA

profiles and cell quotas of these toxigenic species. Samples from the North Sea provided 30 new *Am. languida* strains, all confirming previous morphological, phylogenetic and toxinological (i.e. AZA-38 and -39) records from the area. The 72 new *Az. spinosum* strains represented both Ribotype A in the North Sea and Irish Sea, but Ribotype B was only detected from the North Sea. For the first time, variability in the toxin profile of Ribotype A was confirmed, with different combinations of the three AZA variants (AZA-1 always present, combined with presence/absence of AZA-2 and/or -33), whereas the toxin profile of Ribotype B (AZA-11 and -51) was consistent in all strains. Multiple analyses over 18 months revealed that the AZA profile within all given strains remained stable. In contrast, AZA cell quotas were highly variable among and within *Az. spinosum* strains, and variability of single analogs was as high as 330-fold. These findings confirmed previous studies, but the reasons for the cell quota variability remain unclear. Five new amphidomatacean strains isolated from the 2018 field survey displayed the morphological characteristics of *Az. spinosum*, but exhibited significant DNA sequence differences (clustering closer to *Az. obesum* in phylogenetic trees) and no AZA production. The final taxonomic assignment remains undetermined, and the strains were thus designated as *Az. cf. spinosum*. The newly identified *Az. cf. spinosum* and the description of four new non-toxigenic *Azadinium* species (i.e. *Az. galwayense*, *Az. perforatum*, *Az. perfusorium* and *Az. pseudozhuanum*) highlighted in fact that amphidomatacean biodiversity is still underestimated and that AZA production is rather exceptional within this dinophyte family.

Although qPCR assays for *Az. spinosum* and *Az. poporum* were already available prior to this study, the respective assay for quantification of toxigenic *Amphidoma languida* cells was developed and extensively evaluated in the course of this doctoral thesis project. A quick, cost-effective and high throughput application, coupled with high specificity and quantification limit down to 10 target gene copies per reaction, enables this sensitive assay to detect even single *Am. languida* cells per liter of seawater, and thus is a valuable tool for subsequent biogeographical studies. With respect to multiple newly discovered species and isolated amphidomatacean strains, specificity testing of the three alternative qPCR assays was of utmost importance to test for false-positive or false-negative amplification and therefore to assure reliable detection and quantification in monitoring programs. None of the three assays showed false-positive signals, including for the new non-toxigenic *Az. cf. spinosum*, except for rDNA amplification from a new non-toxigenic *Az. poporum* isolate from the Danish coast. The most concerning result, however, was the significant amplification efficiency difference between *Az. spinosum* Ribotype A and B strains, revealing a

degree of uncertainty for quantification from natural field samples by application of the current *Az. spinosum* assay because both ribotypes have been shown to co-occur in the Norwegian Sea and the North Sea. Although the current *Az. spinosum* and *Az. poporum* assays have not completely lost their validity for field applications, they should be redesigned for improved reliability.

Multiple DNA sample sets, comprising more than 200 field samples from various expeditions between 2015 and 2019 to the eastern North Atlantic, were analyzed by qPCR for the presence and cell abundance of the three toxigenic amphidomatacean species. All three AZA-producers were found to be widely distributed in the area. In terms of positive geographical hits and cell densities (up to 8.3×10^4 cells L⁻¹) *Az. spinosum* was the dominant toxigenic species in Irish coastal waters in summer 2018, underlining the threat for Irish shellfish production. Multiple hits and relatively high cell abundances of *Az. spinosum* were frequently found in the North Sea, as well. *Amphidoma languida* was also widely present and relatively abundant (2.3×10^4 cells L⁻¹) around Ireland at that time, but highest cell density was found in the central North Sea, with an extraordinary abundance of $\sim 1.2 \times 10^5$ cells L⁻¹. This represents the highest ever recorded field abundance for this species and for North Atlantic Amphidomataceae in general. This finding, together with multiple further geographical records, indicated that *Am. languida* may be the dominant AZA producer in the North Sea. On this basis, incorporation of this species is recommended for both the national Irish- and official EU monitoring programs. Several amphidomatacean species have been found in Arctic and Subarctic waters before, and this finding was confirmed in the course of this study. *Amphidoma languida* was the only AZA producing species detected in the Arctic (> 75 °N) close to Spitzbergen in 2015, indicating that this species is able to cope with colder (around 5 °C) water temperatures. In contrast to *Az. spinosum* and *Am. languida*, *Az. poporum* was found in only a few locations and at low cell densities usually < 100 cells L⁻¹, but with one extraordinary signal at Scapa Flow, Orkney Islands in June 2016, corresponding to $\sim 3 \times 10^3$ cells L⁻¹. This indicates an overall much lower potential contribution of this species to AZA contamination in recent years.

Due to continuous sampling at several fixed North Sea stations, this thesis contains detailed qPCR data (in total 245 samples) on the seasonality of all three toxigenic species. The subsequent analysis revealed recurrent occurrence from July to October, consistent with observations at the Irish coastline (Marine Institute, Galway, Ireland), and indicating higher AZP risk in summer and fall. In addition, weekly sampling at the North Sea islands Helgoland and Sylt suggested relatively rapid population increases, demonstrating that sudden bloom events of toxigenic Amphidomataceae leading to rapid shellfish toxicity should be considered for respective monitoring frequency.

First data on the vertical distribution of toxigenic Amphidomataceae presented here revealed no distinct distributional pattern in the water column, and hence pooling of water samples from various depths is an appropriate sampling method. Simultaneous on-board application of alternative technologies during an expedition in 2018 revealed a highly significant correlation between the results of light microscopy of plankton cells and qPCR assays for the detection and enumeration of toxigenic Amphidomataceae, and chemical analysis of AZA composition in the field. Detailed method-specific advantages and disadvantages are presented herein, but in particular the qPCR approach has proven to give solid results by combining high specificity with convenient detection limits.

Laboratory experiments with North Atlantic strains representing all three toxigenic Amphidomataceae (including the first study on *Am. languida*) targeted temperature dependent growth and AZA production. Growth rates and AZA cell quota were inversely related: whereas higher temperatures led to higher growth rates, AZA content per cell decreased with increasing temperatures. Nevertheless, faster growth was shown to overcompensate for lower toxin cell quotas, leading to similar or even higher total AZA content per seawater volume ($\mu\text{g AZA L}^{-1}$) at higher temperatures. This suggests a potentially increasing AZP risk under expected rising ocean temperatures. Highest AZA production was found in *Az. spinosum* Ribotype A (with a characteristic toxin profile of AZA-1, -2 and -33), highlighting a major role of this taxon determining AZP risk in the eastern North Atlantic. Except for *Az. spinosum* Ribotype B strain (containing AZA-11 and -51), all investigated strains showed lower extracellular than intracellular AZA levels. This suggests that AZA is predominantly retained intracellularly, and that screening for cells and intracellular AZAs is an appropriate monitoring method for AZP risk assessment.

In conclusion, extensive research in this doctoral study, including development of a reliable qPCR assay for toxigenic *Am. languida*, with the description of new amphidomatacean species, strains, AZA variants, toxin profiles, adds considerably to the knowledge base on biogeography and variability within the Amphidomataceae. Combining data on AZA cell quota variability with the comprehensive data set on biogeography, seasonality and vertical distribution of the three toxigenic representatives in the North Sea has redefined our view of the role and importance of (toxigenic) Amphidomataceae and AZAs in the North Sea and adjacent areas. Thus, this doctoral thesis study provides a highly valuable baseline for official monitoring and future studies on toxigenic Amphidomataceae.

Zusammenfassung

Azaspirosäuren (engl. AZAs) sind eine Gruppe von lipophilen Biotoxinen, welche im Menschen nach dem Verzehr von kontaminierten Schalentieren zu einer Azaspirosäuren Muschelvergiftung (engl. AZP) führen können. AZA werden von vier Arten der marinen, nanoplanktonischen Familie Amphidomataceae (Dinophyceae) gebildet, namentlich *Azadinium spinosum*, *Az. poporum*, *Az. dexteroporum* und *Amphidoma languida*. Innerhalb dieser Gruppe stellen hauptsächlich *Az. spinosum* (produziert AZA-1, -2 und -33) und - in geringerem Ausmaß - *Az. poporum* (produziert AZA-37) aus dem Nordatlantik eine Gefährdung für die irische Schalentier-Aquakultur dar und unterliegen daher strenger, regelmäßiger Überwachung durch die irischen Behörden. Eine dritte AZA-produzierende Art bekannt aus den Gewässern des Nordatlantik - *Am. languida* - ist ebenfalls in irischen Küstengebieten nachgewiesen, dennoch ist die tatsächliche Gefahr dieser Art und seiner Toxine (AZA-38 und -39) bisher unbekannt. Im Gegensatz zu den Toxinen von *Az. spinosum* und *Az. poporum* sind diese beiden AZA Variationen auch nicht EU-reguliert. Diese drei AZA Produzenten sind zwar ebenso in anderen Gebieten der Nordsee gesichtet worden, allerdings ist die Datenlage zur Biogeographie beschränkt auf relativ wenige Beobachtungen und Studien. Dies macht eine Bewertung des Risikopotentials von Azaspirosäuren Muschelvergiftungen in der Nordsee auf Grundlage des bisherigen Wissensstandes nahezu unmöglich. Hingegen steigt die Bedeutung von Schalentier-Aquakultur als Nahrungsquelle in europäischen Küstengewässern wie der Nordsee zunehmend an, was nicht zuletzt durch Subventionen der Europäischen Kommission (EC) gefördert wird.

Das Ziel dieser Thesis war daher, das Wissen um die Biogeographie der Toxin-produzierenden Amphidomataceae im östlichen Nordatlantik zu erweitern und das aktuelle Risikopotential von AZA-bedingten Muschelvergiftungen unter besonderer Berücksichtigung des globalen Klimawandels zu bewerten. Die Ergebnisse sollen eine Grundlage bieten, um Nahrungsmittelsicherheit und die nachhaltige Nutzung von Nordsee Küstengewässern durch die Aquakultur zu verbessern.

Die Unscheinbarkeit und relativ geringe Zellgröße der Amphidomataceae Arten, sowie das sympatrische Auftreten von toxischen und nicht-toxischen Vertretern der Familie, stellen die größten Problematiken für eine zuverlässige Detektion im Feld dar. Die Verwendung mehrerer Methoden, d.h. Mikroskopie, LC-MS/MS und qPCR, ermöglichte es diese Hürde zu überwinden und führte zu einem breiten Spektrum an neuen Erkenntnissen über (toxische) Amphidomataceae. Isolation und Charakterisierung von insgesamt 102 neuen *Az. spinosum* und *Am. languida*

Stämmen aus dem Nordatlantik in 2016 und 2018 erweiterten signifikant das Wissen um AZA Profile und Zellquoten dieser zwei Arten. Für alle 30 Stämme von *Am. languida* isoliert aus der Nordsee bestätigten die bis dahin erhobenen morphologischen, phylogenetischen und toxinologischen (AZA-38 und -39) Daten aus dem Untersuchungsgebiet. Die 72 *Az. spinosum* Stämme repräsentierten sowohl Ribotyp A aus der Nordsee und den irischen Küstengewässern, als auch Ribotyp B Stämme, welche nur in der Nordsee gefunden wurden. Zum ersten Mal wurde eine Toxin Profil-Variabilität in Ribotyp A Stämmen beobachtet, mit diversen Kombinationen der drei AZA Varianten (AZA-1 stets vorhanden, kombiniert mit Präsenz/Absenz von AZA-2 und/oder -33), wohingegen das typische Toxin Profil von Ribotyp B (AZA-11 und -51) ausnahmslos in allen Stämmen nachgewiesen werden konnte. Mehrfachanalysen über einen Zeitraum von 18 Monaten zeigten, dass das jeweilige Toxin Profil in jedem isolierten Stamm konsistent bestehen blieb. Im Gegensatz dazu waren die AZA Zellquoten zwischen und innerhalb der *Az. spinosum* Stämme höchst variabel, mit bis zu 330-fachen Unterschieden einzelner AZA Komponenten. Dieser Befund bestätigte vorhergehende Studien, dennoch bleibt der Grund für diese hohe Variabilität ungeklärt. Im Rahmen der Feldstudie in 2018 wurden fünf weitere Amphidomataceae Stämme isoliert, welche die gleiche Morphologie, jedoch signifikante DNA Sequenzunterschiede und keine AZA Toxine im Vergleich zu *Az. spinosum* aufweisen. Eine finale taxonomische Einordnung wurde bisher vermieden und die Stämme somit als *Az. cf. spinosum* gekennzeichnet. Taxonomische Untersuchungen während dieser Doktorarbeit, d.h. die Beschreibung von vier neuen, nicht toxigenen Amphidomataceae Arten (*Az. galwayense*, *Az. perforatum*, *Az. perfusorium* und *Az. pseudozhuanum*) und *Az. cf. spinosum*, zeigten deutlich, dass die bisher bekannte Biodiversität wahrscheinlich eine Unterschätzung der Artenvielfalt in der Gruppe darstellt. Dass keine der neuen Arten AZA Produktion aufweist zeigt, dass die Produktion von Toxinen eher eine Ausnahme innerhalb der Amphidomataceae darstellt.

Während qPCR Methoden für *Az. spinosum* und *Az. poporum* bereits verfügbar waren und aktuell verwendet werden, wurde im Rahmen dieser Doktorarbeit die entsprechende Methode zur Quantifizierung von toxigenen *Am. languida* Zellen entwickelt und evaluiert. Aufgrund der hohen Spezifität, sowie einem relativ niedrigen unteren Quantifizierungslimit von zehn Ziel-Gen Kopien pro Reaktion erlaubt diese sensitive Methode die Detektion von selbst einzelnen *Am. languida* Zellen pro Liter und stellte somit eine wichtige Grundlage für folgende Studien zur Biogeographie dar.

Mit der Isolation neuer Arten und Stämmen kam der qPCR Spezifität-Prüfung besondere Bedeutung zu, d.h. auf falsch-negative und falsch-positive Amplifikation zu testen, und somit eine weiterhin zuverlässige Detektion und Quantifizierung zu evaluieren. Keine der drei qPCR Methoden zeigte falsch-positive Signale (einschließlich gegenüber *Az. cf. spinosum*), mit Ausnahme eines neu isolierten, nicht toxischen *Az. poporum* Stammes von der dänischen Küste. Der weitreichendste Befund war jedoch der signifikante Unterschied in der Amplifikationseffizienz der *Az. spinosum* qPCR Methode zwischen Ribotyp A und B, woraus sich eine gewisse Unsicherheit gegenüber der zuverlässigen Quantifizierung dieser Art im Feld ergibt, da beide Ribotypen in Norwegen und der Nordsee sympatrisch auftreten können. Obwohl die aktuelle *Az. spinosum* und *Az. poporum* Methode aufgrund dieser Unsicherheiten nicht viel an Wert verliert, wird dennoch empfohlen, beide in naher Zukunft anzupassen.

Insgesamt wurden 200 Feldproben aus unterschiedlichen Exkursionen in den östlichen Teil des Nordatlantiks zwischen 2015 und 2019 qualitativ und quantitativ auf toxische Amphidomataceae Arten getestet. Alle drei AZA Produzenten waren im Untersuchungsgebiet weit verbreitet. Geographisch am häufigsten und mit höchsten Zellzahlen (bis zu $8,3 \times 10^4$ Zellen pro Liter) war *Azadinium spinosum* die dominante toxische Art in irischen Küstengewässern in 2018, was die bekannte Gefahr für die irische Schalentier-Industrie untermauerte. Jedoch ergaben auch viele Proben aus der Nordsee Signale und relative hohe Zellzahlen von *Az. spinosum*. Ein zu dieser Zeit ebenso weit verbreiteter und abundanter (bis zu $2,3 \times 10^4$ Zellen pro Liter) Vertreter an der irischen Küste war *Am. languida*, die höchsten Zelldichten wurden dennoch in der zentralen Nordsee beobachtet. Bemerkenswert war die außergewöhnlich hohe Abundanz von etwa $1,5 \times 10^5$ Zellen pro Liter an einer Nordsee Station, was die bis dahin höchste beobachtete Zelldichte dieser Art bzw. generell von Amphidomataceae im Nordatlantik ist. Diese hohe Zelldichte, in Kombination mit zahlreichen weiteren geographischen Signalen deutet an, dass *Am. languida* die bedeutsamste toxische Amphidomataceae Art in der Nordsee sein könnte. Anhand dieser Befunde ergibt sich die Empfehlung, diese Art sowie die entsprechenden Toxine in das irische und EU-weite Monitoring Programm einzugliedern. Zusätzlich war *Am. languida* die einzige AZA-produzierende Art, welche 2015 in arktischen Gewässern nahe Spitzbergen ($> 75^\circ\text{N}$) detektiert wurde. Im Gegensatz zu *Az. spinosum* und *Am. languida* wurde *Az. poporum* nur sporadisch und in relativ geringen Abundanzen (i.d.R. nicht mehr als 100 Zellen pro Liter, mit einer Ausnahme von ca. 3×10^3 Zellen pro Liter bei Scapa Flow in Juni 2016) in der Nordsee gefunden und spielte zu dieser Zeit scheinbar eine eher untergeordnete Rolle hinsichtlich des AZP Risikos.

Aufgrund kontinuierlicher Probennahme an mehreren festen Nordsee Stationen stellt diese Doktorarbeit mit insgesamt 245 Proben detaillierte, qPCR basierte Daten zur Saisonalität aller drei toxischen Arten bereit und offenbarte wiederkehrende Signale zwischen Juli und Oktober. Damit konnten Beobachtungen in irischen Küstengewässern durch das Marine Institute (Galway, Irland) bestätigt werden und suggerieren damit ein erhöhtes AZP Risiko im Sommer und Herbst. Zusätzlich zeigte eine wöchentlich-basierte Probennahme vor den Nordseeinseln Helgoland und Sylt, dass die Populationsdichte von toxischen Amphidomataceae von Woche zu Woche signifikant schwanken kann, was in entsprechenden Monitoring Programmen berücksichtigt werden sollte.

Mit dieser Studie werden erste Daten zum Tiefenprofil von toxischen Amphidomataceae geliefert, diese zeigten aber keine konsistenten Verteilungsmuster in der Wassersäule. Die simultane Untersuchung mit Mikroskopie, LC-MS/MS und qPCR an Bord eines Expeditionsschiffes in 2018 offenbarte eine hoch signifikante Korrelation zwischen den Ergebnissen der drei Methoden bezüglich der quantitativen Detektion von toxischen Amphidomataceae und AZA unter Feldbedingungen. Die methoden-spezifischen Vor- und Nachteile sind in dieser Arbeit intensiv diskutiert. Die qPCR lieferte aufgrund der hohen Spezifität und gleichzeitig niedrigem Detektionslimit sehr überzeugende Resultate.

Labor Experimente mit Nordatlantik Stämmen aller drei toxischen Arten, einschließlich der ersten Studie mit *Am. languida*, zielten auf temperatur-bedingtes Wachstum und AZA Produktion ab. Wachstum und AZA Zellquoten verhielten sich dabei gegensätzlich: Während erhöhte Temperaturen zu höheren Wachstumsraten in den Kulturen führte, so sanken gleichzeitig die AZA Zellquoten. Dabei konnte beobachtet werden, dass ein schnelleres Wachstum in der Lage war, niedrigere Zellquoten zu (über-) kompensieren, was zu einem ähnlichen oder sogar höheren AZA Gehalt pro Volumen in höher temperierten Kulturen führte. Dieser Befund lässt vermuten, dass das AZP Risiko aufgrund der zu erwartenden steigenden Ozeantemperaturen in Zukunft ansteigen könnte. Die höchste AZA-Produktion wurde für *Az. spinosum* Ribotyp A (mit traditionellem AZA Profil von AZA-1, -2 und -33) bestimmt, womit die Schlüsselrolle dieser Art in Bezug auf AZP im östlichen Nordatlantik bestätigt wurde. Mit Ausnahme von *Az. spinosum* Ribotyp B (produziert AZA-11 und -51) war der intrazelluläre AZA Anteil pro Zelle in allen untersuchten Stämmen weitaus höher als die entsprechenden extrazellulären Anteile. Dies unterstützte die Annahme, dass das AZP Risiko hauptsächlich durch intrazelluläre Toxine verursacht wird und dass somit die Untersuchung von Zellen und intrazellulären AZA Toxinen eine angemessene Methode ist.

Schlussfolgernd trägt diese Doktorarbeit sowohl aufgrund einer neuen zuverlässigen qPCR Detektionsmethode für *Am. languida*, als auch der Beschreibung neuer Amphidomataceae Arten, Stämmen, AZA Varianten, Toxin Profilen und AZA Zellquoten Variabilität, sowie aufgrund eines weitreichenden Datensatzes zur Biogeographie, Saisonalität und Tiefenprofil signifikant zum Wissen über (toxigene) Amphidomataceae und AZA in der Nordsee und angrenzenden Gebieten bei. Daher bietet die hier dargelegte Thesis eine wertvolle Grundlage für offizielles Monitoring und weitere Studien zu (toxigenen) Amphidomataceae.

1. Introduction

1.1 Harmful microalgae: Role in marine ecosystems, human health and economy

Capable of using the sunlight for photosynthesis and therefore oxygen production, phytoplankton contributes considerably to climatic and organismic processes on this planet by taking up carbon from the atmosphere and making it available for other organisms (Sabine and Feely, 2007; Jeffrey et al., 2011). A fascinating diversity in phytoplanktonic taxa has evolved, allowing them to occupy different habitats and niches, and uncountable interactions with other organisms have been built up. Thus, photosynthetic microalgae are rightly seen as the basis of the food web in marine and freshwater ecosystems. Their major role gets further highlighted, when environmental conditions (e.g. temperature, light and nutrient availability) are exceptionally favorable, leading to strongly increased cell densities in the water column, commonly known as “algal blooms”. These natural phenomena happen frequently, for example in the form of the yearly observed peaks in the dominant diatom abundance in spring (the so-called spring bloom) or density peaks of often dinoflagellate dominated communities in fall, providing nutrients for the whole ecosystem (Cushing, 1959; Longhurst, 1995).

In contrast to such beneficial effects, a number of algal species can have dramatic adverse impacts, if cell density in the water column is rapidly increased to such extent that noxious or toxic effects on their ecosystem, human wellbeing and/or economy are manifest. These outbreaks are commonly known as harmful algal blooms (HABs). Although first hints on harmful algal blooms may be described already in the Bible (Exodus 7: 20-1), detailed knowledge about harmful algae was lacking for centuries (Dale and Yentsch, 1978). Since the creation of a defined research discipline at the First International Conference on Toxic Dinoflagellate Blooms in Boston/Massachusetts in 1974, an incredible number of studies on harmful algal events has increased the awareness of scientists and the general public towards this serious threat (LoCicero, 1975; Hallegraeff et al., 2004). HABs are most prominent in marine coastal waters and negative impacts usually occur at high cell densities, dominating the community structure or even modifying the color of the oceans’ surface (“red tides”). However, harmful effects may also occur at just a few hundred cells per liter of seawater - depending on the respective microalgal species (Lassus et al., 2016). Scientists have repeatedly tried to classify the harmful potential into several categories (Lassus, 1988; Hallegraeff, 1993; Andersen, 1996; Lassus et al., 2016; Kraberg and Stern, 2017). One reasonable

categorization might be the differentiation into two harmful algal groups: The first group shows *direct* negative effects by producing toxic compounds (e.g. *Alexandrium* spp. and *Dinophysis* spp.). On the one hand, these effects can be due to an increased uptake of toxic cells and/or toxins by other organisms like filter-feeders (e.g. mussels) and subsequent accumulation of the toxins in the food web. This may lead to highly concentrated toxin amounts and potentially death, especially in higher trophic organisms and human seafood consumers (Lopes et al., 2013). On the other hand, some microalgae produce highly potent toxins, which intoxicate and kill fish (i.e. ichthyotoxins like e.g. karlotoxins). The threat of these toxic microalgae becomes clear especially in cultured fish: Whereas fish in natural environments are able to actively avoid such bloom areas, trapped fish lack this opportunity and are much more exposed to the harmful conditions (Rossini, 2014). The second major group of harmful microalgae can have *indirect* harmful effects, e.g. by the formation of spines or production of mucus (e.g. *Akashiwo sanguinea*, *Chaetoceros* spp.), which may harm marine fauna and especially fish by clogging their gills. Another indirect effect can be the build-up of high biomass blooms which subsequently, via by bacterial degradation or viral attack, lead to a reduction of oxygen in the water (e.g. *Gonyaulax polygramma*, *Kryptoperidinium foliaceum*). Whereas the first group can show harmful effects due to toxin production already at relatively low cell densities, the harmful potential of the second group is usually related to high biomasses. It is very important to mention that toxic effects on other organisms do not necessarily reflect the key ecological function of compounds produced by microalgae (Rossini, 2014).

Harmful, toxin-producing species are represented in different microalgal groups (like diatoms, dinophytes, haptophytes, raphidophytes and a few other classes of flagellates) and cyanobacteria, and a variety of different toxins and respective symptoms have been associated with seven major seafood poisoning types (**Table 1**). HABs obviously influence ecosystem processes and additionally have impacts on the quality of marine seafood and aquaculture products, and therefore considerable economic consequences. This refers to both, reduction in local seafood consumption and lower export rates (Backer et al., 2015; Sanseverino et al., 2016; Ritzman et al., 2018). Hallegraeff et al. (2017) proposed that fish-killing microalgae have a much greater impact on the economy than those species that lead to shellfish biotoxins contamination. Nevertheless, the latter is of increasing importance in the perspective of a growing world population and demand for produced seafood with simultaneously decreasing natural fish stocks (Wijsman et al., 2019).

Table 1. Selected toxins and biological origin associated with different seafood poisoning syndromes. amnesic shellfish poisoning (ASP), azaspiracid shellfish poisoning (AZP), ciguatera fish poisoning (CFP), diarrhetic shellfish poisoning (DSP), neurotoxic shellfish poisoning (NSP), paralytic shellfish poisoning (PSP), spiroimine shellfish poisoning (SSP). Adapted from Dominguez et al. (2010) and Farabegoli et al. (2018).

Toxin	Biological source	Poisoning syndrome	Mode of action	Major toxin vector / affected organisms
Amphidinols (AMs)	<i>Amphidinium</i> spp.		antifungal, cytotoxic	fish
Azaspiracids (AZAs)	<i>Azadinium</i> spp. <i>Amphidoma languida</i>	AZP	cytotoxic	shellfish
Brevetoxins (BTXs)	<i>Karenia</i> spp.	NSP	sodium channel activation	shellfish
Ciguatoxins (CTXs) & Maitotoxins (MTXs)	<i>Gambierdiscus</i> spp. <i>Fukuyoa yasumotoi</i>	CFP	sodium channel activation	fish
Dinophysistoxins (DTXs) & Okadaic acid (OA)	<i>Dinophysis</i> spp. <i>Prorocentrum</i> spp.	DSP	protein phosphatase inhibition	shellfish
Domoic acid (DA)	<i>Pseudo-nitzschia</i> spp.	ASP	neurotoxic	shellfish
Goniodomines (GDs)	<i>Alexandrium</i> spp.		antifungal, cytotoxic	shellfish
Gymnocines	<i>Karenia mikimotoi</i>		cytotoxic	fish
Gymnodimines (GYMs)	<i>Alexandrium ostenfeldii</i> <i>Karenia selliformis</i>	SSP	acetylcholine receptor inhibition	
Karlotoxins (KmTxS)	<i>Karlodinium veneficum</i> <i>Karlodinium armiger</i>		membrane perforation	fish
Palytoxins (PLTXs) & Ovatoxins (OVTXs)	<i>Ostreopsis</i> spp.		Na/K-ATPase conversion	crabs, fish
Pectenotoxins (PTXs)	<i>Dinophysis</i> spp.	DSP	hepatotoxic	shellfish
Pinnatoxins (PnTXs) & Portimines	<i>Vulcanodinium rugosum</i>	SSP	cytotoxic	shellfish
Prorocentrolides (PcTXs)	<i>Prorocentrum lima</i> <i>Prorocentrum maculosum</i>		acetylcholine receptor inhibition	
Saxitoxins (STXs) & variants	<i>Alexandrium</i> spp. <i>Gymnodinium catenatum</i> <i>Pyrodinium bahamense</i>	PSP	sodium channel blockage	shellfish
Yessotoxins (YTXs) & Adriatoxins (ATXs)	<i>Protoceratium reticulatum</i> <i>Lingulodinium polyedra</i> <i>Gonyaulax</i> spp.	DSP	cytotoxic, neuronal damage	shellfish
Spirolides (SPXs)	<i>Alexandrium ostenfeldii</i>	SSP	acetylcholine receptor inhibition	shellfish

Harmful algal bloom events seem to occur more frequently and intensively in the past decades, with larger geographical extension and a higher species diversity (Van Dolah, 2000; Gobler et al., 2017; Griffith et al., 2019). Although the interplay of factors favoring these outbreaks is still poorly understood, anthropogenic environmental disturbances such as eutrophication and global climate change are widely accepted within the scientific community as important parameters affecting HAB formation (Anderson, 1989; Hallegraeff, 2003; Gobler, 2019).

The increasing attention towards HABs has led to an increasing number of studies on the complex interactions between factors favoring their proliferation (Shumway et al., 2018). Higher perception, modern methodologies, the extension of geographic research sites and management efforts (especially monitoring) started to complement HAB research and were able to minimize cases of illness associated with toxigenic microalgae. However, with each accomplishment, new knowledge gaps appear and highlight the need for further research on harmful algae.

1.2 Azaspiracids - a group of marine biotoxins

In 1995, eight people in the Netherlands suffered an illness after consumption of blue mussels (*Mytilus edulis*), harvested at Killary Harbour at the Irish west coast (McMahon and Silke, 1996). The symptoms (severe gastrointestinal symptoms like stomach cramps, nausea, diarrhea and vomiting) were similar to those of the diarrhetic shellfish poisoning (DSP) caused by lipophilic compounds of the dinoflagellate genus *Dinophysis*, but no DSP toxins were found in the shellfish. The responsible compound was identified two years later by Satake et al. (1998b) and later structurally revised (Nicolaou et al., 2006; Frederick et al., 2007) as a new lipophilic marine biotoxin, azaspiracid (AZA; **Fig. 1**), causing the azaspiracid shellfish poisoning syndrome (AZP). Further cases of unspecific diarrhetic symptoms after consumption of Irish shellfish reported from Italy, France and Ireland were putatively linked to AZP (James et al., 2000). In 2001, a regulatory limit (0.16 mg AZA-1 equivalent kg^{-1} mussel flesh) was set by the EU, based on a risk assessment by the Food Safety Authority of Ireland - FSAI (EU, 2001; FSAI, 2001). AZAs are a major threat in Ireland (**Suppl. Fig. S1**), where accumulation of AZA toxins in e.g. blue mussels (*Mytilus edulis*) have frequently led to toxin concentrations above this regulatory limit and subsequent closures of shellfish production areas (Salas et al., 2011). AZAs are not only present in Ireland, but have been detected in various areas around the globe, including the coast of England (James et al., 2002), Africa (Taleb et al., 2006), Portugal (Vale et al., 2008), Scandinavia (James et al., 2002; Torgersen

et al., 2008), Japan (Ueoka et al., 2009), China (Yao et al., 2010), Chile (López-Rivera et al., 2010), the US (Trainer et al., 2013), Argentina (Turner and Goya, 2015) and New Zealand (Smith et al., 2016). Shellfish farm closures due to exceeded AZA limits are regularly registered for Irish production sites, but exceptionally also for Norway in 2002/03 (Aasen et al., 2004) and also at the Atlantic coast of southern Spain in 2009 (Tillmann et al., 2017a).

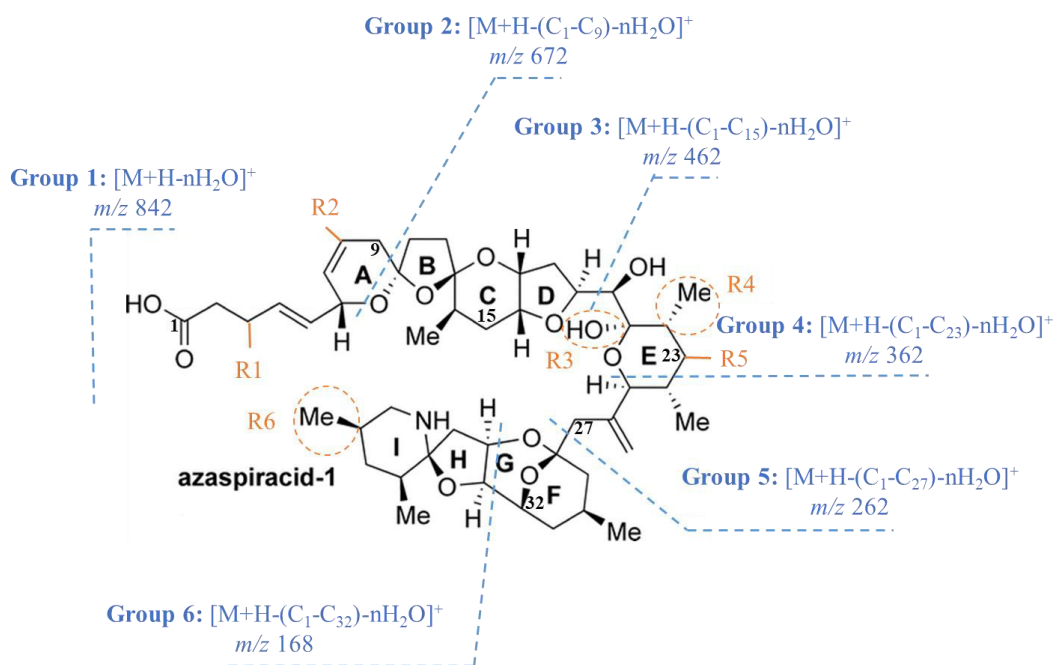


Fig. 1. Chemical structure of an azaspiracid (AZA-1) as revised by Nicolaou et al. (2006) and Frederick et al. (2007). Blue lines indicate the fragmentation pattern of AZA-1 into characteristic AZA fragment groups by LC-MS/MS analysis. Orange “R1-6” refer to molecule modification sites leading to AZA diversity (**Suppl. Table S1**). Adapted from Krock et al. (2019) and Hess et al. (2014).

After the structural elucidation of the first AZA (AZA-1), several analogs of the toxin were isolated from contaminated shellfish, leading to more than 20 described shellfish metabolites reported by Rehmann et al. (2008). Liquid-Chromatography-tandem-Mass-Spectrometry (LC-MS/MS) became a suitable method for the chemical analysis of AZAs in shellfish and replaced the mouse bioassay as the primary monitoring tool in 2011 (EU, 2011). The principle of LC-MS/MS is to separate sample mixtures with multiple components by liquid chromatography and to identify individual compounds by the highly specific detection of the molecule mass and characteristic molecule fragments in the mass spectrometer.

As the basic chemical structure of AZAs is relatively conserved in general, characteristic fragments have been noticed and are used for the detection of individual AZA variants (**Fig. 1**). Molecular modifications in AZAs (usually hydroxylation or methylation; **Suppl. Table S1**) are mostly noted at the biosynthetic end of the molecule, i.e. towards the carboxylic function (Kalaitzis et al., 2010; Krock et al., 2019). However, there were also two modifications described at the opposite end, i.e. the I-ring. The majority of AZAs shows a saturated I-ring and are methylated at the 39-position, resulting in a characteristic group 4 fragment (m/z 362), while some AZAs have an unsaturated I-ring (resulting in a group 4 fragment of m/z 360) or are demethylated (resulting in a group 4 fragment of m/z 348) (Krock et al., 2019). New AZA variants were frequently discovered (Rehmann et al., 2008; Hess et al., 2014) and until 2017, more than 50 AZA analogs were described (**Suppl. Table S1**), which include AZAs of planktonic origin, shellfish metabolites, extraction artefacts as well as proposed but not yet recorded variants. Numerous studies investigated the toxic effects of AZAs on the molecular, cellular and organ level in mice. Several organs have been shown to be negatively affected on the pulmonary, pancreatic, intestinal, hepatic and gastric systems (Twiner et al., 2008; Kilcoyne et al., 2014a; Tillmann et al., 2014c). Beside the effects on cytosolic calcium levels and pH in human lymphocytes (Román et al., 2004; Alfonso et al., 2006) and temporary depletions of ATP (Kellmann et al., 2009), recent studies demonstrated that AZAs significantly affect the mitochondrial hydrogenase activity in human cell lines (Twiner et al., 2014; Pelin et al., 2018; Pelin et al., 2019). These effects in hepatocytes are supposed to derive from an imbalance of intracellular K^+ levels and, in particular, Cl^- ions, as demonstrated by the selective reduction of toxin effects by CFTR chloride channel inhibition (Pelin et al., 2019). However, the actual mode of action of AZAs in humans still remains poorly understood.

The source of AZAs remained unknown for many years, until Tillmann et al. (2009) isolated a previously unidentified small photosynthetic dinoflagellate from the North Sea off the Scottish coast in 2007, then described as a new species - *Azadinium spinosum* - and which was confirmed as the first primary source of AZAs (Krock et al., 2009). The discovery and availability of strains of the AZA-producing dinoflagellate enabled several AZA biotransformation studies with the blue mussel (*M. edulis*) and *Az. spinosum*. Exposure to *Az. spinosum* cells revealed a very rapid accumulation of AZAs with levels exceeding the EU regulatory limit of 0.16 mg AZA kg^{-1} mussel flesh within six hours (Salas et al., 2011; Jauffrais et al., 2012d). Within one week of continuous exposure, AZA levels of up to 0.6 mg kg^{-1} were determined. Furthermore, detoxification kinetic

rates were relatively slow ($T_{1/2}$ of approximately 11 days) suggesting that alarming AZA concentrations may remain for an extended period.

Although mussels also showed the capacity to reduce AZA accumulation by actively decreasing the filtration rate, the rapid accumulation to high levels emphasized the need for the early detection of the producing microalgae in the field (Jauffrais et al., 2012a). Rapid biotransformation (within a few hours of exposure) of AZA-1 and -2 into various metabolites has been described (Jauffrais et al., 2012d). Further research on the effect of dissolved AZAs revealed bioavailability and accumulation exceeding the regulatory limit (Jauffrais et al., 2013a) and demonstrated that AZAs can enter shellfish flesh at least in two ways, either as AZAs ingested from intact cells and digested via the digestive gland or in a dissolved form over the gills. AZAs are also accumulated by other marine organisms: they have been reported in several other bivalves molluscs, including cockles (*C. edule*), oysters (*C. gigas*, *O. edulis*), Manila clams (*T. philippinarum*), razor clams (*E. siliqua*), as well as in a marine sponge (*Echinoclathria* sp.) and the brown crab (*C. pagurus*) (Hess et al., 2003; Torgersen et al., 2008; Ueoka et al., 2009; Furey et al., 2010).

1.3 Amphidomataceae - the source of azaspiracids

With approximately 2,500 species, dinoflagellates (Dinophyceae) represent a major constituent of aquatic food webs and with potentially high cell densities are one of the most important components in both, marine and freshwater ecosystems (Spector, 2012). Most dinoflagellates are planktonic, whereas only 8% are benthic, and 49% of the species are heterotrophic (devoid of plastids), which may be saprophobic, parasitic, holozoic or harbor symbionts (Gómez, 2012). Mixotrophic and heterotrophic dinoflagellates are able to feed on a whole variety of prey items including bacteria, picoeukaryotes, nanoflagellates, diatoms, dinoflagellates, other heterotrophic protists and metazoans. In turn, dinoflagellates themselves are ingested by several predators (Jeong et al., 2010). Thus, dinoflagellates play a very diverse and important role in marine food webs.

Most dinoflagellate genera reveal a cell cortex composed of membranes, thecal plates and microtubules along the cell periphery and the structure, formation and arrangement of the cell cortex display characteristic morphological features (Spector, 2012). Eponymous is the presence of two different flagella, one longitudinal and one transverse flagellum, enabling the cell for its characteristic spiraling forward movement (**Fig. 2**). The transverse flagellum is usually located in a transverse groove (the cingulum), which divides the cell into the upper episome and the lower

hyposome. Dinoflagellates reveal unusual nuclear characteristics such as permanently condensed chromosomes, extraordinary mitosis and the lack of conventional histones and nucleosomes (Taylor (1979); Spector (2012) and references within).

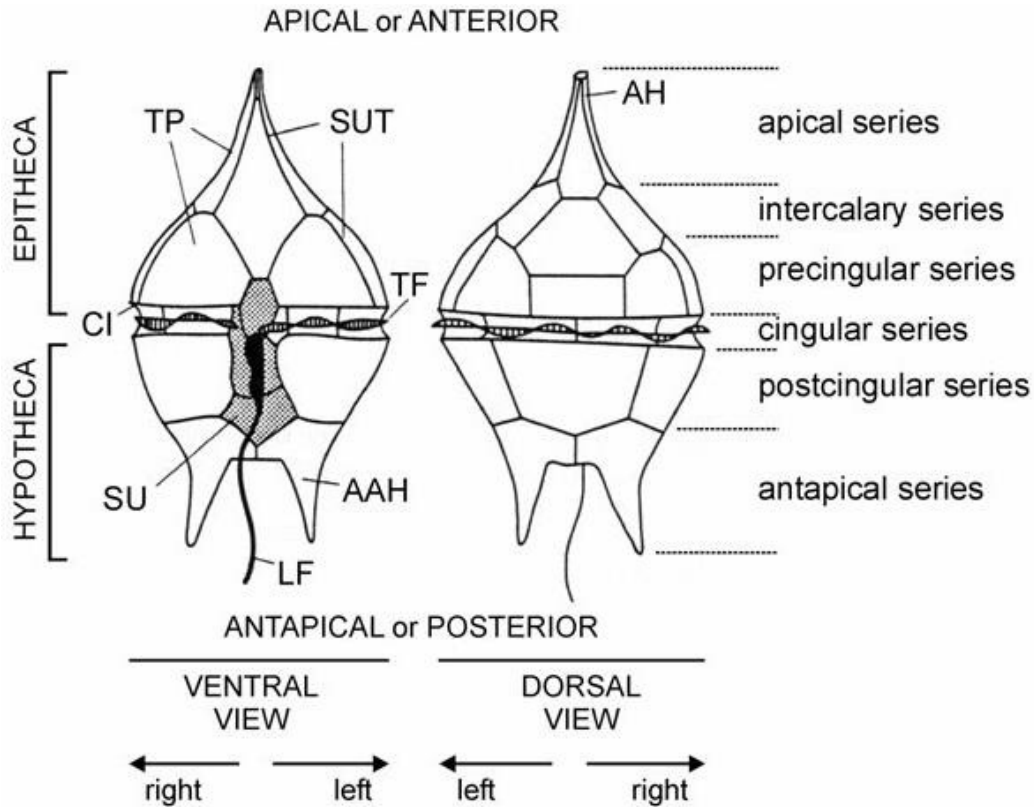


Fig. 2. Principal morphological features of a typical thecate motile dinoflagellate (Streng, 2003). AAH = antapical horn; AH = apical horn; CI = cingulum; LF = longitudinal flagellum; SU = sulcus; SUT = suture between thecal plates; TF = transversal flagellum; TP = thecal plates.

Since *Azadinium spinosum* has been identified as a primary source for AZAs in 2007, intense research revealed a high biodiversity within the genus *Azadinium*. Until 2017, in total 14 species have been described, from which only three, *Az. spinosum*, *Az. poporum* and *Az. dexteroporum* are known azaspiracid producers (Krock et al., 2012; Tillmann and Akselman, 2016; Rossi et al., 2017). However, AZA synthesis is not limited to microalgal species of the genus *Azadinium*. In 2012, a newly described dinoflagellate species - *Amphidoma languida* - was morphologically and phylogenetically characterized as a close relative of the genus *Azadinium*, and both genera (*Azadinium* and *Amphidoma*) together form the family Amphidomataceae (Sournia, 1984; Tillmann et al., 2012a). AZAs have also been detected in *Am. languida*.

Amphidomatacean species are characterized by morphological features as the small cell size (most species approx. 10-16 μm in cell length) and an ovoid to elliptical shape with a hemispheric episome. The latter shows slightly convex sides, which end in a distinct pointed apex. A wide and deep cingulum is present. All species are photosynthetic and contain presumably one single chloroplast, extending into the hypo- and episome. Species can have one or multiple stalked pyrenoids, but several species do not have any. Most visible under scanning electron microscopy (SEM), Amphidomataceae have thecal plates in distinct, specific patterns. *Azadinium* species show a Kofoidian plate pattern of Po, cp, X, 3-4', 2-3a, 6'', 6C, 5S, 6''', 2'''''. Whereas the presence of four apical plates and three intercalary plates is the basic *Azadinium* pattern, a few species (*Az. dalianense*, *Az. zhuanum*) have a reduced number of apical plates with three apical and/or two epithecal intercalary plates. The plate pattern of *Am. languida* is, as for all *Amphidoma* species, characterized by six apical plates but no anterior intercalary plates instead. For all *Azadinium* and *Amphidoma* species, the apical pore complex is characteristic, which is composed of an X-plate and a pore plate with a central round pore covered by a cover plate. The general plate tabulation pattern of five different plate rows revealed the family Amphidomataceae as a member of the dinophycean subclass Peridiniphyceae (Tillmann et al., 2009), but the relationship to the two orders of this subclass (Peridiniales and Gonyaulacales) remains uncertain, since Amphidomataceae show characteristically morphological features of both. Molecular phylogenetic analyses placed amphidomataceans closer to Peridiniales than to Gonyaulacales, but a final conclusion on the order affiliation of Amphidomataceae is lacking (Tillmann et al., 2014a). The three AZA producing amphidomatacean species known to occur in the eastern North Atlantic (AZA producing *Az. dexteroporum* was so far only detected in the Mediterranean) were considered for further research in the course of this PhD and are described in more detail within the following paragraphs.

***Azadinium spinosum* Elbrächter et Tillmann (Tillmann et al., 2009)**

Azadinium spinosum is a rather small photosynthetic dinoflagellate, with a general cell length of 12-16 μm (**Fig. 3A**). The theca is slightly dorsoventrally compressed and the epitheca is larger than the hypotheca and has a characteristic apical pore complex (APC) at the top. One cingulum and one chloroplast can be observed by light microscopy, as well as one large pyrenoid within the episome. The most characteristic and eponymous morphological feature is a small antapical spine at the cells' right side (although an antapical spine was later on also observed in other amphidomatacean species).

The first strain of *Az. spinosum* (3D9) originates from the Scottish east coast in 2007. Since then, this species has been detected at several coastal areas of the north-east Atlantic, including the Irish, Shetland and Norwegian coast, but also in the south Atlantic (Argentina) and Puget Sound (USA) (Akselman and Negri, 2010; Akselman and Negri, 2012; Tillmann et al., 2012b; Kim et al., 2017). *Azadinium spinosum* was also the first amphidomatacean species proven to synthesize azaspiracids, including AZA-1, -2, -33, -34 and -35 (Kilcoyne et al., 2014b). The toxin profile of AZA-1, -2 and -33 seems to be the dominant AZA profile in North Sea strains (Tillmann et al., 2012b; Kilcoyne et al., 2014b). AZA cell quota estimations for *Az. spinosum* are mainly based on laboratory experiments of isolated strains and varied between 1 and 100 fg AZA-1 equiv. cell⁻¹ (Tillmann et al., 2009; Salas et al., 2011; Jauffrais et al., 2013b).

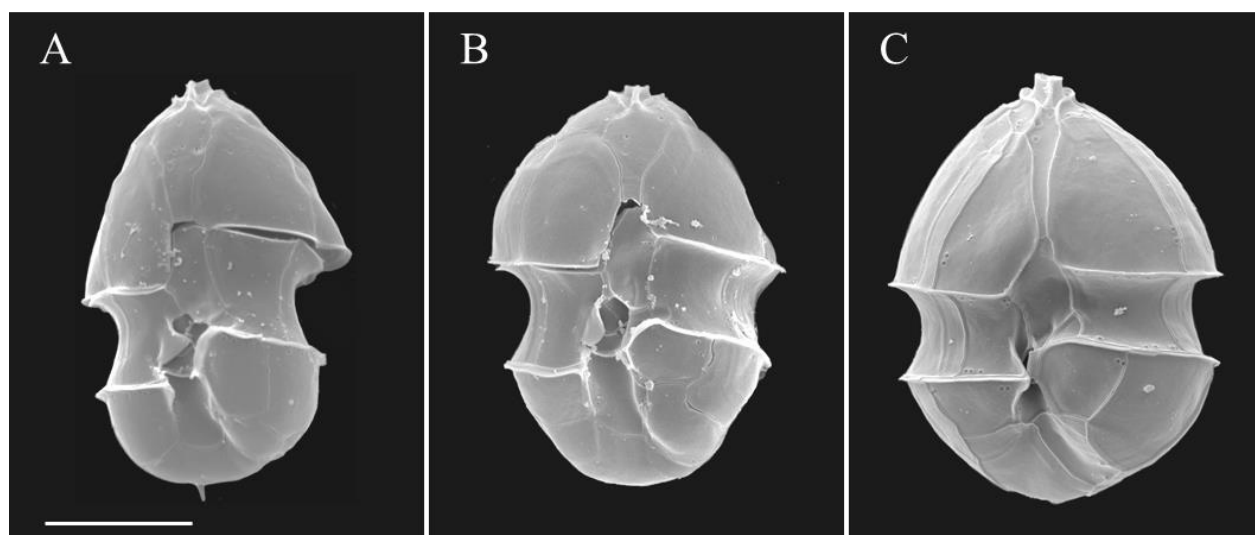


Fig. 3. SEM micrographs of (A) *Az. spinosum*, (B) *Az. poporum* and (C) *Am. languida* in the ventral view. Scale bar: 5 μm . Micrographs by U. Tillmann.

***Azadinium poporum* Tillmann et Elbrächter (Tillmann et al., 2011)**

With a general cell size of 11-16 μm in length and a slight dorsoventrally compression, *Az. poporum* (**Fig. 3B**) is very similar to *Az. spinosum* and other amphidomataceans. However, up to four pyrenoids distributed in both, the epi- and hyposome are visible in LM. The most distinctive morphological feature is the characteristic position of the ventral pore at the left side of the apical pore plate, at the junction with the first two apical plates.

Azadinium poporum was first isolated (type strain UTHC8) in 2008 from the southern North Sea off the Danish coast (Tillmann et al., 2011). Further records revealed a wide distribution area of this species around Ireland, Norway, the Mediterranean, Argentina, Mexico, China, New Zealand and the south-east Pacific (Gu et al., 2013; Luo et al., 2016; Smith et al., 2016; Tillmann et al., 2016; Kim et al., 2017; Luo et al., 2017b; Tillmann et al., 2017c). *Azadinium poporum* strains from China differed slightly in DNA sequence data from the North Sea strains, resulting in the erection of three ribotypes, named A (North Atlantic), B and C (both China Sea) (Gu et al., 2013).

Although this species was originally described as lacking any AZAs, soon Krock et al. (2015) confirmed the newly found variant AZA-37 being produced by the North Sea *Az. poporum* strains. Subsequently, a larger number of different AZAs was detected in other *Az. poporum*. Strains isolated from the Mediterranean and Argentina produced mainly AZA-2, including the first record of a phosphate (AZA-2 phosphate) AZA toxin (Tillmann et al., 2016), whereas the major compound of Chilean strains was AZA-11 (Tillmann et al., 2017c). Chinese strains produce AZA-36, -40 and -41 (Krock et al., 2014). New AZA-59 was recently detected in *Az. poporum* strains from Puget Sound, USA (Kim et al., 2017). In conclusion, *Az. poporum* displays a huge diversity of AZA profiles (AZA-2, -11, -36, -37, -40, -41), including also strains without detectable AZAs (Gu et al., 2013; Krock et al., 2014; Luo et al., 2018).

***Amphidoma languida* Tillmann, Salas et Elbrächter (Tillmann et al., 2012a)**

The size of *Am. languida* is similar to the two previous described species (12.9-15.5 µm in length), however the relatively large cell width of 9.7-14.1 µm gives this species a more ovoid shape (Fig. 3C). In contrast to *Azadinium* spp., *Amphidoma languida* has six apical and no anterior intercalary plates (*Azadinium* has 3-4 apical plates and 2-3 anterior intercalary plates) and a large antapical pore. One large pyrenoid is located within the center of the episome.

Although first described from Bantry Bay (Ireland), observations in samples from the Skagerrak (Denmark), Iceland, Norway, Spain, Argentina and west Indian Ocean indicate, that *Am. languida* is a common amphidomatacean species not only in the North Atlantic, but potentially has a widespread or even global distribution (Tillmann et al., 2015; Tillmann and Akselman, 2016; Tillmann et al., 2017a). In the species description paper, no AZAs were reported for *Am. languida*. In the course of further research, however the new structural variants AZA-38 and -39 were identified being directly synthesized by the type strain (SM1) and apparently being the dominant AZA profile of *Am. languida* (Krock et al., 2012; Tillmann et al., 2015). *Amphidoma languida* has

recently been identified as the causative agent of AZA shellfish contamination above the EU regulatory limit in aquaculture areas of Huelva (southern Spain) in 2009. An alternative AZA profile consisting of AZA-2 and -43 instead of AZA-38 and -39 were found in a Spanish strain, revealing that there is toxin profile variability in *Amphidoma* as well (Tillmann et al., 2017a). The actual threat of this species to humans remains uncertain, because *in vivo* toxicity of AZA-38, -39 and -43 has not been investigated yet. If other representatives of the genus *Amphidoma* synthesize AZAs is unclear, because of the 15 species within the genus, only *Am. languida* has been tested and showed detectable amounts and different AZA analogues (Krock et al., 2012; Tillmann et al., 2017a; Tillmann et al., 2018b).

All AZA producers and AZAs known until the start of this PhD (2017) are summarized in **Table 2**. AZA-2 (detected in *Az. spinosum*, *Az. poporum* and *Am. languida*) and AZA-35 (detected in *Az. spinosum* and *Az. dexteroporum*) are examples that certain AZA variants are not necessarily species-specific traits.

Table 2. Literature review on toxigenic Amphidomataceae and respective AZA (until 2017).

Species	detected AZA*	References
<i>Azadinium spinosum</i>	AZA-1, -2, -33, -34, -35	(Krock et al., 2009; Tillmann et al., 2009; Kilcoyne et al., 2014b)
<i>Azadinium poporum</i>	AZA-2, -11, -36, -37, -40, -41, -59	(Tillmann et al., 2011; Krock et al., 2014; Krock et al., 2015; Kim et al., 2017)
<i>Azadinium dexteroporum</i>	AZA-35, -54, -55, -56, -57, -58, epi-AZA-7	(Percopo et al., 2013; Rossi et al., 2017)
<i>Amphidoma languida</i>	AZA-2, -38, -39, -43	(Krock et al., 2012; Tillmann et al., 2012a; Tillmann et al., 2017a)

* detailed variations in the AZA molecule are indicated in **Fig. 1** and **Suppl. Table S1**.

Since the discovery of the AZA producing organisms, the number of global records of Amphidomataceae (**Fig. 4**) and AZAs increased continuously (López-Rivera et al., 2010; Trainer et al., 2013). This is of course related to an increasing awareness, and a number of studies were performed specifically targeting Amphidomataceae, leading to further method development for investigations of AZAs and their producers under field conditions.

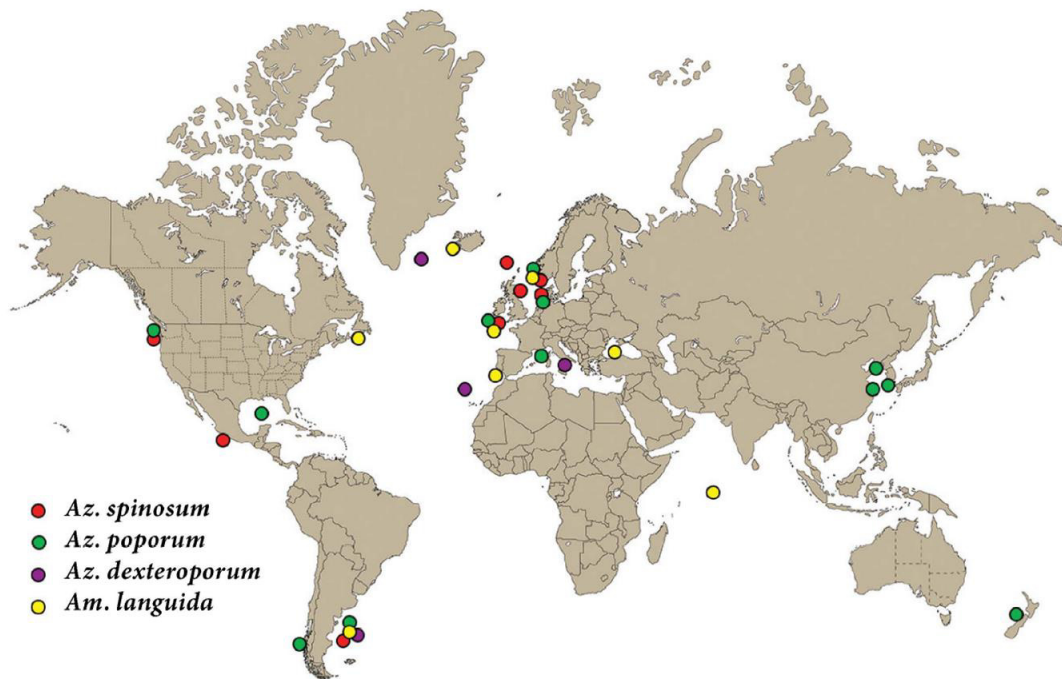


Fig. 4. Global records of toxigenic amphidomatacean species as known until the start of this PhD project (Tillmann, 2018).

Molecular detection of toxigenic Amphidomataceae

One main reason for the late identification of the AZA producers might be their small cell size and inconspicuousness, which make them very difficult to be identified by traditional light microscopy. Nevertheless, especially for field investigations, species identification and differentiation are indispensable for Amphidomataceae, because toxigenic and non-toxigenic representatives are very similar in their size, shape and geographical distributions, which leads to co-occurrence of several species in the same area (Tillmann, 2018). A reliable morphological identification of amphidomatacean species requires enhanced microscopic techniques like electron microscopy, as well as the respective expertise. It then becomes a time-consuming task, especially if other species of similar size and shape, such as *Heterocapsa* spp., are also present in a sample (Tillmann et al., 2010). Due to this high grade of complexity, after more than ten years of research, diversity and global biogeography of Amphidomataceae are still insufficiently known and monitoring of the toxigenic representatives remains challenging.

Since a couple of years molecular tools started to successfully support microscopic and chemical approaches on microorganism species detection to address these limitations and became an ideal

complementary additive for rapid, routine identification of HAB species in field samples (Edvardsen et al., 2013; Penna and Galluzzi, 2013; Eckford-Soper and Daugbjerg, 2015). Starting in the mid 90's, with beginning of the 21th century scientists have realized the potential of rapid, PCR-based methods for the detection of harmful microalgae in addition to shellfish toxicity tests to overcome limitations of microscopic monitoring (Rollo et al., 1995; Penna and Magnani, 1999; Bowers et al., 2000; Coyne et al., 2001; Godhe et al., 2001). The ribosomal DNA (rDNA) region was discovered as being a good target for molecular assays in various marine, toxic microalgae (including dinoflagellates), because these sequences were found to be species-specific and highly conserved regions and exist in high tandem copy numbers (Stryer, 1995; Hershkovitz and Lewis, 1996; Medina et al., 2001). Since then, intense method development took place and molecular assays became available for many harmful microalgae as for example *Pseudo-nitzschia* spp., *Alexandrium* spp., *Ostreopsis* spp. and *Dinophysis* spp. (Galluzzi et al., 2004; Hosoi-Tanabe and Sako, 2005; Andree et al., 2011; Perini et al., 2011; Casabianca et al., 2013). In addition to statements about presence or absence of the target species, by inclusion of DNA-based standard curves, the molecular PCR assays are powerful quantitative (qPCR) tools (Park et al., 2007; Godhe et al., 2008; Casabianca et al., 2013). Together with decreasing costs, qPCR became subsequently also interesting for routine monitoring of toxigenic microalgae (Garneau et al., 2011; Zamor et al., 2012).

To expand biogeographic studies on toxigenic Amphidomataceae, Toebe et al. (2013) designed qPCR assays targeting the large subunit (LSU / 28S) region of the ribosomal DNA for the first three described *Azadinium* species (*Az. spinosum*, *Az. poporum*, *Az. obesum*). Three years later, Smith et al. (2016) added a SYBR-Green based general amphidomatacean real-time PCR assay based on cultures and DNA samples that were available at that time, which allows the detection of all amphidomatacean species. The development of the molecular assays targeting *Az. spinosum* and *Az. poporum* has been a crucial step towards frequent and large-scale observation of these species, and the Marine Institute (Galway, Ireland) incorporated both assays into official Irish monitoring programs. Both species were frequently observed at the Irish coast and thus confirmed their role for the AZP risk in Irish waters (Clarke, 2020). Although specific assays for two of the AZA producing species (*Az. spinosum* and *Az. poporum*) were available and in use, species-specific qPCR assays for toxigenic *Am. languida* and *Az. dexteroporum* are still missing (Smith et al., 2016; Kim et al., 2017; Tillmann et al., 2017c).

1.4 AZA and Amphidomataceae in the North Sea area

The North Sea is part of the eastern North Atlantic, located on the European continental shelf and surrounded by coastlines of several bordering states: The United Kingdom, France, Belgium, the Netherlands, Germany, Denmark, Sweden and Norway. It is connected to the open North Atlantic by the Norwegian Sea in the north and the English Channel in the south. Through the Skagerrak and Kattegat in the east, the North Sea is also connected to the Baltic Sea.

With an approximate size of 1,000 km in length, 600 km in width, a surface area of $7.5 \times 10^5 \text{ km}^2$ and an average depth of $\sim 100 \text{ m}$, the North Sea is a relatively small marine habitat (compared to e.g. the Mediterranean Sea: surface area $\sim 2.5 \times 10^6 \text{ km}^2$, average depth $\sim 1,450 \text{ m}$) (OSPAR, 2000; Boxer and Salah, 2019). Coastal regions as interfaces between the ocean and terrestrial systems offer very unique conditions, since they are influenced by many factors like currents, waves, weather and terrestrial runoffs. The daily tides in the North Sea generate a sea level difference of up to eight meters between low and high tide, creating the largest Wadden Sea area on this planet, which has been inscribed into UNESCO's World Heritage List in 2009.

In terms of salinity, the North Sea area exhibits considerable gradients from higher saline northern parts (salinity ~ 35) towards the more brackish conditions near the southern coast. The latter is influenced by variable freshwater inflows from rivers like the Thames, Humber, Rhine, Weser and Elbe estuaries, leading to significantly lower salinities (Emeis et al., 2015; Sheehan et al., 2020). In addition, rivers do not only represent freshwater inflow, but also nutrient influx, making the shelf area of the southern North Sea, e.g. the German Bight, a highly productive habitat (Joint and Pomroy, 1993; Rick et al., 2006; Charnock et al., 2012).

The North Sea area generally represents a valuable substrate for on-shore aquaculture production, which is well-established by the bordering states (Jansen et al. (2016) and references within), and aquaculture in European coastal waters has a substantial increasing importance for food supply (Eriksen et al., 2014). Therefore, the European Commission (EC) stresses to increase production towards a sustainable, but competitive European aquaculture sector in policy documents such as the Blue Growth Strategy and the Strategic Guidelines for the sustainable development of EU aquaculture (EC, 2012, 2013).

In March 2002, the European Commission defined the maximum permitted limit of AZP toxins (AZA-1, -2 and -3) in bivalve mollusks, echinoderms, tunicates and marine gastropods (whole body or any part edible separately) as $160 \mu\text{g kg}^{-1}$. Although primary considered as the reference method for marine toxin analysis, the mouse bioassay has been replaced in most European

countries by non-invasive methods, particularly by liquid chromatography coupled with tandem mass spectrometry (LC-MS/MS). However, the monitoring of marine biotoxins in aquaculture production areas is not regulated by the EU, but by each member state separately. This results in high flexibility and individual benefits for monitoring systems of the countries, but leads also to a disparity of systems and makes it almost impossible to create an up-to-date scheme, which allows a reliable and transparent comparison on monitoring efforts for the North Sea area.

While European governments implemented more or less frequent monitoring of AZAs in shellfish products (for a list of institutions see **Suppl. Table S2**), the monitoring of the actual producing organisms of AZAs is rather scarce. Personal communication with scientists and collaborators of the respective institutions listed here revealed that only Belgium (A. Troupiotis, M. Derijcke; pers. com.), Denmark (H. Jakobsen, P. Andersen; pers. com.), the UK (A. Turner; pers. com.), the Netherlands (A. Gerssen, M. Poelman; pers. com.), Norway (W. Eikrem; pers. com.) and Sweden (B. Karlsson; pers. com.) Amphidomataceae as a potential threat in general. Actual checking for (toxigenic) Amphidomataceae however, is only performed by the Danish, Dutch and Swedish authorities. However, the techniques used to detect these dinoflagellates are by far not standardized and vary from traditional light microscopy (the Netherlands; A. Gerssen, M. Poelman; pers. com.), over quantitative epifluorescence microscopy (Denmark; H. Jakobsen, P. Andersen; pers. com.) to 18S rDNA metabarcoding (Sweden; B. Karlsson; pers. com.). Most intense and frequent monitoring is performed year round by the Marine Institute in Galway, Ireland, which applies the family-specific amphidomatacean assay, as well as the species-specific qPCR assays on toxigenic *Az. spinosum*, *Az. poporum* and the non-toxigenic *Az. obesum* in addition to traditional light microscopy since 2012 (Clarke, 2020).

Previous observations suggest that toxigenic Amphidomataceae frequently occur in the eastern North Atlantic. However, still little is known about their spatial, temporal and quantitative occurrences, as well as about promoting environmental conditions population growth. Current monitoring of the chemical compounds (AZAs) is implemented in official monitoring programs, the frequent monitoring of the producing species on the other hand is very limited.

The overall motivation of this work was therefore to increase knowledge about the biogeography of toxigenic Amphidomataceae in the eastern North Atlantic by microscopic, chemical and molecular investigations. Supported by physiological studies, the risk potential of AZP in the North Sea and adjacent areas (i.e. the Skagerrak, Kattegat and Belt, the Celtic Sea, as well as the Irish, Scottish and Norwegian coastal waters) was evaluated under the perspective of global change conditions. The results should help to improve safe and sustainable coastal seafood production in the eastern North Atlantic.

2. Objectives

The following research objectives have been addressed:

1) qPCR assay development for toxigenic *Am. languida*

While the species-specific qPCR assays for the molecular detection and quantification of toxigenic *Az. spinosum* and *Az. poporum* are successfully in use, the assay for the third toxigenic species in the North Atlantic, *Amphidoma languida*, is not yet available. As a prerequisite for further biogeographic studies, the aims were

- a) to design a highly specific and sensitive qPCR assay for the detection of *Am. languida*,
- b) to validate both qualitative and quantitative detection,
- c) to validate the assay under field conditions for future study and monitoring applications.

2) Diversity and biogeography of toxigenic Amphidomataceae

Knowledge about the spatial and temporal occurrence of toxigenic Amphidomataceae and respective AZAs in the North Sea and adjacent areas is relatively limited. Thus, the aims were

- a) to investigate the biodiversity of (toxigenic) Amphidomataceae in the North Sea area,
- b) to qualitatively and quantitatively assess the spatial occurrence of the three toxigenic species in various field sample sets originating from excursions in the North Sea,
- c) to qualitatively and quantitatively assess the temporal occurrence of the three toxigenic species via year-round, frequent sampling at fixed North Sea stations,
- d) to validate correlations of estimated species cell densities by qPCR and microscopy with respective measured AZA abundances in the field.

3) Environmental parameters and physiology

In a few previous laboratory settings, temperature has been shown to influence growth-rate and AZA production of toxigenic amphidomatacean species. However, these experiments were limited to *Az. spinosum* and *Az. poporum*, and strains from the North Sea area are not well represented. Therefore, the aims were

- a) to correlate measured temperatures with estimated cell densities of toxigenic amphidomatacean species in the field,
- b) to compare growth and toxin production of several toxigenic amphidomatacean strains from the North Sea area under different temperature regimes, including the first laboratory experiment on toxigenic *Am. languida*.

4) Current AZP risk potential in the North Sea

Based on the collected biogeography, diversity and physiology data during this PhD project, the final objective was to assess the AZP risk potential in the North Sea and adjacent areas under future global change conditions with emphasize on rising ocean temperatures.

3. Results and Discussion

3.1 Diversity of Amphidomataceae

3.1.1 Taxonomic diversity

The complementary approach of morphological analyses and molecular sequencing techniques revealed five new non-toxicogenic amphidomatacean species and increased the known diversity within this family to a total of 33 species. The strains of these new species originate from different geographical regions, supporting the hypothesis that Amphidomataceae is a globally distributed dinophyte family.

The relatively small *Amphidoma parvula* sp. nov. was isolated from the South Atlantic Shelf off Argentina in 2015 and revealed the characteristic plate arrangement of *Amphidoma* with six apical, precingular and postcingular plates, and phylogenetic analyses placed the new species into *Amphidoma* as a sister species of *Am. languida* (Tillmann et al. (2018b); **Fig. 6**).

As part of the present PhD study, samples collected from the western Greenland coast and central Labrador Sea in 2017 revealed new strains of several known species (*Az. obesum*, *Az. trinitatum*, *Az. dexteroporum*) as well as the new species *Azadinium perforatum* sp. nov. (**Publication III**), emphasizing that Amphidomataceae are generally able to cope with colder water temperatures. The new species was morphologically and phylogenetically assigned to the genus *Azadinium*, and differentiated from other *Azadinium* species by the unique presence of thecal pores on the pore plate (**Fig. 5A-C, Fig. 6**).

During a survey in 2018, cell isolations revealed the presence of three new *Azadinium* species in Irish coastal waters (**Publication VI**; note that the proposed new species names used here are preliminary since they are not yet being validly published). *Az. galwayense* sp. nov. shares the characteristic right-side apical position of the ventral pore (**Fig. 5D-F**) as observed in *Am. languida*, *Am. parvula*, *Az. concinnum*, *Az. perforatum*, *Az. perfusorium* and *Az. dexteroporum*, and differs from other *Azadinium* by a characteristic combination of morphological features. For the second new species, *Az. perfusorium* sp. nov. (**Fig. 5G-I**), first on-board investigations by LM led to an initially incorrect identification as *Az. dalianense*, but this species was doubtlessly differentiated from *Az. dalianense* by SEM later and was assigned as a new species supported by DNA sequence analyses (**Fig. 6**). Distinct pyrenoid(s) as seen in **Fig. 5** in Amphidomataceae generally appear prominent in LM, because they are surrounded by a starch sheath.

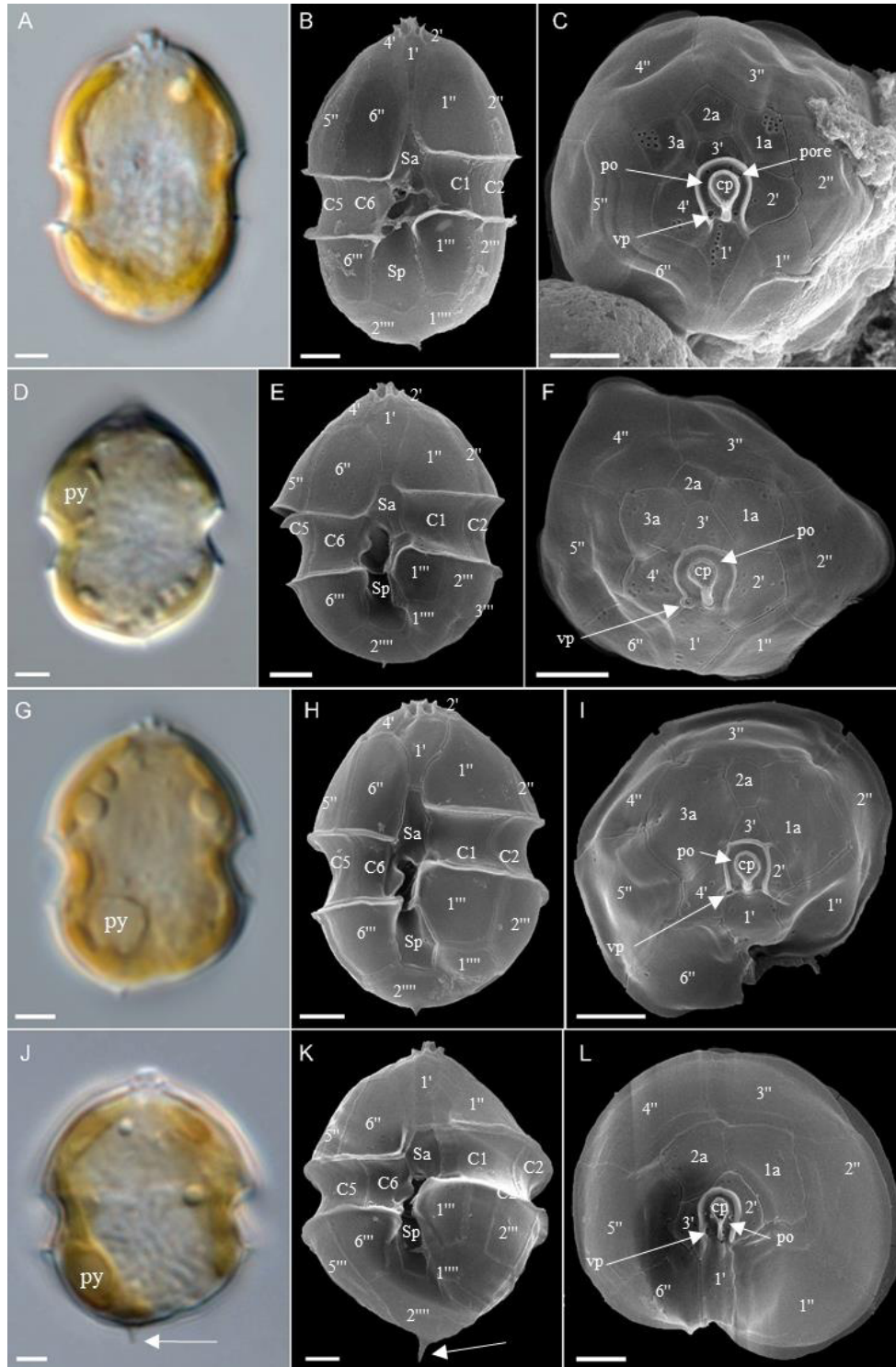


Fig. 5. Micrographs of newly described amphidomatacean species (A-C) *Az. perforatum*, (D-F) *Az. galwayense*, (G-I) *Az. perfusorium* and (J-L) *Az. pseudozhuanum*. (A, D, G, J) LM of formalin fixed cells, py = pyrenoid. (B, E, H, K) SEM Ventral view and (C, F, I, L) apical view. Arrows in J and K indicate the prominent spine in *Az. pseudozhuanum*. Plate labels in SEM micrographs according to the Kofoidian system. cp = cover plate; po = pore plate; Sa = anterior sulcal plate; Sp = posterior sulcal plate; vp = ventral pore. Scale bars = 2 μ m.

The third new species of the survey, *Az. pseudozhuanum* sp. nov. (**Fig. 5J-L**), was found to be morphologically very similar to *Az. zhuanum*, but it could be distinguished by SEM from other *Azadinium* (including *Az. zhuanum*) due to the characteristic plate pattern. In phylogenetic analyses, *Az. pseudozhuanum* and *Az. zhuanum* were represented as a highly supported sister clade, indicating a close relationship of both species (**Fig. 6**). Three newly identified *Azadinium* species and the identification of eight different species (*Az. spinosum*, *Az. poporum*, *Am. languida*, *Az. caudatum*, *Az. obesum*, *Az. pseudozhuanum*, *Az. galwayense* and *Az. perforatum*) plus one so far unknown *Azadinium* species (as seen by LM only) confirmed that Amphidomataceae are an integrated component of the phytoplankton community in Irish coastal waters, supporting the enhanced monitoring efforts by this country (**Publication VI**). The description of in total four new species within the course of this PhD project considerably increased knowledge on the biodiversity of Amphidomataceae (**Objective 2a**) and suggests that an even higher diversity can be expected. Phylogenetic analyses based on concatenated rDNA sequences generally support morphological observations in Amphidomataceae, but dissonant results have also been noticed. Whereas molecular phylogeny (i.e. placement of species in the phylogenetic tree) unequivocally revealed that Amphidomataceae are monophyletic, the trees lack significant statistical support for many of the internal amphidomatacean nodes and thus the evolutionary relationship for the species is not clear yet. As an example, newly described *Az. perforatum* was initially placed (without statistical support) in one branch with *Am. languida* and *Am. parvula*, but with more and new sequence data it is now part of *Azadinium* spp. (**Publications III, VI and VII**).

Even though phylogenetic placement within Amphidomataceae is still not fully solved, rDNA sequence analysis is highly supportive especially in the light of lacking morphological features between or within species. For example, in contrast to significant rDNA sequence differences, significant and consistent morphological differences between the five *Az. dalianense* ribotypes have not been observed so far (**Publication II**). The newly described *Az. cf. spinosum*, which was found to be morphologically identical to *Az. spinosum*, clusters phylogenetically together with *Az. obesum* (**Publication VII, Fig. 6**). Nevertheless, there are also examples for which current molecular phylogeny reflects morphological traits and vice versa. The phylogenetically early diverging group consisting of *Am. languida*, *Am. parvula*, *Az. concinnum*, *Az. perforatum*, *Az. galwayense*, *Az. perforatum* and *Az. dexteroporum* all share the right-side apical position of the ventral pore compared to the other amphidomatacean species, indicating that this might be an ancestral trait in Amphidomataceae (**Publication VII**).

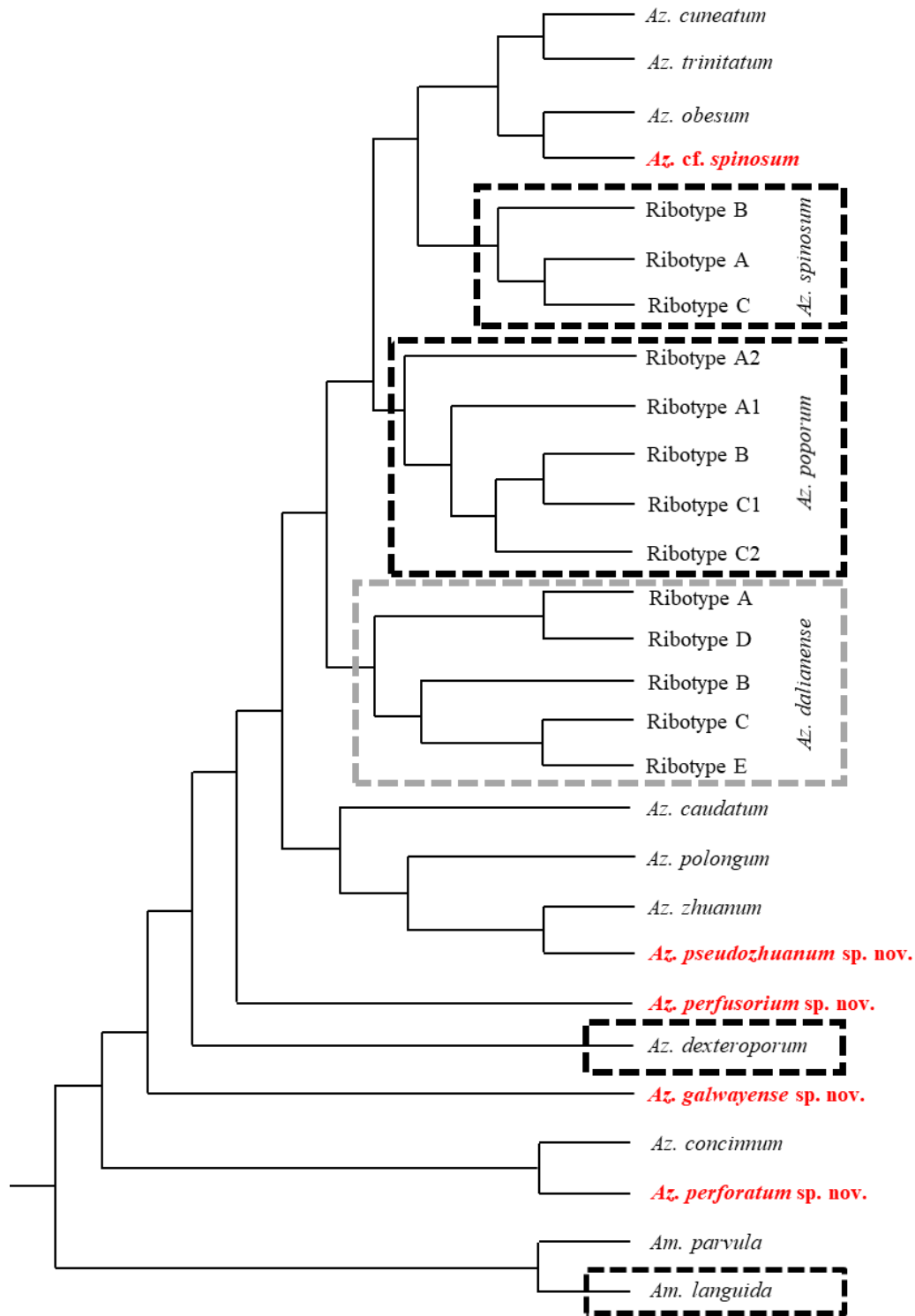


Fig. 6. Current, conceptual molecular phylogeny of Amphidomataceae based on concatenated SSU, ITS1-5.8S-ITS2 and LSU (D1-D2) rDNA sequences (detailed Sanger Sequencing protocol presented in **Suppl. Method I1**). New species described in the course of this PhD are indicated in red. Dashed, black boxes indicate species with toxigenic representatives. The grey dashed box is for better visual presentation of the five known *Az. dalianense* ribotypes. Branch length is not related to genetic distances. Adapted from **Publications VI** and **VII**.

Azadinium zhuanum and *Az. pseudozhuanum* revealed a very similar morphology, which is supported by the close phylogenetic placement (**Fig. 6**). Both species are mainly differentiated by the reduced number of apical plates (from four to three) in *Az. pseudozhuanum*. This feature however, was also observed in *Az. dalianense*, which is phylogenetically placed relatively far apart from *Az. pseudozhuanum*. This indicates that the reduction of the number of apical plates might have happened independently for these species, but needs further investigations and is subject to future studies (**Publication VI**).

Phylogeny of AZA production potential is puzzling at present as the few AZA producing species are scattered over the phylogenetic tree. The toxigenic species *Am. languida* is morphologically and phylogenetically far apart from toxigenic *Az. spinosum* and *Az. poporum*, which for their part are monophyletic together with non-toxigenic *Az. trinitatum*, *Az. cuneatum*, *Az. obesum* and *Az. cf. spinosum* (**Publication VII, Fig. 6**). Separation into different clades therefore raises the question if AZA production is an ancestral trait in Amphidomataceae, how AZA production has actually evolved and what molecular mechanisms determine (non-) toxigenicity. Multiple losses of AZA production ability might be a reason, since there are AZA producing and non-producing ribotypes (as e.g. in *Az. spinosum*) and even strains within the same species and ribotype. This can be seen from the newly isolated non-toxigenic *Az. poporum* strain from the Danish coastline, which clusters together with *Az. poporum* strains from the Mediterranean and France (Ribotype A2), which partially produce AZAs (**Publication II**). Newly described non-toxigenic *Az. cf. spinosum*, which cannot be differentiated morphologically from toxigenic *Az. spinosum*, is placed together with non-toxigenic *Az. obesum*, and final taxonomic placement of new *Az. cf. spinosum* must therefore be further evaluated. In conclusion, phylogeny of AZA production is unclear at present and may become clearer, once the respective (so far unknown) gene cluster(s) coding AZA biosynthesis are identified. Due to this continuously emerging level of complexity in amphidomatacean phylogeny, multi-strain establishment is highly important to fully reveal the biodiversity also at the sub-species level and to reveal new geographical areas for certain species. A summary of all new described species (4) and strains (156) during the course of this PhD is presented in **Table 3**.

First reported from Chinese coastal waters, non-toxigenic *Az. dalianense* has been detected from the French Atlantic coast, in the north-east Pacific and in the south-west Atlantic off Argentina (Kim et al., 2017; Luo et al., 2017b; Tillmann et al., 2018a; Tillmann et al., 2019). The first observation of non-toxigenic *Az. dalianense* in the southern North Sea was reported in 2019 within

this project (**Publication II**), supporting former hypotheses that this is a globally distributed species. Although no significant morphological differences between available strains have been found, DNA sequence analyses revealed evidence for five *Az. dalianense* ribotypes. However, the ribotype clusters do not consistently reflect the geographical distribution. Two strains from the Danish coast revealed phylogenetic placement into the two different ribotypes D and E (**Publication II, Fig. 6**), and such a sympatric occurrence of different *Az. dalianense* ribotypes has been already described for Puget Sound/USA and the Norwegian coast (Kim et al., 2017; Tillmann et al., 2018a).

Table 3. Newly described species and strains of Amphidomataceae sorted by publication (n.a. = not assigned; n.d. = not detected). Strains were usually grown non-axenically at 15 °C, 70 $\mu\text{mol m}^{-2} \text{s}^{-1}$, a 16:8h light:dark cycle and in 1/10 K medium prepared from sterile filtered North Sea water (detailed description of medium preparation in **Suppl. Method I2**).

Species	No. new strains	Ribotype	AZA profile	Survey	Year	Reference
<i>Am. languida</i>	20	n.a.	-38, -39	UTH-16	2016	Publication II
<i>Az. dalianense</i>	2	n.a.	n.d.			
<i>Az. obesum</i>	3	n.a.	n.d.			
<i>Az. poporum</i>	1	A2	n.d.			
<i>Az. dexteroporum</i>	1	n.a.	n.d.	MSM-65	2017	Publication III
<i>Az. obesum</i>	12	n.a.	n.d.			
<i>Az. perforatum</i> sp. nov.	3	n.a.	n.d.			
<i>Az. trinitatum</i>	2	n.a.	n.d.			
<i>Az. caudatum</i>	1	n.a.	n.d.	HE-516	2018	Publication VI
<i>Az. galwayense</i> sp. nov.	3	n.a.	n.d.			
<i>Az. perfusorium</i> sp. nov.	25	n.a.	n.d.			
<i>Az. pseudozhuanum</i> sp. nov.	1	n.a.	n.d.			
<i>Am. languida</i>	10	n.a.	-38, -39	HE-516	2018	Publication VII
<i>Az. spinosum</i>	60	A	-1 (-2, -33)*			
	7	B	-11, -51			
<i>Az. cf. spinosum</i>	5	n.a.	n.d.			

*note that not all *Az. spinosum* Ribotype A strains had all three AZA congeners (-1, -2 and -33), for details see **Publication VII**.

A survey in 2017 revealed the presence of at least eight amphidomatacean species (*Az. obesum*, *Az. trinitatum*, *Az. dexteroporum*, *Az. spinosum*, *Az. polongum*, *Azadinium* spec., *Am. languida* and the new species *Azadinium perforatum*) in western Greenland waters and the Labrador Sea, demonstrating that the amphidomatacean biodiversity in the subarctic is remarkably high (**Publication III**). Sequence analysis of multiple *Az. obesum* strains (12 strains) separated them

into the two known *Az. obesum* clades from the North Atlantic, but uncorrected genetic p-distances between ITS rDNA sequences ($p = 0.002$) revealed a very close relationship. The two new *Az. trinitatum* strains displayed their own, maximum supported branch next to the previous described strains from the North Atlantic, indicating intraspecific variability in this species. The record of *Az. dexteroporum* in the Labrador Sea confirms the presence of this species in the subarctic region, as a strain had been previously established from the Irminger Sea (Tillmann et al., 2015). However, the new strain differs significantly from the Mediterranean type material in terms of morphology and sequence data ($p = 0.038$), indicating cryptic diversity for this species (**Publication III**).

Azadinium caudatum with its two varieties (var. *margalefii* and var. *caudatum*) is the easiest amphidomatacean species to identify due to its relatively large cell size, and it is frequently reported in Irish coastal waters (Dodge and Hermes, 1981; O'Boyle and Raine, 2007). In 2018, a new strain was isolated and confirmed the morphology and close phylogenetic relationship for previous *Az. caudatum* isolates (Nézan et al. (2012); **Publication VI**). Non-toxicity of this species for Irish coastal waters, which was previously reported for a strain isolated at the Scottish coast (Tillmann et al., 2014b), has also been confirmed.

From the survey in 2018, detailed morphological, phylogenetical and toxinological characterization of multiple newly isolated strains of *Am. languida* and *Az. spinosum* considerably increased knowledge on the intraspecific diversity of both species in the North Atlantic (**Publication VII**). In total, 10 new *Am. languida* strains were established from one station in the central North Sea area and all confirmed the previous characterizations of this species (i.e. morphology, LSU rDNA sequence and toxin profile). In contrast, the 72 newly obtained *Az. spinosum* strains revealed a higher complexity of this species in the North Sea area compared to *Am. languida*. Analyses revealed the first sympatric occurrence of *Az. spinosum* Ribotype A (60 strains) and B (7 strains) in the central North Sea. Five strains had the same morphology as *Az. spinosum*, but differed phylogenetically and did not contain any detectable AZA. A non-toxic morphotype of *Az. spinosum* is already known based on strains isolated at the Argentinean coast, designated as Ribotype C (Tillmann et al., 2019). However, the five new strains differed significantly from Ribotype C in terms of rDNA sequences (including CBCs, **Publication VII**) and were provisionally designated as *Az. cf. spinosum*. The final taxonomic level remains to be assigned.

3.1.2 AZA diversity

Chemical analysis (see **Suppl. Method I3**) did not detect any known AZAs in the newly described species (*Az. perforatum*, *Az. perfusorium*, *Az. galwayense*, *Az. pseudozhuanum*; **3.1.1**), increasing the number of non-toxicogenic amphidomatacean species and further highlighting that AZA production in Amphidomataceae is rather exceptional. This is also supported by the first isolate of *Az. caudatum* var. *margalefii* from Irish coastal waters, confirming that this is a non-toxicogenic species (**Publication VI**). No AZAs have been detected in *Am. parvula*, as well (Tillmann et al., 2018b). As it is well described for the genus *Azadinium*, AZA production is therefore not a general feature in *Amphidoma* either. However, only two of in total 16 *Amphidoma* species have been tested for AZAs so far.

Four amphidomatacean species are described to produce AZAs and the currently known produced AZA variants per species are presented here: *Az. spinosum* (AZA-1, -2, -11, -33, -34, -35, -50 and -51), *Az. poporum* (AZA-2, -11, -36, -37, -40, -41, -42, -59 and -62), *Az. dexteroporum* (epi-AZA-7, AZA-35, -54, -55, -56, -57 and -58) and *Am. languida* (AZA-2, -38, -39, -43, -52 and -53) (Krock et al., 2019). More than 20 different AZA congeners have been found in amphidomataceans to date, and new isomers are still frequently found, confirming a high diversity in AZA toxins. Recently, AZA-42 and -62 have been newly described for *Az. poporum* strains by Krock et al. (2019). The latest AZA variant, AZA-63, has been detected in two field samples during a survey in 2016 in Danish coastal waters (**Publication II**). Although the actual producer of AZA-63 could not be identified and the chemical structure can only be proposed (all typical AZA fragments identical with AZA-37, except for a 2 Da downshifted and less complex pseudo-molecular ion cluster), this highlights again the high diversity in AZAs and the still early stages of AZA variant research. Most AZA variants have been detected in *Az. poporum* strains, which might reflect the high number of strains obtained from various geographical areas. However, the AZA variability of *Az. spinosum*, *Az. dexteroporum* and *Am. languida* is also high, although the geographical records for those species are more restricted than for *Az. poporum*.

An extraordinary finding was a new *Az. poporum* strain established from the field survey along the Danish coastline in 2016, which did not show any AZA traces (**Publication II**). Non-toxicogenic *Az. poporum* strains have been previously only reported from the Mediterranean Sea (Krock et al., 2014; Luo et al., 2018), but traces and even high amounts of AZAs were also detected in at least some of those Mediterranean strains (Luo et al., 2017b; Luo et al., 2018). The co-occurrence of toxicogenic and non-toxicogenic strains of one species in the same area is of course challenging for an

accurate risk assessment and would here rather lead to an overestimation of toxigenic *Az. poporum* cells by qPCR analysis, because the current qPCR assay on *Az. poporum* shows (false-) positive signals for this non-toxigenic strain (**this study, Suppl. Table S3**).

The recent isolation of non-toxigenic *Az. cf. spinosum* from the central North Sea revealed the same morphology as known for *Az. spinosum* in the area and therefore increased the complexity for this species, as well (**Publication VII**). A non-toxigenic *Az. spinosum* Ribotype C has been previously reported only from Argentinean coastal waters and it cannot be excluded that they are also present in the North Atlantic phytoplankton assemblage. This of course indicates a potential bias for monitoring of this species in the North Atlantic, when relying only on microscopic analyses. Here however, it could be importantly demonstrated that Ribotype C strains and the new *Az. cf. spinosum* strains do not cause false-positive signals in the *Az. spinosum* specific qPCR assay aiming to target toxigenic cells (**Publication VII**).

These findings also indicate that it is hardly possible to work out species-specific and regional-specific AZA profiles (if existent at all) or non-toxigenicity based on the current data sets. For example, AZA-2 is until now the most widely occurring AZA variant. AZA-2 is produced by three different species, and also by species occurring in very distant areas as for example *Az. poporum*, which is known from Chinese coastal waters (Krock et al., 2014), Argentinean coastal waters (Tillmann et al., 2016), the Mediterranean Sea (Luo et al., 2017b) and the Gulf of Mexico (Luo et al., 2016). AZA-11 was found in the Pacific (Tillmann et al., 2017c), the Mediterranean Sea (Luo et al., 2018) and the North Atlantic (Tillmann et al., 2018a). In contrast, other AZAs like AZA-36 (only detected from *Az. poporum* in Chinese and Korean coastal waters), so far seem to be more local variants (Krock et al., 2012; Krock et al., 2015). However, this is very uncertain since AZAs, which were found in a certain locality only like AZA-40 (Chinese Sea) and AZA-59 (Washington State), have also been detected in the Mediterranean Sea (Luo et al., 2018). Research on AZA producers has been performed in the Northeast Atlantic, the Mediterranean Sea, the Northwest Pacific and partly in the Southwest Atlantic and the Northeast and Southeast Pacific (Krock et al., 2019), but strain numbers and geographical coverage are still limited. The lack of certain AZA producing species and AZAs in other regions might therefore be rather the result of missing studies. To fill the knowledge gaps, extensive strain establishment is an unavoidable task. Recent strain establishment of multiple *Am. languida* and *Az. spinosum* strains from the North Atlantic enabled intense research on AZA variability (**Publication VII**). Ten *Am. languida* strains from a relatively dense population on a central North Sea station confirmed the AZA profile (AZA-38 and -39)

previously described for North Atlantic strains. Whereas a Mediterranean strain of *Am. languida* had a different AZA profile (AZA-2 and -43), no toxin profile variability for the Atlantic population was thus found in any of the in total 30 strains (**Publications II and VII**). The ratio of both AZA congeners (AZA-38 and -39) was found to vary between 0.5 and 1.4, whereas previous analyses (except for one strain) showed a higher proportion of AZA-39 (ratio of 0.4 to 0.7; **Publication II**). A high AZA cell quota variability between strains (ranging about 100-fold from 0.3 to 29.6 fg cell⁻¹) was noticed and confirmed previous investigations on *Am. languida* (ranging more than 1,000-fold from 0.08 to 94 fg cell⁻¹; **Publication II**).

The first *Az. spinosum* strains were isolated from Scotland, Ireland, the Shetland Islands and Denmark, and shared all the same toxin profile of AZA-1, -2 and -33 (Tillmann et al., 2009; Salas et al., 2011; Tillmann et al., 2012b; Krock et al., 2013). *Azadinium spinosum* with the toxin profile consisting of AZA-11 and -51 (Ribotype B) previously described from the Norwegian coast (Tillmann et al., 2018a), has now been confirmed in the central North Sea (**Publication VII**). Notably, of 57 strains isolated in Irish coastal waters in 2018, no Ribotype B strains were detected, but the majority of strains in the central North Sea was Ribotype B. However, no AZA-11 or -51 have been detected in field samples the central North Sea, suggesting a lower AZA cell quota and/or cell abundance (**Publication IV**).

Chemically, the AZA profiles of Ribotype A and B represent couples. AZA-11 and -51 are 3-hydroxylated, whereas there are no substituents at C3 in AZAs of Ribotype A (**Publication VII, Fig. 7**). Furthermore, the base compounds AZA-2 and AZA-11, respectively, are methylated (at C8), whereas AZA-1 is lacking a methylation at C8 and AZA-51 at C24. Hydroxylations or the lack of such might be a common feature in AZA profiles of different ribotypes. AZA-11 and -62, both produced by Chilean *Az. poporum* Ribotype A1 are 3-hydroxylated, whereas Argentinean *Az. poporum* strains (Ribotype C2) produce AZA-2, which does not show 3-hydroxylation (Tillmann et al., 2016; Tillmann et al., 2017c; Krock et al., 2019; Wietkamp et al., 2019a). However, it is too early to state a conclusion on that topic.

The multi-strain comparison highlighted that the total AZA cell quota of *Az. spinosum* Ribotype B seems to be generally lower than of Ribotype A strains (with exceptions), and so far no cell quotas > 15 fg cell⁻¹ were detected in Ribotype B strains, whereas this is frequently found in Ribotype A (Tillmann et al. (2018a); **Publication VII**). Variability in AZA cell quota in *Az. spinosum* (both, Ribotype A and B) was found to be remarkable high (53-fold for Ribotype A, sum of all AZAs). Cell quota variability has been already reported for given strains grown under different conditions

(like temperature, light or nutrients adjustments; Jauffrais et al. (2013b); Dai et al. (2019); Kilcoyne et al. (2019)) or in different growth stages (usually higher AZA cell quotas in the stationary growth phase; Li et al. (2016); Dai et al. (2019); Kilcoyne et al. (2019)). However, the same applied growth conditions still led to cell quota differences within several orders of magnitude, as it was measured for *Az. spinosum* and *Az. poporum* before (Li et al., 2016; Kilcoyne et al., 2019). This high cell quota variability even under identical conditions suggests that there are other, uncontrollable factors present, as for example rhythmic cycles or unknown influences of missing food web interactions (**Publication VII**).

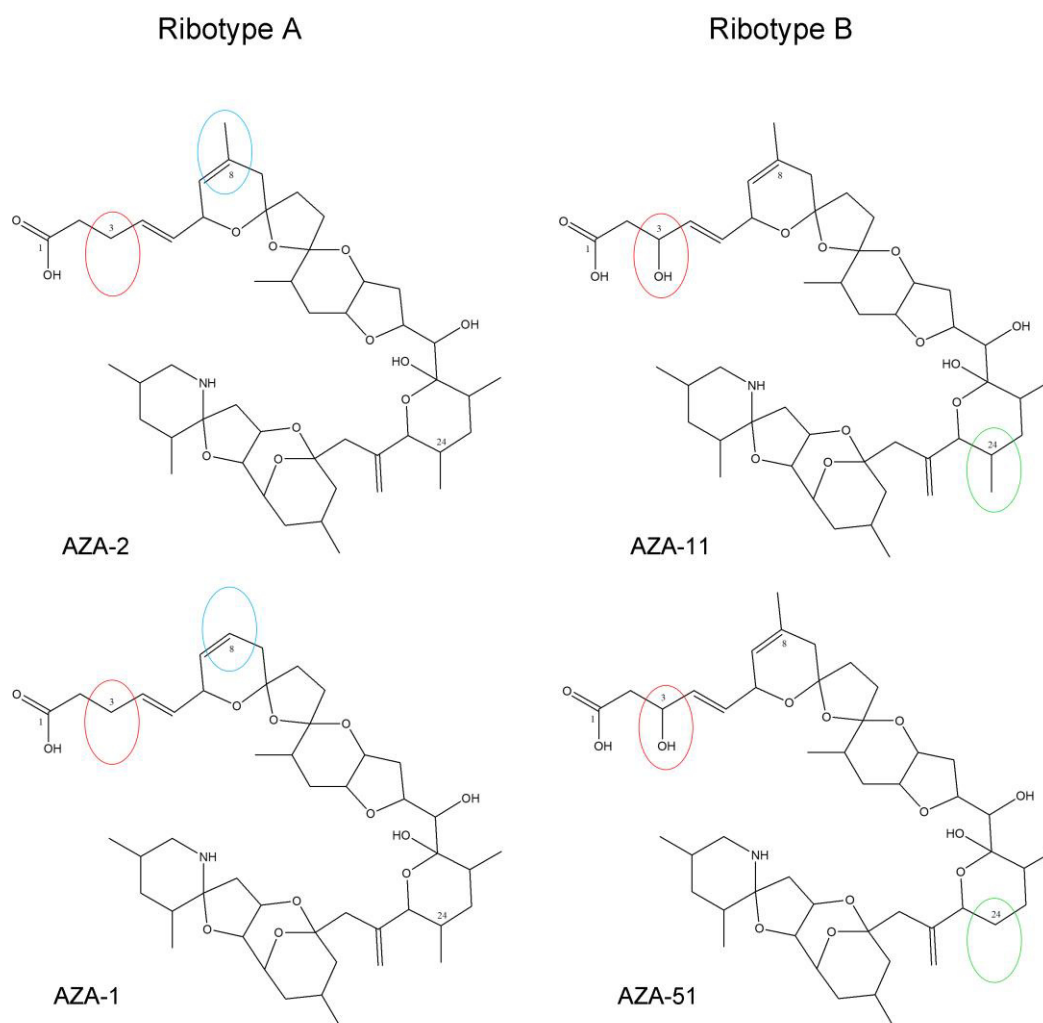


Fig. 7. Planar structures of close related AZA-1, -2, -11 and -51. AZAs of Ribotype B are 3- hydroxylated (red ovals), whereas Ribotype A AZAs are not. AZA profiles of both ribotypes consist of a base compound (AZA-2 and AZA-11, respectively) and a demethylated variant (AZA-1 and AZA-51, respectively). The demethylation site of Ribotype A AZAs is C8 (blue oval) and of Ribotype B C24 (green oval). Fig. from **Publication VII**.

Although high AZA cell quota variability in the three species *Am. languida*, *Az. spinosum* and *Az. poporum* is still puzzling, the toxin profile of multiple strains was found to remain stable over a minimum period of one year, indicating that the toxin profile is genetically fixed (**Publication VII**). Specific toxicity is not yet known for several detected AZA in the field (especially AZA-11, -33, -38, -39 -51), which makes a direct conversion of AZA cell quota to actual toxicity (compared to AZA-1 and -2) not possible at the moment. The respective toxicity tests should be performed soon to enable a more reliable risk assessment on total AZAs in the field. Overall, the presented work significantly increased knowledge on species and AZA diversity in Amphidomataceae and highlights expected to further increase in the future.

3.2 Molecular detection and quantification of toxigenic Amphidomataceae

As a prerequisite for molecular field sample analyses on the three AZA producing species in the North Atlantic, the respective species-specific qPCR assays had to be established. The assays for the detection of toxigenic *Az. spinosum* and *Az. poporum* were already available since 2013 (Toebe et al., 2013) and the family-specific Amphidomataceae assay was established by Smith et al. in 2016.

Table 4. Available real-time PCR assays for Amphidomataceae (adjusted from **Publication I**).

Target species	Target gene	Oligonucleotide type	Sequence (5´-3´)	Product size (bp)	Reference
Amphidomataceae	ITS				Smith et al.
Amp240F		F-Primer	CAACTTTCAGCGACGGATGTCTCG	179	(2016)
Amp418R		R-Primer	AAGCYRCWGGCATAKAGAAGGTAGWGGC		
<i>Am. languida</i>	LSU				Wietkamp et al.
Alan509F		F-Primer	CGGTTACAGGCGAGGAT	60	(2019)
Alan569R		R-Primer	GACATTCACACCTCCGTGGAA		
Alan528		TaqMan MGB probe	6FAM-CTTCTGAGGACATGGTAAC-MGB		
<i>Az. spinosum</i>	LSU				Toebe et al.
Asp48F		F-Primer	TCGTCTTTGTGTCAGGGAGATG	72	(2013)
Asp120R		R-Primer	GGAAACTCCTGAAGGGCTTGT		
Aspin77T		TaqMan MGB probe	6FAM-CGCCCCAAAAGGACTCCT-MGB		
<i>Az. poporum</i>	LSU				Toebe et al.
Apop62F		F-Primer	GATGCTCAAGGTGCCTAGAAAGTC	68	(2013)
Apop148R		R-Primer	CCTGCGTGTCTGGTTGCA		
Apop112		TaqMan MGB probe	6FAM-TTCCAGACGACTCAAA-MGB		
<i>Az. obesum</i>	LSU				Toebe et al.
Aob134F		F-Primer	AGGGATCGATACACAAATGAGTACTG	74	(2013)
Aob208R		R-Primer	AAACTCCAGGGACATGGTAGTCTTA		
Aob163		TaqMan MGB probe	6FAM-AAGACATTCGACCTACCGT-MGB		

In the context of this study, the assay for the third AZA producing species in the North Atlantic, *Am. languida*, was designed and validated (**Objective 1**; for all methodological details see attached **Publication I**). This specific qPCR assay set provided the base for subsequent molecular field investigations on all three known AZA producers in the North Atlantic (**Table 4**).

3.2.1 Assay specificity and ribotypes

The continuous implementation of new species and strains of Amphidomataceae is challenging with respect to assay specificity as there is a risk for false-positive and false-negative qPCR signals, affecting the reliable detection of target cells within field samples. Therefore, it is important to continuously re-evaluate the existing qPCR assay specificity for *Az. spinosum*, *Az. poporum* and *Am. languida* after the isolation of new target strains, but especially for the five new non-toxicogenic amphidomatacean species (Tillmann et al. (2018b), **Publications III** and **VI**). Specificity and sensitivity testing of target and non-target DNA was performed and indicated that all three assays are generally still target-specific (**Suppl. Table S3**).

Directly affecting the assay performance for *Az. poporum* and *Az. spinosum* was the recognition of genetic variability within both species, which is reflected by the identification of “ribotypes”, displaying distinct strain clusters in phylogenetic analyses. Until 2013, three ribotypes (entitled as Ribotype A, B and C) were described within *Az. poporum*. Whereas Ribotype A is assigned to strains from the North Sea area, Ribotypes B and C occur in the Chinese Sea (Gu et al., 2013). DNA sequence differences between ribotypes are also present at the rDNA binding sites of the specific qPCR primers and probe (**Fig. 8**). Several base pair mismatches of the target sequence with primers and probe can have fundamental effects on the assay specificity, sensitivity and therefore on the qualitative and quantitative detection ability (**Publications I** and **V**). *Azadinium poporum* Ribotypes A and B were detected with the same efficiency by the current qPCR assay (despite 1 mismatch in the F-primer for Ribotype A2 and 2 mismatches for Ribotype B), but Ribotype C (3 mismatches with the F-primer) was not detected at all (**Fig. 8A**, **Suppl. Table S3**). A very considerable finding was the isolation of a non-toxicogenic *Az. poporum* strain (LF-14-E12) from Denmark (**Publication II**). Important concerning the qPCR detection, this new non-toxicogenic *Az. poporum* isolate (rDNA sequences identical to Greek and French Ribotype A2 strains) co-occurs with AZA-37 producing strains (Ribotype A1) in the North Sea area. Only one base-pair mismatch was found between the Ribotype A2 strain sequence and the *Az. poporum* qPCR assay (**Fig. 8A**), and this minor mismatch did not diminish the efficiency of the assay (**Suppl. Table S3**).

Therefore, it is important to point out that for *Az. poporum* the assay is not suited to selectively identify and quantify AZA producing strains and may lead to an overestimation of AZA producing *Az. poporum* cells in North Atlantic field samples or to an underestimation if applied in the Mediterranean, respectively.

A

	F-Primer	MGB-Probe	R-Primer
Sequence (5'-3')	GACTTTCTAGGCACCTTGAGCATC	TTTGAGTCGTCTGGAA	CCTGCGTGTCTGGTTGCA
Ribotype A1	-----	-----	-----
Ribotype A2	-----G-----	-----	-----
Ribotype B	-----G-----C-----	-----	-----
Ribotype C	A-----G-----T-----	-----	-----

B

	F-Primer	MGB-Probe	R-Primer
Sequence (5'-3')	CATCTCCCTGACACAAAGACGA	AGGAGTCCTTTTGGGCG	GGAAACTCCTGAAGGG-CTTGT
Ribotype A	-----	-----	-----
Ribotype B	-----	-----C-----	-----T-----G-----
Ribotype C	-----	C--A-----	-----T-----TCA-----CCA
<i>Az. cf. spinosum</i>	-----	T-A-----G-----	T-----T-----A-----

Fig. 8. Base pair mismatches between the ribotype rDNA sequences of (A) *Az. poporum* and (B) *Az. spinosum* with the primers and probe of the respective TaqMan qPCR assays (Publication VII).

In contrast to the *Az. poporum* qPCR applied here (targeting the LSU of *Az. poporum*), a different qPCR assay targeting the *Az. poporum* ITS rDNA was used by Potvin et al. (2013) to quantitatively detect *Az. poporum* in Korean coastal waters between January 2009 and December 2011. The assay has been designed based on the relatively limited number of target sequences available for *Az. poporum* at that time and would have to be re-evaluated in the future with the now available sequence information, specificity testing and quantification ability. Nevertheless, this assay might be a future candidate to test for a reliable detection and quantification of *Az. poporum* in the field, especially in the light of increasing issues of the assay by Toebe et al. (2013) concerning different ribotypes and amplification efficiencies as described above. Genetic differentiation is also present within *Az. spinosum*. First *Az. spinosum* strains isolated around Ireland, Scotland and the Shetland Islands with an AZA profile consisting of AZA-1, -2 and -33 were assigned as Ribotype A (Tillmann et al., 2012b; Kilcoyne et al., 2014b). Ribotype B strains were first identified in Norwegian coastal waters (producing mainly AZA-11 and -51) and later also isolated from the

Argentinean Shelf (one strain, producing AZA-2). Ribotype B is also detected by the current *Az. spinosum* assay, but with less efficiency compared to Ribotype A (Tillmann et al., 2018a; Tillmann et al., 2019) due to bp mismatches with the assay (**Fig. 8B, Suppl. Table S3**). In Norway, Ribotypes A and B have been shown co-occur (Tillmann et al., 2018a), and microscopic and/or LC-MS/MS analysis is needed for their differentiation in such areas.

One important finding was the recent isolation of several non-toxic *Az. spinosum* strains from the Argentinean shelf and the North Atlantic (Tillmann et al. (2019); **Publication VII**). Cells of the Argentinean strains cluster together with *Az. spinosum*, but display an own separated branch next Ribotype A and B strains, and are thus classified as a new ribotype (Ribotype C) of *Az. spinosum* (Tillmann et al., 2019). New non-toxigenic *Az. cf. spinosum* strains from the North Atlantic however, displayed an own branch apart from all other *Az. spinosum* ribotypes. In the current *Az. spinosum* qPCR assay by Toebe et al. (2013), the new non-toxigenic strains (both, the Argentinean and the North Atlantic *Az. cf. spinosum* strains) were not detected *in vitro* (**this study**), which is most likely the result of significant *in silico* mismatches of the reverse primer (7 bp) and the probe (2 bp) with the respective region on the LSU than for Ribotype B (2 bp R-primer, 1 bp probe) (**Fig. 8B**). In terms of the differentiation of toxigenic and non-toxigenic *Az. spinosum*, this excludes false-positive amplifications in the field at least for these strains. However, current and future monitoring on especially *Az. spinosum* Ribotype A and B is directly affected by the unequal qPCR assay specificity and a re-design of the current assay is needed to fully differentiate both ribotypes. Respective new primer sets have been picked and will be tested in the near future, aiming to amplify a sequence on the 28S rDNA, which is identical for Ribotype A and B but excluding Ribotype C, to receive an *Az. spinosum* assay with the same efficiency for the toxigenic ribotypes. Still, even new assays require continuous updates and specificity testing in the future. Concerning *Am. languida*, different ribotypes have not been noticed so far, but of course cannot be ruled out. However, recent multi strain establishment confirmed no significant genetic variability for North Atlantic *Am. languida* (**Publications II and VII**). One observation to mention specifically for *Am. languida* was the difficulty to gain ITS sequences by Sanger Sequencing, because raw sequences often revealed a high degree of overlapping signals. An additional cloning step before DNA sequencing enabled to avoid such signal overlapping, but revealed also significant ITS sequence differences between individual clones (Tillmann et al., 2014a; Tillmann et al., 2015). Such difficulties concerning *Am. languida* ITS sequences have to be kept in mind for potential future ITS applications.

3.2.2 Quantification ability

Quantification of target cells within a field sample via qPCR requires intense beforehand testing and validation of involved chemicals, parameters, workflows etc. Essential tests and measurements for a successful quantification of toxigenic amphidomataceans in the field via qPCR have been described in detail within this thesis (**Publication I**). The quantitative analysis of qPCR data is based on standard curves, which consist of either a dilution series of target DNA or target gene copies. As qPCR amplification after all is directly related to the number of target genes in the reaction volume, the target cell density calculation strongly relies on the calculated DNA cell quota or target gene copy cell quota, respectively. Whereas the DNA based standard curve allows direct conversion into cell numbers, the target gene copy number has to be determined prior to the usage of the gene copy standard curve. In this study, the target gene cell quota was estimated via the DNA cell quota (for details see **Publication I**), and therefore relies on the DNA cell quota and subsequently on the extraction performance of the DNA extraction kit, i.e. a constant extraction efficiency rather than the maximum yield. A constant extraction efficiency (both within and between extraction processes) of the kit is thus most important for a reliable quantification.

Two DNA extraction kits (i.e. the NucleoSpin Plant II and NucleoSpin Soil DNA extraction kit, both Macherey-Nagel, Düren, Germany) were compared in terms of extraction efficiency based on strain cell pellets. Measurements were carried out after two separate extraction processes. The NucleoSpin Soil kit revealed significantly lower standard deviations in relation to the mean DNA cell quota and significantly higher DNA cell quotas (0.9 ± 0.2 and 0.8 ± 0.2 Plant kit vs. 2.6 ± 0.1 and 2.6 ± 0.2 pg cell⁻¹ Soil kit; n=8 each) for the exemplarily tested *Az. spinosum* strain UTH-E2 (**Suppl. Fig. 2**). The NucleoSpin Soil kit was therefore chosen for all DNA extractions in this study. Constant DNA extraction efficiencies between different extraction processes in the progress of this PhD work was confirmed by the application of external positive control (EPC) samples with known cell numbers (10^3 cells), which were present in each extraction set. Furthermore, DNA extraction losses by repeated extractions of samples with known DNA concentration revealed a sufficient recovery rate of $\geq 90\%$ (**Publication I**).

In total, DNA of 13 *Az. spinosum* strains, eight *Az. poporum* strains and five *Am. languida* strains from various geographical locations was extracted with usually six replicates each and DNA cell quota was calculated, which was on average 3.5 pg cell⁻¹ for *Az. spinosum*, 2.9 pg cell⁻¹ for *Az. poporum* and 3.0 pg cell⁻¹ for *Am. languida* (**Suppl. Table S4**). A previous study by Toebe et al. (2013) reported three times higher DNA cell quotas for *Az. spinosum* (9.5 ± 0.3 pg cell⁻¹) and

Az. poporum (9.4 ± 0.3 pg cell⁻¹). This difference might be the result of another DNA measuring method used by the authors, i.e. the NanoDrop, which tends to overestimated double strand DNA (Simbolo et al. (2013), and references within). Exceptionally high DNA cell quotas of 7.7 pg cell⁻¹ and 7.6 pg cell⁻¹ have been measured here in *Az. spinosum* strains 5-F6 and 7-E4, respectively. Both belong to the Ribotype B clade, but no relationship between ribotype and DNA cell quota has been found in general, since Ribotype B strains H-1-D11 (1.4 pg cell⁻¹) and N-16-02 (1.5 pg cell⁻¹) showed significantly lower DNA cell quotas (even lower than most Ribotype A strains). Non-toxigenic *Az. poporum* strain LF-14-E12 (Ribotype A) had a remarkably lower mean DNA cell quota (0.6 pg cell⁻¹) compared to the investigated toxigenic strains. Likewise, non-toxigenic *Az. cf. spinosum* had a significantly lower DNA cell quota (0.6 ± 0.3 pg cell⁻¹ for strain 1-H10 and 0.9 ± 0.3 pg cell⁻¹ for strain 5-B9) compared to toxigenic *Az. spinosum*. However, the respective genetic setting for AZA production does not seem to have a significant influence on DNA cell quota at least for *Az. spinosum*, because both tested non-toxigenic Ribotype C strains (H-1-D4 and H-4-C10) have relatively high DNA cell quotas (5.7 pg cell⁻¹ and 4.3 pg cell⁻¹, respectively). An experiment with *Am. languida* revealed relatively stable DNA cell quota over the entire culture growth cycle (**Publication I**), suggesting that the population growth phase is not related to the DNA cell quota. In conclusion, it is not clear so far, what the reason for these significant differences in DNA cell quotas are.

To more generally evaluate species-specific differences in DNA cell quotas in Amphidomataceae, DNA per cell calculations were performed also for 12 non-toxigenic amphidomatacean species (**Suppl. Table S5**). The analyses revealed similar DNA cell quotas compared to the toxigenic species around 3 pg cell⁻¹. The smallest species in terms of cell size, *Az. concinnum*, had also the lowest DNA cell quota (0.52 ± 0.02 pg cell⁻¹), whereas the largest amphidomatacean species, *Az. caudatum*, had also the significantly highest DNA cell quota (19.03 ± 4.07 pg cell⁻¹). However, if cell size and genome size are in general positively correlated in eukaryotes is contrarily discussed (Doležel et al., 1998; Connolly et al., 2008; Olefeld et al., 2018).

In various microalgal species and strains, the sequential arrangement LSU-ITS1-5.8S-ITS2-SSU on the rDNA has been shown to be present in multiple repetitions (e.g. Wang et al. (2017); Penna and Galluzzi (2013)). The number of those target binding site copies for primers and probe directly affects the amplification in the qPCR reaction: The higher the copy number, the earlier an amplification signal above the detection limit will be seen, and the lower will be the respective C_T value for a given sample. Thus, the rDNA copy number per cell is the determining factor for

PCR-based quantification. Therefore, any strain-specific copy number variability independent from DNA per cell variability will bias quantification (**Publication I** and references within). For several strains of *Az. spinosum* (strains 3D9, N-04-04, N-16-02 and UTH-E2), *Az. poporum* (strains 1-D5, 2-B9, N-39-01 und UTH-D4) and *Am. languida* (strains 2A11, AND-0920, N-12-01 and LF-9-C9), also the rDNA copy numbers per cell were estimated according to detailed descriptions in **Publication I (Suppl. Table S4)**. Overall copy numbers varied slightly between species and were lowest in *Am. languida* cells (716 to 830 copies cell⁻¹) and highest in *Az. spinosum* cells (1,057 to 1,276 copies cell⁻¹), while *Az. poporum* was intermediate but also with the largest range (874 to 1,212 copies cell⁻¹). The calculated copy numbers here confirm findings by Toebe et al. (2013), who reported 1,216 copies cell⁻¹ for *Az. spinosum* and 1,185 copies cell⁻¹ for *Az. poporum*. A variability in rDNA copy numbers has been described for different culturing conditions and growth stages in previous studies on microalgae (Godhe et al., 2008; Galluzzi et al., 2010). Here, one representative *Am. languida* strain was tested but did not show any significant copy number variations over time within a batch culture growth cycle, which indicates that quantification via qPCR in the field might not be biased by the population growth phase (**Publication I**).

The most fundamental finding in this context however, was that the copy numbers between four different strains within each species did not vary significantly (**Publication I, Suppl. Table S4**). No intra-specific copy number variation therefore indicates a reliable quantification of *Az. spinosum*, *Az. poporum* and *Am. languida* cells in the field, based on target DNA or gene copy standard curves. Furthermore, the lower qPCR efficiency for *Az. spinosum* Ribotype B compared to Ribotype A strains (**Suppl. Table S3**) was therefore probably not the result of significant copy number differences and different DNA cell quotas, but most likely caused by the base pair mismatches of the assay with the respective rDNA sequence (**Fig. 8B**). Most problematic is this different detection efficiency in terms of a reliable quantification of *Az. spinosum* cells in the field, because in situations of sympatric occurrence of both ribotypes, the quantification applying either a Ribotype A or B based DNA standard curve will bias the calculated cell abundance.

Potential seawater matrix effects and PCR inhibition were assessed by spiking known numbers of target cells into a defined volume of seawater and performing subsequent qPCR analysis. Calculated cell numbers were repeatedly in good agreement with the number of actual spiked cells, displaying the indispensable baseline for reliable quantitative PCR analyses in the field (**Publications I and IV; Objectives 1b and c**).

3.2.3 Comparative method analysis

Microscopy, species-specific qPCR assays and LC-MS/MS revealed that all three toxigenic North Atlantic species of Amphidomataceae are widely distributed in the North Sea area. In the present study, amphidomatacean species-specific qPCR assays were used for the first time to quantitatively estimate cell densities of all three toxigenic species in the field. The quantification ability of the qPCR assay has been positively evaluated in form of spike experiments, in which LM determined cell numbers of cultured strains were spiked into a field matrix (**Publications I and IV**).

Comparative analyses between LM and qPCR based estimated cell densities in the field during a survey in 2018 revealed that both estimates were generally in the same order of magnitude and showed a highly significant positive correlation ($R = 0.89$, Pearson's product-moment correlation test: $p < 0.001$) (**Fig. 9; Publication IV**).

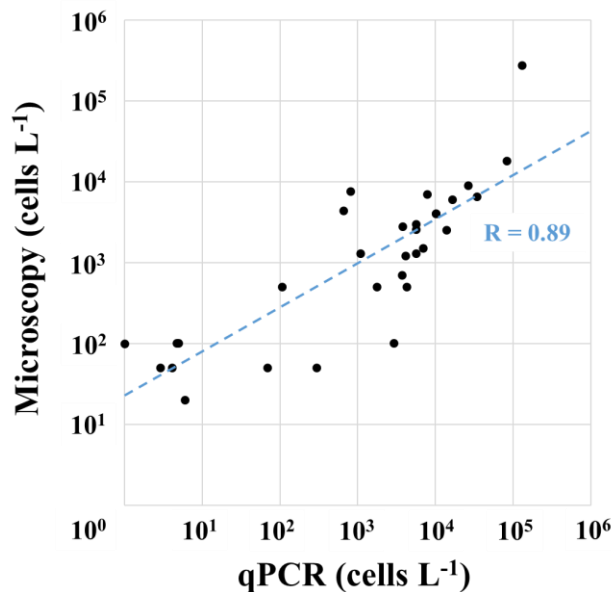


Fig. 9. Correlation between qPCR-based cell abundances (cells L⁻¹) of toxigenic amphidomataceans (x-axis) and microscope-based cell abundances (cells L⁻¹) of all amphidomataceans (y-axis) during the survey HE-516 in the eastern North Atlantic. “R” displays the respective correlation coefficient. Fig. adapted from **Publication IV**.

One reason for discrepancies between microscopy and qPCR for single field samples is based on the fact that amphidomatacean species are hardly possible to distinguish by LM. Whereas the qPCR estimated only cell abundances for the three toxigenic species, LM data were combined amphidomatacean (including toxigenic and non-toxigenic) cell counts (**Publication VII**). For some stations, the proportion of non-toxigenic amphidomatacean cells might have been higher compared

to the toxigenic ones. This could be addressed by for example target-specific, optical markers by Fluorescence *In Situ* Hybridization (FISH). Molecular FISH assays are available for *Az. spinosum* and *Az. poporum* (Toebe et al., 2013), but would have to be subjected to extensive specificity testing, since they have been designed at time when only three amphidomatacean species and only few strains were known. Besides that, FISH has a relatively labor-intensive workflow, making it inappropriate for real-time analyses for example on-board research vessels and in routine monitoring programs. Over- or underestimations of cell numbers by qPCR compared to LM can however, also be the result of lower or respectively higher *in vivo* rDNA copy numbers of the local target population compared to the strain used to calibrate the qPCR assay. Another reason for discrepancies between LM and qPCR could have been the dominance of *Az. spinosum* Ribotype B compared to Ribotype A (in terms of isolated strain numbers) in the North Sea (**Publication VII**). The lower qPCR quantification efficiency of B compared to A strains (**3.2.1**) may have contributed to the comparable lower total amphidomatacean density estimated by qPCR compared to microscopy counts for some stations (**Publication IV**). Despite these uncertainties, LM and qPCR cell abundance estimates were generally in good agreement and can be used complementarily in future studies and monitoring.

qPCR-based cell density estimations enabled also to quantitatively compare qPCR cell counts to the concurrent AZA quantities. In general, qPCR based cell number estimations of *Az. spinosum* and respective AZA-1, -2 and -33 quantities were strongly positive correlated in field samples taken on a survey conducted 2018 in Irish and North Sea coastal waters (**Fig. 10; Publication IV**).

When comparing qPCR-based and LC-MS/MS-based estimated cell quantities, however different cell detection limits of both methods have to be kept in mind. Whereas the qPCR requires theoretically just one target gene copy per sample for amplification, relatively high amounts of particulate AZAs are needed for positive AZA signals in LC-MS/MS. In this study, the LOD for the LC-MS/MS was determined applying an external AZA standard of 100 pg AZA-1 μL^{-1} (certified reference material program of the IMB-NRC, Halifax, Canada) and defined as a signal-to-noise ratio of 3. The LOD was found to be approx. 120 fg AZA μL^{-1} , equivalent to 60 pg per sample, when taking the usual extraction volume of 500 μL acetone into account. Assuming an AZA cell quota of 20 fg cell⁻¹, the “cell detection limit” is 3×10^3 cells per sample. A realistic filtration volume for the field samples of three liters for one sample thus reveals a cell detection limit of $\sim 1 \times 10^3$ cells L⁻¹. This significant difference of the “cell detection limit” between qPCR and LC-MS/MS analysis is obvious during field sample analyses, where stations with estimated

cell densities of less than 10^3 cells L^{-1} by qPCR (cell detection limit of 1 to 3 cells L^{-1}) in most cases did not reveal positive AZA signals during the 2018 survey (**Publication IV**). The depth profiles (Fig. 10 in **Publication IV**) and samples from another survey in 2016 along the Danish coastline (**Publication II**) revealed a similar “threshold” of 10^3 cells L^{-1} . The “cell detection limit” per volume of seawater might be decreased by increasing the filtration volumes, but at some point, this becomes obviously impractical. In addition, bringing LC-MS/MS systems onboard research vessels reveals a much greater logistical effort compared to a microscope or qPCR machine. Nevertheless, the obvious advantage of LC-MS/MS over qPCR or LM is the direct detection of harmful substances like AZAs (which are the major reason for the research on Amphidomataceae), without the need to account for different species, strains, ribotypes or variable AZA cell quotas. As an example, different *Az. spinosum* ribotypes with respective AZA profiles, e.g. Ribotype A (AZA-1, -2 and -33) and Ribotype B (AZA-11 and -51) in the North Sea area are currently impossible to differentiate by qPCR but would clearly be detected separately by chemical detection of their respective AZAs. Advantages and disadvantages of qPCR, LM and LC-MS/MS have to be kept in mind and it would be desirable to simultaneously operate all methods for a reliable risk assessment, but **this study** clearly revealed that the overall results are congruent (**Objective 2d**).

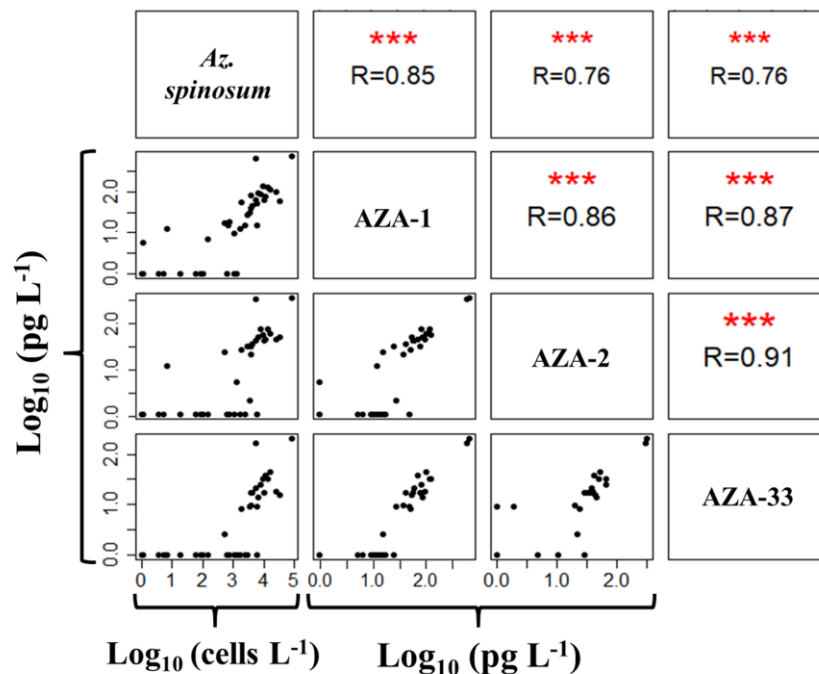


Fig. 10. Pearson correlation matrix of logarithmic qPCR counts (cells L^{-1}) and logarithmic AZA quantities (pg L^{-1}). “R” displays the respective correlation coefficient. Significance levels of respective correlations (Pearson's product-moment correlation test) are indicated by red asterisks (* $p \leq 0.05$, ** $p \leq 0.01$, *** $p \leq 0.001$). Data and figure from **Publication IV**.

The strong correlation between qPCR-based cell abundances of *Az. spinosum* and respective AZA quantities (i.e. AZA-1, -2, 33) further allowed calculation of AZA cell quotas for the *Az. spinosum* field population (**Fig. 11; Publication IV**). A mean calculated AZA-1 cell quota of 17.8 fg cell⁻¹ is in the same range as AZA-1 cell quotas in laboratory grown *Az. spinosum* strains, which are usually between 1 and 20 fg cell⁻¹ (Tillmann et al., 2009; Salas et al., 2011; Tillmann et al., 2019), but can be up to 200 fg cell⁻¹ when grown at 10 °C (Jauffrais et al., 2013b).

Notable is the relatively broad range of the field sample based AZA cell quotas calculated in this study (e.g. AZA-1 cell quota of 2-46 fg cell⁻¹, and AZA-38 and -39 cell quota of 2-101 fg cell⁻¹), which may be the result of multiple factors. These could be methodological (e.g., chemical AZA analyses may include AZAs accumulated in small protistan grazers, detritus or lysed cells) and/or physiological reasons (e.g., cell quotas of *Azadinium* spp. usually increase when growth is limited (Dai et al. (2019); Kilcoyne et al. (2019); **Publication VIII**).

Huge variability in AZA cell quota, nevertheless, has been confirmed in the laboratory by multi strain establishment from the survey in the North Sea in 2018. Species-specific AZA cell quotas within and between *Az. spinosum* and *Am. languida* strains varied significantly with up to 330-fold differences between single AZA congeners and highlighted the need for more studies on the physiology of AZA production (**3.1.2; Publication VII**).

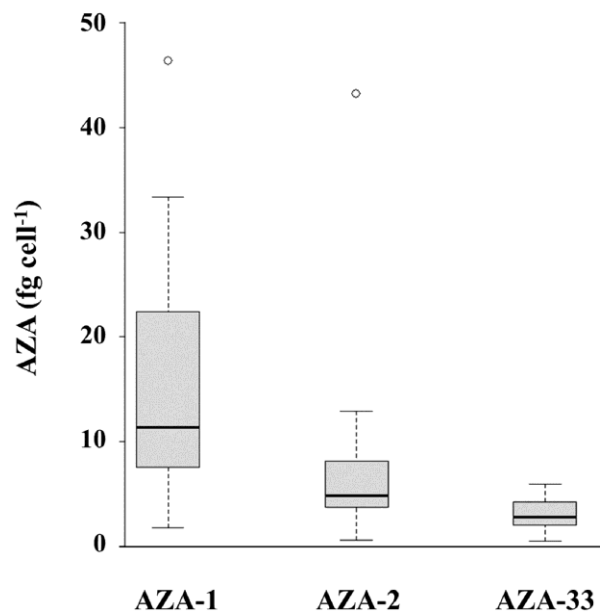


Fig. 11. AZA cell quota for *Az. spinosum* and AZA-1, -2 and -33 based on molecular (qPCR) and chemical (LC-MS/MS) field data. Data and figure from **Publication IV**.

Potential future directions for molecular Amphidomataceae research

The detection and enumeration using DNA/RNA targeting methods has become an integrated tool in (toxic) microalgae research. Thereby, a (still increasing) diversity in techniques has evolved and several of these tools can be considered for amphidomatacean studies in the future.

A supportive additive for field sample analysis in the near future might be the creation of a multiplex/multiprobe qPCR assay for toxigenic Amphidomataceae. Although this most probably goes along with intense adjustments or even complete revisions of the current single species-specific assays, this type of assay offers the simultaneous and therefore time and cost effective detection and quantification of all toxigenic amphidomataceans within a sample (Handy et al., 2006). However, it has to be mentioned here, that the expected frequent description of new species, strains and ribotypes will lead to multiple subsequent assay adjustments and recurrent assay testing. Nevertheless, the Marine Institute is running a duplex qPCR assay for the simultaneous detection of *Az. spinosum* and *Az. poporum* based on the current assay specifications and thus successfully reduces the workload.

Although not yet fully suitable for in-depth (i.e. down to ribotype level) differentiation and quantification of microalgae in the field (Ebenezer et al., 2012), a robust Next-Generation-Sequencing (NGS) workflow with primers targeting specifically all Amphidomataceae would be of use for biodiversity and biogeography analyses of both, toxigenic and non-toxigenic species. First tests in the course of this PhD with the primers covering all Amphidomataceae representatives introduced by Smith et al. (2016) did not reveal convincing results (unpublished), suggesting further method development. NGS is still poorly affordable for regular monitoring purposes, but the costs decreased in the last years and simplification of workflows especially concerning the complex data analysis is in progress (Ebenezer et al., 2012; Mardis, 2017).

During analyses by Digital Droplet PCR (ddPCR), a sample is dispersed as an emulsion into micro-well plates so that a single droplet contains either 0 or 1 target molecule, which will be amplified by PCR and quantification takes place by counting wells that contain PCR products as positive signals (Tewhey et al., 2009; Medlin and Orozco, 2017). The results of qPCR and ddPCR were found to be comparable, with a slightly higher accuracy of the ddPCR, but generally easier usage and (still) lower costs per sample of the qPCR (Te et al., 2015). Due to these relatively marginal differences and the fact that current assays are optimized for qPCR application, the latter might be the preferred option to continue amphidomatacean research for now.

Biosensors are relatively simple, cheap and fast devices coupled with high specificity and sensitivity (Metfies et al., 2005; Orozco et al., 2016). Advantages are the relatively low power requirements and the detection ability of target nucleic acids directly in the field matrix without purification or amplification, making it suitable for direct field application targeting AZA producers in the future (Liao et al., 2007; Medlin and Orozco, 2017).

Microarray detection systems are powerful molecular tools, if not the most powerful ones available today, due to the ability to potentially detect thousands of known targets in one hybridization experiment (Medlin and Orozco, 2017). The target nucleic acids are labeled with a fluorescent dye, hybridized to probes located on the microarray and subsequently scanned by a laser (Cheung et al., 1999; Rick et al., 2001). Microarrays have been developed to identify phytoplankton, including toxigenic microalgae (Metfies and Medlin, 2004; Edvardsen et al., 2013). Probes have to be designed carefully and hybridization conditions have to be set very precisely to avoid false-positive signals (Barra et al., 2013).

At the very beginning of the 21st century, Notomi et al. (2000) introduced a method called loop-mediated isothermal amplification (LAMP) for DNA amplification. The application of at least four specially designed primers and amplification of six distinct sequences from the target DNA lead to a high specificity, without losing sensitivity compared to regular PCRs. Furthermore, the reactions take place at isothermal conditions, thus no thermocycler is needed for amplification, making it attractive for field application. A so-called lateral flow dipstick (LFD) has extended this technique and shows the LAMP result as chromatographic visualization. Although Toldrà et al. (2020) stated that isothermal techniques still require further development, LAMP-LFD might be an interesting candidate for routine monitoring of toxigenic Amphidomataceae in the future, supporting or even replacing qPCR analysis.

In conclusion, the molecular qPCR technique has been evaluated being suitable for the detection and quantification of toxigenic Amphidomataceae in the field, which overcomes the drawbacks of microscopy and LC-MS/MS analysis by its high specificity and sensitivity. Nevertheless, the qualitative and quantitative results of the three methods were in good agreement and the qPCR was thus found to be an appropriate tool for subsequent biogeographic studies in the scope of this work.

3.3 Biogeography of toxigenic Amphidomataceae in the North Sea

3.3.1 qPCR-based spatial distribution and cell abundance

In total, 200 field samples taken during summer excursions in the past years were quantitatively analyzed by qPCR in the course of this PhD project (**Objective 2b**) and revealed the presence of all three AZA-producers known from the North Atlantic, i.e. *Az. spinosum*, *Az. poporum* and *Am. languida* (**Fig. 12, Suppl. Table S6**). The family-specific SYBR Green assay developed by Smith et al. (2016) thereby supported the species-specific assays as a pre-scan method on amphidomatacean DNA in the field samples. All new species and strains of *Azadinium* and *Amphidoma* have been positively tested with this general assay (**Publications II, III, VI and VII**) confirming its reliability to broadly detect amphidomataceans. In this respect, positive amplification signals but lack of signals in the species-specific assays indicate the presence of only non-toxigenic Amphidomataceae in the field samples.

Spatial analyses showed that all three toxigenic amphidomatacean species occurred in the North Sea, but the English Channel, the Scottish waters and the entrance into the Baltic Sea via the Kattegat and Belt area revealed low abundances for toxigenic Amphidomataceae at the respective sampling time (**Publications II and IV**). The cell abundances of the individual species varied significantly between a few cells per liter up to more than 10^5 cells L⁻¹. Generally, *Az. spinosum* and *Am. languida* were more abundant than *Az. poporum*. Maximum cell densities of *Az. spinosum* with 8.3×10^4 cells L⁻¹ were detected in 2018 along the Irish coastline and maximum values for *Am. languida* estimated in the central North Sea in 2018 were even higher (1.2×10^5 cells L⁻¹, **Publication IV**). Maximum cell densities (75 cells L⁻¹) of *Azadinium poporum* were detected at the Limfjord entrance (Denmark) in 2016 (**Publication II**). This finding, together with the relative low number of samples with positive signals, revealed that this species in the last years played only a minor role in the area in terms of AZA contamination risk compared to *Az. spinosum* and *Am. languida*. Although both, *Az. spinosum* and *Am. languida* were widely present along the Irish coast and in the North Sea, *Az. spinosum* was significantly more abundant in most samples taken in Irish coastal waters, while *Am. languida* was generally the dominant species in the North Sea (**Fig. 12**, note the log₁₀ scale).

Extraordinary cell abundances (1.2×10^5 cells L⁻¹) of *Am. languida* in the central North Sea in 2018 represented the highest cell density ever observed for this species and any other amphidomatacean species in North Atlantic waters, underlining the potentially dominant role of toxigenic

Am. languida in the North Sea compared to other amphidomatacean species (**Publication IV**). Nonetheless, even higher amphidomatacean cell densities have been reported from other geographical areas, i.e. up to 10^6 (*Az. polongum*, Peru) or 10^7 (*Az. luciferelloides*, Argentina) cells L^{-1} (Akselman and Negri, 2012; Tillmann and Akselman, 2016; Tillmann et al., 2017b).

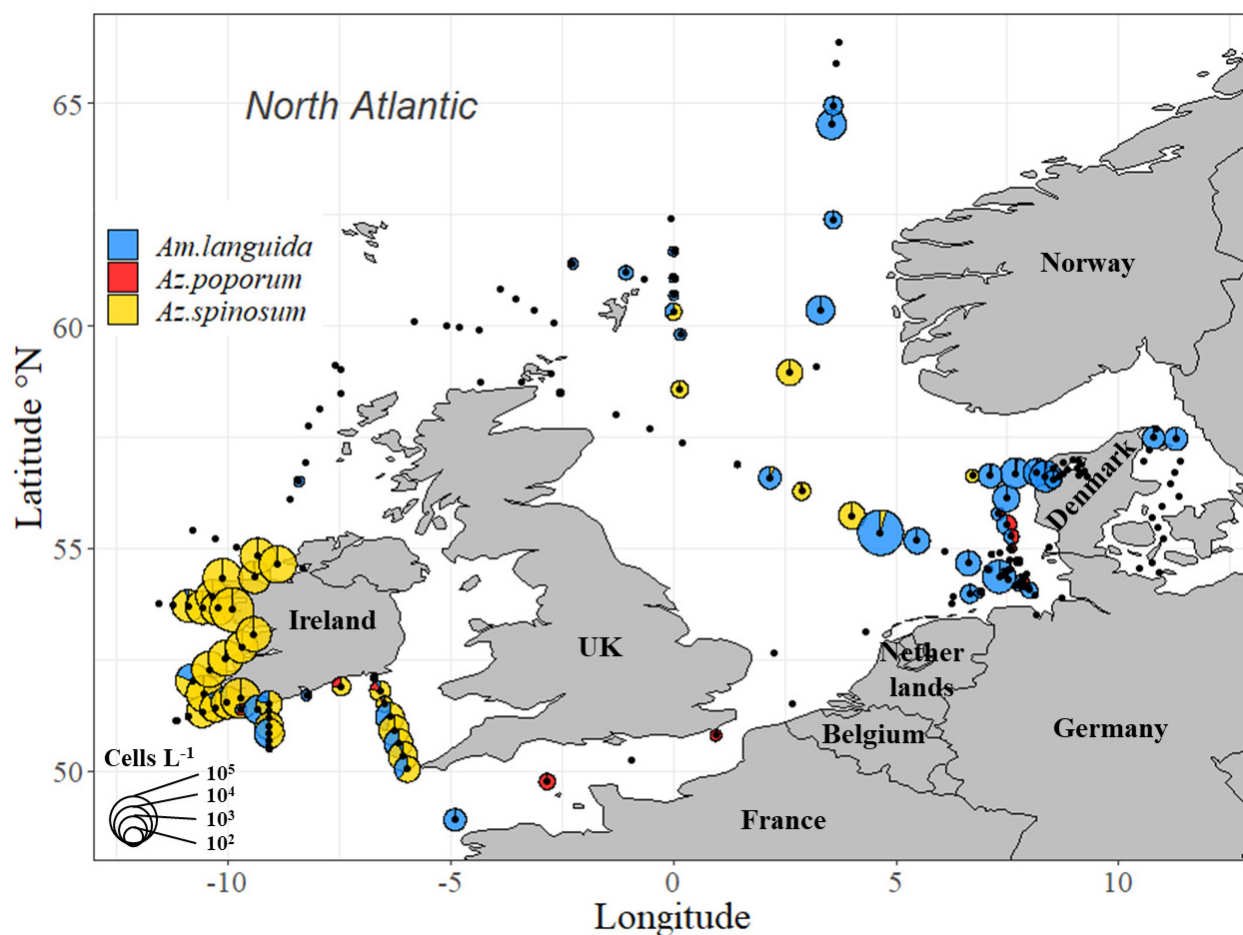


Fig. 12. Pie-charts of cell densities L^{-1} (Log_{10}) of *Az. spinosum* (yellow), *Az. poporum* (red) and *Am. languida* (blue) estimated by qPCR for the investigated field samples in this study. Pie-chart diameters correspond to the respective log_{10} abundances. Data presented in **Suppl. Table S6**.

Presumably, high abundance of toxigenic Amphidomataceae in the (north) western part of the North Sea was already observed a couple of years ago. Between July 2011 and December 2016, more than 20,500 shellfish samples were collected year-round (fortnightly to four-weekly) at representative monitoring points along the coastline of Great Britain by *Cefas* (Centre for Environment, Fisheries and Aquaculture Science) and *SAMS* (Scottish Association for Marine Science) for official biotoxin monitoring (Dhanji-Rapkova et al., 2019). The study represents the

first detailed evaluation of AZAs (-1, -2 and -3) in shellfish from Great Britain over a period of multiple years. Although the AZA producers themselves have not been investigated in that study and therefore no cell abundances are reported, measurements revealed multiple hits for AZA-1 and -2 (and AZA-3 in small proportions) in shellfish even above the EU regulatory limit (up to 433 $\mu\text{g AZA eq. kg}^{-1}$), suggesting temporally high cell densities of *Az. spinosum* Ribotype A. AZA-11 and -51, as well as AZA-38 and -39 were not investigated during that study, thus no conclusions can be made on the presence of *Az. spinosum* Ribotype B and *Am. languida*. Anyway, the high AZA amounts in shellfish indicate the presence of toxigenic Amphidomataceae in the area at that time. This also confirms findings of **this study**, although cell abundances detected in samples taken along the Scottish coast (available only from 2018) were relatively low, not exceeding 50 cells L^{-1} . That is however, in accordance with very few (and low signal) AZA hits monitored in the area the past three years (Andrew Turner, *Cefas*, pers. comm.).

The *Az. spinosum* specific qPCR assay was applied by Paterson (2018) to frequently taken field monitoring samples from Scottish coastal waters between summer 2014 and summer 2015 to survey *Az. spinosum* abundance and seasonality. The target species was only detected in two samples from Scalloway, with maximum reported cell densities of 2,545 cells L^{-1} off the Shetland Islands in August 2014. The cell density of *Az. spinosum* in the order of 2.5×10^3 cells L^{-1} in the area is relatively high compared to findings in **this study** (max. 48 cells L^{-1} in August 2018; HE-517; **Suppl. Table S6**). However, the geographical occurrence of this species around the Shetland Islands does conform with the previous isolation of *Az. spinosum* (Tillmann et al., 2012b) and with findings of **this study**. Together with isolation of another amphidomatacean species (i.e. *Az. polongum*; Tillmann et al. (2012b)), this suggests that Amphidomataceae are common members of the northern North Sea plankton community.

A recent study by Adams et al. (2020) applied the respective qPCR assays to detect and quantify *Az. spinosum* and *Az. poporum* in field samples from inland and coastal waters of the Pacific northwest taken between 2014 and 2018. Both assays revealed cell abundances of up to 156 cells L^{-1} (*Az. spinosum*) and 10,525 cells L^{-1} (*Az. poporum*) estimated by qPCR, indicating that *Az. poporum* is capable of forming higher cell densities in the field compared to findings here. However, this finding was exceptional and general cell densities did not exceed 600 cells L^{-1} , confirming the general pattern described in **this study**.

3.3.2 Vertical distribution

Knowledge on the depth distribution of toxigenic Amphidomataceae is very limited. Previous sampling in the field (e.g. **Publication II**) was performed by pooling the seawater of three different depths (i.e. the deep chlorophyll maximum layer, 10 m and 3m), not allowing statements about depth profiles. During the survey HE-516 in 2018, the vertical distribution on toxigenic AZA producers and their toxins was thus exemplarily analyzed for the first time. At six selected stations, analyzes were performed separately for samples from three depths. The results by qPCR and LC-MS/MS analyzes revealed for some stations large differences in abundance between different depths (e.g. station 71; note the log-scale in **Fig. 13**). However, there was no consistent depth distribution pattern (e.g. neither always concentrated at the surface, nor always concentrated in the deep chlorophyll layer) of toxigenic Amphidomataceae in the water column (**Fig. 13, Publication IV**).

This limited data set however, can only be a first reference on the vertical distribution of these species. Nevertheless, the highest bloom density of *Am. languida* at station 71 was concentrated in the deep layer (29 m), indicating that surface sampling and/or satellite observations (which permeate the surface layer only) are not well suited for Amphidomataceae bloom detection. Pooling (=averaging) different depths to reduce sample number might shift the cell densities per volume of filtered seawater below the “cell detection limit” of the LC-MS/MS, but overall this seems to be a cost and time effective strategy to estimate the occurrence and abundance of AZA producers in the water column (**Publication IV**).

3.3.3 Seasonal occurrence

Although field expeditions gave insights into the spatial distribution of the three toxigenic species, obviously these field samples reveal less information about the temporal occurrence. Time-series sampling of the Irish monitoring program on AZAs revealed that higher shellfish intoxication supposed to happen usually in late summer and fall (R. Salas and D. Clarke; pers. Comm.). The Norwegian Food Safety Authority (NFSA) reports AZA detection in shellfish in several years usually in fall, as well. However, recurrent AZA contamination of Irish shellfish has been noticed also in winter months (McMahon, 1998), indicating that AZA producing species can cope with low water temperatures or that mussel detoxification from AZA contamination in summer/fall takes place at a relatively slow rate, leading to positive AZA hits in a season, where human shellfish consumption supposed to be safe.

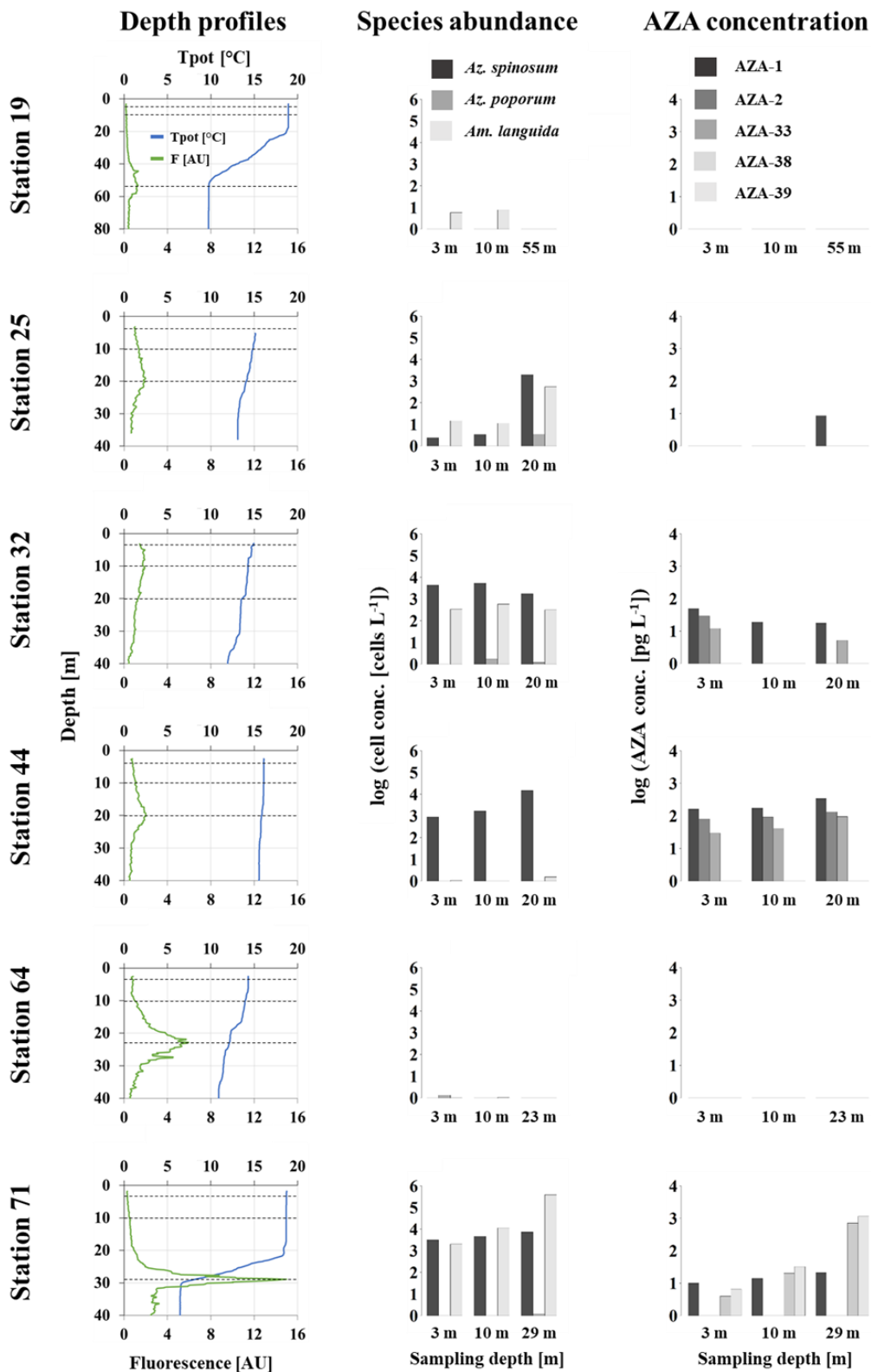


Fig. 13. Depth (m) profiles of potential temperature Tpot (°C), fluorescence (AU), AZA producer abundances (log scale) and respective toxin quantities (log scale) for six selected stations. Dashed lines in the profile plots indicate the depth for the respective samples. Figure from **Publication IV**.

Frequent (weekly or monthly) sampling was performed in 2016, 2018 and 2019 at several locations of the German Bight (Sylt, Helgoland, Cuxhaven, Wilhelmshaven) and Scapa Flow (Orkney Islands, Scotland) to investigate year-round toxigenic amphidomatacean cell abundances (**Suppl. Table S7**). For each of the in total 245 samples, sea surface water was collected at a depth of max. one meter and subsequently filtered with gentle vacuum (<200 mbar) through a 3 µm pore-size polycarbonate filter, which was subsequently stored at -20°C until further processing. DNA extraction and qPCR analysis followed descriptions in **Publication IV**. Both, the family- and the species- specific qPCR assays were applied and the cell density L⁻¹ was calculated. Depending on the filtered water volume (0.5 to 4 L) and extraction volume (30 to 100 µL), the LOD ranged between 1 and 4 cells L⁻¹.

In 2016, all three toxigenic species were detected, but were almost restricted to Scapa Flow and Helgoland in the German Bight (**Fig. 14A-D**). Only one sample from Cuxhaven showed a positive signal for Amphidomataceae (species-specific assays revealed *Az. spinosum*) in August, and samples from Wilhelmshaven did not reveal any amphidomatacean DNA. *Azadinium spinosum* was detected from July to October in Scapa Flow samples, with cell abundances between 9.1 x 10³ cells L⁻¹ (August) to 4.7 x 10⁴ cells L⁻¹ (October). Signals were only found in one month and revealed significant lower numbers in Cuxhaven (1.3 x 10² cells L⁻¹, August) and Helgoland (13 cells L⁻¹, June). *Azadinium poporum* was present at usually a few hundred cells L⁻¹ in Scapa Flow between May and August, with an exceptional maximum cell density of 2.9 x 10³ cells L⁻¹ (June). Much less cells were estimated around Helgoland in June (6 cells L⁻¹) and August (21 cells L⁻¹), and no *Az. poporum* DNA was found in samples from Cuxhaven at all. Also *Am. languida* was present only in relatively low numbers from July to September in Scapa Flow (up to 2.3 x 10² cells L⁻¹), and in July, August and October around Helgoland with an exceptional maximum of 2.5 x 10³ cells L⁻¹ in October. No cells were detected in samples from Cuxhaven either.

In 2018, only *Az. spinosum* was found during three months at Sylt (**Fig. 14E**), with relatively low numbers in May (4 cells L⁻¹), August (15 cells L⁻¹) and October (1.7 x 10² cells L⁻¹). On the other side, it was only *Am. languida* being present at Helgoland (**Fig. 14F**), also in relatively low numbers from July (15 cells L⁻¹) to October (44 cells L⁻¹), with highest abundances of 1.2 x 10² cells L⁻¹ in September.

In 2019, *Am. languida* was the only species detected at Sylt and Helgoland (**Fig. 14G, H**). For Sylt, 57 to 1.8 x 10³ cells L⁻¹ were estimated between July and October, with the peak value in August.

In Helgoland, *Am. languida* was generally lower in abundance (< 100 cells L^{-1}) compared to findings from Sylt samples and irregularly detected in July, October and December (note that no sample was available for November). *Azadinium poporum* has not been detected neither in 2018 nor in 2019 during the stationary sampling.

The results of the species-specific qPCR assays were generally in good agreement with the family-specific SYBR Green assay, showing positive signals for the same samples, which is a demonstration of the general robust methodology. However, in the samples taken at Cuxhaven no toxigenic amphidomatacean DNA has been detected in June, July, September and October, but amplification signals by the family-specific assay revealed the presence of non-toxigenic Amphidomataceae (**Fig. 14D**) (**Publications II, VI and VII**).

In 2016, 2018 and 2019 toxigenic Amphidomataceae in the North Sea were exclusively present in summer and fall (**Objective 2c**). These results are in agreement with those from the summer field excursions (e.g. **Publications II and IV**) and confirm time-series sampling of the Irish and Scottish monitoring program on AZA (and also toxigenic Amphidomataceae for Ireland), as higher shellfish intoxication supposed to happen usually in late summer and fall (R. Salas and D. Clarke; pers. Comm.; Paterson (2018); Dhanji-Rapkova et al. (2019)).

The reasons for preferred occurrence of Amphidomataceae in summer and fall remain unclear but might reflect a general dinoflagellate pattern where many species are better competitors in stratified and nutrient poor conditions, which prevail in summer and fall (Smayda and Reynolds, 2003). Jauffrais et al. (2013b) showed that *Az. spinosum* can grow at various irradiances, and there is evidence that toxigenic Amphidomataceae are able to cope well with lower nutrient concentrations (Kilcoyne et al., 2019). The occurrence and abundance of single amphidomatacean species seem to be very variable in time, as *Az. spinosum* was the exclusive species near Sylt in 2018, whereas *Am. languida* was the only species detected there in 2019.

Overall, not much is known about seasonal dynamics of Amphidomataceae and reasons for the temporal patterns can only be speculated at this point. Nevertheless, **this study** presents the very first qualitative and quantitative data on this issue, indicating that toxigenic Amphidomataceae are recurrently present in the North Sea area. Cell number estimations by qPCR confirmed again that toxigenic amphidomataceans generally occur in relatively low abundances of a few single to a few hundred cells L^{-1} . However, the field survey in 2018 demonstrated that they are also able to generate bloom concentrations of $>10^5$ cells L^{-1} and should thus be considered in monitoring programs of all bordering states of the North Sea (**Publication IV**).

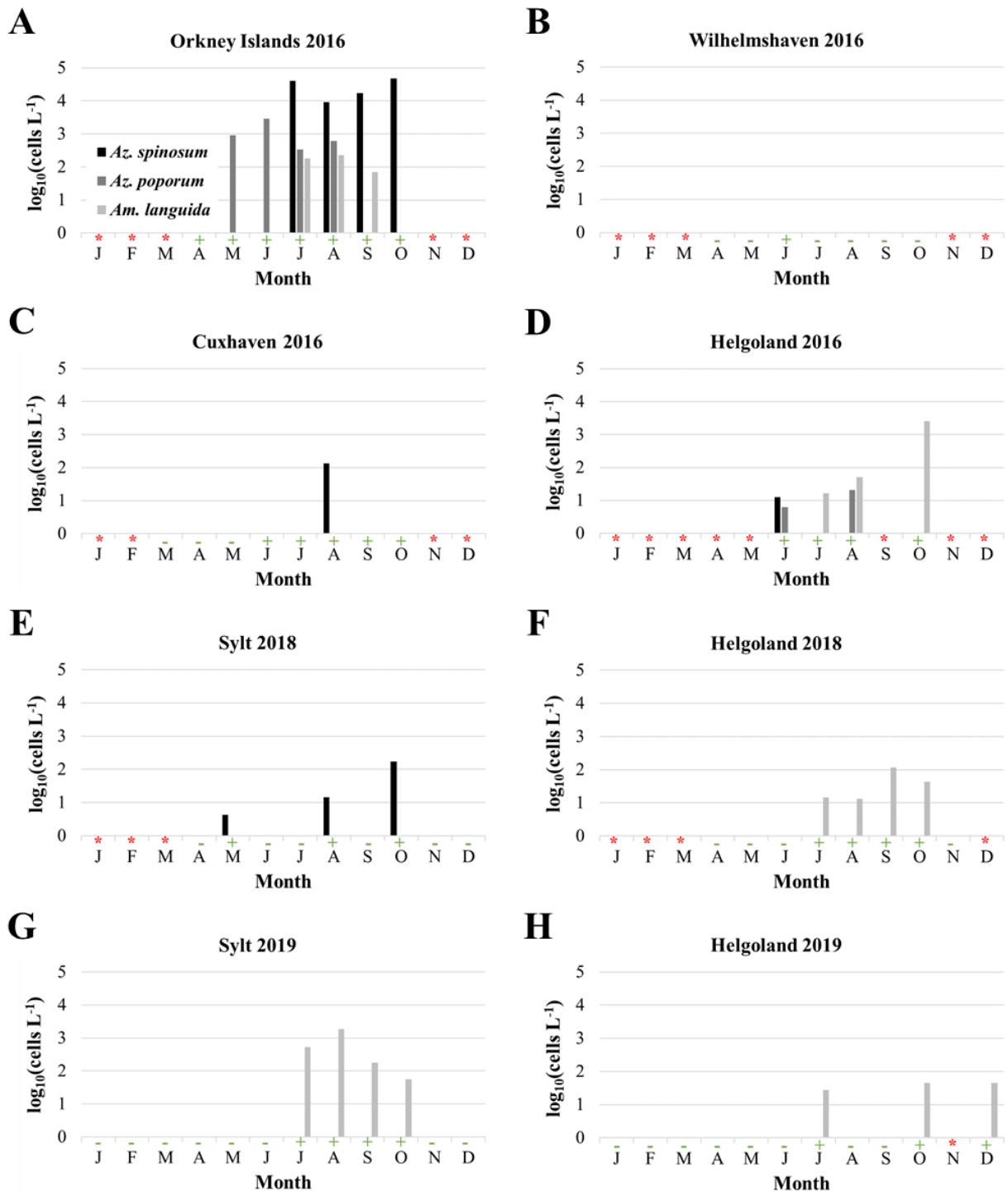


Fig. 14. Monthly presentation of toxigenic amphidomatacean maximum cell densities L^{-1} (\log_{10} transformed) from seawater samples taken between 2016 and 2019 at several locations in the North Sea estimated by qPCR (Suppl. Table S7). +/- qualitative amplification results in the family-specific assay; * no sample available.

In the last couple of years, only a few other studies estimating the temporal dynamics of toxigenic Amphidomataceae by qPCR were published. Between January 2009 and December 2011, frequent field sampling and qPCR analysis was performed by Potvin et al. (2013) to quantitatively assess the dynamics of *Az. poporum* in Shiwha Bay, Korea. With a maximum cell density of 5 cells L⁻¹, cell abundances were generally very low. An application of the *Az. spinosum* qPCR assay was in the frame of the Scottish monitoring program, where Paterson (2018) analyzed series of field samples from Scottish coastal waters collected between summer 2014 and summer 2015 to survey *Az. spinosum* abundance and seasonality. The target species was only detected in two samples, with reported cell densities of 545 cells L⁻¹ (August, 22) and 15 cells L⁻¹ (September, 5) off the Shetland Islands in 2014, but confirmed the presence of *Az. spinosum* in the summer season (**this study**). Qualitative PCR analysis of *Az. poporum* and *Az. spinosum* has been performed between September 2014 and March 2015 in coastal waters of New Zealand (Smith et al., 2016). Whereas *Az. spinosum* has not been detected during this period, positive hits for *Az. poporum* were gained in field samples taken in September and October 2014, as well as in January and February 2015. Strain establishment and DNA sequencing confirmed *Az. poporum* and supported the finding by qPCR, that at least toxigenic *Az. poporum* is present in New Zealand coastal waters.

Recently, Adams et al. (2020) investigated the distribution and abundance of *Az. spinosum* and *Az. poporum* by qPCR on the outer coast and throughout the inland waters of Washington State between 2014 and 2018. Both species were only detected between April and September (with the majority of detections before mid-July), highlighting once more that summer might be the season suitable for toxigenic Amphidomataceae. Furthermore, the authors found a significant inter-annual variability in terms of presence/absence and quantitative data, which was also observed in **this study**. Detectable amplification in 19.0 ± 15.5% (*Az. spinosum*) and 30.2 ± 13.4% (*Az. poporum*) of all collected samples revealed that toxigenic Amphidomataceae are recurrently found, but estimated cell densities of both species did not exceed 600 cells L⁻¹. However, an exceptional high record of 1.1 x 10⁴ cells L⁻¹ for *Az. poporum* in early June 2018 indicated that this species could have been responsible for AZA contamination in mussels (*Mytilus californianus*) measured that time. That *Az. poporum* might considerably contribute to the AZP risk is in contrast to this and other studies, which did not record concerning *Az. poporum* abundances in the field.

In summary, the results of biogeographic analyses revealed *Az. spinosum* and *Am. languida* as the dominant AZA producers in the eastern North Atlantic and a potentially higher AZP risk in summer and fall.

3.4 Toxigenic Amphidomataceae and environmental parameters

3.4.1 Salinity

Previous studies have repeatedly shown the significant effect of salinity on growth and toxin production in dinoflagellates (Flynn et al., 1996; Parkhill and Cembella, 1999; Gedaria et al., 2007). Generally, in both field studies (**Publications II** and **IV**), there was no significant correlation between abundance of the three toxigenic species calculated by microscopy and/or qPCR and salinity. Nevertheless, the detailed data of **Publication II** on the distribution of toxigenic Amphidomataceae and respective AZA along a salinity gradient revealed their presence (albeit in very low abundances) only in the higher-saline northern Kattegat (North Sea), but not in the lower-saline Belt area further south at the Danish east coast. However, a non-toxigenic *Az. obesum* strain was isolated at a salinity of 13 in the Kiel Bight (**Publication II**) indicating that more data is needed to evaluate the potential of Amphidomataceae to thrive in the salinity transition area of North Sea and Baltic Sea.

Previous laboratory studies demonstrated that *Az. spinosum* is able to grow in a range of higher salinities (salinity of 30-40) (Jauffrais et al., 2013b), but experimental data on a potential salinity tolerance of this species towards lower salinities are lacking. Field sample support for occurrence at lower salinities come from positive PCR hits for *Az. spinosum* from inner, low saline (< 30) Norwegian fjords (Tillmann et al., 2018a) and observations of *Azadinium* sp. (likely being *Az. spinosum*) at Irish aquaculture production sites in Bantry and Killary Bay, which underlie temporal freshwater influxes (Salas et al. (2011); Dave Clarke, pers. comm.).

Few laboratory studies indicate that other toxigenic Amphidomataceae are able to cope with or adapt to lower or higher salinities, potentially enabling them to invade new habitats and niches or at least overcome suboptimal periods. Growth was described for a wider range (salinity of 15-35) in a laboratory study on *Az. poporum* by Dai et al. (2019), revealing a potential to expand its habitat to lower saline inshore waters like bays and estuaries. On the other side, *Az. poporum* has not been detected inside the Norwegian fjords (Tillmann et al., 2018a), where salinity can be highly variable due to freshwater inflow. Both laboratory studies by Jauffrais et al. (2013b) on *Az. spinosum* and Dai et al. (2019) on *Az. poporum* revealed only little effects of different salinities on AZA cell quota.

3.4.2 Temperature

Amphidomataceae have been found around the globe in several oceans and in a wide range of water temperatures, spanning from records in cold (6 °C) Argentinean shelf waters as late winter/early spring communities (Akselman and Negri, 2012; Fabro et al., 2020) to tropical temperatures (27 °C) in Brazilian coastal waters (Cavalcante et al., 2018). A number of Amphidomataceae species (i.e. *Az. concinnum*, *Az. cuneatum*, *Am. languida*, *Az. trinitatum*, *Az. perforatum*, *Az. obesum*, *Az. dexteroporum* and including also *Az. spinosum*) were recorded and isolated from cold-water areas such as Greenland, the Irminger Sea, and Iceland (**Publication III**; Tillmann et al. (2014a); Tillmann et al. (2015)). Bloom densities of *Az. luciferelloides* and *Az. cf. spinosum* at the Argentinean Shelf in relative cold waters around 8 °C have been reported (Akselman and Negri, 2012; Tillmann and Akselman, 2016), as well as a bloom of *Az. polongum* in 20 °C coastal waters of Peru (Tillmann et al., 2017b). This suggests that there might be large differences in temperature adaptation, tolerance and optima between Amphidomatacean species. Such differences may also exist for subspecies in different geographical areas: For example, *Az. polongum* was first isolated in relatively cold waters off the Shetland Islands/North Atlantic (Tillmann et al., 2012b), whereas a bloom of *Az. polongum* has been observed in much warmer waters far away in Peru/South Pacific and Coastal waters of Brazil (Tillmann et al., 2017b; Cavalcante et al., 2018). However, in this case it is not clear if this indicates a rather wide temperature tolerance of the species or rather an evolutionary formation of geographically separated ecotypes with different physiological features. This applies also to the toxigenic amphidomatacean representatives. *Azadinium dexteroporum* is known from the relatively warm Mediterranean and was recently also found (together with *Az. cf. poporum*) in Brazilian coastal waters far above 20 °C (Percopo et al., 2013; Cavalcante et al., 2018), but has been detected in the much colder Irminger Sea off Iceland as well (Tillmann et al., 2015). In this case, significant sequence differences between the Mediterranean and the North Atlantic strains indicate cryptic diversity for this species (**Publication III**). *Azadinium spinosum*, first described from the Scotland (Tillmann et al., 2009) and frequently detected in the eastern North Atlantic (**this study**), has been recorded also in the tropical Mexican Pacific (Hernández-Becerril et al., 2012). Records of *Am. languida* are predominant from the eastern North Atlantic (**this study**), but this species was also responsible for AZA contamination of shellfish in the Mediterranean (Tillmann et al., 2012a; Tillmann et al., 2015; Tillmann et al., 2017a) and *Am. languida* have been observed in SEM from a sample collected at the open West Indian Ocean Argentinean shelf as well (Shumway et al., 2018). The widespread geographical occurrence of

Az. poporum is a good example that at least some amphidomatacean species occur under a wide range of temperatures. Furthermore, laboratory experiments with two ribotypes of *Az. poporum* (Ribotype A and C) from the Mediterranean showed that two Ribotype A strains revealed a more narrow temperature tolerance compared to two Ribotype C strains, indicating that the two ribotypes are physiologically different and temperature dependent growth might be ribotype specific (Luo et al., 2018).

Field excursion samples presented here (**Suppl. Table S6**) originate from stations with a wide range of water surface temperatures (i.e. at -1.8 to 18.9 °C). Correlation of *Az. spinosum*, *Az. poporum* and *Am. languida* cell abundances with the water temperature measured on the respective sampling sides did not reveal any significant statistical relationships (Pearson's product-moment correlation tests, $p > 0.05$) (**Objective 3a**). However, there was a noticeable difference between the relatively narrow temperature ranges, in which *Az. spinosum* (13.5 to 17.7 °C) and *Az. poporum* (13.0 to 17.8 °C) were detected, compared to the wider range (4.4 to 18.3 °C) noticed for *Am. languida* (**Fig. 15A-C**). *Amphidoma languida* was the only toxigenic amphidomatacean species detected in low temperatures in eastern North Atlantic waters (< 5 °C) near Spitzbergen in 2015 (PS92, **Fig. 15C, D**). These were the most northern positive signals (i.e. 75° N) reported for this species. In 2012, *Am. languida* have been isolated during a survey in (sub-) Arctic waters from the Irminger Sea (~65° N) (Tillmann et al., 2015), confirmed in 2017 by SEM in the central Labrador Sea (7 °C water temp., ~57° N; **Publication III**) and is now reported from the northern part of the North Sea (**this study; Suppl. Table S6**, HE-517). These findings suggest that this species is at least able to temporarily survive in the low water temperatures. No distinct upper growth limit for the three toxigenic species can be stated from this field data set presented here, since no temperatures significantly higher than 18 °C were measured during sampling in the field in this study.

Aside from these limited, descriptive observations in the field, also relatively little basic laboratory research on temperature dependent growth optima for Amphidomataceae has been performed so far. Inclusion of multiple strains in this type of studies is important especially under the perspective of relatively complex phylogeny with several Ribotypes (and even sub-Ribotypes) for *Az. spinosum* and *Az. poporum*. Experiments with North Sea *Az. spinosum* Ribotype A (traditional toxin profile AZA-1, -2 and -33) were performed by Jauffrais et al. (2012b) and Kilcoyne et al. (2019), but the recently isolated Ribotype B strains from the Norwegian coast with the new toxin profile of AZA-11 and -51 (Tillmann et al., 2018a) have never been subjected to physiological studies.

Previous work on *Az. poporum* included Ribotype A strains from the Mediterranean Sea and the US, but Ribotype A strains from the North Atlantic (the actual type locality of *Az. poporum* Ribotype A) have never been investigated. *Amphidoma languida*, although confirmed to be a widely distributed AZA-producer (AZA-38, -39) in the eastern North Atlantic (Wietkamp et al., 2019a; Wietkamp et al., 2020), have never been targeted in physiological studies.

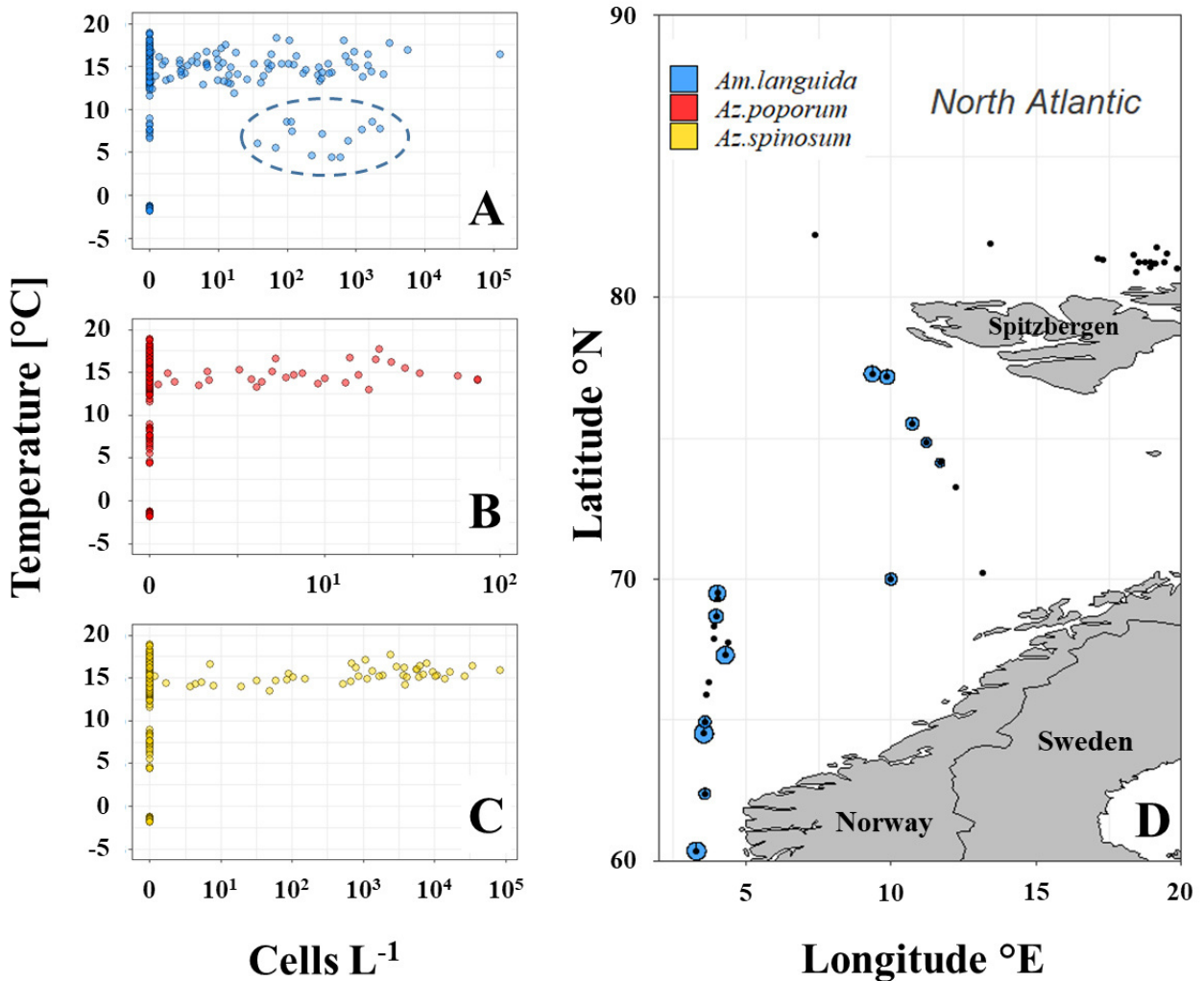


Fig. 15. qPCR counts (cells L⁻¹) and the respective water temperatures for (A) *Am. languida*, (B) *Az. poporum* and (C) *Az. spinosum* for all field samples (Suppl. Table S6). (D) Positive hits for *Am. languida* DNA (blue circles) detected by the species-specific qPCR assay during PS92 in 2015 correspond to the highlighted samples in (A). Pie-chart diameters correspond to the respective log₁₀ abundances. Black dots are stations where no *Am. languida* DNA was detected.

For the first time, two toxigenic *Az. spinosum* strains (representing Ribotype A and Ribotype B), one *Az. poporum* strain (Ribotype A) and one *Am. languida* strain from the North Sea and adjacent areas were investigated in the course of this study (**Publication VII**) and compared in terms of growth and toxin production under different temperature regimes (**Objective 3b**).

The four investigated amphidomatacean strains grew at a wide range of temperatures, with strain-specific differences. *Azadinium poporum* strain UTH-D4 (5 to 22.5 °C, optimum at 20 °C) and *Az. spinosum* strain 7-F4 grew at a wider range (10 to 27.5 °C, optimum at 20 and 25 °C) compared to *Az. spinosum* strain N-05-01 (10 to 20 °C, optimum at 20 °C) and *Am. languida* strain 8-D10 (10 to 20 °C, optimum at 20 °C) (**Publication VII**). Temperature dependent growth rates and AZA cell quotas behaved contrarily. Whereas highest growth rates were noticed at higher temperatures, toxin cell quotas were highest at lower temperatures, probably because the cells had more time to accumulate AZA before cell division. However, the calculation of an “AZA production rate”, i.e. normalizing the AZA cell quotas by the respective growth rate for a given period, revealed that the generally higher growth rates at higher temperatures were able to compensate higher AZA cell quotas in low temperature grown cells. Based on these results it could be expected that the potential AZP risk per defined water volume is similar for cells growing at low and high temperatures.

Highest AZA production at higher temperatures was found in the *Az. spinosum* Ribotype A strain (up to 8 fg cell⁻¹ day⁻¹), highlighting the potentially increasing threat of *Az. spinosum* for the North Sea area in future rising temperature scenarios. AZA cell quotas for *Az. spinosum* Ribotype A were variable, but could be up to 70 fg cell⁻¹, confirming previous studies on AZA cell quotas for this species (**Publication VII**). In contrast, Ribotype B strain N-05-01 did not reveal total AZA cell quotas higher than 10 fg cell⁻¹, which is in accordance with previous cell quota estimations (Tillmann et al. (2018a); **Publication VII**), and showed also a relatively low AZA production (0.5 to 1 fg cell⁻¹ day⁻¹). Also *Az. poporum* showed relatively low AZA production (0.5 to 1 fg cell⁻¹ day⁻¹), similar to *Az. spinosum* Ribotype B. This indicates a potentially higher AZP risk by *Az. spinosum* Ribotype A compared to Ribotype B and *Az. poporum* in the North Sea area, but multiple strains from each species/ribotype should be tested for confirmation. Intraspecific variability in AZA cell quotas between and within strains are frequently found in all toxigenic amphidomatacean species and were also confirmed here, but the responsible reasons remain unknown (**Publication VII**). The mean AZA cell quotas for *Am. languida* were on the same level for all temperatures. The AZA production rates were slightly higher (1 to 1.5 fg cell⁻¹ day⁻¹) compared to *Az. spinosum* Ribotype B and *Az. poporum*.

The proportions of the respective AZA variants per cell overall remained relatively stable between temperatures and from the exponential to the stationary growth phase in *Az. spinosum* Ribotype A (60/30/10% for AZA-1, -2, -33), Ribotype B (70/30% AZA-11, -51) and *Am. languida* (40/60% for AZA-38, -39). This might indicate that there is no up or down regulation of individual toxin variants in the AZA biosynthesis triggered by the growth phase, but this needs more substantial testing.

In contrast to the three other strains, the *Az. spinosum* Ribotype B significantly contributed to particulate dissolved AZA (-11 and -51) levels in the supernatant. In turn, AZA cell quotas in *Az. spinosum* Ribotype A, *Az. poporum* and *Am. languida* were dominated by intracellular AZAs, indicating that monitoring of AZAs in filtrated water samples, as well as monitoring of the producing cells by qPCR and LM is appropriate for AZP risk evaluation.

Amphidoma languida was detected in 5 °C cold water near Spitzbergen in 2015, but the isolated North Sea strain investigated here showed no growth at 5 °C. This demonstrates the importance of multi-strain analysis and may indicate difference in the cell physiology of laboratory-adapted cultures and field populations. More *Am. languida* strains, especially the ones isolated around Iceland, should be used for temperature experiments in the future to evaluate the strain-specific temperature tolerance. However, the data gained in **this study** represent a valuable base line for future physiological studies on the AZA producer *Am. languida*.

Overall, the effect of salinity on growth rates and AZA production seems to be less significant compared to temperature effects, suggesting that temperature plays a more important role in terms of AZP risk at aquaculture production sites.

4. Conclusions and future perspectives

Diversity

New species, strains and AZA variants have been frequently discovered and described for the Amphidomataceae in the past few years, demonstrating a continuous progress in knowledge about this dinophyte family. At the conclusion of the PhD project, in total 33 amphidomatacean species and 63 AZA congeners had been described (**Objective 2**), but knowledge about the taxonomical and toxinological diversity is expected to increase further.

Whereas monophyly of Amphidomataceae is clearly worked out, the molecular phylogeny of species within Amphidomataceae, despite availability of multiple genes and multiple strains for many species, is poorly resolved. Some morphological traits like the location of the ventral pore are mirrored by the current phylogenetic tree, whereas others such as AZA production are not. The current position of *Az. cf. spinosum*, which is morphologically identical to *Az. spinosum*, but based on ITS sequences is more closely related to *Az. obesum*, requires future studies of more strains and species to be fully understood. The fact that all four newly described species lack AZAs confirmed that AZA production is the exception rather than the rule (AZAs are described only for four out of 18 tested species) and the toxigenic trait occurs in several independent branches in the phylogenetic tree. Especially the description of non-toxigenic strains in otherwise toxigenic species (here described for *Az. poporum* and *Az. cf. spinosum*), and even sympatric occurrence with toxigenic strains poses the question of how AZA production is genetically fixed and physiologically manifested in this group of dinoflagellates, but this will be subject to further studies.

Whereas AZA levels in the mid femtogram range (up to ~ 30 fg cell⁻¹) are frequently measured in cultures, high quotas of up to 100 fg cell⁻¹ in *Az. spinosum* could be reached by cultivation in photo bioreactors. Multiple isolations and analyses of *Az. spinosum* and *Am. languida* strains in the course of this study revealed high variability in AZA cell quotas, but reasons for this extraordinary variability remain poorly understood. Whether or not favorable field conditions can lead to extraordinary high AZA cell quotas in toxigenic Amphidomataceae is not currently possible to determine at the cellular level, since single cell AZA measurements cannot be performed to date due to the limit of detection. The femtogram range AZA cell quotas of toxigenic Amphidomataceae are relatively low compared to toxin levels of larger-celled dinoflagellate taxa like *Alexandrium* spp. and *Dinophysis* spp., which are in the picogram-range (Medhioub et al., 2011; Nagai et al., 2011). In addition, AZAs are not the most potent marine biotoxins and no cases of

human death are reported so far. Intraperitoneal mouse potency bioassays revealed relatively high lethal doses of 150 $\mu\text{g kg}^{-1}$ (AZA-1), 110 $\mu\text{g kg}^{-1}$ (AZA-2) and 140 $\mu\text{g kg}^{-1}$ (AZA-3) (Satake et al., 1998a; Ofuji et al., 1999) compared to other dinoflagellate toxins like saxitoxins (e.g. produced by *Alexandrium* spp.) with an IP mouse lethal dose of $\sim 10 \mu\text{g kg}^{-1}$ (Cembella, 2003; Rossini, 2014). Nevertheless, previous human incidents indicate the threat of AZA intoxications. Studies on the biotransformation of AZAs in higher trophic levels (especially shellfish) revealed a rapid (within hours) accumulation and conversion into other variants. The *in vivo* toxicity of a couple of AZA variants (i.e. AZA-11, -33, -38, -39 and -51) is still unknown, but should be determined, since these AZAs are frequently found in the eastern North Atlantic.

In conclusion, further research is needed on species and AZA diversity, biotransformation, AZA variant toxicity and AZA production potential to fully evaluate the risk potential of AZA on seafood production.

Molecular detection of toxigenic Amphidomataceae

AZA production has only been confirmed for four species of the small-celled and therefore inconspicuous Amphidomataceae, hence making application of molecular tools is unavoidable for their routine detection and quantification. Within the scope of this thesis, a quantitative polymerase chain reaction (qPCR) assay for the detection and quantification of toxigenic *Am. languida* was developed and extensively evaluated (**Objective 1**). The highly specific and sensitive assay enables the detection and quantification of down to 1-3 *Am. languida* cells per liter of filtered seawater, which makes it suitable for field applications. Intensive research on DNA extraction efficiency and consistency, on DNA and rDNA copy cell quotas of multiple strains, on varying physiological conditions, as well as seawater matrix effects revealed a reliable, precise enumeration of all three toxigenic amphidomatacean species in the North Atlantic by the species-specific qPCR assays. Overall, the qPCR was found to be a sensitive and robust tool to detect and quantify amphidomataceans in the field, and the full set of qPCR assays for all three toxigenic species from the North Atlantic is now available and in use.

However, it is important to continuously assess the performance of those assays to assure a reliable qualitative and quantitative detection of target cells in the field, especially with respect to a continuous increasing number of newly identified species, strains and ribotypes. That the current *Az. spinosum* qPCR assay amplifies Ribotype B strains (AZA-11 and -51) with less efficiency compared to Ribotype A strains (AZA-1, -2, -33), was a considerable observation during this

project and calls for an assay re-design in the near future. This could be in the form of two separate assays for Ribotype A and B, or one assay covering both ribotypes with the same efficiency. Whereas the first option yields more flexibility, with deeper resolution and therefore comparability to respective AZA measurements, the second assay would be a more time and work efficient choice for routine monitoring. Obviously, both assays would have to assure no false-positive amplification, especially for non-toxicogenic *Az. spinosum* Ribotype C and newly identified *Az. cf. spinosum*.

qPCR quantification data gained in this study had a highly significant correlation with total amphidomatacean cell densities based on live-cell microscopy counting and with chemical analysis of AZAs. The simultaneous coordinated operation of three approaches and instruments - microscopy, LC-MS/MS and qPCR - enabled the validation and comparison of results from different perspectives, with method-specific advantages as being discussed. In combination, the multi-method approach yielded sound and reliable data on diversity, distribution and abundance of toxicogenic Amphidomataceae. In addition, extensive multi strain establishment revealed utmost importance for evaluation of strain- or species- specific differences in terms of morphology, AZA profiles, cell quotas and DNA sequences.

Since the target molecules (DNA, RNA) are universal, several alternative molecular techniques with individual strengths and limitations have been developed in addition to qPCR-based methods for discrimination and enumeration of microalgal species. NGS, ddPCR, biosensors, microarrays and LAMP-LFD are gain increasing popularity for HAB studies as well as for monitoring, and may be implemented as supportive technologies for Amphidomataceae research in the near future.

Biogeography

In the past years, Amphidomataceae have been recorded from several geographical areas around the world and continuous records from new locations suggest a global distribution of this dinophyte family. In the course of this PhD, more than 200 samples from field excursions were analyzed for toxicogenic Amphidomataceae and (for the majority of the samples) also respective AZAs (**Objective 2**). The results of the multi-method approach consisting of microscopy, qPCR, LC-MS/MS and strain establishment coherently confirmed the wide-spread, frequent occurrence and relatively high cell densities of especially *Az. spinosum* and *Am. languida* and respective AZAs in the North Sea area. In contrast, *Az. poporum* was also widely distributed, but with relatively low cell abundances, suggesting a currently minor AZP risk potential of this species for in the area.

Despite covering three years and various field sample data sets, this study can only realistically represent a snapshot concerning the biogeography and abundances of toxigenic Amphidomataceae in the North Sea. Nevertheless, the data clearly show that those species are an explicit component of the microalgae community of the eastern North Atlantic. *Amphidoma languida* was more often recorded and more abundant in the North Sea compared to *Az. spinosum*. Moreover, the highest cell abundance recorded in this thesis ($> 10^5$ cells L^{-1}) were due to a local bloom of *Am. languida* in the central North Sea, indicating a potentially higher AZA intoxication risk by *Am. languida* in the North Sea area. This was also the highest cell density ever recorded for members of the Amphidomataceae in the North Atlantic. The present study provides the methodological basis for a sound and reliable detection and quantification of this species and for more detailed future studies on distribution, abundance and importance of this AZA producer. In any case, based on the yet available data, *Am. languida* and the respective AZA-38 and -39 should be considered to be included into national North Sea monitoring programs.

Frequent sampling over two years on Helgoland and Sylt revealed generally low cell abundances, but clear seasonality with highest densities in late summer and fall. Although mostly present in background cell densities, former and present studies unambiguously showed that blooms of these microalgae with more than 10^5 cells L^{-1} can unexpectedly occur, potentially leading to serious accumulation of AZAs in shellfish. Frequent monitoring of both toxigenic species and AZA toxins is therefore recommendable. One of the main messages from the continuous sampling over two years on fixed North Sea stations is that a risk assessment based on only a few year-round sample sets can be misleading. Ideally, long time series would allow a full evaluation of the biogeographical and temporal distribution potential of amphidomataceans. Seasonal population dynamics might also be triggered by life cycle transitions, but basically nothing is known about bloom initiation of Amphidomataceae in the field. *Azadinium poporum* strain isolation from sediment samples suggested cyst formation and benthic resting stages (Potvin et al., 2012; Gu et al., 2013; Tillmann et al., 2016), but further studies are needed to unambiguously identify amphidomatacean cysts and to study details of cyst formation and life cycles of several amphidomatacean species.

Studies on other toxic dinoflagellates like *Karenia* spp. revealed a distinct daily vertical migration behavior as a result of the need for light and nutrients (Shikata et al., 2015; Hu et al., 2016). First investigations in this study showed that Amphidomataceae were not consistently restricted to a

certain water layer, but the vertical distribution and the potential for vertical migration need to be studied in more detail.

Many countries bordering the North Sea monitor for AZAs in shellfish, but monitoring of toxigenic Amphidomataceae in plankton samples, as it is done for toxigenic *Alexandrium*, *Dinophysis* or *Pseudo-nitzschia* species, is currently not included in most monitoring programs. Plausible reasons for this lack are that monitoring of AZA producing species is time- and labor- intensive, and the implementation of the respective qPCR assays on a regular basis is also a financial burden. It is also not surprising that each country puts monitoring capacity only into what tends to occur within their national or regional waters, i.e. specific attention to potentially toxigenic taxa and toxin composition in plankton and shellfish. This is the obvious reason why the Marine Institute in Ireland invests considerable resources into monitoring of toxigenic Amphidomataceae, because within Europe, Ireland has the most issues with AZA contamination in shellfish. Since 2018, the *Az. spinosum* assay has been officially accredited to ISO 17025 standards and since 2019, the Marine Institute included the species-specific qPCR assay on *Am. languida* into research surveys (Clarke (2020)).

Further investigation on toxigenic Amphidomataceae should include shellfish metabolism of the algae-produced AZAs and frequent monitoring of toxins other than the regulated AZAs, especially locally relevant variants.

Environmental parameters

A field survey along the Danish coastline in 2016 revealed, that toxigenic Amphidomataceae were more restricted to the higher salinity North Sea area compared to lower salinity of the western Baltic Sea. However, Amphidomataceae in general seem to be able to cope with a wide range of salinities. A strain of the non-toxic species *Az. obesum* was isolated from the Baltic Sea (Kiel Bight), and future studies are needed to confirm absence or presence of AZA-producing species in the Baltic Sea. No significant correlation between water temperature and amphidomatacean abundance in the field has been observed in this study (**Objective 3**). A number of amphidomatacean species is able to cope with low water temperatures as has been shown by isolation of *Am. languida*, *Az. concinnum*, *Az. cuneatum*, *Az. perforatum*, *Az. obesum*, *Az. dexteroporum*, *Az. trinitatum* and *Az. spinosum* in cold water areas like Greenland and Iceland. This was further highlighted by the most northern record of AZA producing *Am. languida* ever detected for Amphidomataceae, which is presented in this study. Nevertheless, Amphidomataceae

have also been found in much warmer waters above 25 °C (Cavalcante et al., 2018), indicating a relatively high (potentially species-specific) temperature tolerance. In general, however, not much is known about the temperature dependent occurrence and distribution of this dinophyte family and baseline information on temperature dependent growth and toxin production is available for only a few species and strains. For this reason, temperature experiments were conducted for three AZA producing species of the North Atlantic in the course of this PhD project (**Objective 3**). Higher AZA cell quotas at colder temperatures can be overcompensated by higher growth rates at higher temperatures, potentially leading to a higher AZP risk for *Az. spinosum* under future global change scenarios (**Objective 4**).

The presented PhD study provides new insights into the diversity, biogeography and seasonality of toxigenic Amphidomataceae in the North Sea and adjacent areas, and highlights the use of the molecular qPCR as a valuable tool for the quantitative detection of toxigenic amphidomatacean species in the field. During this project, overall abundance of toxigenic Amphidomataceae and AZAs was low, indicating a generally low AZA contamination risk in shellfish in the eastern North Atlantic at present. Nevertheless, several incidents in the past demonstrate that AZP is a threat for human health and the shellfish industry. The frequent detection of toxigenic Amphidomataceae and AZAs - including the highest yet recorded (toxigenic) amphidomatacean population density - as described here advises caution and frequent monitoring. Especially the bloom of *Am. languida* detected in the central North Sea suggests that this species and respective toxins (AZA-38/-39) should be included for routine monitoring in the area. Temperature-dependent growth experiments suggest a potentially increasing AZP risk in the future due to expected ocean temperature rises. Such physiological data on species-specific temperature related growth and toxin production as presented here are of value for ecosystem modeling and could be implemented to learn more about factors determining harmful amphidomatacean blooms.

Funding

This three-year PhD project, which led to the considerable knowledge expansion in the research field presented here, would not have been possible without the respective financial support. Therefore, I want to sincerely thank the German Ministry for Education and Research (project RIPA ZA, 03F0763A) and the PACES research program of the Alfred-Wegener-Institute as part of the Helmholtz Foundation initiative in Earth and Environment, who funded this study including publication and travel expenses. Furthermore, I thank the Helmholtz Graduate School for Polar and Marine Research (POLMAR) for granting travel expenses, which enabled me to participate and present my research at the International Conference on Harmful Algae (ICHA) in 2018.

Publications

Publication I: New real-time PCR assay for toxigenic *Amphidoma languida*

Molecular detection and quantification of the azaspiracid-producing dinoflagellate *Amphidoma languida* (Amphidomataceae, Dinophyceae). *Journal of Plankton Research*
Wietkamp, S., Tillmann, U., Clarke, D., Toebe, K. (2019)

Publication I describes the design of a new real-time PCR assay for the molecular detection and quantification of the azaspiracid-producing dinoflagellate *Amphidoma languida* within field samples.

The aims were 1) to create and validate a species-specific and highly sensitive qPCR assay on *Am. languida* 2) to assess DNA content and rDNA copy number per cell within and between several *Am. languida* strains (for one strain also over time), which is crucial for qPCR based quantification 3) to investigate potential seawater matrix effects on the assay 4) to test the new assay on DNA samples from the field.

The candidate developed, intensively tested and validated the new qPCR assay (100%). This included spike experiments, DNA content/copy number determination and testing on seawater matrix effects, as well as the respective data analysis. Dr. U. Tillmann (AWI) provided target cells from exponentially growing amphidomatacean cultures. Dr. K. Toebe (AWI) provided introduction to the workflow of a qPCR assay development. D. Clarke (Marine Institute) provided the DNA field sample set and tested of the new assay on a different qPCR instrument. The candidate composed the manuscript (70%) in close cooperation with Dr. U. Tillmann with final edits by the other co-authors.



J. Plankton Res. (2019) 41(2): 101–113. First published online February 5, 2019 doi:10.1093/plankt/fby052

Molecular detection and quantification of the azaspiracid-producing dinoflagellate *Amphidoma languida* (Amphidomataceae, Dinophyceae)

STEPHAN WIETKAMP^{1*}, URBAN TILLMANN¹, DAVE CLARKE² AND KERSTIN TOEBE¹

¹ALFRED-WEGENER-INSTITUTE, HELMHOLTZ CENTRE FOR POLAR AND MARINE RESEARCH, AM HANDELSHAFEN 12, BREMERHAVEN D-27570, GERMANY AND

²MARINE INSTITUTE, RINVILLE, ORANMORE, GALWAY H91 R673, IRELAND

*CORRESPONDING AUTHOR: stephan.wietkamp@awi.de

Received September 10, 2018; editorial decision December 18, 2018; accepted December 19, 2018

Corresponding Editor: Lisa Campbell

Species of the planktonic dinoflagellates *Azadinium* and *Amphidoma* are small, inconspicuous and difficult, if not impossible to be identified and differentiated by light microscopy. Within this group, there are some species that produce the marine biotoxin azaspiracid (AZA) while others are non-toxicogenic, therefore a requirement exists for precise species identification. A quantitative polymerase chain reaction (qPCR) assay for molecular detection and quantification of one of the toxicogenic species, *Amphidoma languida*, was designed and extensively tested. The assay was highly specific and sensitive to detect and quantify down to 10 target gene copies (corresponding to ca. 0.05 cells) per reaction. DNA cell quota and copy number cell⁻¹ were constant for four different *Am. languida* strains, and for one strain they were shown to be stable at various time points throughout the growth cycle. Recovery of known cell numbers of *Am. languida* spiked into natural samples was 95–103%, and the assay was successfully tested on field samples collected from Irish coastal waters. This new qPCR assay is a valuable tool for routine monitoring for the prevention of AZA-shellfish-poisoning caused by the consumption of contaminated shellfish and is a supportive tool for studies on the biogeography of this AZA-producing species.

KEYWORDS: *Amphidomataceae*; quantitative real-time PCR; *Azadinium*; azaspiracid shellfish poisoning (AZP); molecular probes

INTRODUCTION

The azaspiracids (AZA) were identified in 1998 (Satake *et al.*, 1998) as new marine biotoxins, causing the serious seafood toxicity syndrome AZP (azaspiracid shellfish poisoning) in humans. AZA accumulate mainly in shellfish and crabs, and associated symptoms after consumption of contaminated seafood include mainly gastrointestinal health problems, like cramps, vomiting, nausea and severe diarrhea (Botana, 2014; Twiner *et al.*, 2014). AZA levels above the regulatory limit and extended shellfish harvest closures are a recurrent and serious problem mainly in Ireland (Salas *et al.*, 2011). In 2009, the small photosynthetic dinoflagellate *Azadinium spinosum* was described as a new species in a newly erected genus from the North Sea off the Scottish coast and identified as the first source organism producing AZA (Tillmann *et al.*, 2009). Since then, intense research has led to the description of different new AZA congeners and new species of *Azadinium*. To date, 13 *Azadinium* species have been described (Tillmann and Akselman, 2016), from which only three, *A. spinosum*, *A. poporum* and *A. dexteroporum* are known AZA producers (Krock *et al.*, 2012; Rossi *et al.*, 2017). However, AZA are not only produced by *Azadinium*. In 2012, the newly described *Amphidoma languida* was identified morphologically and phylogenetically as a close relative of the genus *Azadinium*, and both, *Azadinium* and *Amphidoma*, are now combined in the family Amphidomataceae (Tillmann *et al.*, 2012). Interestingly, *Amphidoma languida* produces AZA as well. To date, the azaspiracids AZA-2, -38, -39, -43, -52 and -53 with strain-specific AZA profiles have been found in *Am. languida* (Tillmann *et al.*, 2017).

Due to their small cell size (10–15 μm in cell length), most species of Amphidomataceae are difficult to detect and identify by light microscopy. A reliable morphological identification requires enhanced microscopic techniques like electron microscopy and the respective expertise. Thus, it is a time-consuming task, especially when other species of similar size and shape, such as *Heterocapsa* spp., are present in the samples (Tillmann *et al.*, 2009, 2010, 2012). This is probably the main reason why AZA-producing species have been discovered just recently. However, species identification is required for Amphidomataceae because toxigenic and non-toxigenic species are very similar in size and shape as well, and are known to co-occur in the same area (Tillmann *et al.*, 2014, 2015). Therefore, molecular tools are an ideal alternative method for rapid and routine identification of AZA-producing species in field samples. For the first three described *Azadinium* species (*A. spinosum*, *A. poporum* and *A. obesum*), Toebe *et al.* (2013) designed quantitative polymerase chain reaction (qPCR) assays, targeting the large subunit (LSU/28S) region of the ribosomal DNA (rDNA). Three years later, Smith *et al.* (2016) added a gen-

eral Amphidomatacean real-time PCR assay, which allowed the detection of all described Amphidomatacean species that were known until that time, including *Amphidoma languida*.

Although the specific probes for two of the AZA-producing species are available (*A. spinosum* and *A. poporum*; Table I) and in use (Kim *et al.*, 2017; Tillmann *et al.*, 2018a), specific qPCR assays for the toxigenic *A. dexteroporum* and *Am. languida* are still lacking. While toxigenic *A. dexteroporum* have not been identified outside the Mediterranean (Tillmann *et al.*, 2015), *Am. languida* seem to be widely distributed in the North Atlantic (Tillmann, 2018) and have recently been identified as the causative agent of shellfish contamination above the EU regulatory limit in Spain (Tillmann *et al.*, 2017).

The aim of this study is to design and validate a real-time PCR assay for the identification and quantification of the AZA-producing dinoflagellate *Amphidoma languida* within environmental field samples for monitoring applications and to support biogeographical studies on this species.

METHOD

Laboratory cultures and DNA extraction

Genomic DNA was harvested from exponentially growing, unialgal strains grown in 1/10 strength K medium (Keller *et al.*, 1987) at 15°C, a photon flux density of 70 $\mu\text{mol m}^{-2} \text{s}^{-1}$ and a light:dark cycle of 16:8 h. Cells were collected by centrifugation in a 50 mL tube at $3220 \times g$ for 15 min (5810R, Eppendorf, Hamburg, Germany). The supernatant was removed with a pipette. The pellet was resuspended in the remaining overlaying supernatant and subsequently transferred to a 1.5 mL tube and stored at –20°C. DNA was extracted using the NucleoSpin Soil DNA isolation kit (Macherey-Nagel, Düren, Germany) following the manufacturer's instructions. Instead of vortexing the bead tubes, the samples were shaken for 45 s and another 30 s at a speed of 4.0 ms^{-1} in a cell disrupter (FastPrep FP120, MP Biomedicals, Santa Ana, USA). DNA elution was performed twice using 100 μL of the provided elution buffer to increase the overall DNA yield. The DNA was stored at –20°C until further processing. Performance of the Soil kit was checked by analyzing DNA recovery/losses. Therefore, DNA extracts of known DNA concentrations were applied to the extraction procedure as described above. The NucleoSpin Soil kit revealed a $\geq 90\%$ DNA recovery (Table S1) and was subsequently considered to be consistent. Reproducibility of DNA extractions was evaluated with six replicates each for four different strains and revealed relative standard deviations ranging from 4.9 to 8.2% (Table III).

Table I: Sequences of primers and probes for *Amphidoma languida* (this study), the general *Amphidomataceae* assay and other *Azadinium* species from the literature

Target species	Target gene	Oligonucleotide type	Sequence (5'-3')	Product size (bp)	Reference
<i>Amphidoma languida</i>					
	LSU				
Alan509F		F-Primer	CGGTTACAGGCGAGGAT	60	This study
Alan569R		R-Primer	GACATTCACACCTCCGTGGAA		
Alan528		TaqMan MGB probe	6FAM-CTTCTGAGGACATGGTAAC-MGB		
<i>Azadinium</i> and <i>Amphidoma</i> genera					
	ITS				
Amp240F		F-Primer	CAACTTTCAGCGACGGATGTCTCG	179	Smith et al. (2016)
Amp418R		R-Primer	AAGCYRCWGGCATKAGAAGGTAGWGCC		
<i>Azadinium spinosum</i>					
	LSU				
Asp48F		F-Primer	TCGTCTTTGTGTCAGGGAGATG	72	Toebe et al. (2013)
Asp120R		R-Primer	GGAAACTCCTGAAGGGCTTGT		
Aspin77T		TaqMan MGB probe	6FAM-CGCCCAAAGGACTCCT-MGB		
<i>Azadinium poporum</i>					
	LSU				
Apop62F		F-Primer	GATGCTCAAGGTGCCTAGAAAGTC	68	Toebe et al. (2013)
Apop148R		R-Primer	CCTGCGTGTCTGGTTGCA		
Apop112		TaqMan MGB probe	6FAM-TTCCAGACGACTCAAA-MGB		

A large batch of positive extraction-process-controls (EPC) with known cell numbers was prepared and stored at -20°C in 500 μL lysis buffer (buffer SL1, provided by the DNA isolation kit). Each EPC contained 10^3 cells of *Am. languida* (Z-LF-9-C9) and was extracted during each DNA extraction process to check DNA extraction efficiency and consistency. Reproducibility of EPC DNA extractions ($n = 14$) with a relative standard deviation of 7.9% was sufficiently high (Table S2).

Primer and probe design

The software Primer Express V.3.0 (Applied Biosystems by Thermo Fisher Scientific, Waltham, USA) was used to design species-specific primers and the probe, which target the large subunit (LSU/28S) region of the rDNA of *Amphidoma languida* in a real-time PCR assay (Table I). The probe was designed as a TaqMan minor groove binding (MGB)-probe with a 6-FAM reporter dye at the 5'-end and a Black Hole Quencher at the 3'-end (Applied Biosystems by Thermo Fisher Scientific, Waltham, USA). The target positions on the LSU were selected using multiple alignment comparisons within the software MEGA7 V7.0.26 (Kumar et al., 2016). The sequences of the target species *Am. languida*, other Amphidomataceae and further related taxa were obtained from GenBank (<https://www.ncbi.nlm.nih.gov/genbank/>), as well as from unpublished sequences. To confirm the specificity of the designed primers and probe *in silico*, a sequence similarity search was performed using the Basic Local Alignment Search Tool (BLAST) of the National Center for Biotechnology Information (NCBI, <https://blast.ncbi.nlm.nih.gov/Blast.cgi>).

Conditions in real-time assays

A number of different primer sets, where no mismatch with the target-sequence and at least 5% mismatches with non-target sequences were observed, were preliminarily tested in a SYBR Green qPCR assay as a pre-scanning method. The 10 μL SYBR Green qPCR assay for the prescan primer tests contained 5 μL of Fast SYBR Green Master Mix (Applied Biosystems by Thermo Fisher Scientific, Waltham, USA), 0.25 μL of both primers (each 10 μM , for a final concentration of 200 nmol), 3.5 μL of high-grade PCR H_2O and 1 μL of template DNA ($1 \text{ ng } \mu\text{L}^{-1}$). The SYBR Green assays were run in a StepOne Plus real-time PCR cycler (Applied Biosystems by Thermo Fisher Scientific, Waltham, USA) with the following conditions: Stage 1: hold 95°C for 20 s, followed by 40 cycles of Stage 2, Step 1: hold 95°C for 3 s, Step 2: hold 60°C for 30 s, followed by a Melt Curve Stage: Step 1: hold 95°C for 15 s, Step 2: hold 60°C for 60 s, Step 3: hold 95°C for 15 s.

The best performing primer set with the lowest C_T value was then tested for specificity in a TaqMan assay on DNA of various *Am. languida* strains (each at $1 \text{ ng } \mu\text{L}^{-1}$ of DNA), as well as on extracted DNA from a range of non-target microalgae from different geographical regions (Table II). Assays were conducted either with stand alone DNAs or mixtures of DNAs spiked with *Am. languida* DNA.

To find the optimal primer and probe concentrations for the TaqMan assay, six different primer concentrations (600, 700, 800, 900, 1000 and 1200 nM) and three different probe concentrations (100, 200 and 300 nM) were tested. The final 10 μL TaqMan qPCR assay contained 5 μL of $2 \times$ TaqMan Universal PCR Master

Table II: Strains for cross-reactivity testing of the *Amphidoma languida* qPCR assay

Species	Strain	Origin	qPCR result
<i>Amphidoma languida</i>	2 A11	North Atlantic, Iceland	+
<i>Amphidoma languida</i>	AND-A0920	North Atlantic, Spain	+
<i>Amphidoma languida</i>	N-01-01	North Atlantic Norway	+
<i>Amphidoma languida</i>	N-12-01	North Atlantic, Norway	+
<i>Amphidoma languida</i>	N-39-12	Noth Atlantic, Norway	+
<i>Amphidoma languida</i>	N-40-06	North Atlantic, Norway	+
<i>Amphidoma languida</i>	SM1	North Atlantic, Ireland	+
<i>Amphidoma languida</i>	Z-LF-14-E7	North Sea, Denmark	+
<i>Amphidoma languida</i>	Z-LF-14-F2	North Sea, Denmark	+
<i>Amphidoma languida</i>	Z-LF-14-G7	North Sea, Denmark	+
<i>Amphidoma languida</i>	Z-LF-9-C4	North Sea, Denmark	+
<i>Amphidoma languida</i>	Z-LF-9-C9	North Sea, Denmark	+
<i>Amphidoma parvula</i>	H1-E9	South Atlantic, Argentina	–
<i>Azadinium caudatum</i>	AC 1	North Sea, Scotland	–
<i>Azadinium concinnum</i>	1 C6	North Atlantic, Irminger Sea	–
<i>Azadinium cuneatum</i>	3 D6	North Atlantic, Iceland	–
<i>Azadinium cuneatum</i>	35-A2	Northeast Pacific, Puget Sound	–
<i>Azadinium dalianense</i>	121-F6	Northeast Pacific, Puget Sound	–
<i>Azadinium dalianense</i>	48-1-F8	Northeast Pacific, Puget Sound	–
<i>Azadinium dalianense</i>	H-2-G7	South Atlantic, Argentina	–
<i>Azadinium dalianense</i>	N-38-03	North Atlantic, Norway	–
<i>Azadinium dalianense</i>	Z-LF-14-F7	North Sea, Denmark	–
<i>Azadinium dexteroporum</i>	1 D12	North Atlantic, Irminger Sea	–
<i>Azadinium obesum</i>	48-1-F2	Northeast Pacific, Puget Sound	–
<i>Azadinium obesum</i>	2E10	North Sea, Scotland	–
<i>Azadinium obesum</i>	AZA 2D	North Atlantic, Labrador Sea	–
<i>Azadinium obesum</i>	N-41-01	North Atlantic, Norway	–
<i>Azadinium obesum</i>	Z-LF-12-A12	North Sea, Denmark	–
<i>Azadinium obesum</i>	Z-LF-44-C3	Baltic Sea, Germany	–
<i>Azadinium polongum</i>	N-47-01	North Atlantic, Norway	–
<i>Azadinium polongum</i>	Shet B2	North Atlantic, Shetland Islands	–
<i>Azadinium poporum</i>	1 D5	South Pacific, Chile	–
<i>Azadinium poporum</i>	121-E10	Northeast Pacific, Puget Sound	–
<i>Azadinium poporum</i>	18 A1	South Atlantic, Argentina	–
<i>Azadinium poporum</i>	AZ-BH-03	South China Sea, China	–
<i>Azadinium poporum</i>	HJ-2011	East China Sea, Korea	–
<i>Azadinium poporum</i>	N-39-01	North Atlantic, Norway	–
<i>Azadinium poporum</i>	UTH C8	North Sea, Denmark	–
<i>Azadinium poporum</i>	Z-LF-14-E12	North Sea, Denmark	–
<i>Azadinium spinosum</i>	3D9	North Sea, Scotland	–
<i>Azadinium spinosum</i>	H-1-D11	South Atlantic, Argentina	–
<i>Azadinium spinosum</i>	H-4-A10	South Atlantic, Argentina	–
<i>Azadinium spinosum</i>	N-04-01	North Atlantic, Norway	–
<i>Azadinium spinosum</i>	N-05-01	North Atlantic, Norway	–
<i>Azadinium spinosum</i>	Shet F6	North Atlantic, Shetland Islands	–
<i>Azadinium spinosum</i>	SM2	North Atlantic, Ireland	–
<i>Azadinium spinosum</i>	UTH E2	North Sea, Denmark	–
<i>Azadinium trinitatum</i>	A2 D11	North Atlantic, Iceland	–
<i>Azadinium trinitatum</i>	N-39-04	North Atlantic, Norway	–
<i>Alexandrium catenella</i>	MX E11	North Atlantic, western Greenland	–
<i>Alexandrium ostentfeldii</i>	MX D1	North Atlantic, western Greenland	–
<i>Gymnodinium sp.</i>	H-1-A6	South Atlantic, Argentina	–
<i>Heterocapsa minima</i>	JK2	North Atlantic, Ireland	–
<i>Heterocapsa steinii</i>	UTK G7	Baltic Sea, Germany	–
<i>Karlodinium veneficum</i>	E11	Mediterranean, Spain	–
<i>Prorocentrum balticum</i>	CCMP1787	South Pacific, New Zealand	–
<i>Prorocentrum micans</i>	PM A4	Baltic Sea, Germany	–
<i>Scipsiella precaria</i>	SP14	North Sea, Scotland	–

Results show either a positive (+) or no (–) amplification.

Mix, with AmpliTaq Gold DNA polymerase and dNTPs and the passive reference dye ROX (Applied Biosystems by Thermo Fisher Scientific, Waltham, USA), 0.9 µL of both primers (as a final concentration

of 900 nmol), 0.2 µL of the TaqMan MGB probe (as a final concentration of 200 nmol), 2 µL of high-grade PCR H₂O and 1 µL of template DNA (1 ng µL⁻¹). The TaqMan qPCR assay followed these steps: Stage 1: hold

Table III: LSU gene copy number and DNA content cell⁻¹ in four different *Am. languida* strains (n = 6)

Strain	Origin	Mean LSU copy number (no. cell ⁻¹) ± SD	Mean DNA content (pg cell ⁻¹) ± SD
2A11	North Atlantic, Iceland	719 ± 48	2.73 ± 0.18
N-12-01	North Atlantic, Norway	830 ± 93	3.15 ± 0.35
AND-0920	North Atlantic, Spain	777 ± 38	2.95 ± 0.15
Z-LF-9-C9	North Sea, Denmark	829 ± 107	3.15 ± 0.41

95°C for 20 s, followed by 40 cycles of Stage 2, Step 1: hold 95°C for 1 s, Step 2: hold 60°C for 20 s. All reactions were carried out in triplicates within 0.1 mL MicroAmp Fast 96-Well Reaction Plates (Applied Biosystems by Thermo Fisher Scientific, Waltham, USA) on a StepOne Plus real-time PCR cycler (Applied Biosystems by Thermo Fisher Scientific, Waltham, USA) and a sample was considered as positive only if all three replicates of the sample showed a fluorescence signal above the threshold before cycle 37. No-template controls (NTC) containing high-grade PCR H₂O as well as extraction-process-controls (EPC) were present during all PCR runs. For C_T value (threshold cycle), baselines and thresholds were set manually before each qPCR analysis according to the guidelines from Applied Biosystems (Livak, 1997; Ruijter *et al.*, 2009).

Quantification experiments

For DNA-based quantification of cells, standard curves with known DNA concentrations are required in each qPCR run. Two types of standard curves were established: First, a standard curve of 10-fold dilution series of *Am. languida* DNA (10 ng μL⁻¹ to 0.1 pg μL⁻¹) was generated. The DNA from 10⁵ cells was collected from four exponentially growing strains of *Am. languida*. Cell density was estimated by light microscopy (Axiovert 200 M, Zeiss, Germany) counting of settled subsamples of 0.5 mL at a magnification of 400×. The DNA was extracted as described above. The amount of dsDNA of these extracts was measured using the Quantus Fluorometer (Promega, Fitchburg, USA) and DNA cell quota was calculated.

The second standard curve was a 10-fold dilution series of copies of the target amplicon (10⁸ copies μL⁻¹ to 10¹ copies μL⁻¹), which were prepared according to Perini *et al.* (2011). The 681 bp D1-D2 region of the LSU rRNA from purified genomic DNA of *Am. languida* was amplified in a qualitative PCR. Each 20 μL PCR reaction contained 2 μL of 10× HotMaster Taq buffer, 0.1 μL of HotMaster Taq DNA polymerase, 0.2 μL dNTP (10 μM), 0.2 μL of both primers (each 10 μM; Forward primer: D1R; Reverse primer: D2C; (Scholin

et al., 1994)), 16.3 μL of high-grade PCR H₂O and 1 μL of template DNA (10 ng μL⁻¹). PCR was carried out in an Eppendorf Mastercycler (Eppendorf, Hamburg, Germany). Initial denaturation (94°C, 2 min) was followed by 30 cycles of denaturation at 94°C for 30 s, annealing at 55°C for 30 s, elongation at 68°C for 2 min and a final extension at 68°C for 10 min. The amplicon was analyzed and quantified on a Bioanalyzer Instrument (2100 Bioanalyzer, Agilent, Santa Clara, USA) and the number of amplicon copy number per μL was calculated using the following equation:

$$\text{No. molecules } \mu\text{L}^{-1} = (A \times 6.022 \times 10^{23})(B \times 660)^{-1}$$

where A is the amplicon concentration (g μL⁻¹), 6.022×10^{23} is Avogadro's number, B is the number of base pairs of the amplicon and 660 is the average molecular weight of one base pair. Both, the DNA-based and the copy-molecule-based standard curve, were performed in triplicates in all qPCR runs. To account for intraspecific variability, both DNA content and copy numbers per cell were determined for four strains (Z-LF-9-C9, N-12-01, 2A11 and AND-0290).

To additionally test for potential intra-clonal variability in DNA content or DNA copy number cell⁻¹, one of the *Am. languida* strains (Z-LF-9-C9) was sampled in 10 mL duplicates at 10 am and 3 pm for a period of 17 days. For each sampling, the cell density of the culture was determined by microscopy enumeration. The DNA was extracted and measured as described above and the DNA content and copy number cell⁻¹ was calculated.

Spiked seawater samples

To account for potential PCR inhibition effects of a natural seawater matrix, known cell numbers of *Am. languida* were spiked into a natural seawater sample. The sample was prepared from 1 L of water taken at Bremerhaven harbor additionally enriched with 50 mL of *A. poporum* (strain AZ-BH-03, 56.000 cells mL⁻¹) and 50 mL of *Lingulodinium polyedra* (strain 28-4C, 500 cells mL⁻¹). In triplicates, 10⁵, 10⁴, 10³ or 10² cells of *Am.*

languida (strain Z-LF-9-C9) were spiked into 50 mL of the generated seawater matrix. Negative controls without *Am. languida* cells were prepared as well. The tubes were centrifuged and DNA extracted from the pellet as described above.

Subsequent qPCRs with DNA and target molecule based standard curves were performed and the *Am. languida* cell number was calculated as described above. A second spike experiment was performed 2 weeks later, using the same cultures and cell numbers for spiking as described above.

Application of the assay on field samples

In August 2017, a coastal survey (CV17022) of Irish waters was conducted by the Marine Institute (Ireland) on board the RV Celtic Voyager. In total, 66 stations were sampled along a number of transects from the Southeast coast, right round the South coast and up along the West coast (Fig. 4). At each station, 5 L water samples were collected from the observed chlorophyll-maximum-layer with Niskin bottles attached to the deployed CTD instrument. Samples were prefiltered through a 20 µm mesh, subsequently filtered onto 3 µm

TSTP filters (47 mm, Merck, Darmstadt, Germany) and stored at -20°C until further analysis. To wash the collected cells off, the filters were cut into halves, with one half placed in individual 2 mL microtubes containing 1.5 mL of lysis buffer and vortexed for 1 min. The filter papers were discarded, the microtubes were centrifuged at 3220 × g for 5 min and the supernatant was discarded as well. DNA extractions were in accordance with the laboratories ISO-17 025 accredited internal procedures (available at the Marine Institute, SOP No. PHY-055 Vr 1.1). Quantitative PCR was performed on a Roche LightCycler 480 Vr I and II PCR instrument (Roche AG, Basel, Switzerland). Cell number per sample was calculated based on a standard curve of 10-fold dilutions of *Am. languida* DNA as described above using the associated software with the LightCycler instrument.

Statistical analysis

Statistical analyses were performed with parametric (analysis of variances; ANOVA) or non-parametric (Mann–Whitney, Kruskal Wallis, or Spearman correlation) tests, using RStudio ver. 1.1.419, with a *P* < 0.05 level of significance.

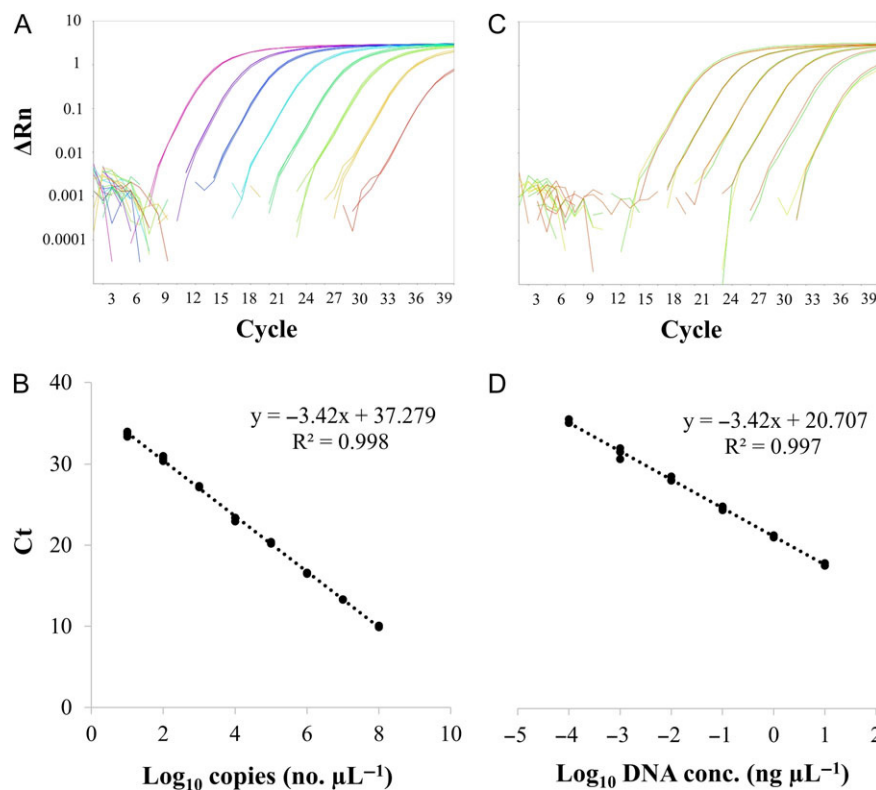


Fig. 1. Amplification of two types of standard curves in the qPCR for *Am. languida* (strain 2A11). The amplification plot and the corresponding standard curve of serial dilutions of rDNA copies produced via PCR amplification of the target region (A, B) and serial dilutions of extracted DNA from known cell numbers (C, D). Measurements have been performed in triplicates, dots may overlap.

RESULTS

Assay and assay specificity

The primer and probe sequences and the amplicon sizes of the newly developed qPCR assay for the detection of *Amphidoma languida* along with the respective information for other AZA-producing species are presented in Table I.

Specificity of the new qPCR assay was tested with target and non-target DNA of a large collection of microalgal species and strains (Table II). All 12 strains of *Am. languida* from different areas of the North Atlantic were detected as single strains or in mixed samples, where no cross-hybridization with any non-target microalgae (multiple

species and strains of other Amphidomatacea, and a representative set of species of other dinophycean genera), neither with single-testing nor within mixed samples. No inhibition of the assay was observed in any of the reactions.

Quantification of *Am. languida* cells

Two types of standard curves were established for quantification of *Am. languida* cells. The first was based on a 10-fold dilution series of target gene copies and the second based on a 10-fold dilution series of DNA extracts of *Am. languida*. The standard curve of target gene copies yielded C_T values between 11.5 ± 0.05 (10^8

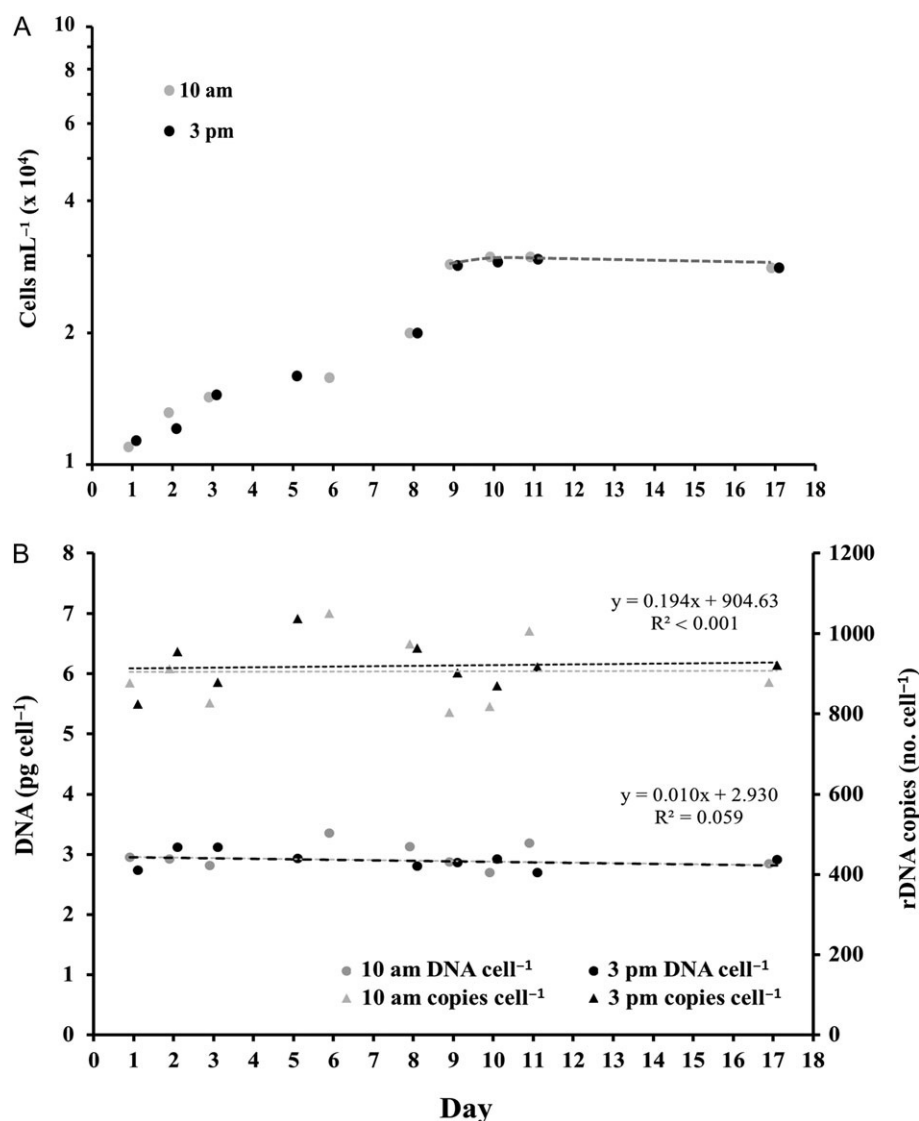


Fig. 2. Culture observation of *Am. languida* over 17 days. Cell density (A), as well as variations in rDNA copy number (triangles) and DNA content (circles) cell⁻¹ (B) over 17 days.

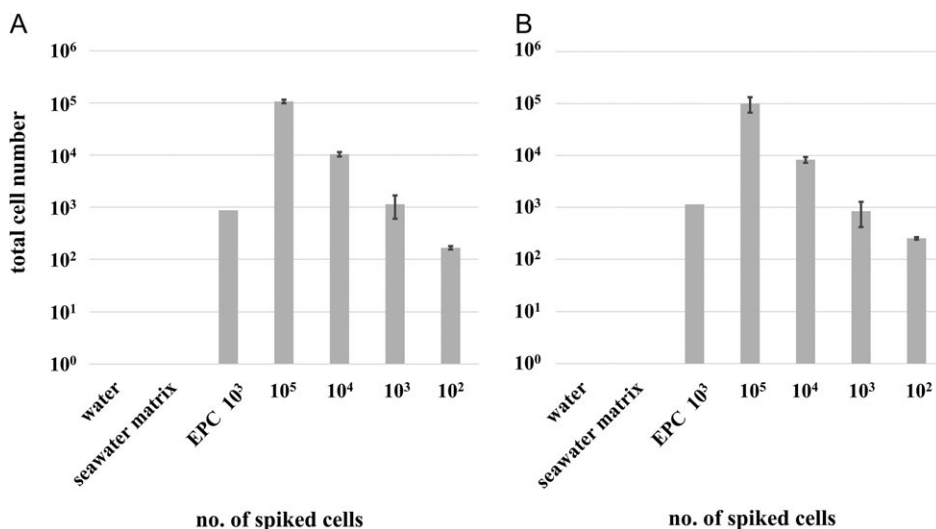


Fig. 3. Cell recovery from C_T values of known cell numbers in qPCR for two independent experiments (**A** and **B**). Spiked samples were prepared in 10-fold dilutions. Milli-Q water and the seawater matrix without *Am. languida* were used as negative controls, EPCs with 10^3 cells of *Am. languida* were included to check for variations between different DNA extractions. Bars represent mean \pm 1 SD ($n = 6$).

copies μL^{-1}) and 36.1 ± 0.56 (10^1 copies μL^{-1}), with an amplification efficiency $E = 96.1\%$ (Fig. 1A and B), calculated according to Bustin *et al.* (2009). The DNA standard curve yielded C_T values between 18.7 ± 0.09 ($10 \text{ ng } \mu\text{L}^{-1}$) and 35.9 ± 0.11 ($10^{-4} \text{ ng } \mu\text{L}^{-1}$), with an amplification efficiency $E = 96.1\%$ (Fig. 1C and D).

DNA copy number and DNA content cell⁻¹

The mean copy number of four different *Am. languida* strains ranged from 719 to 830 cell⁻¹ (Table III) and was not significantly different between strains ($F = 0.057$, $P = 0.981$). Likewise, the mean DNA cell quota ranged from 2.73 to 3.15 pg cell⁻¹ (Table III), without significant differences between strains ($F = 1.705$, $P = 0.218$).

Temporal variability in copy number and DNA content

Potential temporal variability of rDNA copy number and DNA cell quota was extensively analyzed for one strain of *Am. languida* (Z-LF-9-C9) over a time period of 17 days. In batch culture mode, cell density increased from 10×10^3 cells mL^{-1} to 30×10^3 cells mL^{-1} after 17 days of observation, with stationary growth reached at approximately day 9 (Fig. 2A). The rDNA copy number ranged from 805 to 1050 copies cell⁻¹ and did not change significantly with time or cell density (t -test, $P = 0.521$). The DNA cell quota ranged from 2.70 to 3.35 pg cell⁻¹ and did not change significantly with time or cell density either (t -test, $P = 0.473$). Likewise, there was no significant

difference between samples taken at 10 am versus samples taken at 3 pm for both, the rDNA copy number (t -test, $P = 0.476$) and DNA cell quota (t -test, $P = 0.549$) (Fig. 2B).

Limit of quantification and limit of detection

The limit of quantification (LOQ) and the limit of detection (LOD) were estimated from analysis of replicate standard curves ($n = 8$) according to Forootan *et al.* (2017). In the present study, the criterion for LOQ that 95% of the measured values have to be within the interval of mean \pm 2 SD was valid for a target concentration of 10 copies μL^{-1} or 0.1 pg target DNA μL^{-1} , respectively. The respective criterion for LOD, i.e. the lowest target concentration for which at least 95% of replicates are positive, was 10 copies μL^{-1} or 0.1 pg target DNA μL^{-1} as well. With the next dilution below these concentrations (1.0 copies or 0.01 pg target DNA μL^{-1}), no consistent amplification between replicates ($\geq 95\%$) was observed.

Seawater matrix effects

Primer and probe quantification performance under environmental conditions was tested by spiking different amounts of *Am. languida* (strain Z-LF-9-C9) into a natural seawater sample, which was additionally enriched with two non-target microalgae. The concentration of non-target DNA in the seawater matrix without spiked *Am. languida* was $234.7 \pm 6.3 \mu\text{g sample}^{-1}$ ($n = 3$) for the first experiment (Fig. 3, A) and $219.7 \pm 8.2 \mu\text{g sample}^{-1}$ ($n = 3$) for

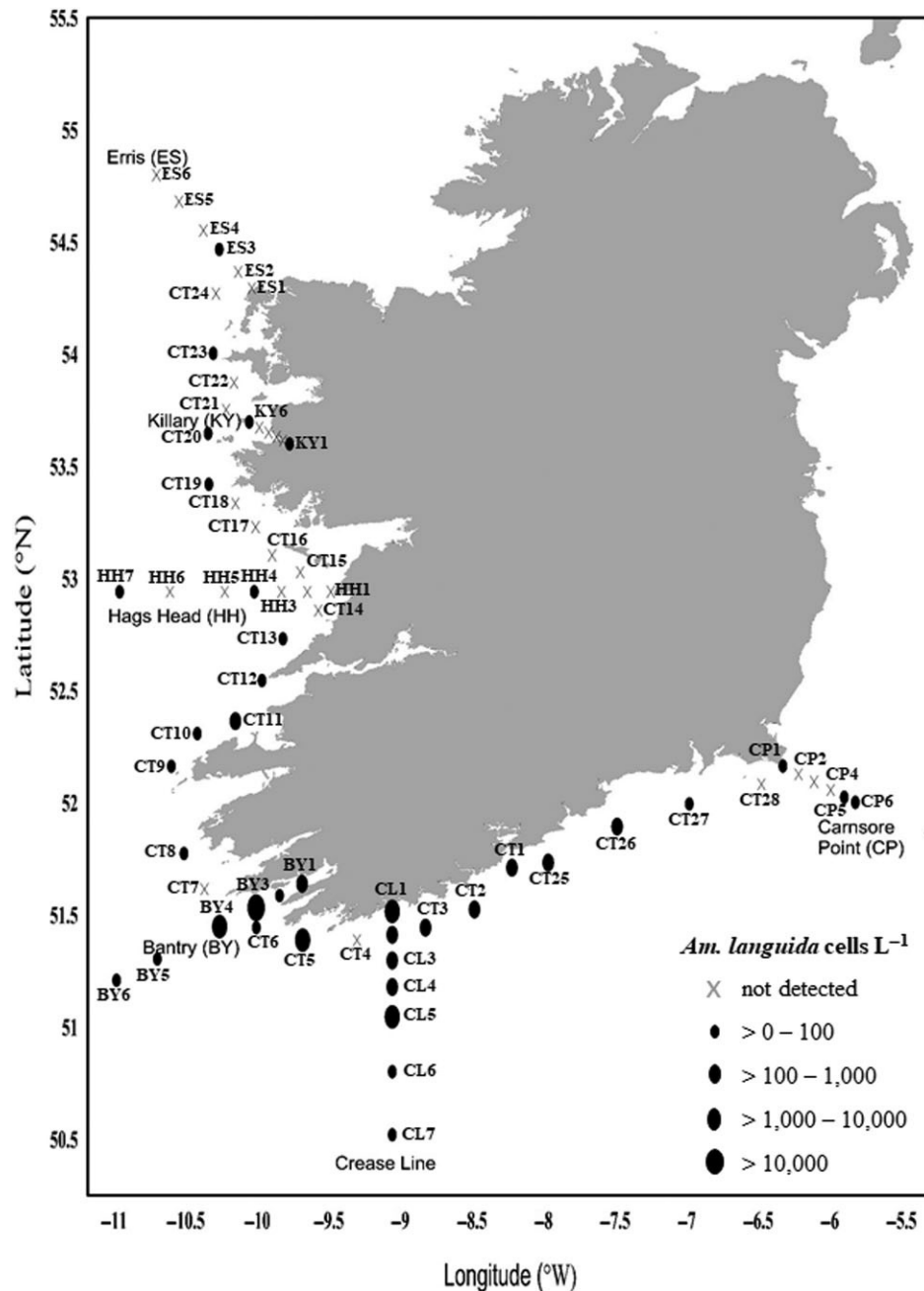


Fig. 4. Sampling locations of the coastal survey (CV17022) in Irish waters in 2017. Stations, where *Am. languida* has been found with the newly developed qPCR assay, are presented as filled circles. Circle size categorizes the amount of cells L⁻¹. Exact qPCR-based cell numbers estimated for each station are given in Table S3.

the second experiment (Fig. 3B). Calculated cell numbers were in good agreement with the actual number of spiked cells. Mean cell recovery rate was $103.0 \pm 9.8\%$ in the first experiment and $95.3 \pm 12.7\%$ in the second experiment with values above 100% mainly occurring at the lowest addition (100 cells).

qPCR application on field samples

On the survey off the Irish coast, *Am. languida* was determined to be present in a number of stations along the south and south-west coast in 2017 (Fig. 4). In particular, *Am. languida* was mainly detected along the southern and south-western sampling locations, with cell concentrations

generally in the range of 5–1000 cells L⁻¹ (Table S3). Higher numbers were exclusively recorded from some stations in the south-east with highest cell concentrations of 8 720 cells L⁻¹ (station BY4) and 22 720 cells L⁻¹ (station BY3). In contrast, in the North-West the target species was detected only in some isolated spots, with cell concentrations not exceeding 20 cells L⁻¹.

DISCUSSION

In this study, a specific and sensitive qPCR assay for the detection and quantification of the AZA-producing species *Amphidoma languida* in field samples is presented.

In general, the quantitative PCR is a highly sensitive tool (Tahir *et al.*, 2017). There are several real-time PCR assay types used in different laboratories and for different research questions. SYBR Green assays contain target-specific primers and an intercalating fluorescent dye, which releases a detectable signal in the qPCR if the primers amplify any DNA amplicon. It is a more economical method compared to the TaqMan chemistry, but also less specific since SYBR Green assays tend to amplify also non-target DNA (Purcell *et al.*, 2011; Mohr *et al.*, 2015). Here, the TaqMan chemistry was chosen, because specific fluorescent probes (additionally to the target-specific primers) enable a highly specific and sensitive amplification of the target molecule. The MGB moiety increases the stability of the probe and raises the melting temperature, which allows the design of shorter, highly specific probes with the same annealing temperature compared to traditional TaqMan probes without the MGB motif (Kutyavin *et al.*, 2000). The new primers and probe for *Am. languida* were designed to amplify a target region on the large subunit (LSU, 28S) of the rDNA. This region worked well previously for the assays on *A. spinosum*, *A. poporum* and *A. obesum* (Toebe *et al.*, 2013). Targeting other regions, e.g. the internal transcribed spacer (ITS) region would be far less suitable, as ITS sequencing for that species revealed surprisingly large intra-genomic variability in this DNA region (Tillmann *et al.*, 2012).

The primers and probe were thoroughly tested for specificity and yielded positive signals only for DNA of the different strains of *Am. languida*. Non-target strains in specificity testing included multiple strains covering almost all species of *Azadinium* and also the only other species of *Amphidoma* where DNA is available, i.e. *Amphidoma parvula* (Tillmann *et al.*, 2018b). Furthermore, for *in silico* probe design, all environmental sequences in GenBank that were identified as *Amphidoma* sp. in the phylogenetic tree presented in Tillmann *et al.* (2018b) were included. In the genus

Amphidoma, there are 11 additional species, where DNA sequences are not yet available, and the probes presented here need to be continuously tested for cross-reactivity once new sequence data of other *Amphidoma* species become available. In addition, for species of *Azadinium*, such as *A. poporum*, *A. dalianense* and *A. spinosum*, recently established new strains revealed considerable intraspecific sequence variability and the presence of different ribotypes (Luo *et al.*, 2017; Tillmann *et al.*, 2018a). The same might be expected for *Am. languida*, so the availability of new strains will again require updates of specificity testing.

With a reliable and reproducible detection and quantification of down to 10 target gene copies (corresponding to ca. 0.05 cells) per reaction, the qPCR assay is highly sensitive. The corresponding final cell detection limit for field samples, of course, depends on a number of adjustable factors. With the precondition of our assay specifications (100 µL DNA extraction volume, 1 µL of extract within a 10 µL assay volume and filtering e.g. 1 L seawater), the limit of quantification would be 2 cells L⁻¹.

Early warning threshold values for *Amphidoma languida* or any other AZA-producing species are not yet defined due to a lack of knowledge and data. Anyhow, given the small cell size and the limited amount of AZA cell⁻¹, cell concentrations critical for AZP are expected to be orders of magnitude higher, i.e. in the range of at least hundreds of cells L⁻¹. Thus, the assay sensitivity is suitable for monitoring purposes and well suited in ecological studies aiming the detection of even low background concentrations. The challenges and problems of reliable quantification of microbial species using the qPCR are addressed in a number of studies (Galluzzi *et al.*, 2004; Godhe *et al.*, 2008; Erdner *et al.*, 2010). Three different issues for quantification are highlighted: (i) DNA extraction performance, (ii) variability in rDNA copy numbers and (iii) assay inhibition effects.

DNA extraction performance

There are several commercial kits on the market for DNA extraction from phytoplankton. DNA extraction performance is especially essential for quantification studies due to the very high impact of uncertainties, and there are ongoing discussions about this topic in the qPCR community (Yuan *et al.*, 2015; Brauge *et al.*, 2018). In the present study, the NucleoSpin Soil DNA isolation kit was used for DNA extraction and purification. Inclusion of EPC of defined *Am. languida* cell numbers for all extraction proceedings revealed a consistent extraction performance of this kit.

rDNA copy number

The qPCR method quantifies the number of target gene copies and therefore, any intraspecific variability and variation in copy number cell⁻¹ is an outstanding factor to consider for qPCR-based quantification and makes enumeration more challenging (Créach *et al.*, 2006; Garneau *et al.*, 2011; Penna and Galluzzi, 2013; Wang *et al.*, 2017). Any mismatch in cell copy number between a field population and the strain used to prepare the qPCR standard curve will bias quantification. For some microalgal species and especially for dinoflagellates, which are known to increase their genome by incorporating copies of several DNA regions (Bachvaroff and Place, 2008), large variability in copy number has been reported for different strains, for different growth stages and culturing conditions (Godhe *et al.*, 2008; Galluzzi *et al.*, 2009).

However, for *Am. languida* the data presented here reveal the same copy number for four different *Am. languida* strains from different geographic origins. Moreover, one representative strain (Z-LF-9-C9) showed no major variability in target gene copy number over time within a batch culture growth cycle.

Inhibition

qPCR amplification of target molecules can be inhibited by several substances common in field samples, such as humic acids, polysaccharides, haem, proteins, polyphenols and others (Gallup, 2011), and it always has to be kept in mind that inhibitors within a field sample set may vary between sites. Inhibitory substances are reduced by washing buffers and spin columns of commercial DNA extraction kits to some extent (Fock-Chow-Tho *et al.*, 2017), but potential matrix effects in field samples are considered by quantifying seawater samples spiked with known amounts of target cells. With two independent experiments using natural seawater (even further enriched with non-target cells), it is shown here, that the qPCR recovers spiked *Am. languida* cells at almost 100% efficiency over a concentration range of four orders of magnitude.

Finally, to investigate the applicability of the assay for field samples, the assay was applied to a field data set of Irish coastal waters and yielded the first abundance data for this species. The assay confirmed the presence of *Am. languida* for the area and revealed the species to be widely distributed along the southern and western Irish coast. qPCR quantification further indicates higher abundance for the south-western part with peak densities off Bantry Bay, the location where the type strain of *Am. languida* was isolated (Tillmann *et al.*, 2012). Peak

densities >22 000 cells L⁻¹ indicate that *Am. languida* might substantially contribute to AZA contamination in Irish mussels and underline the need to include AZA produced by this species in routine seafood monitoring of AZA toxins.

CONCLUSION

Due to its high specificity and sensitivity, the quantitative real-time PCR is a very efficient and rapid tool for the detection and quantification of microorganisms. In this study, a newly developed TaqMan qPCR assay for the detection and enumeration of the AZA-producing marine dinoflagellate *Amphidoma languida* is presented. The high specificity and sensitivity were tested and confirmed, therefore the assay is well suited in monitoring programs. Moreover, it can be a supportive tool for detailed studies on biogeography and spatial and temporal distribution of this AZA-producing species. In the future, the new primers and probe may be integrated with other *Azadinium*-specific probes in a multiplex assay, allowing a simultaneous and thus time- and cost-effective detection and quantification of all known North-Atlantic AZA-producers, *Azadinium spinosum*, *A. poporum* and *Am. languida*.

SUPPLEMENTARY DATA

Supplementary data can be found online at *Journal of Plankton Research* online.

ACKNOWLEDGMENTS

The authors would like to thank Rafael Salas for providing *Am. languida* strain SM1 and David Jaen for providing strain AND-A0920. We thank the technical and scientific crew aboard the RV Celtic Voyager for collecting the field samples during the survey CV17022 in August 2018 and Stephen McGirr for extracting the DNA of the field samples. Furthermore, many thanks go to Katja Metfies for general advices and Uwe John for providing advice concerning the assay design.

FUNDING

This work was supported by funding of the German Ministry for Education and Research (project RIPAZA, 03F0763A) and by the PACES research program of the Alfred-Wegener-Institute as part of the Helmholtz Foundation initiative in Earth and Environment.

REFERENCES

- Bachvaroff, T. R. and Place, A. R. (2008) From stop to start: Tandem gene arrangement, copy number and trans-splicing sites in the dinoflagellate *Amphidinium carterae*. *PLOS ONE*, **3**, e2929.
- Botana, L. M. (2014) *Seafood and Freshwater Toxins: Pharmacology, Physiology, and Detection*, Vol. 3. CRC Press, Boca Raton, USA.
- Brauge, T., Faille, C., Inglebert, G., Dubois, T., Morieux, P., Slomianny, C. and Midelet-Bourdin, G. (2018) Comparative evaluation of DNA extraction methods for amplification by qPCR of superficial vs intracellular DNA from *Bacillus* spores. *Int. J. Food Microbiol.*, **266**, 289–294.
- Bustin, S. A., Benes, V., Garson, J. A., Hellemans, J., Huggett, J., Kubista, M., Mueller, R., Nolan, T. *et al.* (2009) The MIQE guidelines: minimum information for publication of quantitative real-time PCR experiments. *Clin. Chem.*, **55**, 611–622.
- Créach, V., Ernst, A., Sabbe, K., Vanellander, B., Vyverman, W. and Stal Lucas, J. (2006) Using quantitative PCR to determine the distribution of a semicryptic benthic diatom, *Navicula phyllepta* (Bacillariophyceae). *J. Phycol.*, **42**, 1142–1154.
- Erdner, D. L., Percy, L., Keafer, B., Lewis, J. and Anderson, D. M. (2010) A quantitative real-time PCR assay for the identification and enumeration of *Alexandrium* cysts in marine sediments. *Deep Sea Res. II*, **57**, 279–287.
- Fock-Chow-Tho, D., Topp, E., Ibeagha-Awemu, E. A. and Bissonnette, N. (2017) Comparison of commercial DNA extraction kits and quantitative PCR systems for better sensitivity in detecting the causative agent of paratuberculosis in dairy cow fecal samples. *J. Dairy Sci.*, **100**, 572–581.
- Forootan, A., Sjöback, R., Björkman, J., Sjögreen, B., Linz, L. and Kubista, M. (2017) Methods to determine limit of detection and limit of quantification in quantitative real-time PCR (qPCR). *Biomol. Detect. Quantif.*, **12**, 1–6.
- Gallup, J. M. (2011) qPCR inhibition and amplification of difficult templates. In Kennedy, S. and Oswald, N. (eds), *PCR Troubleshooting and Optimization: The Essential Guide*. Caister Academic Press, Norfolk, UK, pp. 23–65.
- Galluzzi, L., Bertozzini, E., Penna, A., Perini, F., Garcés, E. and Magnani, M. (2009) Analysis of rRNA gene content in the Mediterranean dinoflagellate *Alexandrium catenella* and *Alexandrium taylori*: implications for the quantitative real-time PCR-based monitoring methods. *J. Appl. Phycol.*, **22**, 1–9.
- Galluzzi, L., Penna, A., Bertozzini, E., Vila, M., Garcés, E. and Magnani, M. (2004) Development of a real-time PCR assay for rapid detection and quantification of *Alexandrium minutum* (a Dinoflagellate). *Appl. Environ. Microbiol.*, **70**, 1199–1206.
- Gameau, M. E., Schmetzer, A., Countway, P. D., Jones, A. C., Seubert, E. L. and Caron, D. A. (2011) Examination of the seasonal dynamics of the toxic dinoflagellate *Alexandrium catenella* at Redondo Beach, California, by quantitative PCR. *Appl. Environ. Microbiol.*, **77**, 7669–7680.
- Godhe, A., Asplund, M. E., Harnstrom, K., Saravanan, V., Tyagi, A. and Karunasagar, I. (2008) Quantification of diatom and dinoflagellate biomasses in coastal marine seawater samples by real-time PCR. *Appl. Environ. Microbiol.*, **74**, 7174–7182.
- Keller, M. D., Selvin, R. C., Claus, W. and Guillard, R. R. L. (1987) Media for the culture of oceanic ultraphytoplankton. *J. Phycol.*, **23**, 633–638.
- Kim, J. H., Tillmann, U., Adams, N. G., Krock, B., Stutts, W. L., Deeds, J. R., Han, M. S. and Trainer, V. L. (2017) Identification of *Azadinium* species and a new azaspiracid from *Azadinium poporum* in Puget Sound, Washington State, USA. *Harmful Algae*, **68**, 152–167.
- Krock, B., Tillmann, U., Voss, D., Koch, B. P., Salas, R., Witt, M., Potvin, E. and Jeong, H. J. (2012) New azaspiracids in Amphidomataceae (Dinophyceae). *Toxicon*, **60**, 830–839.
- Kumar, S., Stecher, G. and Tamura, K. (2016) MEGA7: molecular evolutionary genetics analysis version 7.0. *Mol. Biol. Evol.*, **33**, 1870–1874.
- Kutyavin, I. V., Afonina, I. A., Mills, A., Gorn, V. V., Lukhtanov, E. A., Belousov, E. S., Singer, M. J., Wallburger, D. K. *et al.* (2000) 3'-minor groove binder-DNA probes increase sequence specificity at PCR extension temperatures. *Nucleic Acids Res.*, **28**, 655–661.
- Livak, K. (1997) ABI Prism 7700 sequence detection system. *User Bull.*, **2**, 1–36.
- Luo, Z. H., Krock, B., Mertens, K. N., Nezan, E., Chomerat, N., Billen, G., Tillmann, U. and Gu, H. (2017) Adding new pieces to the *Azadinium* (Dinophyceae) diversity and biogeography puzzle: Non-toxicogenic *Azadinium zhuanum* sp nov from China, toxicogenic *A. poporum* from the Mediterranean, and a non-toxicogenic *A. dalianense* from the French Atlantic. *Harmful Algae*, **66**, 65–78.
- Mohr, P. G., Moody, N. J. G., Williams, L. M., Hoad, J., Cummins, D. M., Davies, K. R. and Crane, M. (2015) Molecular confirmation of infectious spleen and kidney necrosis virus (ISKNV) in farmed and imported ornamental fish in Australia. *Dis. Aquat. Org.*, **116**, 103–110.
- Penna, A. and Galluzzi, L. (2013) The quantitative real-time PCR applications in the monitoring of marine harmful algal bloom (HAB) species. *Environ. Sci. Pollut. Res.*, **20**, 6851–6862.
- Perini, F., Casabianca, A., Battocchi, C., Accoroni, S., Totti, C. and Penna, A. (2011) New approach using the real-time PCR method for estimation of the toxic marine dinoflagellate *Ostreopsis cf. ovata* in marine environment. *PLoS One*, **6**, e17699.
- Purcell, M. K., Getchell, R. G., McClure, C. A. and Garver, K. A. (2011) Quantitative polymerase chain reaction (PCR) for detection of aquatic animal pathogens in a diagnostic laboratory setting. *J. Aquat. Anim. Health*, **23**, 148–161.
- Rossi, R., Dell'aversano, C., Krock, B., Ciminiello, P., Percopo, L., Tillmann, U., Soprano, V. and Zingone, A. (2017) Mediterranean *Azadinium dexteroporum* (Dinophyceae) produces six novel azaspiracids and azaspiracid-35: a structural study by a multi-platform mass spectrometry approach. *Anal. Bioanal. Chem.*, **409**, 1121–1134.
- Ruijter, J. M., Ramakers, C., Hoogaars, W. M. H., Karlen, Y., Bakker, O., Van Den Hoff, M. J. B. and Moorman, A. F. M. (2009) Amplification efficiency: linking baseline and bias in the analysis of quantitative PCR data. *Nucleic Acids Res.*, **37**, e45.
- Salas, R., Tillmann, U., John, U., Kilcoyne, J., Burson, A., Cantwell, C., Hess, P., Jauffrais, T. *et al.* (2011) The role of *Azadinium spinosum* (Dinophyceae) in the production of azaspiracid shellfish poisoning in mussels. *Harmful Algae*, **10**, 774–783.
- Satake, M., Ofuji, K., Naoki, H., James, K. J., Furey, A., McMahon, T., Silke, J. and Yasumoto, T. (1998) Azaspiracid, a new marine toxin having unique spiro ring assemblies, isolated from Irish mussels, *Mytilus edulis*. *J. Am. Chem. Soc.*, **120**, 9967–9968.
- Scholin, C. A., Herzog, M., Sogin, M. and Anderson, D. M. (1994) Identification of group- and strain-specific genetic markers for globally distributed *Alexandrium* (Dinophyceae). 2. Sequence analysis of a fragment of the LSU rRNA gene. *J. Phycol.*, **30**, 999–1011.
- Smith, K. F., Rhodes, L., Harwood, D. T., Adamson, J., Moisan, C., Munday, R. and Tillmann, U. (2016) Detection of *Azadinium poporum*

- in New Zealand: the use of molecular tools to assist with species isolations. *J. Appl. Phycol.*, **28**, 1125–1132.
- Tahir, D., Bittar, F., Barré-Cardi, H., Sow, D., Dahmani, M., Mediannikov, O., Raoult, D., Davoust, B. *et al.* (2017) Molecular survey of *Dirofilaria immitis* and *Dirofilaria repens* by new real-time TaqMan® PCR assay in dogs and mosquitoes (Diptera: Culicidae) in Corsica (France). *Vet. Parasitol.*, **235**, 1–7.
- Tillmann, U. (2018) Amphidomataceae. In Shumway, S. E., Burkholder, J. A. and Morton, S. L. (eds), *Harmful Algae Blooms, A Compendium Desk Reference*. Wiley, Hoboken, pp. 575–582.
- Tillmann, U. and Akselman, R. (2016) Revisiting the 1991 algal bloom in shelf waters off Argentina: *Azadinium luciferelloides* sp. nov. (Amphidomataceae, Dinophyceae) as the causative species in a diverse community of other amphidomataceans. *Phycol. Res.*, **64**, 160–175.
- Tillmann, U., Edvardsen, B., Krock, B., Smith, K. F., Paterson, R. F. and Voss, D. (2018a) Diversity, distribution, and azaspiracids of Amphidomataceae (Dinophyceae) along the Norwegian coast. *Harmful Algae*, **80**, 15–34.
- Tillmann, U., Elbrächter, M., John, U., Krock, B. and Cembella, A. (2010) *Azadinium obesum* (Dinophyceae), a new nontoxic species in the genus that can produce azaspiracid toxins. *Phycologia*, **49**, 169–182.
- Tillmann, U., Elbrächter, M., Krock, B., John, U. and Cembella, A. (2009) *Azadinium spinosum* gen. et sp. nov. (Dinophyceae) identified as a primary producer of azaspiracid toxins. *Eur. J. Phycol.*, **44**, 63–79.
- Tillmann, U., Gottschling, M., Guinder, V. and Krock, B. (2018b) *Amphidoma parvula* (Amphidomataceae), a new planktonic dinophyte from the Argentine Sea. *Eur. J. Phycol.*, **53**, 14–28.
- Tillmann, U., Gottschling, M., Nezan, E., Krock, B. and Bilien, G. (2014) Morphological and molecular characterization of three new *Azadinium* species (Amphidomataceae, dinophyceae) from the Irminger sea. *Protist*, **165**, 417–444.
- Tillmann, U., Gottschling, M., Nézan, E. and Krock, B. (2015) First records of *Amphidoma languida* and *Azadinium dextroponum* (Amphidomataceae, Dinophyceae) from the Irminger Sea off Iceland. *Mar. Biodivers. Rec.*, **8**, 1–11.
- Tillmann, U., Jaen, D., Fernandez, L., Gottschling, M., Witt, M., Blanco, J. and Krock, B. (2017) *Amphidoma languida* (Amphidomataceae, Dinophyceae) with a novel azaspiracid toxin profile identified as the cause of molluscan contamination at the Atlantic coast of southern Spain. *Harmful Algae*, **62**, 113–126.
- Tillmann, U., Salas, R., Gottschling, M., Krock, B., O'driscoll, D. and Elbrächter, M. (2012) *Amphidoma languida* sp. nov. (Dinophyceae) reveals a close relationship between *Amphidoma* and *Azadinium*. *Protist*, **163**, 701–719.
- Toebe, K., Joshi, A. R., Messtorff, P., Tillmann, U., Cembella, A. and John, U. (2013) Molecular discrimination of taxa within the dinoflagellate genus *Azadinium*, the source of azaspiracid toxins. *J. Plankton Res.*, **35**, 225–230.
- Twiner, M., Hess, P. and Doucette, G. J. (2014) Azaspiracids: toxicology, pharmacology, and risk assessment. In Botana, L. M. (ed.), *Seafood and Freshwater Toxins. Pharmacology, Physiology and Detection*, 3rd edn. CRC Press, Boca Raton, FL, pp. 823–855.
- Wang, C., Zhang, T., Wang, Y., Katz, L. A., Gao, F. and Song, W. (2017) Disentangling sources of variation in SSU rDNA sequences from single cell analyses of ciliates: impact of copy number variation and experimental error. *Proc. R. Soc. B*, **284**, 20170425.
- Yuan, J., Li, M. and Lin, S. (2015) An improved DNA extraction method for efficient and quantitative recovery of phytoplankton diversity in natural assemblages. *PLoS One*, **10**, e0133060.

Publication II: Toxigenic Amphidomataceae in Danish coastal waters

Occurrence and distribution of Amphidomataceae (Dinophyceae) in Danish coastal waters of the North Sea, the Limfjord and the Kattegat/Belt area.

Harmful Algae

Wietkamp, S., Krock, B., Gu, H., Voß, D., Klemm, K., Tillmann, U. (2019)

Publication II deals with the occurrence of amphidomatacean species along the Danish coastline based on field samples from a survey in 2016, with emphasis on the three toxigenic amphidomatacean species *Azadinium spinosum*, *Az. poporum* and *Am. languida*.

The aims of this survey were 1) to investigate the distribution of Amphidomataceae along a salinity gradient, from high saline waters in the eastern North Sea/German Bight towards low salinities in the Danish Limfjord and Kattegat/Baltic Sea. 2) to use and evaluate the molecular qPCR method for the first time in addition to microscopy and toxin analyzes, to detect and quantify all three known AZA-producers from the North Atlantic in the field.

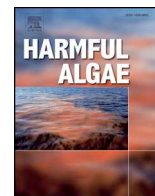
The candidate conducted Sanger Sequencing (50%) and qPCR analysis of the DNA field samples, which were taken in 2016 before the start of the PhD project. Analyses included DNA sequence analysis, molecular pre-screening on Amphidomataceae in the field samples by the family specific SYBR Green qPCR assay, application of the three species-specific qPCR assays on *Azadinium spinosum*, *Az. poporum* and *Am. languida*, post-run quantitative analysis and graphical presentation (100%). Graphical presentation of environmental/CTD data were carried out in collaboration (50%) with D. Voss (ICBM). Contributions by others were on-board microscopy, strain establishment and characterization (Dr. U. Tillmann, AWI), AZA analysis (Dr. B. Krock and T. Krohn, AWI), sampling and general help (A. Müller, AWI; R. Henkel, K. Schwalfenberg and A. Friedrichs, ICBM). Manuscript composition was done by the candidate (70%) in close cooperation with the corresponding author Dr. U. Tillmann and contributions from other co-authors.



ELSEVIER

Contents lists available at ScienceDirect

Harmful Algae

journal homepage: www.elsevier.com/locate/hal

Occurrence and distribution of Amphidomataceae (Dinophyceae) in Danish coastal waters of the North Sea, the Limfjord and the Kattegat/Belt area

Stephan Wietkamp^a, Bernd Krock^a, Haifeng Gu^b, Daniela Voß^c, Kerstin Klemm^a, Urban Tillmann^{a,*}

^a Alfred-Wegener-Institute, Helmholtz Centre for Polar and Marine Research, Am Handelshafen 12, D-27570 Bremerhaven, Germany

^b Third Institute of Oceanography, Ministry of Natural Resources, Xiamen 361005, China

^c Institute for Chemistry and Biology of the Marine Environment (ICBM), Carl von Ossietzky Universität Oldenburg, Schleusenstraße 1, D-26382 Wilhelmshaven, Germany

ARTICLE INFO

Keywords:

Azadinium
Amphidoma
 Azaspiracids
 Denmark
 Limfjord
 Quantitative PCR

ABSTRACT

Some species of the dinophytes *Azadinium* and *Amphidoma* (Amphidomataceae) produce azaspiracids (AZA), lipophilic polyether compounds responsible for Azaspiracid Shellfish Poisoning (AZP) in humans after consumption of contaminated seafood. Toxigenic Amphidomataceae are known to occur in the North Atlantic and the North Sea area, but little is known about their importance in Danish coastal waters. In 2016, 44 Stations were sampled on a survey along the Danish coastline, covering the German Bight, Limfjord, the Kattegat area, Great Belt and Kiel Bight. Samples were analysed by live microscopy, liquid chromatography-tandem mass spectrometry (LC-MS/MS) and quantitative polymerase-chain-reaction (qPCR) on the presence of Amphidomataceae and AZA. Amphidomataceae were widely distributed in the area, but were below detection limit on most of the inner Limfjord stations. Cell abundances of the three toxigenic species, determined with species-specific qPCR assays on *Azadinium spinosum*, *Az. poporum* and *Amphidoma languida*, were generally low and restricted to the North Sea and the northern Kattegat, which was in agreement with the distribution of the generally low AZA abundances in plankton samples. Among the toxigenic species, *Amphidoma languida* was dominant with highest cell densities up to 3×10^3 cells L⁻¹ on North Sea stations and at the western entrance of the Limfjord. Azaspiracids detected in plankton samples include low levels of AZA-1 at one station of the North Sea, and higher levels of AZA-38 and -39 (up to 1.5 ng L⁻¹) in the North Sea and the Limfjord entrance. Furthermore, one new AZA (named AZA-63) was discovered in plankton of two North Sea stations. Morphological, molecular, and toxinological characterisation of 26 newly established strains from the area confirmed the presence of four amphidomatacean species (*Az. obesum*, *Az. dalianense*, *Az. poporum* and *Am. languida*). The single new strain of *Az. poporum* turned out as a member of Ribotype A2, which was previously only known from the Mediterranean. Consistent with some of these Mediterranean A2 strains, but different to the previously established AZA-37 producing *Az. poporum* Ribotype A1 strains from Denmark, the new strain did not contain any AZA. Azaspiracids were also absent in all *Az. obesum* and *Az. dalianense* strains, but AZA-38 and -39 were found in all *Am. languida* strains with total AZA cell quotas ranging from 0.08 up to 94 fg cell⁻¹. In conclusion, AZA-producing microalgae and their respective toxins were low in abundance but widely present in the area, and thus might be considered in local monitoring programs to preserve seafood safety in Danish coastal waters.

1. Introduction

Denmark is almost entirely bordered by the Sea, from the North Sea in the west, Skagerrak in the north, and by the Kattegat and the Belt area to the Baltic Sea on the east side. With a long coastline and many fjords and islands, fishing industry and aquaculture play an important role in the Danish economy. One major natural threat to aquaculture and shellfish industries, however, are harmful microalgal blooms and

the respective biotoxins, which can cause large fish kills or potential health problems in human seafood consumers. Most threatening for Danish waters currently are fish killing species of *Pseudochoctonella*, which since about 20 years has become well established in Scandinavian waters and form recurrent massive blooms in the North Sea and Skagerrak (Jakobsen et al., 2012). Another fish killing algae of concern is *Pseudopfiesteria*, which caused serious fish kills in land-based fish farms in northern Jutland, Denmark (Moestrup et al., 2014).

* Corresponding author.

E-mail address: urban.tillmann@awi.de (U. Tillmann).

<https://doi.org/10.1016/j.hal.2019.101637>

Received 13 March 2019; Received in revised form 12 June 2019; Accepted 25 June 2019

Available online 26 July 2019

1568-9883/ © 2019 Elsevier B.V. All rights reserved.

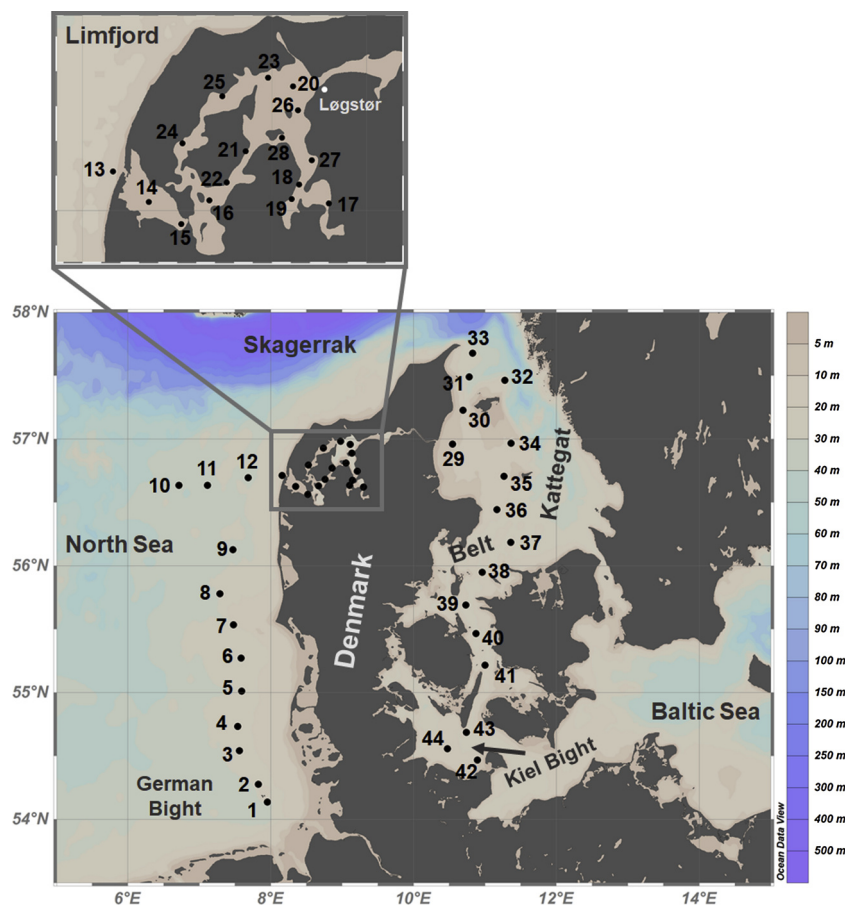


Fig. 1. Location of sampling stations during the UTH-16 expedition.

Microalgal toxins accumulating in shellfish are of concern as well. The Danish shellfish industry is continuously growing and of increasing importance, especially since shellfish farming has been suggested as an effective counteract to reduce particle and nutrient loads of large scale offshore fish farming in Danish coastal waters (Maar et al., 2018). Currently, the most problematic microalgal toxins for the Danish shellfish industry are okadaic acid and related compounds produced by *Dinophysis* spp. (Jørgensen and Andersen, 2007). In 1990, there was a major European incident of diarrhetic shellfish poisoning (DSP) caused by Danish blue mussels harvested in Limfjord, which is the main Danish production area of shellfish. Another long-lasting closure of shellfish harvest due to elevated concentrations of DSP toxins also occurred in 2006 (Jørgensen and Andersen, 2007).

A more recently discovered group of shellfish-contaminating phycotoxins are azaspiracids (AZA), which can lead to Azaspiracid Shellfish Poisoning (AZP) in humans after consumption of contaminated mussels (Twiner et al., 2014). Elevated levels of AZA in shellfish led recurrently to closures of shellfish harvests in Ireland (Salas et al., 2011), and AZA levels above the EU regulatory limit were observed recently in shellfish species harvested at the Spanish Atlantic coast (Tillmann et al., 2017a). Azaspiracids are known to be produced by four (out of ca. 20) dinophyte species of Amphidomataceae, i.e. by *Azadinium spinosum*, *Az. poporum*, *Az. dexteroporum* and *Amphidoma languida* (Krock et al., 2012; Percopo et al., 2013; Tillmann et al., 2009, 2017a). Among those, toxigenic *Az. dexteroporum* is up to now only recorded from the Mediterranean, whereas *Az. poporum*, *Az. spinosum* and *Am. languida* are widely distributed in the North Sea and North Atlantic (Tillmann, 2018; Tillmann et al., 2018).

To date, azaspiracids are known from various European coastal areas, including Irish, Dutch, French, Swedish, Spanish, English and Norwegian coasts (Amzil et al., 2008; Braña Magdalena et al., 2003;

James et al., 2002; Mc Mahon and Silke, 1996; Vale et al., 2008). In Denmark, AZA have been reported in shellfish (Furey et al., 2010) and in plankton (Krock et al., 2009, 2013). Moreover, microscopy and strain establishment revealed the occurrence of toxigenic *Az. spinosum* and *Az. poporum* and their toxic metabolites on the Danish North Sea coastal area (Krock et al., 2013). In fact, *Az. poporum* was originally described from a strain collected in the southern North Sea off the Danish coast (Tillmann et al., 2011). Nevertheless, still little is known about the diversity, distribution, and abundance of Amphidomataceae in the area, and especially about the potential importance of Amphidomataceae in inner waters such as the Limfjord, as well as for low salinity areas on the Danish east coast.

Toxigenic and non-toxic amphidomatacean species are very similar in size and shape, and it is hardly possible to identify and differentiate them by light microscopy. In recent years, molecular tools have contributed significantly to the knowledge about the biogeographical distribution and abundance of various toxic algae (Eckford-Soper and Daugbjerg, 2015; Edvardsen et al., 2013; Penna and Galluzzi, 2013), and molecular assays are also available for Amphidomataceae. In 2013, Toebe et al. (2013) designed a qPCR assay with species-specific primers and probes for the molecular detection of *Az. spinosum* and *Az. poporum*, and recently, Wietkamp et al. (2019) published an assay for the third known AZA producer in the North Sea, *Am. languida*.

To increase the knowledge about the biogeography of Amphidomataceae and in particular about the azaspiracid-producing species in the south-eastern part of the North Sea, an expedition on board the RV Uthörn took place in 2016. One aim of this survey was to investigate diversity, distribution and abundance of Amphidomataceae in Danish coastal waters along the salinity gradient, from high saline waters of the North Sea, through the semi-enclosed Danish Limfjord and the low-saline Kattegat/Belt area down to Kiel Bight/Baltic Sea. In this

study, the molecular qPCR method was used together with field sample AZA analysis and microscopy/strain establishment to specifically detect and quantify the known North Atlantic AZA-producers, *Az. spinosum*, *Az. poporum* and *Am. languida*.

2. Material & methods

2.1. Field campaign

2.1.1. Sampling

Samples were taken along the Danish coast during the survey on *RV Uthörn* (UTH-16) in 2016 from June, 13th till June, 28th. In total, 44 stations were sampled, starting in the German Bight (Fig. 1). Between June, 19th and June, 23rd, several subareas of the Limfjord were sampled in daily excursions from Løgstør. The expedition continued from Løgstør to Kattegat, Great Belt, down to Kiel Bight. At each station, CTD profiles were conducted using a Seabird 'sbe19plus V2' CTD (Sea-Bird Electronics Inc., Seattle, USA) with an attached sampling rosette (6 × 4 L Niskin bottles). The CTD was equipped with an additional fluorescence sensor (SCUFA Fluorometer, Turner Designs, San Jose, USA). Data acquisition was carried out via CTD-client onboard (Seasave V 7.22.2, Sea-Bird Scientific, Bellevue, USA). Post-processing was done with SBE data processing 7.22.5. Temperature was corrected to ITS-90 (Preston-Thomas, 1990). CTD data are available at Pangaea database (Krock et al., 2017). A composite water sample was prepared from two depths (3, 10 m) taken from the Niskin bottles. 5 L of each depth was pre-screened through a 20 µm mesh-size Nitex sieve and pooled.

2.1.2. Live plankton observations of field samples

At selected stations, one liter of the pooled water sample was gently concentrated by gravity filtration using a 3 µm Whatman Nuclepore polycarbonate filter (Ø = 47 mm, GE Healthcare, Little Chalfont, UK). The concentrate was examined using an inverted microscope (Axiovert 200 M, Zeiss, Göttingen, Germany). Samples were screened for cells of *Azadinium* and/or *Amphidoma* at high magnification (640×) based on general cell size and shape, on the presence of a theca, and on the presence of a distinctly pointed apex. Cells of interest were photographed with a digital camera (Axiocam MRc5, Zeiss).

On stations, where cells of Amphidomataceae were detected during live sample observations, cells were subsequently isolated by micro-capillary into wells of 96-well plates filled with 0.2 mL filtered seawater. By the transfer technique, the inclusion of non-target cells was unavoidable. Therefore, the amphidomatacean cells were re-isolated a few times using a stereomicroscope (SZH-ILLD, Olympus, Hamburg, Germany) equipped with dark field illumination into new wells of a 96-well plate. Plates were incubated at 15 °C under a photon flux density of approx. 50 µmol m⁻² s⁻¹ on a 16:8 h light:dark photoperiod in a controlled environment growth chamber (Model MIR 252, Sanyo Electric Biomedical Co., Osaka, Japan).

2.1.3. Azaspiracid analysis of field samples

An amount of 1.5–4 L (depending on particle content) of the pooled and pre-screened water sample was filtered under gentle vacuum (< 200 mbar) through 5 µm pore-size polycarbonate filters (Merck KGaA, Darmstadt, Germany). The filter was placed with its back to the inner wall of a 50 mL centrifuge tube (Sarstedt, Nümbrecht, Germany) and was repeatedly rinsed with 500–1,000 µL methanol until complete decolouration of the filter. The methanolic extract was transferred to a 0.45 µm pore-size spin-filter (Millipore Ultrafree, Eschborn, Germany) and centrifuged for 30 s at 800×g (5415R, Eppendorf, Hamburg, Germany), followed by transfer to an auto-sampler vial and kept at -20 °C until analysis. Mass spectral experiments were performed to survey for a wide array of AZA with an analytical system consisting of a API 4000 Q-Trap, triple quadrupole mass spectrometer (Sciex, Darmstadt, Germany) equipped with a TurboSpray interface coupled to

an Agilent model 1100 LC (Agilent, Waldbronn, Germany). The LC equipment included a solvent reservoir, in-line degasser (G1379A), binary pump (G1311A), refrigerated autosampler (G1329A/G1330B), and temperature-controlled column oven (G1316A). Separation of AZA (5 µL sample injection volume) was performed by reverse-phase chromatography on a C8 phase. The analytical column (50 × 2 mm) was packed with 3 µm Hypersil BDS 120 Å (Phenomenex, Aschaffenburg, Germany) and maintained at 20 °C. The flow rate was 0.2 mL min⁻¹, and gradient elution was performed with two eluents, where eluent A was water and B was acetonitrile/water (95:5 v/v), both containing 2.0 mM ammonium formate and 50 mM formic acid. Initial conditions were 8 min column equilibration with 30% B, followed by a linear gradient to 100% B in 8 min and isocratic elution until 18 min with 100% B then returning to initial conditions until 21 min (total run time: 29 min). Azaspiracid profiles were determined in one period (0–18) min with curtain gas: 10 psi, CAD: medium, ion spray voltage: 5,500 V, temperature: ambient, nebulizer gas: 10 psi, auxiliary gas: off, interface heater: on, declustering potential: 100 V, entrance potential: 10 V, exit potential: 30 V. Single-reaction-monitoring experiments were carried out in positive ion mode by selecting the transitions shown in Supplementary Table S1. A product ion spectrum of the *m/z* value 844 was recorded in the Enhanced Product Ion (EPI) mode in the mass range from *m/z* 150 to 850. Positive ionization and unit resolution mode were used. The following parameters were applied: curtain gas: 10 psi, CAD: medium, ion spray voltage: 5,500 V, temperature: ambient, nebulizer gas: 10 psi, auxiliary gas: off, interface heater: on, declustering potential: 100 V, collision energy spread: 0, 10 V, collision energy: 70 V. The limit of detection (LOD, signal-to-noise ratio = 3) was calculated as 0.24 pg µl⁻¹ sample extract.

2.1.4. Real-time PCR analysis of field samples

Filter concentrates of the pooled water samples were obtained as described in 2.1.3. The filters were attached to the inner wall of a 50 mL plastic centrifuge tube, and repeatedly rinsed with 1 mL pre-heated (60 °C) PL1 DNA lysis buffer of the NucleoSpin Plant II DNA extraction kit (Macherey & Nagel, Düren, Germany). The lysis buffer was subsequently transferred to a 5 mL cryovial pre-filled with 200 µL glass beads (acid-washed, 212–300 µm, Sigma-Aldrich, St. Louis, USA) and stored at -20 °C. DNA of the field samples was extracted using the NucleoSpin Plant II kit according to the manufacturer instructions, with an additional cell disruption step within beat tubes. Therefore, the samples were shaken for 45 s and another 30 s at a speed of 4.0 m s⁻¹ in a FastPrep FP120 cell disrupter (Qbiogene, Carlsbad, USA). Afterwards, 30 µL of the provided elution buffer were spun through the spin column to elute the DNA according to the manufacturer instructions, and subsequently repeated with another 30 µL to increase the DNA yield, leading to a total elution volume of 60 µL.

To pre-scan the field samples for the general occurrence of Amphidomataceae, a SYBR Green real-time PCR assay was performed as described in Smith et al. (2016) with slight variations. The 10 µL SYBR Green assay contained 5 µL of Fast SYBR Green Master Mix (Applied Biosystems by Thermo Fisher Scientific, Waltham, USA), 0.25 µL of both primers (each as a final concentration of 200 nmol), 3.5 µL of high-grade PCR H₂O and 1 µL of template DNA (1 ng µL⁻¹). The assays were run in a StepOne Plus real-time PCR cycler (Applied Biosystems by Thermo Fisher Scientific) with the following conditions: Stage 1: hold 95 °C for 20 s, followed by 40 cycles of Stage 2, Step 1: hold 95 °C for 3 s, Step 2: hold 60 °C for 30 s, followed by a Melt Curve Stage: Step 1: hold 95 °C for 15 s, Step 2: hold 60 °C for 60 s, Step 3: hold 95 °C for 15 s. All measurements were carried out in triplicates and samples were considered as being positive if at least two of the three replicates showed a fluorescence signal above the threshold before cycle 37. No-template controls (NTC), containing high-grade PCR H₂O, as well as positive controls, containing target DNA with known concentrations from exponentially growing amphidomatacean cultures, were present during all PCR runs. A melt curve analysis was always

performed to check the amplification specificity. Samples with amplification above the threshold before cycle 37 were subsequently analysed with the species-specific TaqMan assays for *Az. spinosum*, *Az. poporum* and *Am. languida* as described in Toebe et al. (2013) and Wietkamp et al. (2019). For the species-specific assays, all reactions were carried out in triplicates within 0.1 mL MicroAmp Fast 96-Well Reaction Plates (Applied Biosystems by Thermo Fisher Scientific) and no-template controls (NTC), containing high-grade PCR H₂O, were present during each qPCR run. For determination of the C_T value (threshold cycle), baselines and thresholds were set manually before each qPCR analysis according to the guidelines from Applied Biosystems (Livak, 1997; Ruijter et al., 2009). DNA-based standard curves (10-fold dilution series of target DNA with 10 ng μL⁻¹ to 0.01 pg μL⁻¹) were present for *Az. spinosum*, *Az. poporum* and *Am. languida* during all qPCR runs to calculate cell numbers of the target species. The DNA for the standard curves was gained from known cell numbers of exponentially growing cultures of *Az. spinosum* (3D9), *Az. poporum* (UTH-D4) and *Am. languida* (LF-09-C09). To estimate cell densities of the cultures, cells were settled in counting chambers (0.5 mL subsamples) and counted by light microscopy (Axiovert 200 M, Zeiss) at a magnification of 400 x. DNA extraction for the standard curves was carried out using the NucleoSpin Soil DNA extraction kit (Macherey & Nagel), the amount of dsDNA of these extracts was measured using a Quantus Fluorometer (Promega, Fitchburg, USA) and DNA cell quota was calculated. The limit of detection and of quantification (LOD and LOQ) were defined here following Forootan et al. (2017) as the lowest standard curve DNA concentration, for which all three replicates are within the 95% confidence limits of the curve (LOQ), and for which all three replicates show amplification but values scattered outside the 95% confidence limit of the curve (LOD). For standard curves of all three qPCR assays, the limited resolution of dilutions applied here did not allow to differentiate between LOD and LOQ, which was 0.1 pg μL⁻¹ sample extract.

2.2. Characterisation of Amphidomataceae strains

2.2.1. Culture growth, sampling and extraction of cultured strains

After several weeks of growth, primary isolation plates from the cruise were inspected in the laboratory using a stereomicroscope (SZH-ILLD, Olympus) for the presence of *Azadinium*-like cells as inferred from the typical size, shape, and swimming behavior. From each positively identified well, a clonal strain was established by isolation of single cells with a micro-capillary. Established cultures were thus clonal but not axenic, and were routinely held in 65 mL plastic culture flasks at 15 °C and a photon flux density of 50 μmol m⁻² s⁻¹ on a 16:8 h light:dark photoperiod. The medium was natural, sterile-filtered (0.2 μm VacuCap filters, Pall GmbH, Dreieich, Germany) Antarctic seawater (salinity: 34, pH adjusted to 8.0) and enriched with 1/10 strength K-medium (Keller et al., 1987), slightly modified by omitting the addition of ammonium ions.

For toxin analysis, strains were grown at the standard culture conditions described above. For each harvest, cell density was determined by settling lugol fixed samples and counting > 800 cells under an inverted microscope. Densely grown strains (ranging from 0.5 to 5 × 10⁴ cells mL⁻¹) were harvested by centrifugation (5810 R, Eppendorf) at 3,220 × g for 10 min from 50 mL subsamples. The cell pellet was re-suspended, transferred to a microtube, centrifuged again (5415R, Eppendorf; 16,000 × g, 5 min) and stored at -20 °C until use. For a number of selected strains, growth and harvest procedures were repeated several times to yield a high biomass and to increase the sensitivity of the toxin detection method. Total numbers of harvested cells for all strains are listed in Supplementary Tables S2 and S3. Several cell harvests of each strain were combined in 100 μL acetone. The extraction of cell pellets was repeated four times with 100 μL each and combined cell suspensions were shortly vortexed every 10 min at room temperature five times. Homogenates were centrifuged (5810 R,

Eppendorf) at 15 °C and 3,220 × g for 15 min. Filtrates were then adjusted with acetone to a final volume of 0.5 mL. The extracts were transferred to a 0.45 μm pore-size spin-filter (Millipore Ultrafree, Eschborn, Germany) and centrifuged (5810 R, Eppendorf) at 800 × g for 30 s. The filtrate was transferred into a liquid chromatography (LC) autosampler vial for LC-MS/MS analysis.

For DNA analysis, each strain was grown in 65 mL plastic culture flasks under the standard culture conditions described above. 50 mL of healthy and growing culture (based on stereomicroscopic inspection of the live culture) were harvested by centrifugation (5810 R, Eppendorf; 3,220 × g, 10 min). Each pellet was transferred to a 1.5 mL tube, centrifuged (5415, Eppendorf; 16,000 × g, 5 min) and stored at -20 °C until DNA extraction.

2.2.2. Microscopy observation of cultured strains

2.2.2.1. Light microscopy (LM). Observation of living or fixed cells was carried out with a stereomicroscope (SZH-ILLD, Olympus) and an inverted microscope (Axiovert 200 M, Zeiss). Observation and documentation of live cells at high magnification (1,000 x) was performed using a Zeiss Axioskop 2 (Zeiss) and by recording videos using a digital camera (Gryphax, Jenoptik, Jena, Germany) at full-HD resolution. Single frame micrographs were extracted using Corel Video Studio software (Version X8 pro). Photographs of formalin-fixed cells (1% final concentration) were taken with a digital camera (AxioCam MRc5, Zeiss). Cell length and width of freshly fixed cells (formalin, final concentration 1%) of strains grown at 15 °C were measured at 1,000 x microscopic magnification using Zeiss Axiovision software (Zeiss).

2.2.2.2. Scanning electron microscopy (SEM). For SEM, cells were collected by centrifugation (5810 R, Eppendorf; 3,220 × g, 10 min.) of 15 mL of culture. The supernatant was removed and the cell pellet re-suspended in 60% ethanol in a 2 mL microtube for 1 h at 4 °C to strip off the outer cell membrane. Subsequently, cells were pelleted by centrifugation (5810 R, Eppendorf; 16,000 × g, 5 min) and re-suspended in a 60:40 mixture of deionized water and seawater for 30 min at 4 °C. After centrifugation and removal of the diluted seawater supernatant, cells were fixed with formalin (2% final concentration in a 60:40 mixture of deionized water and seawater) and stored at 4 °C for 3 h. Cells were then collected on polycarbonate filters (Ø = 25 mm, 3 μm pore-size, Merck) in a filter funnel, where all subsequent washing and dehydration steps were carried out. A total of eight washings (2 mL MilliQ-deionized water each) were followed by a dehydration series in ethanol (30, 50, 70, 80, 95, 100%; 10 min each). Filters were dehydrated with hexamethyldisilazane (HMDS), first in 1:1 HMDS:EtOH followed by two times 100% HMDS, and then stored under gentle vacuum in a desiccator. Finally, filters were mounted on stubs, sputter coated (SC500, Emscope, Ashford, UK) with gold-palladium and viewed under a scanning electron microscope (Quanta FEG 200, FEI, Eindhoven, Netherlands). Some SEM micrographs were presented on a black background using Adobe Photoshop 6.0 (Adobe Systems, San Jose, USA).

2.2.3. Chemical analysis of azaspiracids from cultured strains

Extracts of the strains were screened for known AZA in the SRM mode as described above (2.1.3). In addition, precursor ion experiments were performed. Precursors of the characteristic AZA fragments *m/z* 348, *m/z* 360 and *m/z* 362 were scanned in the positive ion mode from *m/z* 400 to 900 under the following conditions: curtain gas: 10 psi, CAD: medium, ion spray voltage: 5,500 V, temperature: ambient, nebulizer gas: 10 psi, auxiliary gas: off, interface heater: on, declustering potential: 100 V, entrance potential: 10 V, collision energy: 70 V, exit potential: 12 V. Product ion spectra of the *m/z* values 830, 842 and 858 were recorded in the Enhanced Product Ion (EPI) mode in the mass range from *m/z* 150 to 930. Positive ionization and unit resolution mode were used. The following parameters were applied: curtain gas: 10 psi, CAD: medium, ion spray voltage: 5,500 V, temperature: ambient,

nebulizer gas: 10 psi, auxiliary gas: off, interface heater: on, declustering potential: 100 V, collision energy spread: 0, 10 V, collision energy: 70 V.

2.2.4. Molecular phylogeny

2.2.4.1. DNA extraction and sequencing of cultured strains. DNA of the cultured strains was extracted as described above (2.1.4) and stored at -20°C until further processing. For the Sanger-Sequencing, the DNA of each sample was quantified with a spectrophotometer (NanoDrop ND-1000, PeqLab Biotechnology GmbH, Erlangen, Germany) and diluted to a final concentration of $10\text{ ng }\mu\text{L}^{-1}$. The DNA was subjected to a polymerase-chain-reaction (PCR) for the following genes: D1/D2 region of 28S/large subunit (LSU) and the Internal Transcribed Spacer region including ITS1, 5.8S rRNA, ITS2, with respective primer sequences summarized in Tillmann et al. (2017a). The reaction mixes were prepared as follows: $16.3\text{ }\mu\text{L}$ of high-grade PCR H_2O , $2.0\text{ }\mu\text{L}$ of Hotmaster Taq PCR Buffer (10X) (Quantabio, Beverly, USA), $0.2\text{ }\mu\text{L}$ of each primer ($10\text{ }\mu\text{M}$), $0.2\text{ }\mu\text{L}$ of dNTP ($10\text{ }\mu\text{M}$) (Quantabio), $0.1\text{ }\mu\text{L}$ of Taq Polymerase (Quantabio) and $1\text{ }\mu\text{L}$ of DNA template ($10\text{ ng }\mu\text{L}^{-1}$) to a final volume of $20\text{ }\mu\text{L}$. Subsequently, the PCR for the LSU and ITS region was performed according the conditions described in Tillmann et al. (2017c). The PCR amplicons were run on a 1% agarose gel in TE buffer at 70 mV for 30 min to verify that the PCR amplicons were of the expected length. The PCR amplicon was purified using the NucleoSpin Gel and PCR clean-up kit (Macherey-Nagel) and sequenced directly in both directions on an ABI PRISM 3730XL (Applied Biosystems by Thermofisher Scientific) as described in Tillmann et al. (2017c).

2.2.4.2. Phylogenetic analysis. Newly obtained LSU and ITS rDNA sequences were incorporated into available *Amphidoma* and *Azadinium* sequences in GenBank (<https://www.ncbi.nlm.nih.gov/genbank/>). Genbank Accession numbers are listed in Supplementary Table S4. All new 17 strains of *Am. languida* with sequence data shared the same LSU rDNA sequences, and thus only eight randomly selected strains were included in the phylogenetic analysis. Sequences were aligned using MAFFT v7.110 (Katoh and Standley, 2013) online program (<http://mafft.cbrc.jp/alignment/server/>) with default settings. Alignments were manually checked with BioEdit v. 7.0.5 (Hall, 1999). For Bayesian inference (BI), the program jModelTest (Posada, 2008) was used to select the most appropriate model of molecular evolution with Akaike Information Criterion (AIC). Bayesian reconstruction of the data matrix was performed using MrBayes 3.2 (Ronquist and Huelsenbeck, 2003) with the best-fitting substitution model (GTR + G). Four Markov chain Monte Carlo (MCMC) chains ran for 6,000,000 generations, sampling every 100 generations. The first 10% of burn-in trees were discarded. A majority rule consensus tree was created in order to examine the posterior probabilities of each clade. Maximum likelihood (ML) analysis were conducted with RaxML v7.2.6 (Stamatakis, 2006) on the T-REX web server (Boc et al., 2012) using the model GTR + G. Node support was assessed with 1,000 bootstrap replicates.

3. Results

3.1. Field data

3.1.1. Hydrography and chemistry

In the three investigated areas, the North Sea coast, the inner Limfjord and the Kattegat/Belt area, different environmental conditions were observed (Fig. 2). CTD data of the North Sea stations (station 1–13) revealed low mean temperatures ($13.86 \pm 0.61^{\circ}\text{C}$) and a constantly high salinity (32.84 ± 0.69). This was in contrast to the Limfjord stations (station 14–28), where a higher mean temperature ($17.50 \pm 0.53^{\circ}\text{C}$) and a broader salinity range (25.92 ± 2.50) was found. The Kattegat/Belt area (station 29–44) showed a clear stratification with higher temperatures in the upper 12 m ($16\text{--}18^{\circ}\text{C}$) and

lower temperatures in the deeper water layer ($6\text{--}12^{\circ}\text{C}$). In contrast, the salinity in the upper layer was relatively low ($14\text{--}20$) compared to the lower layer ($26\text{--}32$). The mean fluorescence was found to be significantly higher within Limfjord (0.1 to 0.5 AU) compared to the North Sea and Kattegat/Belt area ($\leq 0.2\text{ AU}$) with particularly high values at station 18.

3.1.2. Live sample records of Amphidomataceae in field samples

Light microscopy analysis of selected live samples revealed presence of Amphidomataceae in the study area, especially in the North Sea off the Limfjord entry (station 9, 10, 11, 12), at the first inner Limfjord stations (station 14, 15), and also from the last station (station 44) in the Baltic Sea close to Kiel Bight (Fig. 3). Amphidomatacean cells in field samples were not identified to species level.

3.1.3. AZA in field samples

In plankton field samples, AZA-1, -38 and -39 were detected (Fig. 4). Depending on the filtered water volume and filter extraction volume, the limits of detection of the field sample measurements ranged between 24 and 80 pg AZA L^{-1} . Azaspiracids were mainly recorded in the North Sea, the western Limfjord stations, and at two stations of the northern East coast. Highest AZA abundances were recorded in the North Sea on station 9 (AZA-38: 1.10 ng L^{-1} ; AZA-39: 1.47 ng L^{-1}). AZA-1 was detected only at station 10 in low amounts (0.08 ng L^{-1}).

3.1.3.1. Description of AZA-63. In addition to the known AZA described above, in the samples of two stations (9 and 14) a peak with the transition m/z $844 > 826$ was detected (data not shown). The abundance of this compound was estimated as 0.62 ng L^{-1} at station 9 and 0.10 ng L^{-1} at station 14 (both values expressed as AZA-1 equivalents). The collision induced dissociation spectrum (CID) of m/z 844, hereafter named AZA-63 (Fig. 5A), was almost identical with the CID spectrum of AZA-37, except for a 2 Da downshifted and a less complex pseudo-molecular ion cluster, whereas all other typical AZA fragments were identical with AZA-37 (Fig. 5B). The proposed chemical structure of AZA-63 is presented in Fig. 5C.

3.1.4. Real-time PCR results of field samples

The pre-scanning PCR assay targeting the group of Amphidomataceae revealed positive amplifications at almost all stations outside Limfjord. Positive signals inside Limfjord were recorded at station 14 and 15 located at the entrance of the fjord, as well as at station 20, 21 and 28 in the inner fjord (Fig. 4). The species-specific qPCR assays revealed the occurrence of all three targeted species *Az. spinosum*, *Az. poporum* and *Am. languida*. The limit of detection of $0.1\text{ pg target DNA }\mu\text{L}^{-1}$ - considering the DNA extraction volume and the filtered water volume - here corresponded to $1\text{--}3\text{ cells L}^{-1}$. *Azadinium spinosum* was rather low in abundance and mainly present in the North Sea with the highest cell density (31 cells L^{-1}) on station 10. This species was not detected inside Limfjord, and very low cell densities of around 1 cell L^{-1} were found at the Kattegat stations 31 and 32. The species *Azadinium poporum* was also low in abundance with highest densities at station 7 and 12 (approx. 75 cells L^{-1}). It was also present in the western entrance of the Limfjord (station 14, with approx. 20 cells L^{-1}). Like *Az. spinosum*, *Az. poporum* occurred also in the upper Kattegat stations in relatively low amounts (station 31 and 32, approx. $1\text{--}3\text{ cells L}^{-1}$). The species *Amphidoma languida* was found at all stations in the North Sea, except for station 4 and 10. In general, *Am. languida* showed considerably higher cell densities compared to the other two species, with a maximum density of $3 \times 10^3\text{ cells L}^{-1}$ at the entrance of Limfjord (station 14), but it was not found in the inner fjord. In the Kattegat area, *Am. languida* was also present (station 31 and 32), again in significantly higher amounts (approx. 350 cells L^{-1}) compared to *Az. spinosum* and *Az. poporum*. Furthermore, low levels of *Am. languida* (approx. 1 cell L^{-1}) were also found further south at stations 36, 37 and 38.

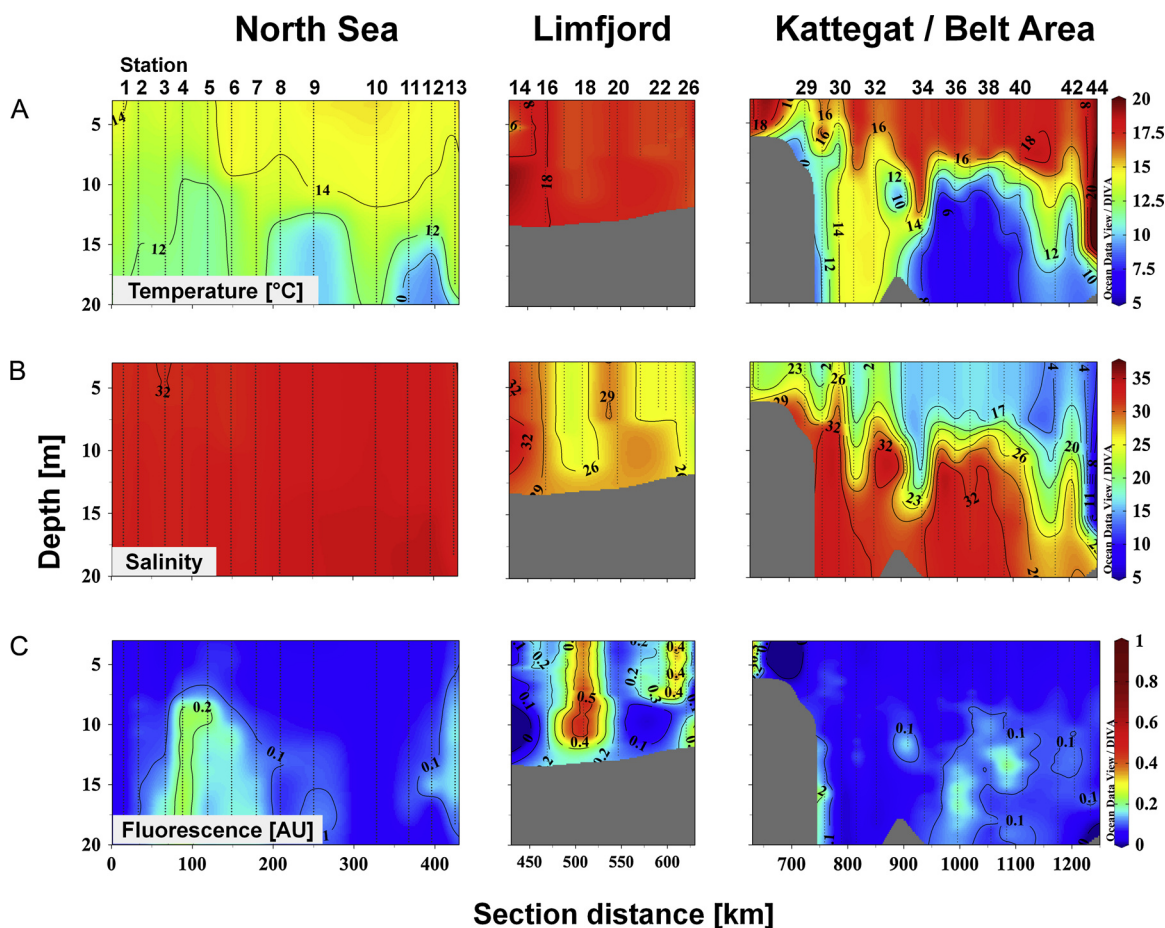


Fig. 2. CTD depth profile of (A) temperature, (B) salinity and (C) chlorophyll fluorescence along the coastal stations 1-44. For the location of the stations see Fig. 1.

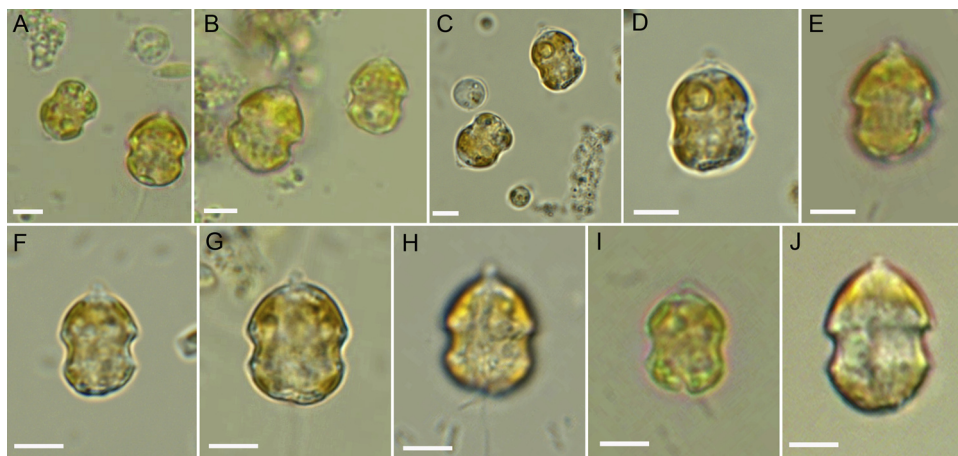


Fig. 3. Amphidomataceae records in live samples of the survey (station 9, 12, 14, 44). Scale bars = 5 µm.

3.2. New strains of Amphidomataceae

Single cell isolation yielded 26 clonal amphidomatacean strains. All strains displayed a similar and conspicuous swimming behavior consisting of a slow movement interrupted by short “jumps” in various directions. Identification of all strains was based on morphology as examined by LM and was confirmed for almost all strains by rDNA sequence comparison (Table 1). For a number of selected strains the morphology was also examined by SEM (Table 1). The newly available 26 strains comprised four species including *Az. dalianense* (2 strains), *Az. obesum* (3 strains), *Az. poporum* (1 strain), and *Am. languida* (20 strains).

3.2.1. Morphology

3.2.1.1. *Azadinium obesum*. Three strains of *Az. obesum* were obtained, two from the North Sea (station 12) and one from the last Baltic Sea station (station 44) close to Kiel Bight. All three strains were indistinguishable in LM and SEM and all shared the morphological features described as distinctive for *Az. obesum* (Fig. 6, Suppl. Figs S1, S2). No pyrenoid was visible using light microscopy (Fig. 6A–C). A detailed SEM examination (Fig. 6D–G) revealed the common *Azadinium* Kofoidian plate pattern (Po, cp, X, 4’, 3a, 6”, 6C, 5S, 6””, 2””) and the ventral pore location at the margin of plate 1’ and 1” (Fig. 6D, E). Epithelial intercalary plates were relatively small and the first of them

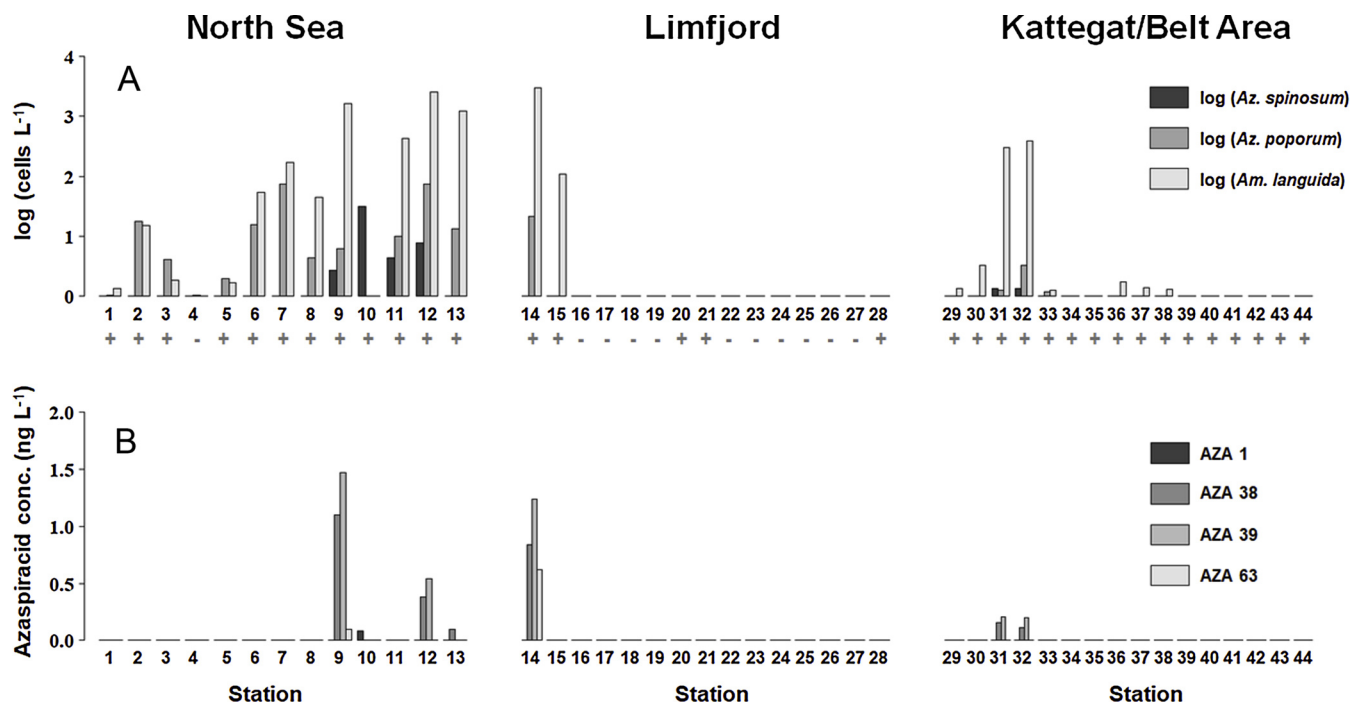


Fig. 4. A: qPCR-based cell densities (cells L⁻¹, log-scale) of *Az. spinosum*, *Az. poporum* and *Am. languida*. Positive (+) or negative (-) amplification in the general amphidomatacean PCR assay is marked below the station number. B: Azaspiracid concentration (ng L⁻¹, linear-scale).

(1a) was not in contact with plate 1'' (Fig. 6E). The small central anterior intercalary plate 2a occurred in two arrangements, either being tetragonal and only contacting plate 3'' of the postcingular series (most common), or being pentagonal and in contact to two plates of the precingular series (3'' and 4'') (Suppl. Fig. S1E).

3.2.1.2. *Azadinium dalianense*. Two of the strains were identified as *Az. dalianense*, one originating from station 9 (North Sea) and one from the Limfjord (station 14). Both strains shared the same morphological features described as distinctive for *Az. dalianense* with an asymmetrically pointed hyposome ending with a small bulb (Fig. 7). At

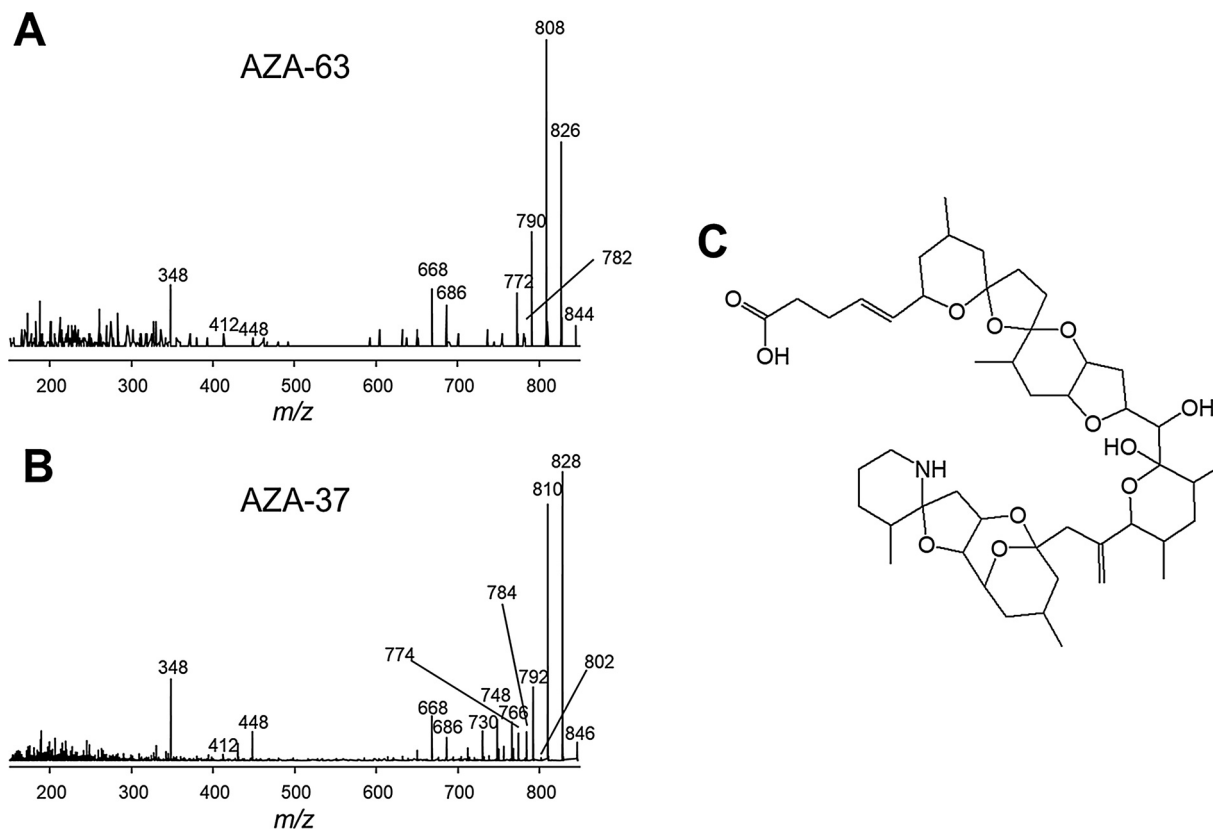


Fig. 5. Collision induced dissociation (CID) spectrum of AZA-63 (A), AZA-37 (B) and the proposed structure of AZA-63 (C).

Table 1

Amphidomatacean strain information (LM = light microscopy, SEM = scanning electron microscopy, LSU = large subunit, ITS = internal transcribed spacer, ND = not detected, – = not analysed).

Species	Strain	Origin Station	Length (µm)	Width (µm)	l/w ratio	N	Morphological analysis	Sequence data	AZA
			Mean ± SD Min-max	Mean ± SD Min-max	Mean ± SD				
<i>Az. dalianense</i>	LF-09-B02	09	16.6 ± 0.9 14.9–18.7	11.9 ± 0.8 10.5–13.9	1.39 ± 0.05	51	LM SEM	LSU, ITS	ND
<i>Az. dalianense</i>	LF-14-F07	14	15.1 ± 1.0 13.2–18.0	10.6 ± 0.8 9.0–12.3	1.43 ± 0.07	50	LM SEM	LSU, ITS	ND
<i>Az. obesum</i>	LF-12-A09	12	15.8 ± 1.1 13.7–18.5	11.6 ± 1.0 9.4–14.2	1.37 ± 0.06	58	LM SEM	LSU, ITS	ND
<i>Az. obesum</i>	LF-12-A12	12	16.2 ± 1.0 14.6–18.6	12.1 ± 0.9 10.2–13.9	1.34 ± 0.07	56	LM SEM	LSU, ITS	ND
<i>Az. obesum</i>	LF-44-C03	44	16.3 ± 1.2 12.5–18.5	12.5 ± 1.2 10.7–17.2	1.31 ± 0.11	58	LM SEM	LSU, ITS	ND
<i>Az. poporum</i>	LF-14-E12	14	14.5 ± 0.9 12.8–16.0	10.1 ± 0.6 9.0–11.4	1.44 ± 0.07	51	LM SEM	LSU, ITS	ND
<i>Am. languida</i>	LF-09-A02	09	–	–	–	–	LM	LSU	AZA-38, -39
<i>Am. languida</i>	LF-09-A03	09	13.7 ± 1.0 10.4–16.4	10.6 ± 0.9 7.5–14.3	1.30 ± 0.09	81	LM	LSU	AZA-38, -39
<i>Am. languida</i>	LF-09-A07	09	13.7 ± 0.8 12.1–15.3	11.1 ± 0.7 9.6–12.6	1.23 ± 0.07	52	LM	LSU	AZA-38, -39
<i>Am. languida</i>	LF-09-B11	09	14.1 ± 0.8 12.4–16.9	11.5 ± 0.8 10.0–13.6	1.23 ± 0.05	54	LM SEM	LSU	AZA-38, -39
<i>Am. languida</i>	LF-09-C02	09	–	–	–	–	LM	–	AZA-38, -39
<i>Am. languida</i>	LF-09-C04	09	13.0 ± 0.9 10.7–14.9	10.1 ± 0.9 8.1–11.7	1.29 ± 0.06	50	LM	LSU	AZA-38, -39
<i>Am. languida</i>	LF-09-C09	09	14.2 ± 0.9 12.6–15.8	11.9 ± 1.0 10.3–14.0	1.19 ± 0.07	21	LM	LSU	AZA-38, -39
<i>Am. languida</i>	LF-09-C10	09	14.5 ± 0.9 11.7–16.3	11.5 ± 0.9 8.8–13.1	1.26 ± 0.08	62	LM SEM	LSU	AZA-38, -39
<i>Am. languida</i>	LF-12-A04	12	–	–	–	–	LM	–	AZA-38, -39
<i>Am. languida</i>	LF-14-E01	14	–	–	–	–	LM	LSU	AZA-38, -39
<i>Am. languida</i>	LF-14-E07	14	13.8 ± 0.7 12.4–15.3	10.9 ± 0.7 9.9–13.3	1.27 ± 0.07	39	LM	LSU	AZA-38, -39
<i>Am. languida</i>	LF-14-F02	14	14.4 ± 0.9 12.4–16.2	12.1 ± 1.1 9.9–14.6	1.19 ± 0.08	54	LM SEM	LSU	AZA-38, -39
<i>Am. languida</i>	LF-14-F04	14	13.6 ± 0.9 11.6–15.8	11.0 ± 0.9 9.6–13.1	1.24 ± 0.07	71	LM	–	AZA-38, -39
<i>Am. languida</i>	LF-14-F06	14	–	–	–	–	LM	LSU	AZA-38, -39
<i>Am. languida</i>	LF-14-F08	14	–	–	–	–	LM	LSU	AZA-38, -39
<i>Am. languida</i>	LF-14-F11	14	–	–	–	–	LM	LSU	AZA-38, -39
<i>Am. languida</i>	LF-14-G01	14	13.9 ± 0.7 13.0–15.0	10.9 ± 1.0 10.0–12.8	1.28 ± 0.06	6	LM	LSU	AZA-38, -39
<i>Am. languida</i>	LF-14-G06	14	–	–	–	–	LM	LSU	AZA-38, -39
<i>Am. languida</i>	LF-14-G07	14	14.6 ± 1.1 12.0–17.1	11.6 ± 0.9 9.2–13.8	1.26 ± 0.05	52	LM	LSU	AZA-38, -39
<i>Am. languida</i>	LF-14-G10	14	–	–	–	–	LM	LSU	AZA-38, -39

the end of this bulb there occasionally was a small spine visible in LM (Fig. 7A). One pyrenoid was consistently located posterior in the hyposome (Fig. 7A, B). SEM revealed the presence of only three apical plates and two large anterior intercalary plates (Fig. 7E). Consistent with the species description plate 2'' and 4'' of the precingular series were distinctly smaller compared to the other precingular plates (Fig. 7E). The ventral pore was located on the left side of the pre plate at the junction of the plates Po, 1' and 2' (Fig. 7G). Cells of both strains examined by SEM had an antapical spine and a small group of pores located on the large antapical plate 2'''' (Fig. 7F). A quantification of the frequency of spine presence (three independent measurements for each strain) revealed a proportion of cells without spine of 68% (n = 90), 69% (n = 16), and 84% (n = 50) for strain LF-09-B02, and 6% (n = 50), 14% (n = 50), and 26% (n = 50) for strain LF-14-F07, respectively.

3.2.1.3. *Azadinium poporum*. One strain from the Limfjord (station 14) was identified as *Az. poporum* (Fig. 8). There was no antapical spine, and pyrenoid(s) were always present in the cell and were located in the episome and/or the hyposome (Fig. 8A, B). SEM (Fig. 8D–G) revealed that all morphological features of strain LF-14-E12 conformed to the

original *A. poporum* description, e.g. the ventral pore was located at the junction of the pore plate and the first two apical plates (Fig. 8E, G).

3.2.1.4. *Amphidoma languida*. With 20 strains, most cell cultures from the survey were obtained from the species *Am. languida* isolated from the North Sea (station 9, 12) and Limfjord (station 14). All strains of *Am. languida* shared an identical morphology as observed in LM (Fig. 9A–C). In accordance with the species description, cells consistently had one large pyrenoid with a starch sheath (visible as a ring-like structure) located in the episome (Fig. 9B). Detailed SEM (Fig. 9D–G) performed for a selected number of strains (Table 1) revealed the Kofoidian plate pattern for the species (Po, cp, X, 6', 0a, 6'', 6C, 5S, 6''', 2''') and the location of the ventral pore at the right side of plate 1' close to the pore plate (Fig. 9E–G). On the hypotheca a large antapical pore was located on the second antapical plate (Fig. 9F). A number of, but not all, cells in the clonal cultures had a round ventral depression located at the anterior tip of the anterior sulcal plate (Fig. 9D).

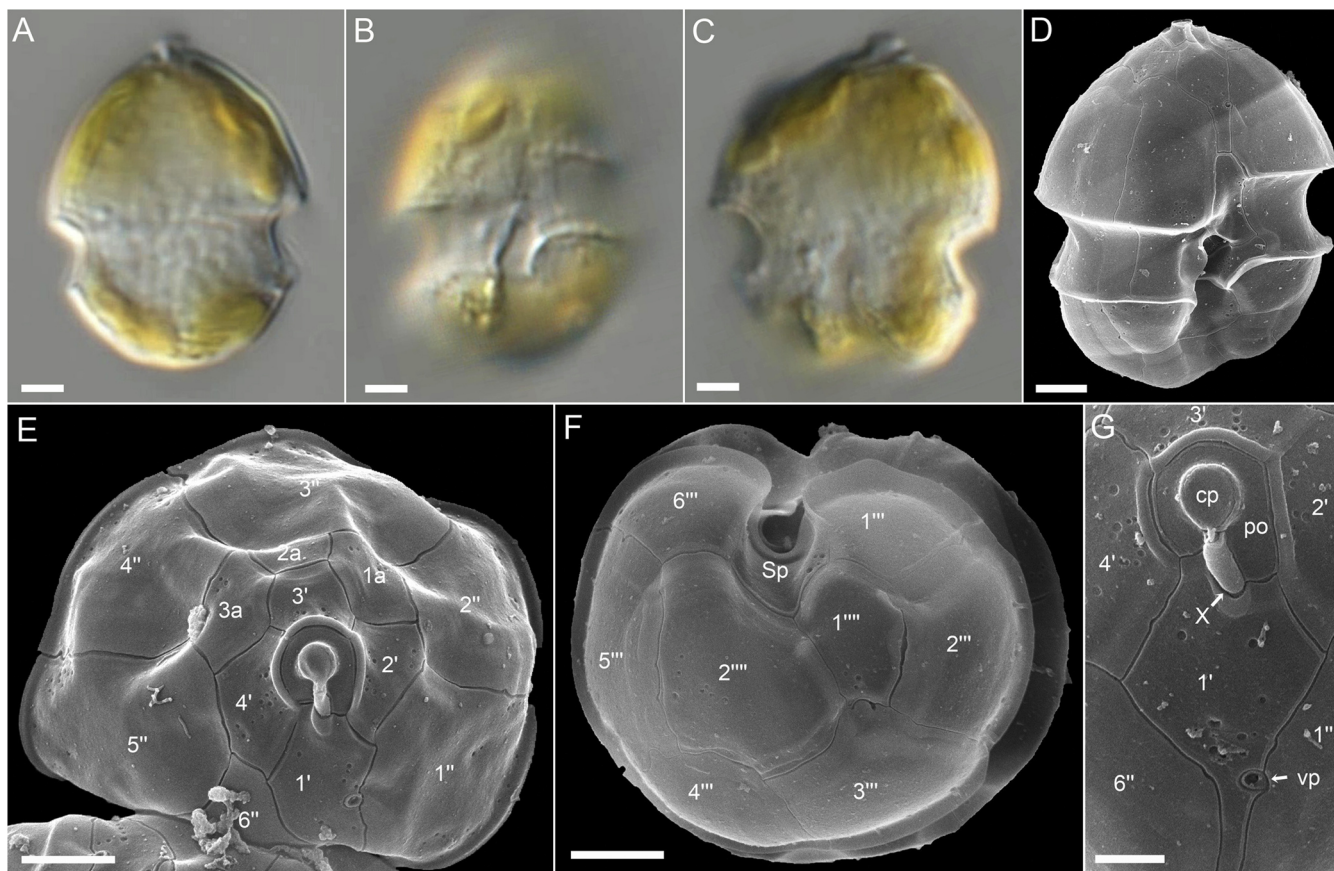


Fig. 6. Light and scanning electron micrographs of *Azadinium obesum* (strain LF-44-C03). (A–C) LM, living cells to illustrate general size and shape. Note the lack of a pyrenoid. (C) Presumably early stage of cell division. (D–G) SEM. (D) Whole cell in ventral lateral view. (E) Epithelial plates in apical view. (F) Hypothecal plates in antapical view. (G) Detailed view of the apical pore complex and the first apical plate. Plate labels according to the Kofoidian system. Sp = posterior sulcal plate, cp = cover plate, X = X-plate, vp = ventral pore, po = pore plate. Scale bars = 2 μm (A–F) or 1 μm (G).

3.2.2. AZA profile of strains

No AZA were detected in both SRM and precursor mode in both strains of *Az. dalianense*, in all three strains of *Az. obesum*, and in the new strain of *Az. poporum* (Table 1, for the respective limits of detection see Suppl. Table S2). All 20 *Am. languida* strains had identical AZA profiles consisting mainly of AZA-38 and AZA-39 (Table 1). Cell quotas of both compounds, however, were quite variable among strains ranging from 0.21 to 33.13 fg cell^{-1} and 0.05 to 61.41 fg cell^{-1} for AZA-38 and -39, respectively (Suppl. Table S3). A few selected strains were independently analysed twice with different biomass and revealed significant intra-strain variability of AZA cell quota as well (Suppl. Table S3). The ratio of AZA-38/39 for most strains was in the range of 0.38 to 0.69. One of the strains (LF-09-C09), however, exceptionally had a higher AZA-38 than AZA-39 cell quota. Two of the strains (LF-12-A04 and LF-14-F11) had an higher AZA-39 cell quota than AZA-38. As an exception, only traces of both AZA-38 and -39 were found in one strain (LF-14-F02), which was confirmed by a second independent analysis (Suppl. Table S3). For almost all *Am. languida* strains the respective phosphate forms of AZA-38 and AZA-39 were found. The peak areas of the phosphates were quite variable among strains and ranged from 0.4% to 28.6% of the respective non-phosphorylated AZA. Interestingly, for two of the strains which only showed traces of AZA-38 (LF-12-A04 and LF-14-F11), AZA-38-phosphate was present in about the same amount as AZA-38. No phosphorylated AZA were found in the strain, which only showed traces of AZA-38 and -39 (LF-14-F02, Suppl. Table S3).

3.2.3. Phylogenetic analysis

In total, LSU sequences of 23 strains and ITS sequences of six strains of Amphidomataceae were gained in this study. ITS amplification and sequencing of *Am. languida* strains failed and was not further analysed here. Sequence data and phylogenetic placement by Bayesian inference analysis (Fig. 10) for all strains confirmed their morphological species determination. All three new *Az. obesum* strains clustered within a well-supported clade with other *Az. obesum* strains from the North Sea, the North Atlantic and the Northeast Pacific. The two new *Az. dalianense* strains fell in two different clades: One strain (LF-09-B02) clustered together with *Az. dalianense* strains from the Northeast Pacific (USA) and the Norwegian coast, referred to as Ribotype D. The second new strain (LF-14-F07) clustered together with *Az. dalianense* strains of Ribotype E from the Southwest Atlantic (Argentina) and the Norwegian coast. Strains from Yellow Sea, China, the North Atlantic (France), and the Northeast Pacific (USA) were classified as Ribotypes A, B and C, respectively. The new *Az. poporum* strain (LF-14-E12) clustered within Ribotype A2, together with strains from the Mediterranean. All 17 new *Am. languida* strains shared identical LSU sequences and fell into the same well-supported clade with strains of Ireland, Iceland and Spain, but were slightly separated from strains isolated from the Norwegian coast.

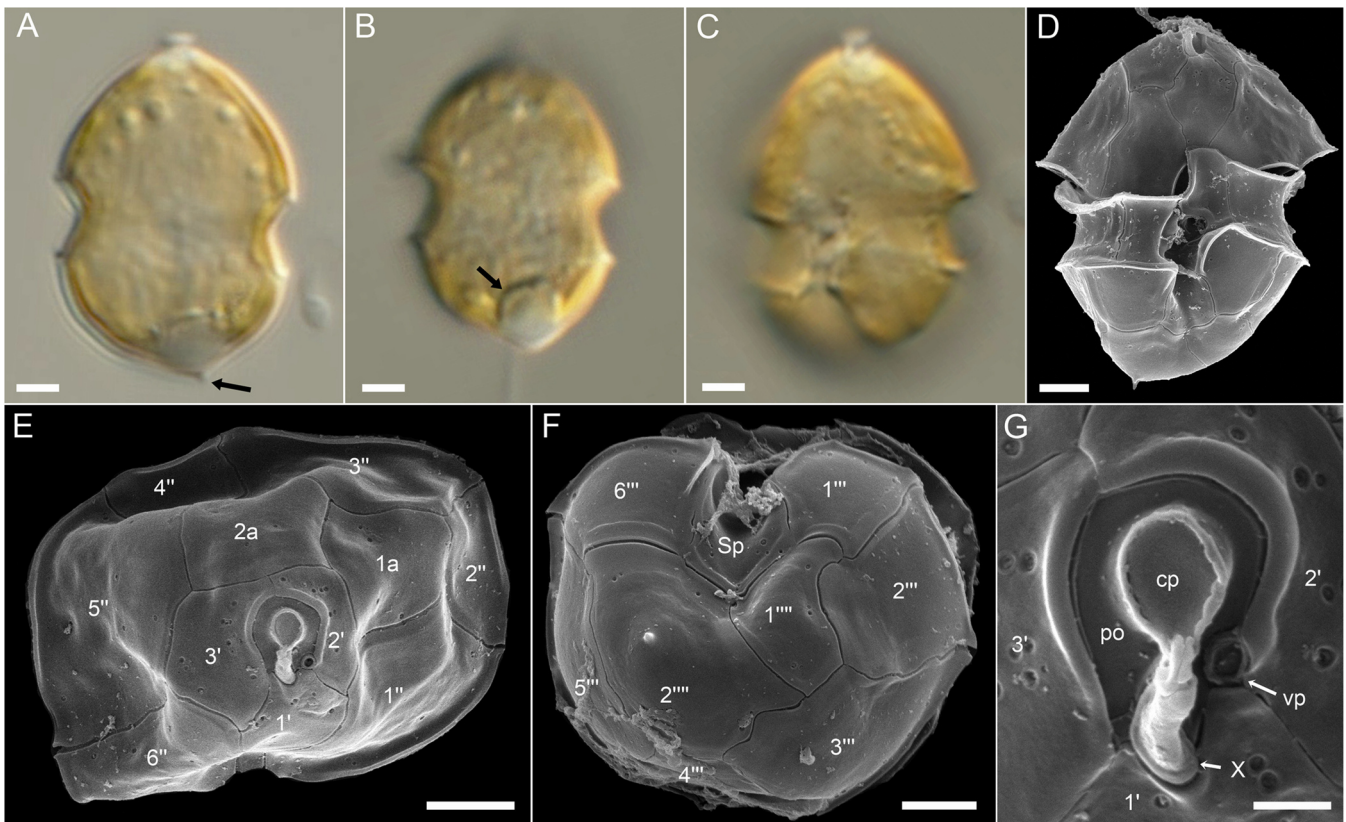


Fig. 7. Light and scanning electron micrographs of *Azadinium dalianense* (strain LF-14-F07). (A–C) LM, living cells to illustrate general size and shape. Note the presence of a small antapical spine (arrow in A) and one pyrenoid located in the hyposome (arrow in B). (D–G) SEM. (D) Whole cell in ventral view. (E) Epithecial plates in apical view. (F) Hypothecal plates in antapical view. (G) Detailed view of the apical pore complex with the ventral pore. Plate labels according to the Kofoidian system. Sp = posterior sulcal plate, cp = cover plate, X = X-plate, vp = ventral pore, po = pore plate. Scale bars = 2 μm (A–F) or 0.5 μm (G).

4. Discussion

4.1. Distribution, diversity and abundances of Amphidomataceae

The pre-scanning real-time PCR assay targeting all amphidomatacean species (Smith et al., 2016) and live microscopy of selected samples revealed that this group of microalgae is present all along the Danish coast. This includes all but one station of the North Sea, the western entrance of Limfjord, and all stations of the Danish east coast from Kattegat through the Belt area down to Kiel Bight. Amphidomataceae were not detected at many of the inner Limfjord stations, including the high chlorophyll central stations 18 and 25. The reasons for this absence remain unclear; higher temperatures of Limfjord compared to the outer coastal area may play a role, but higher temperature was also recorded at the fjord entrance where *Am. languida* was present.

Different to the qualitative PCR assay, qPCR positive hits for the three toxigenic species *Az. spinosum*, *Az. poporum* and *Am. languida* were more restricted. These species were mainly recorded from the North Sea and from the western Limfjord stations, where highest abundances were observed. At the eastern Danish stations, positive hits (and low background abundance) only for the upper Kattegat stations indicate that here these species probably are introduced from the North Sea/Skagerrak, but are not spreading largely into the lower salinity Belt area. It is not clear if decreasing salinities along the Kattegat north-south gradient might represent a physiological barrier for the toxigenic amphidomatacean species. For *Az. spinosum*, culture experiments showing positive growth over a wide range of different salinities (Jaufrais et al., 2013) and positive qPCR signals for *Az. spinosum* for inner, low saline areas of two deep Norwegian Fjords (Tillmann et al., 2018) indicate that this species can cope with or can adapt to lower

salinities. In contrast, *Az. poporum* probably has preferences for higher saline areas as this species was present in Norwegian offshore waters but not in the inner lower saline area of the fjords (Tillmann et al., 2018). In any case, more detailed physiological data related to salinity for different strains of Amphidomataceae are needed to fully evaluate the potential of AZA contamination in the lower saline Baltic areas.

Extended positive pre-scanning PCR signals of Amphidomataceae for the lower saline Belt area down to Kiel Bight clearly indicate that species other than the three toxigenic species are present. This was confirmed by a strain of *Az. obesum*, which was isolated at station 44 in Kiel Bight at a salinity of 13. This strain was grown at a salinity of 15 but was easily adapted to and grown at a salinity of 34 (unpublished). This finding, together with almost identical sequence data of the Baltic strain and other *Az. obesum* strains from other areas indicate that there is not a distinct and separated low salinity population of *Az. obesum* present. No AZA were found in the new *Az. obesum* strains from the North Sea and from Kiel Bight, which confirms previous findings (Kim et al., 2017; Tillmann et al., 2010, 2018) that this species is not toxigenic.

Azadinium dalianense is reported here for the first time in the southern North Sea, which further indicates that this species has a rather widespread global distribution. Besides to the type locality in China, the species is recorded from the French Atlantic coast, in the north-east Pacific (Kim et al., 2017; Luo et al., 2017), along the Norwegian coast (Tillmann et al., 2018), and in the south Atlantic off Argentina (Tillmann et al., 2019). All available strains of the species share the same morphology, but exhibit significant sequence differences. Two different ribotypes were initially distinguished (Kim et al., 2017), but with all sequence information actually available a much broader diversity within *Az. dalianense* with 5 different clusters is evident, but

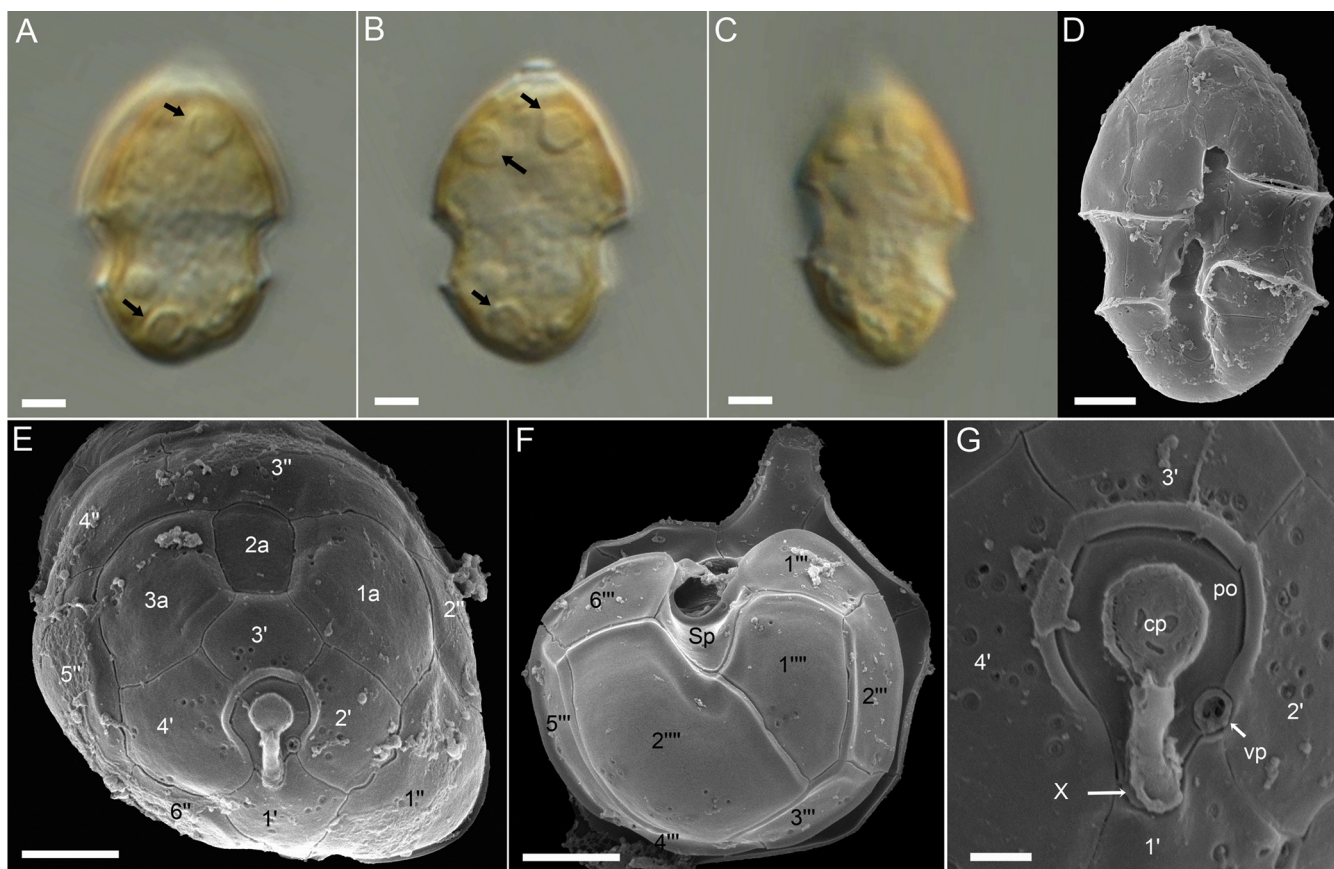


Fig. 8. Light and scanning electron micrographs of *Azadinium poporum* (strain LF-14-E12). (A–C) LM, living cells in ventral (A, B) or lateral (C) view. Note the pyrenoids (arrows in A, B). (D–G) SEM. (D) Whole cell in ventral view. (E) Epithelial plates in apical view. (F) Hypothecal plates in antapical view. (G) Detailed view of the apical pore complex with the ventral pore. Plate labels according to the Kofoidian system. Sp = posterior sulcal plate, cp = cover plate, X = X-plate, vp = ventral pore, po = pore plate. Scale bars = 2 μm (A–F) or 0.5 μm (G).

consistent and significant morphological differences between ribotypes have not been observed so far. Both new strains from Denmark cluster differently, strain LF-09-B02 isolated from the North Sea within Ribotype D and the strain LF-14-F07 isolated from Limfjord within Ribotype E (Fig. 10). Such a sympatric occurrence of different ribotypes in one area has been noted before for Puget Sound, North West Pacific (Kim et al., 2017), and the North Atlantic along the Norwegian coast (Tillmann et al., 2018). All new strains of *Az. dalianense* from Denmark do not produce any known AZA, which supports evidence from other geographical regions that this species is a non-AZA producer.

Generally, the qPCR determined abundances of toxigenic amphidomatacean species were low ranging from 10^1 to 10^3 cells L^{-1} . The species *Amphidoma languida*, with a peak abundance of 3×10^3 cells L^{-1} , was the by far most abundant of the three toxigenic species, which is supported by the relatively large number of *Am. languida* strains obtained from the North Sea and western Limfjord stations. However, maximum abundance in the range of 3×10^3 cells L^{-1} are still low compared to bloom concentrations of Amphidomataceae that may be as high as 10^6 cells L^{-1} (*Az. polongum* bloom in Peru, (Tillmann et al., 2017b) or 10^7 cells L^{-1} (*Az. luciferelloides* in Argentina, (Akselman and Negri, 2012)).

In agreement with the relative high abundance of *Am. languida* in the field samples, the majority of strains obtained in this study were *Am. languida*. Without exception all these strains produce AZA-38 and -39 (albeit one of the strains has only trace amounts of both compounds) indicating that this AZA profile is predominant for North Sea and North Atlantic strains of that species (Krock et al., 2012; Tillmann et al., 2018). The large number of strains furthermore allows evaluating the intraspecific range of AZA cell quota for *Am. languida*, and with

almost 1,000-fold differences, this is remarkably high. The multiple strain analysis further reveal that the ratio of AZA-38 and -39 can be variable, indicating that there are no biosynthetic constraints determining and limiting the ratio of both compounds present in the cells.

4.2. Distribution and abundances of azaspracids

The distribution and abundance of AZA-producing species determined by qPCR reflects the chemically determined presence of AZA. Generally, an AZA-based “cell detection limit” (based on the LOD of the AZA measurements of ca. 40 pg L^{-1} and an assumed cell quota of 10 fg cell^{-1}) of 4×10^3 cells L^{-1} is three orders of magnitude higher than the LOD of the qPCR analysis, which is about 2 cells L^{-1} , and this explain a lack of AZA signals in areas where qPCR signals were low (Fig. 4). AZA-1, which is yet known only from *Az. spinosum* (Tillmann et al., 2009, 2018) was present in low amounts only at station 10, the only station where the qPCR-determined abundance of *Az. spinosum* was > 10 cells L^{-1} . Likewise, the detection of the two congeners AZA-38 and -39, which are up to now only known from *Am. languida* (Krock et al., 2019), corresponds to the highest abundances of *Am. languida* in the field. In the present study, amphidomatacean species-specific PCR assays are used for the first time in a quantitative way. Therefore, cell densities of AZA-producing species can be compared quantitatively to the concurrent AZA quantities. The corresponding AZA cell quota of *Am. languida* based on the cell abundance determined by qPCR and toxin amount determined by LC–MS/MS at station 14 was estimated as ca. 900 fg cell^{-1} . This is relatively high compared to laboratory studies on the AZA content of this species. AZA cell quotas estimated for various *Am. languida* strains range between 2.4 and 38.1 fg cell^{-1}

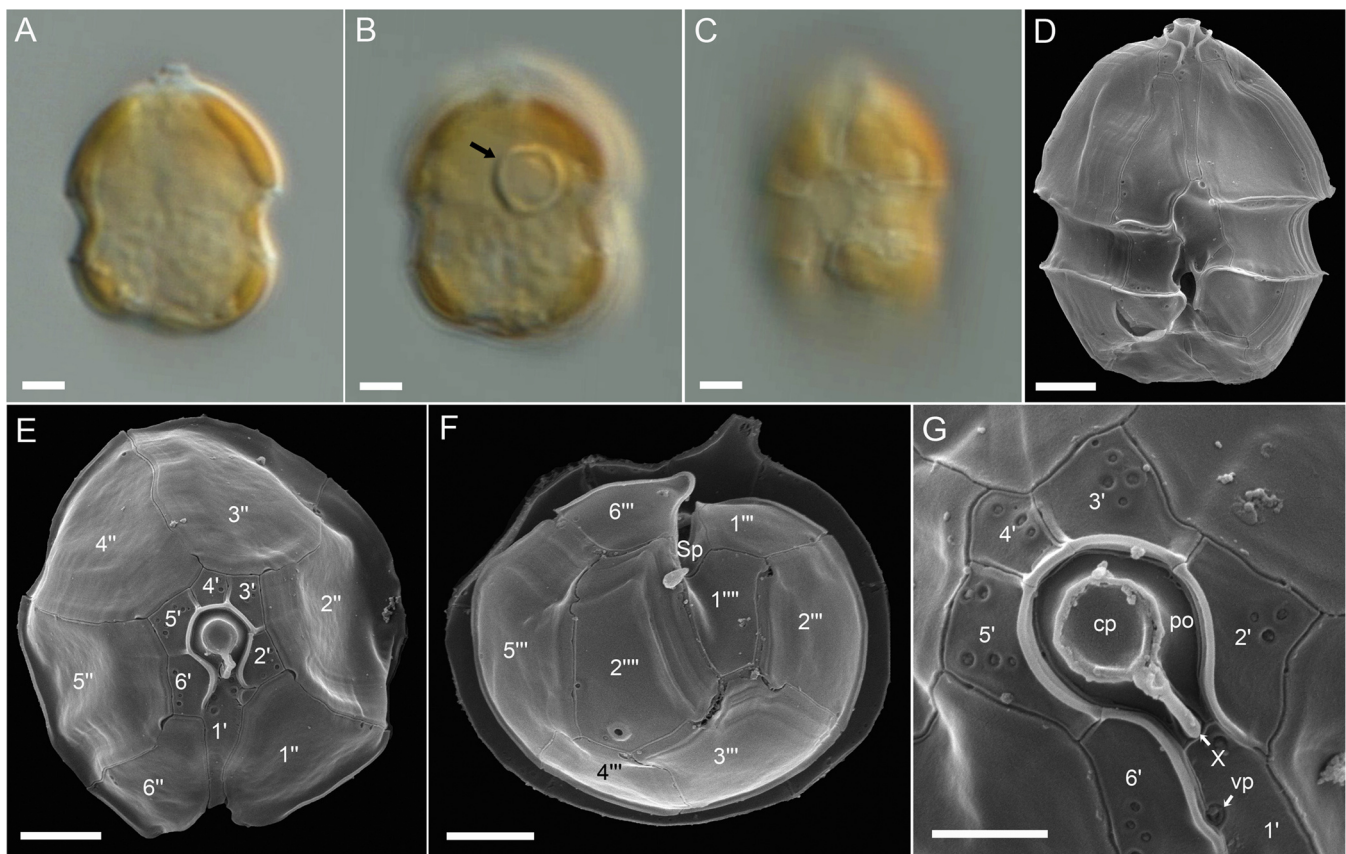


Fig. 9. Light and scanning electron micrographs of *Amphidoma languida* (strain LF-14-F02). (A–C) LM, living cells in ventral (A, B) or ventral lateral lateral (C) view. Note the pyrenoid in the episome (arrow in B). (D–G) SEM. (D) Whole cell in ventral view. (E) Epithelial plates in antapical view. (F) Hypothecal plates in antapical view. (G) Detailed view of the apical pore complex with the ventral pore. Plate labels according to the Kofoidian system. Sp = posterior sulcal plate, cp = cover plate, X = X-plate, vp = ventral pore, po = pore plate. Scale bars = 2 μm (A–F) or 1 μm (G).

(Tillmann et al., 2015, 2017a, 2018), but among the new strains may be as high as ca. 100 fg cell⁻¹ (this study). For AZA-1 and *Az. spinosum* at station 9, a respective cell quota calculation revealed a quota of 2,700 fg AZA cell⁻¹. This is also substantially higher compared to published lab study based AZA cell quotas for this species. These normally are in the range of 10–20 fg cell⁻¹, and only exceptionally can reach ca. 200 fg cell⁻¹ at low temperatures (Jaufrais et al., 2013).

There are multiple factors potentially contributing to such a mismatch between field sample based and laboratory based toxin cell quota estimates. Toxin analysis of field samples may not only include toxins of intact Amphidomataceae cells but also toxins associated with small protistan grazers and/or detritus. Moreover, toxin production of field populations might generally be higher compared to strains grown under artificial conditions in the laboratory. Nutrient concentrations, which often are unrealistically high in cultures or chemical cues of grazers are two examples of factors that are discussed to affect microalgal toxin production (Anderson et al., 1990; Lundholm et al., 2018). And last, but not least, qPCR quantification, which generally is challenging for low target concentrations, can be biased by differences in copy numbers between the strain used to prepare standard curves and the field population (Galluzzi et al., 2010). In the present study, however, the local Limfjord strain LF-09-C09 of *Am. languida* was used for quantification. Adding known numbers of cells of this strain to field samples of a previous study revealed a recovery of almost 100% (Wietkamp et al., 2019). In conclusion, for a clarification of the high calculated cell quota further detailed studies are needed.

In case of *Az. spinosum*, the discrepancy might also be related to specificity of the qPCR assay. The specific primer/probe set for *Az. spinosum* was published by Toebe et al. (2013) based on the DNA of strains that were available at that time. Now, with many more available

strains of *Az. spinosum*, significant genetic variability with at least three different ribotypes within *Az. spinosum* is evident (Tillmann et al., 2019), and that different *Az. spinosum* ribotypes co-occur in the North Sea (southern Norway, Tillmann et al., 2018). It thus has to be kept in mind that sequence differences between the primers/probes and the LSU of the local field sample population may have affected efficiency and therefore quantification (underestimation) of the qPCR assay.

4.3. *Azadinium poporum*

The most interesting finding based on the new Danish strains is that there is a non-AZA producing ribotype of *Az. poporum* present in the area. The species is described based on three strains from the southern Danish North Sea coast (Tillmann et al., 2011). These strains, albeit initially reported as non-AZA producers, are the source of AZA-37 (Krock et al., 2015), which was unknown at the time when the species was described. Over the last years, a significant diversity of *Az. poporum* strains, both in AZA profile and sequence data has become evident (Gu et al., 2013; Krock et al., 2014; Luo et al., 2018), and strains without detectable AZA are known as well (Krock et al., 2014; Luo et al., 2018). A significant number of non-AZA producing strains were recently reported from the Greek Mediterranean area, and interestingly the new Limfjord strain clusters in Ribotype A2 together with those strains (Fig. 10). However, absence of AZA is not consistently related to this ribotype, as traces of AZA are present in some of the Greek strains (Luo et al., 2018), and one Mediterranean Ribotype A2 strain from Corsica (TIO256) produce significant amounts of AZA-2 (Luo et al., 2017). For the North Sea Ribotype A2 strain LF-14-E12, even very high biomass samples did not reveal any traces of AZA indicating that in the southern North Sea a non-toxic ribotype of *Az. poporum* co-occurs with AZA-

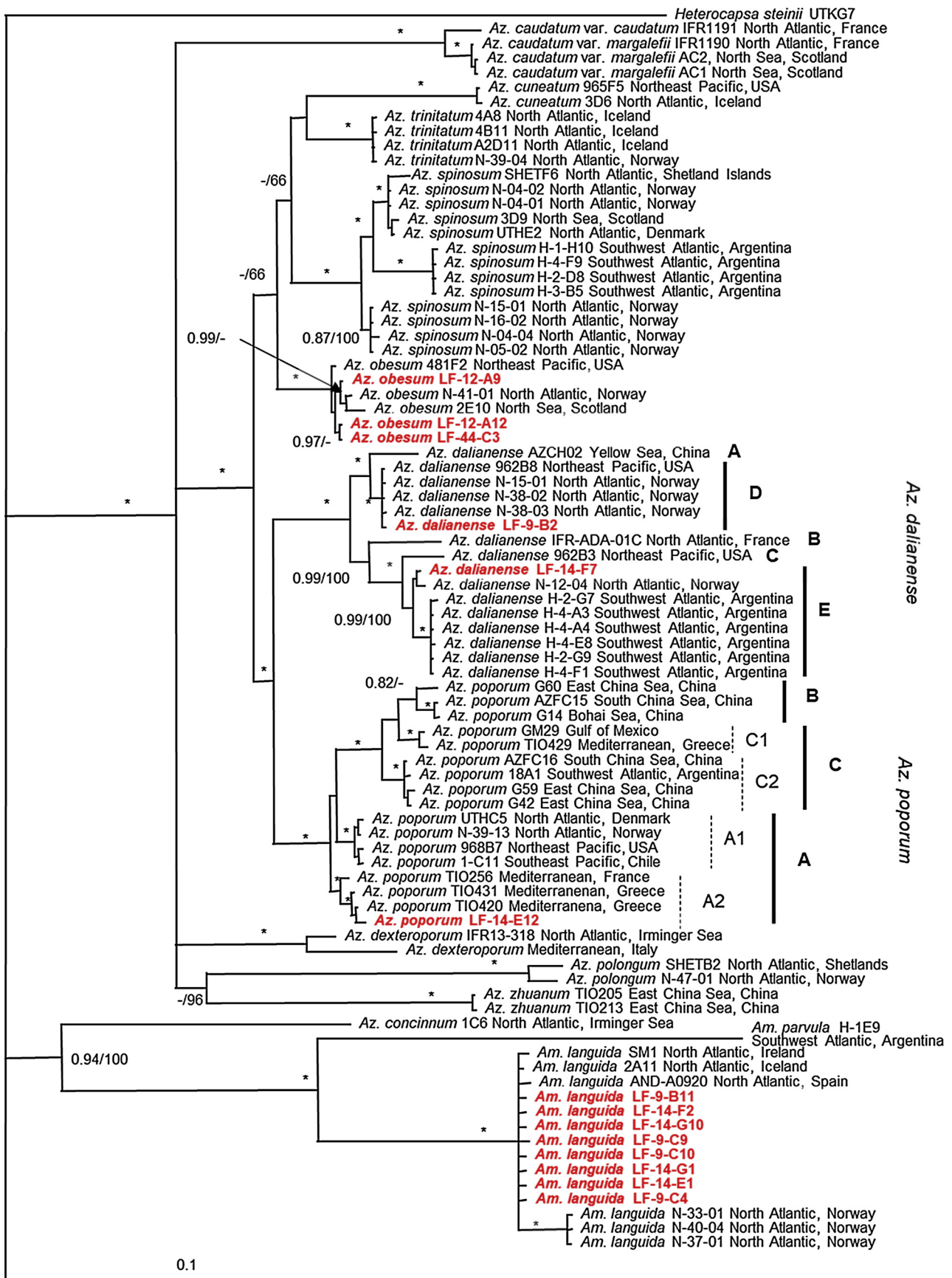


Fig. 10. Phylogeny of *Azadinium obesum*, *Az. dalianense*, *Az. poporum* and *Amphidoma languida* inferred from concatenated SSU, ITS and partial LSU rDNA sequences using Maximum likelihood (ML). *Heterocapsa steinii* was used as outgroup. New sequences are indicated in red. Ribotypes are labeled and marked with vertical lines on the right, with dashed lines indicating subribotypes. Branch lengths are drawn to scale, with the scale bar indicating the number of nucleotide substitutions per site. Numbers on branches are statistical support values to clusters on the right of them (left: Bayesian posterior probabilities; right: ML bootstrap support values). * indicate maximal support (BPP = 1.00 and ML BS = 100). (For interpretation of the references to colour in this figure legend, the reader is referred to the web version of this article).

37 producing Ribotype A strains. Concerning the qPCR quantification of the new *Az. poporum* strain LF-14-E12, there is only one base mismatch within the forward primer sequence, which makes the assay theoretically still suitable for this strain, but further tests have to be performed to confirm that.

4.4. The new AZA-63

Next to AZA-1, -38 and -39, LC-MS/MS analysis of field samples revealed the presence of the new AZA-63 with a pseudo-molecular mass of m/z 844. The record of a mass transition of $844 > 826$ was unexpected, since this mass transition is only known for AZA-4 and -5, and both compounds are exclusively known as shellfish metabolites and not from plankton. Nonetheless, the similarity of its CID spectrum with the one of AZA-37, which is produced by the Ribotype A strains of *A. poporum* in the North Sea (Krock et al., 2012, 2015), is strong evidence that both, AZA-37 and AZA-63 are structurally very similar. AZA-63 is 2 Da smaller than AZA-37, but the CID spectra of both AZA are practically identical up to the fragment m/z 686, which indicates that both AZA share the same structure between C9 and C40 including the lacking double bond in the A-ring. But whereas the pseudo-molecular ion cluster of AZA-37 shows an elimination of CO_2 followed by water losses, which is only observed in 3-hydroxylated AZA (Krock et al., 2012), a loss of CO_2 was not observed in the CID spectrum of AZA-63. The missing CO_2 elimination is clear evidence that AZA-63 is not 3-hydroxylated. The theoretic removal of one oxygen atom from AZA-37 results in a 14 Da lower mass than the mass of AZA-63. The mass difference between the theoretical non-hydroxylated AZA-37 and AZA-63 is equivalent to a methyl (or methylene) group. As the fragments up to m/z 686 are shared among both AZA, the methylation site can only be located between C2 and C8. Taking into account that C8 is methylated in many AZA and no AZA with a methylation of the carboxylic side chain are known, the methylation at C8 is a best guess and a structure of AZA-63 is proposed as 7,8-hydro-8-methyl-AZA-1 (Fig. 5C), but needs unambiguous structural confirmation by NMR.

The low abundance of AZA-63 in the field samples and the unavailability of an AZA-63 producing strain make full structural elucidation via nuclear magnetic resonance spectroscopy of this novel AZA variant impossible. The detection of AZA-63 in field samples at station 9 and 14 coincided with highest cell densities of *Am. languida* estimated by qPCR, but AZA-63 was not found in any of the new *Am. languida* strains. On the other side, *A. poporum* was detected on these stations by molecular markers as well. Given the high structural similarity of AZA-63 and AZA-37, it is reasonable to assume that *A. poporum* is the producing organism of AZA-63 in the North Sea. This, together with the detection of non-AZA Ribotype A2 strain LF-14-E12 in the Limfjord highlights the fact that AZA variability in Atlantic strains of *A. poporum* might be higher than currently known and more strains are needed to fully investigate the AZA profiles present in the North Sea.

5. Conclusion

The multi-method approach combining field sample light microscopy, real-time quantitative PCR, and toxin analysis with strain establishment and characterization coherently confirmed the occurrence and distribution of (toxigenic) amphidomatacean species along the Danish coast. The study further revealed that AZA-producing species were more restricted to the higher saline North Sea area including the western Limfjord, and - in low abundance - to the most northern Kattegat stations. The distribution of AZA-producing species along the Danish coast in 2016 revealed a potential link to salinity, but Amphidomataceae in general seem to be able to cope with a wide range of salinities. In summer 2016, abundance of Amphidomataceae was generally low and AZA toxins were only sporadically detected in low amounts, indicating a low risk of AZA shellfish contamination in the area. However, the toxigenic species are present, and it is well known

that the development of particular plankton species can be sporadic or intermittent, and that unexpected and exceptional bloom events may occur. Future studies should more specifically target temporal variability (time series) of Amphidomataceae and AZA for a thorough evaluation of the AZP risk assessment in Danish waters. Because of the relatively high abundance of *Amphidoma languida* and its toxins in the area, AZA-38 and -39 may be considered for routine toxin analysis as both could be easily included in existing AZA analytical protocols. The application of specific PCR assays to detect and quantify all three North Atlantic AZA producers proved to be a powerful and sensitive tool for biogeographic and also for monitoring studies. Local monitoring programs might thus consider including molecular assays of toxigenic Amphidomataceae as it is current practice for the Irish phytoplankton monitoring program (Dave Clarke, Marine Institute, Galway/Ireland, pers. com.). For implementation, however, it has to be kept in mind that diversity assessment of Amphidomataceae is still ongoing, and thus assay updates ensuring assay specificity are envisaged in the near future. Likewise, a multiplex method allowing a simultaneous and thus time- and cost-effective quantification of all three North-Atlantic AZA-producers is being developed but is not yet available.

Acknowledgements

Captain Lührs and the entire crew of *RV Uthörn* provided assistance and logistical support for the collection of field material used in this study. Per Juel Hansen (Uni Copenhagen) is acknowledged for logistic support, and Rohan Henkel, Kai Schwalfenberg and Anna Friedrichs of ICBM, and Annegret Müller of AWI for their help with onboard work during the cruise and especially Torben Krohn also for toxin extraction and analysis.

Financial support was provided by the PACES research program of the Alfred Wegener Institute as part of the Helmholtz Foundation initiative in Earth and Environment, by the Innovation Fund Denmark through the HABFISH project (Project No. 0603-00449B), and by the German Ministry for Education and Research (project RIPAZA, 03F0763A).[SS]

Appendix A. Supplementary data

Supplementary material related to this article can be found, in the online version, at doi:<https://doi.org/10.1016/j.hal.2019.101637>.

References

- Akselman, R., Negri, R.M., 2012. Blooms of *Azadinium cf. spinosum* Elbrächter et Tillmann (Dinophyceae) in northern shelf waters of Argentina, Southwestern Atlantic. *Harmful Algae* 19, 30–38.
- Amzil, Z., Sibat, M., Royer, F., Savar, V., 2008. First report on azaspiracid and yessotoxin groups detection in French shellfish. *Toxicon* 52 (1), 39–48.
- Anderson, D.M., Kulis, D.M., Sullivan, J.J., Hall, S., Lee, C., 1990. Dynamics and physiology of saxitoxin production by the dinoflagellates *Alexandrium* spp. *Mar. Biol.* 104, 511–524.
- Boc, A., Diallo, A.B., Makarenkov, V., 2012. T-REX: a web server for inferring, validating and visualizing phylogenetic trees and networks. *Nucleic Acids Res.* 40 (W1), W573–W579.
- Braña Magdalena, A., Lehane, M., Kryš, S., Fernández, M.L., Furey, A., James, K.J., 2003. The first identification of azaspiracids in shellfish from France and Spain. *Toxicon* 42 (1), 105–108.
- Eckford-Soper, L.K., Daugbjerg, N., 2015. Development of a multiplex real-time qPCR assay for simultaneous enumeration of up to four marine toxic bloom-forming microalgal species. *Harmful Algae* 48, 37–43.
- Edwardsen, B., Dittami, S.M., Groben, R., Brubak, S., Escalera, L., Rodriguez, F., Reguera, B., Chen, J., Medlin, L.K., 2013. Molecular probes and microarrays for the detection of toxic algae in the genera *Dinophysis* and *Phalacrocoma* (Dinophyta). *Environ. Sci. Pollut. Res. Int.* 20 (10), 6733–6750.
- Forootan, A., Sjöback, R., Björkman, J., Sjögreen, B., Linz, L., Kubista, M., 2017. Methods to determine limit of detection and limit of quantification in quantitative real-time PCR (qPCR). *Biomol. Detect. Quantif.* 12, 1–6.
- Furey, A., O'Doherty, S., O'Callaghan, K., Lehane, M., James, K.J., 2010. Azaspiracid poisoning (AZP) toxins in shellfish: toxicological and health considerations. *Toxicon* 56 (2), 173–190.
- Galluzzi, L., Bertozzini, E., Penna, A., Perini, F., Garcés, E., Magnani, M., 2010. Analysis

- of rRNA gene content in the Mediterranean dinoflagellate *Alexandrium catenella* and *Alexandrium taylori*: implications for the quantitative real-time PCR-based monitoring methods. *J. Appl. Phycol.* 22 (1), 1–9.
- Gu, H., Luo, Z., Krock, B., Witt, M., Tillmann, U., 2013. Morphology, phylogeny and azaspiracid profile of *Azadinium poporum* (Dinophyceae) from the China Sea. *Harmful Algae* 21–22, 64–75.
- Hall, T.A., 1999. BioEdit: A User-Friendly Biological Sequence Alignment Editor and Analysis Program for Windows 95/98/NT. Nucleic Acids Symposium Series. Information Retrieval Ltd., London, pp. 95–98 c1979-c2000.
- Jakobsen, R., Hansen, P.J., Daugbjerg, N., Andersen, N.G., 2012. The fish-killing ditychophyte *Pseudochattonella farcimen*: adaptations leading to bloom formation during early spring in Scandinavian waters. *Harmful Algae* 18, 84–95.
- James, K.J., Furey, A., Lehane, M., Ramstad, H., Aune, T., Hovgaard, P., Morris, S., Higman, W., Satake, M., Yasumoto, T., 2002. First evidence of an extensive northern European distribution of azaspiracid poisoning (AZP) toxins in shellfish. *Toxicol.* 40 (7), 909–915.
- Jauffrais, T., Séchet, V., Herrenknecht, C., Truquet, P., Savar, V., Tillmann, U., Hess, P., 2013. Effect of environmental and nutritional factors on growth and azaspiracid production of the dinoflagellate *Azadinium spinosum*. *Harmful Algae* 27, 138–148.
- Jørgensen, K., Andersen, P., 2007. Relation between the concentration of *Dinophysis acuminata* and diarrhetic shellfish poisoning toxins in blue mussels (*Mytilus edulis*) during a toxic episode in the Limfjord (Denmark), 2006. *J. Shellfish Res.* 26 (4), 1081–1087.
- Katoh, K., Standley, D.M., 2013. MAFFT multiple sequence alignment software version 7: improvements in performance and usability. *Mol. Biol. Evol.* 30 (4), 772–780.
- Keller, M.D., Selvin, R.C., Claus, W., Guillard, R.R.L., 1987. Media for the culture of oceanic ultraphytoplankton. *J. Phycol.* 23 (4), 633–638.
- Kim, J.H., Tillmann, U., Adams, N.G., Krock, B., Stutts, W.L., Deeds, J.R., Han, M.S., Trainer, V.L., 2017. Identification of *Azadinium* species and a new azaspiracid from *Azadinium poporum* in Puget Sound, Washington State, USA. *Harmful Algae* 68, 152–167.
- Krock, B., Tillmann, U., Alpermann, T.J., Voß, D., Zielinski, O., Cembella, A.D., 2013. Phycotoxin composition and distribution in plankton fractions from the German Bight and western Danish coast. *J. Plankton Res.* 35 (5), 1093–1108.
- Krock, B., Tillmann, U., John, U., Cembella, A.D., 2009. Characterization of azaspiracids in plankton size-fractions and isolation of an azaspiracid-producing dinoflagellate from the North Sea. *Harmful Algae* 8 (2), 254–263.
- Krock, B., Tillmann, U., Potvin, É., Jeong, H.J., Drebing, W., Kilcoyne, J., Al-Jorani, A., Twiner, M.J., Göthel, Q., Köck, M., 2015. Structure elucidation and in vitro toxicity of new azaspiracids isolated from the marine dinoflagellate *Azadinium poporum*. *Mar. Drugs* 13 (11), 6687–6702.
- Krock, B., Tillmann, U., Tebben, J., Trefault, N., Gu, H., 2019. Two novel azaspiracids from *Azadinium poporum*, and a comprehensive compilation of azaspiracids produced by Amphidomataceae, (Dinophyceae). *Harmful Algae* 82, 1–8.
- Krock, B., Tillmann, U., Voß, D., Koch, B.P., Salas, R., Witt, M., Potvin, E., Jeong, H.J., 2012. New azaspiracids in Amphidomataceae (Dinophyceae). *Toxicol.* 60 (5), 830–839.
- Krock, B., Tillmann, U., Witt, M., Gu, H.F., 2014. Azaspiracid variability of *Azadinium poporum* (Dinophyceae) from the China Sea. *Harmful Algae* 36, 22–28.
- Krock, B., Zielinski, O., Friedrichs, A., Henkel, R., Schwalfenberger, K., Voß, D., 2017. Physical oceanography during UTHÖRN cruise UT201606 (HAB-DK/Limfjord). PANGAEA. <https://doi.org/10.1594/PANGAEA.874076>.
- Livak, K., 1997. ABI Prism 7700 sequence detection system. *User Bull.* 2, 1–36.
- Lundholm, N., Krock, B., John, U., Skov, J., Cheng, J., Pančić, M., Wohlrab, S., Rigby, K., Nielsen, T.G., Selander, E., 2018. Induction of domoic acid production in diatoms - types of grazers and diatoms are important. *Harmful Algae* 79, 64–73.
- Luo, Z., Krock, B., Giannakourou, A., Venetsanopoulou, A., Pagou, K., Tillmann, U., Gu, H., 2018. Sympatric occurrence of two *Azadinium poporum* ribotypes in the Eastern Mediterranean Sea. *Harmful Algae* 78, 75–85.
- Luo, Z.H., Krock, B., Mertens, K.N., Nézan, E., Chomérat, N., Billen, G., Tillmann, U., Gu, H., 2017. Adding new pieces to the *Azadinium* (Dinophyceae) diversity and biogeography puzzle: Non-toxicogenic *Azadinium zhuanum* sp. nov. from China, toxicogenic *A. poporum* from the Mediterranean, and a non-toxicogenic *A. dalianense* from the French Atlantic. *Harmful Algae* 66, 65–78.
- Maar, M., Larsen, J., Dahl, K., Riemann, B., 2018. Modelling the environmental impacts of future offshore fish farms in the inner Danish waters. *Aquacult. Env. Interact.* 10, 115–133.
- Mc Mahon, T., Silke, J., 1996. Winter toxicity of unknown aetiology in mussels. *Harmful Algae News* 14 (2), 1998.
- Moestrup, Ø., Hansen, G., Daugbjerg, N., Lundholm, N., Overton, J., Vestergård, M., Steenfeldt, S.J., Calado, A.J., Hansen, P.J., 2014. The dinoflagellates *Pfiesteria shumwayae* and *Luciella masanensis* cause fish kills in recirculation fish farms in Denmark. *Harmful Algae* 32, 33–39.
- Penna, A., Galluzzi, L., 2013. The quantitative real-time PCR applications in the monitoring of marine harmful algal bloom (HAB) species. *Environ. Sci. Pollut. Res.* 20 (10), 6851–6862.
- Percopo, I., Siano, R., Rossi, R., Soprano, V., Sarno, D., Zingone, A., 2013. A new potentially toxic *Azadinium* species (Dinophyceae) from the Mediterranean Sea, *A. dexteroporium* sp. nov. *J. Phycol.* 49 (5), 950–966.
- Posada, D., 2008. jModelTest: phylogenetic model averaging. *Mol. Biol. Evol.* 25 (7), 1253–1256.
- Preston-Thomas, H., 1990. The international temperature scale of 1990 (ITS-90). *Metrologia* 27 (1), 3.
- Ronquist, F., Huelsenbeck, J.P., 2003. MrBayes 3: bayesian phylogenetic inference under mixed models. *Bioinformatics* 19 (12), 1572–1574.
- Ruijter, J.M., Ramakers, C., Hoogaars, W.M.H., Karlen, Y., Bakker, O., van den Hoff, M.J.B., Moorman, A.F.M., 2009. Amplification efficiency: linking baseline and bias in the analysis of quantitative PCR data. *Nucleic Acids Res.* 37 (6), e45.
- Salas, R., Tillmann, U., John, U., Kilcoyne, J., Bursan, A., Cantwell, C., Hess, P., Jauffrais, T., Silke, J., 2011. The role of *Azadinium spinosum* (Dinophyceae) in the production of azaspiracid shellfish poisoning in mussels. *Harmful Algae* 10 (6), 774–783.
- Smith, K.F., Rhodes, L., Harwood, D.T., Adamson, J., Moisan, C., Munday, R., Tillmann, U., 2016. Detection of *Azadinium poporum* in New Zealand: the use of molecular tools to assist with species isolations. *J. Appl. Phycol.* 28 (2), 1125–1132.
- Stamatakis, A., 2006. RAxML-VI-HPC: maximum likelihood-based phylogenetic analyses with thousands of taxa and mixed models. *Bioinformatics* 22 (21), 2688–2690.
- Tillmann, U., 2018. Amphidomataceae. In: Shumway, S.E., Burkholder, J.A., Morton, S.L. (Eds.), *Harmful Algae Blooms, A Compendium Desk Reference*. Wiley, Hoboken, pp. 575–582.
- Tillmann, U., Edvardsen, B., Krock, B., Smith, K.F., Paterson, R.F., Voß, D., 2018. Diversity, distribution, and azaspiracids of Amphidomataceae (Dinophyceae) along the Norwegian coast. *Harmful Algae* 80, 15–34.
- Tillmann, U., Elbrächter, M., John, U., Krock, B., 2011. A new non-toxic species in the dinoflagellate genus *Azadinium*: *A. poporum* sp. nov. *Eur. J. Phycol.* 46 (1), 74–87.
- Tillmann, U., Elbrächter, M., John, U., Krock, B., Cembella, A., 2010. *Azadinium obesum* (Dinophyceae), a new nontoxic species in the genus that can produce azaspiracid toxins. *Phycologia* 49 (2), 169–182.
- Tillmann, U., Elbrächter, M., Krock, B., John, U., Cembella, A., 2009. *Azadinium spinosum* gen. et sp. nov. (Dinophyceae) identified as a primary producer of azaspiracid toxins. *Eur. J. Phycol.* 44 (1), 63–79.
- Tillmann, U., Gottschling, M., Krock, B., Smith, K.F., Gunder, V., 2019. High abundance of Amphidomataceae (Dinophyceae) during the 2015 spring bloom of the Argentinean Shelf and a new, non-toxicogenic ribotype of *Azadinium spinosum*. *Harmful Algae* 84, 244–260.
- Tillmann, U., Gottschling, M., Nézan, E., Krock, B., 2015. First records of *Amphidoma languida* and *Azadinium dexteroporium* (Amphidomataceae, Dinophyceae) from the Irminger Sea off Iceland. *Mar. Biodivers. Rec.* 8, 1–11.
- Tillmann, U., Jaén, D., Fernández, L., Gottschling, M., Witt, M., Blanco, J., Krock, B., 2017a. *Amphidoma languida* (Amphidomataceae, Dinophyceae) with a novel azaspiracid toxin profile identified as the cause of mollusc contamination at the Atlantic coast of southern Spain. *Harmful Algae* 62, 113–126.
- Tillmann, U., Sánchez-Ramírez, S., Krock, B., Bernal-Jiménez, A., 2017b. A bloom of *Azadinium polongum* in coastal waters off Peru. *Rev. Biol. Mar. Oceanogr.* 52 (3), 591–610.
- Tillmann, U., Trefault, N., Krock, B., Parada-Pozo, G., De la Iglesia, R., Vásquez, M., 2017c. Identification of *Azadinium poporum* (Dinophyceae) in the Southeast Pacific: morphology, molecular phylogeny, and azaspiracid profile characterization. *J. Plankton Res.* 39 (2), 350–367.
- Toebe, K., Joshi, A.R., Messtorff, P., Tillmann, U., Cembella, A., John, U., 2013. Molecular discrimination of taxa within the dinoflagellate genus *Azadinium*, the source of azaspiracid toxins. *J. Plankton Res.* 35 (1), 225–230.
- Twiner, M.J., Hess, P., Doucette, G., 2014. Azaspiracids: toxicology, pharmacology, and risk assessment. *Seafood and Freshwater Toxins*. pp. 823–855.
- Vale, P., Biré, R., Hess, P., 2008. Confirmation by LC-MS/MS of azaspiracids in shellfish from the Portuguese north-western coast. *Toxicol.* 51 (8), 1449–1456.
- Wietkamp, S., Tillmann, U., Clarke, D., Toebe, K., 2019. Molecular detection and quantification of the azaspiracid-producing dinoflagellate *Amphidoma languida* (Amphidomataceae, Dinophyceae). *J. Plankton Res.* 41 (2), 101–113.

Publication III: Amphidomataceae in Greenland and *Az. perforatum* sp. nov.

Amphidomataceae (Dinophyceae) in the western Greenland area, including description of *Azadinium perforatum* sp. nov. *Phycologia*

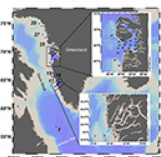
Tillmann, U., Wietkamp, S., Krock, B., Tillmann, A., Voss, D., Gu, H. (2020)

Publication III describes a field study on Amphidomataceae conducted in the central Labrador Sea and western Greenland coast in 2017.

The aims of this study were 1) to assess the occurrence, diversity and abundance of Amphidomataceae in high latitudes and 2) to investigate especially the toxigenic amphidomatacean species.

Taxonomic research in high latitudes have a long history, and current dramatic temperature rises especially at the north pole potentially lead to significant changes in phytoplankton diversity, distribution, community structure, growth and life cycles. Results indicated the presence of Amphidomataceae (with at least eight species) detected by microscopy, which was subsequently confirmed by many positive hits for DNA analyses in the family-specific qPCR assay. However, field sample toxin analyses were negative for AZA. Species-specific qPCR assays revealed the occurrence of toxigenic *Az. poporum* and *Am. languida* at just a very few stations and in very low abundances. In addition, a so far unknown dinoflagellate has been isolated and turned out as a new amphidomatacean species, named *Azadinium perforatum* sp. nov.

The candidate contributed to this study by analyzing filtered seawater samples from each station on the presence of amphidomatacean DNA via the family- and species-specific qPCR assays (100%). Furthermore, he performed DNA sequencing and data analysis of LSU, ITS and SSU sequences for molecular characterization of 18 established strains (90%). He contributed to the manuscript preparation (25%) led by Dr. U. Tillmann (AWI) with focus on the molecular part.






Amphidomataceae (Dinophyceae) in the western Greenland area, including description of *Azadinium perforatum* sp. nov.

Urban Tillmann, Stephan Wietkamp, Bernd Krock, Anette Tillmann, Daniela Voss & Haifeng Gu

To cite this article: Urban Tillmann, Stephan Wietkamp, Bernd Krock, Anette Tillmann, Daniela Voss & Haifeng Gu (2020) Amphidomataceae (Dinophyceae) in the western Greenland area, including description of *Azadinium perforatum* sp. nov., *Phycologia*, 59:1, 63-88, DOI: [10.1080/00318884.2019.1670013](https://doi.org/10.1080/00318884.2019.1670013)


To link to this article: <https://doi.org/10.1080/00318884.2019.1670013>

 View supplementary material 

 Published online: 02 Dec 2019.

 Submit your article to this journal 

 Article views: 68

 View related articles 

 View Crossmark data 



Amphidomataceae (Dinophyceae) in the western Greenland area, including description of *Azadinium perforatum* sp. nov.

URBAN TILLMANN¹, STEPHAN WIETKAMP¹, BERND KROCK¹, ANETTE TILLMANN¹, DANIELA VOSS², AND HAIFENG GU ³

¹Alfred-Wegener-Institute, Helmholtz Centre for Polar and Marine Research, Am Handelshafen 12, Bremerhaven, D-27570, Germany

²Institute for Chemistry and Biology of the Marine Environment (ICBM), Carl von Ossietzky Universität Oldenburg, Schleusenstraße 1, Wilhelmshaven, D-26382, Germany

³Third Institute of Oceanography, Ministry of Natural Resources, Xiamen, 361005, China

ABSTRACT

Azaspiracids (AZA) are lipophilic marine biotoxins associated with shellfish poisoning which are produced by some species of Amphidomataceae. Diversity and global biogeography of this family are still poorly known. In summer 2017 plankton samples were collected from the central Labrador Sea and western Greenland coast from 64° N (Gothaab Fjord) to 75° N for the presence of Amphidomataceae and AZA. In the central Labrador Sea, light microscopy revealed small *Azadinium*-like cells (9200 cells l⁻¹). Clonal strains established from plankton samples and scanning electron microscopy of fixed plankton samples revealed at least eight species of Amphidomataceae: *Azadinium obesum*, *Az. trinitatum*, *Az. dexteroporum*, *Az. spinosum*, *Az. polongum*, *Amphidoma languida*, *Azadinium* spec., and a new species described here as *Azadinium perforatum* sp. nov. The new species differed from other *Azadinium* species by the presence of thecal pores on the pore plate. All samples, including cultured strains, filtered seawater samples, and solid phase adsorption toxin tracking (SPATT) samplers deployed during the expedition in a continuous water-sampling system (FerryBox), were negative for AZA. DNA samples and PCR assays were positive for Amphidomataceae from most stations, whereas species-specific assays for three toxigenic species were rarely positive (two stations for *Az. poporum*, one station for *Am. languida*). The results highlight the presence of Amphidomataceae in the area but the lack of toxins and low abundance of toxigenic species currently indicate a low risk of toxic Amphidomataceae blooms in Arctic coastal waters.

ARTICLE HISTORY

Received 16 May 2019
Accepted 17 September 2019
Published online 02
December 2019

KEYWORDS

Amphidoma; Azaspiracids;
New species; Subarctic

INTRODUCTION


Biodiversity and biogeography research of high latitude phytoplankton have a long history, starting with the first exploratory expeditions in the mid-19th and early twentieth century (Brandt & Apstein 1908; Cleve 1873; Cleve & Grunow 1880; Ehrenberg 1843; Gran 1929; Grontved & Seidenfaden 1938; Lebour 1925). Extensive lists of plankton species from these survey reports are still the basis for contemporary taxonomic research in the Arctic. Such historical work and also more recent taxonomic studies are needed as an indispensable baseline in order to fully evaluate potential change in species diversity, and distribution and community composition in the area. This is of special importance for Arctic and subarctic areas, as significant and rapid temperature changes unprecedented in the observational record are occurring. Temperatures in the Arctic are increasing at a rate of two to three times the global average temperature in the past 150 years (Wassmann *et al.* 2011). Along with decreasing ice cover and increasing solar irradiance, temperature increases are expected to expand the spatial and temporal windows for survival, life cycle transitions and growth of a variety of plankton species, including those responsible for toxic, or harmful, algal blooms (HABs).

Current knowledge of Arctic plankton species diversity is biased towards large species collected and observed by classical plankton nets and light microscopy. Thus, species < 20 µm account for fewer than 20% of species in a more recent assessment of pan-Arctic biodiversity (Poulin *et al.* 2011). Recent biodiversity assessments of the area are based mainly on high throughput sequencing (Metfies *et al.* 2012; Elferink *et al.* 2017; Kiliyas *et al.* 2013, 2014; Wolf *et al.* 2015). While this approach reveals high diversity, especially in low size fractions (Elferink *et al.* 2017), high throughput sequencing still lacks species-level taxonomic resolution. However, species identification is especially necessary where closely related toxic and non-toxic species occur. Moreover, molecular diversity estimates always reveal a high degree of molecular signatures which cannot be linked to defined morphospecies (Medinger *et al.* 2010; Xiao *et al.* 2014), and this underlines the continuous and even increasing need for alpha taxonomy.

Azadinium and *Amphidoma* are the only genera of Amphidomataceae. They are good examples of small-sized nanoplankton described in the last decade, whose distribution and species diversity are not yet fully explored. This dinophycean family is of particular interest because some species produce

CONTACT Urban Tillmann  urban.tillmann@awi.de

Colour versions of one or more of the figures in the article can be found online at www.tandfonline.com/uphy.

 Supplemental data for this article can be accessed on the publisher's website.

© 2019 International Phycological Society

azaspiracids (AZA), a group of lipophilic compounds which accumulate in shellfish (Hess *et al.* 2014; Twiner *et al.* 2014). The presence of AZA in field plankton samples and/or shellfish in Arctic and subarctic areas has not yet been reported, but that might reflect a lack of targeted studies. In any case, there is evidence for the presence of Amphidomataceae in cold northern waters. The non-toxigenic *Azadinium caudatum* (Halldal) Nézan & Chomérat was described from the northern Norwegian coast in winter (Halldal 1953) and is common, and at times numerous, along the Norwegian coast (Thronsen *et al.* 2007). A dinophyte described as *Gonyaulax parva* Ramsfjell from the central Norwegian Sea towards Iceland (Ramsfjell 1959) is almost certainly a species of *Azadinium* (see discussion in Tillmann *et al.* 2014a); furthermore, other species from the Canadian Arctic (Bérard-Therriault *et al.* 1999; Holmes 1956), labelled as '*Goniaulax gracilis*' (which was depicted and invalidly described by J. Schiller in 1935), probably refers to a species of *Azadinium* (see discussion in Tillmann *et al.* 2014a). Finally, three new, but non-toxigenic, species of *Azadinium*, *Az. trinitatum* Tillmann & Nézan, *Az. cuneatum* Tillmann & Nézan, and *Az. concinnum* Tillmann & Nézan, were recently described from the North Atlantic Ocean around Iceland and the Irminger Sea (Tillmann *et al.* 2014a). In addition, toxigenic *Amphidoma languida* Tillmann, Salas & Elbrächter (producing AZA-38 and -39) and non-toxigenic *Az. dexteroporum* Percopo & Zingone were isolated from the area as well (Tillmann *et al.* 2015). Presence, diversity and distribution of Amphidomataceae on the western Greenland coast are currently unknown. A main reason for a lack of records and distribution data is that many species of Amphidomataceae are small (<20 µm cell length) and inconspicuous, and thus often go unnoticed in routine light microscopy. Amphidomataceae are thus a good example of the necessity of applying specific molecular detection tools. A family-specific molecular PCR assay detecting all Amphidomataceae (Smith *et al.* 2016) and species-specific qPCR assays for three of the toxigenic species (Toebe *et al.* 2013; Wietkamp *et al.* 2019a) are both available. From a chemical perspective, detection of AZA using LC-MS/MS can be a complementary and sensitive analytical tool for records of toxigenic Amphidomataceae, especially when long-term Solid Phase Adsorption Toxin Tracking (SPATT) deployments allow for integration and amplification of low signal levels.

On a research survey on the *RV Maria S. Merian* to the west coast of Greenland, we combined traditional onboard live microscopy with qPCR molecular detection and LC-MS/MS analysis (both discrete plankton samples and continuously deployed SPATT samplers) to specifically investigate the presence, diversity and distribution of amphidomatacean species. This baseline information evaluates the risk potential of azaspiric acid shellfish poisoning (AZP) in subarctic and Arctic waters.

MATERIAL & METHODS

Hydrographic observations and sampling

Data were collected from 25 June to 19 July 2017 onboard *RV Maria S. Merian* (MSM65) in the central Labrador Sea and along the western coast of Greenland (Fig. 1). At each station, CTD profiles were conducted using a Seabird 'sbe911+' CTD (Sea-Bird Electronics Inc., Seattle, Washington, USA) attached to

a sampling rosette. The CTD was equipped with a chlorophyll fluorescence sensor (Fluorometer, WET Labs, Philomath, Oregon, USA). Data acquisition was carried out via CTD-client on-board; post-processing was done with Seasoft V2. Temperature was corrected to ITS-90 (Preston-Thomas 1990). A total of 50 CTD stations (Fig. 1) from the central Labrador Sea and along the western coast of Greenland were sampled from specific depths using Niskin bottles. CTD Profiles are available at Pangaea (Zielinski *et al.* 2018). Data from surface waters (Fig. 2) represent the upper 5 m of each CTD cast. Graphics were generated using Ocean Data View (ODV) software (Schlitzer 2018).

Besides CTD casts at each station, surface water of the whole cruise track was investigated for temperature, salinity (model SBE45, Sea-Bird Electronics Inc., Seattle, Washington, USA) and fluorescence (model cyclops 7, Turner Design Inc., San Jose, California, USA) using a Pocket FerryBox (4H Jena, Jena, Germany). Data are available on request. The outlet of the FerryBox offers further options for sampling, e.g., for toxins.

Sample processing

Niskin bottle samples from three depths (3 m, 10 m, and depth of the chlorophyll maximum) were fixed with Lugol's iodine (1% final concentration). For quantitative plankton counts, samples of these three depths were pooled, and 50 ml and 10 ml were settled in Utermöhl sedimentation chambers and counted with an IMR inverted microscope (Olympus, Hamburg, Germany). Counted subsample volume and magnification were adjusted for each species or protist group depending on the respective abundance. In addition, mixed water samples from three depths were used for on-board living plankton microscope observations. A 1-l sample was pre-screened (20 µm Nitex mesh) and gently concentrated by gravity filtration using a 5-µm polycarbonate filter (47-mm diameter, Millipore, Eschborn, Germany). A subsample was fixed with formaldehyde (1% final concentration) for later SEM analysis, and the rest was examined using an inverted microscope (Axiovert 200M, Zeiss, Göttingen, Germany). Samples were screened for cells of *Azadinium* and *Amphidoma* at high magnification (x640) based on general cell size and shape, on the presence of a theca, and on the presence of a distinctly pointed apex. Cells of interest were photographed with a digital camera (AxioCam MRc5, Zeiss).

DNA extraction and PCR analysis

Plankton samples were collected at each station with Niskin bottles from 3 m, 10 m and from the chlorophyll maximum layer. Three litres of seawater from each depth were pre-screened through a 20-µm mesh Nitex sieve, and subsequently pooled. An amount of 3–5 l (depending on particle content) was filtered under gentle vacuum (< 200 mbar) through 5-µm pore-size polycarbonate filters (47-mm diameter, Millipore). Filters were attached to the inner wall of a 50-ml plastic centrifuge tube, and repeatedly rinsed with 1 ml pre-heated (60 °C) DNA lysis buffer (PL 1 buffer of the NucleoSpin Plant II kit, Macherey & Nagel, Düren, Germany). The lysis buffer was subsequently transferred into a 5-ml cryovial prefilled with 200-mg glass beads (acid-washed, grain size 212–300 µm, Sigma Aldrich, St. Louis, Missouri, USA) and stored at –20 °C. Not later than 1 week

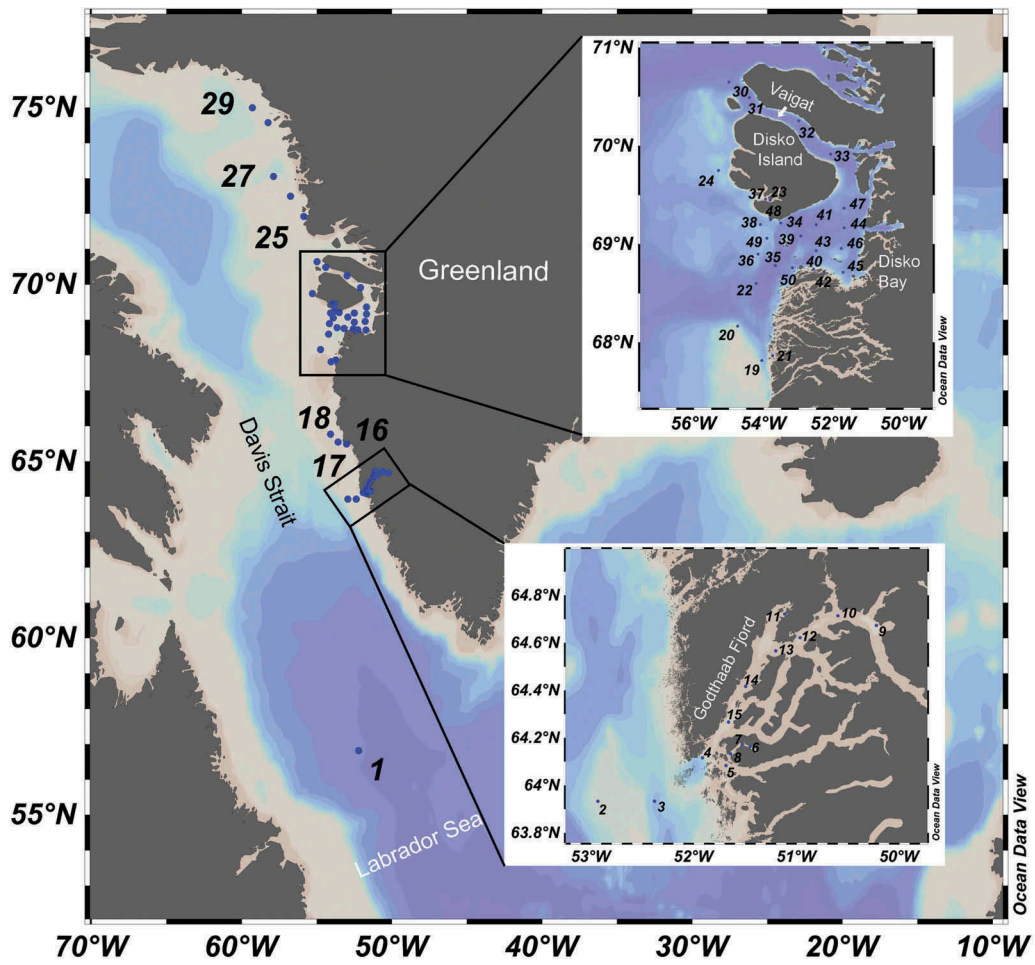


Fig. 1. Map of investigated area and location of stations of RV *Maria S. Merian* MSM65 cruise, 2017. Range in colours corresponds to different contour lines of water depth.

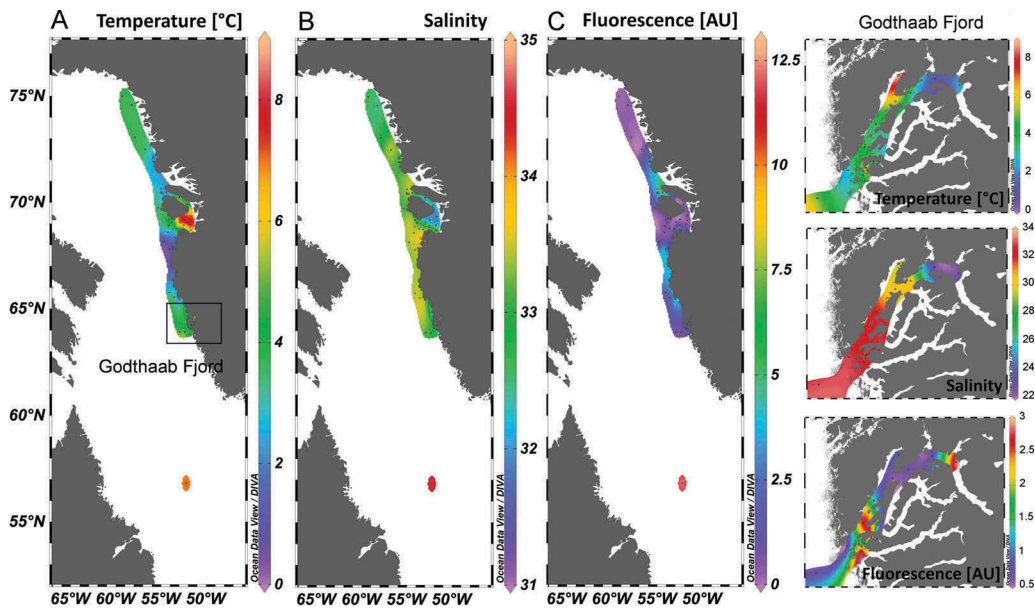


Fig. 2. Temperature (A), salinity (B) and fluorescence (C) in surface waters over the whole transect of the MSM65 campaign. The right panel shows cut-outs of the Godthaab Fjord area.

after sampling, DNA was extracted using the NucleoSpin Plant II kit (Macherey & Nagel) according to manufacturer's instructions.

SYBR Green PCR assays with family-specific amphidomatacean primers introduced by Smith *et al.* (2016) were performed on DNA extracts as a molecular pre-scanning method. One reaction contained 5 μl of Fast SYBR Green Master Mix (Applied Biosystems by Thermo Fisher Scientific, Waltham, Massachusetts, USA), 3.5 μl of high-grade PCR H_2O , 0.25 μl of both primers (each 10 μM , at a final concentration of 200 nM) and 1 μl of template DNA. Plates were analysed on a StepOne Plus real-time PCR cycler (Applied Biosystems by Thermo Fisher Scientific) following these steps: initial preheating to 95 °C for 20 s, 40 cycles of 3 s at 95 °C and 30 s at 60 °C. The subsequent melt curve was performed for 15 s at 95 °C, 60 s at 60 °C and 15 s at 95 °C. Positive controls with known DNA concentrations as well as no-template controls (NTC) containing high-grade, nuclease-free water, were present in all PCR reactions. Primer performance and reactions were evaluated in terms of specificity and sensitivity. Melt-curve analysis was done for every reaction. Samples were analysed in triplicate, and were considered positive if at least two of the three replicates showed a fluorescence signal above the threshold before cycle 37.

Samples which showed positive results in the SYBR Green assay were tested with specific TaqMan qPCR assays on *Az. spinosum*, *Az. poporum* and *Am. languida* as described in Toebe *et al.* (2013) and Wietkamp *et al.* (2019a). Measurements were performed in triplicate. Each run contained non-template controls (NTC) and positive controls. Quantitative analyses were based on DNA standard curves as tenfold dilution series of target species' DNA (10 ng μl^{-1} to 10 fg μl^{-1}) from cultures of *Az. spinosum* (3D9), *Az. poporum* (UTH-D4) and *Am. languida* (Z-LF-9-C9). For the limits of detection (LOD) and of quantification (LOQ), the definitions of Forootan *et al.* (2017) were applied. However, for standard curves of all three qPCR assays, the limited resolution of dilutions applied here did not allow differentiating between LOD and LOQ, which was 0.1 pg μl^{-1} sample extract.

Azaspiracids

For AZA analysis of field plankton samples from discrete depths, samples were prepared and filtered as described above. Filters were placed with their back to the inner wall of a 50-ml centrifuge tube (Sarstedt, Nümbrecht, Germany), and were repeatedly rinsed with 500–1000 μl methanol until complete decolouration of the filters. The methanolic extracts were transferred to a spin-filter (Ultrafree, 0.45- μm pore-size, Millipore, Eschborn, Germany), centrifuged for 30 s at 800 x g, followed by transfer into autosampler vials and stored at –20 °C until measurement.

Additional samples were taken using a FerryBox continuous sampling system. Solid Phase Adsorption Toxin Tracking (SPATT) bags (100- μm mesh, 10 g HP-20) were placed in a 7.5-l plastic container that was fed by the outflow of a FerryBox system at a flow rate of *c.* 2 litres min^{-1} , which in turn was supplied by the ship seawater system. During the entire expedition, three SPATT bags were deployed: SP1: 26 June (station 2) – 04 July (station 16), Labrador Sea – Godthaab Fjord (Nuup Kargerlua); SP2: 04 July (station 16) – 11 July (station 31),

Maniitsoq transect north – Vaigat (Sullorsuaq Strait); and SP3: 11 July (station 31) – 17 July (station 50), Vaigat – Disko Bay (Qeqertarsuup tunua).

Mass spectral experiments were performed to survey a wide array of AZA with an analytical system consisting of triple quadrupole mass spectrometer (API 4000 QTrap, Sciex, Darmstadt, Germany) equipped with a TurboSpray interface coupled to LC equipment (model LC 1100, Agilent, Waldbronn, Germany) that included a solvent reservoir, in-line degasser (G1379A), binary pump (G1311A), refrigerated autosampler (G1329A/G1330B), and temperature-controlled column oven (G1316A). Separation of AZA (5- μl sample injection volume) was performed by reverse-phase chromatography on a C8 phase. The analytical column (50 \times 2 mm) was packed with 3 μm Hypersil BDS 120 Å (Phenomenex, Aschaffenburg, Germany) and maintained at 20 °C. The flow rate was 0.2 ml min^{-1} , and gradient elution was performed with two eluents, where eluent A was water and eluent B was acetonitrile/water (95:5 v/v), both containing 2.0 mM ammonium formate and 50 mM formic acid. Initial conditions were 8-min column equilibration with 30% B, followed by a linear gradient to 100% B in 8 min and isocratic elution until 18 min with 100% B then returning to initial conditions until 21 min (total run time: 29 min). AZA profiles were determined in the selected reaction monitoring (SRM) mode in one period (0–18) min with curtain gas: 10 psi, CAD: medium, ion spray voltage: 5500 V, temperature: ambient, nebuliser gas: 10 psi, auxiliary gas: off, interface heater: on, declustering potential: 100 V, entrance potential: 10 V, exit potential: 30 V. SRM experiments were carried out in positive-ion mode by selecting the transitions shown in Table S1.

On-board isolation and culture

On the first station in the central Labrador Sea, cells of Amphidomataceae were detected during the on-board live sample observations and were subsequently isolated using micro-capillaries into wells of 96-well plates filled with 0.2 ml filtered seawater. Cells were subsequently re-isolated a few times using a SZH-ILLD stereomicroscope (Olympus) equipped with dark field illumination into new wells of a 96-well plate. Plates were incubated at 10 °C under a photon flux density of *c.* 50 $\mu\text{mol m}^{-2} \text{s}^{-1}$ in a 16:8 h light:dark photoperiod in a controlled environment growth chamber (Model MIR 252, Sanyo Biomedical, Wood Dale, Illinois, USA).

Characterisation of Amphidomataceae strains

After 4 weeks of growth, primary isolation plates from the cruise were inspected in the laboratory using a SZH-ILLD stereomicroscope (Olympus) for presence of *Azadinium*/*Amphidoma*-like cells as inferred from typical size, shape, and swimming behaviour. From each well with amphidomatacean cells, a clonal strain was established by isolation of single cells by micro-capillary. Established cultures were thus clonal but not axenic, and were routinely held in 70-ml plastic culture flasks at 15 °C in a natural seawater medium prepared with sterile filtered (0.2 μm VacuCap filters, Pall Life Sciences, Dreieich, Germany) Antarctic seawater (salinity, 34; pH adjusted to 8.0), and enriched with 1/10 strength K-medium

(Keller *et al.* 1987) which was slightly modified by omitting ammonium ions.

For toxin analysis, strains were grown at 15 °C under a photon flux density of 50 $\mu\text{mol m}^{-2} \text{s}^{-1}$ on a 16:8 h light:dark photoperiod. For each harvest, cell density was determined by settling Lugol-fixed samples and counting > 800 cells using an inverted microscope. Densely grown strains (ranging from 0.5–5 $\times 10^4$ cells ml^{-1}) were harvested by centrifugation (5810R, Eppendorf, Hamburg, Germany) of 50-ml subsamples at 3220 $\times g$ for 10 min. The cell pellet was resuspended, transferred into a microtube, centrifuged again (5415, Eppendorf, 16,000 $\times g$, 5 min), and stored frozen (–20 °C) until use. For selected strains, growth and harvest procedures were repeated several times to yield a high biomass and consequently lower the cell quota-based limit of detection. Numbers of cells harvested for these strains are listed in Table S2. Several cell harvests of each strain were combined in 100 μl of acetone. Extraction of cell pellets was repeated four times with 100 μl each and combined cell suspensions were vortexed every 10 min for 1 h at room temperature. Homogenates were centrifuged (5810 R, Eppendorf) at 15 °C and 3220 $\times g$ for 15 min. Filtrates were then adjusted with acetone to a final volume of 0.5 ml. The extracts were transferred to a 0.45- μm pore-size spin-filter (Millipore) and centrifuged (5415R, Eppendorf) at 800 $\times g$ for 30 s, with the resulting filtrate being transferred into a liquid chromatography (LC) autosampler vial for LC-MS/MS analysis.

For DNA extraction, each strain was grown in 70-ml plastic culture flasks under the standard culture conditions described above. Aliquots of 50 ml of healthy and growing culture (based on stereomicroscopic inspection of the live culture) were harvested by centrifugation (5819R, Eppendorf, 3000 $\times g$, 10 min). Each pellet was transferred into a microtube, again centrifuged (5415, Eppendorf, 16,000 $\times g$, 5 min), and stored at –80 °C until DNA extraction.

MICROSCOPY

Observation of living and fixed cells was carried out with a SZH-ILLD stereomicroscope (Olympus) and an Axiovert 200 M inverted microscope (Zeiss). Observation and documentation of live cells at x1000 magnification were performed using an Axioskop 2 (Zeiss) and by recording videos using a Gryphax digital camera (Jenoptik, Jena, Germany) at full-HD resolution. Single frame micrographs were extracted using Corel VideoStudio software (Version X8 Pro). Photographs of formaldehyde-fixed cells (1% final concentration) were taken with an Axiocam MRc5 digital camera (Zeiss).

Cell length and width were measured at x1000 magnification using Axiovision software (Zeiss) and freshly fixed cells (formaldehyde, final concentration 1%) of strains growing at 15 °C.

For scanning electron microscopy (SEM), cells were collected by centrifugation (5810R, Eppendorf, 3220 $\times g$, 10 min) of 15 ml of culture. The supernatant was removed and the cell pellet resuspended in 60% ethanol in a 2-ml microtube for 1 h, at 4 °C to strip off the outer cell membrane. Subsequently, cells were pelleted by centrifugation (5415R, Eppendorf, 16,000 $\times g$, 5 min) and resuspended in a 60:40 mixture of deionised water and seawater for 30 min at 4 °C. After centrifugation and removal of the

diluted seawater supernatant, cells were fixed with formaldehyde (2% final concentration in a 60:40 mixture of deionised water and seawater) and stored at 4 °C for 3 h. Cells were then collected on polycarbonate filters (Millipore, 25-mm diameter, 3- μm pore-size) in a filter funnel where all subsequent washing and dehydration steps were carried out. Eight washings (2-ml MilliQ-deionised water each) were followed by a dehydration series in ethanol (30%, 50%, 70%, 80%, 95%, 100%; 10 min each). Filters were dehydrated with hexamethyldisilazane (HMDS), first in 1:1 HMDS:EtOH, followed by twice in 100% HMDS, and then stored under gentle vacuum in a desiccator. Finally, filters were mounted on stubs, sputter coated (SC500, Emscope, Ashford, UK) with gold-palladium and viewed with a Quanta FEG 200 scanning electron microscope (FEI, Eindhoven, Netherlands). Some SEM micrographs were presented on a black background using Adobe Photoshop 6.0 (Adobe Systems, San Jose, California, USA). Labelling of dinophyte thecal plates was done according to the Kofoidian system.

Molecular phylogeny

DNA extraction was performed using the NucleoSpin Plant II kit (Macherey & Nagel) according to manufacturer's instructions. Sequencing reactions of the 18S/small subunit (SSU), the Internal Transcribed Spacer region (ITS1, 5.8S rRNA, ITS2) and the D1/D2 region of 28S/large subunit (LSU) were performed as follows: polymerase chain reaction (PCR) was performed to amplify the aforementioned regions from the DNA extracts. Each reaction contained 16.3 μl ultra-pure H_2O , 2.0 μl HotMasterTaq buffer (5Prime, Hamburg, Germany), 0.2 μl dNTPs (10 μM), 0.2 μl of each primer (10 μM), 0.1 μl of Taq Polymerase (Quantabio, Beverly, Massachusetts, USA) and 1.0 μl of extracted DNA template (10 $\text{ng } \mu\text{l}^{-1}$) to a final reaction volume of 20 μl . PCR conditions for the amplification of the LSU and ITS were set as described in Wietkamp *et al.* (2019b) using the following primer sets: DirF (5'-ACC CGC TGA ATT TAA GCA TA-3') and D2CR (5'-CCT TGG TCC GTG TTT CAA GA-3') for LSU; ITSa (5'-CCA AGC TTC TAG ATC GTA ACA AGG (ACT)TC CGT AGG T-3') and ITSb (5'-CCT GCA GTC GAC A(GT)A TGC TTA A(AG)T TCA GC(AG) GG-3') for ITS. For SSU amplifications, the following settings were used: initialisation at 94 °C for 5 min; 30 cycles of 94 °C for 2 min, 55 °C for 2 min, 68 °C for 3 min; a final extension at 68 °C for 10 min. Forward and reverse primers for SSU amplification were: 1F (5' – AAC CTG GTT GAT CCT GCC AGT – 3') and 1528R (5' – TGA TCC TTC TGC AGG TTC ACC TAC – 3').

Phylogenetic analysis

Newly obtained SSU, ITS and/or partial LSU rDNA sequences were incorporated into available *Amphidoma*, *Azadinium* and closely-related sequences in GenBank (<https://www.ncbi.nlm.nih.gov/genbank/>). Genbank accession numbers are listed in Table S3. Concatenated sequences were aligned using MAFFT v7.110 (Katoh & Standley 2013) online program (<http://mafft.cbrc.jp/alignment/server/>). Alignments were manually checked with BioEdit v7.0.5 (Hall 1999). For Bayesian inference (BI), jModelTest (Posada 2008) was used to select the most

appropriate model of molecular evolution using Akaike Information Criterion (AIC). Bayesian reconstruction of the data matrix was performed using MrBayes 3.2 (Ronquist & Huelsenbeck 2003) with the best-fitting substitution model (GTR+G). Four Markov chain Monte Carlo (MCMC) chains were run for 4,000,000 generations, sampling every 100 generations. Convergence diagnostics were estimated graphically using 'are we there yet?' (<http://ceb.scs.fsu.edu/awty>; Nylander *et al.* 2008), and the first 10% of burn-in trees were discarded. A majority-rule consensus tree was created to examine posterior probabilities of each clade. Maximum-likelihood (ML) analyses were conducted with RaxML v7.2.6 (Stamatakis 2006) on the T-REX web server (Boc *et al.* 2012) using the model GTR+G. Node support was assessed with 1000 bootstrap replicates.

Multiple ITS rDNA sequences of selected new strains were aligned with available *Amphidoma* and *Azadinium* sequences in GenBank using MAFFT v7.110 (Katoh & Standley 2013) online program with default settings. Completed alignments were imported into PAUP* v4b10 (Swofford 2002) to estimate divergence rates using simple uncorrected pairwise (p) distance matrices.

Chemical analysis of azaspiracids

Extracts of strains were screened for known AZA in the SRM mode as described above. In addition, precursor ion experiments were performed. Precursors of the characteristic AZA fragments m/z 348, m/z 360 and m/z 362 were scanned in the positive-ion mode from m/z 400 to 900 under the following conditions: curtain gas, 10 psi; CAD, medium; ion spray voltage, 5500 V; temperature, ambient; nebuliser gas, 10 psi; auxiliary gas, off; interface heater, on; declustering potential, 100 V; entrance potential, 10 V; collision energy, 70 V; exit potential, 12 V. Product ion spectra of the m/z values 830, 842 and 858 were recorded in the Enhanced Product Ion (EPI) mode in the mass range from m/z 150 to 930. Positive ionisation and unit resolution mode were used. The following parameters were applied: curtain gas: 10 psi, CAD: medium, ion spray voltage: 5500 V, temperature: ambient, nebulizer gas: 10 psi, auxiliary gas: off, interface heater: on, declustering potential: 100 V, collision energy spread: 0, 10 V, collision energy: 70 V, exit potential, 12 V.

RESULTS

Hydrography

Surface temperature values ranged from *c.* 0.6 °C to 8.5 °C (Fig. 2). Highest surface temperatures were found in the Labrador Sea (Station 1) and the Disco Bay area, whereas the coastline had lower temperature (0.6 °C to 4.5 °C). Salinity values ranged from *c.* 22 to 35, with the lowest salinities found in the inner fjord section of Godthaab Fjord (*c.* 22) and Disco Bay, close to Jacobshaven (Illusiat; *c.* 31; Fig. 2). High fluorescence signals were identified in the Labrador Sea (*c.* 12 AU), at the entrance of the Vaigat area (4–5 AU), and within outer and inner section of the Godthaab Fjord (*c.* 3 AU; Fig. 2).

General plankton composition

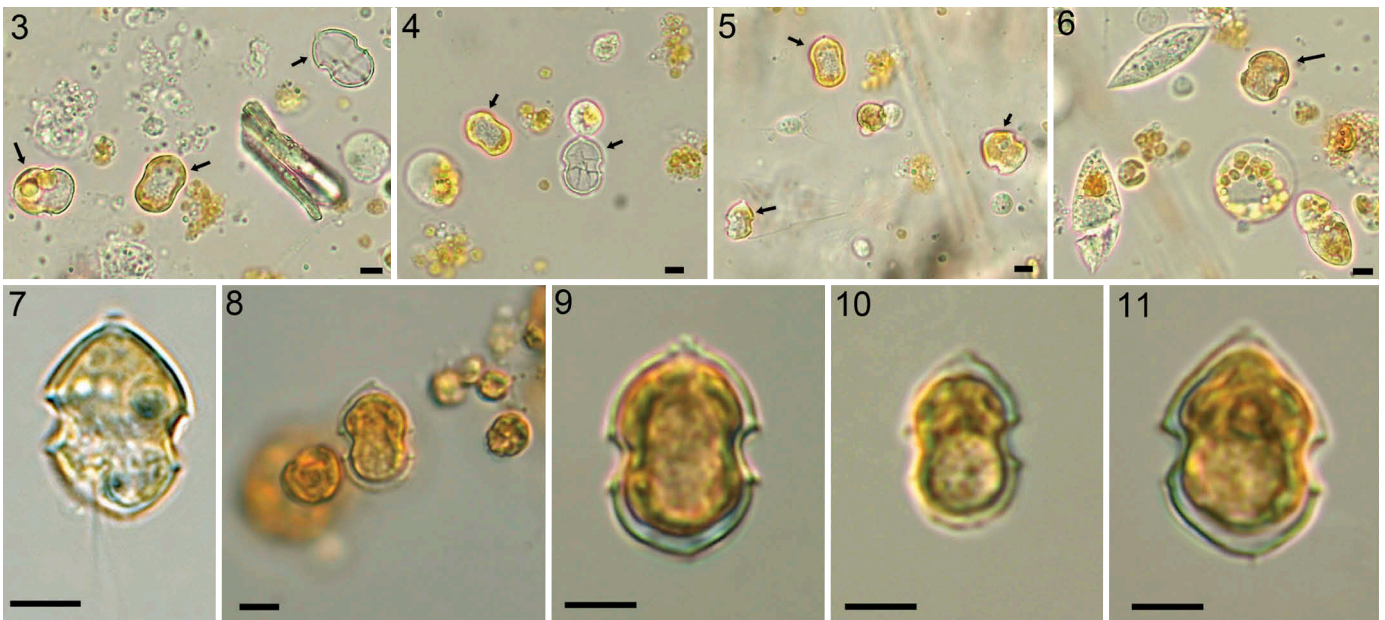
Phytoplankton composition and abundance determined from net tows and quantitative Uthermöhl counts revealed a high diversity of microplankton and locally quite different communities. This reflected late spring bloom dominance by diatoms, and/or high biomass of colonial flagellates such as *Phaeocystis pouchetii* (Harriot) Lagerheim and/or *Dinobryon balticum* (Schütt) Lemmermann, or post-bloom communities dominated by low densities of various dinoflagellate species. The first station in the open Labrador Sea revealed a high biomass of micro- and nanoplankton with noticeably high abundance of a small species of *Prorocentrum* and of an unknown haptophyte species. Along the Greenland coast and inside Godthaab Fjord and Disko Bay, plankton communities had high abundance of different species of flagellates and diatoms. Among the latter, there was a conspicuous bloom of *Chaetoceros debilis* Cleve in certain parts of the Godthaab Fjord, and locally high abundance of *Thalassiosira* spp. or *Chaetoceros socialis* H.S. Lauder in other parts of the study area. The most important and abundant flagellate species were two colony-forming species: the haptophyte *Phaeocystis pouchetii* and the chrysophyte *Dinobryon balticum*. Dinoflagellate communities consisted mainly of a highly diverse community of heterotrophic species (e.g., *Gyrodinium* spp., *Protoperidinium* spp., *Amphidinium* spp.) or undetermined species of unknown trophic status, whereas photosynthetic dinoflagellates (e.g., *Protoceratium reticulatum* (Claparède & Lachmann) Bütschli, *Dinophysis* spp., *Alexandrium* spp., *Margalefidinium* sp., *Heterocapsa* spp.) were generally of low abundance and biomass.

On-board microscopy records of Amphidomataceae

On-board microscopy using live samples revealed the presence of Amphidomataceae at the first station in the central Labrador Sea (Figs 3–11). Identification was based on size, shape, and the presence of a distinctly pointed apex. No attempt was made to identify cells to species. Quantitative plankton counts using the sedimentation technique and Lugol-fixed samples revealed abundant, small, thecate dinoflagellates classified as *Azadinium/Amphidoma* (Figs 8–11) of 9200 cells ml⁻¹. For all other stations inspected along the Greenland coast, no microscopic records of Amphidomataceae were noted with certainty.

PCR assays

Of the 50 stations sampled, 33 were positive with the SYBR Green amphidomatacean PCR assay (Fig. 12). In Godthaab Fjord, negative hits were restricted to a few inner stations. Whereas most of the transit stations off the coast (stations 16–21, 25–27) were negative, Amphidomataceae were present at the two northernmost stations, and at all but four stations in the Disko Bay area. Positive hits of the species-specific qPCR assays were much more restricted. Considering the DNA extraction volume and the filtered water volume, the limit of detection of 0.1 pg target DNA µl⁻¹ corresponded here to *c.* 0.4–0.6 cells l⁻¹.



Figs 3–11. Records of Amphidomataceae from the central Labrador Sea (station 1).

Figs 3–7. Living samples with amphidomatacean cells or empty thecae (both designated by arrows). Scale bars = 5 μm.

Figs 8–11. Amphidomatacean cells in Lugol-fixed Utermöhl samples. Scale bars = 5 μm.

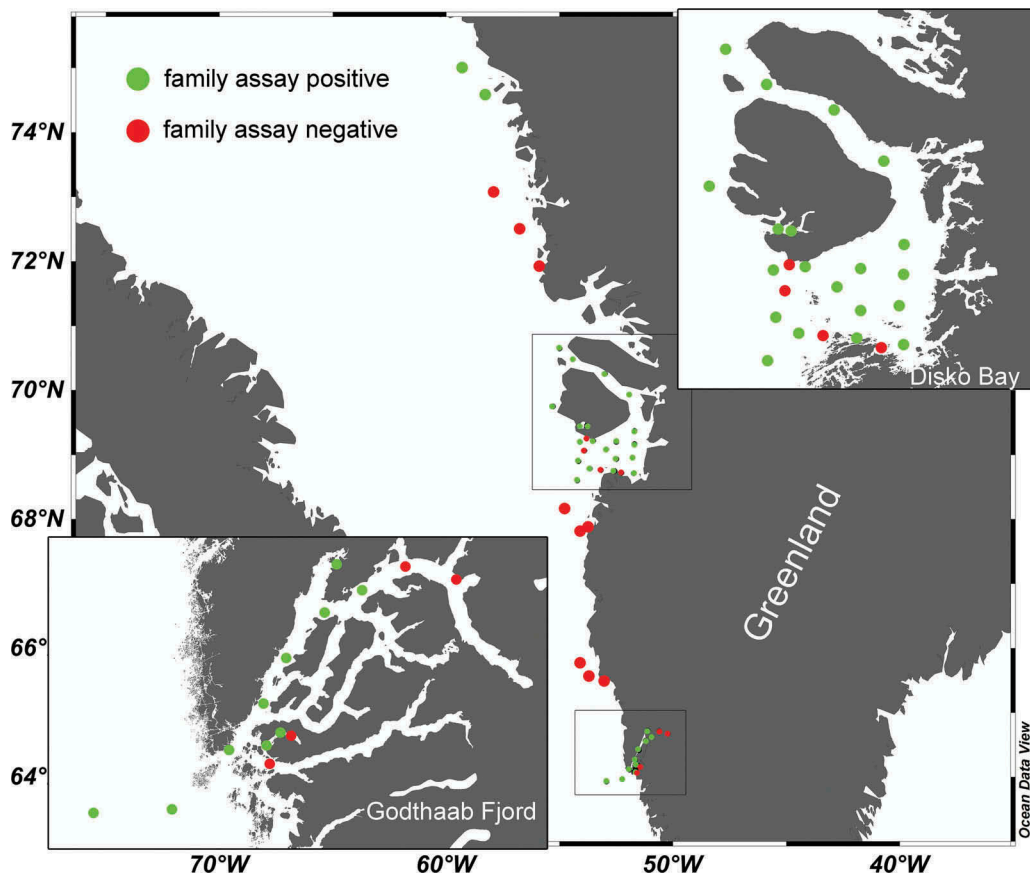


Fig. 12. Map showing PCR presence (green) or absence (red) of positive signals using Amphidomataceae family primers.

All samples were negative for *Az. spinosum* Elbrächter & Tillmann. *Amphidoma languida* was detected only at the first station in the central Labrador Sea with 117 cells l⁻¹. Positive

records with background abundance (1–2 cells l⁻¹) for *Az. poporum* Tillmann & Elbrächter occurred at stations 14 and 22 only.

AZA in field samples

None of the known AZA listed in Table S1 was detected in the 5–20 µm size fractions of seawater samples. The limits of detection (signal-to-noise ratio = 3) of these measurements ranged between 7 and 12 pg l⁻¹ seawater depending on water volume filtered and filter extraction volume. In addition to plankton samples, solid phase adsorption toxin tracking (SPATT) bags were continuously employed in a FerryBox sampling surface water throughout the expedition, but did not contain AZA above the LOD of 6 pg g⁻¹ resin.

Azadinium, new strains

On-board single-cell isolation yielded 18 clonal amphidoma-tacean strains. All strains displayed a similar and conspicuous swimming behaviour consisting of a slow movement interrupted by short ‘jumps’ in various directions. Identification of all strains was based on morphology as examined by LM and SEM and was confirmed for all strains by rRNA sequence comparison (Table 1). The newly available strains comprised four species including *Az. obesum* Tillmann & Elbrächter (12 strains), *Az. trinitatum* (two strains), *Az. dexteroporum* (one strain), and three strains of a new species.

Azadinium perforatum Tillmann, Wietkamp & H.Gu sp. nov. Figs 13–41

DESCRIPTION: Small photosynthetic thecate Dinophyceae; cells 14.6 to 20.0 µm long and 9.9 to 14.4 µm wide; cingulum broad (c. 20% of cell length) and postmedian; epitheca conical and ending in a small but distinctly pointed apical pore; hypotheca hemispherical with a very broad and long sulcus and with a single, very small antapical spine; tabulation formula: Po, cp, X, 6', 0a, 6'', 6C, 5S, 6''', 2''''; thecal pores present on the pore plate; a ventral pore located on the right ventral side in a notch of the pore plate.

HOLOTYPE: SEM stub prepared from clonal strain AZA-2H (designated CEDiT2019H103), deposited at the Senckenberg Research Institute and Natural History Museum, Centre of Excellence for Dinophyte Taxonomy (Wilhelmshaven, Germany).

ISOTYPES: Formalin-fixed sample prepared from clonal strain AZA-2H (designated CEDiT2019I104) deposited at the Senckenberg Research Institute and Natural History Museum, Centre of Excellence for Dinophyte Taxonomy (Wilhelmshaven, Germany)

TYPE LOCALITY: Central Labrador Sea (56°49.42'N; 52°13.15'W).

HABITAT: Marine plankton.

STRAIN ESTABLISHMENT: Sampled and isolated by U. Tillmann on 28 June 2017.

ETYMOLOGY: The epithet (Latin *perforatus* – pierced, penetrated) is inspired by the presence of small pores on the pore plate.

Morphology

Using light and electron microscopy, all three clonal strains identified as *Az. perforatum* sp. nov. (AZA-2C, AZA-2E, AZA-2H) were identical in terms of morphology and plate pattern. The selected strain AZA-2H is described in detail.

Cells of *Az. perforatum* sp. nov. were ovoid and slightly dorsoventrally compressed (Figs 13–22). Cells of strain AZA-

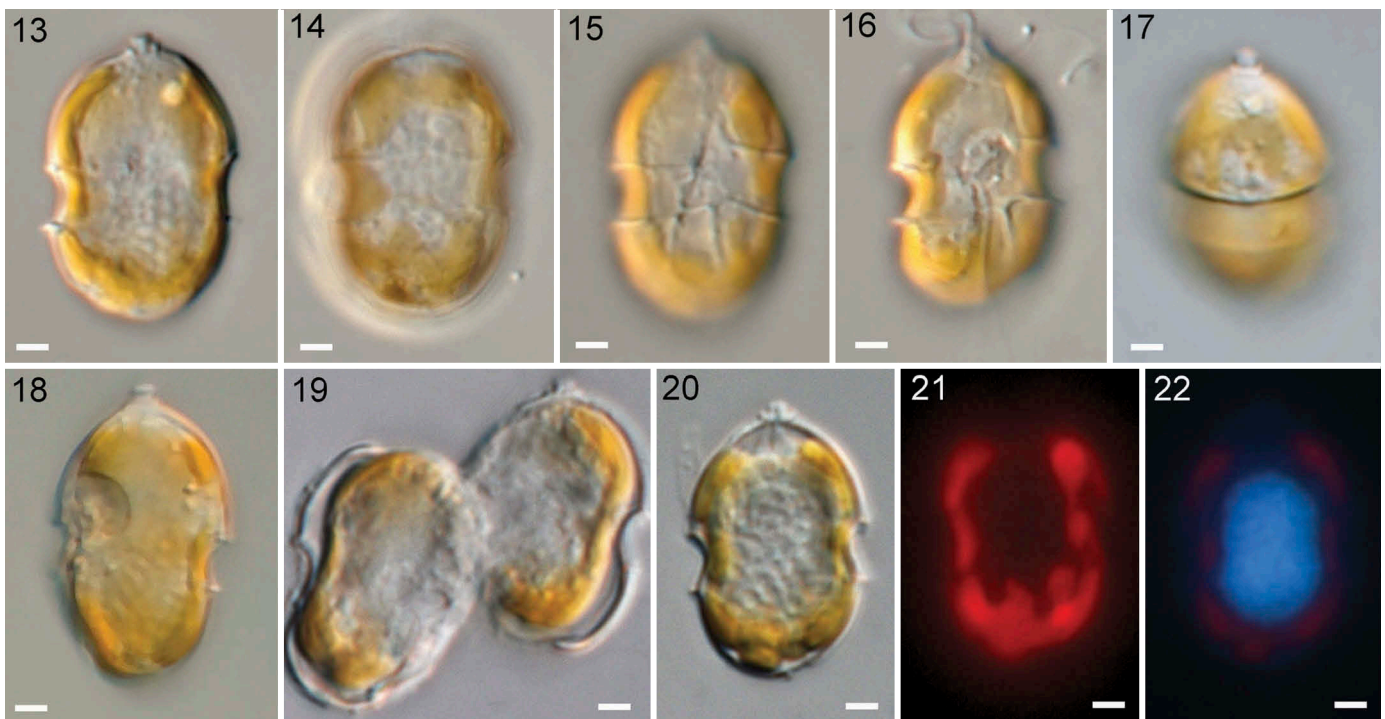
Table 1. Strain information. All strains were analysed by light microscopy and scanning electron microscopy. For none of the strains were azaspiracids detected. For all strains, LSU and ITS sequence data were obtained, and for all three *Az. perforatum* strains there are also SSU sequences (see Supplementary Table S3).

Species	Strain	Length (µm)	Width (µm)	l/w ratio	
		Mean ± s Min-max	Mean ± s Min-max	Mean ± s	n
<i>Az. obesum</i>	AZA-1B	15.3 ± 1.0 13.1–17.0	11.6 ± 1.0 9.2–13.8	1.33 ± 0.05	53
<i>Az. obesum</i>	AZA-1C	14.8 ± 0.8 13.2–16.4	10.8 ± 0.8 9.3–12.7	1.37 ± 0.06	53
<i>Az. obesum</i>	AZA-1F	15.8 ± 0.9 13.3–18.0	12.0 ± 0.8 10.2–14.1	1.32 ± 0.05	51
<i>Az. obesum</i>	AZA-1G	14.9 ± 0.9 12.4–16.7	11.0 ± 0.7 9.7–12.4	1.36 ± 0.06	50
<i>Az. obesum</i>	AZA-2B2	14.5 ± 0.9 12.9–16.4	10.7 ± 0.8 9.2–12.8	1.36 ± 0.06	54
<i>Az. obesum</i>	AZA-2D	15.2 ± 0.8 14.0–17.3	11.4 ± 0.9 9.7–13.9	1.34 ± 0.06	53
<i>Az. obesum</i>	AZA-2G	15.6 ± 0.8 13.7–17.1	11.9 ± 0.8 10.6–13.8	1.31 ± 0.05	54
<i>Az. obesum</i>	AZA-ZE4	16.1 ± 1.0 14.1–17.7	12.2 ± 1.1 10.0–14.3	1.32 ± 0.06	53
<i>Az. obesum</i>	AZA-ZE7	16.6 ± 2.3 12.4–22.2	13.3 ± 2.6 8.8–20.0	1.26 ± 0.08	82
<i>Az. obesum</i>	AZA-ZE8	15.3 ± 0.9 13.8–17.5	11.1 ± 0.9 9.7–13.4	1.37 ± 0.06	53
<i>Az. obesum</i>	AZA-ZE9	15.3 ± 1.3 13.2–17.3	11.0 ± 0.8 9.5–12.8	1.40 ± 0.06	52
<i>Az. obesum</i>	AZA-ZE11	15.5 ± 0.9 13.6–17.3	11.8 ± 0.8 10.3–13.6	1.32 ± 0.06	52
<i>Az. trinitatum</i>	AZA-2F	13.7 ± 0.8 12.1–15.4	9.2 ± 0.7 7.6–11.3	1.50 ± 0.08	44
<i>Az. trinitatum</i>	AZA-ZE10	13.5 ± 0.8 12.0–15.9	9.3 ± 0.6 8.1–10.8	1.46 ± 0.07	50
<i>Az. dexteroporum</i>	AZA-2B1	10.5 ± 0.7 9.1–13.2	7.5 ± 0.6 6.5–10.0	1.40 ± 0.06	57
<i>Az. perforatum</i>	AZA-2C	17.6 ± 1.1 14.6–19.2	12.0 ± 0.8 9.9–13.5	1.47 ± 0.05	59
<i>Az. perforatum</i>	AZA-2E	17.8 ± 1.1 15.5–19.5	12.3 ± 0.9 10.4–14.0	1.45 ± 0.06	56
<i>Az. perforatum</i>	AZA-2H	18.0 ± 0.9 15.3–20.0	12.6 ± 0.9 9.9–14.4	1.49 ± 0.07	84

2H had a mean length of 18.0 µm (15.3 to 20.0 µm, n = 84) and a mean width of 12.6 µm (9.9 to 14.4 µm, n = 84), resulting in a mean length:width ratio of about 1.5 (Table 1). The dome-shaped episome terminated in a distinctly acuminate apical pore (Figs 13, 17, 18). The episome was slightly longer than the hemispherical hyposome. The broad cingulum was thus slightly postmedian in position, descending but only slightly displaced (Figs 15, 16).

A single large, lobed and reticulate chloroplast expanded through the entire cell (Figs 13–18, 21) and no indication of a pyrenoid was visible using LM. The large, ellipsoid nucleus was positioned in cell centre (Figs 13, 20, 22). Cytokinesis occurred in motile cells and was of the desmoschisis type in which the parental theca was shared between the two sister cells (Fig. 19).

Thecal plates were thin, but could be clearly observed in light microscopy (Figs 13–20), and were stainable with calcofluor white (not shown). However, because of the delicateness of the plates, the Kofoidian pattern was better resolved by SEM (Figs 23–37, all prepared from the holotype SEM stub).



Figs 13–22. *Azadinium perforatum* sp. nov. (strain AZA-2H): LM of living (Figs 13–18) and formaldehyde-fixed (Figs 19–22) cells.

Figs 13–18. Living cells showing general size and shape. Scale bars = 2 μ m.

Fig. 19. Formalin fixed cell, late stage of cell division (desmoschisis). Scale bar = 2 μ m.

Figs 20–22. Same cell stained with DAPI in brightfield (Fig. 20), with blue light excitation (Fig. 21) to show chloroplast shape and location, or with UV excitation (Fig. 22) to indicate nuclear shape and location. Scale bars = 2 μ m.

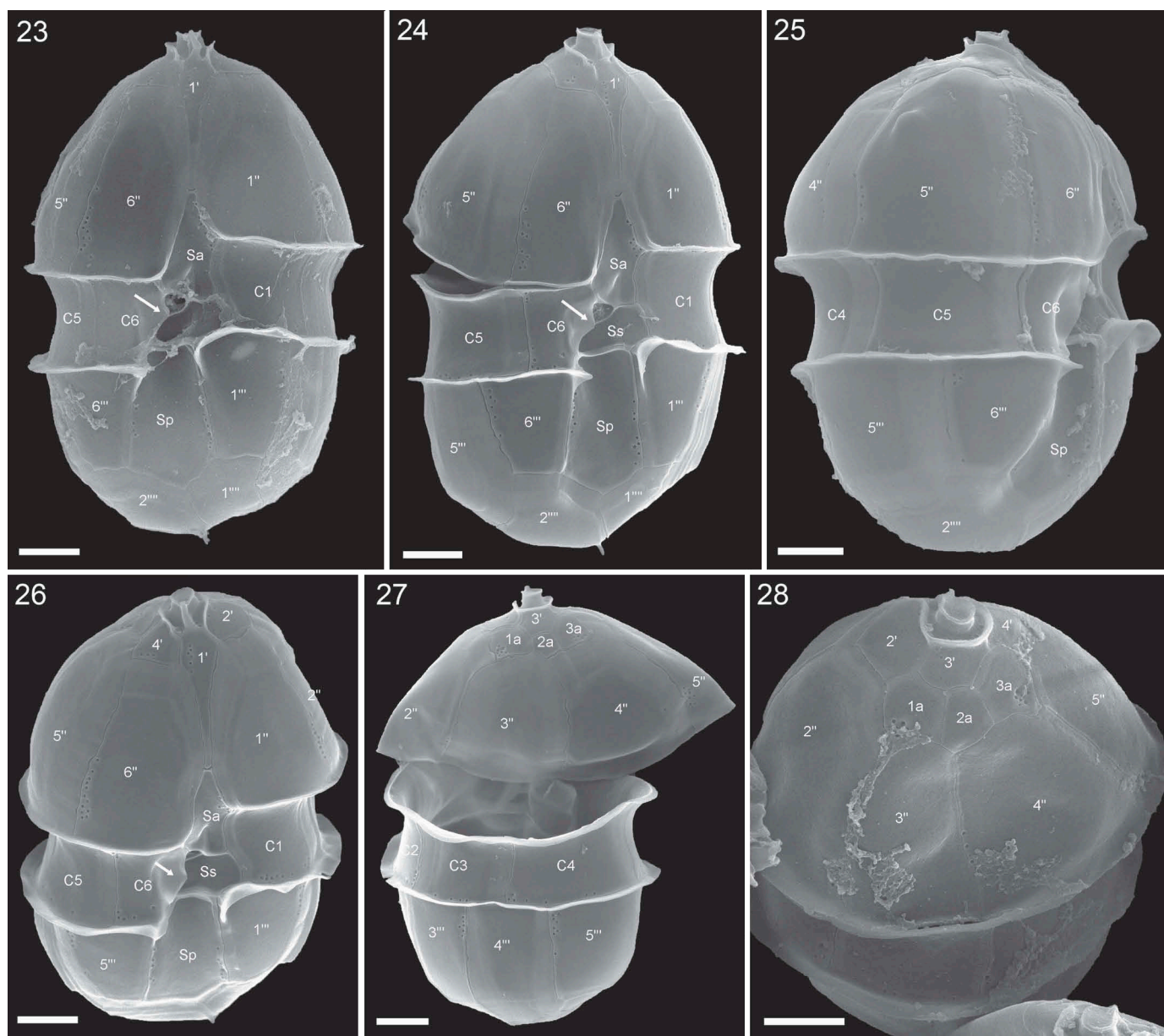
The plate formula was Po, cp, X, 4', 3a, 6'', 6C, 5S, 6''', 2'''' and is schematically drawn in Figs 38–41. Plates were generally smooth, but growth bands of thecal plates were occasionally faintly visible as striated rows running parallel to plate sutures (e.g., Figs 24–27). The presence of these growth bands was restricted to certain sutures.

The acuminate epitheca terminated in the prominent apical pore complex (APC; Figs 23–28) which was composed of three plates: a pore plate (Po) covered by a cover plate (cp), and the canal plate X (Figs 29–31). The pore plate was teardrop-shaped and confined by a collar formed by edges of the apical plates. The collar was narrow and raised, and thus was distinct in LM (Fig. 20). On the tapered ventral side of the pore plate, the collar was open. In the centre of the apical pore plate (Po), a teardrop-shaped pore emerged which was covered by a cover plate (cp). A small X-plate was located where the pore plate abutted the first apical plate. Internal views to determine the exact shape of the X-plate were not obtained. From the exterior, the X-plate had a characteristic three-dimensional structure with finger-like protrusions contacting the apical cover plate (Figs 30, 31). In addition to the APC, the epitheca was composed of 13 thecal plates forming rows of four apical, three anterior intercalary, and six precingular plates (Fig. 29). The six-sided first apical plate was elongated rhomboid or diamond-shaped with a narrow posterior part (Fig. 32). The other three apical plates were small and six-sided, with the dorsal plate 3' being smaller than lateral plates 2' and 4' (Fig. 29). The sutures of plate 3' to its neighbouring apical plates were very short so that the epithecal intercalary plates almost contacted the pore plate. Three small anterior

intercalary plates were symmetrically arranged on the dorsal side of the epitheca (Figs 27, 28, 29, 33) with the middle intercalary plate 2a slightly smaller than the others. All three intercalary plates were five-sided and in contact with two precingular plates. All six precingular plates were of almost equal size, taller than wide, and arranged symmetrically with the suture between plate 3'' and 4'' in mid-dorsal position. Both ventrally-located precingular plates (1'' and 6'') were four-sided, and all other precingulars were five-sided.

The hypotheca was composed of six postcingular and two antapical plates (Fig. 35). Of the six postcingular plates, the two ventrally-located plates were slightly narrower than the other postcingular plates. All postcingular plates were rather long with the lateral and dorsal postcingular plates longer than the two ventral postcingular plates (Figs 23–25). Both antapical plates extended on the dorsal side towards the sulcus. They were different in size with the larger plate 2'''' bearing a minute antapical spine located almost in the middle of the cell close to the suture between plates 1'''' and 2'''' (Figs 23, 24, 35).

The cingulum was wide, about one-fifth of total cell length, and was only slightly displaced by about one-third of its width (Figs 23, 24). There were six cingular plates (Fig. 36). Five of the cingular plates were of comparable size, but the right cingular plate C6 was distinctly narrower and invaded the sulcal area on its left side with an irregularly shaped wing-like extension (arrows in Figs 23, 24, 26). The central sulcal area was deeply concave and the sulcus extended with a slightly concave plate (Sp) along most of the hypotheca. The small central sulcal plates were difficult to resolve because of the internal vaulted structure of the flagellar pore region. Nevertheless, five sulcal plates were



Figs 23–28. SEM of *Azadinium perforatum* sp. nov. (strain AZA-2H).

Fig. 23. Theca in ventral view. Scale bar = 2 μ m.

Figs 24, 25. Thecae in right lateral view. Scale bar = 2 μ m.

Fig. 26. Theca in apical right lateral view. Scale bar = 2 μ m.

Fig. 27. Theca in dorsal view. Scale bar = 2 μ m.

Fig. 28. Theca in apical dorsal view. Scale bar = 2 μ m.

identified (Figs 36, 37). The large anterior sulcal plate (Sa) was asymmetrical pentagonal and partly intruded the epitheca with a triangular, tapered anterior part (Figs 23, 24, 26). Two small plates, namely a median sulcal (Sm) and a right sulcal (Sd) plate formed the inverted part of the sulcus (Figs 36, 37). A broad left sulcal plate (Ss) ran horizontally from C1 to C6, thereby separating the posterior sulcal plate (Sp) from the other sulcal plates. The large posterior sulcal plate was approximately twice as long as wide, and triangular at its posterior end (Figs 23–26).

Thecal plates had a limited number of thecal pores of diameter about 0.1 μ m. On precingular, cingular, and postcingular plates the pores were arranged mainly as rows

parallel to some plate sutures (Figs 23–28). The first apical plate had a characteristic anterior row of five to ten pores (Figs 29, 30, 32), whereas pores on other apical and intercalary plates were scattered and ranged from zero to eight pores per plate (Figs 29, 33). The median intercalary plate 2a was usually free of pores, but occasionally one pore occurred (Figs 29, 33). Dorsal plates 3'' and 4''' of the pre- and postcingular series were free of pores. A few small pores were present on the second antapical plate, whereas the first antapical plate had no pores (Fig. 35). Some pores were consistently present on all three larger sulcal plates, i.e., on Sa, Ss and Sp (Figs 23, 24, 26).



Figs 29–37. *Azadinium perforatum* sp. nov. (strain AZA-2H): SEM micrographs of different cells to illustrate epithelial plate arrangement.

Fig. 29. Apical view. Scale bar = 2 μ m.

Fig. 30. Detailed view of apical pore complex in central view. Scale bar = 1 μ m.

Fig. 31. Detailed view of apical pore complex in apical view. Scale bar = 0.5 μ m.

Fig. 32. Ventral view of first apical plate. Scale bar = 1 μ m.

Figs 33, 34. Detailed dorsal view of apical and anterior intercalary plates. Note Fig. 34 suggests that plate 3' and 2a are fused. Scale bars = 1 μ m.

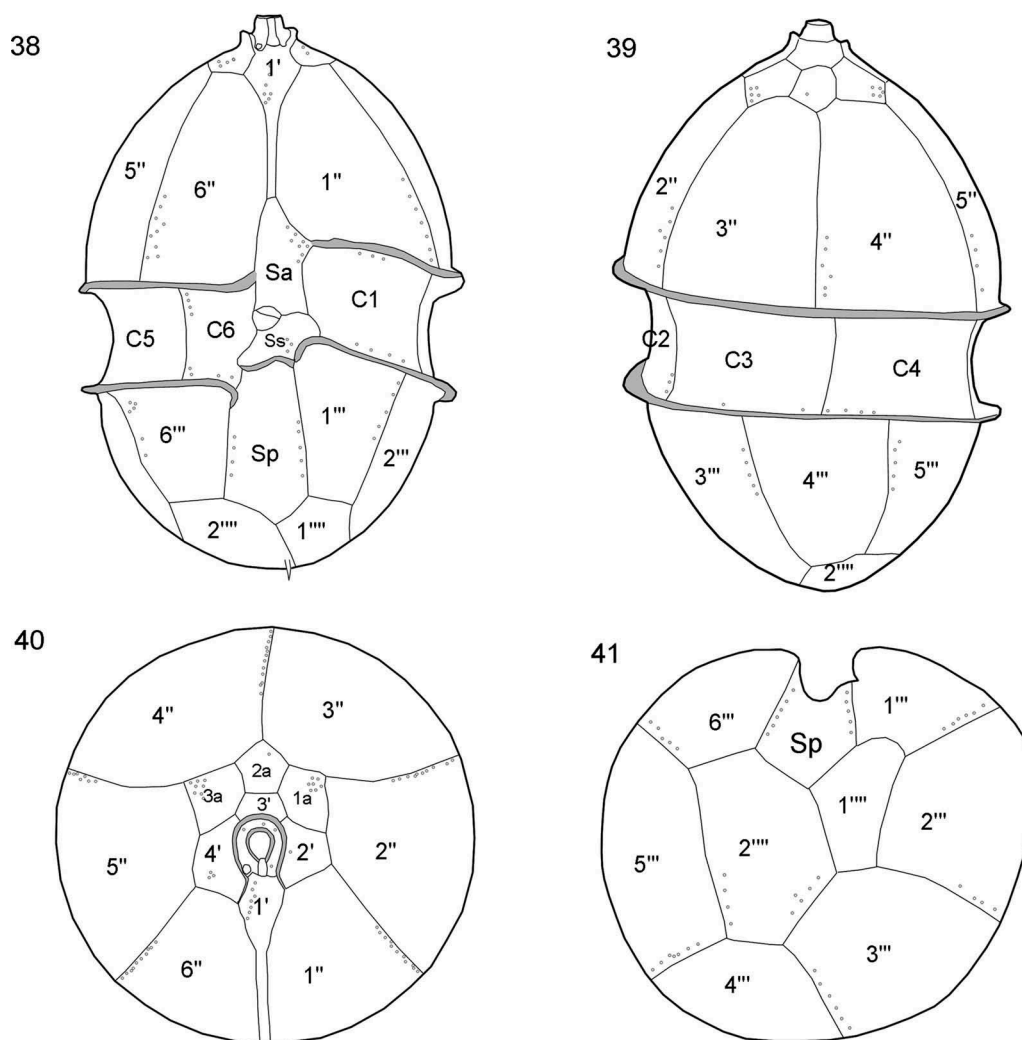
Fig. 35. Antapical view of hypothecal plates. Scale bar = 2 μ m.

Fig. 36. Dorsal/apical view of hypotheca showing series of cingular plates with interior view of sulcal plates. Scale bar = 2 μ m.

Fig. 37. Details of sulcal plate arrangement in external view. Scale bar = 1 μ m.

The plate pattern shown in Figs 38–41 was standard; however, some variation occurred in culture. A common (but not quantified) variation was the lack of a suture between plates 3'

and 2a, leading to a single elongated dorsal apical plate extending posteriorly between, and separating the two remaining anterior intercalary plates (Fig. 34).



Figs 38–41. *Azadinium perforatum* sp. nov. Schematic illustrations of tabulation. Plate labels according to Kofoidian system. Positions of thecal pores indicated in Figs 38–41 as small grey circles; position of small antapical spine indicated in Fig. 38.

Fig. 38. Ventral view.

Fig. 39. Dorsal view.

Fig. 40. Apical view.

Fig. 41. Antapical view.

Morphology of other strains

Azadinium obesum Tillmann & Elbrächter

Figs 42–52

With 12 new strains, *Azadinium obesum* (Figs 42–52) was the species most often obtained from single-cell isolation at station 1. All strains of *Az. obesum* shared identical morphology in LM and SEM. No pyrenoid was visible using light microscopy (Figs 42–44). SEM revealed the Kofoidian plate pattern, Po, cp, X, 4', 3a, 6'', 6C, 5S, 6''', 2''', and plate size and arrangement as described for the type species (Figs 46–52). As a distinctive morphological feature, the ventral pore was located on the left margin of plate 1' (Figs 46, 50). For all strains of *Az. obesum*, plate 2a was present in both quadra- (i.e. in contact with one precingular plate) and penta-configuration (in contact with two precingular plates; Figs 49, 50). Epithecal intercalary plates

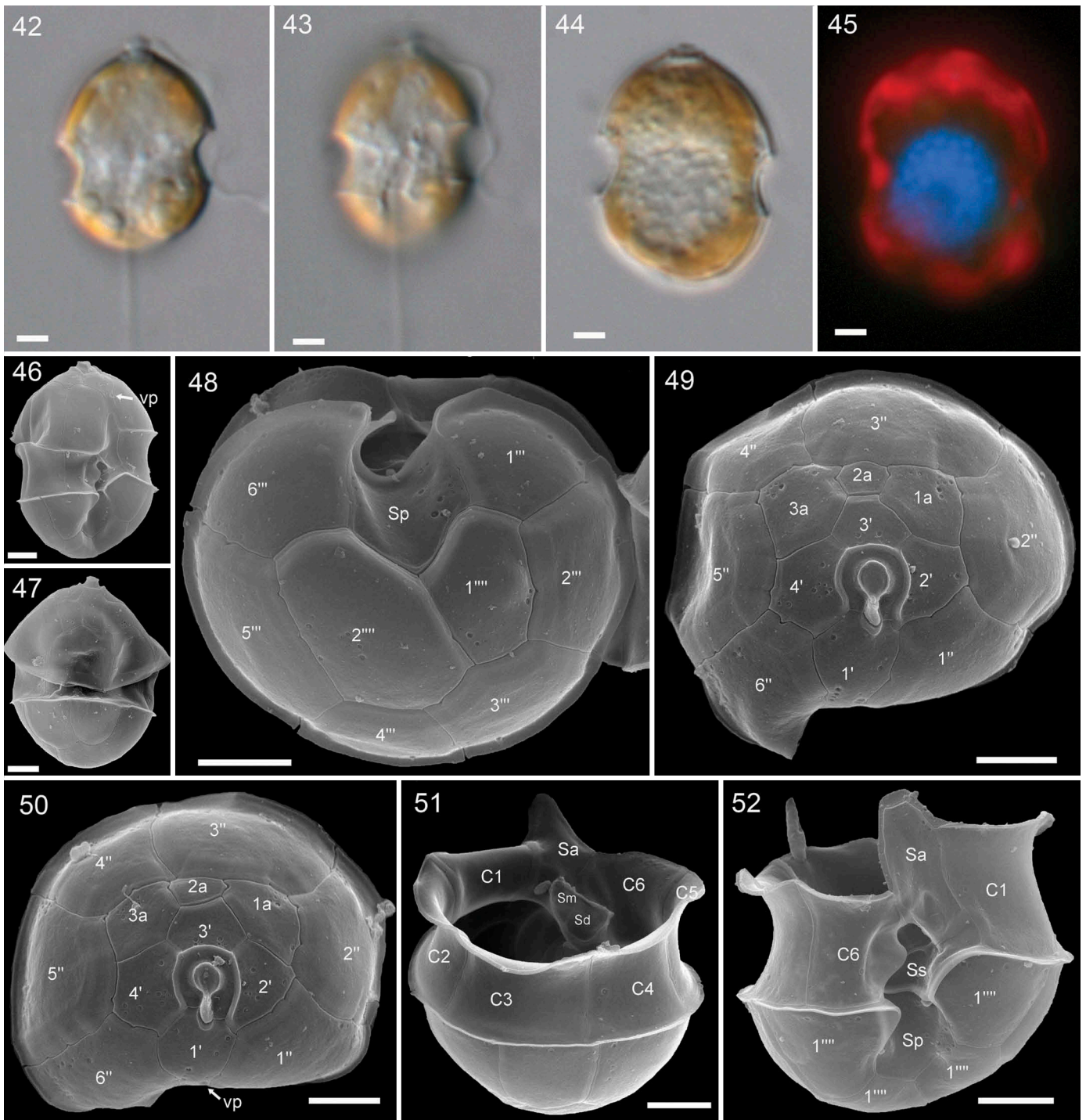
were relatively small, and the first (1a) was not in contact with plate 1'' (Figs 49, 50).

Azadinium dexteroporum Percopo & Zingone

Figs 53–62

One strain was identified as *Azadinium dexteroporum* (Figs 53–62). Cells of strain AZA-2B1 were distinctly smaller than other strains (Table 1). In LM, the very broad and excavated cingulum, acuminate apex, distinct antapical spine, and relatively small pyrenoid visible by its starch cup, were observed (Figs 53–55). Dividing cells retained their motility throughout mitosis and cytokinesis, the latter being of the desmoschisis type, i.e., parental theca shared by the two sister cells (Fig. 56).

The Kofoidian plate pattern and most plate details (Figs 57–62) conformed to the species description. The distinctly smaller central intercalary plate 2a was quadrangular



Figs 42–52. Light and scanning electron micrographs of *Azadinium obesum* (strain AZA-2D). vp, ventral pore.

Figs 42, 43. LM, living cells in ventral view. Scale bars = 2 μ m.

Figs 44, 45. Formalin fixed cells in brightfield (Fig. 44) or with calcofluor staining and epifluorescence (UV excitation; Fig. 45) to illustrate shape and location of nucleus (blue) and chloroplast (red). Scale bars = 2 μ m.

Fig. 46. SEM of theca in ventral view. Scale bar = 2 μ m.

Fig. 47. SEM of theca in dorsal view. Scale bar = 2 μ m.

Fig. 48. Hypothecal plates in antapical view. Scale bar = 2 μ m.

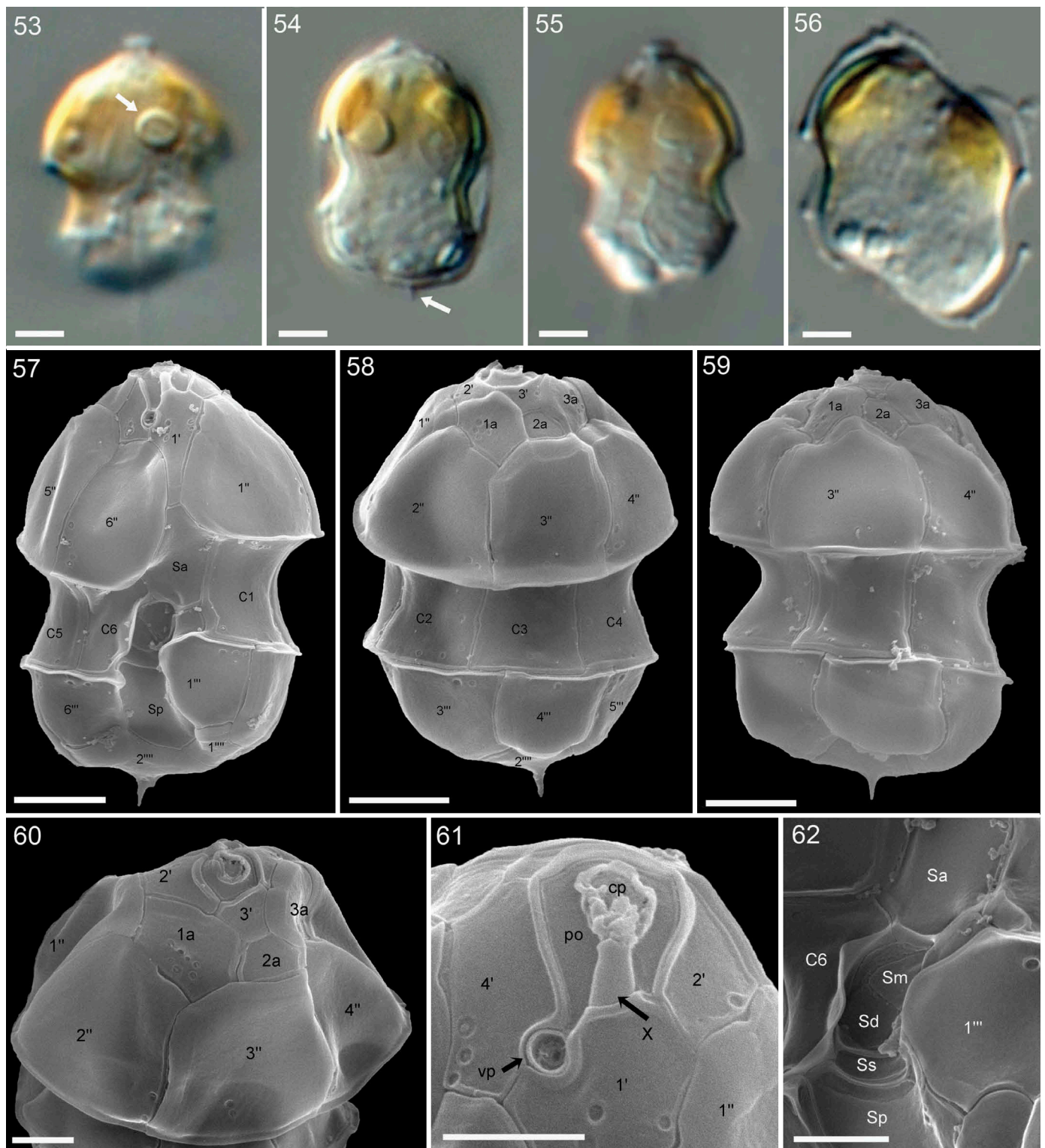
Figs 49, 50. Epithecal plates in apical view. Note plate 2a in quadra (Fig. 49) or penta (Fig. 50) configuration. Scale bars = 2 μ m.

Fig. 51. Dorsal/apical view of hypotheca showing series of cingular plates with an interior view of sulcal plates. Scale bar = 2 μ m.

Fig. 52. Hypotheca in ventral view showing details of sulcal plates. Scale bar = 2 μ m.

and often almost symmetrically located above plate 3'' (Figs 58, 60). However, a penta-configuration (i.e., plate 2a was pentagonal) was also present, with plate 2a contacting plates 3'' and 4'' (Figs 58, 59). Different from the Mediterranean type

strain, plate 2a of the Labrador Sea strain (AZA-2B1) was not concave, although at times the thick plate overgrowth of adjoining plates gave a slightly sunken appearance to this plate (Fig. 58). As the most characteristic feature, the ventral



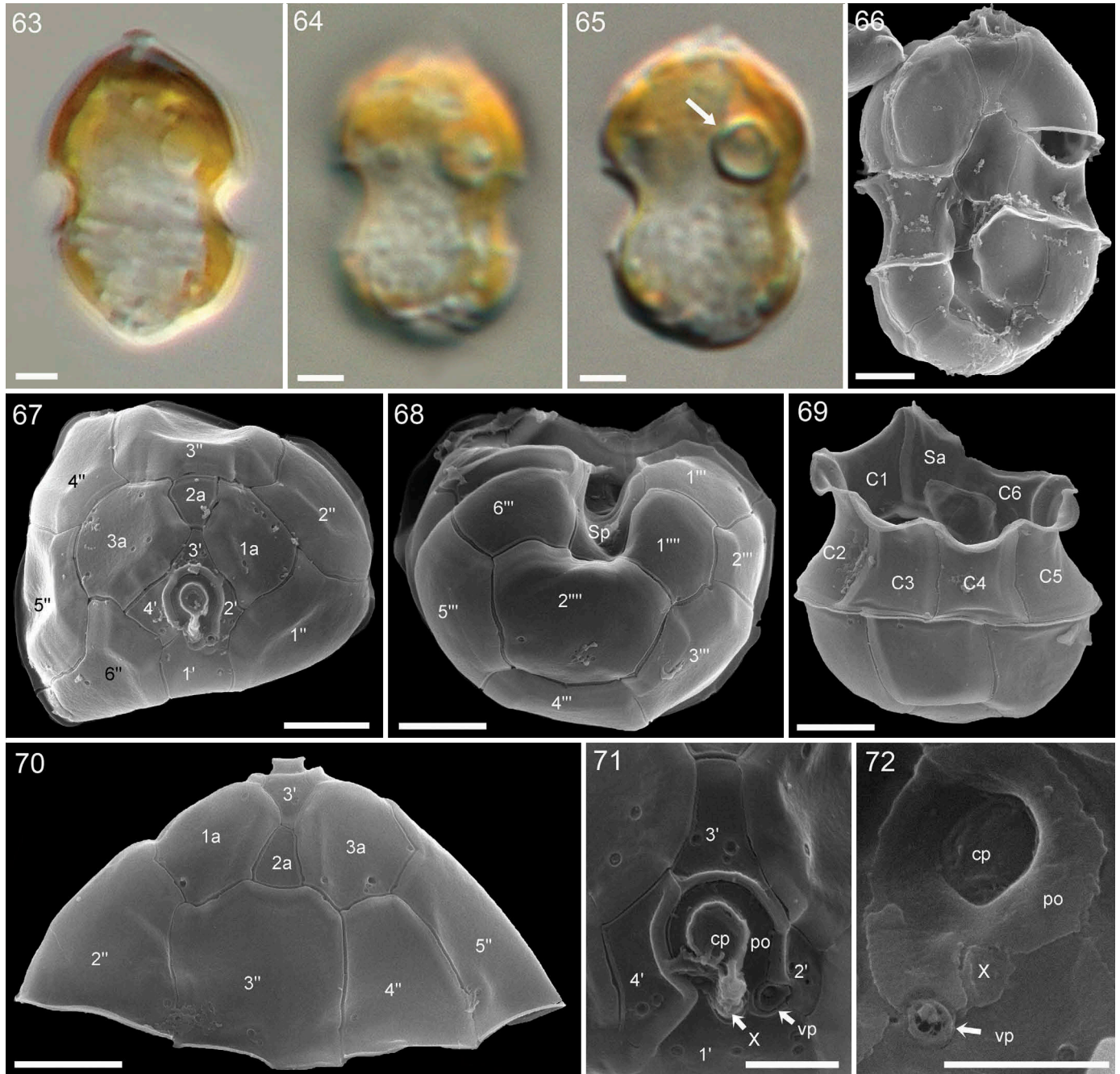
Figs 53–62. Light and scanning electron micrographs of *Azadinium dexteroporum* (strain AZA-2B1). cp, cover plate; X, X-plate; vp, ventral pore; po, pore plate.
Figs 53–56. LM, living cells showing general size and shape, one pyrenoid (arrow in Fig. 53) in episome, and presence of an antapical spine (arrow in Fig. 54). Scale bars = 2 μm.
Fig. 56. Dividing cell in late stage of desmoschisis. Scale bar = 2 μm.
Fig. 57. SEM of theca in ventral view. Scale bar = 2 μm.
Figs 58, 59. SEM of thecae in or dorsal view. Note plate 2a in quadra (Fig. 58) or penta (Fig. 59) configuration. Scale bars = 2 μm.
Fig. 60. Detailed dorsal view of apical area showing a plain plate 2a. Scale bar = 1 μm.
Fig. 61. Detailed view of apical pore complex showing position of ventral pore. Scale bar = 1 μm.
Fig. 62. Details of sulcal plate arrangement in external view. Scale bar = 1 μm.

pore (vp) was located at the distal end of the somewhat elongated right side of the asymmetric pore plate (Fig. 61). As has been observed in the central sulcal region of the type strain, occasionally an additional structure was visible above Sm and Sd (Fig. 62). However, it could not be verified if this represented an additional sulcal platelet, or an internal outgrowth of plate C6 extending to both central sulcal plates.

Azadinium trinitatum Tillmann & Nézan

Figs 63–72

Two strains of *Azadinium trinitatum* (AZA-2F, AZA-ZE10) were obtained. Cells varied in shape with an epitheca ranging from conical to more dome-shaped. Viewed by LM (Figs 63–65), one pyrenoid was located in the episome. SEM examination



Figs 63–72. Light and scanning electron micrographs of *Azadinium trinitatum* (strain AZA-2F). cp, cover plate; X, X-plate; vp, ventral pore; po, pore plate.

Figs 63–65. LM, living cells showing general size and shape, and one pyrenoid (arrow in Fig. 65) in episome. Scale bars = 2 μ m.

Fig. 66. SEM of theca in ventral view. Scale bar = 2 μ m.

Fig. 67. Epithecical plates in apical view. Scale bar = 2 μ m.

Fig. 68. Hypothecal plates in antapical view. Scale bar = 2 μ m.

Fig. 69. Dorsal view of hypotheca showing series of cingular plates with an interior view of sulcal plates. Scale bar = 2 μ m.

Fig. 70. Epitheca in dorsal view. Scale bar = 2 μ m.

Fig. 71. Detailed view of apical pore complex in external view. Scale bar = 1 μ m.

Fig. 72. Detailed view of apical pore complex in internal view. Scale bar = 1 μ m.

(Figs 66–72) showed most morphological details described for the type strain, i.e., presence of relatively small apical plates, a broad contact of plates 1a and 1", and a ventral pore located at the left lateral side of the pore plate in a cavity of the 1' plate at the tip of an elongated side of a slightly asymmetric pore plate. However, different from the type strain from Iceland, both cultured strains from the Labrador Sea lacked any indication of an antapical spine on plate 2'''.

AZA analysis strains

All strains tested were negative for AZA. The limits of detection (LOD) in the SRM mode for the targeted analysis of known AZA ranged between 0.7 and 23 ag cell⁻¹, depending on analysed biomass. LOD in the less sensitive precursor ion mode for the search of unknown AZA variants ranged between 29 and 596 ag cell⁻¹ (Table S2).

Sequence data and phylogeny

Three strains of *Az. perforatum* (AZA-2C, -2E, -2H) shared identical SSU rDNA sequences.

For LSU rDNA sequence comparison, *Az. dexteroporum* strain AZA-2B1 shared identical sequences with strain 1-D12 and differed from the type strain at nine positions (92.54% similarity for 624 bp). The AZA-ZE10 strain of *Az. trinitatum* differed from AZA-2F at three positions (99.60% similarity, out of 742 bp) and differed from N-39-04 at five positions (99.33% similarity, for 742 bp). Various strains of *Az. obesum* (AZA-1B, -1F, -2B2, -2D, -2G, -ZE8, -ZE9) and the type strain 2E10 shared identical sequences, and strains AZA-1C, -1G, -ZE7 shared identical sequences, too. They differed from each other at three positions (99.59% similarity, for 730 bp). *Az. perforatum* strains AZA-2C and -2H shared identical sequences and differed from AZA-2E at only one position (99.84% similarity, for 619 bp).

For ITS rDNA sequence comparison, *Az. dexteroporum* strain AZA-2B1 differed from strain 1-D12 at one position (99.81% similarity, for 529 bp) and from the type strain at 23 positions (95.60% similarity, for 529 bp). Strain *Az. trinitatum* (AZA-ZE10) differed from AZA-2F at three positions (99.45% similarity, for 544 bp) and differed from N-39-04 at four

positions (99.26% similarity, for 544 bp). Various strains of *Az. obesum* (AZA-1F, -2D, -2G, -ZE4, -ZE8, -ZE9) and the type strain 2E10 had identical sequences as did strains AZA-1C, -1G. They differed at three positions (99.46% similarity, for 560 bp). *Az. perforatum* strain AZA-2H differed from AZA-2C and -2E at three and four positions (99.51% and 99.35% similarity, for 616 bp). Uncorrected pairwise genetic distances for selected *Azadinium* and *Amphidoma* strains and species based on ITS rDNA sequences ranged from 0.002 to 0.319 (Table 2).

Maximum likelihood (ML) and Bayesian inference (BI) analysis based on combined SSU, ITS and partial LSU rDNA sequences yielded similar phylogenetic trees. The BI tree is illustrated in Fig. 73. The family Amphidomataceae was well resolved with moderate support (0.75 BPP/100 BS). The new species *Az. perforatum* was monophyletic with maximal support (1.0 BPP/100 BS) and was a sister clade to *Amphidoma parvula* and *Am. languida* with strong support (0.97 BPP/100 BS). The group diverged earlier than other species of Amphidomataceae, followed by *Azadinium concinnum*, with moderate support (0.7 BPP/100 BS). All other *Azadinium* species grouped with moderate support (0.82 BPP/100 BS). *Azadinium dexteroporum* strain AZA-2B1 grouped with strain 1-D12 with maximal support, which was a sister clade to the type strain from Italy. Both new *Az. trinitatum* strains (AZA-ZE10 and -2F) grouped with maximal support, and made a sister clade of strains from Norway and Iceland, with maximal support. All *Az. obesum* strains grouped with maximal support. The group consisted of two clades formed by strains from the North Atlantic Ocean with strong support (0.94 BPP/100 BS and 0.99 BPP/100 BS, respectively), and a third clade was formed by a strain from northeast Pacific Ocean.

Azadinium spp. in the Labrador Sea field sample Figs 74–109

SEM analysis of the concentrated formaldehyde-fixed bottle sample of station 1 in the central Labrador Sea confirmed the presence of species for which culture strains were obtained, i.e. *Az. perforatum*, *Az. dexteroporum*, *Az. obesum* and *Az. trinitatum*. Cells of *Az. obesum* in the field sample were most easily

Table 2. Uncorrected genetic *p*-distance between ITS rDNA sequences of some selected *Azadinium*/*Amphidoma* species/strains. Asterisks (*) denote strains obtained in this study.

	<i>Az. dexteroporum</i> AZA-2B1*	<i>Az. dexteroporum</i> (type)	<i>Az. obesum</i> AZA-1G*	<i>Az. obesum</i> 2E10	<i>Az. trinitatum</i> AZA-2F*	<i>Az. trinitatum</i> 4B11	<i>Az. concinnum</i> 1C6	<i>Az. perforatum</i> AZA-2H*	<i>Am. languida</i> SM1	<i>Am. parvula</i> H-1E9
<i>Az. dexteroporum</i> AZA-2B1*	-									
<i>Az. dexteroporum</i> (type)	0.038	-								
<i>Az. obesum</i> AZA-1G*	0.143	0.146	-							
<i>Az. obesum</i> 2E10	0.142	0.144	0.002	-						
<i>Az. trinitatum</i> AZA-2F*	0.151	0.156	0.055	0.053	-					
<i>Az. trinitatum</i> 4B11	0.150	0.154	0.047	0.046	0.006	-				
<i>Az. concinnum</i> 1C6	0.276	0.261	0.251	0.253	0.250	0.250	-			
<i>Az. perforatum</i> AZA-2H*	0.270	0.277	0.258	0.258	0.277	0.272	0.293	-		
<i>Am. languida</i> SM1	0.295	0.286	0.290	0.292	0.294	0.293	0.277	0.325	-	
<i>Am. parvula</i> H-1E9	0.312	0.302	0.307	0.309	0.319	0.317	0.285	0.295	0.206	-

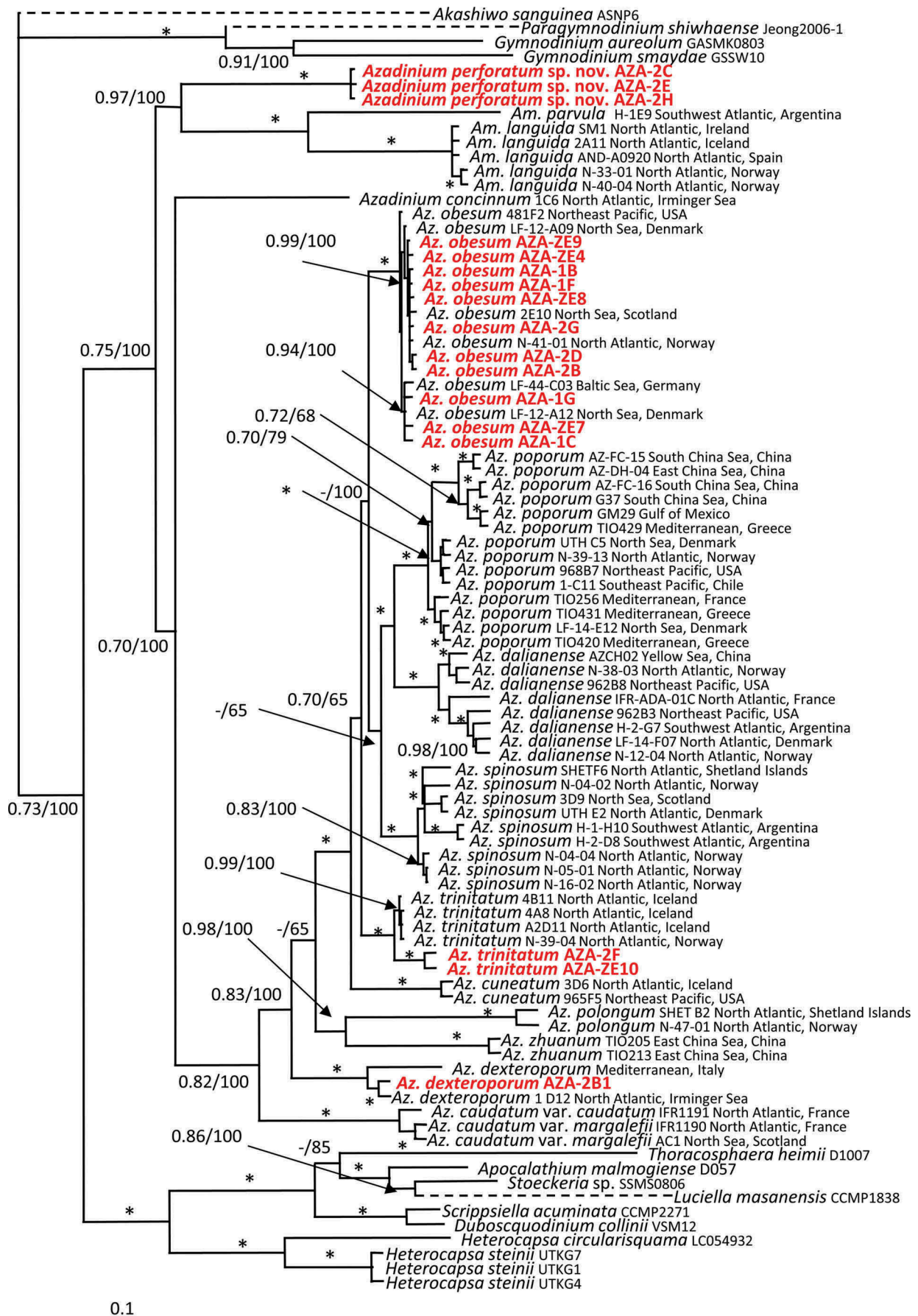
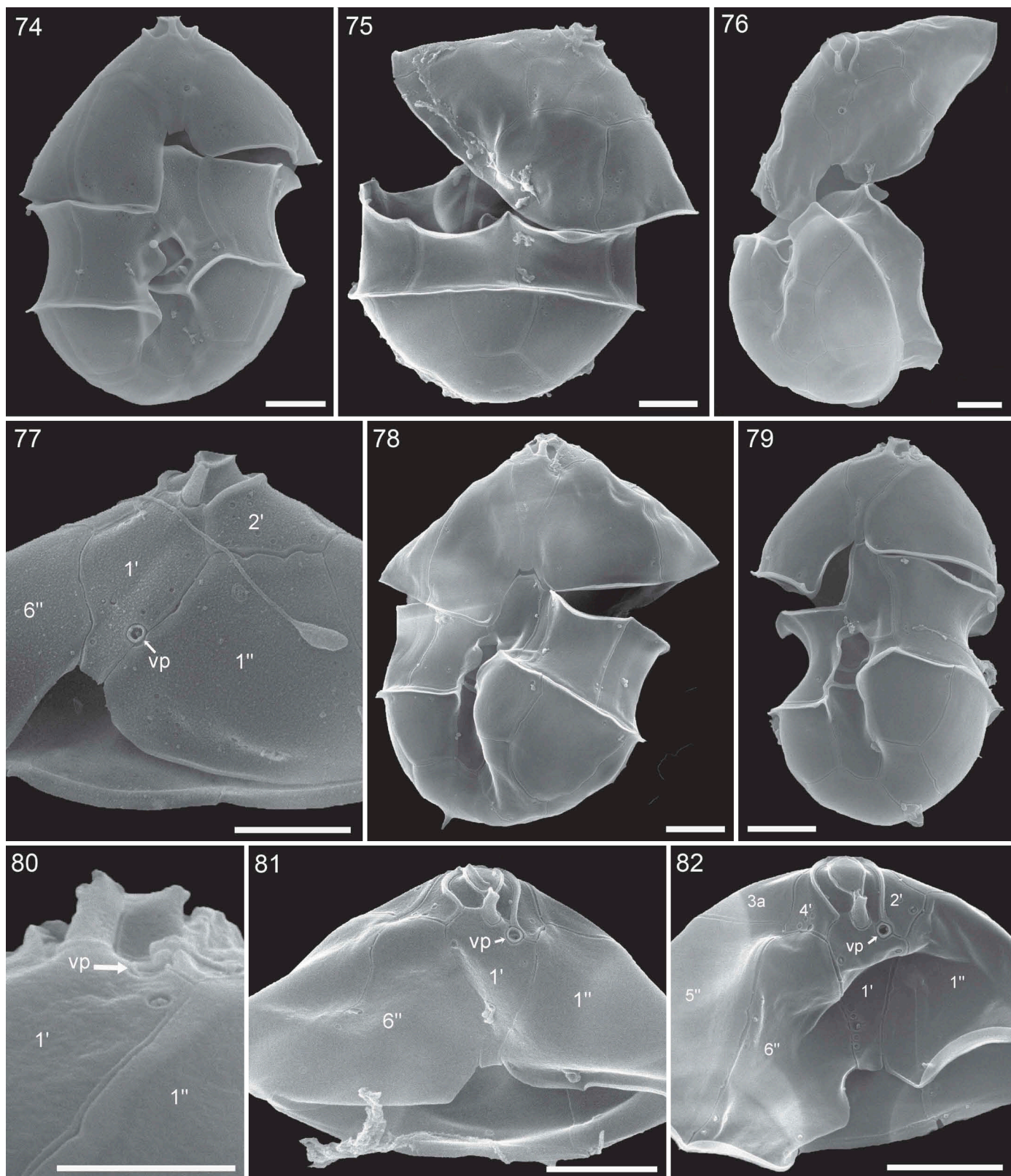


Fig. 73. Molecular phylogeny of *Azadinium* and *Amphidoma* inferred from concatenated SSU, partial LSU and ITS rDNA sequences using Bayesian inference (BI). New sequences of *Azadinium perforatum*, *Az. dexteroporum*, *Az. trinitatum* and *Az. obesum* indicated in red. Scale bar indicates number of nucleotide substitutions per site. Numbers on branches are statistical support values (left, Bayesian posterior probabilities; right, ML bootstrap support values). Asterisks (*) indicate maximal support (pp = 1.00 in BI and bootstrap = 100% in ML, respectively). Dashed lines indicate half-length.



Figs 74–82. SEM, field sample from station 1. vp, ventral pore.

Fig. 74. *Azadinium obesum* in ventral view. Scale bar = 2 μ m.

Fig. 75. *Azadinium obesum* in dorsal view. Scale bar = 2 μ m.

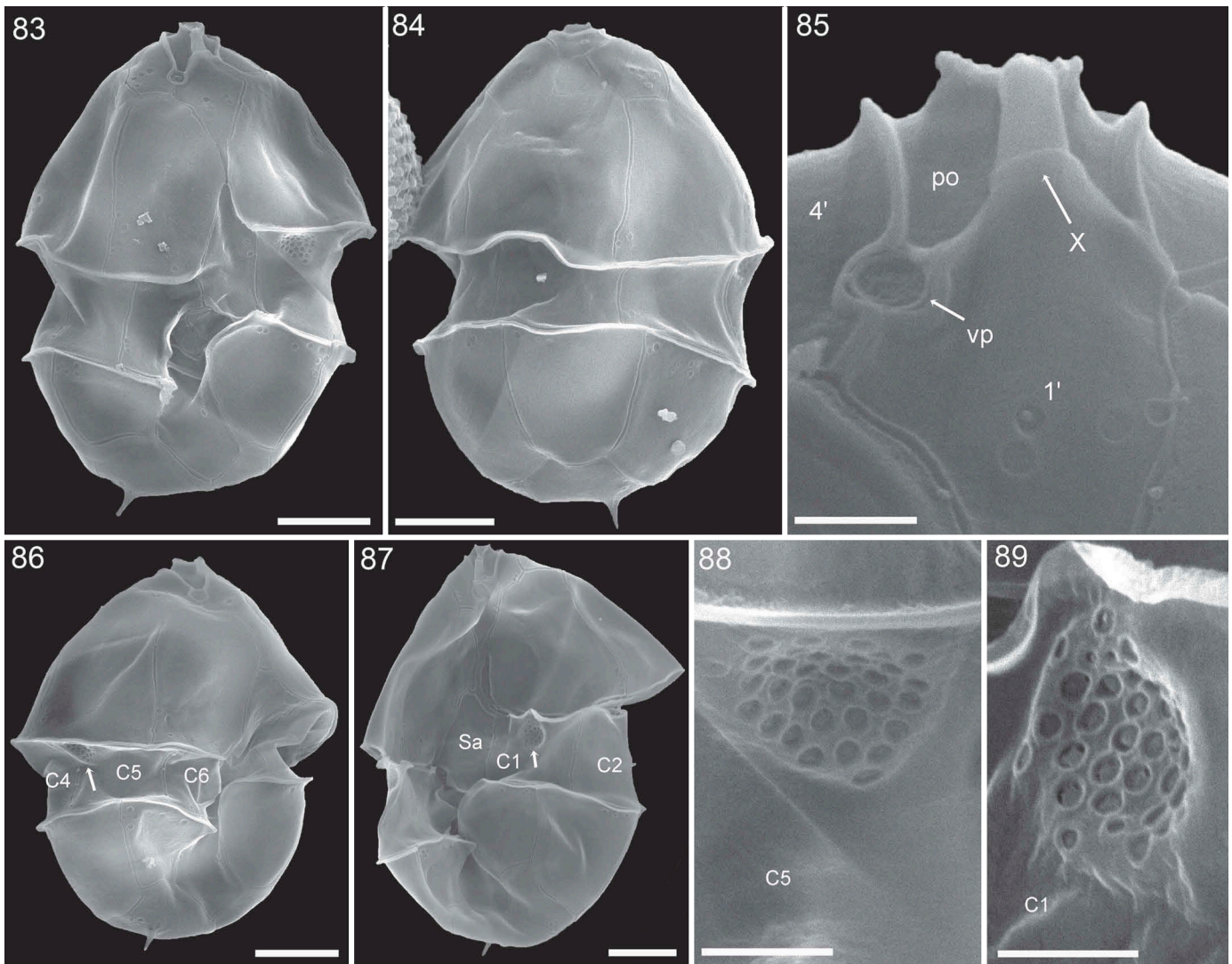
Fig. 76. Unfolded thecae of *Az. obesum* allowing antapical/lateral view of hypotheca and ventral view of epitheca. Scale bar = 2 μ m.

Fig. 77. Epitheca of *Azadinium obesum* in ventral view showing position of ventral pore. Scale bar = 2 μ m.

Figs 78, 79. *Azadinium trinitatum* in ventral view. Note presence (Fig. 78) or absence (Fig. 79) of antapical spine. Scale bars = 2 μ m.

Fig. 80. Detailed apical view of cell shown in Fig. 79 indicating position of ventral pore. Scale bar = 1 μ m.

Figs 81, 82. Epitheca of *Azadinium trinitatum* in ventral view showing position of ventral pore and small lateral apical plates. Scale bars = 2 μ m.



Figs 83–89. SEM, field sample from station 1, *Azadinium dexteroporum*. X, X-plate; vp, ventral pore; po, pore plate.

Fig. 83. Cell in ventral view. Scale bar = 2 μ m.

Fig. 84. Cell in dorsal view. Scale bar = 2 μ m.

Fig. 85. Detailed view of apical pore complex showing position of ventral pore. Scale bar = 0.5 μ m.

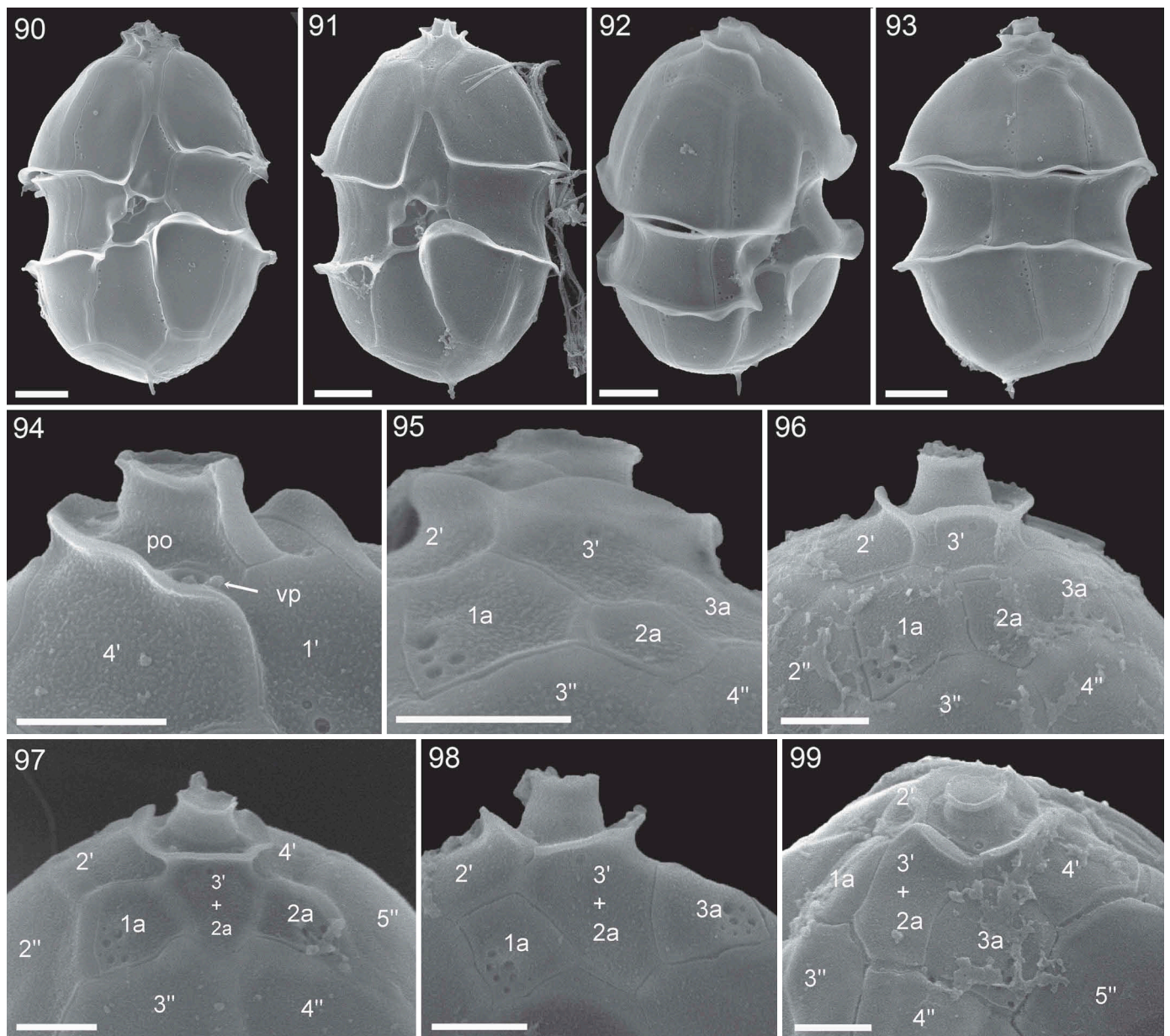
Figs 86, 87. Cells in ventral view indicating position of pore fields (arrows) on cingular plates C5 (Fig. 86) and C1 (Fig. 87). Scale bars = 2 μ m.

Figs 88, 89. Detailed view of cingular pore fields. Scale bars = 0.5 μ m.

identified by shape, position of ventral pore, by lack of a spine, and the small anterior intercalary plates with the missing contact of plates 1a and 1" (Figs 74–77). Identifying specimens of *Az. trinitatum* (Figs 78–82) was difficult and required simultaneous visibility of both the ventral pore and the narrow apical plates to differentiate the species from *Az. poporum* and *Az. dalianense*. Most cells identified as *Az. trinitatum* lacked a spine (Fig. 79), but a single cell with a spine, likely representing *Az. trinitatum*, was observed (Fig. 78). Cells of *Az. dexteroporum* (Figs 83–89) were easily detected by their small size and peculiar position of the ventral pore. All cells attributed to *Az. dexteroporum* in dorsal view had a plane median intercalary plate 2a (Fig. 84). Cells of the field sample had a conspicuous roundish field of thecal pores on cingular plates C1 and C5 (Figs 86–89). Specimens of the new species *Az. perforatum* (Figs 90–99) were regularly observed in the field sample, and these conformed to the morphological description of strain

AZA-2H. Just as for cells of the isolated strains, specimens of field samples were observed with fused dorsal apical plates 3' and 2a (Figs 97–99).

In addition to species confirmed by established strains, additional species were identified. A single specimen of *Az. spinosum* was recorded based on presence of a spine and position of the ventral pore (Figs 100, 101). With ventral pore position resembling *Az. spinosum*, but with an elongated pore plate and large lateral apical plates, a few cells were identified as *Az. polongum* Tillmann (Figs 102, 103). Although appearing wrinkled and unfortunately blurred in SEM, two cells were identified as *Am. languida* based on the ventral pore position (Figs 104, 105) or by the presence of an antapical pore (Fig. 106). Moreover, a number of epithelial cell fragments were observed where apical plate number and arrangement conformed to *Az. dalianense* Z. Luo, H. Gu & Tillmann, but where the position of the



Figs 90–99. SEM, field sample of station 1, *Azadinium perforatum* sp. nov. vp, ventral pore; po, pore plate.

Figs 90, 91. Cells in ventral view. Scale bars = 2 μ m.

Fig. 92. Cell in left lateral view. Scale bar = 2 μ m.

Fig. 93. Cell in dorsal view. Scale bar = 2 μ m.

Fig. 94. Detailed view of apical pore complex showing position of ventral pore. Scale bar = 1 μ m.

Figs 95–99. Detailed dorsal view of apical area. Note suture between plates 3' and 2a in Figs 95 and 96, which is missing in 97–99. Scale bars = 1 μ m.

ventral pore was distinct, and located on the suture of plates 1' and 2' (Figs 107–109). Whole cell views of such cells were not available, and further observation is needed to characterise this potential new species.

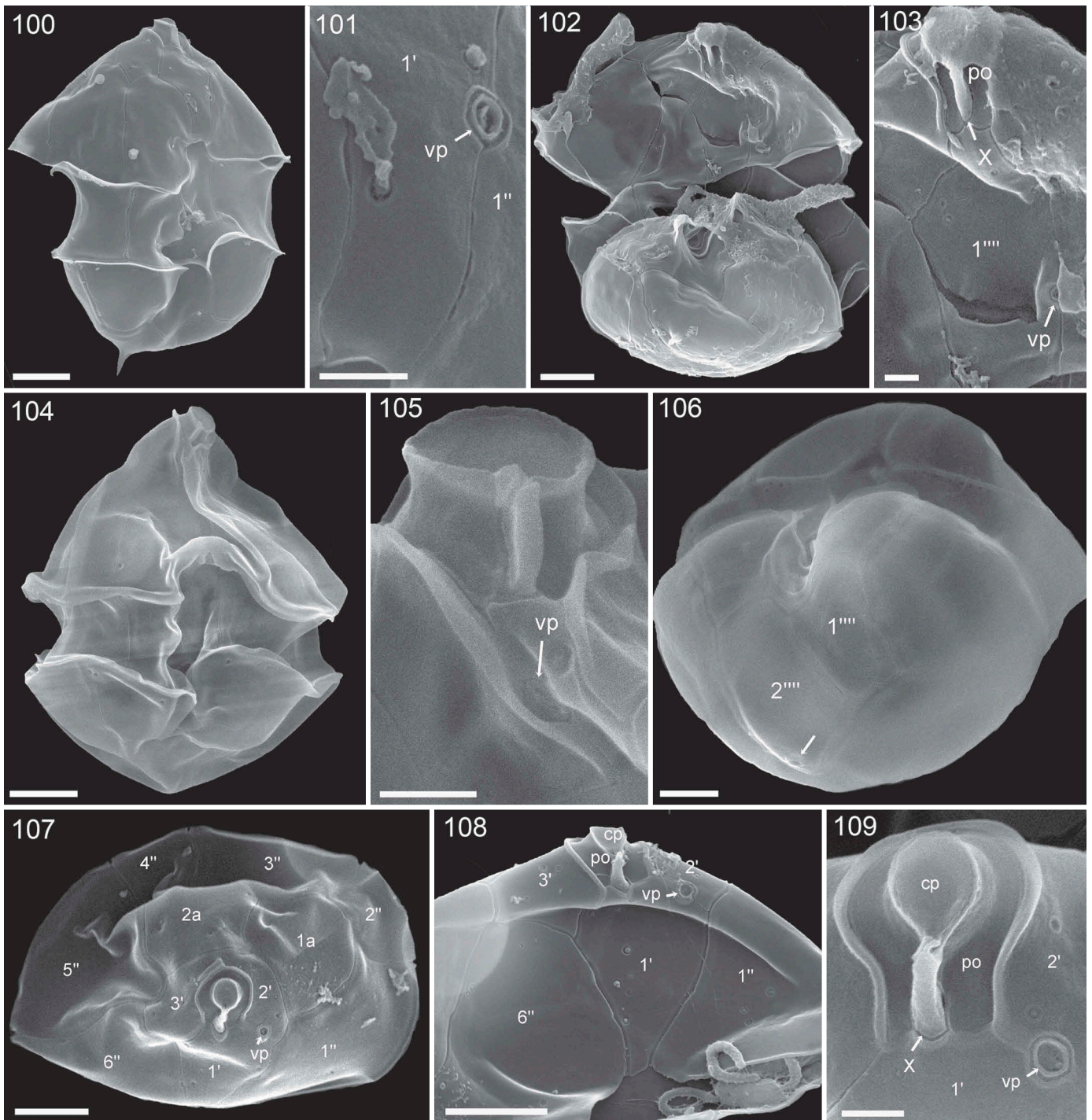
DISCUSSION

In the first study of Amphidomataceae in subarctic areas (Tillmann *et al.* 2014a), seven randomly isolated strains represented as many as five species, three of which were newly described. With the present study and the description of

a new *Azadinium* species, we demonstrate that the biodiversity of Amphidomataceae in the subarctic is remarkably large.

Azadinium perforatum sp. nov.

Morphological and molecular sequencing approaches clearly show that three of the newly established strains from the Labrador Sea represent a new species. The new taxon belongs to the genus *Azadinium* as it conforms to all features described as characteristic for the genus, including the plate pattern with four apical and three epithelial intercalary plates, both six post- and precingular plates, and two antapical plates



Figs 100–109. SEM, field sample of station 1. cp, cover plate; X, X-plate; vp, ventral pore; po, pore plate.

Fig. 100. *Azadinium spinosum* in ventral view. Scale bar = 2 μ m.

Fig. 101. *Azadinium spinosum*. Detailed view of the ventral area of the same cell shown in Fig. 100 to illustrate the position of the ventral pore. Scale bar = 0.5 μ m.

Fig. 102. *Azadinium polongum* in ventral view. Scale bar = 2 μ m.

Fig. 103. Detailed view of cell in Fig. 102 showing position of ventral pore and shape of the pore plate. Scale bar = 0.5 μ m.

Fig. 104. *Amphidoma languida* in ventral view. Scale bar = 2 μ m.

Fig. 105. Detailed view of cell in Fig. 104 showing position of ventral pore.

Fig. 106. *Amphidoma languida* in ventral/antapical view showing position of antapical pore (arrow). Scale bar = 2 μ m.

Figs 107–109. Epithecae of *Azadinium* sp. in ventral/apical view. Note peculiar position of ventral pore located in middle of suture of plates 1' and 2', and presence of three apical plates and two anterior intercalary plates. Scale bars = 2 μ m (107, 108) and 0.5 μ m (109).

(Tillmann et al. 2009). Although *Az. perforatum* resembles several other species of *Azadinium* in size and overall shape, it possesses a distinctive and unique combination of features,

which unambiguously differentiate this species from others (Table 3). Previous work on *Azadinium* and *Amphidoma* emphasised that the position of the ventral pore (vp) is

Table 3. Compilation of morphological features of species of *Azadinium* (including *Az. perforatum*) with a ventral pore located at the right side of the pore plate.

	<i>Az. caudatum</i> var. <i>margalefii</i>	<i>Az.</i> <i>dexteroporum</i>	<i>Az.</i> <i>concinnum</i>	<i>Az.</i> <i>luciferelloides</i>	<i>Az.</i> <i>zhuanum</i>	<i>Az.</i> <i>perforatum</i>
Length range μm (mean)	25.0–42.1	7.0–10.0 (8.5)	8.0–11.5 (9.5)	9.4–14.1 [†] (11.1)	16.8–21.6 (18.5)	15.3–20.0 (18.0)
Width range μm (mean)	18.4–30.0	5.0–8.0 (6.2)	5.6–8.3 (6.6)	6.6–10.1 [†] (7.9)	12.5–18.8 (14.8)	9.9–14.4 (12.6)
L/W ratio	1.2	1.4	1.4	1.4	1.3	1.5
Antapical projection	short horn, long spine	spine	spine	spine	spine	tiny spine
Stalked pyrenoid	none	1	none	unknown	1	none
1'' in contact 1a	yes	yes	no	yes	yes	no
Number of apicals and intercalary plates	4, 3	4, 3	4, 3	4, 3	3, 2	4, 3
Ventral pore position	pore plate, right side, inside Po	end of pore plate, right side	pore plate, right side	pore plate, right side	pore plate, right side	pore plate, right side
Pore plate symmetry	suture to 1' almost symmetric	suture to 1' strongly asymmetric, left side more apical	suture to 1' almost symmetric	suture to 1' almost symmetric	suture to 1' almost symmetric	suture to 1' almost symmetric
Thecal pores on pore plate	no	no	no	no	no	yes
Relative size of first and last intercalary	small	small	very small	small	large	small
Relative size of apical plates	medium	small	small	small	medium	medium
Size and arrangement of precingular plates	Plate 3'' mid-dorsal, plates 2'' and 4'' small	Plate 3'' mid-dorsal	Large, symmetrically arranged, plate 3'' and 4'' mid-dorsal	Plate 3'' mid-dorsal	Plate 3'' mid-dorsal	Large, symmetrically arranged, plate, 3'' and 4'' mid-dorsal
Records	Mediterranean, North Sea, Atlantic	Mediterranean, North Atlantic, South Atlantic	North Atlantic	South Atlantic	East China Sea, Yellow Sea	Labrador Sea
Reference [‡]	a, b	c, d	e	f	g	This study

[†] Based on SEM only. [‡] a, Nézan *et al.* (2012); b, Tillmann *et al.* (2014b); c, Percopo *et al.* (2013); d, Tillmann *et al.* (2015); e, Tillmann *et al.* (2014a); f, Tillmann & Akselmann (2016); g, Luo *et al.* (2017)

diagnostic for species discrimination, although two new species of *Amphidoma*, *Am. parvula* Tillmann & Gottschling and *Am. alata* Tillmann, lack such a ventral pore (Tillmann 2018a; Tillmann *et al.* 2018b). The amphidomatacean vp is larger than regular thecal pores, surrounded by a platelet-like structure, and has different and species-specific positions on the ventral part of the epitheca. With the vp on the right side of the pore plate, *Az. perforatum* is distinct from *Az. spinosum*, *Az. obesum*, *Az. polongum*, and *Az. asperum* Tillmann (vp on the left side of plate 1'), from *Az. poporum*, *Az. dalianense*, *Az. trinitatum*, *Az. cuneatum* (vp on left side of pore plate), and *Az. caudatum* var. *caudatum* (Halldal) Nézan & Chomérat (vp on right side of plate 1'; see Table 3 in Tillmann *et al.* 2014a). Species that have a vp positioned similarly to *Az. perforatum* (on the cells' right side of the pore plate) are *Az. caudatum* var. *margalefii* (Rampi) Nézan & Chomérat, *Az. concinnum*, *Az. dexteroporum*, *Az. luciferelloides* Tillmann & Akselman, and *Az. zhuanum* Z.Luo, Tillmann & H.Gu (Table 3). These species also have an antapical spine. In *Az. perforatum*, this spine was distinctly tiny, a feature consistent with field specimens (Figs 90–93). Notably, *Az. perforatum* is differentiated from all other *Azadinium* by its unique feature of thecal pores on the pore plate.

Although *Az. perforatum* is larger, it shares some morphological features with *Az. concinnum*, e.g., lack of a stalked pyrenoid, presence of small anterior intercalary plates, and lack of contact between the first precingular

plate and the small first anterior intercalary plate. Otherwise, this feature is found only in *Az. obesum* and *Az. cuneatum* (Tillmann *et al.* 2014a). Moreover, precingular plates of both *Az. perforatum* and *Az. concinnum* are rather large and symmetrically arranged, and both plates 3'' and 4'' are in mid-dorsal position, also seen in species of *Amphidoma* (Dodge & Saunders 1985; Tillmann *et al.* 2012; Tillmann 2018a). It is thus interesting to note that in previous phylogenetic analyses *Az. concinnum* had a rather basal position outside of all other *Azadinium* (Tillmann *et al.* 2019), not unlike the current phylogenetic analysis (Fig. 73). The seemingly large difference in epithelial plate arrangement (*Amphidoma* has six apical plates and no apical intercalary plate, whereas *Azadinium* species have only 3–4 apical plates but 2–3 apical intercalary plates) may also be explained by the fact that there is only one fewer epithelial plate in *Amphidoma*. It is conceivable that the intercalary plates of *Azadinium* are homologous to at least some of the apical plates in *Amphidoma* (Tillmann *et al.* 2014a). In this respect, it is important to note that for *Az. perforatum* a common plate variation was a fusion of apical plates 3' and 2a (Fig. 34), and this deviation was also common among field specimens (Figs 97–99). Next to the number of apical and intercalary plates, another consistent (at least for species of *Amphidoma* studied by SEM) morphological difference between *Azadinium* and *Amphidoma* was recently highlighted (Tillmann 2018a): both differ in

the detailed arrangement of the median sulcal area. For species of *Amphidoma*, the contact between plates Sa and C6 is long and covers almost the whole cingulum width, while for species of *Azadinium* this contact is more narrow, much less than one-third of cingulum width. In this respect, the sulcal area of both *Az. concinnum* and *Az. perforatum* are of the ‘*Azadinium*’ type.

While morphology of *Az. concinnum* and *Az. perforatum*, with their small apical and intercalary plates and the large and symmetrically arranged precingular plates, may indicate a similar and somewhat interim position of both species between *Azadinium* and *Amphidoma*, our phylogenetic analysis shows no close relationship between these species. The new *Az. perforatum* is placed outside of *Azadinium* as a sister clade to *Amphidoma*, whereas *Az. concinnum* is placed at the base within *Azadinium* but only moderately supported. The position of *Az. perforatum* thus indicates higher diversity within Amphidomataceae, potentially also at generic level. However, considering the morphological data and the currently unclear position of *Az. concinnum*, we argue that it is premature to erect a new genus for *Az. perforatum*. In the future, new species/strains of Amphidomataceae and/or new sequences of other marker genes may allow for a more differentiated evaluation of the generic diversity and evolution of the family.

In terms of symmetric precingular plates and relatively small apical and anterior intercalary plates, another similar species was described in 1959 as *Gonyaulax parva* from the Norwegian Sea and Iceland (Ramsfjell 1959). The plate pattern of this species corresponds to the plate tabulation of *Azadinium* and thus should be transferred to *Azadinium* at a later stage. The new species *Az. perforatum* differs from *G. parva* by its different shape (more elongated/slender for *Az. perforatum* than the broader *G. parva*) and by presence of the antapical spine.

The new species *Az. perforatum* is similar in shape to the sketch of a taxon from the Labrador Sea listed by Holmes (1956) as ‘*Goniaulax gracilis* Schiller’. However, this name is just briefly mentioned as ‘uncertain species’ by Schiller (1935) without any description or diagnosis, and is thus not validly described (ICN Art. 38.1). Moreover, the description by Holmes indicates that the Labrador Sea cells are smaller (10–15 µm long) and have a different length:width ratio. In addition, his drawings indicate that the anterior sulcal plate is vaulted and extends close to the apex. Holmes’ observations may thus refer to another undescribed small amphidomatacean species in the area. The name ‘*Goniaulax gracilis*’ sensu Schiller (and thus, likely a member of Amphidomataceae) is also linked to some pictures of small dinophytes in Bérard-Therriault *et al.* (1999; page 216, Fig. 90 a–c, g, i, l). The four LM images probably show species of Amphidomataceae, but no substantiating details are visible. One of the two SEM images (Fig. 90 i) probably represents a species of *Amphidoma* (*Am. languida*?), and the second cell (Fig. 90 l) is probably *Azadinium*, but with a distinct cell outline and a different development and position of the antapical spine than in *Azadinium perforatum*. ‘*Goniaulax gracilis*’ sensu Schiller is also mentioned briefly in a species list (without illustrations) by Smayda (1958) from Jan Mayen (North Atlantic) and by Hsiao (1983) from the Canadian Arctic, which may be

interpreted as evidence that small species of Amphidomataceae are common in cold-water, northern plankton communities.

Amphidomataceae in Labrador Sea and coastal Greenland waters

Positive hits of the SYBR Green PCR assay indicate that Amphidomataceae are widely distributed in the study area, covering quite different regions including the open, deep Labrador Sea, inland fjord areas such as Godthaab Fjord, Disko Bay and the two northernmost stations. The amphidomatacean SYBR Green PCR assay was not performed quantitatively but relatively high Ct values [cycle threshold (Ct) > 27] indicate a rather low cell abundance for all Greenland stations. Slightly lower Ct values (Ct: 27–30) were observed inside Disko Bay, indicating higher densities than in stations further outside (Ct: 30–33). Generally, low abundance corresponds to a lack of firm identification of amphidomatacean cells during quantitative Utermöhl counts for these stations. A lack of microscopic confirmation does not contradict low PCR signals as the microscopy sample volume was limited (50 ml) and single amphidomatacean cells might easily go unnoticed in the larger group of small unidentified dinoflagellates. Thus, the data underline the advantage of molecular detection at low abundance of this small and inconspicuous group of microalgae.

In the whole Greenland area, only two stations were positive with the species-specific qPCR assays, and both indicate the presence of low background levels of *Azadinium poporum*. This species has a wide distribution in the Mediterranean Sea, the Pacific and the Atlantic (Tillmann 2018b). The northern record reported here needs to be confirmed by more direct methods, as false-positive qPCR reactions cannot be ruled out. Nevertheless, *in silico* sequence comparison of all other known amphidomatacean species with *Az. poporum* primers and probe (Wietkamp, unpublished) identified at least seven base pair mismatch. This underlines the high specificity of the assay, and indicates that risk of a false-positive cross-reaction is low.

The first station in the central Labrador Sea was distinct from the more coastal Greenland stations and had a total plankton biomass approximately three times higher than the Greenland station with the highest biomass (estimated from Utermöhl counts and volume-carbon conversion, unpublished data). In contrast to most coastal Greenlandic stations, diatoms in the central Labrador Sea were of low abundance (absolute and relative) and comprised only 0.6% of total plankton biomass. Plankton at station 1 was dominated by small (< 20 µm) unidentified flagellates (1.7 × 10⁶ l⁻¹). Most intriguing was the dominance of a c. 25 µm large unidentified haptophyte with a short, stiff haptonema and the very unusual presence of c. 20 small chloroplasts. Dinoflagellates made up about one-third of the biomass at station 1 with a high density of small athecate species, most of which could not be identified to species level. In contrast to the coastal Greenlandic stations, a significant number of toxigenic cells of *Dinophysis acuminata* (330 l⁻¹) were present and confirmed the presence of relatively high levels of pectenotoxin-2 (Krock, unpublished). The most abundant phototrophic dinoflagellate was a yet undetermined small

(10–15 μm) *Prorocentrum* (64×10^3 cells l^{-1}). Within this diverse community, Amphidomataceae were fairly abundant (9.2×10^3 cells l^{-1}) as estimated by quantitative LM, and confirmed by an exceptionally strong signal of the SYBR Green PCR assay ($\text{Ct } 19.85 \pm 0.06$, $n = 3$). The first station in the central Labrador Sea was the only station where the toxigenic species *Am. languida* was recorded by the specific qPCR assay, yielding an abundance of *c.* 120 cells l^{-1} , which is in the lower range of cell densities determined for this species along the Danish coast (Wietkamp *et al.* 2019b). In any case, amphidomatacean abundance in the central Labrador Sea in June is lower than bloom concentrations of Amphidomataceae that may be as high as 10^6 cells l^{-1} (*Az. polongum* bloom in Peru; Tillmann *et al.* 2017) or 3×10^5 to 1×10^7 cells l^{-1} (Amphidomataceae spring bloom densities on Argentine Shelf; Akselman & Negri 2012; Tillmann *et al.* 2019).

Based on both, field-sample-SEM and the amphidomatacean strains established from station 1, a large diversity of Amphidomataceae in the central Labrador Sea is evident. Next to strain-based records of *Az. obesum*, *Az. trinitatum*, *Az. dexteroporum*, and *Az. perforatum*, SEM indicates the presence of *Az. spinosum*, *Am. languida*, and *Az. polongum*. Moreover, another probably yet undescribed species is present whose apical plate number and arrangement conform to *Az. dalianense* (Luo *et al.* 2013), but the position on the ventral pore is different (Figs 107–109). However, no whole-cell views were obtained, and more studies are needed for a more detailed morphological description of this potentially new species.

The ability to establish multiple strains of *Az. obesum*, *Az. trinitatum* and *Az. perforatum* indicates that these are the dominant Amphidomataceae in the summer community of the Labrador Sea. *Azadinium obesum* is known from the North Atlantic Ocean (Tillmann *et al.* 2010, 2018a) and *Az. trinitatum* is known from the Iceland area (Tillmann *et al.* 2014a); thus, their presence in the Labrador Sea was not unexpected.

The new Labrador strains of *Az. trinitatum* form a well-supported sister clade to the Icelandic strains of the species. Uncorrected genetic distance of ITS rDNA between both clades is relatively low (0.006, Table 2), but nevertheless indicates significant intraspecific variability in *Az. trinitatum*. This is supported by the fact that the new strains lack an antapical spine, which is present in Icelandic populations (Tillmann *et al.* 2014a).

The Labrador Sea record of *Az. dexteroporum*, together with a previously established strain from the Irminger Sea (Tillmann *et al.* 2015), confirm the presence of this species in the subarctic region. The new Labrador Sea strain differs significantly from the Mediterranean type material in terms of sequence data (ITS rDNA genetic distance = 0.038, Table 2) and by the presence of a plain median intercalary plate; this plate is distinctly concave in the Mediterranean strain (Percopo *et al.* 2013). All of these facts indicate cryptic diversity for *Az. dexteroporum*, and taxonomic assessment of this diversity should be the objective of future research.

One single cell, most likely representing *Az. spinosum*, was identified in the SEM sample from station 1, but the *Az. spinosum*-specific qPCR assay was negative. This might be explained by abundance below the qPCR detection limit of approx. 0.5 cells l^{-1} . Moreover, recent studies have revealed

significant intraspecific variability in *Az. spinosum* in terms of rDNA sequence data (Tillmann *et al.* 2018a, 2019), which likely affects the primer/probe binding efficiency. If *Az. spinosum* in the Labrador Sea is from a different ribotype than that of the *Az. spinosum* strains/ribotype used to design the assay, the assay efficiency and thus detection and quantification of the qPCR method would be affected.

Azaspiracids

No azaspiracids were detected in discrete plankton samples from the study area. A lack of AZA at the first station, where a cell density of 120 cells l^{-1} of the toxigenic *Am. languida* was determined by qPCR, may be explained by the detection limit of the chemical method. Combining the LOD of the AZA measurements (10 pg l^{-1}) and the highest AZA cell quota of *Am. languida* reported in the literature, of 100 fg cell $^{-1}$ (Wietkamp *et al.* 2019b), yields a ‘cell detection limit’ of 100 cells l^{-1} , which is only slightly lower than the qPCR-determined abundance. Absence of AZA in field samples also agrees with the lack of AZA production of all newly established strains of *Az. obesum*, *Az. trinitatum*, *Az. dexteroporum* and *Az. perforatum*. For *Az. obesum* and *Az. trinitatum*, this confirms previous study results that neither species are AZA producers (Tillmann *et al.* 2014a; Wietkamp *et al.* 2019b). AZA has unambiguously been described for type strains of *Az. dexteroporum* from the Mediterranean Sea (Rossi *et al.* 2017). However, another strain (1-D12) isolated from the subarctic Irminger Sea lacked AZA (Tillmann *et al.* 2015). Absence of AZA in the new Labrador Sea strains confirms this finding and suggests non-toxicity of *Az. dexteroporum* from the North Atlantic Ocean. A comparable situation with both producing and non-producing strains, with significant levels of sequence differences, can be seen in *Az. poporum* (Luo *et al.* 2018; Wietkamp *et al.* 2019b) and *Az. spinosum* (Tillmann *et al.* 2019). None of the high biomass samples of all three clonal strains of *Az. perforatum* revealed AZA, indicating that this new species likely does not produce AZA. However, with the aforementioned strain variability in *Az. dexteroporum* and the recently discovered intraspecific variability in AZA expression for *Az. poporum* and *Az. spinosum* (Luo *et al.* 2018; Tillmann *et al.* 2019; Wietkamp *et al.* 2019b), more studies and strains of *Az. perforatum* are needed for confirmation. In any case, with 10 non-toxic species versus four known AZA producers, it is evident that AZA production within Amphidomataceae is the exception rather than the rule.

Azaspiracids were also lacking in the SPATT samples from the FerryBox flow-through system. SPATT samplers specifically adsorb large, lipophilic molecules such as AZA (Fux *et al.* 2009; MacKenzie *et al.* 2004), and with long-term deployment (here for about 1 week) allow for integrative sampling to detect minute amounts of these molecules. A lack of AZA detection in SPATT samples thus strengthens the conclusion that abundance and significance of toxigenic Amphidomataceae in June–July for the western Greenland area are low.

ACKNOWLEDGEMENTS

We thank chief scientist Oliver Zielinski, Captain Maaß and the crew of RV *Maria S. Merian* for assistance and logistical support with the collection of field material used in this study. Anne Müller and

Thomas Max are acknowledged for their help with on-board work during the cruise and especially for DNA and toxin extraction. Torben Krohn (AWI) kindly assisted with AZA sample preparation and analysis. Thanks to Marc Gottschling (Uni München) for helpful discussions.

FUNDING

This work was supported by the PACES research program of the Alfred Wegener Institute as part of the Helmholtz Foundation initiative in Earth and Environment, and by the German Ministry for Education and Research (project RIPAZA) under grant number 03F0763A.

ORCID

Haifeng Gu  <http://orcid.org/0000-0002-2350-9171>

REFERENCES

- Akselman R. & Negri R.M. 2012. Blooms of *Azadinium* cf. *spinosum* Elbrächter et Tillmann (Dinophyceae) in northern shelf waters of Argentina, Southwestern Atlantic. *Harmful Algae* 19: 30–38. DOI: [10.1016/j.hal.2012.05.004](https://doi.org/10.1016/j.hal.2012.05.004).
- Bérard-Therriault L., Poulin M. & Bossé L. 1999. *Guide d'identification du phytoplancton marin de l'estuaire et du golfe de Saint-Laurent incluant également certaines protozoaires. Publication spéciale canadienne des sciences halieutiques et aquatiques* 128. NRC Research Press, Ottawa, Canada. 387 pp.
- Boc A., Diallo A.B. & Makarenkov V. 2012. T-REX: a web server for inferring, validating and visualizing phylogenetic trees and networks. *Nucleic Acids Research* 40: 573–579. DOI: [10.1093/nar/gks485](https://doi.org/10.1093/nar/gks485).
- Brandt K. & Apstein C. [eds] 1908. *Nordisches Plankton*. Lipsius & Tischer, Kiel, Leipzig, Germany. 356pp.
- Cleve P.T. 1873. On diatoms of the Arctic Sea. *Bihang Kongelige Svenska Vetenskapelige Akademie Handlingar* 1(13): 1–28.
- Cleve P.T. & Grunow A. 1880. Beiträge zur Kenntniss der arktischen Diatomeen. *Kongiga Svenska Vetenskaps-Akademiens Handlingar* 17: 1–122.
- Dodge J.D. & Saunders R.D. 1985. An SEM study of *Amphidoma nucula* (Dinophyceae) and description of the thecal plates in *A. caudata*. *Archiv Für Protistenkunde* 129: 89–99. DOI: [10.1016/S0003-9365\(85\)80012-9](https://doi.org/10.1016/S0003-9365(85)80012-9).
- Ehrenberg C.G. 1843. Über neue Anschauungen des kleinsten nördlichen Polarlebens. *Deutsche Akademie Der Wissenschaften Zu Berlin Monatsberichte* 1843: 522–529.
- Elferink S., Neuhaus S., Wohlrab S., Toebe K., Voß D., Gottschling M., Lundholm N., Krock B., Koch B.P., Zielinski O. *et al.* 2017. Molecular diversity patterns among various phytoplankton size-fractions in West Greenland in late summer. *Deep-Sea Research Part I* 121: 54–69. DOI: [10.1016/j.dsr.2016.11.002](https://doi.org/10.1016/j.dsr.2016.11.002).
- Forootan A., Sjöback R., Björkman J., Sjögreen B., Linz L. & Kubista M. 2017. Methods to determine limit of detection and limit of quantification in quantitative real-time PCR (qPCR). *Biomolecular Detection and Quantification* 12: 1–6. DOI: [10.1016/j.bdq.2017.04.001](https://doi.org/10.1016/j.bdq.2017.04.001).
- Fux E., Biré R. & Hess P. 2009. Comparative accumulation and composition of lipophilic marine biotoxins in passive samplers and in mussels (*M. edulis*) on the west coast of Ireland. *Harmful Algae* 8: 523–537. DOI: [10.1016/j.hal.2008.10.007](https://doi.org/10.1016/j.hal.2008.10.007).
- Gran H.H. 1929. Quantitative plankton investigations carried out during the expedition with the “Michael Sars”, July – Sept. 1924. *Rapports Et Procès-verbaux Des Réunions/Conseil Permanent International pour l'Exploration de la Mer* 56: 1–50.
- Grontved J. & Seidenfaden G. 1938. The phytoplankton of the waters west of Greenland. *Meddelelser Om Grønland* 82(5): 1–380.
- Hall T. 1999. BioEdit: a user-friendly biological sequence alignment editor and analysis program for windows 95/98/NT. *Nucleic Acids Symposium Series* 41: 95–98.
- Haldal P. 1953. Phytoplankton investigations from weather Ship M in the Norwegian Sea, 1948–49. *Hvalrådets Skrifter* 38: 1–91.
- Hess P., McCarron P., Krock B., Kilcoyne J. & Miles C.O. 2014. Azaspiracids: chemistry, biosynthesis, metabolism, and detection. In: *Seafood and freshwater toxins*, (Ed. by L.M. Botana), pp. 799–821. CRC Press, Boca Raton, Florida, USA.
- Holmes R.W. 1956. The annual cycle of phytoplankton in the Labrador Sea, 1950–1951. *Bulletin of the Bingham Oceanographic Collection* 16: 1–74.
- Hsiao S.I.C. 1983. A checklist of marine phytoplankton and sea ice microalgae recorded from Arctic Canada. *Nova Hedwigia* 37: 225–313.
- Katoh K. & Standley D.M. 2013. MAFFT multiple sequence alignment software version 7: improvements in performance and usability. *Molecular Biology and Evolution* 30: 772–780. DOI: [10.1093/molbev/mst010](https://doi.org/10.1093/molbev/mst010).
- Keller M.D., Selvin R.C., Claus W. & Guillard R.R.L. 1987. Media for the culture of oceanic ultraphytoplankton. *Journal of Phycology* 23: 633–638. DOI: [10.1111/j.1529-8817.1987.tb04217.x](https://doi.org/10.1111/j.1529-8817.1987.tb04217.x).
- Kilias E., Kattner G., Wolf C., Frickenhaus S. & Metfies K. 2014. A molecular survey of protist diversity through the central Arctic Ocean. *Polar Biology* 37: 1271–1287. DOI: [10.1007/s00300-014-1519-5](https://doi.org/10.1007/s00300-014-1519-5).
- Kilias E., Wolf C., Nöthig E.-M., Peeken I. & Metfies K. 2013. Protist distribution in the western Fram Strait in summer 2010 based on 454-pyrosequencing of 18S rDNA. *Journal of Phycology* 49: 996–1010. DOI: [10.1111/jpy.12109](https://doi.org/10.1111/jpy.12109).
- Lebour M.V. 1925. *The dinoflagellates of the northern seas*. The Marine Biological Association of the United Kingdom, Plymouth, UK. 250 pp.
- Luo Z., Gu H., Krock B. & Tillmann U. 2013. *Azadinium dalianense*, a new dinoflagellate from the Yellow Sea, China. *Phycologia* 52: 625–636. DOI: [10.2216/13-178.1](https://doi.org/10.2216/13-178.1).
- Luo Z., Krock B., Giannakourou A., Venetsanopoulou A., Pagou K., Tillmann U. & Gu H. 2018. Sympatric occurrence of two *Azadinium poporum* ribotypes in the eastern Mediterranean Sea. *Harmful Algae* 78: 75–85. DOI: [10.1016/j.hal.2018.08.003](https://doi.org/10.1016/j.hal.2018.08.003).
- Luo Z., Krock B., Mertens K.N., Nézan E., Chomérat N., Bilien G., Tillmann U. & Gu H. 2017. Adding new pieces to the *Azadinium* (Dinophyceae) diversity and biogeography puzzle: non-toxicogenic *Azadinium zhuanium* sp. nov. from China, toxicogenic *A. poporum* from the Mediterranean, and a non-toxicogenic *A. dalianense* from the French Atlantic. *Harmful Algae* 66: 65–78. DOI: [10.1016/j.hal.2017.05.001](https://doi.org/10.1016/j.hal.2017.05.001).
- MacKenzie L., Beuzenberg V., Holland P., McNabb P. & Selwood A.I. 2004. Solid phase adsorption toxin tracking (SPATT): a new monitoring tool that simulates the biotoxin contamination of filter feeding bivalves. *Toxicon* 44: 901–918. DOI: [10.1016/j.toxicon.2004.08.020](https://doi.org/10.1016/j.toxicon.2004.08.020).
- Medinger R., Nolte V., Pandey R.V., Jost S., Ottenwaelder B., Schloetterer C. & Boenigk J. 2010. Diversity in a hidden world: potential and limitation of next-generation sequencing for surveys of molecular diversity of eucaryotic microorganisms. *Molecular Ecology* 19: 32–40.
- Metfies K., Von Appen W.J., Kilias E., Nicolaus A. & Nöthig E.M. 2012. Biogeography and photosynthetic Biomass of Arctic Marine Pico-Eukaryotes during Summer of the Record Sea Ice Minimum 2012. *PloS One* 11: e0148512.
- Nézan E., Tillmann U., Bilien G., Boulben S., Chèze K., Zentz F., Salas R. & Chomérat N. 2012. Taxonomic revision of the dinoflagellate *Amphidoma caudata*: transfer to the genus *Azadinium* (Dinophyceae) and proposal of two varieties, based on morphological and molecular phylogenetic analyses. *Journal of Phycology* 48: 925–939. DOI: [10.1111/j.1529-8817.2012.01159.x](https://doi.org/10.1111/j.1529-8817.2012.01159.x).
- Nylander J.A., Wilgenbusch J.C., Warren D.L. & Swofford D.L. 2008. AWTY (are we there yet?): a system for graphical exploration of MCMC convergence in Bayesian phylogenetics. *Bioinformatics* 24: 581–583. DOI: [10.1093/bioinformatics/btm388](https://doi.org/10.1093/bioinformatics/btm388).
- Percopo I., Siano R., Rossi R., Soprano V., Sarno D. & Zingone A. 2013. A new potentially toxic *Azadinium* species (Dinophyceae) from the Mediterranean Sea, *A. dexteroporum* sp. nov. *Journal of Phycology* 49: 950–966. DOI: [10.1111/jpy.12104](https://doi.org/10.1111/jpy.12104).
- Posada D. 2008. ModelTest: Phylogenetic model averaging. *Molecular Biology and Evolution* 25: 1253–1256. DOI: [10.1093/molbev/msn083](https://doi.org/10.1093/molbev/msn083).
- Poulin M., Daugbjerg N., Gradinger R., Ilyash L., Ratkova T. & Von Quillfeldt C. 2011. The pan-Arctic biodiversity of marine pelagic and sea-ice unicellular eukaryotes: a first-attempt assessment. *Marine Biodiversity* 41: 13–28. DOI: [10.1007/s12526-010-0058-8](https://doi.org/10.1007/s12526-010-0058-8).

- Preston-Thomas H. 1990. The international temperature scale of 1990 (ITS-90). *Metrologia* 27: 3–10. DOI: [10.1088/0026-1394/27/1/002](https://doi.org/10.1088/0026-1394/27/1/002).
- Ramsfjell E. 1959. Two new phytoplankton species from the Norwegian Sea, the diatom *Coscinosira poroseriata*, and the dinoflagellate. *Gonyaulax Parva*. *Nytt Magazin for Botanikk* 7: 175–177.
- Ronquist F. & Huelsenbeck J.P. 2003. MrBayes 3: Bayesian phylogenetic inference under mixed models. *Bioinformatics* 19: 1572–1574. DOI: [10.1093/bioinformatics/btg180](https://doi.org/10.1093/bioinformatics/btg180).
- Rossi R., Dell'Aversano C., Krock B., Ciminiello P., Percopo I., Tillmann U., Soprano V. & Zingone A. 2017. Mediterranean *Azadinium dexteroporum* (Dinophyceae) produces AZA-35 and six novel azaspiracids: a structural study by a multi-platform mass spectrometry approach. *Analytical and Bioanalytical Chemistry* 409: 1121–1134. DOI: [10.1007/s00216-016-0037-4](https://doi.org/10.1007/s00216-016-0037-4).
- Schiller J. 1935. Dinoflagellatae (Peridineae) in monographischer Behandlung. In: *Dr. L. Rabenhorst's Kryptogamen-Flora von Deutschland, Österreich und der Schweiz*, (Ed. by L. Rabenhorst), pp. 1–320. Akademische Verlagsgesellschaft, Leipzig, Germany.
- Schlitzer R. 2018. Ocean data view. <https://odv.awi.de>.
- Smayda T.J. 1958. Phytoplankton studies around Jan Mayen Island March - April, 1955. *Nytt Magazin for Botanikk* 6: 75–96.
- Smith K.F., Rhodes L., Harwood D.T., Adamson J., Moisan C., Munday R. & Tillmann U. 2016. Detection of *Azadinium poporum* in New Zealand: The use of molecular tools to assist with species isolations. *Journal of Applied Phycology* 28: 1125–1132. DOI: [10.1007/s10811-015-0667-5](https://doi.org/10.1007/s10811-015-0667-5).
- Stamatakis A. 2006. RAxML-VI-HPC: Maximum likelihood-based phylogenetic analyses with thousands of taxa and mixed models. *Bioinformatics* 22: 2688–2690. DOI: [10.1093/bioinformatics/btl446](https://doi.org/10.1093/bioinformatics/btl446).
- Swofford D.L. 2002. *PAUP*: phylogenetic analysis using parsimony (* and other methods)*, version 4.0b10. Sinauer Associates, Sunderland, Massachusetts, USA.
- Thronsdon J., Hasle G.R. & Tangen K. 2007. *Phytoplankton of Norwegian coastal waters*. Almatier Forlag AS, Oslo, Norway. 343 pp.
- Tillmann U. 2018a. Electron microscopy of a 1991 spring plankton sample from the Argentinean shelf reveals the presence of four new species of Amphidomataceae (Dinophyceae). *Phycological Research* 66: 269–290. DOI: [10.1111/pre.12225](https://doi.org/10.1111/pre.12225).
- Tillmann U. 2018b. Amphidomataceae. In: *Harmful Algae Blooms, a compendium desk reference*, (Ed. by S.E. Shumway, J.A. Burkholder & S.L. Morton), pp. 575–582. Wiley, Hoboken, New Jersey, USA.
- Tillmann U. & Akselman R. 2016. Revisiting the 1991 algal bloom in shelf waters off Argentina: *Azadinium luciferelloides* sp. nov. (Amphidomataceae, Dinophyceae) as the causative species in a diverse community of other amphidomataceans. *Phycological Research* 64: 160–175. DOI: [10.1111/pre.2016.64.issue-3](https://doi.org/10.1111/pre.2016.64.issue-3).
- Tillmann U., Edvardsen B., Krock B., Smith K.F., Paterson R.F. & Voß D. 2018a. Diversity, distribution, and azaspiracids of Amphidomataceae (Dinophyceae) along the Norwegian coast. *Harmful Algae* 80: 15–34. DOI: [10.1016/j.hal.2018.08.011](https://doi.org/10.1016/j.hal.2018.08.011).
- Tillmann U., Elbrächter M., John U., Krock B. & Cembella A. 2010. *Azadinium obesum* (Dinophyceae), a new nontoxic species in the genus that can produce azaspiracid toxins. *Phycologia* 49: 169–182. DOI: [10.2216/PH09-35.1](https://doi.org/10.2216/PH09-35.1).
- Tillmann U., Elbrächter M., Krock B., John U. & Cembella A. 2009. *Azadinium spinosum* gen. et sp. nov. (Dinophyceae) identified as a primary producer of azaspiracid toxins. *European Journal of Phycology* 44: 63–79. DOI: [10.1080/09670260802578534](https://doi.org/10.1080/09670260802578534).
- Tillmann U., Gottschling M., Guinder V. & Krock B. 2018b. *Amphidoma parvula* (Amphidomataceae), a new planktonic dinophyte from the Argentine Sea. *European Journal of Phycology* 53: 14–28. DOI: [10.1080/09670262.2017.1346205](https://doi.org/10.1080/09670262.2017.1346205).
- Tillmann U., Gottschling M., Krock B., Smith K.F. & Guinder V. 2019. High abundance of Amphidomataceae (Dinophyceae) during the 2015 spring bloom of the Argentinean Shelf and a new, non-toxicogenic ribotype of *Azadinium spinosum*. *Harmful Algae* 84: 244–260. DOI: [10.1016/j.hal.2019.01.008](https://doi.org/10.1016/j.hal.2019.01.008).
- Tillmann U., Gottschling M., Nézan E. & Krock B. 2015. First record of *Azadinium dexteroporum* and *Amphidoma languida* (Amphidomataceae, Dinophyceae) from the Irminger Sea off Iceland. *Marine Biodiversity Records* 8: 1–11. DOI: [10.1017/S1755267215001128](https://doi.org/10.1017/S1755267215001128).
- Tillmann U., Gottschling M., Nézan E., Krock B. & Bilien G. 2014a. Morphological and molecular characterization of three new *Azadinium* species (Amphidomataceae, Dinophyceae) from the Irminger Sea. *Protist* 165: 417–444. DOI: [10.1016/j.protis.2014.04.004](https://doi.org/10.1016/j.protis.2014.04.004).
- Tillmann U., Krock B. & Taylor B. 2014b. *Azadinium caudatum* var. *margalefii*, a poorly known member of the toxicogenic genus *Azadinium* (Dinophyceae). *Marine Biology Research* 10: 941–956. DOI: [10.1080/17451000.2013.866252](https://doi.org/10.1080/17451000.2013.866252).
- Tillmann U., Salas R., Gottschling M., Krock B., O'Driscoll D. & Elbrächter M. 2012. *Amphidoma languida* sp. nov. (Dinophyceae) reveals a close relationship between *Amphidoma* and *Azadinium*. *Protist* 163: 701–719. DOI: [10.1016/j.protis.2011.10.005](https://doi.org/10.1016/j.protis.2011.10.005).
- Tillmann U., Sánchez-Ramírez S., Krock B. & Bernales-Jiménez A. 2017. A bloom of *Azadinium polongum* in coastal waters off Peru. *Revista De Biología Marina Y Oceanografía* 52: 591–610. DOI: [10.4067/S0718-19572017000300015](https://doi.org/10.4067/S0718-19572017000300015).
- Toebe K., Joshi A.R., Messtorff P., Tillmann U., Cembella A. & John U. 2013. Molecular discrimination of taxa within the dinoflagellate genus *Azadinium*, the source of azaspiracid toxins. *Journal of Plankton Research* 35: 225–230. DOI: [10.1093/plankt/fbs077](https://doi.org/10.1093/plankt/fbs077).
- Twiner M., Hess P. & Doucette G.J. 2014. Azaspiracids: toxicology, pharmacology, and risk assessment. In: *Seafood and freshwater toxins*, (Ed. by L.M. Botana), pp. 823–855. CRC Press, Boca Raton, Florida, USA.
- Wassmann P., Duarte C.M., Agustí S. & Sejr M.K. 2011. Footprints of climate change in the Arctic marine ecosystem. *Global Change Biology* 17: 1235–1249. DOI: [10.1111/gcb.2010.17.issue-2](https://doi.org/10.1111/gcb.2010.17.issue-2).
- Wietkamp S., Krock B., Gu H., Voß D., Klemm K. & Tillmann U. 2019b. Occurrence and distribution of Amphidomataceae (Dinophyceae) in Danish coastal waters of the North Sea, the Limfjord, and the Kattegat/Belt area. *Harmful Algae* 88: 101637. DOI: [10.1016/j.hal.2019.101637](https://doi.org/10.1016/j.hal.2019.101637).
- Wietkamp S., Tillmann U., Clarke D. & Toebe K. 2019a. Molecular determination and quantification of the toxicogenic dinoflagellate *Amphidoma languida* (Amphidomataceae, Dinophyceae). *Journal of Plankton Research* 41: 101–113. DOI: [10.1093/plankt/fby052](https://doi.org/10.1093/plankt/fby052).
- Wolf C., Kiliás E. & Metfies K. 2015. Protists in the polar regions: comparing occurrence in the Arctic and Southern Oceans using pyrosequencing. *Polar Research* 34: 23225. DOI: [10.3402/polar.v34.23225](https://doi.org/10.3402/polar.v34.23225).
- Xiao X., Sogge H., Lagesen K., Tooming-Klunderud A., Jakobsen K.S. & Rohrlack T. 2014. Use of high throughput sequencing and light microscopy show contrasting results in a study of phytoplankton occurrence in a freshwater environment. *PLoS One* 9: e106510. DOI: [10.1371/journal.pone.0106510](https://doi.org/10.1371/journal.pone.0106510).
- Zielinski O., Braun A., Henkel R., Mascarenhas V.J., Meier D. & Voß D. 2018. *Physical oceanography during Maria S. Merian cruise MSM65 (GREENHAB II)*. Institute for Chemistry and Biology of the Marine Environment, Carl-von-Ossietzky University of Oldenburg, Germany. PANGAEA. DOI: [10.1594/PANGAEA.886181](https://doi.org/10.1594/PANGAEA.886181).

Publication IV: AZA producers in North Atlantic waters in 2018

Distribution and abundance of azaspiracid-producing dinophyte species and their toxins in North Atlantic and North Sea waters in summer 2018. *PLoS ONE*

Wietkamp, S., Krock, B., Clarke, D., Voss, D., Salas, R., Kilcoyne, J., Tillmann, U. (2020)

Publication IV presents results of a field study on Amphidomataceae in Irish and North Sea coastal waters, where the three toxigenic amphidomatacean species *Azadinium spinosum*, *Az. poporum* and *Am. languida* are frequently detected.

The aims were 1) to validate and test the performance of all available species-specific qPCR assays in the field by specificity and spike tests 2) to increase knowledge about the biogeography of the toxigenic species in the area and 3) to evaluate the multi-method approach of applying on-board microscopy, LC-MS/MS and qPCR.

71 coastal stations were sampled and analyzed tested on the presence and abundance of those three species and respective AZA. The species and AZA known to be produced by them (AZA-1, -2, -33, -38 and -39) were detected and data of microscopic, chemical and molecular analyses were well correlated.

The candidate conducted on-board sampling and qPCR analysis of the DNA field samples, as well as the spike experiments (100%). On-board sampling for AZA measurements (Dr. B. Krock, AWI) was also done by the candidate (50%), with the help of L. Hintze and K. Krapf (both AWI). Further technical support came from D. Clarke, R. Salas, C. Cusack, P. Hynes and J. Silke (MI). Further analyses and figures were prepared by the candidate (70%), except for graphical presentations of CTD data (collaboration with D. Voss, ICBM) and light microscopy images of species (Dr. U. Tillmann, AWI). Manuscript composition and preparation was done by the candidate (70%) in close cooperation with the corresponding author Dr. U. Tillmann and contributions by other co-authors.

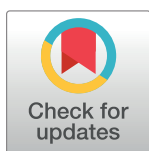
RESEARCH ARTICLE

Distribution and abundance of azaspiracid-producing dinophyte species and their toxins in North Atlantic and North Sea waters in summer 2018

Stephan Wietkamp¹, Bernd Krock¹, Dave Clarke², Daniela Voß³, Rafael Salas², Jane Kilcoyne², Urban Tillmann^{1*}

1 Alfred-Wegener-Institute, Helmholtz Centre for Polar and Marine Research, Bremerhaven, Germany, **2** Marine Institute, Galway, Ireland, **3** Institute for Chemistry and Biology of the Marine Environment (ICBM), Carl von Ossietzky Universität Oldenburg, Wilhelmshaven, Germany

* urban.tillmann@awi.de



OPEN ACCESS

Citation: Wietkamp S, Krock B, Clarke D, Voß D, Salas R, Kilcoyne J, et al. (2020) Distribution and abundance of azaspiracid-producing dinophyte species and their toxins in North Atlantic and North Sea waters in summer 2018. PLoS ONE 15(6): e0235015. <https://doi.org/10.1371/journal.pone.0235015>

Editor: Raffaella Casotti, Stazione Zoologica Anton Dohrn, ITALY

Received: March 16, 2020

Accepted: June 5, 2020

Published: June 19, 2020

Peer Review History: PLOS recognizes the benefits of transparency in the peer review process; therefore, we enable the publication of all of the content of peer review and author responses alongside final, published articles. The editorial history of this article is available here: <https://doi.org/10.1371/journal.pone.0235015>

Copyright: © 2020 Wietkamp et al. This is an open access article distributed under the terms of the [Creative Commons Attribution License](https://creativecommons.org/licenses/by/4.0/), which permits unrestricted use, distribution, and reproduction in any medium, provided the original author and source are credited.

Data Availability Statement: Cruise CTD data are available at <https://doi.org/10.1594/PANGAEA>.

Abstract

Representatives of the marine dinophyte family Amphidomataceae produce lipophilic phyco toxins called azaspiracids (AZA) which may cause azaspiracid shellfish poisoning (AZP) in humans after consumption of contaminated seafood. Three of the four known toxigenic species are observed frequently in the eastern North Atlantic. In 2018, a research survey was performed to strengthen knowledge on the distribution and abundance of toxigenic Amphidomataceae and their respective toxins in Irish coastal waters and in the North Sea. Species-specific quantification of the three toxigenic species (*Azadinium spinosum*, *Azadinium poporum* and *Amphidoma languida*) was based on recently developed qPCR assays, whose performance was successfully validated and tested with specificity tests and spike experiments. The multi-method approach of on-board live microscopy, qPCR assays and chemical AZA-analysis revealed the presence of Amphidomataceae in the North Atlantic including the three targeted toxigenic species and their respective AZA analogues (AZA-1, -2, -33, -38, -39). *Azadinium spinosum* was detected at the majority of Irish stations with a peak density of 8.3×10^4 cells L⁻¹ and AZA (AZA-1, -2, -33) abundances up to 1,274 pg L⁻¹. *Amphidoma languida* was also present at most Irish stations but appeared in highest abundance in a bloom at a central North Sea station with a density of 1.2×10^5 cells L⁻¹ and an AZA (AZA-38, -39) abundances of 618 pg L⁻¹. *Azadinium poporum* was detected sporadically at the Irish south coast and North Sea and was rather low in abundance during this study. The results confirmed the wide distribution and frequent occurrence of the target species in the North Atlantic area and revealed, for the first time, bloom abundances of toxigenic Amphidomataceae in this area. This emphasizes the importance of future studies and monitoring of amphidomatacean species and their respective AZA analogues in the North Atlantic.

896405. All other relevant data are within the paper and its Supporting Information files

Funding: This work was supported by funding of the German Ministry for Education and Research (project RIPAZA, 03F0763A) and by the PACES II research program of the Alfred-Wegener-Institute as part of the Helmholtz Foundation initiative in Earth and Environment.

Competing interests: The authors have declared that no competing interests exist.

Introduction

Marine toxic microalgae are of concern for human health and aquaculture industries worldwide. Higher cell densities of harmful algae may occur at any time of the year, when conditions are favorable, but the complex interplay of both biotic and abiotic factors determining these outbreaks are still not fully understood [1, 2]. These harmful algal blooms can cause the death of aquatic organisms, including large fish-kills, or may lead to accumulation of toxic compounds within the aquatic food web. Elevated phycotoxin levels have the potential to cause human intoxications after consumption of contaminated seafood and therefore can have negative economic and health impacts on a global scale [3].

Since shellfish (e.g., oysters, blue mussels) are becoming increasingly important as a nutritious and sustainable food source for humans, a large number of studies have focused on toxins produced by certain phytoplankton species, which accumulate in shellfish. Well-known examples of those toxic algal compounds are yessotoxins (YTX, produced by e.g., *Protocera-tium reticulatum*), diarrhetic-shellfish-poisoning toxins (DSP, produced by e.g., *Dinophysis* spp.) and paralytic-shellfish-poisoning toxins (PSP, produced by e.g., *Alexandrium* spp.) [4–7]. While these toxins have been thoroughly studied since the 1970s and 80s, another group of microalgal toxins, azaspiracids (AZA), which were more recently discovered [8], are now known to also accumulate in shellfish. These lipophilic polyether toxins are responsible for the so-called azaspiracid-shellfish-poisoning (AZP) syndrome, which is characterized by several gastrointestinal symptoms in humans after consumption of contaminated shellfish [9]. In 2002, the EU set a regulatory limit of 160 $\mu\text{g kg}^{-1}$ AZA equivalents (AZA-1, -2 and -3) in whole shellfish, or any edible part. AZA contamination is a major problem for shellfish producers in Ireland, where AZA levels above the threshold have been recurrently reported [10, 11] in a number of species of bivalve molluscan shellfish including mussels, oysters, clams and cockles. The regulatory limit has also been exceeded in Norway in 2002/2003, leading to first closures of mussel farms at the entire south coast due to AZA contamination [12]. More recently, AZA were found, for the first time, along the Atlantic coast of southern Spain with elevated levels observed in molluscan shellfish [13].

It took 10 years after the structural elucidation of AZA-1 [8] until a source organism of AZA was identified, using on-board microscopy and LC-MS/MS (Liquid-Chromatography coupled with tandem Mass Spectrometry) [14]. The causative organism was later described as *Azadinium spinosum*, a new dinophyte species within a newly erected genus [15]. Since then, two other AZA producing species of *Azadinium* have been described i.e., *Az. poporum* and *Az. dexteroporum* [16–19]. In addition, one species of the closely related genus *Amphidoma* (which, together with *Azadinium*, are included in the family Amphidomataceae), *Am. languida* also produces AZA [13, 19]. However, the currently known diversity of Amphidomataceae is much larger with 23 species in the family described to date, and most of those species were assigned as non-toxicogenic based on cultured strains [20–22]. One main reason for the late discovery of these tiny unicellular organisms (most are ~ 10–15 μm in cell length) is their inconspicuousness, which challenges their detection and morphological description using traditional light microscopy. The recent development of molecular-based methods increasingly supports the detection of such inconspicuous organisms, predominantly in the context of harmful microalgae [23–26]. Particularly, quantitative polymerase chain reaction (qPCR) methodology gained momentum due to its high specificity and sensitivity [27]. By including standard curves of target DNA, the sensitive, qualitative detection is complemented with quantitative estimations of the target organism. Currently, the detection and quantification of toxic microalgae via qPCR has become a standard procedure in many studies and monitoring programs [28–30].

PCR-based assays have also been designed for Amphidomataceae. Toebe et al. [31] and Wietkamp et al. [32] developed specific TaqMan assays for three toxigenic species within this family (*Az. spinosum*, *Az. poporum* and *Am. languida*), and Smith et al. [33] designed a SYBR Green assay targeting the DNA of all amphidomatacean species. These qPCR assays have been used to detect Amphidomataceae in field samples, for example on research surveys along the Danish coastline [34], the Norwegian coast [35], the Irish coastline [32], the Argentine shelf [36] and in western Greenland [22], or are in use for the regular monitoring of *Az. spinosum* and *Az. poporum* in Irish coastal waters [37]. In 2018, the Marine Institute (Galway/Ireland) became the first laboratory internationally to validate and accredit the method for *Az. spinosum* detection in a routine monitoring programme to ISO 17025 standards. In these studies, the molecular qPCR assays assisted investigations on toxigenic Amphidomataceae and indicated their presence at many sites with low cell densities, when microscopy or LC-MS/MS were hardly able to detect the species or their respective toxins.

However, qPCR technology has some limitations. Obviously, a specific assay can only be designed if target sequences and reference target DNA (e.g., from cultured strains) is available. Moreover, new strains of similar or closely related species need to be included in updated specificity tests to avoid false positive results. The respective assay also requires recurrent validation by applying it to new strains of the target species. The latter mainly refers to a reliable DNA-based quantification of target cells, because different strains may vary in their ribosomal DNA (rDNA) copy number, which would strongly bias the quantification performance [38–40]. The reliable quantification of target DNA by qPCR within field samples is one of the most crucial factors, because (as already described) even the “gold standard”—microscopy—has drawbacks when it comes to inconspicuous organisms and the validation of the qPCR assay within the field matrix becomes challenging. Therefore, the combination of analytical methods with individual advantages has become a popular approach in studies on harmful microalgae to compensate limitations of single techniques [41–45].

Three of the four known AZA producing species (i.e., *Az. spinosum*, *Az. poporum* and *Am. languida*) are present in the North Sea. *Azadinium spinosum* was first isolated and described from the east coast of Scotland [15], and further strains were established originating from Ireland, Denmark and the Shetland Islands. All these strains share the same toxin profile (AZA-1, -2 and -33) and almost identical ITS sequences [46, 47]. Assigned as Ribotype A, these strains are clearly delimited from Norwegian strains with a toxin profile of mainly AZA-11 and -51, which form a different ribotype, Ribotype B [35]. Recently, Tillmann et al. [36] found evidence for a third ribotype (Ribotype C), consisting of *Az. spinosum* strains collected at the Argentinian Shelf in 2015, where no AZA were detected.

The second toxigenic species, *Az. poporum* was first described from the Danish North Sea coast [16], but is now known to occur in numerous regions around the globe [48] showing different toxin profiles and DNA sequences, with several ribotypes also identified [20, 49, 50].

The first strain of *Am. languida* was isolated from Bantry Bay at the Irish south-west coast in 2009 [51], but there is evidence that this species is widely distributed in the North Atlantic and North Sea [13, 34, 35]. Although no known AZA were found initially in the first *Am. languida* strain, two newly described AZA (AZA-38 and -39) were subsequently assigned as the dominant toxins of this species [19]. However, a different toxin profile was observed in an *Am. languida* strain from the Andalusian coast of Spain in 2017, consisting of AZA-2 and -43 [13], and AZA-52 and -53 have been detected in a few *Am. languida* strains from the Norwegian coast [35].

Although (toxigenic) Amphidomataceae are present in the North Sea and adjacent Atlantic areas, little is known about their spatial and temporal distribution. The aim of this study was to gain detailed data about the distribution and abundance of toxigenic Amphidomataceae and

AZA in the North Sea and in Irish coastal waters, and to provide information on the AZP risk in these regions. Therefore, in summer 2018, a research survey in the North Sea, the Celtic Sea and Irish coastal waters was undertaken. The vessel was equipped with light microscopes, a triple-quadrupole LC-MS/MS and a qPCR instrument for on-board visual-, chemical- and molecular-based detection and quantification of toxigenic Amphidomataceae and their toxins.

Materials and methods

Field campaign

The necessary field permits for this study complying with all relevant regulations were issued from The Netherlands (Rijksdienst voor Ondernemend Nederland), Belgium (Royaume de Belgique, Service public fédéral Affaires étrangères), France (Ministère des Affaires Étrangères et du Développement International), Ireland (Department of Foreign Affairs and Trade), and the United Kingdom (Foreign & Commonwealth Office) via the German Embassy and are available upon request.

Data were collected during the survey (HE-516) on-board *RV Heincke* between 17th July and 15th August, 2018. Starting in the German Bight, the vessel piloted through the English Channel, northwards towards the Irish south coast and then on a clockwise trajectory around the southwest, west and northwest coasts of Ireland, across to the Outer Hebrides and south of Orkney Islands in Scotland and returned to the German Bight again via a long southeastward transect through the North Sea. In total, 75 stations were sampled (station number and positions are listed in [S2 Table](#)), including six defined station transects ([Fig 1](#)). CTD profiles were recorded at each station using a Seabird 'sbe911+' CTD (Sea-Bird Electronics, Inc. Seattle, USA) with a sampling rosette (on-board device). A chlorophyll fluorescence sensor (Eco AFL-FL SN1365, Sea-Bird Electronics, former WET labs, Bellevue, USA) was attached to the CTD and used for the detection of chlorophyll maxima in the water column. CTD data were stored and processed using Seasave V 7.23.2. Temperature (potential T in °C) was calculated according ITS-90 [52]. Water samples were collected with Niskin bottles attached to the CTD

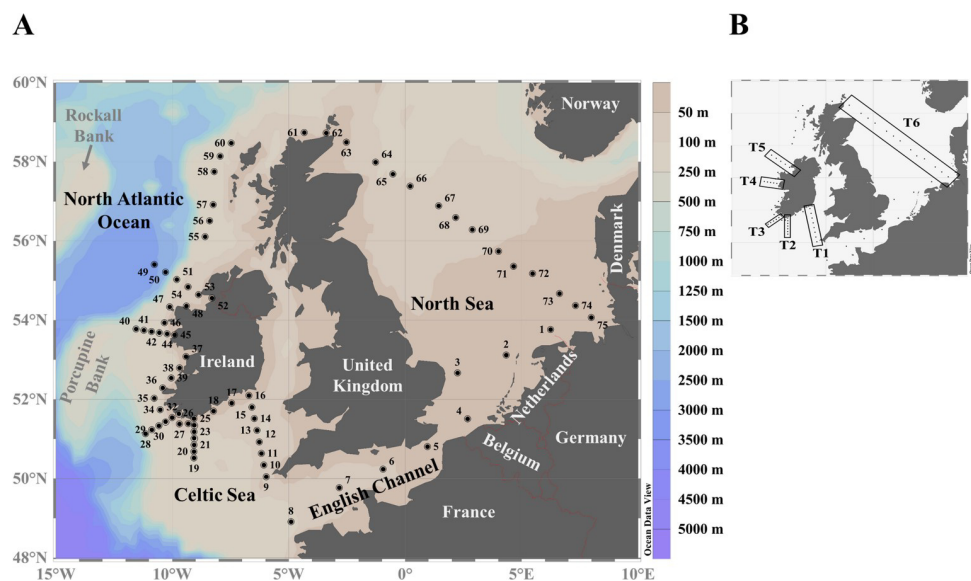


Fig 1. A: Study area and sampling locations during the survey HE-516. B: Transects (T1 –T6) referred to in the text are indicated by black rectangles.

<https://doi.org/10.1371/journal.pone.0235015.g001>

from discrete depths during the upward casts. CTD data sets are available at Pangaea [53]. For field data correlations as well as visualization (S1 Fig), CTD profile data for temperature, salinity and fluorescence were averaged from the surface down to the maximum sampling depth.

At each station, plankton samples were collected with 10 L Niskin bottles at 3 m, 10 m and the deep-chlorophyll-maximum (DCM) layer. Five litres of seawater from each depth were filtered through a 20 μm mesh-size Nitex sieve, and the three depth samples were subsequently pooled and well mixed.

On-board microscopy. A defined volume (between 0.5 and 1 L) of the pooled water sample was gently concentrated by gravity filtration using a 3 μm Whatman polycarbonate filter (47 mm diameter, GE Healthcare, Little Chalfont, UK). The living plankton concentrate was collected in a flat (10 mm) 5 mL Utermöhl chamber and examined using an inverted microscope (Axiovert 200M, Zeiss, Göttingen, Germany). Cells were preliminarily identified as *Azadinium* and/or *Amphidoma* at high magnification (640 x) based on general cell size and shape, on the presence of a theca, and on the presence of a distinctly pointed apex. Cells of interest were photographed with a digital camera (AxioCam MRC5, Zeiss).

At 45 selected stations, the concentrated live samples were also used for a semi-quantitative estimation of Amphidomataceae cell densities. After at least one hour of sedimentation, the total number of amphidomatacean cells (without further differentiation into species or subgroups) was determined for a defined subarea of the chamber using 640 x and/or 1,000 x magnification. Assuming all cells of interest had settled to the bottom and taking the subarea/total chamber area ratio and the concentrated water volume into account, the Amphidomataceae cell abundance per L was calculated. The limit of detection of this counting procedure ranged (depending on the counted subarea and the sample volume) from ~ 20 to 50 cells L^{-1} .

DNA sampling. For DNA analysis, between 0.8–6.0 L (depending on the particle content) of the pooled water sample was filtered under gentle vacuum (< 200 mbar) through 3 μm pore-size polycarbonate filters (Merck KGaA, Darmstadt, Germany). For six randomly selected stations (19, 25, 32, 44, 64 and 71), the samples of the three different depths were not pooled, but analyzed separately. The filters containing the 3 μm phytoplankton fraction were placed inside a 50 mL plastic centrifuge tube (Sarstedt, Nümbrecht, Germany), extended along its inner side wall and vortexed with 30 mL of the 3 μm pre-filtered seawater for 1 min to resuspend the filtered particulate matter. The filter was removed and the 50 mL tube was then centrifuged (5415R, Eppendorf, Hamburg, Germany) at $3,220 \times g$ for 15 min. The supernatant was discarded and the remaining cell pellet was subsequently collected in bead tubes together with 500 μL of the SL1 lysis buffer, both provided by the NucleoSpin Soil DNA extraction kit (Macherey & Nagel, Düren, Germany). The DNA was extracted immediately on-board according to the DNA kit manufacturer's instructions with a slight variation. Instead of vortexing, the bead tubes were shaken in a cell disrupter (FastPrep FP120, Thermo-Savant, Illkirch, France) for 45 s initially and then for another 30 s, both run times at a speed of 4 ms^{-1} . DNA elution was performed using $2 \times 50 \mu\text{L}$ of the provided elution buffer (to a final elution volume of 100 μL) to maximize the overall DNA yield. The DNA was stored at -20°C until further processing.

AZA sampling. For AZA analysis, between 0.8–6.0 L (depending on the particle content) of the pooled water sample were filtered as described above. For the six selected stations (19, 25, 32, 44, 64 and 71), samples from all three depths were processed separately for AZA toxin analysis. Each filter was placed into a 50 mL centrifuge tube and extracted by a series of 0.5–1 mL methanol washes until complete filter discoloration. The extracts were subsequently transferred to a spin-filter (0.45 μm pore size, Millipore Ultrafree, Eschborn, Germany) and centrifuged (5415R, Eppendorf) for 30 s at $800 \times g$. The filtrate was then transferred to autosampler vials and immediately analyzed by LC-MS/MS.

Sample processing

qPCR. Real-time qPCR with species-specific assays for *Az. spinosum*, *Az. poporum* and *Am. languida* was performed daily on-board as described in Toebe et al. [31] and Wietkamp et al. [32] using a Roche LightCycler 96 (Roche, Penzberg, Germany). All reactions were carried out in duplicate. Prepared positive Extraction Process Controls (EPC), which contained the DNA of each target species, as well as negative EPCs (0.4 μm filtered, sterilized seawater) were included during all PCR runs. The positive controls contained 10^3 cells of each target species and the DNA of these cell pellets was extracted daily together with the field samples. This was to account for potential extraction efficiency variability between separate DNA extraction procedures, visible by comparing the C_T (Cycle Threshold) values of the EPC samples between qPCR runs.

The final determination of cell densities of the three species for each sample (including samples of the spike experiment) was performed in technical triplicate after the survey at the Alfred-Wegener-Institute (Bremerhaven, Germany) according to procedures described previously [32]. C_T values of the three technical replicates per sample were averaged and used for cell abundance calculation. The limit of quantification (LOQ) and the limit of detection (LOD) for these qPCR analyses were defined following Forootan et al. [54]. The LOQ referred to the lowest standard curve concentration, for which all three replicates showed amplification and are within the 95% confidence interval. The LOD was referred to the lowest standard curve concentration, for which all three replicates showed amplification but values are outside the 95% confidence interval of the standard curve. For the standard curves of all three qPCR assays on the field samples, the resolution of dilutions applied did not allow differentiation between LOD and LOQ, which were both $0.1 \text{ pg } \mu\text{L}^{-1}$.

Evaluation of qPCR performance. *qPCR assay specificity.* DNA of recently discovered target and non-target species and/or strains from Norway [35] and Denmark [32] was applied to the current qPCR assays on *Az. spinosum* and *Az. poporum*, to check whether the assays are still species-specific. Cell isolates of the respective species/strains were cultured and collected as described in Tillmann et al. [36]. For each sample, the DNA was extracted from cell pellets according to the procedures for the field samples, and normalized to a concentration of $1 \text{ ng } \mu\text{L}^{-1}$ for comparability of the amplification performance. Each sample was analyzed in triplicate in each of the qPCR assays. The specificity was evaluated by comparing the respective mean C_T values to known target strains (UTH-D4, *Az. poporum* and 3D9, *Az. spinosum*; Table 1), which were used to design the original assay [31].

Spike experiments. To evaluate the qPCR assay performance in the field and to account for potential inhibition effects on the qPCR assay, known cell numbers of living cells of *Am. languida* (strain Z-LF-09-C9), *Az. spinosum* (strain 3D9) and *Az. poporum* (strain UTH-D4) were spiked on-board into a natural seawater matrix, taken at 20 m depth at station 3. Known target cell abundances were adjusted with the help of microscopic counts (magnification of 200 x) of 0.5 mL culture subsamples, settled at the bottom of counting chambers. The absence of the three species in the seawater matrix was confirmed by light microscopy and qPCR. In four replicates, 1 L seawater matrix each was spiked with three different total cell quantities (10^2 , 10^3 or 10^4 cells) of all species, so that all three species were present. Negative controls, without added target cells, were also prepared. The spiked seawater sample was subsequently filtered through 3 μm filters, as described for the field samples, and then stored at -20°C until further processing. DNA of the spiked samples was extracted and species-specific qPCR assays were applied as described for the field samples.

LC-MS/MS. Water was deionized and purified (Milli-Q, Millipore, Eschborn, Germany) to $18 \text{ M}\Omega \text{ cm}^{-1}$ or higher quality. Formic acid (90%, p.a.), acetic acid (96%, p.a.) and

Table 1. Strains used for specificity tests, including respective results of the qPCR assays. n.a.: not analysed; ND: not detected.

Species	Strain	Toxin profile	Ribotype	Reference	Result of the <i>Az. poporum</i> assay	Result of the <i>Az. spinosum</i> assay
<i>Am. languida</i>	N-01-01	AZA-38, -39	n.a.	[35]	ND	ND
<i>Am. languida</i>	N-01-02	AZA-38, -39	n.a.	[35]	ND	ND
<i>Am. languida</i>	N-40-03	AZA-39, -52	n.a.	[35]	ND	ND
<i>Az. dalianense</i>	N-12-04	ND	B	[35]	ND	ND
<i>Az. dalianense</i>	N-38-02	ND	A	[35]	ND	ND
<i>Az. obesum</i>	N-41-01	ND	n.a.	[35]	ND	ND
<i>Az. polongum</i>	N-47-01	ND	n.a.	[35]	ND	ND
<i>Az. poporum</i>	LF-14-E12	ND	A	[55]	C _T = 15.4	ND
<i>Az. poporum</i>	N-39-03	AZA-37	A	[35]	C _T = 15.5	ND
<i>Az. poporum</i>	N-39-13	AZA-37	A	[35]	C _T = 15.6	ND
<i>Az. poporum</i>	UTH-D4	AZA-37	A	[56]	C _T = 15.3	ND
<i>Az. spinosum</i>	3D9	AZA-1, -2, -33	A	[15]	ND	C _T = 19.3
<i>Az. spinosum</i>	N-04-01	AZA-1, -2, -33	A	[35]	ND	C _T = 19.4
<i>Az. spinosum</i>	N-04-04	AZA-11, -51	B	[35]	ND	C _T = 25.7
<i>Az. spinosum</i>	N-05-01	AZA-11, -51	B	[35]	ND	C _T = 26.8
<i>Az. spinosum</i>	N-16-02	AZA-11, -51	B	[35]	ND	C _T = 25.2
<i>Az. trinitatum</i>	N-39-04	ND	n.a.	[35]	ND	ND

<https://doi.org/10.1371/journal.pone.0235015.t001>

ammonium formate (98%, p.a.) were from Merck (Darmstadt, Germany). The solvents, methanol and acetonitrile, were high performance liquid chromatography (HPLC) grade (Merck, Darmstadt, Germany). Selected Reaction Monitoring (SRM) measurements were performed on-board monitoring for a wide array of AZA. The analytical system consisted of a API 4000 Q Trap triple quadrupole mass spectrometer equipped with a TurboSpray[®] interface (Sciex, Darmstadt, Germany) coupled to a model 1100 LC (Agilent, Waldbronn, Germany). The LC equipment included a solvent reservoir, in-line degasser (G1379A), binary pump (G1311A), refrigerated autosampler (G1329A/G1330B), and temperature-controlled column oven (G1316A).

Separation of AZA (5 µL sample injection volume) was performed by reverse-phase chromatography on a C8 phase. The analytical column (50 × 2 mm) was packed with 3 µm Hypersil BDS 120 Å (Phenomenex, Aschaffenburg, Germany) and maintained at 20°C. The flow rate was 0.2 mL min⁻¹ and gradient elution was performed with two eluants, wherein eluant A was water and B was acetonitrile/water (95:5 v/v), and both contained 2 mM ammonium formate and 50 mM formic acid. A gradient elution was employed, starting with 30% B, rising to 100% B over 8 mins, held for 10 min, then decreased to 30% B over 3 min and held for 8 min to equilibrate the system. The profile of AZA was determined in one period (0–18 min) with curtain gas: 10 psi, CAD: medium, ion spray voltage: 5500 V, ambient temperature; nebulizer gas at 10 psi, auxiliary gas was off, the interface heater was on, the declustering potential at 100 V, the entrance potential at 10 V, and the exit potential at 30 V. The SRM experiments were carried out in positive ion mode by selecting the transitions shown in [S1 Table](#). AZA were calibrated against an external standard solution of AZA-1 (certified reference material programme of the IMB-NRC, Halifax, Canada) and expressed as AZA-1 equivalents.

LODs for all congeners were defined as a signal-to-noise ratio = 3, evaluated individually for each sample.

Statistics. Statistics were computed using the open source program “R”, version 3.4.3 [57]. Correlations between microscopic, qPCR, AZA and environmental data, as well as significance tests were performed with the implemented “pairs” and “corr test” functions (Pearson’s

product-moment correlation test), respectively. The presented maps in this study were generated using the program “Ocean Data View” (ODV), version 5.1.0 [58].

Results

Hydrography and chemistry

Mean temperature (S1A Fig) of the upper layer was highest in the German Bight and the North Sea entrance of the English Channel, reaching 18.5°C at Helgoland (station 75) and 18.9°C at station 4. Intermediate values (~ 15.5°C) were observed at the Irish coast and the central North Sea stations, whereas low mean temperatures (< 13.5°C) were measured along the Scottish coast, at northern North Sea stations, and at the western entrance of the English Channel (station 8). Salinity (S1B Fig) revealed higher values in the upper layer (≥ 35) at stations off the coastline compared to coastal stations, with maxima of 35 in the central North Sea (stations 67–69) and 35.4 at Irish outer areas (stations 28, 40 and 49). Lower salinity values, down to 32.8, were obtained mainly in the German Bight (stations 1, 73, 74 and 75). Fluorescence values (S1C Fig) indicated higher densities of phototrophic organisms along the Irish west coast (up to 5.6 AU). A minimum fluorescence (0.4 AU) was measured at station 20, which was located on a transect at the Irish south coast. Mean fluorescence values in the upper layer in the range from 2 to 4 AU were observed in the German Bight (stations 1, 2, 71, 72, 74 and 75), Irish waters (stations 33, 34, 38, 39 and 47) and two stations (10 and 11) close to the coast of south west Wales.

Depth profiles for transect stations (Fig 1B) are presented in S2 Fig. For all transects there was a thermocline between the first 20 to 40 meters and a deeper water layer (S2A Fig), with stronger thermoclines occurring in transects T1, T2 and T6, where temperature differences of up to 10°C were recorded. Salinity (S2B Fig) increased with distance from the Irish coastline. Higher salinity at the respective stations were not limited to the surface but were measured over the whole downcast of the CTD up to 100 m depth where maximum values exceeded salinity levels of 35.4. There were generally lower salinities along the North Sea transect, with minima (≤ 34.6) recorded in the German Bight (stations 71–75). Fluorescence measurements (S2C Fig) revealed values mostly in the range from 0 to 4 AU. Values higher than 4 AU were infrequently detected and limited to certain water layers (e.g., station 10, 10–20 m depth). Peak values were found at station 11 (> 10 AU), 71 (> 9 AU) and 72 (> 13 AU) as a deep (30–40 m) chlorophyll layer.

Live sample records of Amphidomataceae

On-board microscopy using live samples revealed the presence of various species of Amphidomataceae. Species identification using light microscopy (LM) for the majority of species in this family is difficult and would require confirmation by scanning electron microscopy (SEM), but the detailed microscopical observation revealed the presence of at least nine different amphidomatacean species for the study area, including *Az. cf. zhuanum*, *Am. languida*, *Az. caudatum* (both varieties *Az. caudatum* var. *margalefii* and *Az. caudatum* var. *caudatum*), *Az. spinosum*, and *Az. obesum* (Fig 2). For a number of selected stations covering the western coast of Ireland, the eastern seaboard of Scotland, and the whole North Sea transect (S2 Table), the abundance of total amphidomatacean cells was estimated using a semi-quantitative LM method. Densities of all Amphidomataceae-like cells were estimated to range from “undetected” (i.e., below the detection limit of ~ 20–50 cells L⁻¹) to a maximum of 2.7 x 10⁵ cells L⁻¹ in the central North Sea. Highest density estimates for the Irish west coast were 1.8 x 10⁴ cells L⁻¹ (S2 Table).

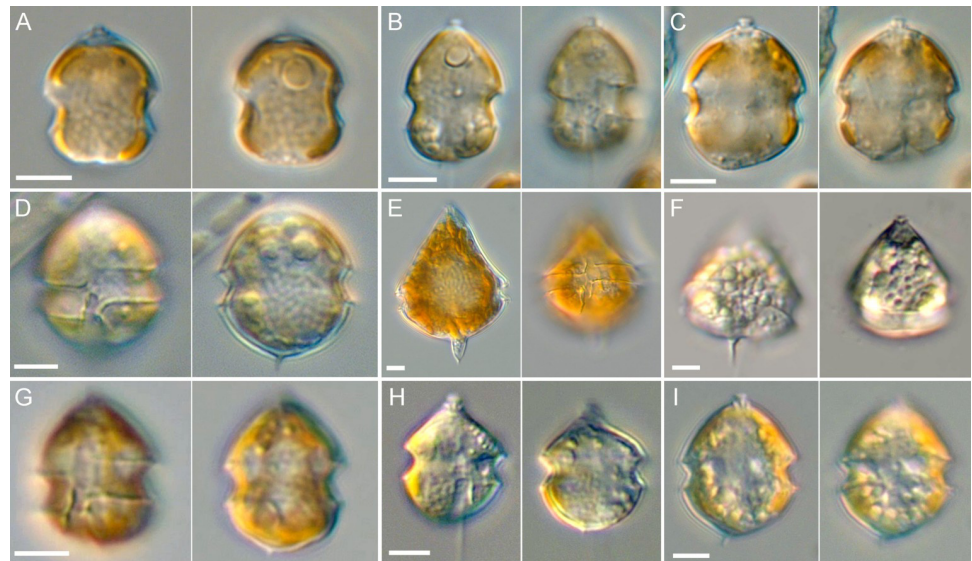


Fig 2. Diversity of Amphidomataceae as recorded during HE-516 by live on-board light microscopy. A: *Amphidoma languida*; B: *Azadinium spinosum*; C: *Az. obesum*; D: *Az. cf. zhuanum*; E: *Az. caudatum* var. *caudatum*; F: *Az. caudatum* var. *margalefii*; G: *Az. spec. 1*; H: *Az. spec. 2*; I: *Az. spec. 3*. Scale bars = 2 μm .

<https://doi.org/10.1371/journal.pone.0235015.g002>

qPCR assay performance

Specificity tests on qPCR assays. Application of several recently isolated target and non-target species/strains to the current *Az. spinosum* and *Az. poporum* qPCR assay revealed no amplification of non-target species DNA in both assays (Table 1). Newly isolated strains of *Az. poporum* from Norway (N-39-03 and N-39-13; Ribotype A1) revealed the same amplification efficiency ($C_T = 15.5$ and 15.6) as the reference strain UTH-D4 ($C_T = 15.3$). Likewise, DNA of the newly obtained strain from the Danish coast (LF-14-E12; Ribotype A2) was amplified with the same efficiency ($C_T = 15.4$).

The Norwegian strain of *Az. spinosum*, belonging to Ribotype A (N-04-01), showed a similar amplification efficiency ($C_T = 19.4$) as the reference strain 3D9 ($C_T = 19.3$; also Ribotype A), whereas the Norwegian strains assigned as Ribotype B (N-04-04, N-05-01 and N-16-02) revealed less efficiency ($C_T = 25.7$, 26.8 and 25.2).

Spike experiment. The on-board qPCR assay performance was tested for the three species-specific qPCR assays targeting *Az. spinosum*, *Az. poporum* and *Am. languida* by performing spike experiments (Fig 3). The recovery rate for different cell numbers of *Az. spinosum* and *Am. languida* ranged from 89 to 93%, the rate for *Az. poporum* was higher with a range from 93 to 111%.

Negative controls did not show any detectable amplification. Taking the filtered water volume and the DNA extraction volume into account, the LOD and LOQ was 3 cells L^{-1} for the three assays.

qPCR analyses of field samples

All three investigated toxigenic species (*Az. spinosum*, *Az. poporum* and *Am. languida*) were detected by qPCR (Fig 4). Considering the DNA extraction volume and filtered water volume, the limit of detection for the qPCR of $0.1 \text{ pg target DNA } \mu\text{L}^{-1}$ for all three species corresponded to 1 to 3 cells L^{-1} in the field samples.

Azadinium spinosum was found at almost all stations along the Irish south and west coast. This species was also detected at five stations (67–71) in the central North Sea, but was not

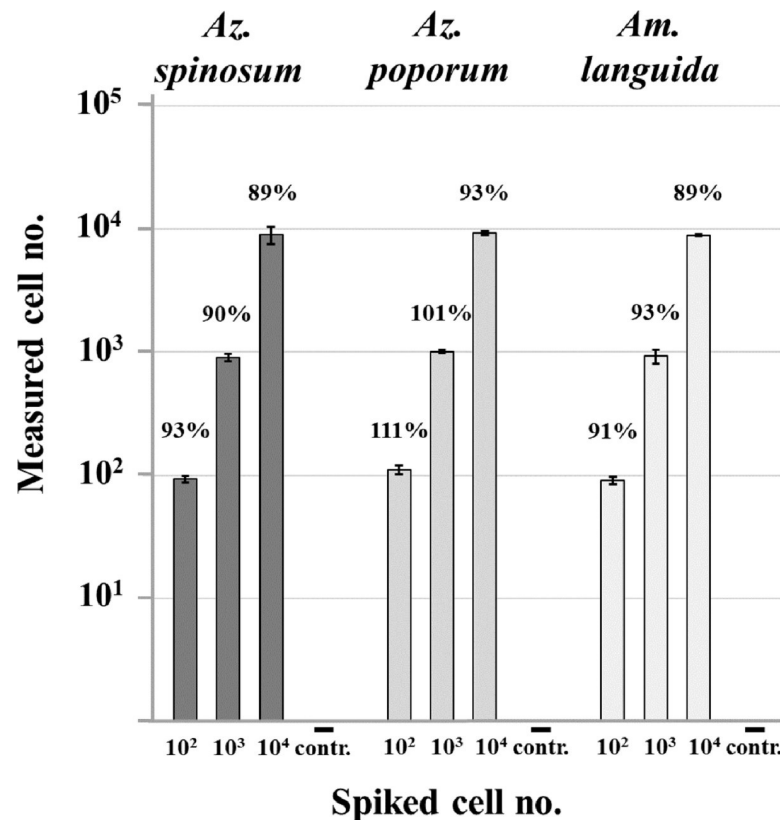


Fig 3. Spike experiment: qPCR quantification of AZA-producer within environmental matrix. Standard deviation is presented for each bar ($n = 4$). Numbers above the bars represent the percentage of recovery. Negative controls (-contr.) did not contain any target cells.

<https://doi.org/10.1371/journal.pone.0235015.g003>

detected in the English Channel or in the Scottish coastal waters. *Azadinium poporum* was recorded at 18 stations. This species was mainly present along the southern Irish coast, at stations along the North Sea transect (stations 64, 65 and 69) and at two stations (stations 5 and 7) located in the English Channel, where *Az. poporum* was the sole toxigenic amphidomatacean species present. *Azadinium poporum* was not detected along the Irish west or Scottish coasts. *Amphidoma languida* was detected at majority of all stations (42 in total). It was present throughout the whole study area, with exceptions at stations inside the English Channel and a couple of stations off the Scottish coast. It was the only toxigenic amphidomatacean species detected in the German Bight and off the Outer Hebrides/Scotland. qPCR quantification revealed higher densities of *Az. spinosum* along the Irish south and west coasts, with peak cell densities at the coastal stations 31 (3.4×10^4 cells L^{-1}), 45 (8.3×10^4 cells L^{-1}), and 47 (2.6×10^4 cells L^{-1}) (S2 Table). Relatively high abundances of 6.2×10^3 cells L^{-1} were also found in the central North Sea (station 71) and along a northward transect from the English Channel to the southern Irish coast (station 9–13). Overall, lower cell densities of the three targeted species were observed in the North Sea compared to the Irish stations.

Amphidoma languida was widely distributed, but in the Atlantic this species was lower in abundance than *Az. spinosum* (S2 Table). In the Atlantic area cell abundances of *Am. languida* rarely exceeded 10^3 cells L^{-1} . In the North Sea, however, a maximum cell density of 1.2×10^5 cells L^{-1} was observed at the central station 71, which was the highest cell density of any of the three targeted species using qPCR during the survey.

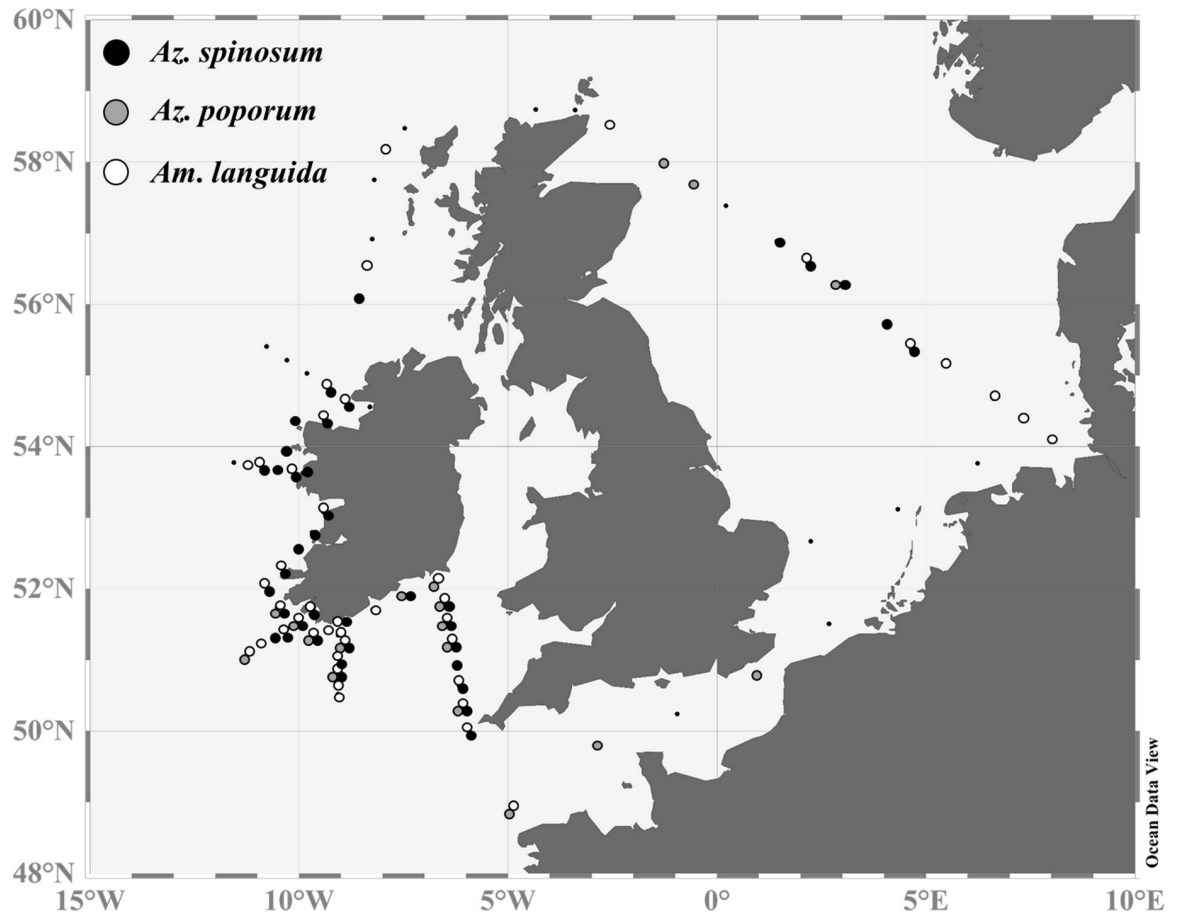


Fig 4. qPCR qualitative results. Positive hits for the species are indicated by black (*Az. spinosum*), grey (*Az. poporum*) and white (*Am. languida*) dots. Stations, where none of the three species were detected, are presented as smaller black dots.

<https://doi.org/10.1371/journal.pone.0235015.g004>

Plotting species abundance along six station transects (Fig 1B) revealed that *Az. spinosum* was more abundant at the south-western and western transects (up to 8.3×10^4 cells L^{-1} at station 45, T4) than along the southern stations, where a maximum of 2.4×10^3 cells L^{-1} was found at station 12, T1 (Fig 5). The peak density on the North Sea transect (T6) was 6×10^3 cells L^{-1} at station 71. In contrast, *Am. languida* (although generally in lower cell densities than *Az. spinosum*) was more abundant along the south-western Irish coast (up to 1.5×10^3 cells L^{-1} at stations 26 and 35) compared to the western stations with a maximum of 1×10^2 cells L^{-1} at station 42. Stations on the North Sea transect (T6) revealed higher abundance of *Am. languida* in the North Sea area compared to Irish waters, and especially at stations in the central North Sea and towards the German Bight (stations 71–75, with the peak density of 1.2×10^5 cells L^{-1} at station 71) (Fig 5). In T1 and T2, the southern Ireland transects, cell densities of both species (*Az. spinosum* and *Am. languida*) were higher in the middle stations of each transect. However, for the south-western and western transects T3–T5, highest cell densities were observed at the stations closer to shore (Fig 5).

Chemical detection of AZA in field samples

In total, five AZA (AZA-1, -2, -33, -38 and -39) congeners were detected by LC-MS/MS within the 3–20 μm size plankton fraction. The individually determined LOD of single compounds (depending on the filtration and extraction volume) was in the range 5–50 $pg L^{-1}$. AZA-1 was

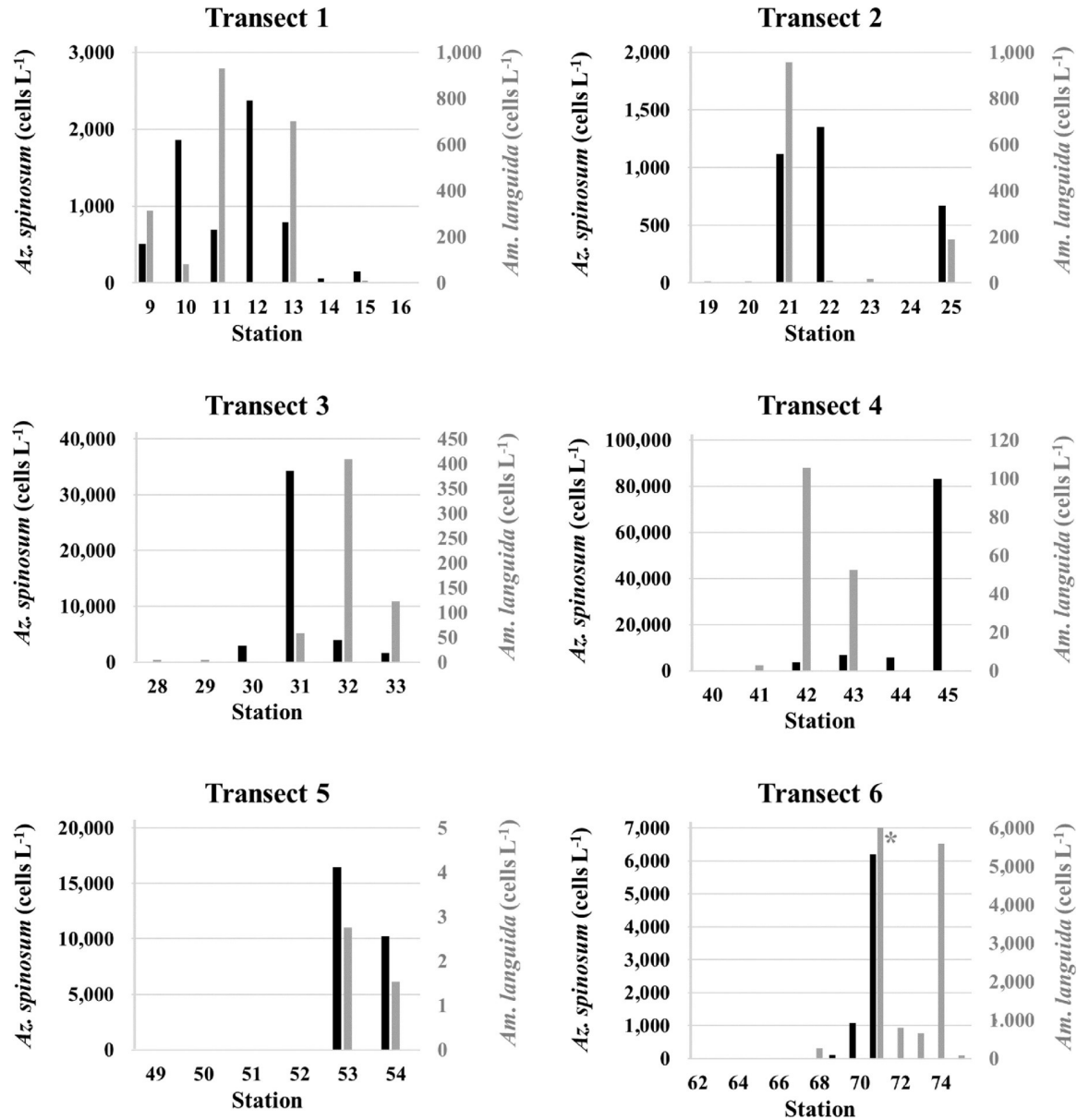


Fig 5. Cell numbers (cells L⁻¹) estimated by qPCR for *Az. spinosum* (black bars) and *Am. languida* (grey bars) for the six transects (T1 -T6) shown in Fig 1B. Cell number calculation based on mean C_T values of three technical replicates. The peak cell density (> 120,000 cells L⁻¹) of *Am. languida* at station 71 is not shown, but indicated by the grey asterisk in T6.

<https://doi.org/10.1371/journal.pone.0235015.g005>

detected at 31 stations, with a mean amount (samples with AZA-1 ≥ LOD) of 87 pg L⁻¹ and peak values of 676 and 745 pg L⁻¹ at the western Irish stations 44 and 45, respectively (S2 Table). At most stations, where AZA-1 was detected, AZA-2 and AZA-33 were also observed but generally at lower quantities compared to AZA-1 (mean AZA-2: 62 pg L⁻¹; mean AZA-33: 37 pg L⁻¹). Peak values with 325 pg L⁻¹ (AZA-2) and 204 pg L⁻¹ (AZA-33) were recorded at stations 44 and 45 (S2 Table). AZA-38 and -39 were less prevalent and only detected at two stations in the central North Sea. Rather high levels of AZA-38 (234 pg L⁻¹) and AZA-39 (384 pg L⁻¹) were measured at station 71, whereas levels of these two compounds at the neighboring station 72 were lower (S2 Table).

Comparative method analysis of field data

There was no significant correlation between any of the measured environmental parameters (temperature, salinity and oxygen) with neither amphidomatacean abundances calculated by microscopy or qPCR, nor with AZA quantities measured by LC-MS/MS.

Microscopy and qPCR. Cell density (cells L⁻¹) estimates obtained by semi-quantitative live-microscopy counts (as total Amphidomataceae) and qPCR (sum of the three species-specific assays) revealed similar biogeographical patterns (Fig 6A and 6B and S2 Table). Both methods revealed high abundances along the Irish west coast, with peak cell estimates of 1.8 x 10⁴ cells L⁻¹ based on microscopy, and 8 x 10⁴ cells L⁻¹ based on qPCR at station 45. In the North Sea both methods identified maximum densities at station 71 where 2.8 x 10⁵ cells L⁻¹ (microscopy) and 1.3 x 10⁵ cells L⁻¹ (qPCR) were recorded.

Total Amphidomataceae (microscopy) and toxigenic species (qPCR) generally were in the same order of magnitude and were positively correlated (R = 0.89, Pearson's product-moment correlation test: p < 0.001) (Fig 7). The discrepancy between qPCR estimates and microscopic counts was generally higher for the North Sea stations than for the stations located along the Irish west coast.

qPCR and AZA. qPCR abundance and toxin data are compared under the assumption that AZA-1, -2 and -33 are produced by *Az. spinosum*, whereas AZA-38 and -39 are produced by *Am. languida*. Both species-specific qPCR data for *Az. spinosum* and *Am. languida*, and their respective toxins, revealed similar biogeographical patterns (Fig 6C–6F). qPCR cell density estimates of *Az. spinosum* were positively correlated (R = 0.76 to 0.85) to AZA-1, -2 and -33 quantities (Fig 8), and Pearson's product-moment correlation tests revealed highly significant correlations (p ≤ 0.001) between the four variables. A number of samples revealed positive qPCR hits for *Az. spinosum*, but no AZAs were detected. This was the case in eight stations for AZA-1, in 17 stations for AZA-2 and 19 stations for AZA-33 (Fig 8 and S2 Table). There was only one station (station 24) where AZA was detected (12 pg L⁻¹ AZA-1), but no qPCR amplification for *Az. spinosum* DNA was observed. Positive and highly significant correlations (R = 0.86 to 0.91; p ≤ 0.001) were found also between AZA-1, -2 and -33 levels.

AZA-38 and -39 were only detected at two stations (stations 71 and 72) and thus the correlation of cell number estimates of *Am. languida* by qPCR and AZA-38 and -39 were not calculated.

Field data estimates of AZAs and qPCR-based cell densities allowed calculation of AZA cell quotas. Mean cell quotas for *Az. spinosum* and AZA-1, -2 and -33 were 17.8 ± 9.9, 8.3 ± 11.0 and 3.0 ± 1.5 fg cell⁻¹, respectively (Fig 9). Maximum values for AZA-1, -2 and -33 were 46.4, 43.2 and 5.9 fg cell⁻¹, respectively. The respective AZA cell quotas of *Am. languida*, calculated for the two North Sea stations where AZA-38 and -39 were detected, revealed 1.9 and 3.1 fg cell⁻¹ for AZA-38 and -39 at station 71, and 101.0 and 92.3 fg cell⁻¹ for station 72.

The depth distribution of AZA and toxigenic Amphidomataceae, as estimated on six selected stations (19, 25, 32, 44, 64 and 71), was quite variable between stations. At station 25, 44, and 71 most cells were found at the Deep-Chlorophyll-Maximum (DCM) layer (note the log-scale in Fig 10). Station 71 showed the highest cell density for toxigenic *Am. languida*, but also relatively high amounts of *Az. spinosum*. The CTD depth profile revealed almost a constant salinity value between the surface and 40 m. A distinct thermocline at ~ 27 m depth was observed with a sudden decrease of the potential temperature from 18 to 6.5°C. Around the thermocline an exceptional high phytoplankton biomass was present, as indicated by distinct peaks in fluorescence (~ 15 AU) and oxygen (~ 340 μmol L⁻¹, oxygen data can be found at [53]).

At station 19 there was a deep (~ 55 m) thermocline with a weak fluorescence signal and at station 64 there was a strong fluorescence signal at 23 m depth. At both stations, the few cells of toxigenic Amphidomataceae were recorded in the sub-surface samples only. Higher cell

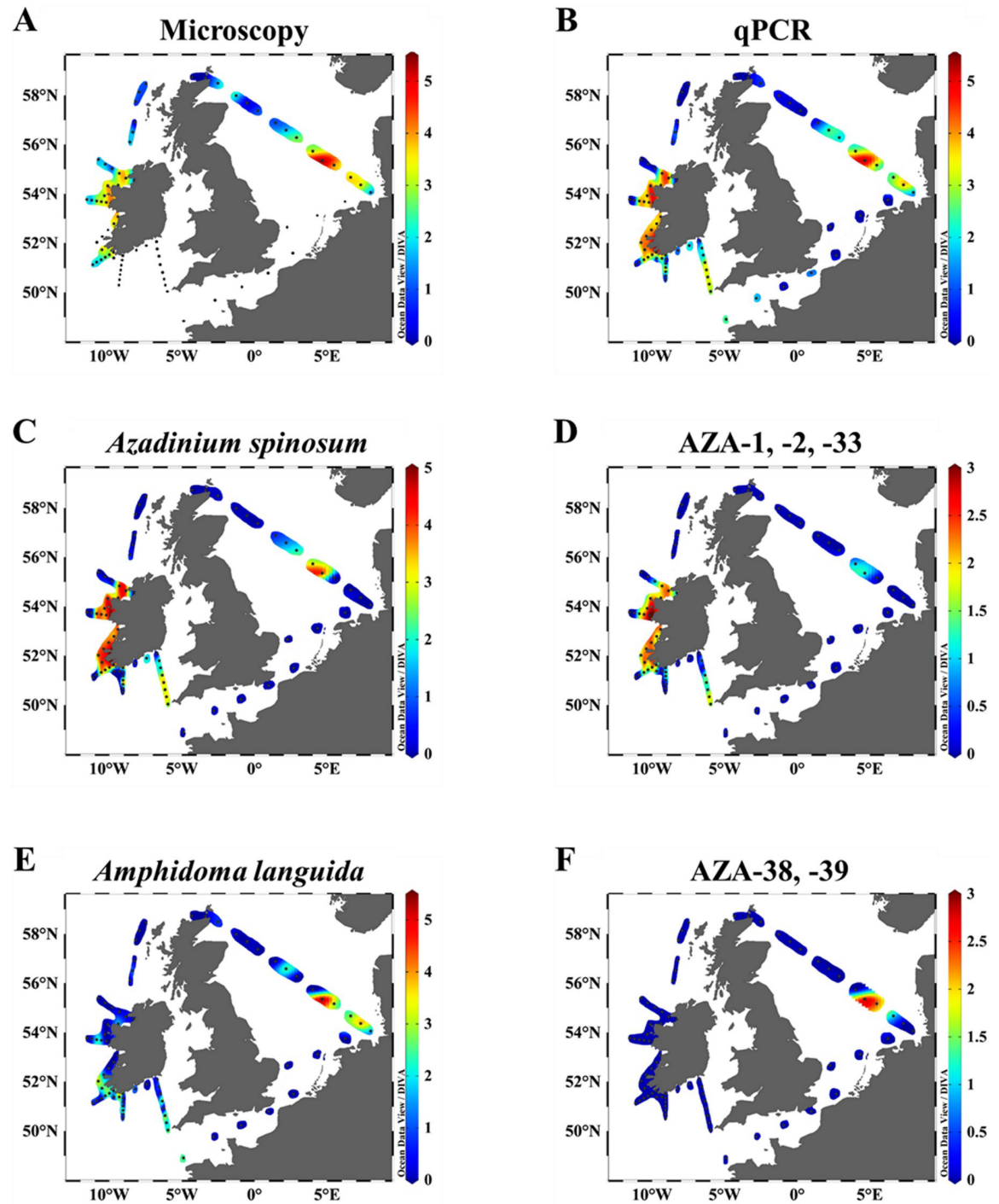


Fig 6. Graphical visualization of general agreement between on-board light microscopy, qPCR, and chemical AZA quantification. Color code refers to the logarithmic scale (\log_{10}). A–B: Abundances of amphidomatacean cells L^{-1} by (A) light microscopy and (B) qPCR estimations. C–D: Cells L^{-1} of *Azadinium spinosum* estimated by qPCR (C) and AZA quantities ($pg L^{-1}$) of AZA-1, -2 and -33 (D) measured by LC-MS/MS. E–F: Cell numbers L^{-1} of *Amphidoma languida* estimated by qPCR (E) and AZA quantities ($pg L^{-1}$) of AZA-38 and AZA-39 (F) measured by LC-MS/MS.

<https://doi.org/10.1371/journal.pone.0235015.g006>

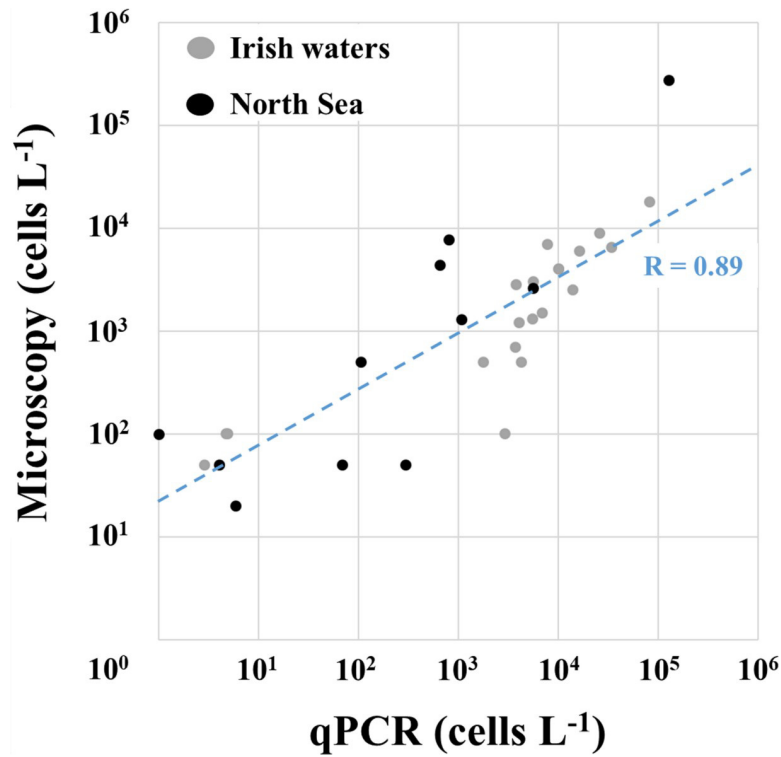


Fig 7. Correlation between microscopic (x-axis) and qPCR (y-axis) calculated cell numbers L^{-1} . Dots indicate the sample area of either Irish waters (grey) or the North Sea (black). “R” displays the respective correlation coefficient.

<https://doi.org/10.1371/journal.pone.0235015.g007>

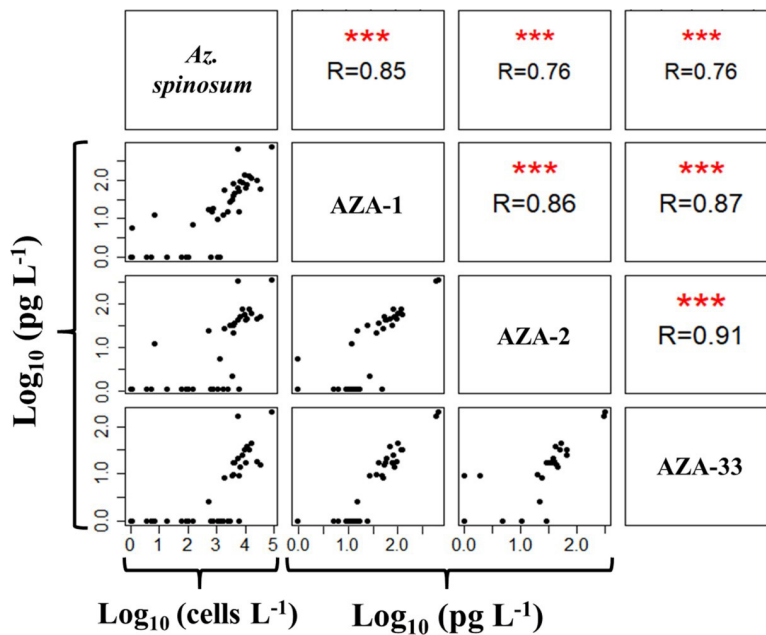


Fig 8. Pearson correlation matrix of logarithmic qPCR counts ($cells L^{-1}$) and logarithmic AZA quantities ($pg L^{-1}$). “R” displays the respective correlation coefficient. Significance levels of respective correlations (Pearson’s product-moment correlation test) are indicated by red asterisks (* $p \leq 0.05$, ** $p \leq 0.01$, *** $p \leq 0.001$).

<https://doi.org/10.1371/journal.pone.0235015.g008>

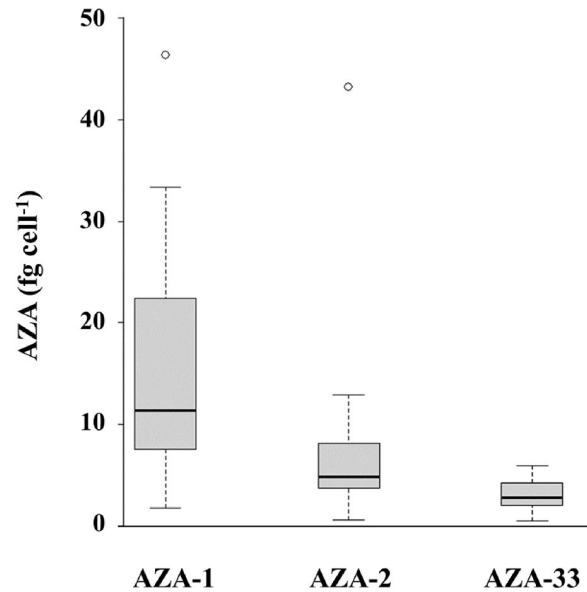


Fig 9. AZA cell quota for *Az. spinosum* and AZA-1, -2 and -33 based on molecular (qPCR) and chemical (LC-MS/MS) field observations.

<https://doi.org/10.1371/journal.pone.0235015.g009>

densities of toxigenic species in the upper 10 m were also observed at station 32, where neither a thermocline nor a deep chlorophyll maximum was observed. The depth-distribution pattern of AZA mirrored the cell distribution, but for samples with lower cell density estimates (e.g., stations 19 and 64) no AZAs were detected.

Discussion

Amphidomataceae and AZA in the North Atlantic: Distribution and abundance

Microscopy, species-specific qPCR assays and LC-MS/MS revealed that Amphidomataceae, and especially all three North Atlantic toxigenic species, are widely distributed in Irish coastal waters, the Celtic Sea and the North Sea. All three species identified and quantified using qPCR revealed different abundances, with *Az. spinosum* and *Am. languida* being more abundant and widespread compared to *Az. poporum*.

Amphidoma languida. *Am. languida* was detected at most stations. Most notably, the highest amphidomatacean cell abundance, of more than 10^5 cells L^{-1} observed at station 71 in the North Sea transect, was mainly dominated by *Am. languida*. AZA-38 and -39, the two AZA-congeners known to be produced by North Atlantic strains of *Am. languida* [59], were also detected at these North Sea stations, with relatively high toxin levels of 234 $pg L^{-1}$ and 384 $pg L^{-1}$, respectively.

This peak of amphidomatacean abundance in the North Sea at station 71 was associated with a dense and deep (~ 30 m) chlorophyll patch extending from stations 71 to 72. While *Am. languida* was much more abundant at station 71 compared to 72, fluorescence was much higher at station 72, which may indicate that different plankton communities or different development stages were sampled. In any case, this subsurface bloom appeared close to the shelf break where water depth decreased from > 100 m to ~ 50 – 40 m (S2C Fig). This shelf area off the German Bight is generally regarded as a highly productive habitat [60, 61]. Summer subsurface chlorophyll peaks have been observed previously to be prominent in the stratified

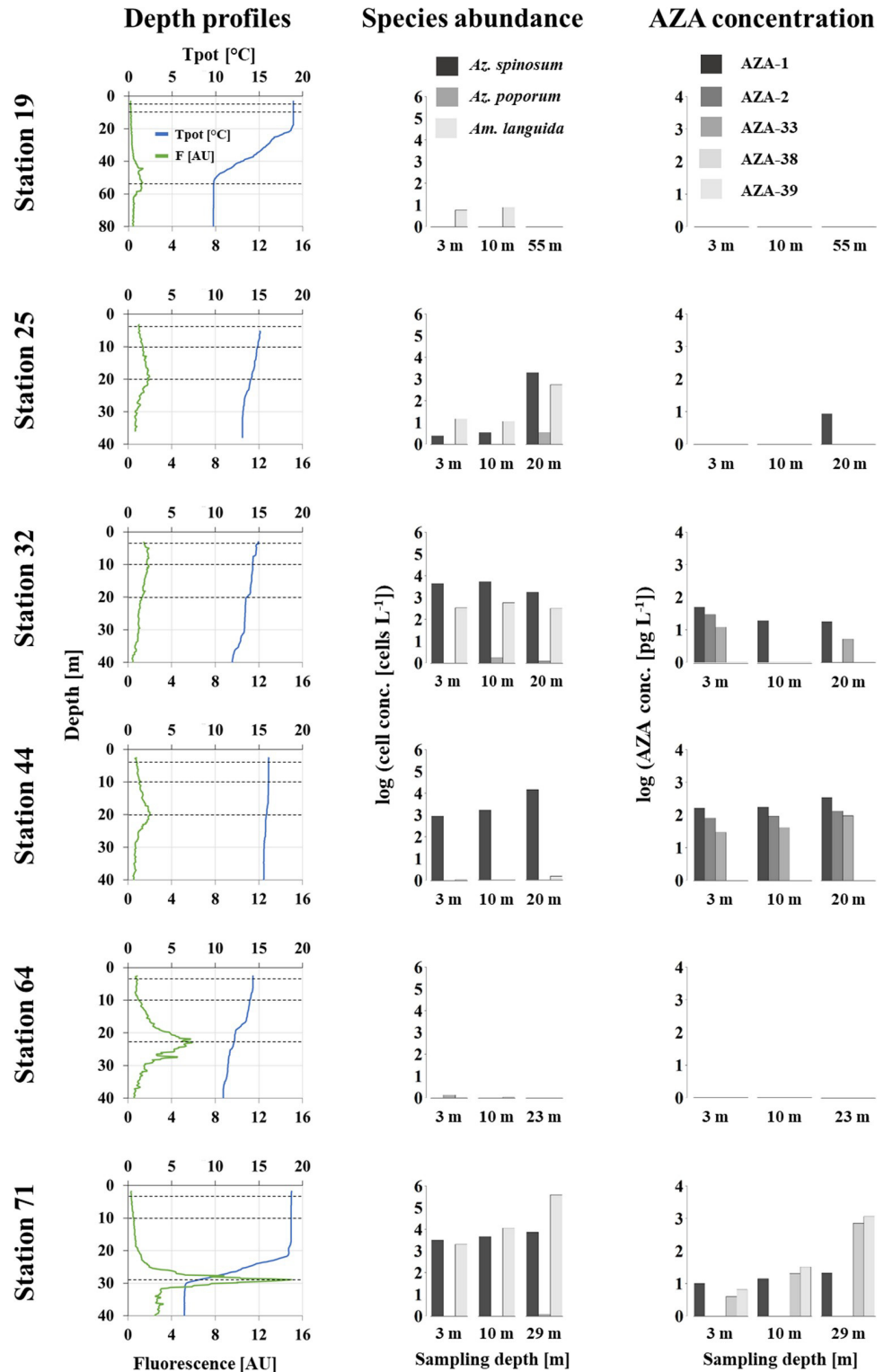


Fig 10. Depth (m) profiles of potential temperature Tpot (°C), fluorescence (AU), AZA-producer abundances and respective toxin quantities for six selected stations. Dashed lines in the profile plots indicate the depth for the respective samples.

<https://doi.org/10.1371/journal.pone.0235015.g010>

regions of the North Sea, to be patchily distributed both in time and space, and to be dominated by dinoflagellates and not by diatoms [62]. For the formation of such blooms a 'tidal pumping' mechanism entailing the fortnightly sweep of the tidal mixing front from shallow to deep water and thereby injecting nutrient-rich bottom water into the pycnocline layer, has been discussed [63].

The maximum *Am. languida* density of this North Sea bloom of $>10^5$ cells L^{-1} is the highest density of an amphidomatacean species yet reported from the North Atlantic and/or North Sea waters. Blooms of other Amphidomataceae in other geographical regions have been found at even higher abundances, with records up to 10^6 (*Az. polongum*, Peru) or up to 10^7 (*Az. luciferelloides*, Argentina) cells L^{-1} [64, 65].

Based on the present findings, *Am. languida* appear to be the dominant AZA-producers in the central North Sea and the German Bight compared to *Az. spinosum* and/or *Az. poporum*, however, this survey is only a snapshot in time. In any case, a dominance of *Am. languida* over *Az. spinosum* for the North Sea matches with data from a previous field study on toxigenic Amphidomataceae in the North Sea [34]. *Amphidoma languida* was also widely present around the Irish coast. Application of the *Am. languida* specific qPCR assay on samples taken on a 2017 Irish coastline survey (CV17022) revealed overall cell abundances of up to $\sim 1.5 \times 10^3$ cells L^{-1} with peak densities of up to 2.3×10^4 cells L^{-1} along the Irish coastline [32]. Together with the present results these data sets indicate a frequent occurrence and significant abundance of *Am. languida* at the Irish southern and south-western coastline and emphasize the potential risk for shellfish contamination with *Am. languida* specific AZA in these production areas. However, different to the high levels of AZA-38 and -39 found in the central North Sea, these two *Am. languida* specific AZA congeners were not detected around Ireland (Fig 6F and S2 Table), which might be explained by the limit of detection for the chemical method which may not be sensitive enough to detect the prevalent but low abundances. Nevertheless, with the emerging importance of the presence of *Am. languida* in the North Sea and the Irish Atlantic the routine surveillance of both *Am. languida* cells (applying the specific qPCR assay) and the presence of AZA-38 and -39 should be considered. Both are currently not regulated by the European Union (EU) in routine monitoring programs. Importantly, however, actual *in vivo* toxicity of AZA-38 and -39 is still unknown and has to be investigated.

Azadinium spinosum. *Azadinium spinosum* showed a distribution similar to *Am. languida* and both species co-occur in Irish coastal waters as well as in the North Sea. Peak cell densities and levels of AZA congeners typically produced by *Az. spinosum* (i.e., AZA-1, -2 and -33) were clearly concentrated at the Irish southwestern and western coastline (Fig 6C). This underlines the special threat of *Az. spinosum* to Irish aquaculture [11]. Previous laboratory growth studies revealed that *Az. spinosum* are able to cope with a wide range of environmental conditions. Temperature had the most significant impact on the growth of a North Sea strain and indicated higher growth rates at relatively high temperatures of $22^\circ C$ [66], however toxin production was significantly higher at lower temperatures [66, 67]. Therefore, water temperatures of 13 to $17^\circ C$, as observed in this study, are likely to be suboptimal for rapid cell division and formation of extensive *Az. spinosum* blooms. On the other hand, the strong thermocline, as observed in the central North Sea at station 71 (Fig 10), had relatively high temperatures of $\sim 18^\circ C$ and thus might have favored the high cell densities of *Az. spinosum* and *Am. languida*.

The presence of *Az. spinosum* cells in the North Atlantic area off the west coast of Ireland have been observed previously [11]. A transatlantic survey conducted in 2014 from Galway (west coast Ireland), revealed the presence of *Az. spinosum* cells at several stations along a transect through the North Atlantic area, up to the Bight Fracture zone, where the highest cell density observed was 1.3×10^4 cell L^{-1} at a station in the Porcupine bank and the second highest cell density was observed at 1×10^4 cells L^{-1} between the Edoras and Fangorn Banks past the

Rockall Bank [68]. Along the Irish coastline, prevalent abiotic parameters, like wind direction and prevailing winds, could allow for bloom formation by concentration of plankton inside bays, even under suboptimal growth conditions. This might be of special importance for the south-west coastal bays, which are open directly to these western-southwesterly winds. Dinoflagellates are associated with the thermocline and surface mixed layer brought into the bays by downwelling pulses [69, 70]. Data using satellite tracked drifting buoys on the north west European shelf [71] reveal that water mass circulation around the Celtic Sea follows a highly organized thermohaline circulation. This circulation advects water through the south and west of the region of St. George's Channel. This flow is directed south into the Celtic Sea and west along the southern Irish coast [72]. Furthermore, there is evidence that this flow extends around the south-western tip of Ireland [71–73]. Typical northeastward winds in the region probably play an important role in the wind driven advection of plankton into the bays of the south-west of Ireland [74]. This circulation pattern may explain why the higher cell densities were found at the inner stations of transects along the southwest and west coast of Ireland (T3, T5) and further offshore in southern Ireland transects (T1 and T2, Fig 5). Nevertheless, the impact of abiotic factors on the growth and bloom formation of toxigenic Amphidomataceae remains poorly known and additional studies should be conducted to address this knowledge gap.

qPCR records of *Az. spinosum* coincide with LC-MS/MS records of the AZA congeners produced by Irish and North Sea strains (i.e., AZA-1, -2 and -33). Both data sets were significantly correlated and allowed the calculation of the field population AZA cell quota. With a mean AZA-1 cell quota of 17.8 fg cell⁻¹ (Fig 9) the field measurements are in the same range as laboratory measurements of isolated strains, which typically vary between ~ 1 and 20 fg cell⁻¹ [11, 15, 36] and were higher (up to 200 fg cell⁻¹) when grown at 10° C [66]. The range of AZA cell quota as estimated here (e.g. AZA-1 cell quota ranging from 2–46 fg cell⁻¹, and AZA-38/-39 cell quota ranging from 2–101 fg cell⁻¹) likely include methodological issues (e.g., chemical AZA analyses may include AZA accumulated in small protistan grazers). There may also be physiological reasons e.g., cell quotas of *Azadinium* spp. usually increase when growth is limited/stagnant [67, 75]. The toxin profile of AZA-1, -2 and -33 is typical of Irish, Scottish and Shetland strains [46], which in phylogenetic trees form a well-supported ribotype (Ribotype A) [35]. Other co-occurring *Az. spinosum* strains from the Norwegian coast, however, cluster in another *Az. spinosum* ribotype (Ribotype B) and have a fundamentally different AZA profile consisting mainly of AZA-11 and -51 [35]. In the present study, only AZA-1, -2 and -33, but no AZA-11 or -51 were detected, suggesting that Ribotype B was not present, or perhaps in low abundance. First and yet unpublished characterization of multiple *Az. spinosum* strains established from the survey confirm that strains from Ireland are exclusively of Ribotype A, whereas the majority of *Az. spinosum* strains from the central North Sea are of Ribotype B.

Azadinium poporum. Based on various records around the world, *Az. poporum* seems to be the most widely distributed species of Amphidomataceae [48]. The species doubtlessly is also present in the North Sea and Irish waters but during the survey it was restricted to the southern Irish coast and the North Sea in very low abundances (< 60 cells L⁻¹) compared to the other toxigenic Amphidomataceae. Previous Irish coastline surveys conducted in 2012 and 2016 to 2019 have also shown low abundance or complete absence of *Az. poporum* in samples [68]. Notably, it was the only toxigenic amphidomatacean species detected in the English Channel. This area is known for its seasonal dynamics, spatial heterogeneity and inter-annual variability of harmful algae [76], so more data are needed to evaluate the importance of local weather conditions and current circulation pattern for the occurrence and abundance of Amphidomataceae in the English Channel.

Vertical distribution of AZA producers. Little is known about the depth distribution of AZA-producing species. Original data, as obtained here at three different depths at six stations, revealed variable patterns in species depth distribution. Highest densities of toxigenic Amphidomataceae at the deep-chlorophyll-layer in the North Sea indicate that surface water sampling and/or satellite observations are less well suited for the detection of such Amphidomatacean blooms. In any case, the limited depth-distribution data set presented here indicates that reducing the number of samples by pooling (= averaging) different depths seems to be a justified strategy to estimate the occurrence and abundance of AZA producers in the water column. While this method might in some cases shift cell densities per volume of filtered seawater below the “cell detection limit” of the LC-MS/MS, overall it is a cost and time effective sampling procedure.

Critical evaluation of qPCR quantification. The spike experiments for all three toxigenic species with an average recovery efficiency of ~ 94% of the target cells over a range of 10^2 to 10^4 target cells per L revealed a very robust assay design and reliability of the quantitative field data calculations. Specific qPCR is thus confirmed to be a valuable tool for the detection and enumeration of low abundant species [77]. In addition to this and previous Amphidomataceae qPCR spike-recovery experiments [32], a direct comparison of qPCR quantification with other independent quantification methods over a larger data set is desirable. Comparison with optical detection and quantification using target-specific, optical markers, for example by fluorescence *in situ* hybridization (FISH), seems to be the most straightforward strategy. Molecular FISH assays for toxigenic *Az. spinosum* and *Az. poporum* are available but labour-intensive [31]. More important, however, these assays were designed at a time when only three species and a limited number of strains were known. Extensive testing would be needed to exclude cross reactivity of these FISH assays with any of the currently known species, most of which are non-toxigenic amphidomatacean species.

Nevertheless, qPCR data can be compared to the semi-quantitative microscopy quantification of live amphidomatacean cells, even if the latter method captures all Amphidomataceae (including toxigenic and non-toxigenic species), whereas qPCR specifically quantifies the three toxigenic species only. With all these limitations in mind, there is generally a good agreement in cell abundances between both methods. However, some discrepancies between microscopy and qPCR analysis were observed for some stations. Higher cell estimates by live microscopy can easily be due to varying levels of non-toxigenic amphidomatacean species, which undoubtedly are present (Fig 2) but not included in the qPCR estimates. Moreover, lower *in vivo* rDNA copy numbers of the local target population than of the strain used to calibrate the qPCR assay can easily lead to a qPCR underestimation of the actual cell densities and vice versa [39]. Higher cell densities calculated by qPCR compared to microscopic counting might also be due to limitations of the live counting method, if not all cells present in the sedimentation chamber sink to the bottom and/or are identified correctly as members of Amphidomataceae.

qPCR-based cell abundances and AZA levels measured by LC-MS/MS in the field samples were also well correlated. This could be demonstrated adequately for *Az. spinosum* and its corresponding toxins AZA-1, -2 and -33. Out of 44 stations, where *Az. spinosum* was detected by qPCR, 35 stations also revealed its synthesized AZAs. The non-correlation of 20% was likely due to the higher detection limit of LC-MS/MS. The mean limit of detection for AZA-1 in the field samples was 13.2 pg L^{-1} . Given the calculated AZA cell quota of $17.8 \text{ fg cell}^{-1}$ (AZA-1 produced by *Az. spinosum*, this study), the “cell detection limit” corresponds to $\sim 1 \times 10^3 \text{ cells L}^{-1}$. Such a “threshold” can also be seen from the depth profile samples (Fig 10): cell densities calculated by qPCR above a density of $\sim 1 \times 10^3 \text{ cells L}^{-1}$ correspond to positive AZA measurements, whereas almost no AZA was recorded for qPCR cell abundance levels $< 1 \times 10^3 \text{ cells L}^{-1}$ (S2

[Table](#)). Of all field samples, only three stations revealed AZA-1 signals although the qPCR estimated cell densities below 500 cells L⁻¹. Toxin accumulation in small protistan grazers and/or bound to decaying cells or detritus may be an explanation.

Conclusion

Live cell microscopy, chemical AZA analysis and qPCR assays revealed that toxigenic Amphidomataceae and AZA were widely distributed in summer 2018 in the eastern North Atlantic. Quantification of three toxigenic amphidomatacean species was based on qPCR assays, whose performance was challenged using extended specificity testing and spike-recovery experiments. qPCR quantification data had a highly significant correlation with total amphidomatacean cell densities based on live-cell microscopy counting and with chemical analysis of AZAs. Whereas *Az. poporum* occurred only in very low densities at a few stations, higher abundances of *Az. spinosum* were detected along the Irish coastline and therefore underline the importance of current monitoring programs on that species performed by the Marine Institute (Galway, Ireland). *Amphidoma languida* revealed highest cell densities in the central North Sea, indicating this may be the dominant toxigenic amphidomatacean species in the North Sea area. However, this species was also detected at many stations in Irish waters and its surveillance should thus be incorporated into the Irish, as well as EU monitoring programs.

The on-board availability and (almost) real time operation of three approaches and instruments—microscopy, LC-MS/MS and qPCR—was successful and enabled the validation and comparison of results from different perspectives. In combination, the multi-method approach yielded sound and reliable data on diversity, distribution and abundance of toxigenic Amphidomataceae in the area.

Supporting information

S1 Table. Mass transitions m/z (Q1>Q3 mass) and their respective AZA.

(PDF)

S2 Table. Species counts (cells L⁻¹) based on qPCR (cell number calculation based on mean C_T values of three technical replicates) and microscopy, as well as toxin amount (pg L⁻¹) based on LC-MS/MS for each station. n.d. = not detected; n.a. = no data available.

(PDF)

S1 Fig. Geographical distribution of temperature (A), salinity (B) and fluorescence (C) averaged for the upper layer defined as the maximum sampling depth at each station.

(TIF)

S2 Fig. Depth profiles of temperature (A), salinity (B) and fluorescence (C) for the six defined sampling transects T1 –T6 as indicated in [Fig 1B](#).

(TIF)

Acknowledgments

The authors thank Caroline Cusack, Paula Hynes and Joe Silke (Marine Institute, Galway, Ireland), as well as Luisa Hintze and Karina Krapf (AWI, Bremerhaven, Germany) for on-board technical support on sampling and chemical analyzes of AZA samples. Thanks go also to Rohan Henkel (ICBM, Wilhelmshaven, Germany) for on-board CTD operation, data formatting and processing. We further thank Captain Diecks and the entire crew on *RV Heincke* for support and assistance during the field sampling campaign in this study.

Author Contributions

Conceptualization: Stephan Wietkamp, Bernd Krock, Urban Tillmann.

Data curation: Bernd Krock.

Formal analysis: Stephan Wietkamp.

Funding acquisition: Bernd Krock, Urban Tillmann.

Investigation: Stephan Wietkamp, Bernd Krock, Dave Clarke, Daniela Voß, Jane Kilcoyne, Urban Tillmann.

Methodology: Stephan Wietkamp, Dave Clarke, Rafael Salas.

Project administration: Bernd Krock, Urban Tillmann.

Resources: Dave Clarke.

Supervision: Bernd Krock, Urban Tillmann.

Validation: Stephan Wietkamp, Bernd Krock, Dave Clarke, Urban Tillmann.

Visualization: Stephan Wietkamp, Daniela Voß, Urban Tillmann.

Writing – original draft: Stephan Wietkamp, Urban Tillmann.

Writing – review & editing: Stephan Wietkamp, Bernd Krock, Dave Clarke, Daniela Voß, Rafael Salas, Jane Kilcoyne, Urban Tillmann.

References

1. Trainer VL, Moore SK, Hallegraef G, Kudela RM, Clement A, Mardones JI, et al. Pelagic harmful algal blooms and climate change: lessons from nature's experiments with extremes. *Harmful Algae*. 2020; 91:101591. <https://doi.org/10.1016/j.hal.2019.03.009> PMID: [32057339](https://pubmed.ncbi.nlm.nih.gov/32057339/)
2. Wells ML, Karlson B. Harmful algal blooms in a changing ocean. In: Glibert PM, Berdalet E, Burford MA, Pitcher GC, Zhou M, editors. *Global Ecology and Oceanography of Harmful Algal Blooms*. Cham: Springer; 2018. p. 77–90.
3. Botana LM. *Seafood and freshwater toxins—pharmacology, physiology, and detection*. Boca Raton: CRC Press; 2014. 1197 p.
4. Anderson DM, Alpermann TJ, Cembella AD, Collos Y, Masseret E, Montresor M. The globally distributed genus *Alexandrium*: multifaceted roles in marine ecosystems and impacts on human health. *Harmful Algae*. 2012; 14:10–35. <https://doi.org/10.1016/j.hal.2011.10.012> PMID: [22308102](https://pubmed.ncbi.nlm.nih.gov/22308102/)
5. Hinder SL, Hays GC, Brooks CJ, Davies AP, Edwards M, Walne AW, et al. Toxic marine microalgae and shellfish poisoning in the British isles: history, review of epidemiology, and future implications. *Environ Health*. 2011; 10(1):54.
6. Nielsen LT, Hansen PJ, Krock B, Vismann B. Accumulation, transformation and breakdown of DSP toxins from the toxic dinoflagellate *Dinophysis acuta* in blue mussels, *Mytilus edulis*. *Toxicon*. 2016; 117:84–93. <https://doi.org/10.1016/j.toxicon.2016.03.021> PMID: [27045361](https://pubmed.ncbi.nlm.nih.gov/27045361/)
7. Satake M, MacKenzie L, Yasumoto T. Identification of *Protoceratium reticulatum* as the biogenetic origin of yessotoxin. *Nat Toxins*. 1997; 5:164–7. <https://doi.org/10.1002/nt.7> PMID: [9407560](https://pubmed.ncbi.nlm.nih.gov/9407560/)
8. Satake M, Ofuji K, James K, Furey A, Yasumoto T. New toxic events caused by Irish mussels. In: Reguera B, Blanco J, Fernández ML, Wyatt T, editors. *Harmful Algae*. Santiago de Compostela: Xunta de Galicia and International Oceanographic Commission of UNESCO; 1998. p. 468–9.
9. Twiner M, Hess P, Doucette GJ. Azaspiracids: Toxicology, pharmacology, and risk assessment. In: Botana LM, editor. *Seafood and Freshwater Toxins*. Boca Raton, USA: CRC Press; 2014. p. 823–55.
10. Anonymous. Regulation (EC) No 853/2004 of the European Parliament and of the Council of 29 April 2004 laying down specific hygiene rules for on the hygiene of foodstuffs. *Off J Eur Union* 2004; 30:1–151.
11. Salas R, Tillmann U, John U, Kilcoyne J, Burson A, Cantwell C, et al. The role of *Azadinium spinosum* (Dinophyceae) in the production of azaspiracid shellfish poisoning in mussels. *Harmful Algae*. 2011; 10:774–83.

12. Aasen J, Torgersen T, Dahl E, Naustvoll L. Confirmation of azaspiracids in mussels in Norwegian coastal areas, and full profile at one location. Proceedings of the 5th International Conference on Molluscan Shellfish Safety, Galway, Ireland, June 14–18. 2004:162–9.
13. Tillmann U, Jaen D, Fernández L, Gottschling M, Witt M, Blanco J, et al. Amphidoma languida (Amphidomataceae, Dinophyceae) with a novel azaspiracid toxin profile identified as the cause of molluscan contamination at the Atlantic coast of southern Spain. Harmful Algae. 2017; 62:113–26. <https://doi.org/10.1016/j.hal.2016.12.001> PMID: 28118886
14. Krock B, Tillmann U, John U, Cembella AD. Characterization of azaspiracids in plankton size-fractions and isolation of an azaspiracid-producing dinoflagellate from the North Sea. Harmful Algae. 2009; 8:254–63.
15. Tillmann U, Elbrächter M, Krock B, John U, Cembella A. Azadinium spinosum gen. et sp. nov. (Dinophyceae) identified as a primary producer of azaspiracid toxins. Eur J Phycol. 2009; 44(1):63–79.
16. Tillmann U, Elbrächter M, John U, Krock B. A new non-toxic species in the dinoflagellate genus Azadinium: A. poporum sp. nov. Eur J Phycol. 2011; 46(1):74–87.
17. Percopo I, Siano R, Rossi R, Soprano V, Sarno D, Zingone A. A new potentially toxic Azadinium species (Dinophyceae) from the Mediterranean Sea, A. dexteroporum sp. nov. J Phycol. 2013; 49(5):950–66. <https://doi.org/10.1111/jpy.12104> PMID: 27007318
18. Rossi R, Dell'Aversano C, Krock B, Ciminiello P, Percopo I, Tillmann U, et al. Mediterranean Azadinium dexteroporum (Dinophyceae) produces AZA-35 and six novel azaspiracids: a structural study by a multi-platform mass spectrometry approach. Anal Bioanal Chem. 2017; 409:1121–34. <https://doi.org/10.1007/s00216-016-0037-4> PMID: 27822651
19. Krock B, Tillmann U, Voß D, Koch BP, Salas R, Witt M, et al. New azaspiracids in Amphidomataceae (Dinophyceae): proposed structures. Toxicon. 2012; 60:830–9. <https://doi.org/10.1016/j.toxicon.2012.05.007> PMID: 22643573
20. Luo Z, Krock B, Mertens K, Nézan E, Chomérat N, Bilien G, et al. Adding new pieces to the Azadinium (Dinophyceae) diversity and biogeography puzzle: non-toxic Azadinium zhuanum sp. nov. from China, toxigenic A. poporum from the Mediterranean, and a non-toxic Azadinium dalianense from the French Atlantic. Harmful Algae. 2017; 66:65–78. <https://doi.org/10.1016/j.hal.2017.05.001> PMID: 28602255
21. Tillmann U, Akselman R. Revisiting the 1991 algal bloom in shelf waters off Argentina: Azadinium luciferelloides sp. nov. (Amphidomataceae, Dinophyceae) as the causative species in a diverse community of other amphidomataceans. Phycol Res. 2016; 64:160–75.
22. Tillmann U, Wietkamp S, Krock B, Tillmann A, Voß D, Gu H. Amphidomataceae (Dinophyceae) in the western Greenland area, including the description of Azadinium perforatum sp. nov. Phycologia. 2020; 59(1):63–88.
23. Battocchi C, Totti C, Vila M, Masó M, Capellacci S, Accoroni S, et al. Monitoring toxic microalgae Ostreopsis (dinoflagellate) species in coastal waters of the Mediterranean Sea using molecular PCR-based assay combined with light microscopy. Mar Poll Bull. 2010; 60(7):1074–84.
24. Ebenezer V, Medlin LK, Ki J-S. Molecular detection, quantification, and diversity evaluation of microalgae. Mar Biotechnol. 2012; 14(2):129–42. <https://doi.org/10.1007/s10126-011-9427-y> PMID: 22200918
25. Eckford-Soper LK, Daugbjerg N. Development of a multiplex real-time qPCR assay for simultaneous enumeration of up to four marine toxic bloom-forming microalgal species. Harmful Algae. 2015; 48:37–43. <https://doi.org/10.1016/j.hal.2015.06.009> PMID: 29724474
26. Hatfield RG, Bean T, Turner AD, Lees DN, Lowther J, Lewis A, et al. Development of a TaqMan qPCR assay for detection of Alexandrium spp. and application to Harmful Algal Bloom monitoring. Toxicon. 2019; 2:100011
27. Penna A, Galluzzi L. The quantitative real-time PCR applications in the monitoring of marine harmful algal bloom (HAB) species. Environ Sci Pollut Res. 2013; 20(10):6851–62.
28. Engesmo A, Strand D, Gran-Stadniczeňko S, Edvardsen B, Medlin LK, Eikrem W. Development of a qPCR assay to detect and quantify ichthyotoxic flagellates along the Norwegian coast, and the first Norwegian record of Fibrocapsa japonica (Raphidophyceae). Harmful Algae. 2018; 75:105–17. <https://doi.org/10.1016/j.hal.2018.04.007> PMID: 29778220
29. Perini F, Bastianini M, Capellacci S, Pugliese L, DiPoi E, Cabrini M, et al. Molecular methods for cost-efficient monitoring of HAB (harmful algal bloom) dinoflagellate resting cysts. Mar Pollut Bull. 2018.
30. Ruvindy R, Bolch CJ, Mackenzie L, Smith KF, Murray SA. qPCR assays for the detection and quantification of multiple Paralytic Shellfish Toxin-producing species of Alexandrium. Front Microbiol. 2018; 9.
31. Toebe K, Joshi AR, Messtorff P, Tillmann U, Cembella A, John U. Molecular discrimination of taxa within the dinoflagellate genus Azadinium, the source of azaspiracid toxins. J Plankton Res. 2013; 35(1):225–30.

32. Wietkamp S, Tillmann U, Clarke D, Toebe K. Molecular determination and quantification of the toxigenic dinoflagellate *Amphidoma languida* (Amphidomataceae, Dinophyceae). *J Plankton Res.* 2019; 41(2):101–13.
33. Smith KF, Rhodes L, Harwood DT, Adamson J, Moisan C, Munday R, et al. Detection of *Azadinium poporum* in New Zealand: the use of molecular tools to assist with species isolations. *J Appl Phycol.* 2016; 28:1125–32.
34. Wietkamp S, Krock B, Gu H, Voß D, Klemm K, Tillmann U. Occurrence and distribution of Amphidomataceae (Dinophyceae) in Danish coastal waters of the North Sea, the Limfjord, and the Kattegat/Belt area. *Harmful Algae.* 2019; 88:101637. <https://doi.org/10.1016/j.hal.2019.101637> PMID: 31582159
35. Tillmann U, Edvardsen B, Krock B, Smith KF, Paterson RF, Voß D. Diversity, distribution, and azaspiracids of Amphidomataceae (Dinophyceae) along the Norwegian coast. *Harmful Algae.* 2018; 80:15–34. <https://doi.org/10.1016/j.hal.2018.08.011> PMID: 30502808
36. Tillmann U, Gottschling M, Krock B, Smith KF, Guinder V. High abundance of Amphidomataceae (Dinophyceae) during the 2015 spring bloom of the Argentinean Shelf and a new, non-toxicogenic ribotype of *Azadinium spinosum*. *Harmful Algae.* 2019; 84:244–60. <https://doi.org/10.1016/j.hal.2019.01.008> PMID: 31128809
37. Clarke D, Salas R, Hynes P, McCarthy A, Walsh D, Silke J. PCR assays for the detection of ASP, DSP, PSP and AZP toxigenic producing phytoplanktonic species in Irish coastal waters. In: Hess P, editor. *Proceedings of the 18th Conference on Harmful Algae Blooms, Nantes, 2018.* Nantes, France: ISSHA; 2020. in press.
38. Casabianca S, Casabianca A, Riobó P, Franco JM, Vila M, Penna A. Quantification of the toxic dinoflagellate *Ostreopsis* spp. by qPCR assay in marine aerosol. *Environ Sci Technol.* 2013; 47(8):3788–98. <https://doi.org/10.1021/es305018s> PMID: 23480590
39. Galluzzi L, Bertozzini E, Penna A, Perini F, Garcés E, Magnani M. Analysis of rRNA gene content in the Mediterranean dinoflagellate *Alexandrium catenella* and *Alexandrium taylori*: implications for the quantitative real-time PCR-based monitoring methods. *J Appl Phycol.* 2010; 22:1–9.
40. Perini F, Casabianca A, Battocchi C, Accoroni S, Totti C, Penna A. New approach using the real-time PCR method for estimation of the toxic marine dinoflagellate *Ostreopsis cf. ovata* in marine environment. *PLoS One.* 2011; 6:e17699. <https://doi.org/10.1371/journal.pone.0017699> PMID: 21408606
41. Berdalet E, Tester PA, Chinain M, Fraga S, Lemée R, Litaker W, et al. Harmful algal blooms in benthic systems: recent progress and future research. *Oceanography.* 2017; 30(1):36–45.
42. Busch JA, Andrée KB, Diogène J, Fernández-Tejedor M, Toebe K, John U, et al. Toxigenic algae and associated phycotoxins in two coastal embayments in the Ebro Delta (NW Mediterranean). *Harmful Algae.* 2016; 55(55):191–201.
43. Fu M, Chen G, Zhang C, Wang Y, Sun R, Zhou J. Rapid and sensitive detection method for *Karlodinium veneficum* by recombinase polymerase amplification coupled with lateral flow dipstick. *Harmful Algae.* 2019; 84:1–9. <https://doi.org/10.1016/j.hal.2019.01.011> PMID: 31128793
44. Toldrà A, Jauset-Rubio M, Andrée KB, Fernández-Tejedor M, Diogène J, Katakis I, et al. Detection and quantification of the toxic marine microalgae *Karlodinium veneficum* and *Karlodinium armiger* using recombinase polymerase amplification and enzyme-linked oligonucleotide assay. *Anal Chim Acta.* 2018; 1039:140–8. <https://doi.org/10.1016/j.aca.2018.07.057> PMID: 30322545
45. Zamyadi A, Romanis C, Mills T, Neilan B, Choo F, Coral LA, et al. Diagnosing water treatment critical control points for cyanobacterial removal: exploring benefits of combined microscopy, next-generation sequencing, and cell integrity methods. *Water Res.* 2019; 152:96–105. <https://doi.org/10.1016/j.watres.2019.01.002> PMID: 30665164
46. Tillmann U, Söhner S, Nézan E, Krock B. First record of *Azadinium* from the Shetland Islands including the description of *A. polongum* sp. nov. *Harmful Algae.* 2012; 20:142–55.
47. Tillmann U, Salas R, Jauffrais T, Hess P, Silke J. AZA: the producing organisms—biology and trophic transfer. In: Botana LM, editor. *Seafood and Freshwater Toxins.* Boca Raton, USA: CRC Press; 2014. p. 773–98.
48. Tillmann U. Amphidomataceae. In: Shumway SE, Burkholder JA, Morton SL, editors. *Harmful Algae Blooms, a Compendium Desk Reference.* Hoboken: Wiley; 2018. p. 575–82.
49. Luo Z, Krock B, Giannakourou A, Venetsanopoulou A, Pagou K, Tillmann U, et al. Sympatric occurrence of two *Azadinium poporum* ribotypes in the Eastern Mediterranean Sea. *Harmful Algae.* 2018; 78:75–85. <https://doi.org/10.1016/j.hal.2018.08.003> PMID: 30196927
50. Krock B, Tillmann U, Tebben J, Trefaults N, Gu H. Two novel azaspiracids from *Azadinium poporum*, and a comprehensive compilation of azaspiracids produced by Amphidomataceae (Dinophyceae) *Harmful Algae.* 2019; 82:1–8. <https://doi.org/10.1016/j.hal.2018.12.005> PMID: 30928006

51. Tillmann U, Salas R, Gottschling M, Krock B, O'Driscoll D, Elbrächter M. *Amphidoma languida* sp. nov. (Dinophyceae) reveals a close relationship between *Amphidoma* and *Azadinium*. *Protist*. 2012; 163(5):701–19. <https://doi.org/10.1016/j.protis.2011.10.005> PMID: 22130577
52. Preston-Thomas H. The international temperature scale of 1990 (ITS-90). *Metrologia*. 1990; 27(1):3–10.
53. Krock B, Wisotzki A. Physical oceanography during HEINCKE cruise HE516. Alfred Wegener Institute, Helmholtz Centre for Polar and Marine Research, Bremerhaven., PANGAEA. 2018:<https://doi.org/10.1594/PANGAEA.896405>.
54. Forootan A, Sjöback R, Björkman J, Sjögreen B, Linz L, Kubista M. Methods to determine limit of detection and limit of quantification in quantitative real-time PCR (qPCR). *Biomol Detect Quantif*. 2017; 12:1–6. <https://doi.org/10.1016/j.bdq.2017.04.001> PMID: 28702366
55. Wietkamp S, Krock B, Gu H, Voß D, Klemm K, Tillmann U. Occurrence and distribution of Amphidomataceae (Dinophyceae) in Danish coastal waters of the North Sea, the Limfjord and the Kattegat/Belt area. *Harmful Algae*. 2019; 88:101637. <https://doi.org/10.1016/j.hal.2019.101637> PMID: 31582159
56. Krock B, Tillmann U, Potvin É, Jeong HJ, Drebing W, Kilcoyne J, et al. Structure elucidation and in vitro toxicity of new azaspiracids isolated from the marine dinoflagellate *Azadinium poporum*. *Mar Drugs*. 2015; 13(11):6687–702. <https://doi.org/10.3390/md13116687> PMID: 26528990
57. R-Core-Team. R: a language and environment for statistical computing. 2017.
58. Schlitzer R. Ocean data view. <http://odvawide>. 2018.
59. Tillmann U, Gottschling M, Nézan E, Krock B. First record of *Azadinium dexteroporum* and *Amphidoma languida* (Amphidomataceae, Dinophyceae) from the Irminger Sea off Iceland. *Marine Biodiversity Records*. 2015; 8(e142):1–11.
60. Joint I, Pomroy A. Phytoplankton biomass and production in the southern North Sea. *Mar Ecol Prog Ser*. 1993; 99(1–2):169–82.
61. Charnock H, Dyer KR, Huthnance JM, Liss P, Simpson BH. *Understanding the North Sea System*: Springer Science and Business Media; 1994.
62. Richardson K, Visser AW, Bo Pedersen F. Subsurface phytoplankton blooms fuel pelagic production in the North Sea. *J Plankton Res*. 2000; 22(9):1663–74.
63. Bo Pedersen F. The oceanographic and biological tidal cycle succession in shallow sea fronts in the North Sea and the English Channel. *Estuar Coast Shelf Sci*. 1994; 38(3):249–69.
64. Akselman R, Negri RM. Blooms of *Azadinium* cf. *spinosum* Elbrächter et Tillmann (Dinophyceae) in northern shelf waters of Argentina, southwestern Atlantic. *Harmful Algae*. 2012; 19:30–8.
65. Tillmann U, Sánchez Ramírez S, Krock B, Bernales Jiménez A. A bloom of *Azadinium polongum* in coastal waters off Peru. *Rev Biol Mar Oceanogr*. 2017; 52(3):591–610.
66. Jauffrais T, Séchet V, Herrenknecht C, Truquet P, Véronique S, Tillmann U, et al. Effect of environmental and nutritional factors on growth and azaspiracid production of the dinoflagellate *Azadinium spinosum*. *Harmful Algae*. 2013; 27:138–48.
67. Kilcoyne J, McCoy A, Burrell S, Krock B, Tillmann U. Effect of temperature, growth media, and photoperiod on growth and toxin production of *Azadinium spinosum*. *Mar Drugs*. 2019; 17(498): <https://doi.org/10.3390/md17090489> PMID: 31443393
68. Clarke D. New insights and perspectives from 20 years of monitoring algal events in Irish coastal waters. In: Clarke D, Gilmartin M, editors. *Proceedings of the 11th Irish Shellfish Safety Workshop, Marine Environment and Health Series No. 41, 2020*. Galway, Ireland: Marine Institute; 2020. in press
69. Raine R. A review of the biophysical interactions relevant to the promotion of HABs in stratified systems: the case study of Ireland. *Deep Sea Res Part II Top Stud Oceanogr*. 2014; 101:21–31.
70. Berdalet E, McManus MA, Ross ON, Burchard H, Chavez FP, Jaffe JS, et al. Understanding harmful algae in stratified systems: review of progress and future directions. *Deep Sea Res Part II Top Stud Oceanogr*. 2014; 101:4–20.
71. Hill AE, Brown J, Fernand L, J. H, Horsburgh KJ, Proctor R, et al. Thermohaline circulation of shallow tidal seas. *Geophys Res Lett*. 2008; 35:L11605.
72. Brown J, Carrillo L, Fernand L, Horsburgh KJ, Hill AE, Young EF, et al. Observations of the physical structure and seasonal jet-like circulation of the Celtic Sea and St. George's Channel of the Irish Sea. *Cont Shelf Res*. 2003; 23:533–61.
73. Raine R, McMahon T. Physical dynamics on the continental shelf off southwestern Ireland and their influence on coastal phytoplankton blooms. *Cont Shelf Res*. 1998; 18(8):883–914.
74. Raine R, O'Mahoney J, McMahon T, Roden C. Hydrography and phytoplankton of waters off southwest Ireland. *Estuar Coast Shelf Sci*. 1990; 30:579–96.

75. Dai X, Bill BD, Adams NG, Tillmann U, Sloan C, Lu D, et al. The effect of temperature and salinity on growth rate and azaspiracid concentration in two strains of *Azadinium poporum* (Dinophyceae) from Puget Sound, Washington State. *Harmful Algae*. 2019; 89:101665. <https://doi.org/10.1016/j.hal.2019.101665> PMID: 31672233
76. Husson B, Hernández-Fariñas T, Le Gendre R, Schapira M, Chapelle A. Two decades of *Pseudonitzschia* spp. blooms and king scallop (*Pecten maximus*) contamination by domoic acid along the French Atlantic and English Channel coasts: seasonal dynamics, spatial heterogeneity and interannual variability. *Harmful Algae*. 2016; 51(26–39).
77. Huang H-L, Shao Q-W, Zhu X-J, Luo J, Meng R, Zhou C-X, et al. Distribution of *Karlodinium veneficum* in the coastal region of Xiangshan Bay in the East China Sea, as detected by a real-time quantitative PCR assay of ribosomal ITS sequence. *Harmful Algae*. 2019; 81(65–76).

Publication V: qPCR assay for Amphidomataceae

qPCR assay for Amphidomataceae: State of the art and new challenges.

ICHA 2018 Proceedings

Tillmann, U., Wietkamp, S., Gu, H., Clarke, D., Smith, K. (in press)

Publication V represents a short-paper for the *ICHA 2018 proceedings* issue and is based on the respective special session hold during the *ICHA* (International Conference on Harmful Algae) in Nantes, France 2018. It briefly summarizes the status of the available qPCR assays for the molecular detection and enumeration of toxigenic Amphidomataceae in the field at that time, as well as accompanying challenges, which are picked up and intensively discussed within the presented thesis.

This short-paper highlights the qPCR as an advantageous tool for national monitoring programs targeting toxigenic Amphidomataceae as it is year-round performed by the Marine Institute in Galway, Ireland. A frequently increasing number of newly identified species, strains and ribotypes within this dinophyte family however requires continuous assay updating.

The candidate contributed to this publication let by Dr. U. Tillmann (AWI) by the preparation of the summarizing table on available Amphidomataceae qPCR assays (100%), by manuscript preparation (40%) and performed the final style formatting (50%) together with the corresponding author.

qPCR assay for Amphidomataceae: State of the art and new challenges

Urban Tillmann^{1*}, Stephan Wietkamp¹, Haifeng Gu², Dave Clarke³, Kirsty Smith⁴

¹ Alfred Wegener Institute, Am Handelshafen 12, 27570 Bremerhaven, Germany;

² Third Institute of Oceanography, State Oceanic Administration, Xiamen 361005, China;

³ Marine Institute, Rinville, Oranmore, Galway H91R673, Ireland;

⁴ Cawthron Institute, Privat Bag 2, Nelson 7042, New Zealand.

* corresponding author's email: urban.tillmann@awi.de

Current status: Accepted to be published in 2020 in the ICHA 2018 Proceedings

(ISBN - n°. 978-87-990827-7-3), Copenhagen DK (IOC & ISSHA)

Abstract

Azaspiracids (AZA) are a group of lipophilic toxins, which are produced by a few species of the marine nanoplanktonic dinoflagellate genera *Azadinium* and *Amphidoma* (Amphidomataceae). Amphidomataceae were found to be globally distributed in coastal waters and new areas of occurrence are regularly discovered. The AZA toxins accumulate mainly in shellfish and - when consumed by humans - may cause health problems. Given this serious threat, appropriate detection methods enabling a fast identification and quantification for these toxigenic species are needed. AZA-producing species are small and inconspicuous and difficult - if not impossible - to be identified by traditional microscopy. Therefore, a number of molecular detection and quantification assays have been developed and are in use. We here evaluate the current state of the art of amphidomatacean qPCR assays and identify new challenges, which are important to be continuously assessed for reliable qualitative and quantitative detection.

Keywords: *Azadinium*, *Amphidoma*, molecular detection, qPCR assays, ribotypes.

Introduction

Amphidomataceae are a family of dinoflagellates which are known for the production of azaspiracids (AZA), a group of lipophilic polyketide toxins that can accumulate in shellfish and may cause human health problems (Twiner et al., 2014). Azaspiracids are a major problem in Ireland, where AZA concentrations in shellfish above the EU regulatory limit ($0.16 \mu\text{g g}^{-1}$ mussel flesh) are recurrently registered (Salas et al., 2011). The resulting long-lasting closures of shellfish farms lead to high economic losses and are a major threat for the Irish shellfish industry. In 2009, the first source organism of AZA, the small thecate dinoflagellate *Azadinium spinosum* was identified and described as a new species in a new genus within the family of Amphidomataceae (Tillmann et al., 2009). Since then, knowledge on the diversity of Amphidomataceae has increased rapidly, and currently there are 26 described species. Among the 13 Amphidomataceae species tested so far, only four have been found to produce AZA, i.e., *Az. spinosum*, *Az. poporum*, *Az. dexteroporum*, and *Amphidoma languida* (Krock et al., 2019), and based on phylogenetic data the toxigenic species do not represent a distinct clade (Tillmann et al., 2018a). All species of Amphidomataceae show distinct morphological features, but morphological species identification in most cases requires scanning electron microscopy. This, together with a high number of very similar and small non-toxigenic species in the group, makes routine detection and quantification of the toxigenic Amphidomatacean species in field samples challenging and almost impossible using light microscopy. Thus, other alternative and innovative methods are needed for a more routine and fast identification and enumeration of Amphidomataceae in field samples.

State of the art and new challenges

Card-fish probes using *in situ* hybridization are available for a few *Azadinium* species (Toebe et al., 2013), but have never been applied in the field, probably because of the complex sample treatment protocol. In contrast, molecular qPCR assays for detection and quantification are now commonly used for a large number of toxic microalgae (Engesmo et al., 2018; Ruvindy et al., 2018) and a number of assays are also available for Amphidomataceae (**Table 1**). In 2016, Smith et al. designed one SYBR Green real-time PCR assay targeting the common intergenic transcribed spacer (ITS) regions of all species of *Azadinium* and *Amphidoma*. Furthermore, species-specific TaqMan qPCR assays are available for four species: The non-toxigenic *Az. obesum* and the

toxigenic species *Az. spinosum*, *Az. poporum* and *Am. languida* (Toebe et al., 2013; Wietkamp et al., 2019b).

These assays are now regularly used by the Marine Institute in Galway/Ireland, where the *Az. spinosum* assay is now an integrated part of the Irish monitoring program, which has recently undergone in-house validation and is now accredited to ISO 17025 standards. The assays have also been tested for the Scottish monitoring program (Paterson, 2018) and used in various field sample surveys, including the Puget Sound area (Kim et al., 2017), the Norwegian coast (Tillmann et al., 2018a), Irish coastal waters (Wietkamp et al., 2019b) or in Argentinean coastal waters (Tillmann et al., 2019). One general and major challenge of all qPCR assays is a reliable quantification (Bonk et al., 2018). Quantification in qPCR is based on standard curves prepared using the DNA of target species cells and can either be dilution series of target DNA or of the amplified PCR product of the specific target gene.

Table 1. Available real-time PCR assays for Amphidomataceae detection and quantification.

Target species	Target gene	Oligonucleotide type	Sequence (5'-3')	Product size (bp)	Reference
Amphidomataceae	ITS				Smith et al.
Amp240F		F-Primer	CAACTTTCAGCGACGGATGTCTCG	179	(2016)
Amp418R		R-Primer	AAGCYRCWGGCATKAGAAGGTAGWGGC		
<i>Am. languida</i>	LSU				Wietkamp et al.
Alan509F		F-Primer	CGGTTACAGGCGAGGAT	60	(2019)
Alan569R		R-Primer	GACATTCACACCTCCGTGGAA		
Alan528		TaqMan MGB probe	6FAM-CTTCTGAGGACATGGTAAC-MGB		
<i>Az. spinosum</i>	LSU				Toebe et al.
Asp48F		F-Primer	TCGTCTTTGTGTCAGGGAGATG	72	(2013)
Asp120R		R-Primer	GGAAACTCCTGAAGGGCTTGT		
Aspin77T		TaqMan MGB probe	6FAM-CGCCCCAAAAGGACTCCT-MGB		
<i>Az. poporum</i>	LSU				Toebe et al.
Apop62F		F-Primer	GATGCTCAAGGTGCCTAGAAAGTC	68	(2013)
Apop148R		R-Primer	CCTGCGTGTCTGGTTGCA		
Apop112		TaqMan MGB probe	6FAM-TTCCAGACGACTCAAA-MGB		
<i>Az. obesum</i>	LSU				Toebe et al.
Aob134F		F-Primer	AGGGATCGATACACAAATGAGTACTG	74	(2013)
Aob208R		R-Primer	AAACTCCAGGGACATGGTAGTCTTA		
Aob163		TaqMan MGB probe	6FAM-AAGACATTGACCTACCGT-MGB		

Therefore, any variability in these numbers (i.e. DNA copy number) between species and strains will bias the quantification of field populations (Galluzzi et al., 2010; Eckford-Soper and Daugbjerg, 2015; Nishimura et al., 2016). Intra- and inter-specific differences in the number of target molecules for the qPCR in the genome of microorganisms have been observed for a number of dinoflagellate species (Perini et al., 2011; Macé et al., 2018) and thus needs to be carefully assessed for Amphidomataceae as well. Variability of copy number for Amphidomataceae is not well known yet and definitely has to be determined using multiple strains and different physiological stages of toxigenic species in the near future, as has been recently performed for *Amphidoma languida* (Wietkamp et al., 2019b).

Another general problem and challenge of using the qPCR for detection and enumeration of target cells is the assay specificity, which needs to be extensively tested using non-target species and strains to reduce false positive signals. However, there is also the risk of false negative results. This is especially important in the Amphidomataceae, where new species and new strains are almost continuously discovered and established.

When the original assays were designed, the known species and available strains were quite limited compared to what we have just a few years later. For one of the toxigenic species, *Az. poporum*, the qPCR assay was designed based on the only three Danish strains available at that time. With now more than 70 described strains we know that *Az. poporum* has a very wide distribution, and a high intraspecific variability in sequence data with three major ribotypes and some significant further sub-groups is evident. The parent strains for the assay from Denmark belong to ribotype A1 and there are significant differences to the other ribotypes. Variation also occurs in the large subunit (LSU) region of the rDNA, the target of the qPCR respective assay, where all other ribotypes have 1 – 3 base pair mismatches with the forward primer of the current specific *Az. poporum* assay (**Fig. 1 A**). Therefore, new primers and probes need to be tested in order to quantitatively catch all ribotypes of *Az. poporum* that we now are aware of.

The same problem becomes evident for another important toxigenic species, *Az. spinosum*. The qPCR assay was designed based on two strains from the North Sea, but in the meantime many new strains revealed intraspecific variability as well, and currently three ribotypes of *Az. spinosum* are defined. Not only the DNA sequences, but also AZA toxin profiles differ among ribotypes. Strains from ribotype A produce AZA-1, -2 and -33, strains from ribotype B produce either AZA-11 and

AZA-51 or just AZA-2, and strains of ribotype C lack any detectable AZA (Tillmann et al., 2019). As it is the case for *Az. poporum*, there are base pair mismatches with primers and probe of the qPCR assay for *Az. spinosum* ribotypes as well. Strains of the AZA producing ribotype B have two mismatches with the reverse primer and one with the probe, and the non AZA-producing ribotype C has six mismatches with the reverse primer (Fig. 1 B).

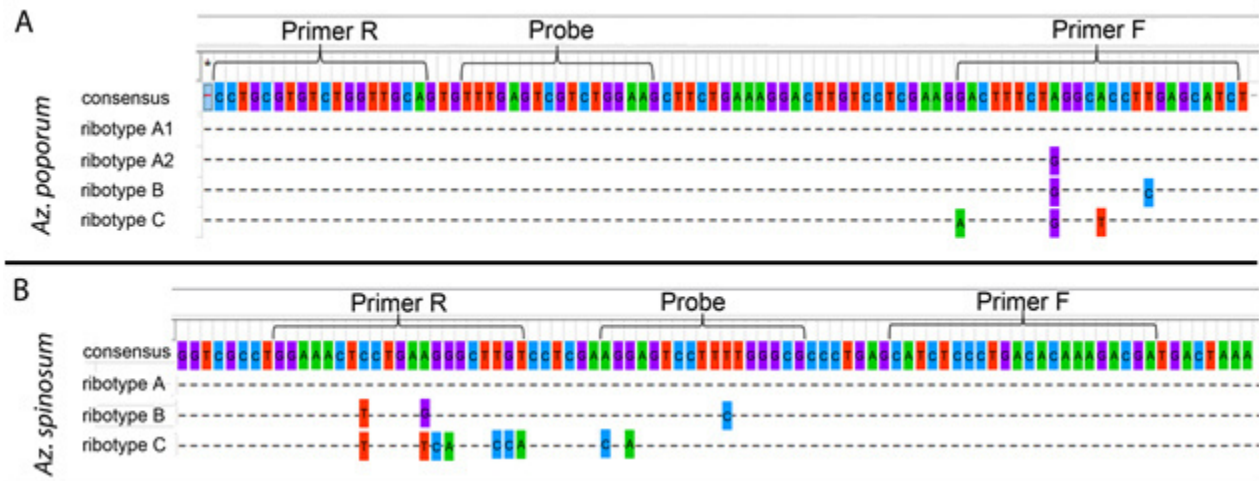


Fig. 1: Base pair mismatches between ribotypes of (A) *Az. poporum* and (B) *Az. spinosum* with the primers and probe of the respective TaqMan qPCR assays.

Preliminary laboratory tests (Smith and Tillmann, unpublished) confirmed the concern that new strains of *Az. spinosum* are not detected efficiently, and this has a serious impact for monitoring programs, which rely on the currently used *Az. spinosum* qPCR assay. Therefore, there is a need to re-design the *Az. spinosum* assay in order to fully capture and quantify more strains of this important toxigenic species. In this particular case, it may also be advised to specifically design new primers and probes, which enable the user to target ribotypes A and B (AZA producing strains), but not ribotype C (non-AZA producing strains).

Conclusion

In conclusion, the Amphidomataceae family, which includes only a few toxigenic species, is an obvious case, where molecular tools are needed for routine detection and quantification. A number of qPCR assays for this group has been published and is in use, but it is important to continuously assess those assays for reliable quantitative detection, especially in light of a still increasing number of newly identified species, strains and ribotypes in this group.

Acknowledgements

This work was supported by funding of the German Ministry for Education and Research (project RIPAZA, 03F0763A) and by the PACES research program of the Alfred-Wegener-Institute as part of the Helmholtz Foundation initiative in Earth and Environment.

Publication VI: Description of three new *Azadinium* species

Morphological and molecular characterization of three new *Azadinium* species revealed a high diversity of non-toxigenic species of Amphidomataceae (Dinophyceae) in Irish waters, North East Atlantic *Phycological Research*

Salas, R., Tillmann, U., Gu, H., Wietkamp, S., Krock, B., Clarke, D. (submitted)

Publication VI contains the description of three new *Azadinium* species (i.e. *Azadinium perfusorium* sp. nov., *Azadinium galwayense* sp. nov. and *Az. pseudozhuanum* sp. nov.), isolated during the field campaign HE-516 in Irish, Scottish and North Sea waters in 2018, as well as the first isolation of another known non-toxic species from Irish waters - *Az. caudatum* var. *margalefii*. The aim of this study was to characterize the three new species based on morphological, chemical (AZA) and molecular analyses. Previous studies on the biodiversity of amphidomataceans led frequently to descriptions of new species fostering the notion that Amphidomataceae are a highly diverse taxonomic group. Three new *Azadinium* species isolated in 2018 increased the number of known *Azadinium* species to 17, underlining that current knowledge probably still underestimates amphidomatacean biodiversity.

The candidate supported this study by performing DNA sequencing and toxin analysis of most isolates (>80%) of the established strains. Furthermore, he performed specificity testing of the current qPCR assays on *Az. spinosum*, *Az. poporum* and *Am. languida* with DNA of the three new species and the new isolate of *Az. caudatum* var. *margalefii* (100%) and compared the findings with D. Clarke (MI). The candidate contributed to the manuscript preparation (20%) led by R. Salas (MI) with focus on the sequencing, AZA and qPCR part.

Article (*Phycological Research* submission format)

Morphological and molecular characterization of three new *Azadinium* species revealed a high diversity of non-toxicogenic species of Amphidomataceae (Dinophyceae) in Irish waters, North East Atlantic

Rafael Salas^{1*}, Urban Tillmann^{2*}, Haifeng Gu³, Stephan Wietkamp², Bernd Krock², Dave Clarke¹

Affiliations:

¹ Marine Institute, Rinville, Oranmore, H91 R673, Co. Galway, Republic of Ireland

² Alfred Wegener Institut-Helmholtz Zentrum für Polar- und Meeresforschung Am Handelshafen 12, D-27570 Bremerhaven, Germany

³ Third Institute of Oceanography, Ministry of Natural Resources, Xiamen 361005, People's Republic of China

*Corresponding authors:

Urban Tillmann: phone +4947148311470; e-mail: urban.tillmann@awi.de

Rafael Salas: phone +3539187241; email: rafael.salas@marine.ie

Running title: Three new *Azadinium* species

SUMMARY

Shellfish contamination with azaspiracids (AZA), which are lipophilic marine biotoxins produced by marine dinoflagellates, is a major and recurrent problem for the Irish shellfish industry. AZA are produced by certain species of Amphidomataceae, but the species diversity of this group of microalgae in Irish waters is poorly known. Here we present a morphological and molecular characterization of multiple new strains of non-toxicogenic *Azadinium* isolated on an oceanographic survey in 2018. One strain of *Azadinium caudatum* var. *margalefii* (first strain for the area) confirmed non-toxicogenicity of Atlantic populations of this species. Moreover, three new non-toxicogenic *Azadinium* species are described from the North East Atlantic: *Azadinium galwayense* sp. nov., *Azadinium perfusorium* sp. nov. and *Azadinium pseudozhuanum* sp. nov.. *Azadinium galwayense* differed from other *Azadinium* by a characteristic combination regarding presence and location of the ventral pore (on the right side of the pore plate), of a pyrenoid (located in the episome), and by a pentagonal shape of the median epithelial intercalary plate 2a, and lack of contact between plates 1" and 1a. *Azadinium perfusorium* shared the same vp position as *Az. galwayense* and differed by a characteristic combination of a pyrenoid located in the hyposome, a tetragonal shape of plate 2a, and a relatively large size of the two lateral epithelial intercalary plates. *Azadinium pseudozhuanum* was unique by the combination of its vp position (on the right side of the pore plate) and presence of three apical and two intercalary plates. Molecular phylogeny confirmed the distinctiveness of these three new species and their placement in *Azadinium*. DNA of these new species was shown not to cause false-positive signals in specific qPCR assays in use to detect and quantify toxicogenic amphidomatacean species. The present finding significantly increased knowledge on the diversity of *Azadinium* species in the North East Atlantic.

Keywords: new species; Azaspiracids; Phylogeny; Biogeography

INTRODUCTION

The Amphidomataceae are an increasingly growing family of dinophyceans since the initial discovery of *Azadinium spinosum* Elbrächter et Tillmann (Tillmann et al., 2009) as the putative causative organism of azaspiracid (AZA) toxins (Krock et al., 2009). These small nano-planktonic dinoflagellates are difficult to identify under light microscopy (LM) and likely to have been misidentified in the past for other small gymnodinoid species or small armoured species e.g. of *Heterocapsa* (Tillmann et al., 2011; Salas et al., 2014). Thus far, the genus *Azadinium* comprises 13 species (Tillmann et al., 2020), and most have been described in the last decade alone (Tillmann et al. 2009; 2010; 2011; 2012b; 2014a; 2020; Tillmann and Akselman 2016; Tillmann 2018; Luo et al. 2013; 2017b; Percopo et al. 2013).

Amphidomatacean toxins were first detected in contaminated shellfish (blue mussels - *Mytilus edulis*) in 1995, from a batch of mussels harvested in Killary harbour in the West coast of Ireland (McMahon and Silke 1996) following an outbreak of human illness in the Netherlands after consumption of contaminated mussels from this area. The toxin was provisionally named KT (Killary Toxin) after the origin location of the mussels, but after its isolation and chemical characterization from shellfish (Satake et al. 1998; Ofuji et al. 1999) the name was changed to “Azaspiracids” (AZA) which better describes this lipophilic polyether molecule composed of a secondary amine (denoted by the prefix “aza-“ in IUPAC nomenclature), a three spiro assemblies and a carboxylic acid. The development of routine chemical analysis for the main AZA detected in shellfish (AZA-1, -2, -3) as a monitoring tool in the 2000s have shown that concentrations above the EU regulatory level of 160 micrograms of azaspiracid equivalents per kilogram (Anonymous, 2004) are often found in Irish shellfish, mainly in mussels, and occasionally in oysters (*Crassostrea gigas*), cockles (*Cerastoderma edule*) and clams (*Spisula solida*) which is a serious problem for the Irish aquaculture industry (Salas et al., 2011; Clarke, 2020).

The taxonomic diversity and wide geographical range of Amphidomataceae is also matched by a large chemical diversity (Tillmann *et al.* 2016), and the list of AZA produced by these species has increased continuously and now comprise 26 AZA variants (Krock et al. 2019). AZA toxins obviously have a worldwide distribution (Braña Magdalena et al. 2003; Taleb et al. 2006; Torgersen et al. 2008; Vale et al. 2008; Amzil et al. 2008; Ueoka et al. 2009; Yao et al. 2010; Álvarez et al. 2010; López Rivera et al. 2010; Krock et al. 2013; Trainer et al. 2013; Turner & Goya 2015), but Ireland to this day remains the most affected country globally by these toxins. However, little is known on the species diversity of Amphidomataceae in Irish waters. The

relatively large and easy to determine taxon recorded as *Amphidoma caudata*, which in fact is a species of *Azadinium* (Nézan et al. 2012), is known to occur in Irish coastal waters for a long time (Dodge 1981; O’Boyle and Raine 2007). A local strain of *Azadinium spinosum* was isolated from Bantry Bay, southern Ireland (Salas et al. 2011), and based on the prevailing toxin profile in shellfish with dominance of AZA congeners typical for *Az. spinosum* (i.e. AZA-1 and -2) (James et al. 2002). Based on the continuous record of *Az. spinosum* presence in the Irish monitoring program using specific PCR assays (Tillmann et al. 2014c, Clarke et al. in press.) this species is assumed to be the dominant source of AZA in Ireland (Salas et al. 2011; Wietkamp et al. 2020). However, at times there does appear to be mismatch between AZA in shellfish and LM monitoring reports of “*Azadinium* sp.” in Ireland (Tillmann et al. 2014c), therefore the presence of additional AZA source organisms in Irish waters cannot be ruled out. Another toxigenic species present in Ireland is *Amphidoma languida* Tillmann, Salas & Elbrächter, which was originally described based on a strain obtained from Bantry Bay, Southern Ireland (Tillmann et al. 2012a) and which is widely distributed around Ireland (Wietkamp et al. 2019b; 2020). Current morphology-confirmed diversity estimates of Irish Amphidomataceae include three species only (*Az. spinosum*, *Az. caudatum* (both varieties) and *Am. languida*), which is low compared to a recent Amphidomatacean diversity estimate from Norwegian coastal waters where the presence of seven species was documented (Tillmann et al., 2018a).

Detailed knowledge on the local species inventory is important to identify other yet unknown sources of AZA and/or to evaluate the potential of local non-toxigenic species/strains for false positive signals either in LM based and/or PCR methods used in Irish monitoring programs. Therefore, in summer 2018, a research survey in the North Sea, the Celtic Sea and Irish coastal waters was undertaken. The specific focus of this survey was to increase knowledge about the diversity and distribution of Amphidomataceae and their respective toxins in Irish coastal waters and in the North Sea. Field data of this survey including qPCR-based abundance and distribution of toxigenic Amphidomatacean species and their toxins are presented elsewhere (Wietkamp et al. 2020). In addition to these field samples, diversity of Amphidomatacean in the area was studied by on-board cell isolation and establishment of a large number of clonal Amphidomatacean strains. In the present paper, the focus is a morphological, toxinological, and phylogenetic description of various non-toxigenic species/strains obtained during this survey, including the formal description of three new species of the genus *Azadinium*, supplemented by a brief presentation of the first Irish strain of *Az. caudatum* var. *margalefii* (Halldal) Nézan & Chomérat.

MATERIALS AND METHODS

Sample collection and isolation of strains

Plankton samples were collected during the Oceanographic survey AZAHAB (Fig. 1) (RV Heincke) between the 17th July and 15th August 2018 (for a full set of stations see Wietkamp et al. 2020).

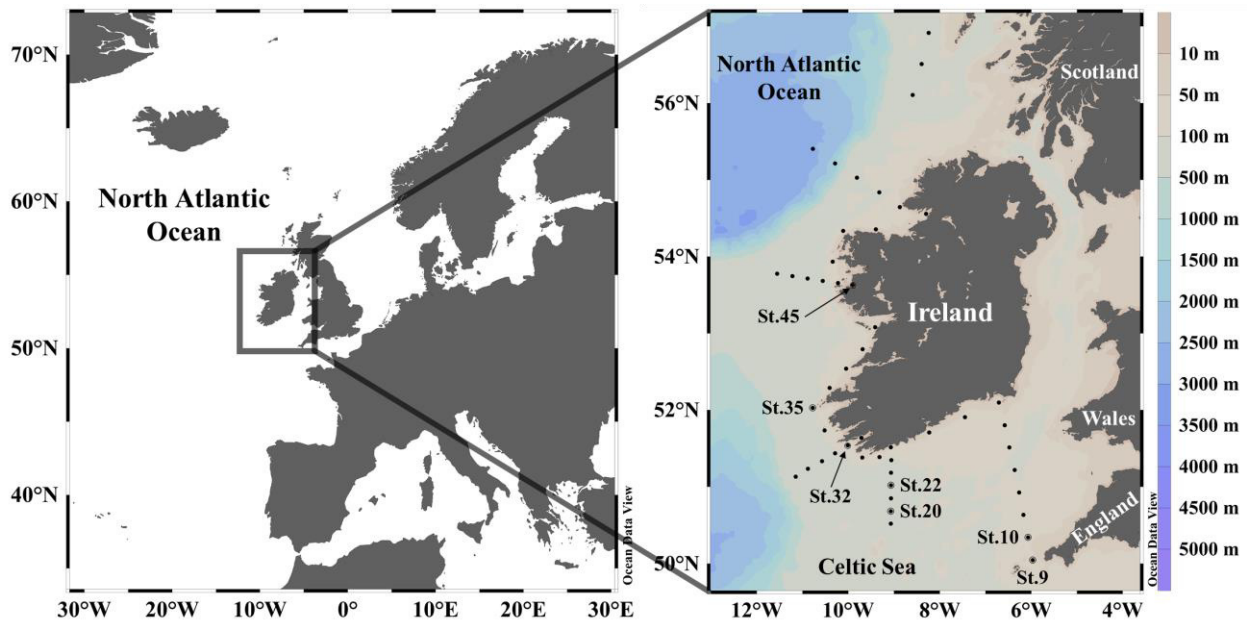


Fig. 1: Map of Ireland showing sample stations where *Azadinium* strains were isolated.

For live cell documentation and isolation Niskin bottle samples from three depth of the upper 30 m water column were mixed, pre-screened with 20 μm gauze and gently concentrated onto 3 μm pore size polycarbonate filter (TSTP, Millipore, Darmstadt, Germany) under gentle vacuum. *Azadinium/Amphidoma* cells were photographed using a video camera (Gryphax, Jenoptik, Jena, Germany) attached to an inverted microscope (Axiovert 200M, Zeiss, Oberkochen, Germany). Cell isolation was carried out using inverted microscopes (IX-51, Olympus, Southend-on-Sea, UK; or Axiovert 200M, Zeiss). Single cells were isolated by micropipetting and placed individually in single wells of 96 well plates (Corning, New York, NY, US) prefilled with 200 μm of filtered sea water from the sampling site. Preliminary strains were kept in a temperature-controlled incubator (Model MIR 252, Sanyo Electric Biomedical Co., Osaka, Japan) at 15 $^{\circ}\text{C}$ and 16:8 L:D light cycle at a photon flux density of about 50 $\mu\text{E m}^{-2} \text{s}^{-1}$. Primary isolation plates from the cruise were inspected in the laboratory using a stereomicroscope (SZHILLD, Olympus) for the presence of

Azadinium-like cells as inferred from the typical size, shape, and swimming behavior. From each positively identified well, a clonal strain was established by isolation of single cells with a microcapillary. Established cultures were thus clonal but not axenic, and were routinely held in 65 mL plastic culture flasks at 15 °C and a photon flux density of 50 $\mu\text{mol m}^{-2} \text{s}^{-1}$ on a 16:8 h light:dark photocycle. The medium was natural, sterile-filtered (0.2 μm VacuCap filters, Pall GmbH, Dreieich, Germany) Antarctic seawater (salinity: 34, pH adjusted to 8.0) and enriched with 1/10 strength K-medium (Keller et al. 1987), slightly modified by omitting the addition of ammonium ions.

Morphological characterization of strains

Light microscopy (LM) observations of live or preserved material of the different Amphidomataceae strains were carried out using differential interference contrast (DIC) or epifluorescence and high resolution (up to 1000x magnification) Axiovert 200M and Axioskop 2 (both Zeiss; both coupled with a digital camera (MRC5, Zeiss) and a video camera (Gryphax, Jenoptik, Jena, Germany)), or BX-53 (Olympus, Southend-on-Sea, UK) coupled with a digital camera DP72 (Olympus). Cell length and width of > 50 randomly chosen cells were measured at 1000x magnification in the Axioskop 2 and the Olympus BX-53 microscopes using Axiovision software (Zeiss) or Cell Sens software dimensions (Olympus) in newly fixed cells (formaldehyde, final concentration 1%). For scanning electron microscopy (SEM) cells were collected by centrifugation (5810 R, Eppendorf, Hamburg, Germany; 3,220 \times g, 10 min.) of 15 mL of culture. The supernatant was removed and the cell pellet resuspended in 60% ethanol in a 2 mL microtube for 1 h at 4 °C to strip off the outer cell membrane. Subsequently, cells were pelleted by centrifugation (5415R, Eppendorf, 16,000 \times g, 5 min) and cells were fixed with formaldehyde (2% final concentration in a 60:40 mixture of deionised water and seawater) and stored at 4 °C for 3 h. Finally, cells were collected on polycarbonate filters (25 mm \varnothing , 3 μm pore-size, Merck Millipore, Billerica, USA) in a filter funnel where all subsequent washing and dehydration steps were carried out. Eight washings (2 mL deionized water each) were followed by a dehydration series in ethanol (30%, 50%, 70%, 80%, 95%, 100%; 10 min each). Filters were finally dehydrated with hexamethyldisilazane (HMDS), initially 1:1 HMDS:EtOH followed by 2 \times 100% HMDS, and stored under gentle vacuum in a desiccator. Filters were mounted on stubs, sputter coated (Emscope SC500, Ashford, UK) and Quorum SC7620 (Quorum Tech, Sussex, UK) with gold-palladium targets and viewed under a scanning electron microscope (FEI Quanta FEG 200, Eindhoven, the

Netherlands or a Hitachi FlexSEM 1000 (Hitachi, Maidenhead, UK). SEM micrographs were presented on a black background using Adobe Photoshop 6.0 (Adobe Systems, San Jose, CA, USA) or GIMP2.10.14 (Spencer Kimball, Peter Mattis and GIMP dev. team).

AZA analysis of strains

For AZA analysis, strain cultures were grown at 15 °C, a photon flux density of 50 $\mu\text{mol m}^{-2} \text{s}^{-1}$ and a 16:8 h light/dark photoperiod. For each harvest, cell density was determined by settling Lugol's fixed samples and counting >400 cells under an inverted microscope in order to calculate toxin cell quota. Densely grown strains (ranging from ca. $1 - 7 \times 10^4$ cells mL^{-1}) were harvested by centrifugation (5810R, Eppendorf, Hamburg, Germany) at 3,220 x g for 10 min of 50 mL subsamples. The cell pellet was resuspended, transferred to a microtube, centrifuged again (Eppendorf 5415, 16,000 x g, 5 min), and stored frozen (-20 °C) until use. For a number of selected strains, growth and harvest procedures were repeated several times to yield a high biomass for an increased sensitivity of the toxin detection method. Total number of cells harvested for these strains is listed in Table S1 (Supporting Information).

Cell pellets were extracted with 500 μL acetone and were vortexed every 10 min during one hour at room temperature. Homogenates were centrifuged (Eppendorf 5810 R) at 15 °C and 3,220 x g for 15 min. Filtrates were then adjusted with acetone to a final volume of 0.5 mL. The extracts were transferred to a 0.45 μm pore-size spin-filter (Millipore Ultrafree, Millipore, Burlington, USA) and centrifuged (Eppendorf 5415 R) at 800 x g for 30 s, with the resulting filtrate transferred into a liquid chromatography (LC) autosampler vial for LC-MS/MS analysis.

Extracts of strains were screened for known AZA in the selected reaction monitoring (SRM) mode with an analytical system consisting of triple quadrupole mass spectrometer (API 4000 QTrap, Sciex, Darmstadt, Germany) equipped with a TurboSpray interface coupled to LC equipment (model LC 1100, Agilent, Waldbronn, Germany) that included a solvent reservoir, inline degasser (G1379A), binary pump (G1311A), refrigerated autosampler (G1329A/G1330B), and temperature-controlled column oven (G1316A). Separation of AZA (5- μL sample injection volume) was performed by reverse-phase chromatography on a C8 phase. The analytical column (50 \times 2 mm) was packed with 3 μm Hypersil BDS 120 Å (Phenomenex, Aschaffenburg, Germany) and maintained at 20 °C. The flow rate was 0.2 mL min^{-1} , and gradient elution was performed with two eluents, where eluent A was water and eluent B was acetonitrile/water (95:5 v/v), both containing 2.0 mM ammonium formate and 50 mM formic acid. Initial conditions were 8-min

column equilibration with 30% B, followed by a linear gradient to 100% B in 8 min and isocratic elution until 18 min with 100% B then returning to initial conditions until 21 min (total run time: 29 min). AZA profiles were determined in the SRM mode in one period (0–18) min with curtain gas: 10 psi, CAD: medium, ion spray voltage: 5,500 V, temperature: ambient, nebuliser gas: 10 psi, auxiliary gas: off, interface heater: on, declustering potential: 100 V, entrance potential: 10 V, exit potential: 30 V. SRM experiments were carried out in positive ion mode by selecting the transitions shown in Table S2 (Supporting Information).

In addition, precursor ion experiments were performed. Precursors of the characteristic AZA fragments m/z 348, m/z 350, m/z 360, m/z 362 and m/z 378 were scanned in the positive-ion mode from m/z 500 to 1,000 under the following conditions: curtain gas, 10 psi; CAD, medium; ion spray voltage, 5,500 V; temperature, ambient; nebuliser gas, 10 psi; auxiliary gas, off; interface heater, on; declustering potential, 100 V; entrance potential, 10 V; collision energy, 70 V; exit potential, 12 V.

Molecular Phylogeny

DNA extraction

For one part of DNA extraction, conducted at the Alfred-Wegener-Institute (Helmholtz Center for Polar- and Marine Research, Bremerhaven, Germany), a number of selected strains (Tab. 1) was grown in 70 mL plastic culture flasks at 15 °C under a photon flux density of 70 $\mu\text{mol m}^{-2} \text{s}^{-1}$ on a 16:8 h light:dark photoperiod.

Ten to 50 mL of healthy and growing culture (based on stereomicroscopic inspection of the live culture) were harvested by centrifugation (Eppendorf 5810R; 3,220 x g, 10 min). The supernatant was discarded and the remaining cell pellet was subsequently re-suspended and transferred to a 1.5 mL microtube together with 500 μL of the SL1 lysis buffer, both provided by the DNA extraction kit. The DNA extraction followed the manufacturer's instructions of the NucleoSpin Soil DNA extraction kit (Macherey & Nagel, Düren, Germany), with a slight variation. The bead tubes were shaken, rather than vortexed, for 45 s and another 30 s at a speed of 4.0 ms^{-1} in a cell disrupter (FastPrep FP120, Thermo-Savant, Illkirch, France).

For the second part of DNA extraction, conducted at Marine Institute (Galway, Ireland), 5 - 30 mL aliquots were collected in 50 mL centrifuge tubes from strains (Tab. 1) which were in exponential growth, and centrifuged (5804, Eppendorf) for 15 min at 3,230 x g. The majority of the supernatant was removed, leaving the cell pellet in approximately 1 mL of volume. The cell pellet was re-

suspended by vortexing and transferred to a 1.5 mL microtube which was centrifuged (Minispin, Eppendorf) for 5 min at 12,200 x g, and the supernatant discarded. DNA was extracted using the Qiagen Plant Mini DNeasy extraction kit (Qiagen, Manchester, England) in accordance with the manufacturer's protocols with minor modifications. Cellular disruption was achieved by adding glass beads (2 different diameter sizes of 0.75-1.0mm ϕ and 0.25-0.5mm ϕ) with 400 μ L of API lysis buffer (supplied with extraction kit) and placed in a bead mill mixer (MM400, Retsch, Haan Germany) for 2 min at a frequency of 25/s Hz. The microtubes were transferred to a thermomixer (Comfort, Eppendorf) for an incubation period of 15 min at 65 °C with shaking, and the supernatant transferred to a QIAcube (Qiagen) for automated DNA extraction.

For both parts, 2 x 50 μ L of the provided elution buffer was used (to a final elution volume of 100 μ L) to maximize the overall DNA yield. The DNA of all extracts was stored at -20 °C until further processing.

DNA Sequencing

Sanger-Sequencing of strain DNA was performed for the 18S/small subunit (SSU), the Internal Transcribed Spacer region (ITS1, 5.8S rRNA, ITS2) and the D1/D2 region of 28S/large subunit (LSU) using the following primer sets: 1F (5' - AAC CTG GTT GAT CCT GCC AGT - 3') and 1528R (5' - TGA TCC TTC TGC AGG TTC ACC TAC - 3') for SSU; ITSa (5' - CCA AGC TTC TAG ATC GTA ACA AGG (ACT)TC CGT AGG T - 3') and ITSb (5' - CCT GCA GTC GAC A(GT)A TGC TTA A(AG)T TCA GC(AG) GG - 3'), or ITS1 (5' - TCC GTA GGT GAA CCT GCG G - 3') and ITS4 (5' - TCC TCC GCT TAT TGA TAT GC - 3') for ITS; DirF (5' - ACC CGC TGA ATT TAA GCA TA-3') and D2CR (5' - CCT TGG TCC GTG TTT CAA GA - 3') for LSU. One part of the final sequences was gained by sending extracted DNA to Eurofins sequencing facilities (Eurofins Genomics, Ebersberg, Germany), where sequences were generated on an ABI 3730 XL sequencer (Applied Biosystems by Thermo Fisher Scientific, Waltham, Massachusetts, USA) according to internal sequencing procedures.

The second part of the sequences was generated at Marine Institute. For PCR, the GoTaq Hot Start Polymerase (Promega, Wisconsin, USA) kit was used, where the PCR reaction mixture contained 11.42 μ L water (molecular biology grade), 0.08 dNTPs (25 μ M), 0.2 μ L of 0.1 μ M Forward and Reverse primers, 4 μ L GoTaq buffer (5x), 0.1 μ L of Taq Polymerase, 2 μ L of MgCl₂ (2.5 mM) and 2 μ L of DNA template to a final reaction volume of 20 μ L. PCR products were generated using a PCRmax Cyclyer (AC 296, Thermofisher Scientific) with the following conditions for each of the

regions. For ITS; 95 °C at 2 min; 10 cycles of: 95 °C at 50 s, 58 °C at 40 s, 72 °C at 1 min; 30 cycles of 95 °C at 45 s, 50 °C at 45 s, 72 °C at 1 min and a final step of 72 °C at 5 min. For LSU cycling parameters; 95 °C at 2 min; 30 cycles of: 95 °C at 30s, 55 °C at 30s, 72 °C at 2 min and a final step of 72 °C at 10 min. For the SSU region, the cycling parameters were; 95 °C at 5 min; 30 cycles of: 95 °C at 2 min, 55 °C at 2 min, 72 °C at 3 min and a final step of 72 °C at 10 min. The generated PCR products were checked on a 2% agarose gel (in TBE buffer, 80 mV, 30 min) to check if amplification was successful and the DNA integrity. Aliquots of the generated PCR products were forwarded on for sequencing to SequiServe (Vatterstetten, Germany).

The third part of sequences was generated at the Alfred-Wegener-Institute. Each PCR reaction contained 16.3 µL ultra-pure H₂O, 2.0 µL HotMaster Taq buffer (5Prime, Hamburg, Germany), 0.2 µL dNTPs (10 µM), 0.2 µL of each primer (10 µM), 0.1 µL of Taq Polymerase (Quantabio, Beverly, Massachusetts, USA) and 1.0 µL of extracted DNA template (10 ng µL⁻¹) to a final reaction volume of 20 µL. PCR were conducted in a Nexus Gradient Mastercycler (Eppendorf) with conditions described in Tillmann et al. (2020). The PCR amplicons were checked on a 1% agarose gel (in TE buffer, 70 mV, 30 min) to verify the expected length. The PCR amplicon was purified using the NucleoSpin Gel and PCR clean-up kit (Macherey-Nagel) and sequenced directly in both directions on an ABI PRISM 3730XL (Applied Biosystems by Thermofisher Scientific) as described in Tillmann et al. (2017c). Raw sequence data were processed using the CLC Genomics Workbench 12 (Qiagen, Hilden, Germany).

Phylogenetic analysis

Newly obtained SSU, ITS-5.8S and/or partial LSU rRNA gene sequences were incorporated into available *Amphidoma*, *Azadinium* and a few outgroup sequences in GenBank (<https://www.ncbi.nlm.nih.gov/genbank/>). GenBank accession numbers are listed in Table S3 (Supporting Information). Concatenated sequences were aligned using MAFFT v7.110 (Kato and Standley 2013) online program (<http://mafft.cbrc.jp/alignment/server/>). Alignments were manually checked with BioEdit v. 7.0.5 (Hall 1999). Completed alignments of ITS-5.8S rRNA gene sequences were imported into PAUP *4b10 software (Swofford 2002) to estimate divergence rates using simple uncorrected pairwise (p) distance matrices. The secondary structures of ITS2 sequences of *Az. zhuanum* strain TIO205 and *Az. pseudozhuanum* strain 32-R1 were predicted using the Mfold program (Zuker 2003). (<http://mfold.rit.albany.edu/?q=mfold/RNA-Folding-Form>).

For Bayesian inference (BI), the program jModelTest (Posada 2008) was used to select the most appropriate model of molecular evolution with Akaike Information Criterion (AIC). Bayesian reconstruction of the data matrix was performed using MrBayes 3.2 (Ronquist and Huelsenbeck 2003) with the best-fitting substitution model (GTR+G). Four Markov chain Monte Carlo (MCMC) chains ran for 10,000,000 generations, sampling every 1000 generations. The convergence of the MCMC chains was examined in TRACER 1.7 (Rambaut et al. 2018), and the first 10% of the samples were discarded as ‘burn-in’, well after stationarity had been reached. A majority rule consensus tree was created in order to examine the posterior probabilities of each clade. Maximum likelihood (ML) analyses were conducted with RaxML v7.2.6 (Stamatakis 2006) on the T-REX web server (Boc et al. 2012). Data were analyzed using the GTR+CAT approximation and the rapid hill-climbing algorithm was used. Node support was assessed with 1000 bootstrap replicates.

qPCR assay specificity

DNA of strains 2-D1, 5-B8, 6-B4 (*Az. perfusorium*), strain 9-E13 (*Az. caudatum* var. *margalefii*), strain 32-R1 (*Az. pseudozhuanum*) and strains 35-R4, 35-R6 and 35-R7 (*Az. galwayense*) was applied to the current species-specific qPCR assays for *Az. spinosum*, *Az. poporum* (Toebe et al. 2013) and *Am. languida* (Wietkamp et al. 2019b), as well as to the general Amphidomataceae assay (Smith et al. 2016) to check whether the assays might reveal false-positive/false negative signals for the new species/strains. The DNA was normalized to a concentration of 1 ng μL^{-1} and tested in three technical replicates each for amplification in the four qPCR assays according to the procedures described in Wietkamp *et al.* (2020). Positive controls contained 1 ng μL^{-1} of DNA of each target species (*Az. spinosum*: strain 3D9; *Az. poporum*: strain UTHD4; *Am. languida*: strain Z-LF-9-C9). The limit of quantification (LOQ) and the limit of detection (LOD) for these qPCR analyses were defined as described in Wietkamp et al. (2020). For the standard curves of all three species-specific qPCR assays, the resolution of dilutions applied did not allow differentiation between LOD and LOQ, which were both 0.1 pg μL^{-1} .

RESULTS

Onboard high resolution LM of live samples revealed a high diversity of Amphidomataceae in Irish waters (Fig. 2). While LM observation do not allow certain species level identification for many of the species in Fig. 2, isolation and SEM characterization of clonal strains was used to better

describe the species diversity. On-board single cell isolation yielded ~ 100 new clonal amphidomatacean strains.

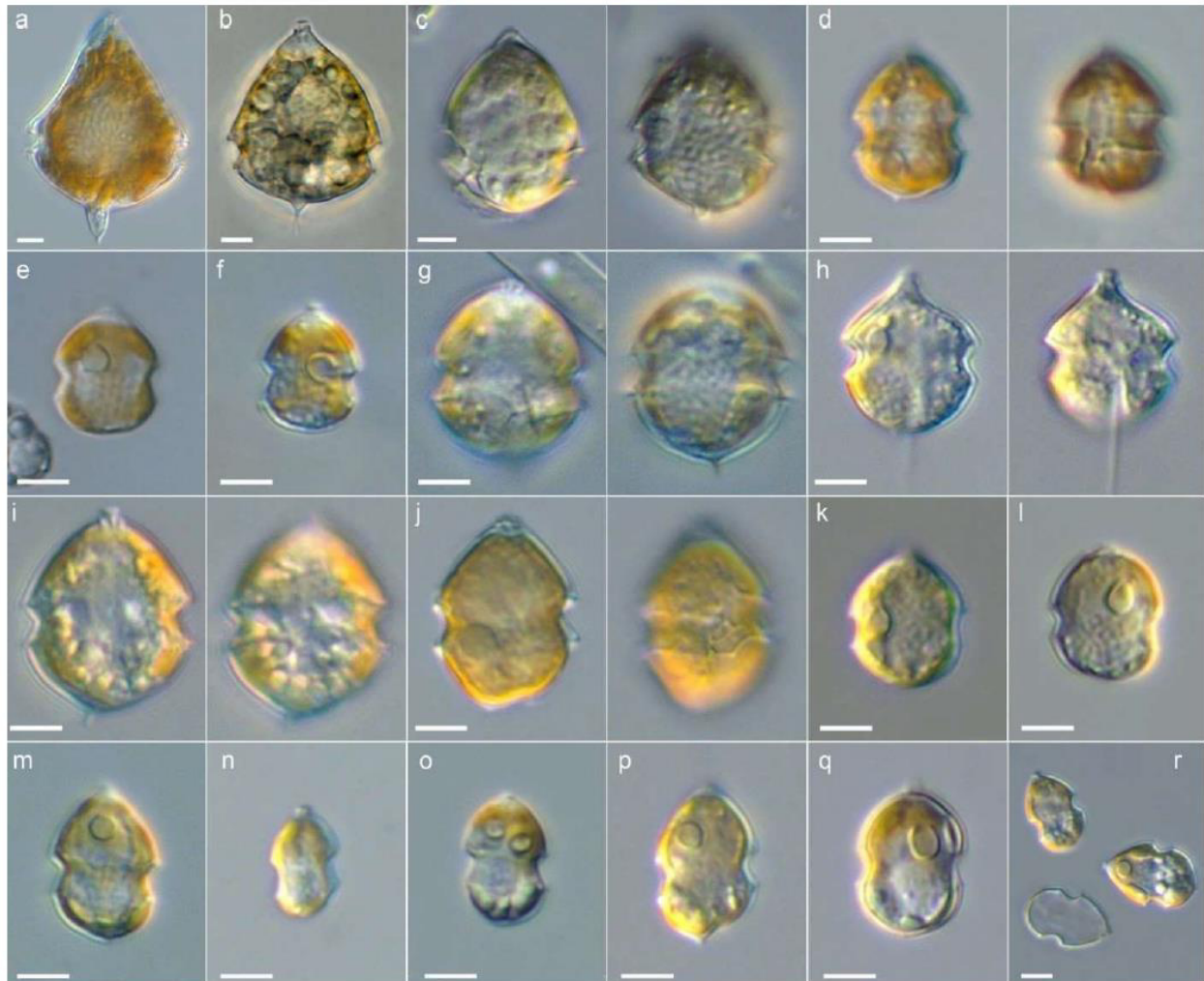


Figure 2: Diversity of Amphidomataceae in Irish waters as recorded during HE-516 by live onboard light microscopy. (a) *Az. caudatum* var. *caudatum*. (b) *Az. caudatum* var. *margalefii*. (c) Two different focal planes of an unidentified *Azadinium* sp. (d) Two focal planes of *Az.* cf. *perfusorium*. (e, f) Two different cells of *Amphidoma languida*. (g) Two focal planes of *Az.* cf. *pseudozhuanum*. (h) Two focal planes of a yet undescribed *Azadinium* sp. (*Az.* spec. 1). (i) Two different focal planes of an unidentified amphidomatacean species. (j) Two different focal planes of an unidentified *Azadinium* sp. (k, l) Two different cells of an unidentified amphidomatacean species. (m–o) Unidentified cells of *Azadinium* sp. (p–r) Different cells of *Azadinium* cf. *spinosum*. Scale bars: 5 μ m.

Table 1: Compilation of information about *Azadinium* strains obtained in this study.

Species	Strain	Origin station	Length (μm) Mean \pm SD Min-max	Width (μm) Mean \pm SD Min-max	l/w ratio Mean \pm SD	N	Morphological analysis	Sequence data
<i>Az. perpusorium</i>	5-B8	35	14.2 \pm 0.7 12.9-15.7	10.7 \pm 0.7 9.3-12.0	1.33 \pm 0.05	53	LM SEM	SSU, LSU, ITS
<i>Az. perpusorium</i>	2-D1	35	14.9 \pm 1.0 13.2-18.0	11.3 \pm 0.9 9.0-13.1	1.32 \pm 0.06	52	LM SEM	SSU, LSU, ITS
<i>Az. perpusorium</i>	6-B4	45	14.4 \pm 1.0 12.2-16.8	10.5 \pm 0.9 8.9-12.7	1.37 \pm 0.06	75	LM SEM	SSU, LSU, ITS
<i>Az. perpusorium</i>	6-C8	22	14.5 \pm 1.0 11.8-16.5	10.9 \pm 1.0 8.9-13.2	1.33 \pm 0.06	60	LM SEM	- LSU, ITS
<i>Az. perpusorium</i>	9-R1	9	14.8 \pm 1.1 13.04-17.51	11.3 \pm 1.3 9.07-13.51	1.32 \pm 0.08	57	LM SEM	- LSU, ITS
<i>Az. perpusorium</i>	35-R3	35	-	-	-	-	LM	- LSU, ITS
<i>Az. perpusorium</i>	9-R2	9	13.7 \pm 1.1 11.49-15.85	10.3 \pm 1.1 8.26-12.44	1.33 \pm 0.07	52	LM SEM	- LSU -
<i>Az. perpusorium</i>	10-R1	10	13.9 \pm 0.9 12.28-16.33	10.3 \pm 0.8 8.76-11.94	1.36 \pm 0.07	51	LM SEM	- LSU -
<i>Az. perpusorium</i>	10-R2	10	13.4 \pm 1.0 11.53-15.76	10.0 \pm 0.9 8.58-12.85	1.35 \pm 0.07	55	LM SEM	- LSU -
<i>Az. perpusorium</i>	10-R3	10	13.5 \pm 0.8 12.16-15.51	10.0 \pm 0.9 9.06-12.09	1.31 \pm 0.07	50	LM SEM	- LSU -
<i>Az. perpusorium</i>	35-R2	35	-	-	-	-	LM	- LSU -
<i>Az. perpusorium</i>	6-A8	22	14.2 \pm 0.9 11.9-16.1	10.2 \pm 0.7 8.9-11.9	1.39 \pm 0.07	50	LM SEM	- - -
<i>Az. perpusorium</i>	6-B7	35	13.8 \pm 0.8 12.2-15.2	10.3 \pm 0.8 9.0-12.4	1.34 \pm 0.07	50	LM SEM	- - -
<i>Az. perpusorium</i>	6-D2	35	14.6 \pm 1.0 12.2-16.4	10.8 \pm 1.0 9.2-12.3	1.36 \pm 0.07	50	LM SEM	- - -
<i>Az. perpusorium</i>	4-F9	22	14.4 \pm 0.9 11.4-15.9	10.9 \pm 0.8 9.2-12.4	1.32 \pm 0.05	50	LM SEM	- - -
<i>Az. perpusorium</i>	4-H7	35	15.0 \pm 0.8 13.5-16.6	11.2 \pm 0.7 9.8-12.1	1.34 \pm 0.06	50	LM SEM	- - -
<i>Az. perpusorium</i>	3-F6	35	14.9 \pm 0.9 12.8-16.8	11.2 \pm 0.8 9.7-12.7	1.33 \pm 0.06	52	LM SEM	- - -
<i>Az. perpusorium</i>	2-C7	22	14.7 \pm 0.9 13.1-16.6	10.6 \pm 0.7 9.3-12.4	1.39 \pm 0.07	50	LM SEM	- - -
<i>Az. perpusorium</i>	6-G12	22	14.6 \pm 1.0 12.2-16.4	10.8 \pm 0.7 9.2-12.3	1.36 \pm 0.07	50	LM	- - -
<i>Az. perpusorium</i>	5-B4	35	14.8 \pm 1.0 12.5-17.1	11.2 \pm 1.0 9.2-13.3	1.33 \pm 0.06	52	LM	- - -
<i>Az. perpusorium</i>	2-A1	35	-	-	-	-	LM	- - -
<i>Az. perpusorium</i>	5-B10	22	-	-	-	-	LM	- - -
<i>Az. perpusorium</i>	6-C3	22	-	-	-	-	LM	- - -
<i>Az. perpusorium</i>	6-C11	35	-	-	-	-	LM	- - -
<i>Az. perpusorium</i>	6-D8	35	-	-	-	-	LM	- - -
<i>Az. perpusorium</i>	6-G3	22	-	-	-	-	LM	- - -
<i>Az. galwayense</i>	35-R4	35	13.7 \pm 1.1 11.9-15.8	9.8 \pm 0.8 8.3-12.5	1.40 \pm 0.08	51	LM, SEM	SSU, LSU, ITS
<i>Az. galwayense</i>	35-R6	35	14.3 \pm 1.3 11.4-16.7	10.8 \pm 1.1 8.6-14.1	1.33 \pm 0.06	50	LM, SEM	SSU, LSU, ITS
<i>Az. galwayense</i>	35-R7	35	14.1 \pm 1.3 11.5-18.4	10.6 \pm 1.3 8.5-15.1	1.34 \pm 0.10	47	LM, SEM	SSU, LSU, ITS
<i>Az. pseudozhuanum</i>	32-R1	32	17.2 \pm 1.2 14.9-20.1	14.2 \pm 1.3 12.3-17.5	1.21 \pm 0.07	49	LM, SEM	- LSU, ITS
<i>Az. caudatum</i>	9-E13	20	28.5 \pm 2.4 23.7-32.0	22.8 \pm 2.3 18.2-26.6	1.25 \pm 0.06	52	LM, SEM	SSU, LSU, ITS

New strains of toxigenic species (*Az. spinosum*, *Am. languida*) will be presented in detail elsewhere (Tillmann et al. in prep). Here, we report on the identity of 31 non-toxicogenic strains which were identified based on morphology as examined by LM and SEM (selected strains) and conformed for a number of strains by rRNA sequence comparison (Tab. 1). One strain of *Azadinium caudatum* var. *margalefii* was isolated from stat. 20 (Tab. 1, Fig. 1). Three strains, all originating from stat. 35, were identified as a new species described here as *Azadinium galwayense* spec. nov.. One strain isolated from stat. 32 (Tab. 1, Fig. 1) was described as *Azadinium pseudozhuanum* spec. nov.. The majority of strains (26) isolated from stat 9, 10, 20, 22, 34, 35 and 45 (Tab. 1, Fig. 1) were found to represent another new species, *Azadinium perfusorium* spec. nov.

Description of new species

Azadinium galwayense Salas et Tillmann sp. nov.

Figures 3–6, Figure S1 in the Supporting information.

Description: Small photosynthetic thecate Dinophyceae; cells 11.4 to 18.4 µm long and 8.3 to 15.1 µm wide; cingulum broad and postmedian; epitheca conical and ending in a small but distinctly pointed apical pore; hypotheca hemispherical with a very broad and long sulcus and with a single conspicuous antapical spine slightly angled to the right; tabulation formula: Po, cp, X, 4', 3a, 6'', 6C, 5S, 6''', 2''''; a ventral pore located outside the right side of the pore plate. The median epithecal intercalary plate 2a pentagonal and the first precingular plate (1'') without contact to the first epithecal intercalary plate (1a).

Holotype: SEM stub prepared from strain 35-7R (designated CEDiT2020H115) deposited at the Senckenberg Research Institute and Natural History Museum, Centre of Excellence for Dinophyte Taxonomy (Wilhelmshaven, Germany).

Isotype: Formalin-fixed sample prepared from clonal strain 35-R7 (designated CEDiT2020I116) deposited at the Senckenberg Research Institute and Natural History Museum, Centre of Excellence for Dinophyte Taxonomy (Wilhelmshaven, Germany).

Type locality: North East Atlantic, West of Ireland (52° 1.854' N; 10° 46.284' W)

Etymology: The epithet galwayense honors the county of Galway in the west of Ireland where the first azaspiracid toxins were discovered from blue mussels grown in Killary Harbour in 1995 and where the Irish Marine Institute main laboratory is located.

Detailed description

All three strains of *Az. galwayense* obtained in the present study (35-R4, 35-R6, 35-R7) were identical in terms of morphology and plate pattern. Strain 35-R7 was selected to prepare the type material and is described in detail. Cells were small, ovoid in shape and slightly compressed ventrally. Newly formalin preserved cells range in size from 11.5–18.4 μm in length (mean length: $14.1 \pm 1.3 \mu\text{m}$; $n=47$) and 8.5 – 15.1 μm in width (mean width: $10.6 \pm 1.3 \mu\text{m}$; $n=47$) and a median length:width ratio of 1.34 ± 0.10 (Tab. 1).

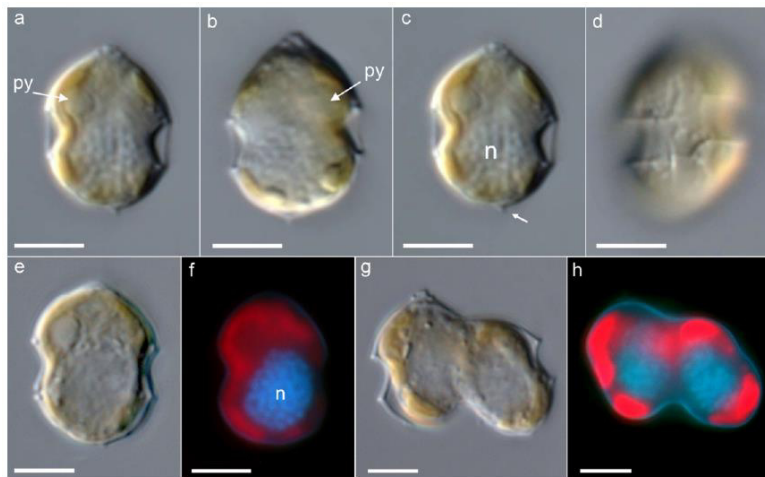


Figure 3: *Azadinium galwayense* sp. nov. (strain 35-R7). LM of formalin fixed cells. (a–d) General size and shape. (a, b) Arrow showing a pyrenoid (py) in the episome. (c) Nucleus (n) size and shape and antapical spine (arrow). (d) Note the wide cingulum. (e–h) Formalin fixed cells stained with DAPI in brightfield (e) and with UV light excitation (f) to indicate shape, size and location of the nucleus (n) and the chloroplast. (g, h) Late stage of cell division (desmoschisis) in brightfield (g) and with UV light excitation (h). Scale bars: 5 μm .

The cells had a dome shaped episome bearing a prominent apical pore complex (APC) (Fig. 3c, g). The hyposome was rounded ending on an antapical spine. The cingulum was broad and deeply excavated, located in a post-median position and with a slight descending displacement from left to right in ventral view (Fig. 3d) of about 1/3 of the cingulum. A single chloroplast was visible and occupied the periphery of the cell (Fig. 3f, h). There was a single pyrenoid surrounded by a starch sheath in the left side of the episome (Fig. 3a, b). The nucleus with condensed and clearly visible chromosomes was large and round to ellipsoid and was sub-centrally located occupying a large part of the hyposome and a small part of the episome (Fig. 3c, f, h). Cells divided with an oblique

fission line by desmoschisis, i.e. parent thecal plates were shared by the sister cells (Fig. 3g, h). No cyst formation was noticed in cultures.

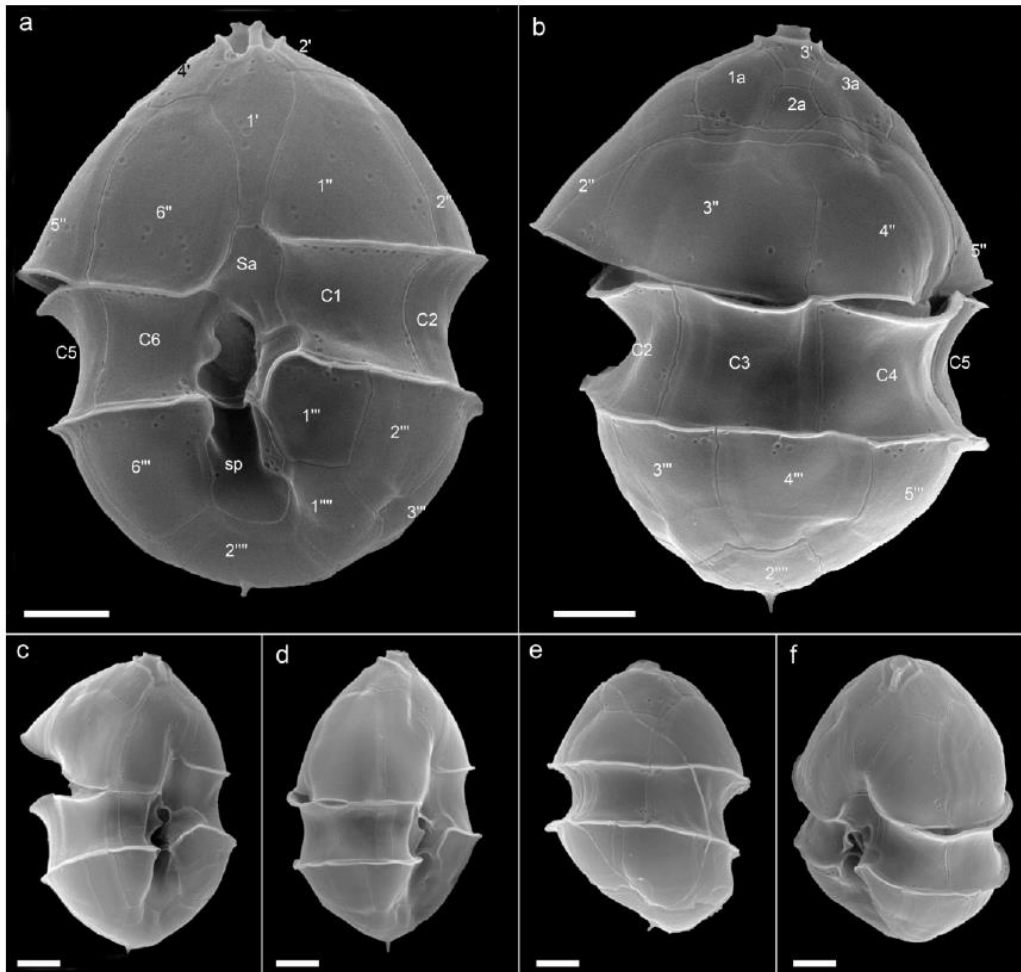


Figure 4: *Azadinium galwayense* sp. nov. (strain 35-R7). SEM micrographs of different thecae in (a) dorsal and (b) ventral view. (c–f). Lateral views. Scale bars: 2µm.

Azadinium galwayense had the plate pattern Po, cp, X, 4' 3a, 6'', 6C, 5S, 6''', 2'''' (Figs 4–6). The epitheca in apical view (Fig. 5a, b) showed a ventral pore (vp) in the right side of the APC, located between the 1' and 4' apical plate sutures and the pore plate (Po). The APC consisted of Po, a cover plate (cp) and X-plate (or canal plate). The Po were surrounded by a prominent and horse-shoe shaped rim (Fig. 5b). Four apical plates surrounded the APC. The 1' apical plate was widest at the point where the sutures between 4' and 6'' and 2' and 1'' plates met ventrally and narrowed as it extended towards the sulcal area (Fig. 4a). Plates 2' and 4' were rhomboid in shape, and plate 3' was small and hexagonal with very small sutures to the lateral apical plates 2' and 4'. The 1'' pre-

cingular plate was never in contact with the first intercalary plate (1a) ($n = 50$). The second intercalary plate (2a) was pentagonal and contacted both precingular plates 3'' and 4'' (Figs 4b). The cingulum was wide and excavated and consisted of six plates. Sutures of the cingular plates coincided with the sutures of the precingular plates (Fig. 4a, b). In lateral view (Fig. 5a, c), *Az. galwayense* was slightly dorso-ventrally flattened. The sulcal area consisted of five sulcal plates (Fig. 5d). The anterior sulcal plate (Sa) was large, rectangular, occupied a large part of the cingular area, and was in touch with the first and sixth cingular plates, and extended slightly into the epitheca. The posterior sulcal plate (Sp) extended about 2/3rds the distance from the cingulum to the antapex.

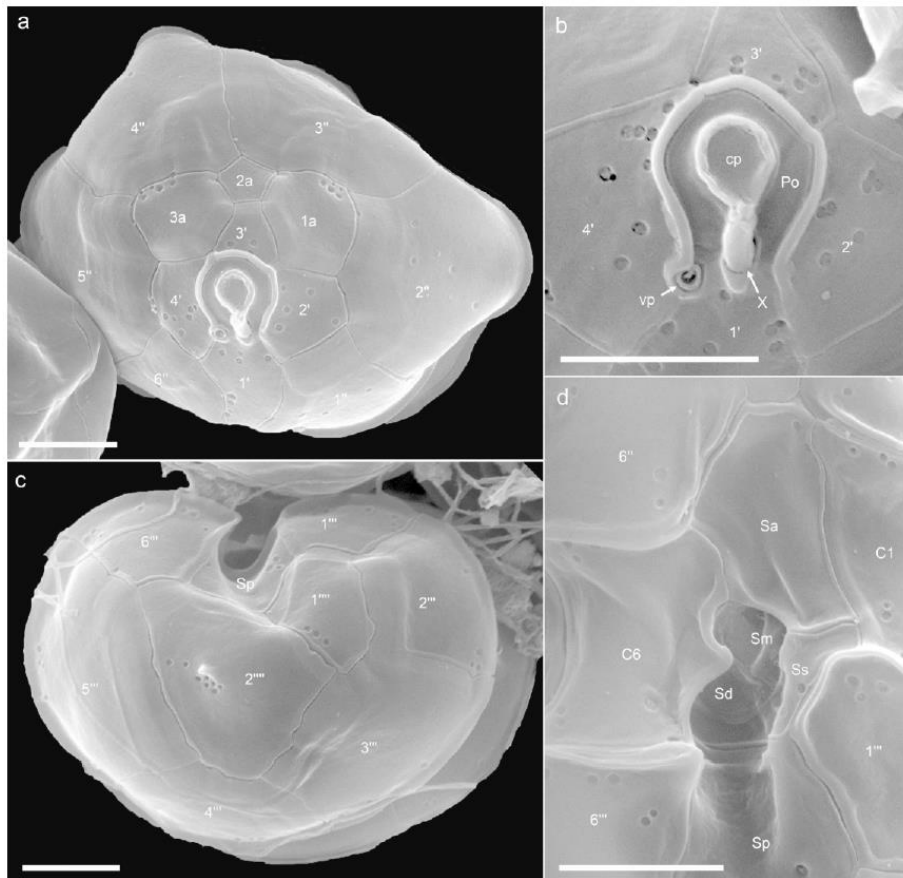


Figure 5: *Azadinium galwayense* sp. nov. (strain 35-R7). SEM micrographs of different thecae. (a) Epithecatal plates in apical view. (b) Detailed view of the apical pore complex (APC). (c) Hypothecal plates in antapical view. (d) Detailed view of the sulcal plates. cp, cover plate; Po, pore plate; Sa, anterior sulcal plate; Sp, posterior sulcal plate; Ss, left sulcal plate; Sm, median sulcal plate; Sd, right sulcal plate; X, X-plate. Scale bars: 2 μ m.

The left sulcal plate (Ss) was broad, anteriorly located to the Sp and running transversally from plate C1 to C6. The central sulcal area was made of two smaller sulcal plates Sm and Sd (Fig. 5d, Fig. S1 in the Supporting Information). The hyposome consisted of six post-cingular and two

antapical plates. Plates 3''' and 5''' were the widest and 1''' the narrowest. The 2''' plate was the largest of the two antapical plates and the one bearing a conspicuous spine.

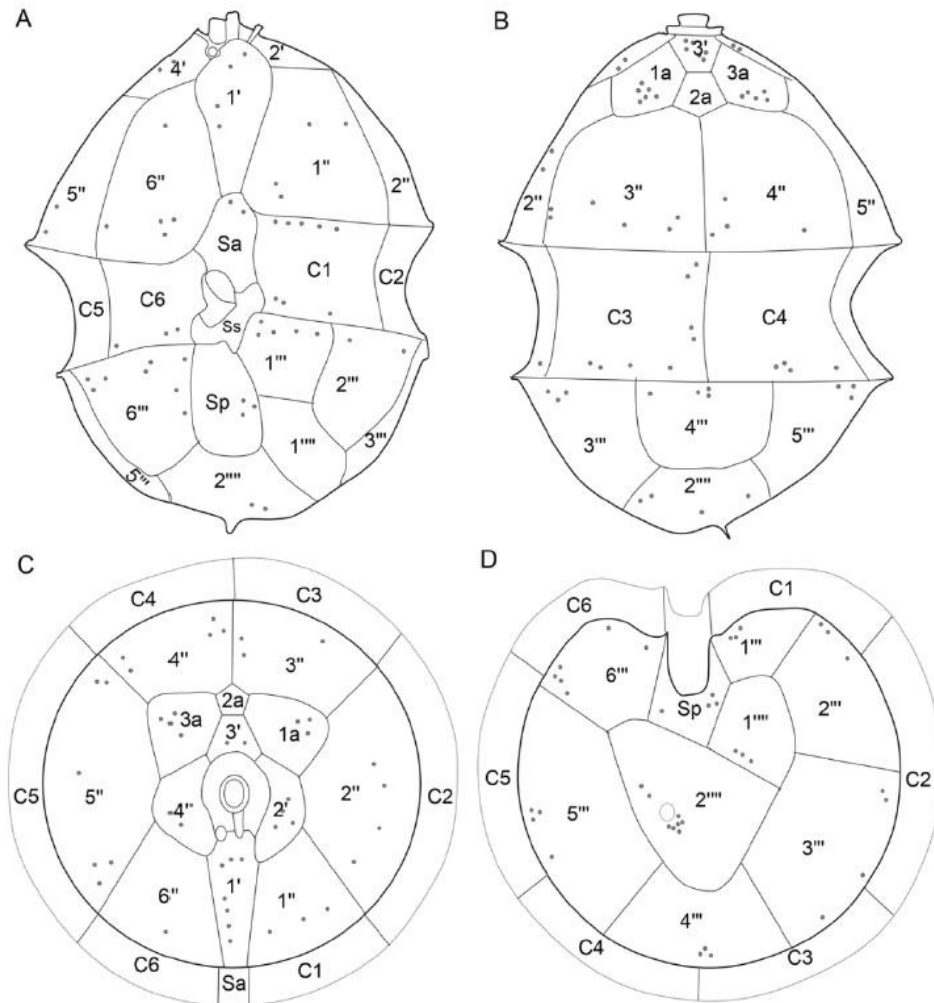


Figure 6: *Azadinium galwayense* sp. nov. (strain 35-R7): Schematic illustration of thecal plates. (a) Ventral view. (b) Dorsal view. (c) Apical view. (d) Antapical view. Plate labels according to the Kofoidian system. Abbreviations of sulcal plates: Sa, anterior sulcal plate; Sp, posterior sulcal plate; Ss, left sulcal plate.

The thecal plates were smooth and thecal pores of slightly varying diameter (range 0.09 – 0.16 μm , mean $0.12 \pm 0.02 \mu\text{m}$, $n = 20$) were found scattered on many plates (Figs 4–6, Fig. S1 in the Supporting Information). Thecal pores were found in varying numbers and positions in plates of the both the epitheca and hypotheca and were most conspicuous in the four apical plates and in the 1a and 3a intercalary plates. Plate 2a plate was always consistently free of pores (Figs 4b, 5a). Long rows of almost evenly spaced thecal pores were present along the episome-cingular sutures but not

in the hyposome-cingular boundary (Fig. 4a, b). On the hypothecal plates the pores were positioned closer to the sutures with other plates, and they were especially bunched together around the spine in the 2^{'''} (Fig. 5c) and dorsally positioned to the spine.

Azadinium perfusorium Tillmann et Salas sp. nov.

Figures 7–10, Figures S2–S5 in the Supporting information.

Description: Small photosynthetic thecate Dinophyceae; cells 11.5 to 18.0 µm long and 8.3 to 13.5 µm wide; cingulum broad and median; epitheca conical and ending in a small but distinctly pointed apical pore; hypotheca hemispherical with a very broad and long sulcus and with a single antapical spine; tabulation formula: Po, cp, X, 4', 3a, 6'', 6C, 5S, 6''', 2''''; a ventral pore located on the right ventral side of the pore plate at the junction of apical plates 1' and 4'. Apical plate 4' larger and extend more ventrally than apical plate 2'. Epithecal intercalary plates 1a and 3a large and plate 2a small and tetragonal.

Holotype: SEM stub (designated CEDiT2020H117) prepared from strain 5-B8 deposited at the Senckenberg Research Institute and Natural History Museum, Centre of Excellence for Dinophyte Taxonomy (Wilhelmshaven, Germany) illustrated in Figures 7 to 10.

Isotype: Formalin-fixed sample prepared from clonal strain 5-B8 (designated CEDiT2020I118) deposited at the Senckenberg Research Institute and Natural History Museum, Centre of Excellence for Dinophyte Taxonomy (Wilhelmshaven, Germany).

Type locality: North East Atlantic, West of Ireland (52° 1.854' N; 10° 46.284' W)

Etymology: The epithet (lat, *perfusorius*: superficial, cursory) is inspired by the almost identical light microscopy appearance of this species and *Azadinium dalianense* (antapical spine, pyrenoid located in the hyposome), such that the field sample specimens initially (and obviously cursory) were misidentified as *Azadinium dalianense*.

Detailed description

All 25 strains identified as *Az. perfusorium* were inspected with LM (Tab. 1) and were identical in size, shape, presence of antapical spine, and presence and position of the pyrenoid. A selected number of strains inspected by SEM revealed all other morphological details as being identical as well. Cells of strain 5-B8, from which the holotype was prepared, is described and depicted in detail. Cells of *Az. perfusorium* strain 5-B8 ranged in size from 12.9 – 15.7 µm in length (mean length: 14.2 ± 0.7µm; n = 53) and 9.3 – 12.0 µm width (mean width: 10.7 ± 0.7 µm; n = 53) and

had a length:width ratio of 1.33 ± 0.05 . Cells were ovoid in outline, almost round in diameter, and had a dome shaped episome and a rounded hyposome (Fig. 7). The cingulum was wide and excavated, slightly postmedian in position, and descending with a slight displacement of about 1/3 of the cingulum width (Fig. 7f). A single chloroplast was reticulate and parietally arranged (Fig. 7f, g). A single large pyrenoid visible by a starch sheath was invariably located on the right side of the hyposome (Fig. 7b, c, d, e). The nucleus was round to slightly ovoid and almost centrally located (Fig. 7h, i, j). Cells divided by desmoschisis with an oblique fission line (Fig. S2 j–n in the Supporting Information). No cyst formation was noticed in cultures.

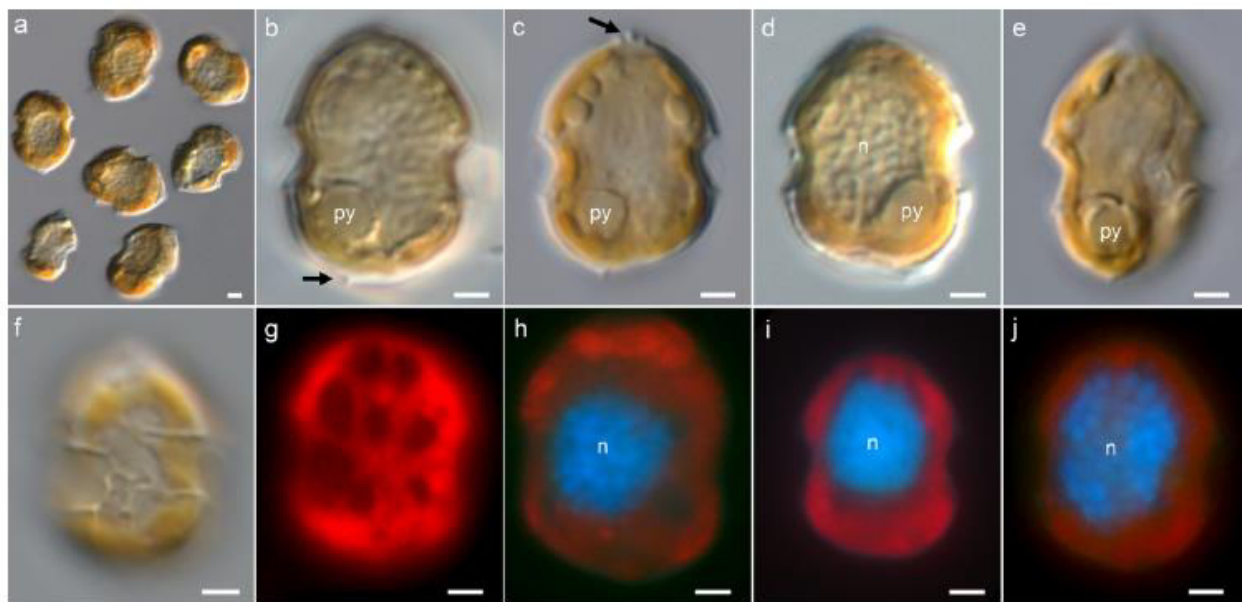


Figure 7: *Azadinium perfusorium* sp. nov. (strain 5B-8). LM of formalin fixed cells. (a–f) General size and shape. Note the pyrenoid (py) located in the hyposome, the antapical spine (black arrow in b) and the prominent apical pore complex (black arrow in c). (d) Nucleus (n) size and position. (e) Cell in lateral view. (f) Ventral view, note the wide cingulum. (g) Cell with blue light excitation showing the reticulate chloroplasts. (h–j) Formalin fixed and DAPI stained cells with UV light excitation to indicate shape, size and location of the nucleus (n). Scale bars: 2 μ m.

SEM revealed the thecal plate pattern (Po, cp, X, 4' 3a, 6'', 6C, 5S, 6''', 2''') and other thecal plate details (Figs 8–10, Figs S2–S5 in the Supporting Information). In the epitheca there were four apical plates and six precingular plates. The APC had a horse-shoe shape and consisted of Po, cp and a X-plate (Figs 8a, b, 9a, c). The Po had an obvious raised surrounding rim which was formed by the lateral and dorsal apical plates and which was open ventrally (Fig. 9a, c). A small X-plate was located centrally between plates 1' and Po and its outer structure was connected with the cp

through a finger-like protrusion (Fig. 9c). The vp was located on the right ventral end of Po at the junction of plates 1' and 4' (Fig. 9a, c). The four apical plates were quite different in shape and size. The ventral 1' plate was wide anteriorly and narrowed towards the anterior sulcal plate (Fig. 8a). Apical plates 2' and 4' were small and pentagonal (plate 2') or hexagonal (plate 4'). Both lateral apical plates had a very short suture with the hexagonal dorsal apical plate 3'. Plate 4' was distinctly asymmetrical in shape and extended more lateral than plate 2' into the ventral area (Fig. 9a).

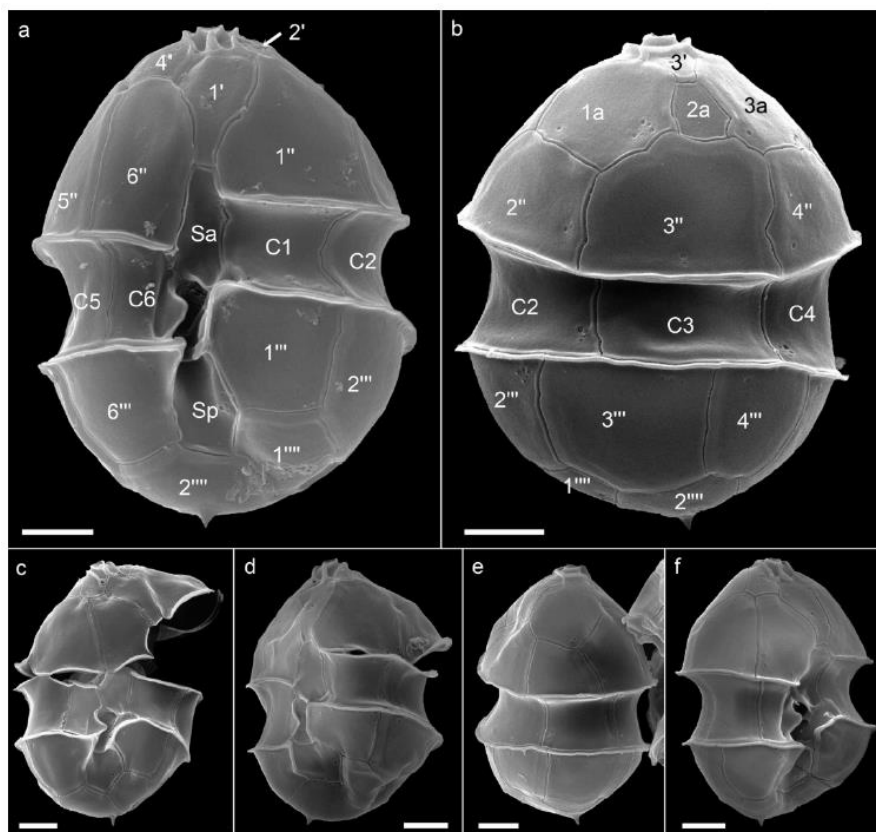


Figure 8: *Azadinium perfusorium* sp. nov. (strain 5-B8). SEM micrographs of different cells in (a) ventral and (b) dorsal view. (c) Ventral view. (d) Left lateral - ventral view. (e) right lateral view. (f) right lateral - ventral view. Scale bars: 2 μ m.

Among the series of three anterior intercalary plates both lateral plates 1a and 3a had a large size. The central epithelial intercalary plate 2a was much smaller and tetragonal in shape and symmetrically located above precingular plate 3'' (Figs 8b, 9a). The first epithelial intercalary plate 1a was always in contact with the dorsally located precingular plate (1'') whereas plate 3a on the cell's right side was disconnected from the ventral precingular plate 6'' by the lanceolate end of plate 4' (Fig. 9a).

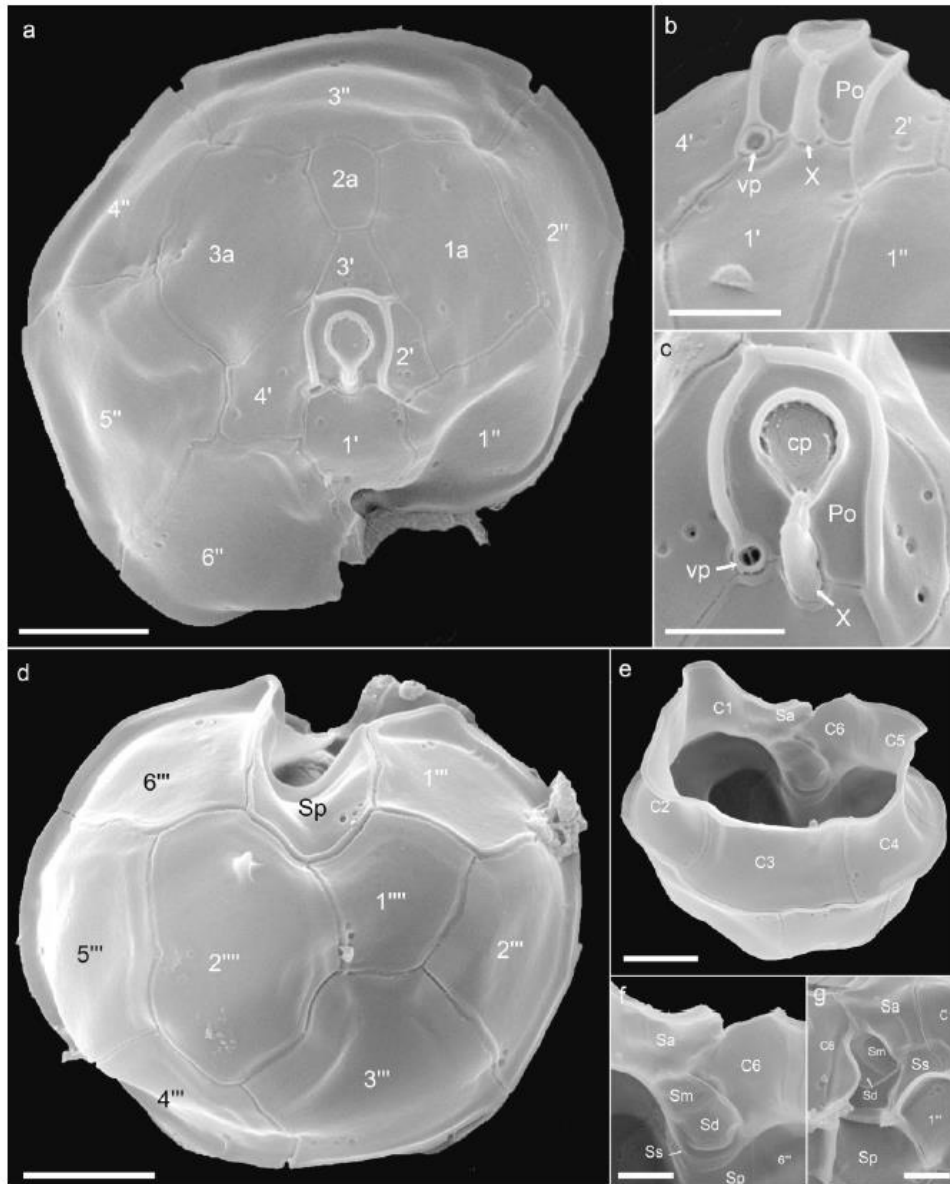


Figure 9: *Azadinium perfusorium* sp. nov. (strain 5-B8). SEM micrographs of different thecae. (a) Epithecal plates in apical view (b, c) Detailed view of the apical pore complex (APC) in (b) ventral or (c) apical view. (d) Hypothecal plates in antapical view. (e) Hypotheca in apical-dorsal view showing cingular plates. (f, g) Detailed view of sulcal plates in internal (f) or outside (g) view. cp, cover plate; Po, pore plate; Sa, anterior sulcal plate; Sp, posterior sulcal plate; Ss, left sulcal plate; Sm, median sulcal plate; Sd, right sulcal plate; X, X-plate. Scale bars: 2 μm.

The cingulum with small lists on both sides consisted of six cingular plates (Fig. 9e) which were lined up in position with the precingular plates. In the sulcal area there were five sulcal plates (Fig. 9e, g). The anterior sulcal plate (Sa) was narrow, and extended into the epitheca, whereas the

posterior sulcal plate (Sp) was wide and extended into the hypotheca (Fig. 8a). Below the Sa, a left sulcal plate (ss) extended across the sulcal area from C1 to C6 (Fig. 9f, g). Two small plates (Sm and Sd) formed a concave shaped vaulted center and were surrounded by Sa, Ss and C6 (Fig. 9f, g).

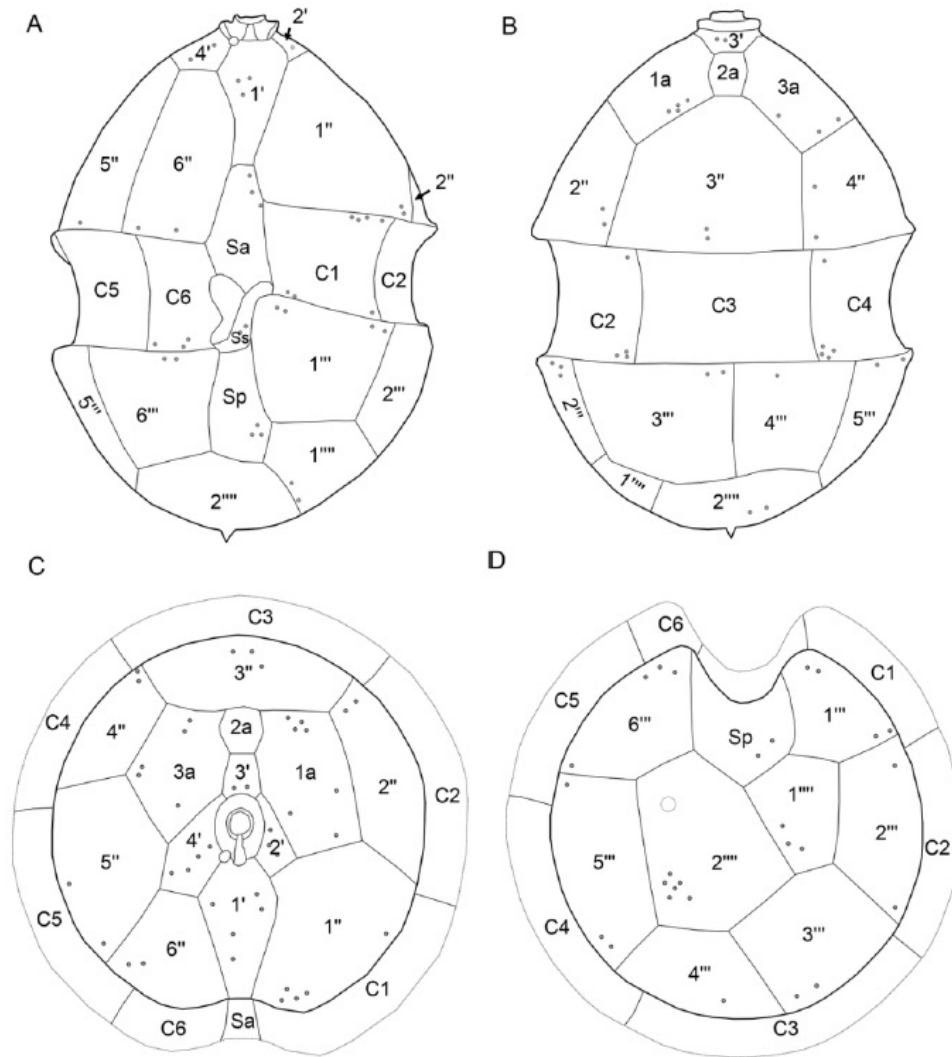


Figure 10: *Azadinium perfusorium* sp. nov. (strain 5-B8). Schematic illustration of thecal plates. (a) Ventral view. (b) Dorsal view. (c) Apical view. (d) Antapical view. Plate labels according to the Kofoidian system. Abbreviations of sulcal plates: Sa, anterior sulcal plate; Sp, posterior sulcal plate; Ss, left sulcal plate.

The hypotheca consisted of six postcingular and two antapical plates (Fig. 9d). The large and hexagonal plate 2''' bore a single antapical spine which was in a ventral position close to the Sp plate (Fig. 9d). Plate 1''' plate was smaller and pentagonal in shape (Fig. 9d).

The thecal plates were smooth and thecal pores were sparsely scattered around the cells' plates (Figs 7–9). Thecal pores ranged in diameter from 0.09 to 0.16 μm (mean: $0.11 \pm 0.02 \mu\text{m}$, $n = 20$). Plate 2a plate was consistently free of thecal pores (Figs 7n, p, 8a). On the hypotheca, thecal pores on postcingular plates were positioned closer to the cingulum. A cluster of pores was located on the dorsal side of plate 2''' distant from the antapical spine (Fig. 9d) situated on a more ventral position and closer to the posterior sulcal plate.

Azadinium pseudozhuanum Salas, Tillmann & H.Gu sp. nov.

Figures 11–13, Figures S6, S7 in the Supporting information.

Description: small photosynthetic thecate dinophyceae; cells 14.9 to 20.1 μm long and 12.3 to 17.5 μm wide; cingulum broad and postmedian; epitheca conical and ending in a small but distinctive apical pore; hypotheca semicircular with a long sulcus bearing a single long and robust antapical spine; tabulation formula: Po, cp, X, 3', 2a, 6'', 6C, 5S, 6''', 2''''; a ventral pore located in the right side of the apical pore plate. Anterior intercalary plate 1a larger than 2a.

Holotype: SEM stub (designated CEDiT2020H119) prepared from clonal strain 32-R1, deposited at the Senckenberg Research Institute and Natural History Museum, Centre of Excellence for Dinophyte taxonomy (Wilhelmshaven, Germany) illustrated in Figures 11 to 13.

Isotype: Formalin-fixed sample prepared from clonal strain 32-R1 (designated CEDiT2020I120) deposited at the Senckenberg Research Institute and Natural History Museum, Centre of Excellence for Dinophyte Taxonomy (Wilhelmshaven, Germany)

Type Locality: North East Atlantic, West of Ireland ($51^{\circ} 32.520' \text{N}$; $10^{\circ} 0.600' \text{W}$)

Etymology: The epithet *pseudozhuanum* is employed here because of the close resemblance with *Az. zhuanum* in both light and scanning electron microscopy. Both species share important morphological characters like the large antapical spine, a pyrenoid that can be found in either the epitheca or hypotheca, and both have only two intercalary plates.

Detailed description

Cells of *Az. pseudozhuanum* (32-R1) were small, round to ovoid in shape and slightly compressed ventrally. Cells ranged in size from 14.9–20.1 μm in length (mean length: $17.2 \pm 1.2 \mu\text{m}$; $n = 49$) and 12.3–17.5 μm in width (mean width: $14.2 \pm 1.3 \mu\text{m}$; $n = 49$) and a median length:width ratio of 1.21 ± 0.07 (Tab. 1). The cells' episome was conical bearing a prominent apical pore complex

(APC) (Fig. 11a, e). The hyposome was hemispherical bearing a long and robust antapical spine (Fig 11 c, d, h). The cingulum was broad and deeply excavated, post median and slightly offset of about 1/3 of the cingulum width (Fig. 11b).

A single chloroplast was parietally arranged around the periphery of the cell (Fig.11j). There was a single pyrenoid surrounded by a starch sheath and this could be positioned in the episome left side or hyposome right side (Fig. 11e–g). Exceptionally, cells with two pyrenoids were also recorded (Fig. 11h). The round nucleus with clearly visible chromosomes was consistently located in the hyposome (Fig. 11 k, l). During cell division the nucleus was elongated in an anterior/posterior axis occupying part of the episome (Fig. 11m, o). Cells divided by desmoschisis with an oblique fission line (Fig. 11n).

The dominant thecal plate pattern of *Az. pseudozhuanum* was Po, cp, X, 3', 2a, 6'', 6C, 5S, 6''', 2'''' (Figs 11p–r, 12, 13, Fig. S6 in the Supporting Information). The epitheca in apical view (Fig. 12a, d) revealed the location of the ventral pore inside the right side of the pore plate. The APC consisted of Po, a cover plate (cp), and the X-plate (or canal plate) (Fig. 12d). The Po were surrounded by a prominent horse-shoe shaped rim (Fig. 12a, e). Three apical plates surrounded the APC. The 1' plate was long and narrow, somewhat rectangular in shape (Figs 11p, q; 12a, b). Plate 2' extended from the Po on the left side ventrally all the way around the Po to a mid to right-dorsal position. The 3' plate was rhomboid in shape (Fig. 12a, b). The anterior intercalary plates were located in a dorsal position with the suture between the 1a and 2a generally in a mid-dorsal position and in contact with the 2' plate. The 1a plate was generally larger than the 2a plate and pentagonal in shape and not in contact with plate 3'. In contrast, the 2a was quadrangular and straddles between the 2' and 3' plates (Fig. 12a, b).

The precingular plates were roughly of similar size except for the 5'' plate which was slightly larger (Fig. 12a, b), the mid-dorsal 3'' plate was the only precingular plate in contact with both intercalary plates.

The cingulum was wide and excavated and consisted of six plates (Fig. 11 p, q). The sulcal area consisted of five plates (Fig. 12g). The anterior sulcal (Sa) was large and extended slightly into the epitheca. The left sulcal (Ss) was located below the Sa and extended across from C1 to C6 in a slightly downward trajectory. The median sulcal (Sm) and right sulcal (Sd) were located in the sulcal central area and were the smallest of the series (Fig. 12g). The posterior sulcal (Sp) plate below the Ss extended into the hypotheca 1/2 to 2/3 of the hypothecal length and was pentagonal in shape (Fig. 11p, q).

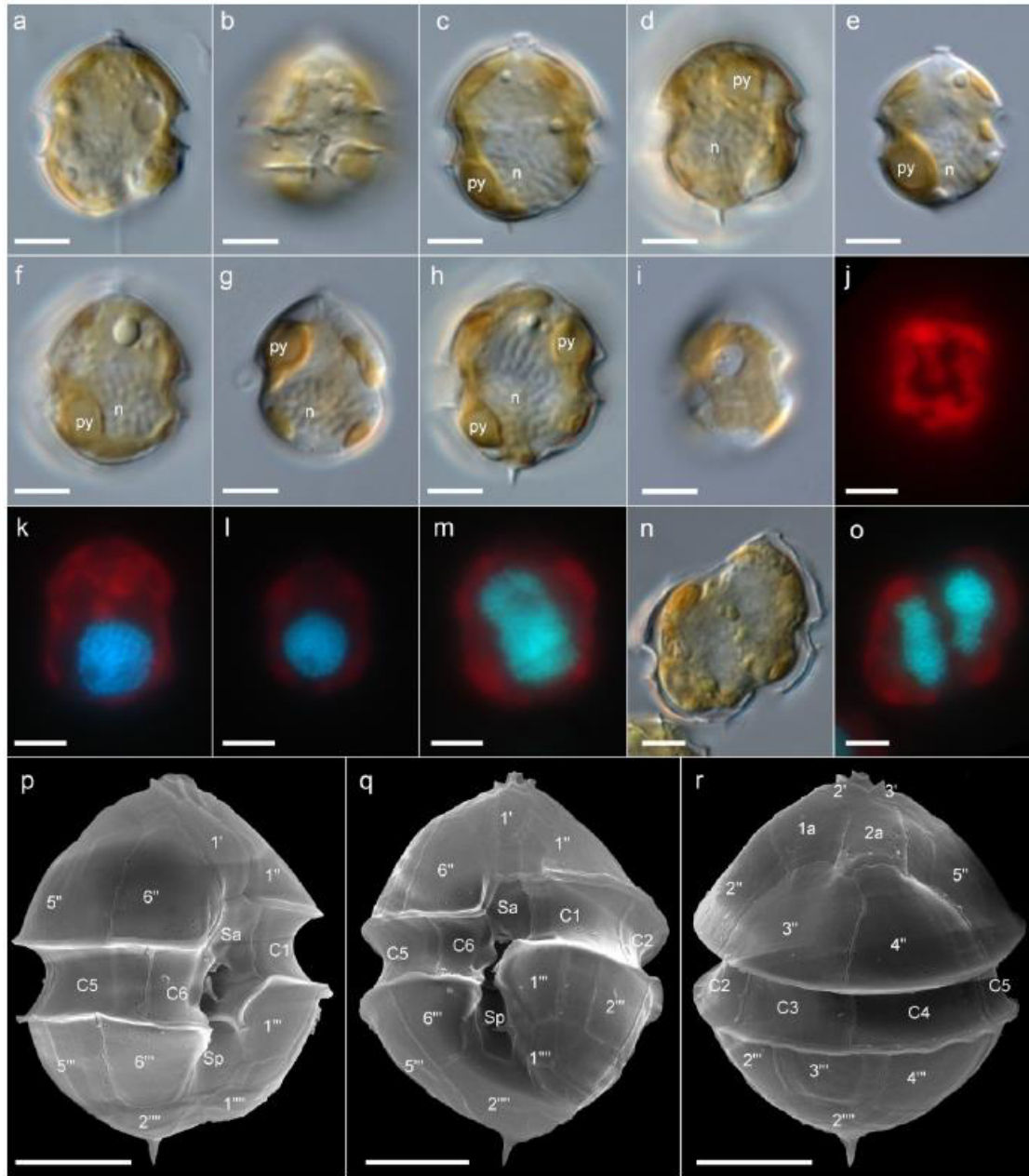


Figure 11: *Azadinium pseudozhuanum* sp. nov. (strain 32-R1). LM of living (a–i) or formaldehyde fixed cells (j–o), or SEM images (p–r). (a–i) General size and shape. Note the broad cingulum (b), the prominent apical pore complex (arrow in a), and the prominent antapical spine (arrows in c, d, h). (c–g) Position of pyrenoid (py) either in the episome (d, g) or hyposome (c, e, f). (g) Cell (presumably in early stage of cell division) with two pyrenoids. (i) Note the parietally arranged and reticulate chloroplast. (j) Formaldehyde fixed cells viewed with blue light excitation to indicate shape of the chloroplast. (k–m) DAPI stained cells observed under UV light excitation showing position, shape and size of the nucleus. (m) Cell in early stage of cell division, note the elongated nucleus. (n, o) Late stage of cell division (desmoschisis) in brightfield (n) and with UV light excitation (o). (p–r) SEM of different theca in (p) right lateral view, (q) ventral view, and (r) dorsal view. Scale bars: 5µm.

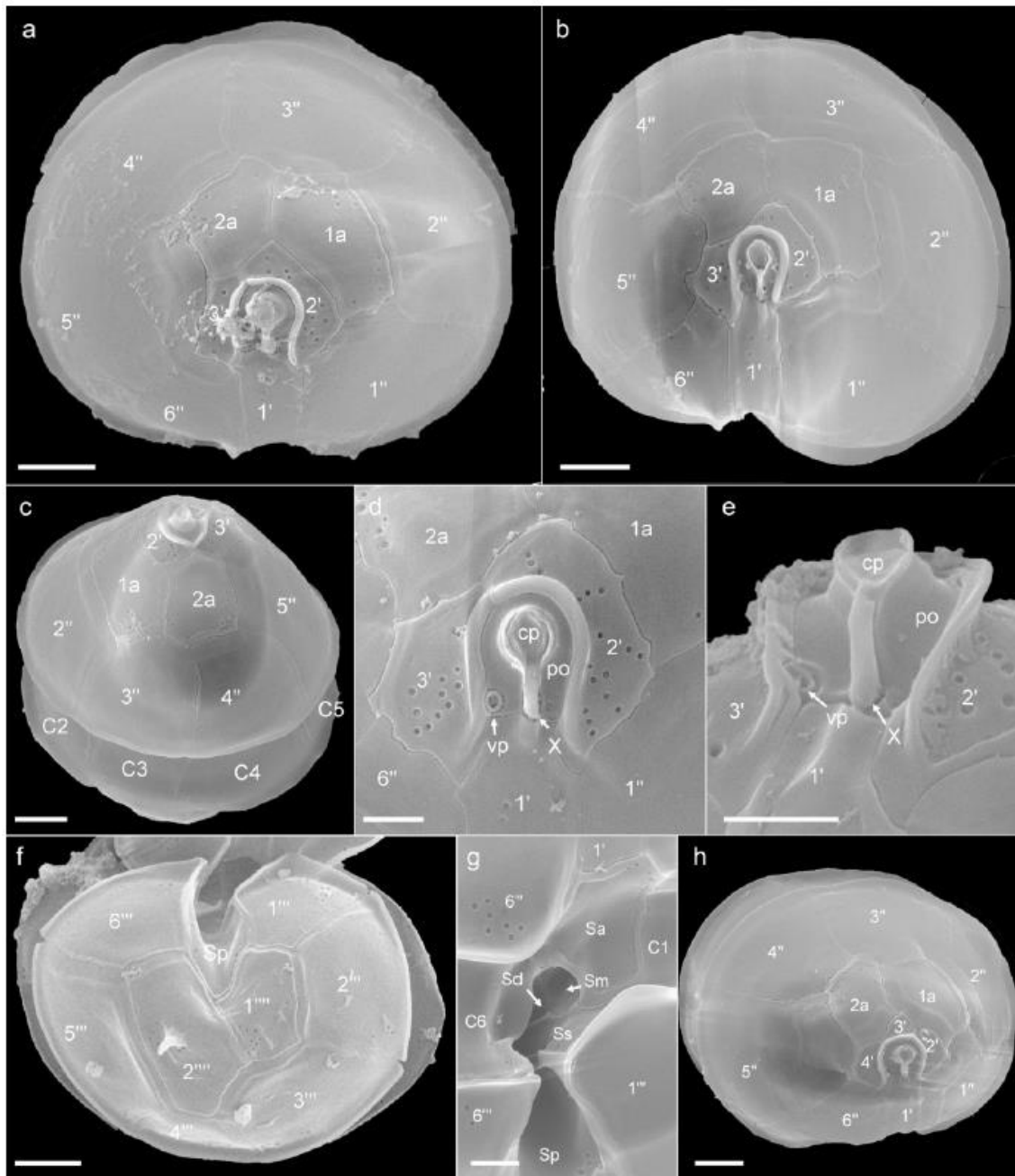


Figure 12: *Azadinium pseudozhuanum* sp. nov. (strain 32-R1). SEM images of different thecae. (a, b) Epithelial plates in apical view. (c) Epitheca in dorsal view. (d, e) Detailed view of the apical pore complex (APC) in apical (d) and ventral (e) view. (f) Hypothecal plates in antapical view. (g) Detailed view of sulcal plates. (h) Apical view of epithelial plates showing a deviating plate pattern with four apical plates. cp, cover plate; Po, pore plate; Sa, anterior sulcal plate; Sp, posterior sulcal plate; Ss, left sulcal plate; Sm, median sulcal plate; Sd, right sulcal plate; X, X-plate. Scale bars: 5 μ m.

The hypotheca consisted of six post-cingular plates and two antapical plates (Fig. 12f). The 2^{'''} plate was the largest of the two antapical plates and the one bearing a large conspicuous spine. The spine was quite robust and supported by ridges and several pores were found clustered around its base.

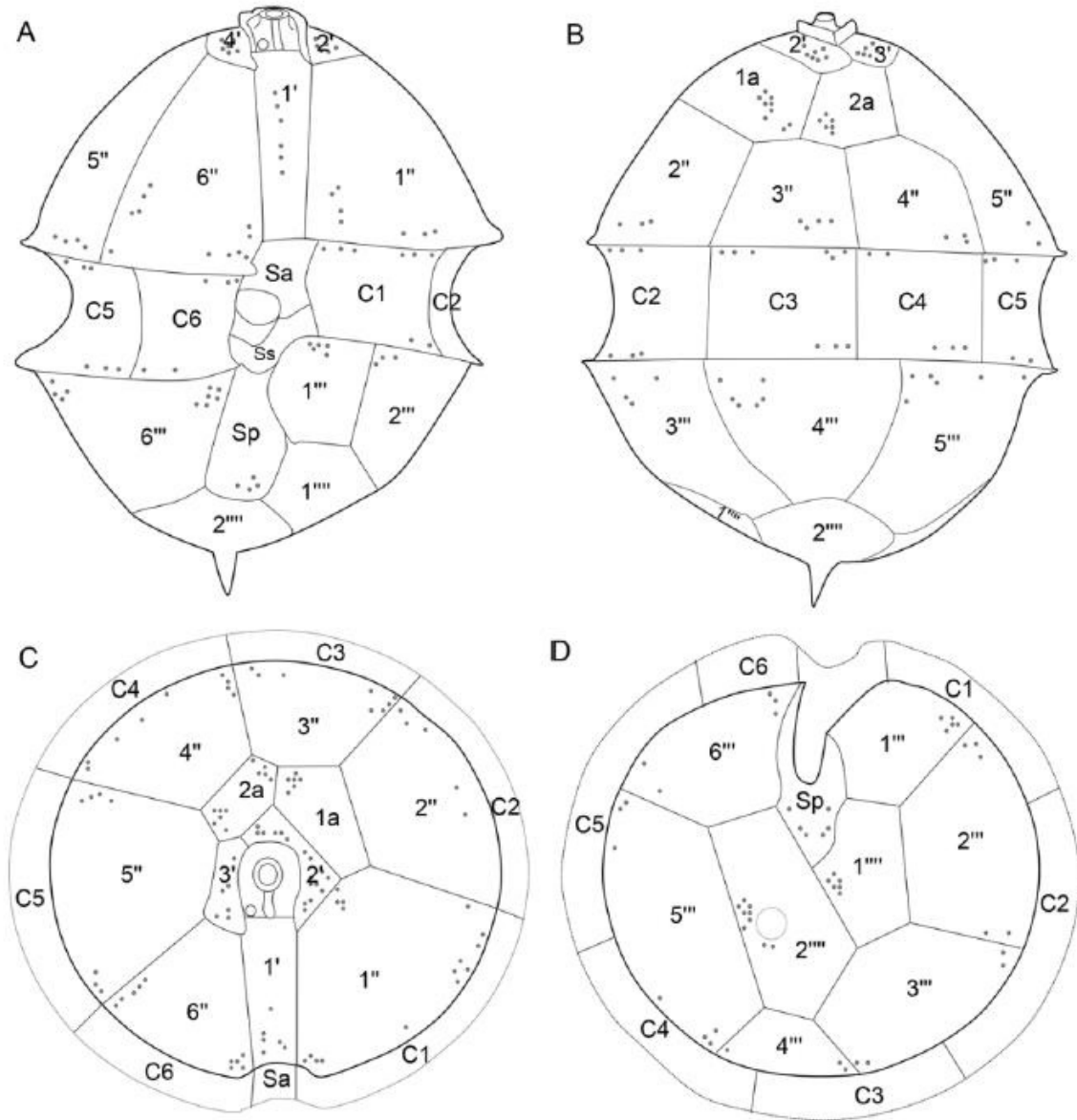


Figure 13: *Azadinium pseudozhuanum* sp. nov. (strain 32-R1). Schematic illustration of thecal plates. (a) Ventral view. (b) Dorsal view. (c) Apical view. (d) Antapical view. Plate labels according to the Kofoidian system. Abbreviations of sulcal plates: Sa, anterior sulcal plate; Sp, posterior sulcal plate; Ss, left sulcal plate.

The thecal plates were smooth and scattered by thecal pores of slightly varying size with pore diameter varying between 0.09 and 0.14 μm (mean: 0.12 ± 0.01 , $n = 20$). Pores were most prominent in the apical series (Fig. 12d) and in the antapical plates (Fig. 12f), where several pores were characteristically scattered around the base of the spine.

In the cultured material of strain 32-R1, deviations from the dominant plate pattern described above were regularly encountered. Variability in the number of plates was most obvious for epithelial plates (Fig. 12h, Fig. S7 in the Supporting Information). To quantitatively estimate the number of plates in apical and epithelial intercalary plate series, a SEM stub was systematically scanned, and the number of plates in each series was scored for cells, in which all plates of a series were visible. This procedure was performed two times for independently grown cultures in Ireland and Germany. Both quantifications of epithelial plates yielded similar results (Tab. 2). Overall, 86% of all cells had three apical plates, whereas for 14% of cells four apical plates were present. The dominant combination of three apical and two epithelial intercalary plates were present for 70 % of cells. Deviating numbers of precingular, postcingular or antapical plates were rarely observed as well but were not quantified.

Table 2: % quantification of apical and epithelial intercalary plates per cell for *Az. pseudozhuanum* grown in Ireland (Q1) or Germany (Q2). The dominant plate pattern of three apical and two intercalary plates is highlighted in grey.

no apical plates	3			4			
no intercalary plates	1	2	3	1	2	3	n
Q1	14.5%	62.0%	3.6%	3.6%	14.5%	1.8%	55
Q2	8.0%	75.0%	8.0%	1.0%	11.0%	0%	100
overall	10.3%	70.4%	4.5%	1.9%	12.2%	0.6%	155

Azadinium caudatum var. *margalefii*

A single strain of *Az. caudatum* var. *margalefii* (9-E13) was obtained during this survey from station 20. Both varieties, var. *margalefii* and var. *caudatum*, were identified in plankton samples (Fig. 2) but only this variety survived in culture (Fig. 14). The size was $28.5 \pm 2.4 \mu\text{m}$ in length and $22.8 \pm 2.3 \mu\text{m}$ in width (Tab. 1). Plate pattern and arrangement (Fig. 14f, k) was identical to the description of Nézan et al. (2012).

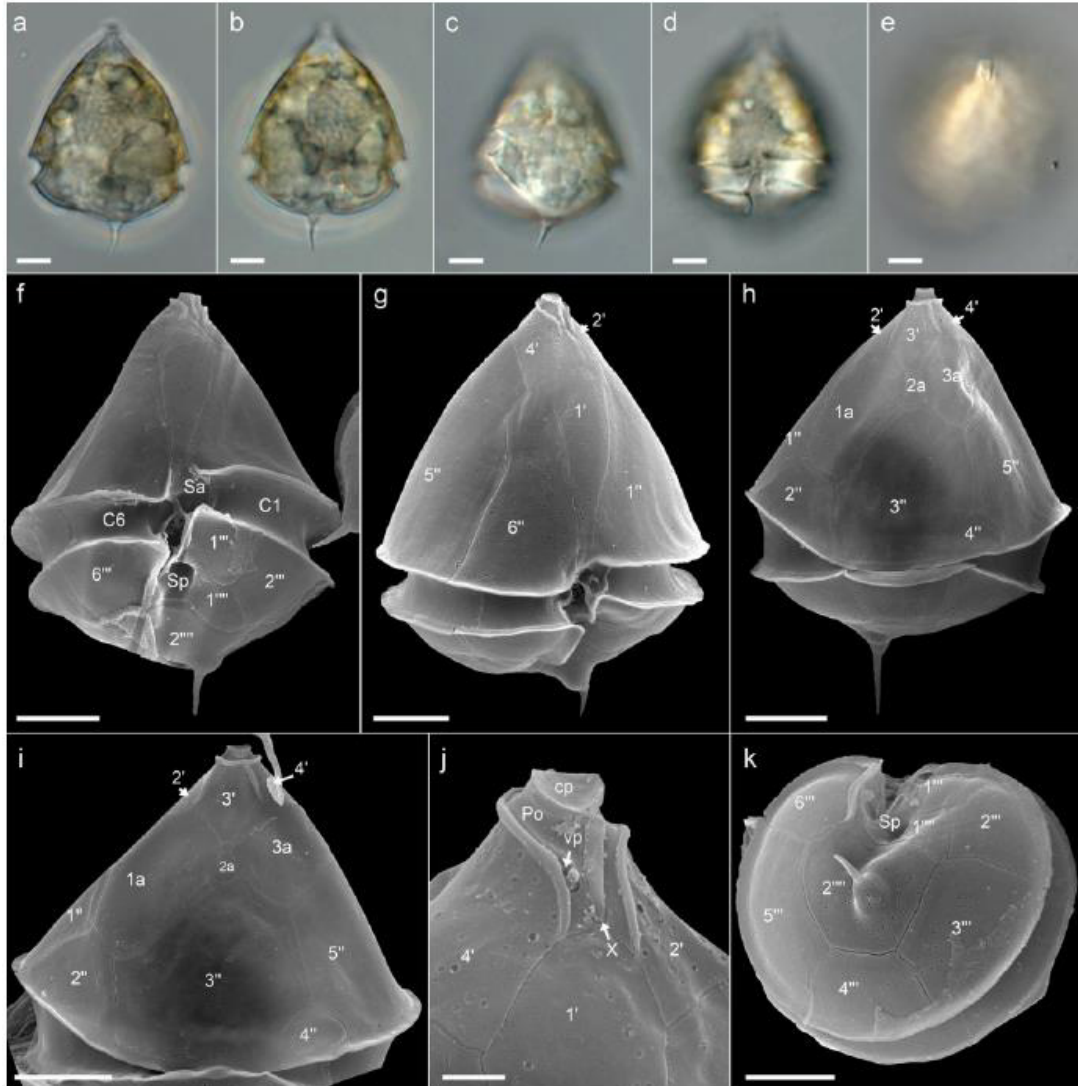


Figure 14: *Azadinium caudatum* var. *margalefii* (strain 9-E13). LM of living cells (a–e) and SEM images (f–g). (a–e) General size and shape. (f–h) SEM of whole theca in (f, g) ventral or (h) dorsal view. (i) Epithecal plates in dorsal view. (j) Detailed ventral view of the apical pore complex (APC). (k) Hypothecal plates in antapical view. cp, cover plate; Po, pore plate; Sa, anterior sulcal plate; Sp, posterior sulcal plate; vp, ventral pore; X, X-plate. Scale bars: 5 μm .

Azspiracid analysis

All strains were negative for AZA. The limits of detection (LOD) in the SRM mode for the targeted analysis of known AZA for the three highest biomass samples was 0.001 fg cell⁻¹ for *Az. galwayense* and *Az. perfusorium*, and 0.003 and 0.17 fg cell⁻¹ for *Az. pseudozhuanum* strain 32-R1 and *Az. caudatum* var. *margalefii* strain 9-E13, respectively (Tab. S2 in the Supporting Information). All LOD data including LOD in the less sensitive precursor ion mode for the search of unknown AZA variants are listed in Table S2 in the Supporting Information.

Molecular results

Sequence data and phylogeny.

For SSU rRNA gene sequences comparison, all three strains of *Az. perfusorium* (5-B8, 2-D1, 6-B4) selected for SSU sequencing shared identical sequences, and three strains of *Az. galwayense* (35-R4, 35-R6, 35-R7) shared 99.9% similarity. *Azadinium perfusorium* shared 99.4% similarity with *Az. galwayense*.

For LSU rRNA gene sequences comparison, all three strains of *Az. galwayense* (35-R4, 35-R6, 35-R7) shared identical sequences. All ten strains of *Az. perfusorium* selected for LSU sequencing shared identical sequences, too. *Azadinium galwayense* shared 95.0% similarity with *Az. perfusorium*. *Azadinium caudatum* var. *margalefii* strains 9-E13 and AC1 (from Scotland) shared identical sequences. *Az. pseudozhuanum* strain 32-R1 and *Az. zhuanum* strain TIO205 (from China) shared 97.1% similarity.

For ITS-5.8S rRNA gene sequences comparison, all three strains of *Az. galwayense* shared identical sequences. All six strains of *Az. perfusorium* selected for ITS sequencing shared identical sequences, too. *Azadinium caudatum* var. *margalefii* strains 9-E13 and AC1 (from Scotland) shared 99.7% similarity. *Az. pseudozhuanum* strain 32-R1 and *Az. zhuanum* strain TIO205 (from China) only shared 89.6% similarity. Uncorrected pairwise genetic distances among some selected *Azadinium* and *Amphidoma* strains and species based on ITS-5.8S rRNA gene sequences ranged from 0.05 to 0.30 (Tab. 3).

Table 3: Uncorrected genetic p-distance between ITS-5.8S rRNA gene sequences of selected *Azadinium/Amphidoma* species/strains. Asterisks (*) denote strains obtained in this study.

	Italy	1C6	A2D11	UTHC8	3D6	2E10	AZCH02	3D9	SHETB2	SM1	5-B8	35-R7	9-E13	TIO205	32-R1	H-1E9
<i>Az. dexteroporum</i> Italy	-															
<i>Az. concinnum</i> 1C6	0.26	-														
<i>Az. trinitatum</i> A2D11	0.15	0.25	-													
<i>Az. poporum</i> UTHC8	0.15	0.27	0.07	-												
<i>Az. cuneatum</i> 3D6	0.15	0.26	0.09	0.08	-											
<i>Az. obesum</i> 2E10	0.14	0.26	0.05	0.05	0.07	-										
<i>Az. dalianense</i> AZCH02	0.16	0.28	0.09	0.08	0.11	0.07	-									
<i>Az. spinosum</i> 3D9	0.16	0.25	0.06	0.08	0.10	0.05	0.09	-								
<i>Az. polongum</i> SHETB2	0.21	0.27	0.18	0.17	0.18	0.16	0.19	0.16	-							
<i>Am. languida</i> SM1	0.28	0.26	0.28	0.27	0.26	0.27	0.28	0.29	0.28	-						
<i>Az. perfusorium</i> 5-B8*	0.10	0.24	0.11	0.12	0.13	0.10	0.13	0.12	0.18	0.26	-					
<i>Az. galwayense</i> 35-R7*	0.10	0.23	0.11	0.12	0.12	0.10	0.12	0.11	0.17	0.25	0.06	-				
<i>Az. caudatum</i> 9-E13*	0.18	0.26	0.17	0.18	0.19	0.17	0.18	0.17	0.22	0.27	0.16	0.15	-			
<i>Az. zhuanum</i> TIO205	0.20	0.28	0.16	0.18	0.18	0.16	0.18	0.17	0.22	0.27	0.16	0.16	0.21	-		
<i>Az. pseudozhuanum</i> 32-R1*	0.23	0.29	0.19	0.20	0.21	0.19	0.22	0.20	0.25	0.27	0.18	0.18	0.23	0.11	-	
<i>Am. parvula</i> H-1E9	0.29	0.26	0.28	0.28	0.29	0.28	0.29	0.28	0.28	0.19	0.26	0.25	0.27	0.28	0.29	-
<i>Az. perforatum</i> AZA2H	0.28	0.28	0.28	0.29	0.28	0.27	0.27	0.28	0.30	0.30	0.26	0.24	0.28	0.30	0.29	0.28

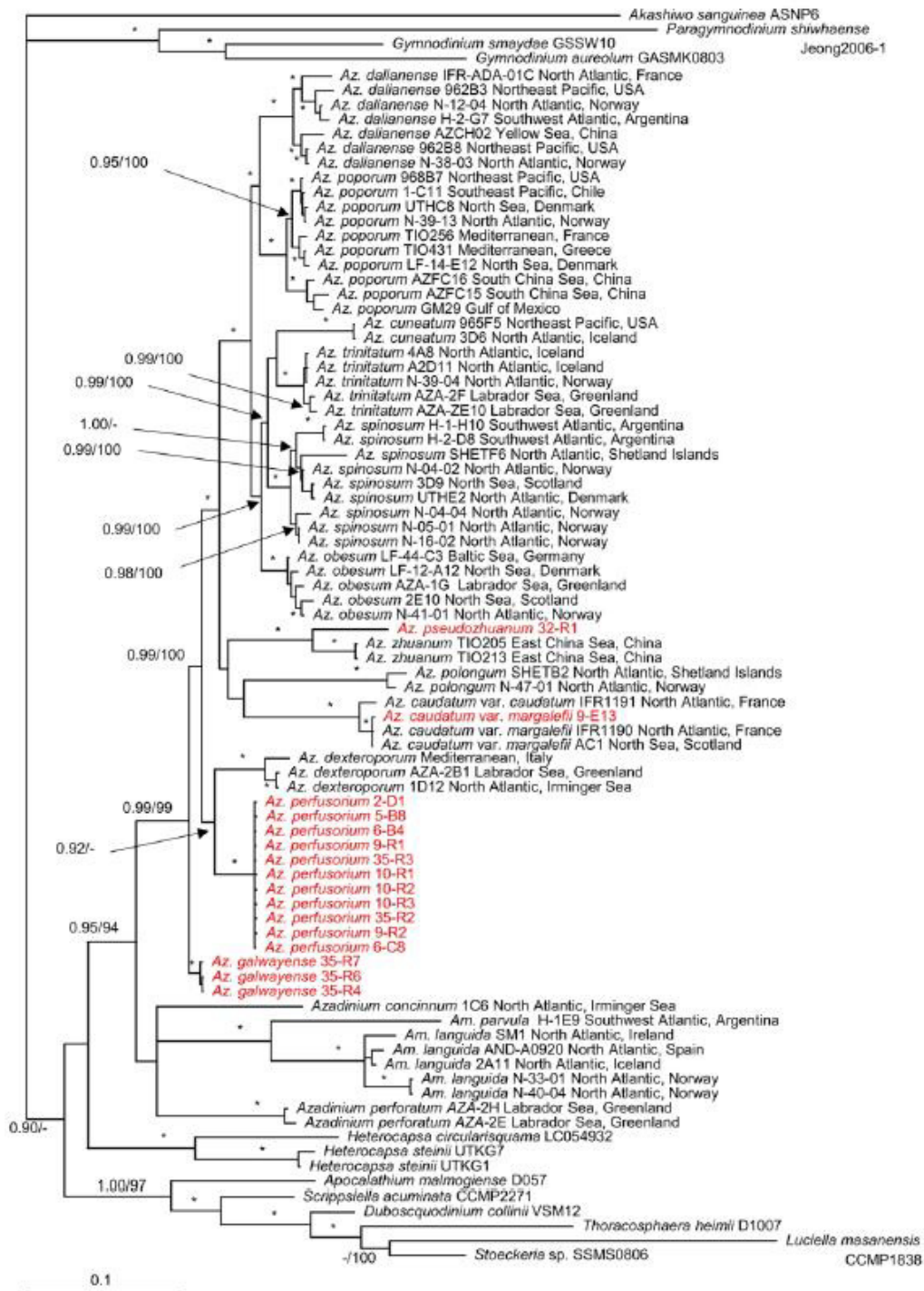


Figure 15: Molecular phylogeny of *Azadinium* and *Amphidoma* inferred from concatenated SSU, ITS-5.8S and partial LSU rRNA gene sequences using Bayesian inference (BI). New sequences of *Azadinium perfusorium*, *Az. galwayense*, *Az. caudatum* and *Az. zhuanium* are indicated in red. Scale bar indicates number of nucleotide substitutions per site. Numbers on branches are statistical support values (left, Bayesian posterior probabilities; right, ML bootstrap support values). Bootstrap values >50% and posterior probabilities above 0.9 are shown. Asterisks (*) indicate maximal support (pp = 1.00 in BI and bootstrap = 100% in ML, respectively).

The maximum likelihood (ML) and Bayesian inference (BI) analysis based on concatenated SSU, ITS-5.8S and partial LSU rRNA gene sequences yielded similar phylogenetic trees. The BI tree was illustrated in Fig. 15. The family Amphidomataceae was well resolved with strong support (0.95 BPP /94 BS) consisting of two clades. The first clade comprising *Amphidoma* and two *Azadinium* species (*Az. concinnum* and *Az. perforatum*) was not supported, and the second clade comprising all other *Azadinium* species was well supported (0.99 BPP /99 BS). The new species *Az. galwayense* was monophyletic with maximal support (1.0 BPP /100 BS) and diverged earliest in the second clade, followed by *Az. perfusorium* which was monophyletic too with maximal support and formed a sister clade of *Azadinium dexteroporum* with low support (0.92 BPP /16 BS). The new *Az. caudatum* var. *margalefii* strain 9-E13 grouped together with other two strains of *Az. caudatum* var. *margalefii* with maximal support and made a sister clade of *Az. caudatum* var. *caudatum* with maximal support. The single strain of *Az. pseudozhuanum* formed a sister clade of *Az. zhuanum* with maximal support.

The ITS2 secondary structure of *Az. pseudozhuanum* strain 32-R1 and *Az. zhuanum* strain TIO205 was predicted. Both of them showed four main helices (I, II, III, IV) and displayed at least one compensatory base change (CBCs, compensatory change on both side of a helix pairing) in helices II, III and IV (Fig. S8 in the Supporting Information).

qPCR assay specificity

No amplification in the current *Az. spinosum*, *Az. poporum* and *Am. languida* qPCR assays was observed for any of the selected non-target strains of *Az. galwayense*, *Az. perfusorium*, *Az. pseudozhuanum* and *Az. caudatum* var. *margalefii*. In contrast, the amphidomatacean (family-specific) assay revealed positive signals for all these tested (target) strains.

Discussion

The three new species - Morphology

Both morphological and molecular sequencing approaches clearly show that among the newly established strains from Irish waters there are three new species of *Azadinium*. The new species *Az. galwayense*, *Az. perfusorium* and *Az. pseudozhuanum* conform with all features described as characteristic for the genus *Azadinium* (Tillmann et al. 2009). They are very similar to several other species of *Azadinium* in size and overall shape, but all three possesses distinctive and unique combination of features, which unambiguously differentiate them from other *Azadinium*. Previous

work on *Azadinium* underline the importance of the ventral pore (vp) position as diagnostic feature for species discrimination. The amphidomatacean vp is larger than regular thecal pores, surrounded by a platelet-like structure, and has different and species-specific positions on the ventral part of the epitheca (Tillmann et al. 2012a, Tillmann and Akselman 2016). All three new species have the vp on the cells' right side of the pore plate and thus are distinct from *Az. spinosum*, *Az. obesum*, *Az. polongum*, and *Az. asperum* Tillmann (vp on the left side of plate 1'), from *Az. poporum*, *Az. dalianense*, *Az. trinitatum*, *Az. cuneatum* (vp on the left side of the pore plate), and *Az. caudatum* var. *caudatum* (Halldal) Nézan & Chomérat (vp on the right side of plate 1'; see table 3 in Tillmann et al, 2014a). There is one species likely to be *Azadinium* where the vp position is unknown: *Gonyaulax parva* Ramsfjell described from the Norwegian Sea and Iceland (Ramsfjell, 1959) corresponds to the plate tabulation of *Azadinium* (and thus should be transferred to *Azadinium* at a later stage) but differs from the newly described species by its absence of an antapical spine and because all three intercalary plates of *G. parva* are of the small size type (Ramsfjell 1959). Thus we are left for a detailed comparison with species that have the vp on the cells' right side of the pore plate, which are *Az. caudatum* var. *margalefii* (Rampi) Nézan & Chomérat, *Az. concinnum*, *Az. dexteroporum*, *Az. luciferelloides* Tillmann & Akselman, *Az. zhuanum* Z.Luo, Tillmann & H.Gu, and *Az. perforatum* Tillmann, Wietkamp & H.Gu (Tab. 4). Of those, *Azadinium caudatum* var. *margalefii* is not listed in Table 4 because this taxon is easily recognizable even in light microscopy as distinctly different to all new species in terms of general size and shape of the cell and of the antapical spine (compare Fig. 14 with 4, 8, and 11).

For a morphological differentiation of the new *Az. pseudozhuanum* from other *Azadinium* species it is most important that *Az. pseudozhuanum* is almost unique by having a reduced number of apical (three) and epithecal intercalary plates (two) compared to the typical pattern of other *Azadinium* which have four apical and three epithecal intercalary plates. The combination of *Az. pseudozhuanum* in epithecal plate number is also found in *Az. dalianense* (Luo et al. 2013), but this species has a different position of the ventral pore (on the left side of Po in *Az. dalianense*). The only other species with a reduction in epithecal plate number is *Az. zhuanum*, but here the dominant plate pattern consist of four apical and two intercalary plates (Luo et al., 2017b). Without doubt, however, *Az. zhuanum* and *Az. pseudozhuanum* are very similar species and share e.g. the same cell shape, the same variable pyrenoid position, the presence of a remarkably large and solid spine, or the rather rectangular shape of the first apical plate.

Table 4: Compilation of morphological features of small species of *Azadinium* (including the tree new species) with a ventral pore located on the cells right side of the pore plate.

	<i>Az. thuanum</i>	<i>Az. pseudochuanum</i>	<i>Az. dexteroporum</i>	<i>Az. perforatum</i>	<i>Az. concinnum</i>	<i>Az. luciferelloides</i>	<i>Az. gabovense</i>	<i>Az. perfulsorium</i>
length range (mean)	16.8–21.6 (18.5)	14.9–20.1 (17.2)	7.0–10.0 (8.5)	15.3–20.0 (18.0)	8.0–11.5 (9.5)	9.4–14.1 † (11.1)	11.4–18.4 (13.7)	11.3–18.0 (14.2)
width range (mean)	12.5–18.8 (14.8)	12.3–17.5 (14.2)	5.0–8.0 (6.2)	9.9–14.4 (12.6)	5.6–8.3 (6.6)	6.6–10.1 † (7.9)	8.3–15.1 (10.6)	8.3–13.5 (10.7)
L/W ratio	1.3	1.2	1.4	1.5	1.4	1.4	1.3	1.3
nucleus	round anterior	round posterior	round posterior	ellipsoid median	round posterior	not reported	round oval posterior	round oval median
antapical projection	spine	spine	spine	tiny spine	spine	spine	spine	spine
stalked pyrenoid	1, epi-OR, hyposome	1, epi-OR, hyposome	1, episome	none	none	unknown	1, episome	1, hyposome
1" in contact 1a	yes	yes	yes	no	no	yes	no	yes
Nr. apicals and intercalaries	4, 2	3, 2	4, 3	4, 3	4, 3	4, 3	4, 3	4, 3
ventral pore position	pore plate, right side	pore plate, right side	end of pore plate, right side	pore plate, notch in <i>pg</i>	pore plate, notch in <i>pg</i>	pore plate, notch in <i>pg</i>	pore plate, right side	pore plate, right side, notch in <i>pg</i>
pore plate symmetry	symmetric	symmetric	asymmetric	symmetric	symmetric	symmetric	symmetric	symmetric
thecal pores on the pore plate	no	no	no	yes	no	no	no	no
relative size 1a/3a	large	large	small	small	very small	small	small	large
configuration 2a	no plate 2a	no plate 2a	quadra (penta) §	penta	penta	quadra (penta) ††	penta	quadra
relative size apical plates	medium	medium	small	medium	small	small	medium	medium
size and arrangement of precingular plates	plate 3" mid-dorsal	plate 3" mid-dorsal	plate 3" mid-dorsal	large, symmetrically arranged, plate 3" mid-dorsal	large, symmetrically arranged, plate 3" mid-dorsal	plate 3" mid-dorsal	both plates 3" and 4" mid-dorsal	plate 3" mid-dorsal
records	East China Sea Yellow Sea	North Atlantic	Mediterranean, North and South Atlantic	Labrador Sea	North Atlantic	South Atlantic	North Atlantic	North Atlantic
Reference §§	a	this study	b, c	d	e	f	this study	this study

† based on SEM only.

§ Both configurations observed. The authentic strain from the Mediterranean had a quadra 2a, but in in strain from the Labrador Sea both quadra and penta 2a were documented (Tillmann et al. 2020).

†† based on a field population. Quadra was the dominant configuration, but pentagonal 2a plates were also recorded (Tillmann and Akselmann 2016).

§§ a, Luo et al.; b, Tillmann et al. (2014b); c, Percopo et al. (2013); d Tillmann et al. (2020); e, Tillmann et al. (2014a); f, Tillmann & Akselmann (2016).

However, both species differ in the position of the nucleus, which is consistently located in the episome for *Az. zhuanum* (Luo et al. 2017) but in the hyposome of *Az. pseudozhuanum*, although during cell division slightly deviating positions and shapes of the nucleus can be observed. With respect to the different number of apical plates (three for *Az. pseudozhuanum* versus four in *Az. zhuanum*) it is important to discuss the variability in plate pattern observed for both species in culture. For *Az. zhuanum* strain TIO205 6% of cells had only three apical plates (Luo et al. 2017) and for *Az. pseudozhuanum* about 14% of cells had four apical plates (Tab. 2). Intraclonal variability of plate pattern seems to be very common in cultured strain of *Azadinium* and other dinophyte species (Balech, 1977; Elbrächter and Meyer, 2001; Tillmann et al., 2010) but has also been reported, albeit at lower frequency, for dinophyte field populations (Tillmann and Akselman 2016; Tillmann et al. 2017a). To conclude, with a consistently different nucleus position and the different dominant pattern of apical plate number we differentiate both taxa on the species level, and this conclusion is supported by the significant differences in sequences data including the presence of CBS between *Az. zhuanum* and *Az. pseudozhuanum*, as will be discussed below.

Based on the presence of four apical plates in basal *Azadinium* species (*Az. concinnum*, *Az. perforatum*, *Az. galwayense*, *Az. perfusorium*, see Fig. 15, a reduction of apical plates seems to be a derived character state. Plate topology of apical plates of *Az. zhuanum*, *Az. pseudozhuanum* and *Az. dalianense* indicate that the transition from four to three apical plates is due to a fusion of plates 2' and 3'. For *Az. dalianense* and *Az. pseudozhuanum* this fusion seems to have happened independently, as both are rather unrelated in the phylogenetic tree (Fig. 15). Both species also have only two large intercalary plates, and thus the loss of the small central intercalary plate and the reduction of apical plates seem to be topologically related. A reduction of plate 2a seem to be the first step as both *Az. zhuanum* and *Az. pseudozhuanum* share this feature. With respect to the subsequent fusion of plates 2' and 3', *Az. zhuanum* and *Az. pseudozhuanum* might be in an evolutionary “early” and “late” stage in a transition of four to three apical plates, respectively.

Both *Az. galwayense* and *Az. perfusorium* may be differentiated from each other at the LM level using the location of the pyrenoid, which consistently is anterior in *Az. galwayense* and posterior in *Az. perfusorium*. However, this trait is of little help differentiating the new species from other *Azadinium*. In fact, pyrenoid position of *Az. perfusorium* is identical to *Az. dalianense* (as is the presence of an antapical spine) (Luo et al. 2013; Kim et al. 2017; Wietkamp et al. 2019a) such that this new species initially on board was cursorily identified as *Az. dalianense*. Moreover, in *Az. zhuanum* and *Az. pseudozhuanum* there is intra-clonal variability in pyrenoid position (Luo et al.

2017; this study: Fig. 11). For some *Azadinium* species in culture, the number of pyrenoids was found to be variable as well (Tillmann et al. 2014a; Kim et al. 2017), and all this variability speaks against considering pyrenoid position/number as a reliable taxonomic character.

Thus, details of thecal plates are additionally needed as diagnostic traits. Both *Az. galwayense* and *Az. perfusorium* differ from both *Az. zhuanum* and *Az. pseudozhuanum* by the differing number in apical plates (Luo et al. 2017; this study). *Azadinium dexteroporum* is smaller than *Az. galwayense* or *Az. perfusorium* and can be differentiated from both new species by its most characteristic feature, i.e. the vp, which is located at the distal end of the more or less elongated right side of an asymmetric pore plate (Percopo et al. 2013; Tillmann et al. 2015; 2020). The recently described *Az. perforatum* (Tillmann et al. 2020) is slightly larger and slender compared to *Az. galwayense* and *Az. perfusorium* and has a very tiny spine. Moreover, this species is unique by the presence of thecal pores on the pore plate (Tillmann et al. 2020). Different to the new species, *Azadinium concinnum* lacks a pyrenoid with starch sheath, and this species has very small lateral, dorsal apical plates and intercalary plates and thus all symmetrically arranged precingular plates are very high (Tillmann et al. 2014a). A differentiation of both *Az. galwayense* and *Az. perfusorium* from *Az. luciferelloides* has to be based on SEM observations only, as for this species no live material and/or LM pictures are available (Tillmann and Akselman 2016) to evaluate the presence/absence of a pyrenoid and supporting confirmation based on sequence data is currently not possible. These three species may have rather subtle differences, such as the presence (*Az. galwayense*) or absence (*Az. perfusorium*, *Az. luciferelloides*) of thecal pores closely around the base of the antapical spine, whether the vp is partly located in a notch of the pore plate (*Az. luciferelloides*, *Az. perfusorium*) or not (*Az. galwayense*,) or whether the plate Sa is distinctly invading the epitheca (*Az. luciferelloides* and *Az. perfusorium*) or to a much lesser degree (*Az. galwayense*). However, in SEM there are also distinct differences in epithelial plate size and arrangement among these three species (Fig. 16).

These differences refer to (1) the arrangement of the medium intercalary plate 2a (pentagonal, i.e. penta-configuration; or tetragonal, i.e. quadra-configuration) and (2) whether there is contact between plates 1" and 1a or not. *Azadinium galwayense* differs from *Az. luciferelloides* and *Az. perfusorium* by its invariable penta-configuration of plate 2a and, related to that, by the dorsal position of both precingular plates 3" and 4" (Fig. 16a, b). For *Az. luciferelloides* plate 2a usually has a quadra-configuration and is in contact to plate 3" of the precingular plates only (Fig. 16c, d), although among field specimen rarely an asymmetrical penta- configuration of plate 2a was

observed (Tillmann and Akselman 2016). Moreover, *Az. galwayense* is unique among *galwayense/luciferelloides/perfusorium* by a lack of contact between plate 1'' and 1a (Fig. 16a, b) which is present for both *Az. luciferelloides* and *Az. perfusorium*. Such a lack of contact between these two plates in *Azadinium* is otherwise present in *Az. obesum* and *Az. cuneatum*. A lack of contact between plate 1a and 1'' was also noted in a field population of *Az. polongum* from Peru (Tillmann et al. 2017a), whereas such a contact is consistently present in the type material of *Az. polongum* (Tillmann et al. 2012b).

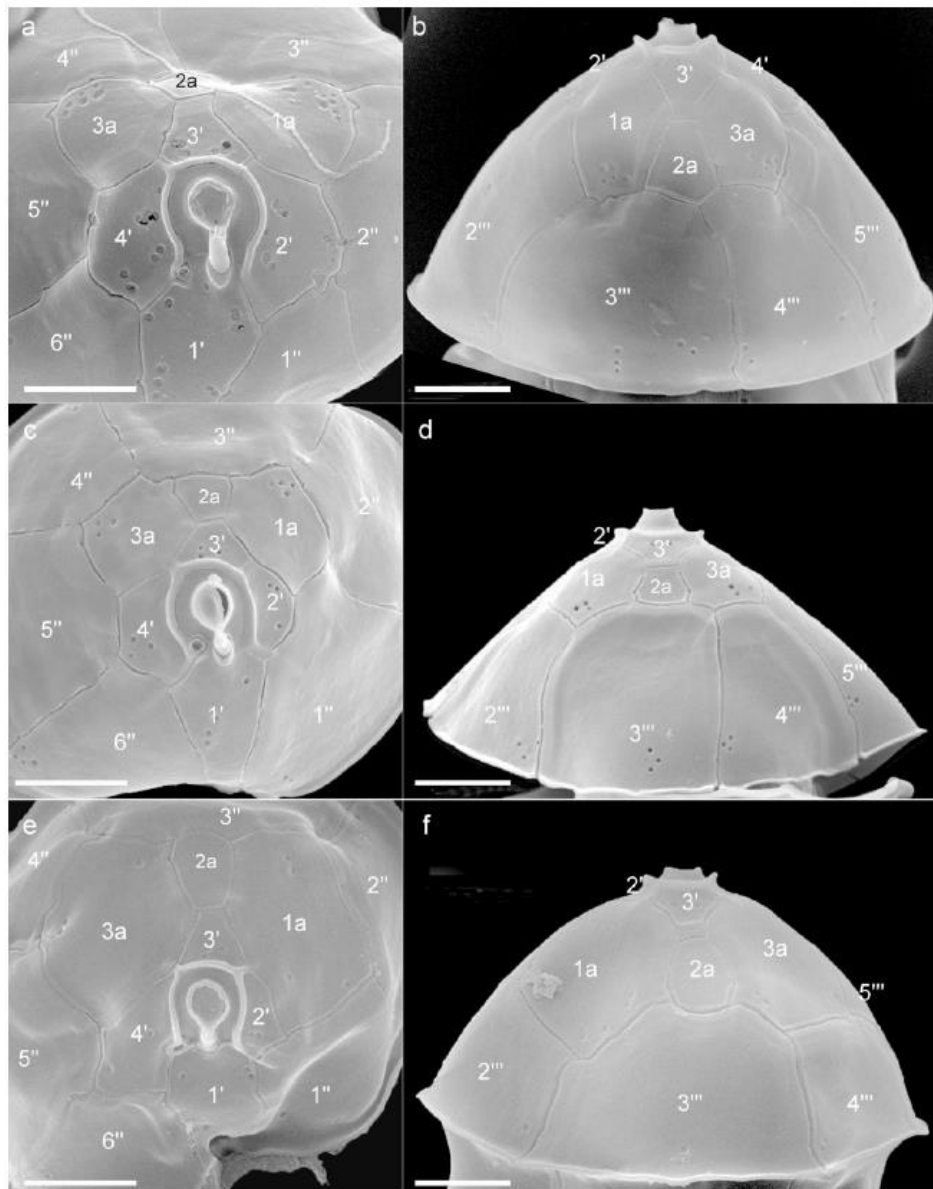


Figure 16: Comparison of epithelial plates of (a, b) *Az. galwayense*, (c, d) *Az. luciferelloides*, and (e, f) *Az. perfusorium*. Scale bars: 2 μ m.

However, with a lack of sequence data for the Peru field population its conspecificity with *Az. polongum* is unclear at present. The outstanding and most important difference between *Az. perfusorium* and *Az. luciferelloides* is the size of the lateral anterior intercalary plates 1a and 3a, which are distinctly and consistently larger in *Az. perfusorium* compared to the small size in *Az. luciferelloides* (Fig. 16c, d). We consider this stable trait as sufficient morphological evidence to differentiate *Az. perfusorium* from *Az. luciferelloides*, but further attempt to obtain sequence data of *Az. luciferelloides* are needed for verification.

The three new species – Molecular phylogeny

The morphological diagnosis of *Az. galwayense* and *Az. perfusorium* as new species is clearly supported by the molecular phylogenetic analysis, as strains from these species are placed in well-defined separate clusters in the phylogenetic tree (Fig. 15). *Az. pseudozhuanum* forms a sister clade with the morphological similar *Az. zhuanum* with maximal support. The genetic distance between *Az. zhuanum* and *Az. pseudozhuanum* based on ITS-5.8S rRNA gene sequences reaches 0.11, compared to 0.06 between *Az. galwayense* and *Az. perfusorium*. Moreover, at least three CBCs in ITS2 (Fig S8 in the Supporting Information) were revealed between *Az. pseudozhuanum* and *Az. zhuanum*. This further support that they belong to different species, as single CBC in helix III have been suggested to indicate gamete incompatibility and therefore separate species (Coleman 2009). However, high genetic distances within dinoflagellate species has been reported previously. For instance, genetic distances based on ITS-5.8S rRNA gene sequences among *Akashiwo sanguinea* ribotypes are higher than 0.14 but in this case no morphological differences could be identified yet, and therefore *A. sanguinea* is currently designated as a cryptic species complex (Luo et al., 2017a). Generally, adding the new sequences in the phylogenetic analysis fosters previous notions of the monophyly of Amphidomataceae. However, as noted previously (Tillmann et al. 2018b; 2020), both *Azadinium concinnum* and *Azadinium perforatum* are placed in a clade with *Amphidoma languida* and *Am. parvula*, but without any statistical support. In the *Azadinium* clade, *Az. galwayense* is the earliest diverging species followed by a clade where *Az. perfusorium* and *Az. dexteroporum* are sister groups. Species of these early diverging Amphidomataceae groups, i.e. *Am. languida*, *Az. concinnum*, *Az. perforatum*, *Az. galwayense*, *Az. perfusorium* and *Az. dexteroporum* share a right-side apical position of the ventral pore indicating that this is an ancestral trait in Amphidomataceae. Morphological agreements of *Az. galwayense* with *Az. concinnum* and *Az. perforatum* with respect to a symmetrically arranged pentagonal plate 2a above the two

symmetrical dorsal precingular plates 2" and 3" (Tab.4) are not reflected in the current molecular tree. Generally, the currently unresolved position of e.g. *Az. concinnum* in phylogenetic trees being either within the genus *Azadinium* (Tillmann et al. 2020) or outside *Azadinium* and more close to *Amphidoma* (this study), the limited number of strains available for *Az. concinnum* and *Az. perforatum*, and the current lack of sequence data especially for additional species of *Amphidoma* prevent from a final conclusion about the generic level differentiation within Amphidomataceae.

Diversity of Amphidomataceae in Irish waters

The present description of three new species of *Azadinium* from Irish coastal waters add significantly to the knowledge on the diversity of Amphidomataceae in the area. Known since many years in Ireland is the large and easy to identify species *Az. caudatum* with both varieties (var. *margalefii* and var. *caudatum*) (Dodge 1981; O'Boyle and Raine 2007), which is regularly recorded in the Irish plankton monitoring program. The new strain of *Az. caudatum* var. *margalefii* now, based on LCMS/MS analysis, indicates that Irish populations of the taxon are non-toxigenic confirming previous analyses of a Scottish strain (Tillmann et al. 2014b).

All strains of the three new species lack any AZA, which foster the notion that AZA production for Amphidomataceae (now known for only four of the 16 species tested so far) is more the exception than the rule. However, strain variability on AZA production potential is known for *Az. dexteroporum*, where a Mediterranean strain is a producer of various AZA (Rossi et al. 2017) whereas two strains from the North Atlantic with slightly different sequence data compared to the authentic *Az. dexteroporum* strain are not (Tillmann et al. 2015; 2020). It thus may be premature to claim non-toxigenicity for the species level, but at least for *Az. perfusorium* with multiple strains from multiple station it is quite likely that non-toxigenicity of Irish populations of this species is a stable trait.

The diversity of Amphidomataceae in Irish waters also includes toxigenic species. Both *Azadinium spinosum* and *Amphidoma languida* are known to be present in the area based on studies on a single strain each (Salas et al. 2011; Tillmann et al. 2012a) isolated from Bantry Bay in Southern Ireland. In addition, both species are repeatedly recorded using specific qPCR assays of field surveys (Wietkamp et al. 2019b; 2020) and/or the Irish monitoring program (Clarke 2020; Clarke et al. in press). The third AZA producing species of the North Atlantic, *Az. poporum*, has been recorded from the area based on positive qPCR signals before (Wietkamp et al. 2020), but local strains are not yet available for confirmation. Another non-toxigenic species, *Az. obesum*, also can be added

to the Irish list of species, as this species is regularly detected by its specific PCR probe (Clarke et al. in press) and for which we have unpublished SEM confirmation (R. Salas unpublished) from a western Ireland plankton sample. LM micrographs obtained on-board of the AZAHAB cruise indicate at least one more yet undescribed Amphidomatacean species (*Az. spec. 1*) characterized by a fairly asymmetric shape of the epitheca (Fig. 2h). In conclusion, the diversity of Amphidomataceae in Irish waters is high and comprise the presence of at least nine different species (*Az. spinosum*, *Az. poporum*, *Am languida*, *Az. caudatum*, *Az. obesum*, *Az. pseudozhuanum* spec. nov., *Az. galwayense* spec. nov., *Az. perfusorium* spec. nov. and *Az. spec. 1*). A high diversity of Amphidomataceae has been reported before from various areas including North Pacific coastal waters (Kim et al. 2017), North Atlantic Subarctic waters (Tillmann et al. 2020), the Norwegian coast (Tillmann et al. 2018a) or the Argentinean shelf (Tillmann and Akselman 2016; Tillmann 2018; Tillmann et al. 2019), and thus seem to be the rule and not an exception.

Abundance of non-toxigenic species in the Irish coastal area are poorly known (except that it is known that *Az. caudatum* is regularly present but never in high abundances). The high number of strains of *Az. perfusorium* obtained from five different stations indicate that non-AZA producers are widespread and potentially abundant as well: This, of course complicates any LM based early warning plankton monitoring program aiming at detecting alarming levels of toxigenic Amphidomataceae, as small non-toxigenic species including *Az. galwayense*, *Az. pseudozhuanum* and *Az. perfusorium* can hardly be distinguished by routine LM from *Azadinium spinosum*. The presence of other yet undetermined AZA producing species in the area can of course not be ruled out, but the lack of new toxigenic species among the multiple new isolates of the survey provide evidence that monitoring the previously known Atlantic AZA producers (*Az. spinosum*, *Az. poporum*, *Am. languida*) using existing specific molecular detection methods is adequate from an AZA early warning perspective. Testing DNA of the three new *Azadinium* species with all three specific qPCR assays (*Az. spinosum*, *Az. poporum*, *Am. languida*) also exclude false-positive cross reactivity of the new non-toxigenic species with the AZA-producer detection assays.

Acknowledgements:

The authors thank Caroline Cusack, Paula Hynes and Joe Silke (Marine Institute, Galway, Ireland), as well as Luisa Hintze and Karina Krapf (AWI, Bremerhaven, Germany) for on-board technical support. Thomas Max and Anne Müller (both AWI Bremerhaven, Germany) are thanked for continued support in laboratory work and AZA analysis. This work was supported by funding of the German Ministry for Education and Research (project RIPA ZA, 03F0763A) and by the PACES II research program of the Alfred-Wegener-Institute as part of the Helmholtz Foundation initiative in Earth and Environment.

Supporting Information

Additional Supporting Information may be found in the online version of this article at the publisher's web-site:

Figure S1: *Az. galwayense* sp. nov. (strain 35-R7), additional micrographs

Figure S2: *Az. perfusorium* sp. nov. (strain 5-B8), additional SEM micrographs

Figure S3: *Az. perfusorium* sp. nov. (strain 5-B8), additional detailed SEM micrographs

Figure S4: *Az. perfusorium* sp. nov. (strain 2-D1), micrographs

Figure S5: *Az. perfusorium* sp. nov. (strain 2-D1), detailed SEM micrographs

Figure S6: *Az. pseudozhuanum* sp. nov. (strain 32-R1), epithelial plate pattern

Figure S7: *Az. pseudozhuanum* (strain 32-R1), deviating epithelial plate configurations

Figure S8: ITS secondary structure of *Az. pseudozhuanum* and *Az. zhuanum*

Table S1: Limit of detections AZA analyses

Table S2: Selected reaction monitoring (SRM) transitions for AZA analyses

Table S3: Genbank accession numbers

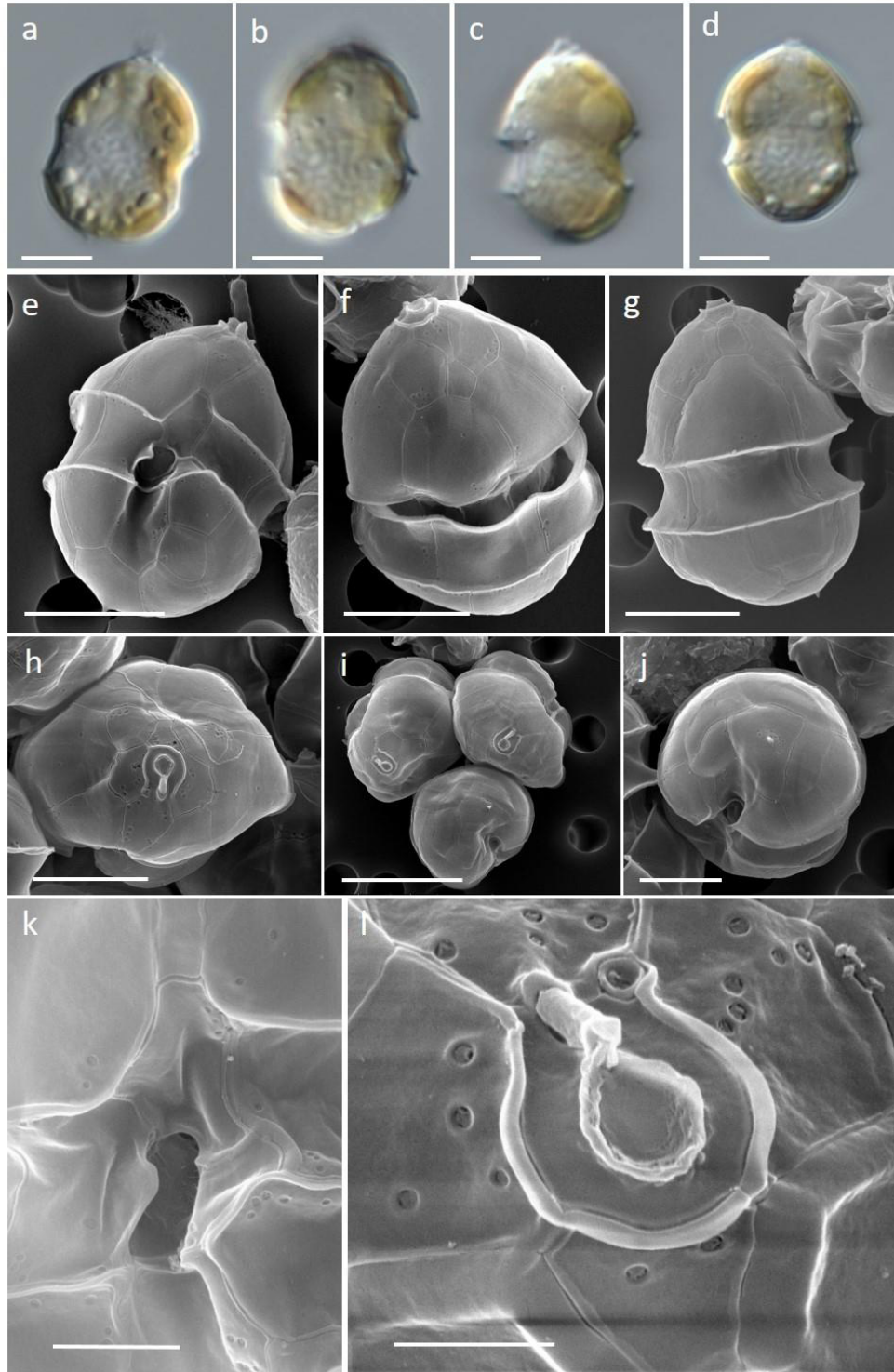


Figure S1. *Azadinium galwayense* strain 35-R7. (a–d) LM of formaldehyde fixed cells. (e–l) SEM micrographs of different cells in (e) ventral view, (f–g) dorsal view (h) apical view. (i) Three cells in apical and antapical view. (j) Cell in antapical view. (k) Detailed view of sulcal plates. (l) Apical dorsal view of apical pore complex (APC) and the ventral pore (vp). Scale bars: 5 μm (a–h, j), 10 μm (i), 2 μm (k) or 1 μm (l).

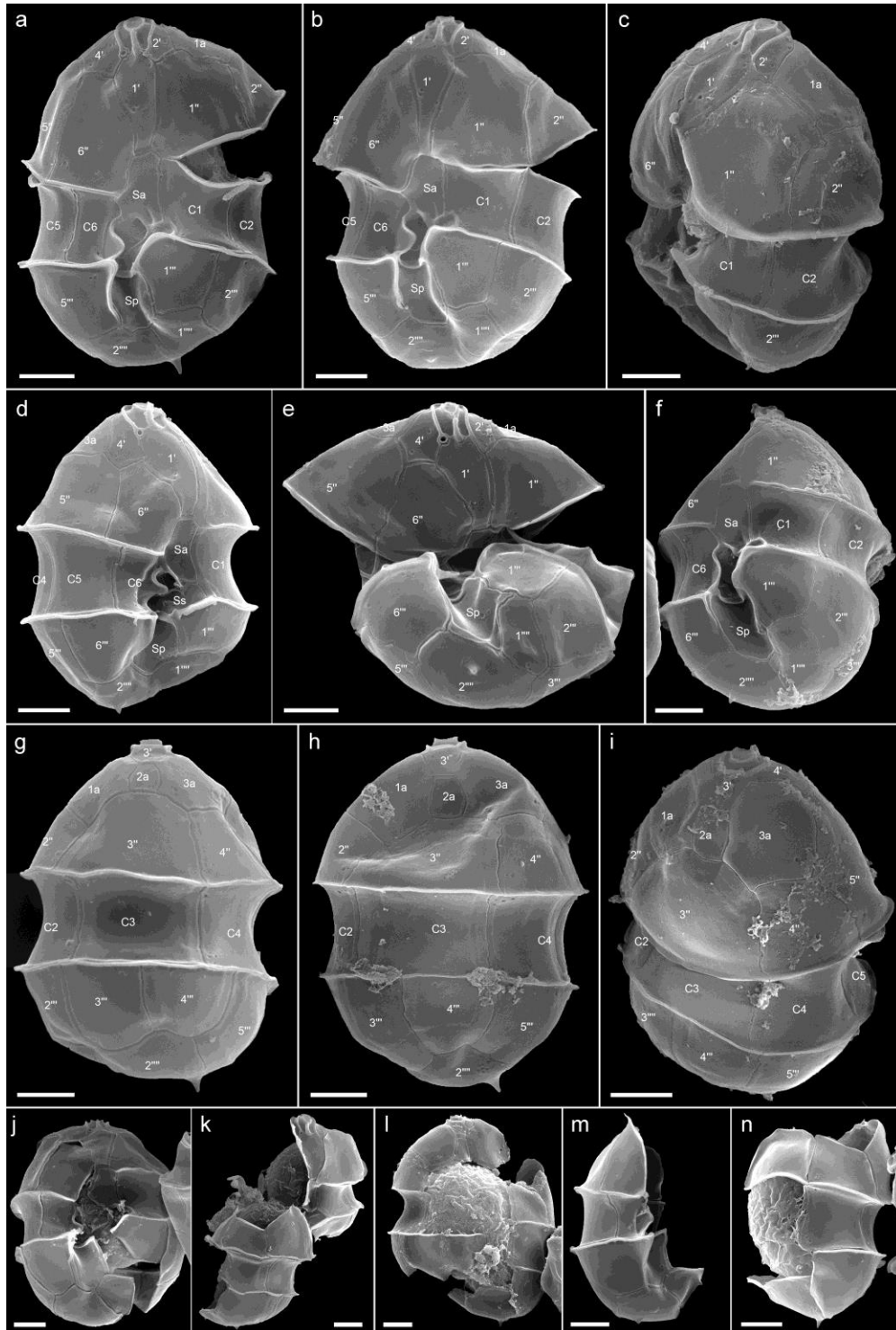


Figure S2. *Azadinium perfusorium* strain 5-B8, SEM micrographs of different cells in (a, b) ventral view, (c) left lateral view, (d) right lateral view, (e) ventral view, (f) ventral antapical view, and (g–i) dorsal view. (j–n) Different stages of dividing cells in (j, k) ventral and (l) dorsal view. (m, n) Presumably newly divided cells with half of the parent thecal plates in (m) ventral or (n) dorsal view. Scale bars: 2 μ m.

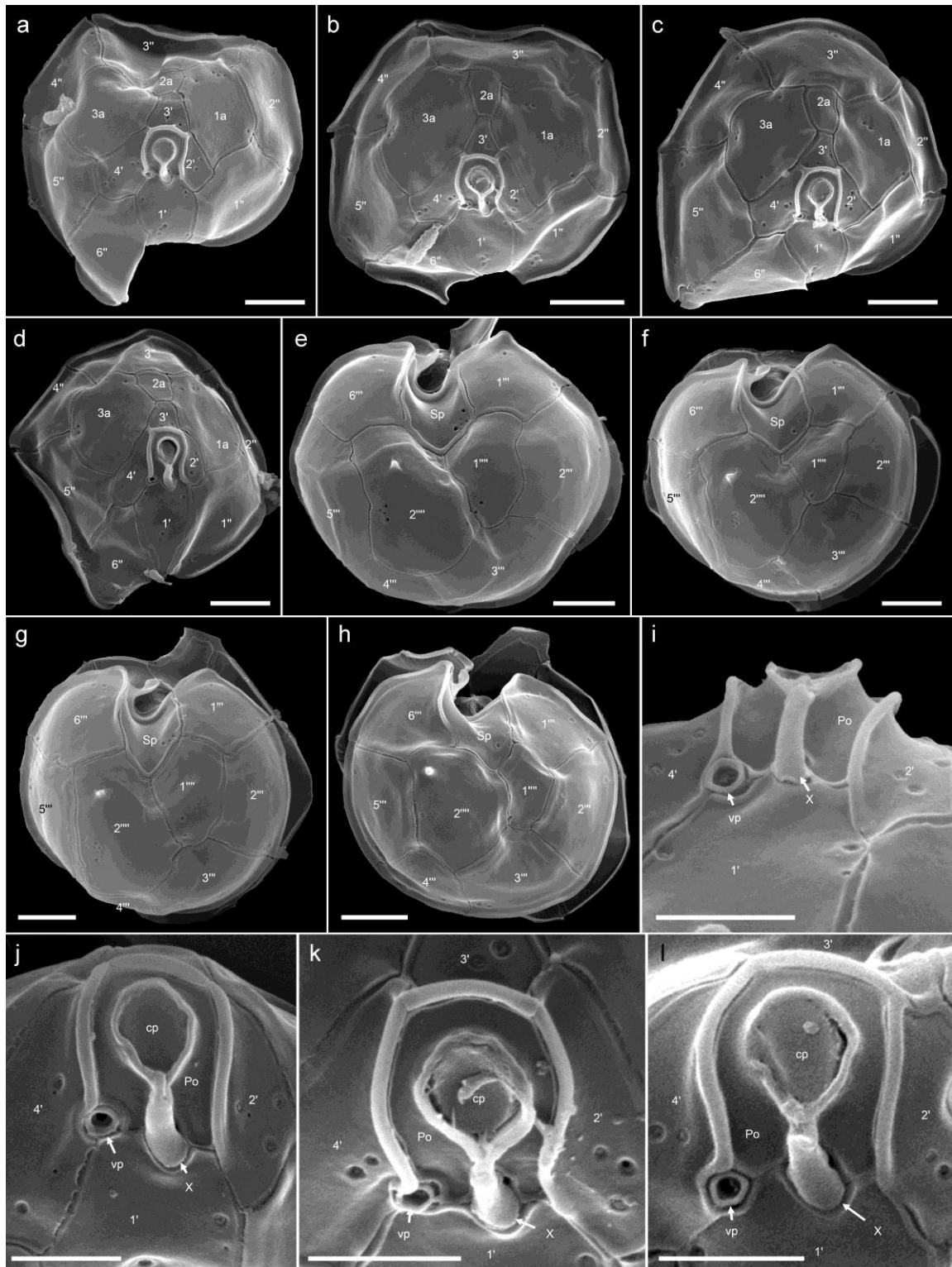


Figure S3. *Azadinium perfuscatorum* strain 5-B8. SEM of different cells in (a–d) apical view showing epithelial plates. (e–h) Antapical view of hypothecal plates. (i–l) Detailed views of the apical pore complex in (i) ventral or (j–l) apical view. vp, ventral pore; Po, pore plate; X, X-plate; cp, cover plate. Scale bars: 2 μm (a–h) or 1 μm (i–l).

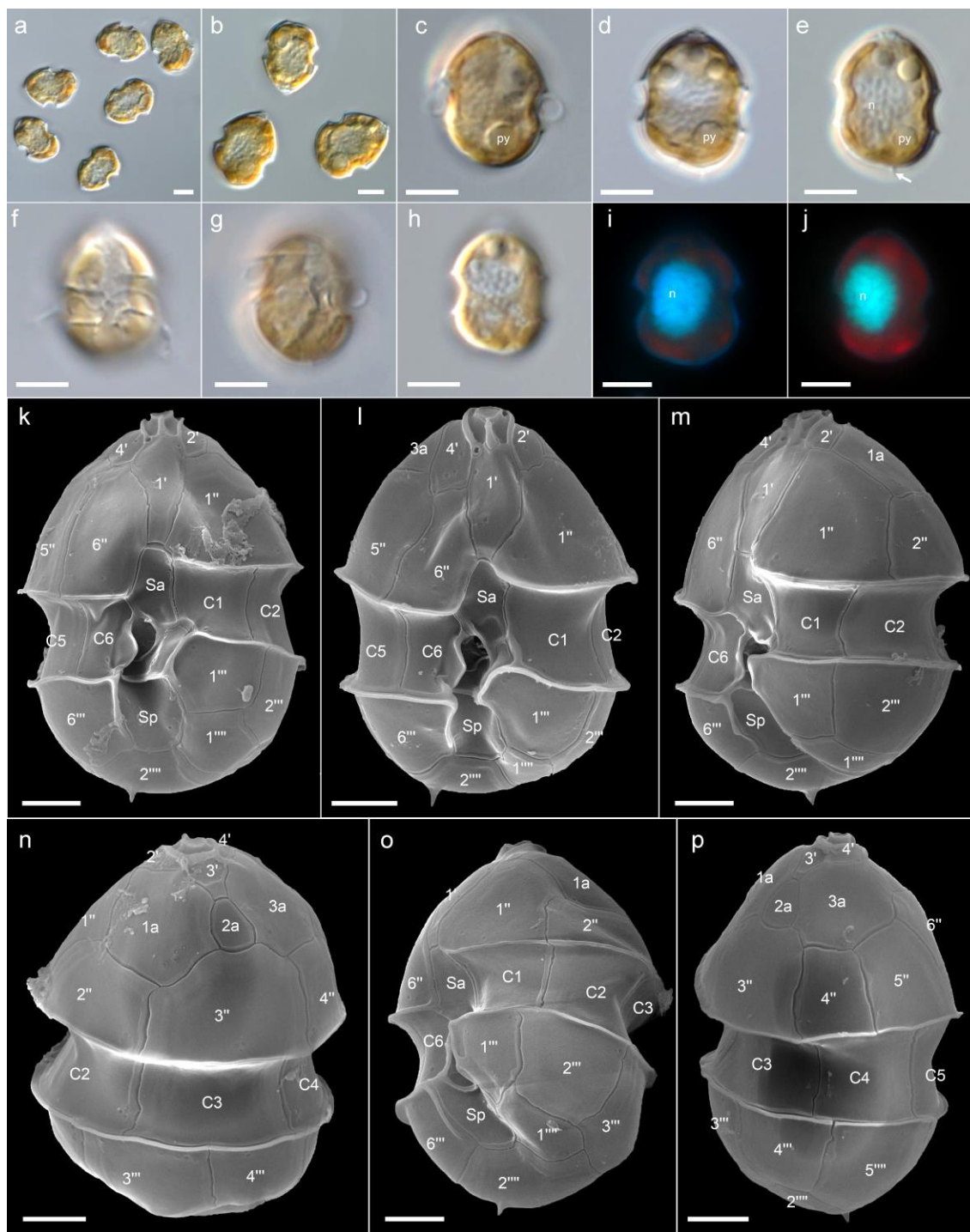


Figure S4. *Azadinium perusorium* strain 2-D1. (a–j) LM of formaldehyde fixed (a, b, i, j) or living cells (d–h). (a–h) General size and shape indicating the position of the pyrenoid (py), the antapical spine (arrow in e). (i, j) Cells stained with DAPI and viewed with UV excitation to indicate size, shape and location of the nucleus. (k–p) SEM of different cells in (k, l) ventral view, (m) left lateral view, (n) dorsal view, (o) lateral antapical view, or (p) in right lateral view. Scale bars: 5 μm (a–i) or 2 μm (k–p).

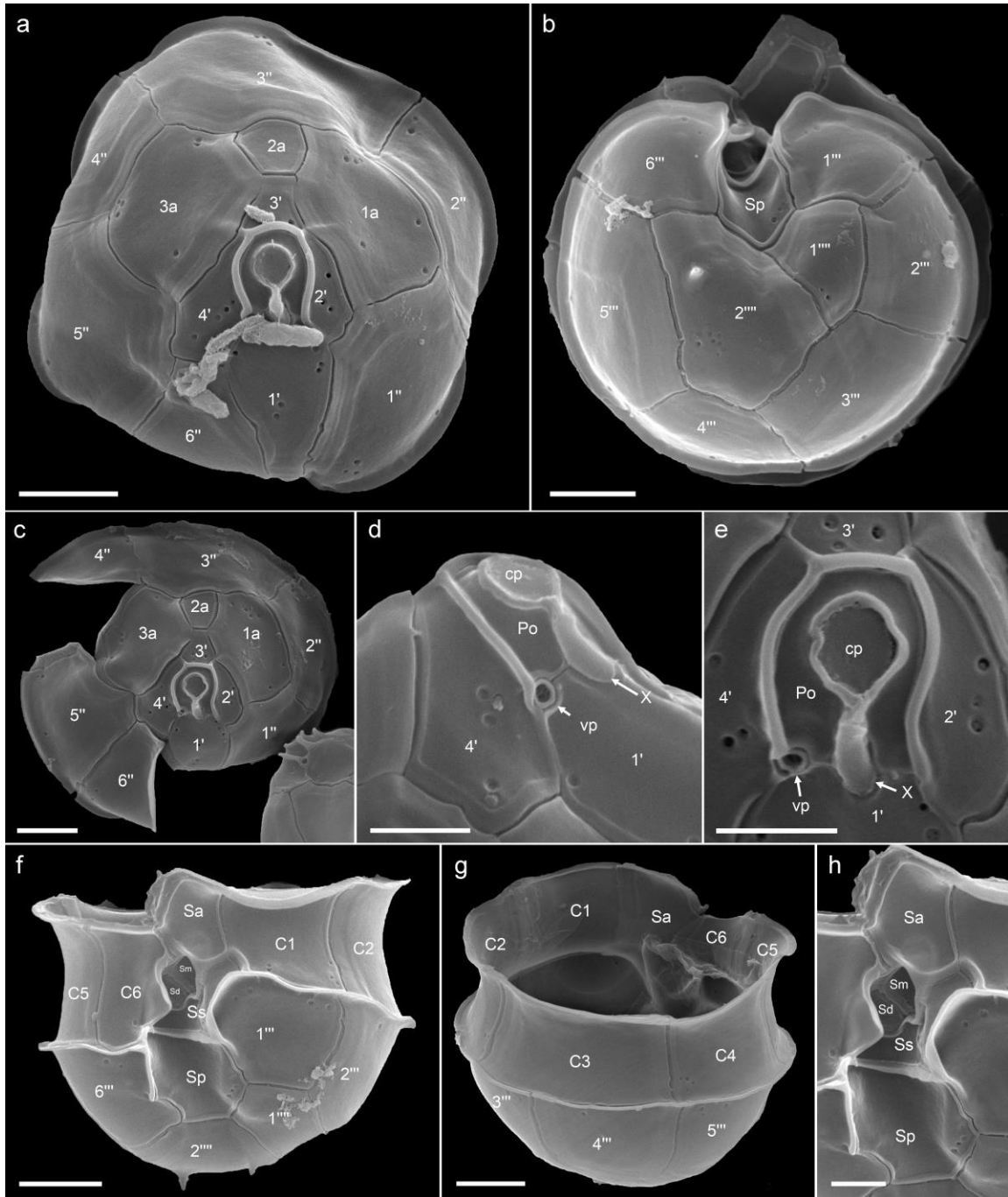


Figure S5. *Azadinium perfuscatorum* strain 2-D1. SEM micrographs of different cells. (a, c) Apical view of epithelial plates. (b) antapical view of hypothecal plates, (d) Apical pore complex (APC) in ventral lateral view. (e) Detailed apical view of the APC. (f) hypotheca in ventral view. (g) hypotheca in apical dorsal view showing cingular plates. (h) Detailed view of sulcal plates. vp, ventral pore; Po, pore plate; X, X-plate; cp, cover plate; Sa, anterior sulcal plate; Sp, posterior sulcal plate; Ss, left sulcal plate; Sm, median sulcal plate; Sd, right sulcal plate. Scale bars: 2 μ m (a–c, f, g) or 1 μ m (d, e, h).

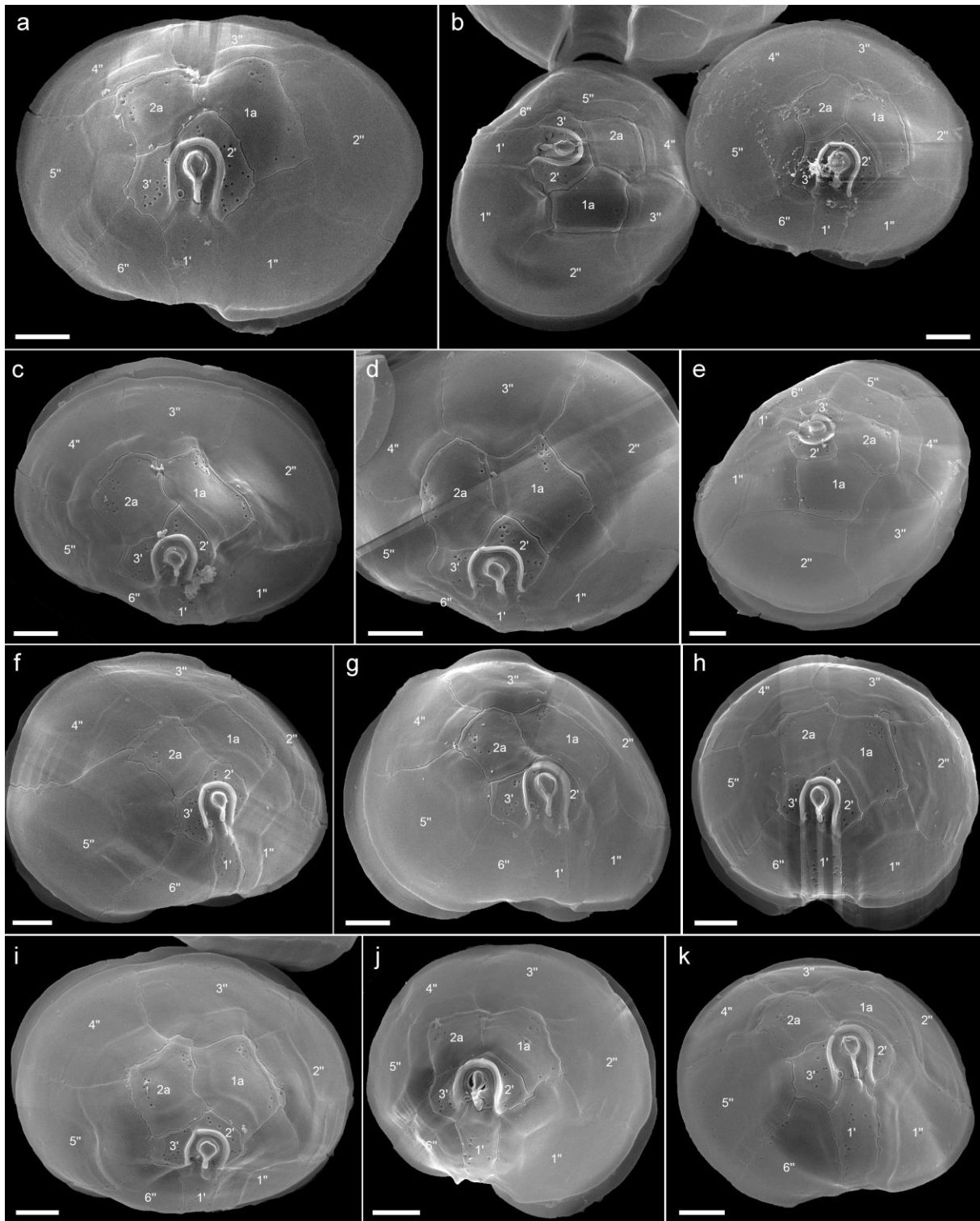


Figure S6. *Azadinium pseudozhuanum* strain 32-R1. (a-k) SEM micrographs of different cells in apical view illustrating epithelial plate configuration. Scale bars: 2 μ m.

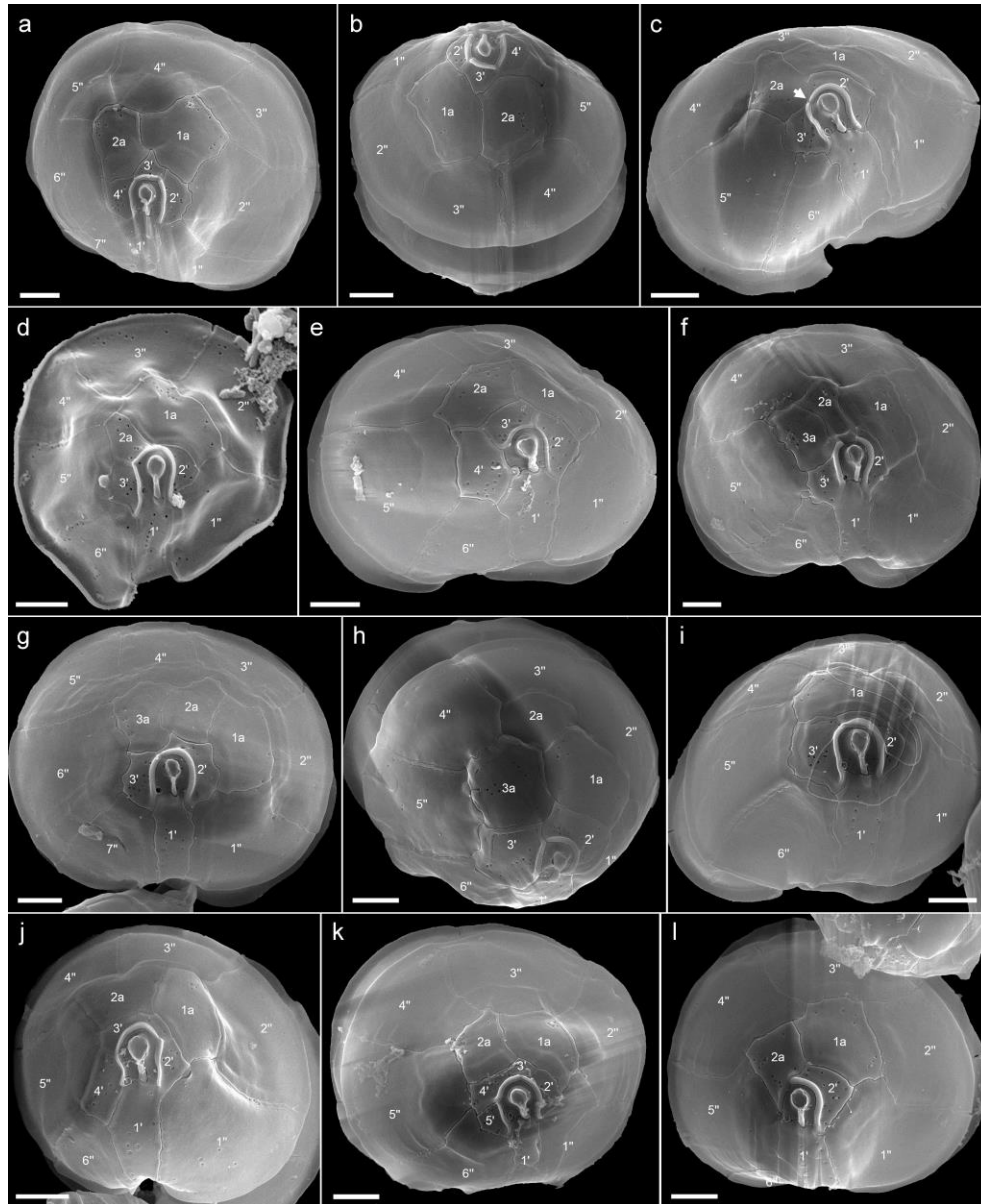


Figure S7. *Azadinium pseudozhuanum* strain 32-R1. (a–l) SEM micrographs of different cells in apical view illustrating deviations from the dominant epithelial plate configuration. (a, b) Four instead of three apical plates in (a) apical or (b) dorsal view. Note that in (a) there are also seven instead of six precingular plates. (c, d) Three apical and two anterior intercalary plates, but here with contact of plate 2a with the pore plate (arrow in c). (e) Four apical plates. Note the lack of the rim around the pore plate along the suture of plate 4'. (f–h) Three apical and three anterior intercalary plates. Note that in (g) plate 2a is in contact to the pore plate and there are seven precingular plates, and that in (h) the plate 2a is without contact to apical plates. (i) Three apical plates and only one anterior intercalary plate. (j) Four apical plates of unusual size and arrangement. (k, l) Aberrant pattern of five (k) and only two (l) apical plates. Scale bars: 2 μ m.

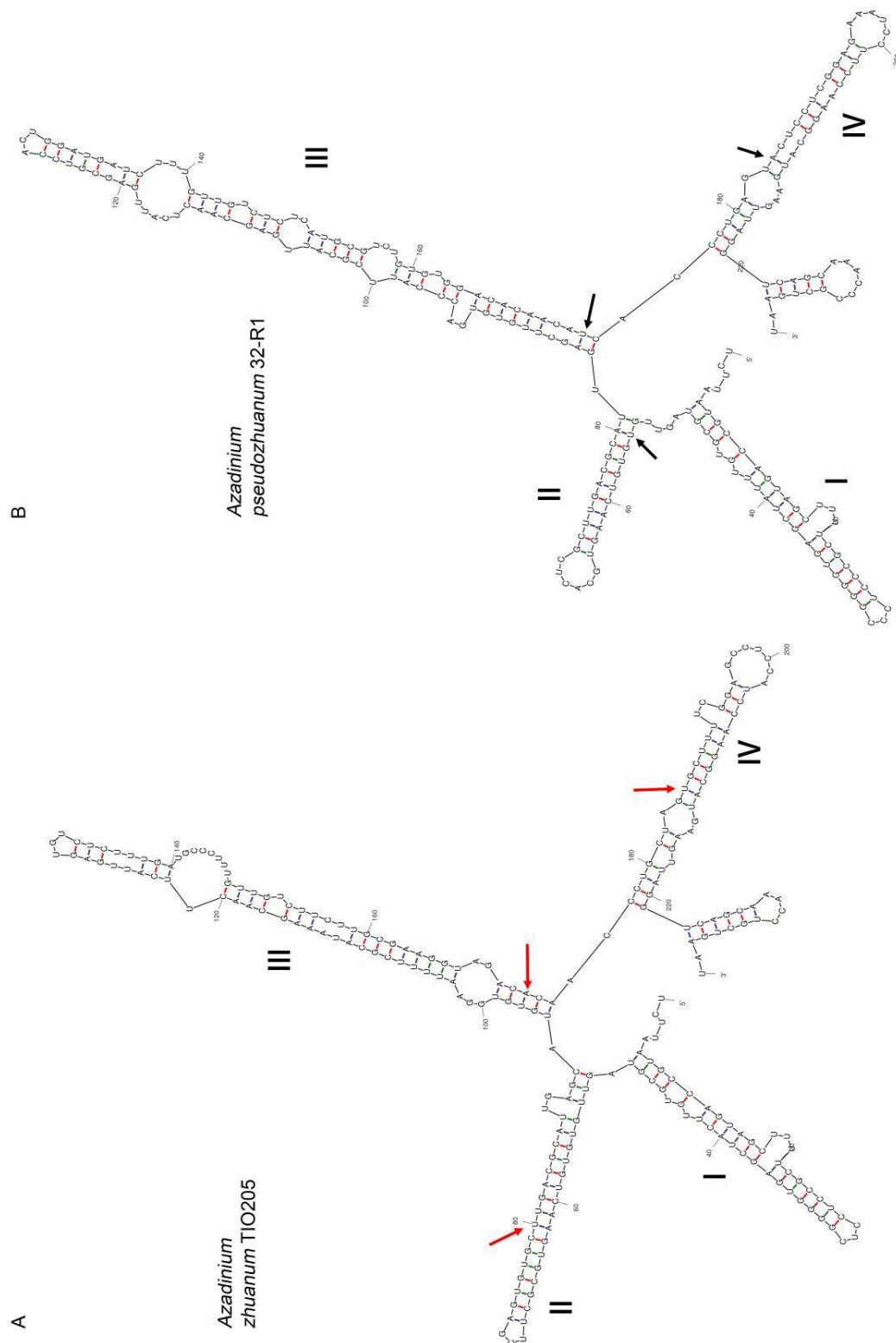


Figure S8. ITS2 secondary structure model of (a) *Az. zhuanum* strain TIO205 and (b) *Az. pseudozhuanum* strain 32-R1 showing four helices (I, II, III and IV). The location of compensatory base pair changes (CBC) are indicated by red and black arrows, respectively.

Table S1: AZA analysis of all strains: Limit of detection (LOD); LOD SRM: LOD in selected reaction monitoring, refers to detection of known AZA. LOD PREC: LOD in precursor mode, refers to detection of yet unknown AZA with AZA typical fragment ions of m/z 348, m/z 350, m/z 360, m/z 362 and m/z 378.

Species	Strain	Origin station	pellet date	pellet cells	LOD SRM (fg/cell)	LOD PREC (fg/cell)
<i>Az. perfusorium</i>	5-B8	35	collection	47,801,400	0.001	0.052
<i>Az. perfusorium</i>	6-C8	22	collection	47,977,950	0.001	0.052
<i>Az. perfusorium</i>	6-B4	45	collection	48,051,400	0.001	0.052
<i>Az. perfusorium</i>	2-D1	35	17.9.18	3,186,018	0.021	n.a.
<i>Az. perfusorium</i>	5-B4	35	17.9.18	592,748	0.115	n.a.
<i>Az. perfusorium</i>	4-H7	35	17.9.18	2,278,373	0.030	n.a.
<i>Az. perfusorium</i>	2-C7	22	11.9.18	1,500,000	0.045	n.a.
<i>Az. perfusorium</i>	4-F9	22	17.9.18	1,092,878	0.062	n.a.
<i>Az. perfusorium</i>	3-F6	35	17.9.18	2,908,167	0.023	n.a.
<i>Az. perfusorium</i>	6-G12	22	17.9.18	3,028,569	0.023	n.a.
<i>Az. perfusorium</i>	6-B7	35	5.10.18	1,505,000	0.021	n.a.
<i>Az. perfusorium</i>	6-A8	22	5.10.18	1,363,650	0.023	n.a.
<i>Az. perfusorium</i>	6-D2	35	5.10.18	1,808,400	0.017	n.a.
<i>Az. perfusorium</i>	6-C3	22	5.10.18	1,737,700	0.018	n.a.
<i>Az. perfusorium</i>	6-C11	35	5.10.19	1,949,750	0.016	n.a.
<i>Az. perfusorium</i>	6-D8	35	5.10.19	2,044,000	0.015	n.a.
<i>Az. perfusorium</i>	6-G3	22	5.10.18	795,200	0.039	n.a.
<i>Az. perfusorium</i>	5-B10	22	25.9.18	2,070,500	0.023	n.a.
<i>Az. perfusorium</i>	9-R1	9	6.1.20	7,966,900	0.003	0.409
<i>Az. perfusorium</i>	9-R2	9	collection	7,410,000	0.003	0.441
<i>Az. perfusorium</i>	10-R1	10	6.1.20	8,040,500	0.003	0.405
<i>Az. perfusorium</i>	10-R2	10	collection	11,795,000	0.002	0.276
<i>Az. perfusorium</i>	10-R3	10	collection	8,806,250	0.003	0.422
<i>Az. perfusorium</i>	35-R2	35	6.1.20	8,821,000	0.003	0.370
<i>Az. perfusorium</i>	35-R3	35	collection	10,580,000	0.002	0.308
<i>Az. galwayense</i>	35-R4	35	collection	23,606,050	0.001	0.106
<i>Az. galwayense</i>	35-R6	35	collection	19,640,000	0.001	0.127
<i>Az. galwayense</i>	35-R7	35	collection	20,410,700	0.001	0.123
<i>Az. pseudozhuanum</i>	32-R1	32	collection	5,854,650	0.003	0.576
<i>Az. caudatum</i>	9-E13	20	19.11.18	148,500	0.174	16.849

Table S2: Selected reaction monitoring (SRM) transitions monitored for AZAs in the strains.

Mass transition	Toxin	Collision energy [V]
716>698	AZA-33	40
816>798	AZA-39, AZA-34	40
816>348	AZA-39	70
828>658	AZA-3, AZA-58	70
828>810	AZA-3, AZA-43	40
830>812	AZA-38, AZA-35	40
830>348	AZA-38	70
842>672	AZA-1	70
842>824	AZA-1, AZA-40	40
842>348	AZA-40	70
844>826	AZA-4, AZA-5, AZA-56	40
846>828	AZA-37	40
846>348	AZA-37	70
854>836	AZA-41	40
854>670	AZA-41	70
854>360	AZA-41	70
856>672	Me-AZA-1, AZA-2	70
856>838	AZA-2	40
858>840	AZA-7, AZA-8, AZA-9, AZA-10, AZA-36	40
858>348	AZA-36	70
860>842	AZA-59	40
868>850	AZA-55	40
868>362	AZA-55	70
870>852	Me-AZA-2, AZA-42, AZA-54, AZA-62	40
870>360	AZA-42	40
872>854	AZA-11, AZA-12	40
872>362	AZA-11, AZA-12	70
884>866	AZA-57	40
922>904	AZA-1 phosphate	40
936>918	AZA-2 phosphate	40
938>920	AZA-36 phosphate	40
940>842	AZA-59 phosphate	40
952>818	AZA-11 phosphate	40

Table S3: Species used for the molecular analyses based on SSU, ITS1–5.8S–ITS2 and LSU sequences, including strain designation, geographic origin and GenBank accession number.

Species Name	Strain No.	Locality (Lat., Long)	GenBank No (SSU/ITS/LSU)	Ribotype	Reference
<i>Amphidoma languida</i>	SM1	North Atlantic, Ireland (51°39'N, 09°35'E)	JN615412 / JQ247699 / JN615413		Tillmann et al., 2012a
	2A11	North Atlantic, Iceland (65°27'N, 24°39'W)	KR362880 / KR362882 / KR362885		Tillmann et al., 2015
	AND-A0920	eastern North Atlantic, Spain, (37°11'N, 07°02'W)	KX671042 / KX671038 / KX671043		Tillmann et al., 2017
	N-33-01	North Atlantic, Norway (61°07'N, 04°28'E)	LS974133 / - / LS974132		Tillmann et al., 2018a
	N-40-04	North Atlantic, Norway (62°43'N, 06°03'E)	LS974145 / - / LS974144		Tillmann et al., 2018a
<i>Amphidoma parvula</i>	H-1E9	Southwest Atlantic, Argentina (41°56'S, 57°43.2'W)	KY996792		Tillmann et al., 2018b
<i>Azadinium caudatum</i> var. <i>caudatum</i>	IFR1191 [IFR10-332, IFR10-330, IFR11-033]	North Atlantic, France (47°50'N, 03°57'W)	JQ247701 / JQ247700 / JQ247702		Nézan et al., 2012
	AC1	North Atlantic, UK–Scotland (58°38'N, 03°36'W)	- / JQ247705 / JQ247709		Nézan et al., 2012
<i>Azadinium caudatum</i> var. <i>margaleffi</i>	IFR1190 [IFR10-020, IFR1140]	North Atlantic, France (47°50'N, 03°57'W)	JQ247707 / JQ247704 / JQ247708		Nézan et al., 2012
	9-E13	North Atlantic, Ireland (50° 41' N, 9° 4' W)	MT644696/MT644669/MT644680		this study
	IC6	North Atlantic, Irminger Sea, (62°14'N, 37°27'W)	- / KJ481829 / KJ481830		Tillmann et al., 2014
<i>Azadinium cuneatum</i>	3D6	North Atlantic, Iceland (65°27'N, 24°39'W)	KJ481822 / KJ481823 / KJ481824		Tillmann et al., 2014
	965F5	Northeast Pacific, USA (47°49'N, 122°48'W)	- / KY404225 / KY404225		Kim et al., 2017
<i>Azadinium dalmanense</i>	AZCH02	East China Sea, China (39°15'N, 122°36'E)	KF543360 / KF543358 / KF543359		Luo et al., 2013
	IFR-ADA-01C	North Atlantic, France	- / MF033117 / MF033126		Luo et al., 2017
	962B3	Northeast Pacific, USA (47°23'N, 122°58'W)	- / KY404221 (ITS+LSU)		Kim et al., 2017
	962B8	Northeast Pacific, USA (47°23'N, 122°58'W)	- / KY404222 (ITS+LSU)		Kim et al., 2017
	N-38-03	North Atlantic, Norway (62°20'N, 05°22'E)	LS974153 (SSU+ITS+LSU)		Tillmann et al., 2018
	N-12-04	North Atlantic, Norway (60°05'N, 04°54'E)	- / LS974150 (ITS+LSU)		Tillmann et al., 2018
	H-2-G7	South Atlantic, Argentina (41°06'S, 57°43'W)	- / MK405513 (ITS+LSU)		Tillmann et al., 2019
	n.inf.	Mediterranean Sea, Gulf of Naples (40°49'N, 14°15'W)	- / KJ179946 / KJ179945		Percopo et al., 2013
	IFR13-318, IFR13-133	North Atlantic, Irminger Sea	- / KR362889 / KR362887		Tillmann et al., 2015
	AZA-2-B1	Labrador Sea, Greenland (56°49'N, 52°13'W)	- / MK882968 / MK882952		Tillmann et al., 2020

Table S3: Continued

Species Name	Strain No.	Locality (Lat., Long)	GenBank No (SSU/ITS/LSU)	Ribotype	Reference
<i>Azadinium gahwayense</i>	35-R4	North Atlantic, Ireland (52° 1' N, 10° 46' W)	MT644697/MT644670/MT644681		this study
	35-R6	North Atlantic, Ireland (52° 1' N, 10° 46' W)	MT644698/MT644671/MT644682		this study
	35-R7	North Atlantic, Ireland (52° 1' N, 10° 46' W)	MT644699/MT644672/MT644683		this study
<i>Azadinium obesum</i>	2E10	North Atlantic, UK-Scotland (57°04'N, 02°30'W)	GQ914935 / FJ766093 / GQ914936		Tillmann et al., 2010
	LF-12-A12	North Atlantic, Denmark (56°41'N, 07°41'E)	- / MK612412 / MK613128		Wietkamp et al., 2019
	LF-44-C03	North Atlantic, Denmark (54°33'N, 10°29'E)	- / MK612413 / MK613126		Wietkamp et al., 2019
	AZA-1G	Labrador Sea, Greenland (56°49'N, 52°13'W)	- / MK882967 / MK882951		Tillmann et al., 2020
	N-41-01		LS974154 / - / LS974155		Tillmann et al., 2018
	AZA-2E	Labrador Sea, Greenland (56°49'N, 52°13'W)	MK883042 / MK882971 / MK882956		Tillmann et al., 2020
	AZA-2H	Labrador Sea, Greenland (56°49'N, 52°13'W)	MK883043 / MK882974 / MK882959		Tillmann et al., 2020
<i>Azadinium perfusorium</i>	2-D1	North Atlantic, Ireland (52° 1' N, 10° 46' W)	MT644700/MT644673/MT644684		this study
	5-B8	North Atlantic, Ireland (52° 1' N, 10° 46' W)	MT644701/MT644674/MT644685		this study
	6-B4	North Atlantic, Ireland (53° 37' N, 9° 54' W)	MT644702/MT644675/MT644686		this study
	10-R1	North Atlantic, UK (50° 20' N, 6° 4' W)	MT644690		this study
	10-R2	North Atlantic, UK (50° 20' N, 6° 4' W)	MT644691		this study
	10-R3	North Atlantic, UK (50° 20' N, 6° 4' W)	MT644692		this study
	35-R2	North Atlantic, Ireland (52° 1' N, -10° 46' W)	MT644693		this study
	9-R2	North Atlantic, UK (50° 2' N, 5° 58' W)	MT644689		this study
	6-C8	North Atlantic, Ireland (51° 1' N, 9° 4' W)	- / MT644676/MT644687		this study
	9-R1	North Atlantic, UK (50° 2' N, 5° 58' W)	- / MT644677/MT644688		this study
	35-R3	North Atlantic, Ireland (52° 1' N, 10° 46' W)	- / MT644678/MT644694		this study
<i>Azadinium pseudo-zhuanum</i>	32-R1	North Atlantic, Ireland (51° 32' N, 10° 0' W)	- / MT644679/MT644695		this study
<i>Azadinium polongum</i>	SHEB2	North Atlantic, Shetland Islands (60°13' N, 01°00' W)	JX559886 (SSU+ITS+LSU)		Tillmann et al., 2012b
	N-47-01	North Atlantic, Norway (63°58' N, 08°37' E)	- / LS974156 (ITS+LSU)		Tillmann et al., 2018
<i>Azadinium poporum</i>	UTHC8	North Atlantic, Denmark (56°15' N, 07°28' E)	HQ324898 / HQ324890 / HQ324894	A	Tillmann et al., 2011
	TIO256	Mediterranean, France (42°08' N, 09°32' E)	MF033112 / MF033116 / MF033123	A	Luo et al., 2017
	1-C11	Southeast Pacific, Chile	- / KX133011 / KX133014	A	Tillmann et al., 2017
	968B7	North-East Pacific USA (47°49' N, 122°48' W)	- / KY404217 (ITS+LSU)	A	Kim et al., 2017
	AZFC15	South China Sea, China (21°30' N, 108°14' E)	- / KC286569 / KC286550	B	Gu et al., 2013

Table S3: Continued

Species Name	Strain No.	Locality (Lat., Long)	GenBank No (SSU/ITS/LSU)	Ribotype	Reference
<i>Azadinium spinosum</i>	AZFC16	South China Sea, China (21°30'N, 108°14'E)	- / KC286579 / KC286556	C	Gu et al., 2013
	GM29	Gulf of Mexico, USA	- / KU686476 / KU686475	C	Luo et al., 2016
	TIO431	Mediterranean Sea, Greece (39°30'N, 20°15'E)	- / MH685508 / MH685486	A	Luo et al., 2018
	N-39-13	North Atlantic, Norway (62°28'N, 05°46'E)	LS974158 (SSU+ITS+LSU)	A	Tillmann et al., 2018
	LF-14-E12	North Atlantic, Denmark (56°37'N, 08°20'E)	- / MK612414 / MK613129	A	Wietkamp et al., 2019
	3D9	North Atlantic, UK–Scotland (57°04'N, 02°30'W)	FJ217814 / FJ217816 / FJ217815		Tillmann et al., 2009
	SHETF6	North Atlantic, Shetland Islands (60°13'N, 01°00'W)	JX559885 (SSU+ITS+LSU)		Tillmann et al., 2012b
	UTHE2	North Atlantic, Denmark (56°15'N, 07°28'E)	HQ324900 / HQ324892 / HQ324896		Tillmann et al., 2011
	N-04-02	North Atlantic, Norway (58°15'N, 06°24'E)	LS974160 (SSU+ITS+LSU)		Tillmann et al., 2018
	H-1-H10	South Atlantic, Argentina (41°06'S, 57°43'W)	- / MK405497 (ITS+LSU)		Tillmann et al., 2019
	H-2-D8	South Atlantic, Argentina (41°06'S, 57°43'W)	- / MK405500 (ITS+LSU)		Tillmann et al., 2019
	N-05-01	North Atlantic, Norway	LS974163 (SSU+ITS+LSU)		Tillmann et al., 2018
N-16-02	North Atlantic, Norway (60°52'N, 04°34'E)	LS974168 (SSU+ITS+LSU)		Tillmann et al., 2018	
N-04-04	North Atlantic, Norway (58°15'N, 06°24'E)	LS974162 / - / LS974161		Tillmann et al., 2018	
<i>Azadinium trinitatum</i>	4A8	North Atlantic, Iceland (64°43'N, 24°02'W)	KJ481808 / KJ481809 / KJ481810		Tillmann et al., 2014
	A2D11	North Atlantic, Iceland (64°43'N, 24°02'W)	KJ481803 / KJ481806 / KJ481807		Tillmann et al., 2014
	N-39-04	North Atlantic, Norway (62°28'N, 05°46'E)	LS974170 (SSU+ITS+LSU)		Tillmann et al., 2018
	AZA-2F	Labrador Sea, Greenland (56°49'N, 52°13'W)	- / MK882972 / MK882957		Tillmann et al., 2020
	AZA-Z-E10	Labrador Sea, Greenland (56°49'N, 52°13'W)	- / MK882979 / MK882964		Tillmann et al., 2020
	TIO205	East China Sea, China (27°28'N, 121°03'E)	MF033110 / MF033114 / MF033120		Luo et al., 2017
TIO213	East China Sea, China (27°28'N, 121°03'E)	MF033111 / MF033115 / MF033121		Luo et al., 2017	
<i>Azadinium zhuanum</i>	TIO205	East China Sea, China (27°28'N, 121°03'E)	MF033110 / MF033114 / MF033120		Luo et al., 2017
	TIO213	East China Sea, China (27°28'N, 121°03'E)	MF033111 / MF033115 / MF033121		Luo et al., 2017

Publication VII: New amphidomatacean strains from the North Atlantic

Multiple new strains of Amphidomataceae (Dinophyceae) from the North Atlantic revealed a high toxin profile variability of *Azadinium spinosum* and a new non-toxicogenic *Az. cf. spinosum* *Microorganisms*

Tillmann, U., Wietkamp, S., Gu, H., Krock, B., Salas, R., Clarke, D. (submitted)

Publication VII contains the description of multiple new toxicogenic *Amphidoma languida* and *Azadinium spinosum* strains isolated during the field campaign HE-516 in Irish, Scottish and North Sea waters in 2018. Moreover, five non-toxicogenic strains, which conformed in morphology with *Azadinium spinosum* were characterized and, based on molecular phylogenetic analyses, were designated as *Az. cf. spinosum*.

Previous studies on the intra-specific variation of Amphidomataceae, as characterized by slightly different morphology, DNA sequences and AZA profiles, led to the erection of different ribotypes within the species *Az. spinosum* and *Az. poporum*. So far, non-toxicogenic *Az. spinosum* were only reported from field samples taken off Argentina. The finding of *Az. cf. spinosum*, which were morphologically identical to *Az. spinosum*, but were negative for AZA, increased the number of intra-specific variants.

The candidate contributed to this study by performing DNA extraction, sequencing and toxin analysis of all 82 established strains (100%). He performed specificity testing of the current qPCR assays on *Az. spinosum*, *Az. poporum* and *Am. languida* with DNA of the new strains (100%). He contributed to the manuscript preparation (25%) led by Dr. U. Tillmann (AWI) with focus on the sequencing, qPCR and AZA part.

Multiple new strains of Amphidomataceae (Dinophyceae) from the North Atlantic revealed a high toxin profile variability of *Azadinium spinosum* and a new non-toxigenic *Az. cf. spinosum*

Urban Tillmann^{1*}, Stephan Wietkamp¹, Haifeng Gu^{2,3}, Bernd Krock¹, Rafael Salas⁴, Dave Clarke⁴

¹ Alfred Wegener Institute, Helmholtz Center for Polar and Marine Research, Am Handelshafen 12, D-27570 Bremerhaven, Germany

² Third Institute of Oceanography, Ministry of Natural Resources, Xiamen 361005, People's Republic of China

³ School of Marine Sciences, Nanjing University of Information Science and Technology, Nanjing, 210044, China

⁴ Marine Institute, Rinville, Oranmore, Co.Galway, H91 R673, Republic of Ireland

* Correspondence: urban.tillmann@awi.de; Tel.: +49 9471 4831 1470

Received: date; Accepted: date; Published: date

Abstract: Azaspiracids (AZA) are a group of lipophilic toxins, which are produced by a few species of the marine nanoplanktonic dinoflagellates *Azadinium* and *Amphidoma* (Amphidomataceae). A survey was conducted in 2018 to increase knowledge on the diversity and distribution of amphidomatacean species and their toxins in Irish and North Sea waters (North Atlantic). We here present a detailed morphological, phylogenetic, and toxinological characterizations of 82 new strains representing the potential AZA producers *Azadinium spinosum* and *Amphidoma languida*. A total of ten new strains of *Am. languida* were obtained from the North Sea and all conformed in terms of morphology and toxin profile (AZA-38 and-39) with previous records from the area. Within 72 strains assigned to *Az. spinosum* there were strains of two distinct ribotypes (A and B) which consistently differed in their toxin profile (dominated by AZA-1 and-2 in ribotype A, and by AZA-11 and -51 in ribotype B strains). Five strains conformed in morphology with *Az. spinosum*, but no AZA could be detected in these strains. Moreover, they

revealed significant nucleotide differences compared to known *Az. spinosum* sequences and clustered apart from all other *Az. spinosum* strains within the phylogenetic tree, and therefore were provisionally designated as *Az. cf. spinosum*. These *Az. cf. spinosum* strains without detectable AZA were shown not to cause amplification in the species-specific qPCR assay developed to detect and quantify *Az. spinosum*. As shown here for the first time, AZA profiles differed between strains of *Az. spinosum* ribotype A in presence/absence of AZA-1, -2 and/or AZA-33, with the majority of strains having all three AZA congeners, and others having only AZA-1, AZA-1 and -2, or AZA-1 and -33. In contrast, no AZA profile variability was observed in ribotype B strains. Multiple AZA analyses of a period of up to 18 months showed that toxin profiles (including absence of AZA for *Az. cf. spinosum* strains) were consistent and stable over time. Total AZA cell quotas were highly variable both among and within strains, with quotas ranging from 0.1 to 63 fg AZA cell⁻¹. Cell quota variability of single AZA compounds for *Az. spinosum* strains could be as high as 330-fold, but the underlying causes for the extraordinary large variability of AZA cell quotas is poorly understood.

Keywords: azaspiracids; toxin profile; toxin cell quota; variability; ribotype

1. Introduction

Azaspiracids (AZA) are polyether lipophilic marine biotoxins that accumulate in filter-feeding bivalves. AZA have been associated with human incidents of shellfish poisoning since the first intoxication case in 1995 attributed to Irish mussels (McMahon and Silke, 1996; Satake et al., 1998a). To date seven human azaspiracid shellfish poisoning (AZP) events have been confirmed in The Netherlands, Ireland, Italy, France, the UK and the US (Twiner et al., 2008; Twiner et al., 2014), and each of these AZP events have been traced to contaminated Irish shellfish.

Although AZA now have been reported in shellfish and/or plankton samples from numerous geographical sites of the Atlantic (James et al., 2002; Braña Magdalena et al., 2003; Amzil et al., 2008; Vale et al., 2008; Turner and Goya, 2015; Dhanji-Rapkova et al., 2019) or Pacific (Ueoka et al., 2009; Alvarez et al., 2010; López-Rivera et al., 2010; Yao et al., 2010; Trainer et al., 2013), Ireland with its important shellfish industry remains the country most seriously affected by AZA related problems. AZA concentrations above the EU threshold level of 0.16 mg kg⁻¹ shellfish meat have exceptionally been recorded in Norway in 2002/2003 (Aasen et al., 2004) and along the Atlantic coast of southern Spain in 2009 (Tillmann et al., 2017a). However, elevated AZA levels in Ireland have led to recurrent and extended production site closures with severe economic consequences for the shellfish industry since 2002 (Salas et al., 2011; Kilcoyne et al., 2014a). Accordingly, there is a need to increase knowledge on the diversity and distribution of AZA-producing species in order to allow better identification and quantification of these species in national monitoring programs. Moreover, detailed knowledge on the biology, toxin profile, cell quota and the regulating factors of local populations is required for better understanding of bloom formation, bloom dynamics and bloom impacts on shellfish and the marine environment.

With the formal description of the new small dinoflagellate *Azadinium spinosum* Elbrächter & Tillmann (Amphidomataceae), the first source organism of AZA was identified (Tillmann et al., 2009). Amphidomataceae include *Azadinium* and the closely related genus *Amphidoma*, and now more than 30 amphidomatacean species are known, of which only four, *Az. spinosum*, *Az. poporum* Tillmann & Elbrächter, *Az. dexteroporum* Percopo & Zingone, and *Amphidoma languida* Tillmann, Salas & Elbrächter, are known to produce AZA (Krock et al., 2012; Tillmann et al., 2012a; Rossi et al., 2017). The first strains of *Az. spinosum* originating from Scotland, Denmark and the Shetland Islands all share the same toxin profile, i.e., AZA-1, -2 and -33 (Tillmann et al., 2012b; Tillmann et al., 2014c), as did the first and only strain isolated from Irish waters in 2011 (Salas et al., 2011).

However, more recent studies revealed significant intraspecific variability within *Az. spinosum* by identifying a new ribotype B, which has a fundamentally different toxin profile consisting of AZA-11 and -51 (Tillmann et al., 2018a). Moreover, another *Az. spinosum* ribotype (assigned as ribotype C) identified from the Argentinean shelf does not contain any AZA (Tillmann et al., 2019). Toxigenic specimen of ribotype B are of special concern, as sequence data and actual testing show that such strains are not quantitatively captured by the current *Az. spinosum* qPCR assay (Tillmann et al. (2018a), Publication V), whose design was based on ribotype A strains (Toebe et al., 2013). Considering the large number of amphidomatacean species known today and the high intraspecific variability of gene sequences and toxin production potential (Tillmann et al., 2015; Luo et al., 2018; Tillmann et al., 2018a), it is remarkable that knowledge of the diversity in Irish waters is based on two strains only, i.e. one strain of *Az. spinosum* (Salas et al., 2011) and one strain of *Am. languida* (Tillmann et al., 2012a). Detailed knowledge on the local species inventory, however, is important to identify other yet unknown sources of AZA and/or to evaluate the potential of local non-toxigenic species/strains for false positive signals either in LM based and/or PCR based monitoring programs. Moreover, potential intraspecific variability of the presumably most important Irish AZA-producer, *Az. spinosum*, is completely unknown for Irish waters at present. Therefore, in summer 2018, a research survey in the Celtic Sea, in Irish coastal waters and in the North Sea was undertaken. The specific focus of this survey was to increase knowledge about the diversity and distribution of Amphidomataceae and their respective toxins in Irish coastal waters and in the North Sea. Field data of this survey including qPCR-based abundance and distribution of toxigenic amphidomatacean species and their toxins are presented elsewhere (Wietkamp et al., 2020). Next to field-sample data, on-board cell isolation and establishment of a large number of clonal amphidomatacean strains aimed at a better description of amphidomatacean diversity in the area. From 113 successfully isolated new strains from the survey, also non-toxigenic strain of four species (three of them new species) are presented elsewhere (Publication VI). The focus of the present paper is to present detailed morphological, phylogenetic, and toxinological characterizations of 82 new strains representing the potential AZA producers *Az. spinosum* and *Am. languida*.

2. Materials and Methods

2.1.1 Sampling

Samples were collected during the survey (HE-516) on-board *RV Heincke* between 17th July and 15th August, 2018 covering the South- and West coast of Ireland and the North Sea (for a full list of stations see Wietkamp et al. (2020); CTD data are stored in Pangaea (Krock and Wisotzki, 2018)). At each station, plankton samples were collected with 10 L Niskin bottles at 3 m, 10 m and the depth-chlorophyll-maximum (DCM) layer. Five liters of seawater from each depth were filtered through a 20 µm mesh-size Nitex sieve, pooled, and well mixed.

2.1.3 On board microscopy

Mixed bottle samples were used for on board microscopical observation and documentation of live cells of Amphidomataceae. One-liter samples were pre-screened (20 µm Nitex mesh), gently concentrated by gravity filtration using a 3-µm polycarbonate filter (47 mm diameter, GE Healthcare, Little Chalfont, UK), and examined using an inverted microscope (Axiovert 200M, Zeiss, Göttingen, Germany). Cells of *Azadinium* and/or *Amphidoma* were pre-identified at high magnification (640X) based on general cell size and shape, on the presence of a theca, and on the presence of a distinctly pointed apex. Cells of interest were photographed with a digital camera (AxioCam MRc5, Zeiss).

2.1.4 Onboard isolation and culture

Pre-identified cells of Amphidomataceae detected during the onboard live sample observations were isolated by micro-capillary into wells of 96-well plates filled with 0.2 mL filtered seawater from the sampling side. Plates were incubated at 15 °C under a photon flux density of approx. 50 µmol m⁻² s⁻¹ on a 16:8 h light:dark photocycle in a controlled environment growth chamber (Model MIR 252, Sanyo Biomedical, Wood Dale, USA).

2.2 Characterisation of Amphidomataceae strains

2.2.1 Culture growth, sampling and extraction

Isolation plates from the cruise were inspected after two weeks using a stereomicroscope (SZH-ILLD, Olympus, Hamburg, Germany) for the presence of *Azadinium*-like cells as inferred from the typical size, shape, and swimming behavior. From each positively identified well, a clonal strain was established by isolation of single cells via micro-capillary and established cultures were

thus clonal but not axenic. The clonal cultures were maintained in 70 mL plastic culture flasks at 15 °C in a natural seawater medium prepared with sterile-filtered (0.2 µm VacuCap filters, Pall Life Sciences, Dreieich, Germany) Antarctic seawater (salinity: 34, pH adjusted to 8.0) and enriched with 1/10 strength K-medium [(Keller et al., 1987); slightly modified by omitting addition of ammonium ions].

For DNA extraction, each strain was grown in 70 mL plastic culture flasks at 15 °C under a photon flux density of 70 µmol m⁻² s⁻¹ on a 16:8 h light:dark photoperiod. Fifty mL of healthy and growing culture (based on stereomicroscopic inspection of the live culture) were harvested by centrifugation (Eppendorf 5810R, Eppendorf, Hamburg, Germany; 3,220 x g, 10 min). Each pellet was transferred to a microtube, again centrifuged (Eppendorf 5415; 16,000 x g, 5 min), and stored frozen in 500 µL SL1 lysis buffer (provided by the DNA extraction kit) at –80 °C until DNA extraction.

For toxin analysis, strains were grown under the standard culture conditions described above. For each harvest, cell density was determined by settling Lugol's fixed samples and counting >400 cells under an inverted microscope in order to calculate toxin cell quota. Densely grown strains (ranging from ca. 1 – 7 x 10⁴ cells mL⁻¹) were harvested by centrifugation (Eppendorf 5810R) at 3,220 x g for 10 min of 50 mL subsamples. The cell pellet was resuspended, transferred to a microtube, centrifuged again (Eppendorf 5415, 16,000 x g, 5 min), and stored frozen (–20 °C) until use. For a number of selected strains, growth and harvest procedures were repeated several times to yield a high biomass for an increased sensitivity of the toxin detection method. Total number of cells harvested for these strains is listed in Supplementary Tab. S2. A number of selected strains of *Azadinium spinosum* were sampled and analyzed for their AZA profile several times at various time points in a period of up to 18 months after isolation to evaluate temporal stability of the toxin profile.

Cell pellets were extracted with 500 µL acetone and were vortexed every 10 min during one hour at room temperature. Homogenates were centrifuged (Eppendorf 5810 R) at 15 °C and 3,220 x g for 15 min. Filtrates were then adjusted with acetone to a final volume of 0.5 mL. The extracts were transferred to a 0.45 µm pore-size spin-filter (Millipore Ultrafree, Millipore, Burlington, USA) and centrifuged (Eppendorf 5415 R) at 800 x g for 30 s, with the resulting filtrate transferred into a liquid chromatography (LC) autosampler vial for LC-MS/MS analysis.

2.2.2 Microscopy

Light microscopy (LM)

Observation of living or fixed cells was carried out with an inverted microscope (Axiovert 200 M, Zeiss) or a compound microscope (Axioskop 2, Zeiss) by recording videos using a digital camera (Gryphax, Jenoptik, Jena, Germany) at full-HD resolution. Single frame micrographs were extracted using Corel Video Studio software (Version X8 pro). The shape and location of the nucleus was determined after staining of formalin-fixed cells with 4'-6-diamidino-2-phenylindole (DAPI, 0.1 $\mu\text{g mL}^{-1}$ final concentration) for 10 min. Cell length and width were measured at 1,000X microscopic magnification using Zeiss Axiovision software (Zeiss) and photographs of formaldehyde-fixed cells (1% final concentration) of strains growing at 15 °C taken with a digital camera (AxioCam MRc5, Zeiss).

Scanning electron microscopy (SEM)

For SEM, cells were collected by centrifugation (Eppendorf 5810R; 3,220 x g, 10 min) of 15 mL of culture. The supernatant was removed and the cell pellet re-suspended in 60% ethanol in a 2 mL microtube for 1 h at 4 °C to strip off the outer cell membrane. Subsequently, cells were pelleted by centrifugation (Eppendorf 5415 R, 16,000 x g, 5 min) and re-suspended in a 60:40 mixture of deionized water and seawater for 30 min at 4 °C. After centrifugation and removal of the diluted seawater supernatant, cells were fixed with formaldehyde (2% final concentration in a 60:40 mixture of deionized water and seawater) and stored at 4 °C for 3 h. Cells were then collected on polycarbonate filters (Millipore, 25 mm \varnothing , 3 mm pore-size) in a filter funnel where all subsequent washing and dehydration steps were carried out. A total of eight washings (2 mL deionized water each) were followed by a dehydration series in ethanol (30, 50, 70, 80, 95, 100%; 10 min each). Filters were dehydrated with hexamethyldisilazane (HMDS), first in 1:1 HMDS:EtOH followed by two times 100% HMDS, and then stored under gentle vacuum in a desiccator. Finally, filters were mounted on stubs, sputtercoated (SC500, Emscope, Ashford, UK) with gold-palladium and viewed under a scanning electron microscope (Quanta FEG 200, FEI, Eindhoven, Netherlands). Some SEM micrographs were presented on a black background using Adobe Photoshop 6.0 (Adobe Systems, San Jose, USA).

2.2.3 Molecular phylogeny

PCR amplification and DNA sequencing

The cell pellets for DNA extraction were collected in individual bead tubes together with 500 μL of the SL1 lysis buffer, both provided by the NucleoSpin Soil DNA extraction kit (Macherey & Nagel, Düren, Germany). The DNA extraction followed the manufacturer's instructions, with a slight variation. The bead tubes were not vortexed but shaken for 45 s and another 30 s at a speed of 4.0 m s^{-1} in a cell disrupter (FastPrep FP120, Thermo-Savant, Illkirch, France). For DNA elution, 2 x 50 μL of the provided elution buffer were used (to a final elution volume of 100 μL) to maximize the overall DNA yield. DNA was stored at $-20 \text{ }^\circ\text{C}$ until further processing.

Sanger-Sequencing of strain DNA was performed for the 18S/small subunit (SSU), the Internal Transcribed Spacer region (ITS1, 5.8S rRNA, ITS2) and the D1/D2 region of 28S/large subunit (LSU), using the following primer sets: 1F (5' – AAC CTG GTT GAT CCT GCC AGT – 3') and 1528R (5' – TGA TCC TTC TGC AGG TTC ACC TAC – 3') for SSU; ITSa (5' -CCA AGC TTC TAG ATC GTA ACA AGG (ACT)TC CGT AGG T-3') and ITSb (5' -CCT GCA GTC GAC A(GT)A TGC TTA A(AG)T TCA GC(AG) GG-3') for ITS; DirF (5' -ACC CGC TGA ATT TAA GCA TA-3') and D2CR (5' -CCT TGG TCC GTG TTT CAA GA-3') for LSU.

One part of the final sequences was gained by sending extracted DNA and primers to Eurofins sequencing facilities (Eurofins Genomics, Ebersberg, Germany), where sequences were generated on an ABI 3730 XL sequencer (Applied Biosystems by Thermo Fisher Scientific, Waltham, Massachusetts, USA) according to internal sequencing procedures.

The second part of sequences was generated at the Alfred-Wegener-Institute (Helmholtz Center for Polar- and Marine Research, Bremerhaven, Germany). Each PCR reaction contained 16.3 μL ultra-pure H_2O , 2.0 μL HotMaster Taq buffer (5Prime, Hamburg, Germany), 0.2 μL dNTPs (10 μM), 0.2 μL of each primer (10 μM), 0.1 μL of Taq Polymerase (Quantabio, Beverly, Massachusetts, USA) and 1.0 μL of extracted DNA template (10 $\text{ng } \mu\text{L}^{-1}$) to a final reaction volume of 20 μL . PCR were conducted in a Nexus Gradient Mastercycler (Eppendorf) with conditions described in Tillmann et al. (2020). The PCR amplicons were checked on a 1% agarose gel (in TE buffer, 70 mV, 30 min) to verify the expected length. The PCR amplicon was purified using the NucleoSpin Gel and PCR clean-up kit (Macherey-Nagel) and sequenced directly in both directions on an ABI PRISM 3730XL (Applied Biosystems by ThermoFisher Scientific) as described in Tillmann et al. (2017c). Raw sequence data were processed using the CLC Genomics Workbench 12 (Qiagen, Hilden, Germany).

Phylogenetic analyses

Newly obtained SSU, ITS1-5.8S-ITS2 and/or partial LSU rRNA gene sequences were incorporated into available *Amphidoma*, *Azadinium* and closely related sequences in GenBank. GenBank accession numbers are listed in Supplementary Table S3. Concatenated sequences were aligned using MAFFT v7.110 (Katoh and Standley, 2013) online program (<http://mafft.cbrc.jp/alignment/server/>). Alignments were manually checked with BioEdit v. 7.0.5 (Hall, 1999). Completed alignments of ITS1-5.8S-ITS2 sequences were imported into PAUP *4b10 software (Swofford, 2002) to estimate divergence rates using simple uncorrected pairwise (p) distance matrices. The secondary structures of ITS2 sequences of five strains of *Az. spinosum* or *Az. cf. spinosum* were predicted using the Mfold program (Zuker, 2003) (<http://mfold.rit.albany.edu/?q=mfold/RNA-Folding-Form>).

For Bayesian inference (BI), the program jModelTest (Posada, 2008) was used to select the most appropriate model of molecular evolution with Akaike Information Criterion (AIC). Bayesian reconstruction of the data matrix was performed using MrBayes 3.2 (Ronquist and Huelsenbeck, 2003) with the best-fitting substitution model (GTR+G). Four Markov chain Monte Carlo (MCMC) chains ran for 10,000,000 generations, sampling every 1,000 generations. The convergence of the MCMC chains was examined in TRACER 1.7 (Rambaut et al., 2018), and the first 10% of the samples were discarded as ‘burn-in’, well after stationarity had been reached. A majority rule consensus tree was created in order to examine the posterior probabilities of each clade. Maximum likelihood (ML) analyses were conducted with RaxML v7.2.6 (Stamatakis, 2006) on the T-REX web server (Boc et al., 2012). Data were analyzed using the GTR+G approximation and the rapid hill-climbing algorithm was used. Node support was assessed with 1,000 bootstrap replicates.

qPCR assay specificity of newly obtained strains

Newly obtained strain DNA sequences were aligned with the primer and probe sequences of the current *Az. spinosum* qPCR assay using MEGA7 (Kumar et al., 2016) to look *in silico* for base pair (bp) mismatches, which potentially affect the assay specificity.

Subsequently, DNA of newly obtained *Az. spinosum* ribotype A (4-F8, 5-C11, 6-G8), ribotype B (5-F3, 8-B8), *Az. cf. spinosum* (1-H10, 2-A3, 5-B9, 5-D3, 6-A1) and *Am. languida* (5-F11, 8-D10) strains was subjected to *in vitro* specificity testing with the current qPCR assays for *Az. spinosum*, *Az. poporum* and *Am. languida* following the detailed descriptions in Wietkamp et al. (2020).

2.2.4 Chemical analysis of azaspiracids

Extracts of strains were screened for known AZA in the selected reaction monitoring (SRM) mode with an analytical system consisting of triple quadrupole mass spectrometer (API 4000 QTrap, Sciex, Darmstadt, Germany) equipped with a TurboSpray interface coupled to LC equipment (model LC 1100, Agilent, Waldbronn, Germany) that included a solvent reservoir, inline degasser (G1379A), binary pump (G1311A), refrigerated autosampler (G1329A/G1330B), and temperature-controlled column oven (G1316A). Separation of AZA (5 μ L sample injection volume) was performed by reverse-phase chromatography on a C8 phase. The analytical column (50 \times 2 mm) was packed with 3 μ m Hypersil BDS 120 Å (Phenomenex, Aschaffenburg, Germany) and maintained at 20 °C. The flow rate was 0.2 mL min⁻¹, and gradient elution was performed with two eluents, where eluent A was water and eluent B was acetonitrile/water (95:5 v/v), both containing 2.0 mM ammonium formate and 50 mM formic acid. Initial conditions were 8-min column equilibration with 30% B, followed by a linear gradient to 100% B in 8 min and isocratic elution until 18 min with 100% B then returning to initial conditions until 21 min (total run time: 29 min). AZA profiles were determined in the SRM mode in one period (0–18) min with curtain gas: 10 psi, CAD: medium, ion spray voltage: 5,500 V, temperature: ambient, nebuliser gas: 10 psi, auxiliary gas: off, interface heater: on, declustering potential: 100 V, entrance potential: 10 V, exit potential: 30 V. SRM experiments were carried out in positive ion mode by selecting the transitions shown in Supplementary Table S1.

In addition, precursor ion experiments were performed. Precursors of the characteristic AZA fragments m/z 348, m/z 350, m/z 360, m/z 362 and m/z 378 were scanned in the positive-ion mode from m/z 500 to 1,000 under the following conditions: curtain gas, 10 psi; CAD, medium; ion spray voltage, 5,500 V; temperature, ambient; nebuliser gas, 10 psi; auxiliary gas, off; interface heater, on; declustering potential, 100 V; entrance potential, 10 V; collision energy, 70 V; exit potential, 12 V. Collision induced dissociation (CID) spectra of the m/z values 716, 830, 842, 856, 858 and 872 were recorded in the Enhanced Product Ion (EPI) mode in the mass range from m/z 150 to 930. Positive ionization and unit resolution mode were used. The following parameters were applied: curtain gas: 10 psi, CAD: medium, ion spray voltage: 5,500 V, temperature: ambient, nebulizer gas: 10 psi, auxiliary gas: off, interface heater: on, declustering potential: 100 V, collision energy spread: 0, 10 V, collision energy: 70 V, exit potential, 12 V.

2.3 Statistics

Data of AZA cell quota and ratios were plotted using the box-whisker plot option of Microsoft Excel using median, and first and third quartile, and plotting all data points. Outliers were defined as outside 1.5 x interquartile range. AZA cell quota and AZA ratios were tested for normal distribution by Shapiro-Wilk tests. Based on these results all AZA cell quota and ratios were tested by One-Way-ANOVA on ranks (Kruskal-Wallis test). Statistical testing was performed using Statistica (version 9.1, StatSoft, Tulsa, USA).

3. Results

A total of 113 new strains of Amphidomataceae was obtained from the Irish coast and from the central North Sea (Tab. 1). Of those, a total of 31 non-toxigenic strains representing *Azadinium caudatum* var. *margalefii* (1 strain), as well as three new species *Az. pseudozhuanum* (1 strain), *Az. galwayense* (3 strains) and *Az. perfusorium* (26 strains), are reported elsewhere (Publication V). The remaining 82 new strains representing potentially toxigenic *Az. spinosum* and *Am. languida* strains (Tab. 1), are reported here. Within strains designated as *Az. spinosum* we identified strains of toxigenic ribotypes A and B, as well as five new strains without detectable AZA. The latter revealed significant nucleotide differences compared to known *Az. spinosum* sequences and therefore also clustered apart from other *Az. spinosum* strains within the phylogenetic tree. These strains are subsequently designated as *Az. cf. spinosum*.

Strains were obtained from the Irish coast and from the central North Sea (Fig. 1), with multiple strains of *Az. spinosum* obtained from stations 35, 45, and 71. All five *Az. cf. spinosum* strains originated from station 35, and new strains of *Am. languida* exclusively originated from the central North Sea station 71 (Fig. 1). All strains were analysed for their AZA profiles, most were investigated morphologically using LM or SEM, and sequence data were obtained for a selected number of strains (a detailed compilation of information on each strain can be found in Supplementary Tables S4 and S5).

Table 1. Summary of Amphidomataceae strains obtained during the filed sample campaign HE-516 in summer 2018.

Genus	Species	No. of strains	Reference
<i>Azadinium</i>	<i>caudatum</i> var. <i>margalefii</i>	1	Salas et al. subm.
<i>Azadinium</i>	<i>pseudozhuanum</i> sp. nov.	1	Salas et al. subm.
<i>Azadinium</i>	<i>galwayense</i> sp. nov.	3	Salas et al. subm.
<i>Azadinium</i>	<i>perfusorium</i> sp. nov.	26	Salas et al. subm
<i>Azadinium</i>	<i>spinosum</i> ribotype A	60	this paper
<i>Azadinium</i>	<i>spinosum</i> ribotype B	7	this paper
<i>Azadinium</i>	cf. <i>spinosum</i>	5	this paper
<i>Amphidoma</i>	<i>languida</i>	10	this paper

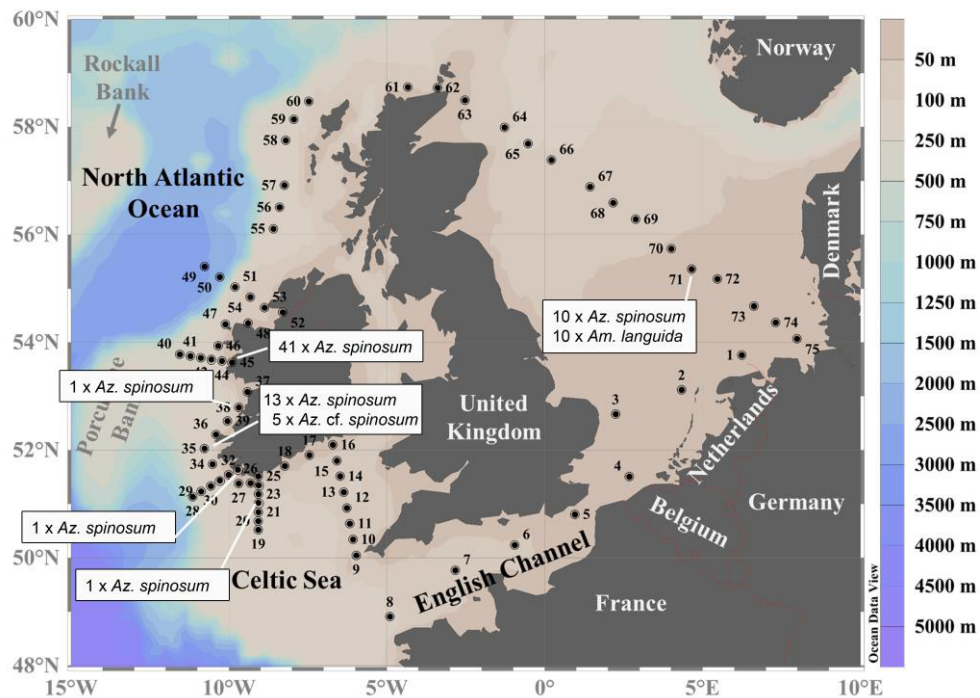


Figure 1. Map of the study area highlighting sample stations where *Azadinium* and *Amphidoma* strains were isolated.

3.1. Phylogeny of strains

All 24 *Az. spinosum* strains producing AZA-1 (and -2, -33) for which sequence data were generated shared identical LSU and ITS rDNA sequences except for two strains, which showed one bp difference in LSU sequences. Likewise, all seven *Az. spinosum* strains producing AZA-11 (and -51) shared identical LSU and ITS rDNA sequences. The two different *Az. spinosum* groups differed from each other in LSU by seven bp and in ITS by 11bp. The five non-toxicogenic *Az. cf. spinosum* strains differed from each other in LSU by six bp. In ITS, four of them shared identical sequences but differed from strain 5-B9 by 13 bp. In contrast, all strains of *Am. languida* shared identical sequences.

Genetic distances were less than 0.04 among *Az. spinosum* ribotypes A, B and C, but varied from 0.05 to 0.07 when compared with *Az. cf. spinosum* sequences. Moreover, ITS genetic distances ≤ 0.04 were calculated between *Az. cf. spinosum* and *Az. obesum* (0.03–0.04). Lower p-distances were also seen between *Az. obesum* and *Az. trinitatum* (0.05–0.06), or *Az. poporum* (0.05) (Supplementary Table S6).

The ITS2 secondary structure of five strains, representing ribotypes A, B, C and *Az. cf. spinosum* (two strains) was predicted. All of them showed four main helices (I, II, III, IV) but the number of loops in Helices II and III varied markedly. There was one compensatory base change (CBC, compensatory change on both side of a helix pairing) in helix IV between ribotypes A/ B/C and *Az. cf. spinosum* strains (Table 2, Fig. S1).

Table 2: Presence and location of CBC among *Azadinium spinosum* (ribotype A, B, and C) and/or *Az. cf. spinosum* (*cf.*) strains.

Strains	7-D3 (B)	H-4-G1 (C)	1-H10 (<i>cf.</i>)	5-B9 (<i>cf.</i>)
3D9 (A)	no	no	Helix IV	Helix IV
7-D3 (B)		no	Helix IV	Helix IV
H-4-G1 (C)			Helix IV	Helix IV
1-H10 (<i>cf.</i>)				no

The maximum likelihood (ML) and Bayesian inference (BI) analysis based on concatenated SSU, ITS-5.8S and partial LSU rRNA gene sequences yielded similar phylogenetic trees. The BI tree is illustrated in Fig. 2. The family Amphidomataceae was well resolved with maximal support (1.0 Bayesian posterior probability (BPP) and 100 bootstrap support (BS)) consisting of two clades. The first clade consisted of *Amphidoma parvula* and *Am. languida* with maximal support. New strains of *Am. languida* grouped together with strains from elsewhere with maximal support. The second clade comprised all *Azadinium* species but received low support. Two *Azadinium* species (*Az. concinnum* and *Az. perforatum*) diverged early and formed a sister clade with the remaining *Azadinium* species, which formed a monophyletic group with maximal support. *Azadinium spinosum* consisted of three ribotypes with maximal support. Ribotype A included strains 6-A10, 4-G9, 3-B4 and 5-C11 with low BPP but high BS (98). Ribotype B included strains 5-G8 and 7-D3 with strong support (0.96 BPP /100 BS). The five non-toxicogenic *Az. cf. spinosum* strains were well resolved and consisted of two clades. One of them comprised strains 6-A1, 5-D3, 2-A3, 1-H10 and another comprised strain 5-B9. They were closest to *Az. obesum* with low support.

qPCR assay specificity with newly obtained strains

In silico specificity checking for newly obtained *Az. spinosum* ribotype A strains did not show any base pair mismatches with the primers and probe of the current *Az. spinosum* qPCR assay. Sequences of the new ribotype B strains revealed one bp mismatch with the probe and two bp mismatches with the reverse primer. *Azadinium cf. spinosum* sequences had three bp mismatches with both, the probe and the reverse primer (Tab. 3).

In vitro testing of new *Az. spinosum* ribotype A strains showed the same amplification efficiency ($C_T = 18.4$ for strains 4-F8 and 5-C11, $C_T = 19.4$ for strain 6-G8) as the ribotype A reference strains (Supplementary Table S7). DNA of the newly obtained ribotype B strains was amplified with less efficiency compared to the ribotype A DNA. However, the same efficiency ($C_T = 25.6$ for strain 5-F3 and $C_T = 25.4$ for strain 8-B8) was observed compared to the ribotype B reference strains. None of the newly isolated *Az. cf. spinosum* strains was amplified in the *Az. spinosum* qPCR assay. DNA of the newly obtained *Am. languida* strains showed the same amplification efficiency ($C_T = 20.7$ for strains 5-F11, $C_T = 20.4$ for strain 8-D10) as the reference strains (Supplementary Table S7).

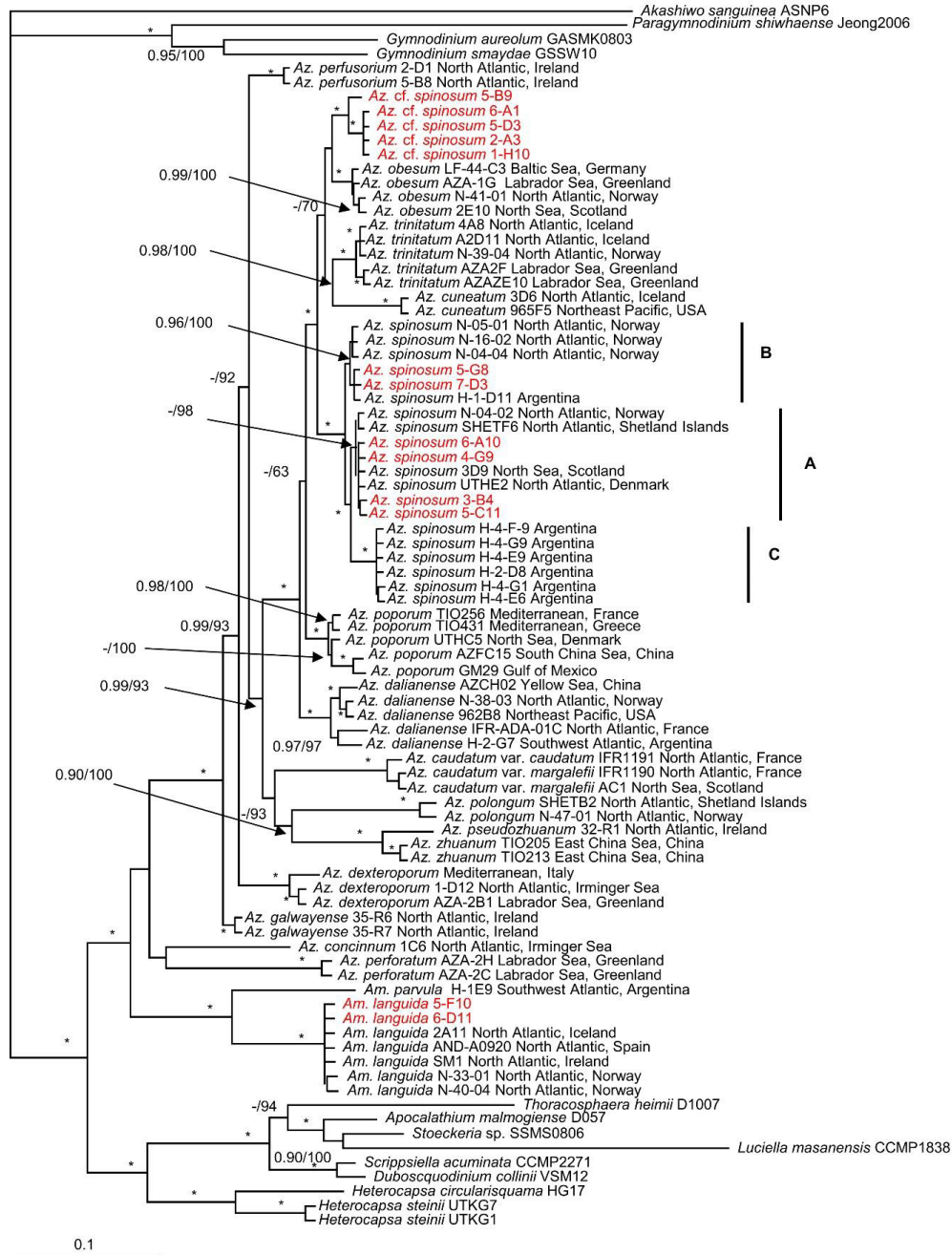


Figure 2: Molecular phylogeny of *Azadinium* and *Amphidoma* inferred from concatenated SSU, ITS-5.8S and partial LSU rRNA gene sequences using Bayesian inference (BI). New sequences of *Azadinium spinosum*, *Az. cf. spinosum*, and *Amphidoma languida* are indicated in red. Ribotypes of *Az. spinosum* are marked with A, B, and C. Scale bar indicates number of nucleotide substitutions per site. Numbers on branches are statistical support values (left, Bayesian posterior probabilities; right, ML bootstrap support values). Bootstrap values >50% and posterior probabilities above 0.9 are shown. Asterisks (*) indicate maximal support (pp = 1.00 in BI and bootstrap = 100% in ML, respectively).

Table 3: Sequence alignment of the *Az. spinosum* specific qPCR primers and probe with the respective ribotype homologous. Base-pair differences to the primer or probe sequence are highlighted in yellow.

	F-Primer	Probe	R-Primer
Sequence	CATCTCCCTGACACAAAGACGA	AGGAGTCCTTTTGGGCG	GGAAACTCCTGAAGGGCTTGT
ribotype A	-----	-----	-----
ribotype B	-----	-----C-----	-----T-----G-----
ribotype C	-----	C-A-----	-----T-----TCA-----CCA
<i>Az. cf. spinosum</i>	-----	T-A-----G-----	T-----T-----A-----

Application of all tested *Az. spinosum*, *Az. cf. spinosum* and *Am. languida* strains did not reveal any detectable false-positive amplifications (Supplementary Table S7). LOD was 0.1 pg target DNA μL^{-1} for all three qPCR assays.

3.2 Morphological identification

Morphological identification of the strains conformed their phylogenetic placement, and morphology of *Az. spinosum* (ribotypes A and B), *Az. cf. spinosum* and *Am. languida* are shown below.

Azadinium spinosum

Ribotype A: All strains assigned to ribotype A in our phylogenetic placement were similar in size (Tab. S4), shape and general appearance (Fig. 3 A–D, G, H). Cells of all *Az. spinosum* ribotype A strains consistently had an antapical spine (Fig. 3 A, B, G, H, L). One large pyrenoid with a starch sheath (visible as a ring-like structure) was located in the episome (Fig. 3 B–D). The nucleus was generally round to slightly ellipsoid but could be more elongated as well (Fig. 3 E, F). All cells of all strains which were examined with SEM (Tab. S4) had a conspicuous ventral pore on the left suture of plate 1' (Fig. 3 G, I) and the thecal plate pattern of epi- and hypotheca typical for the species (Fig. 3 K, L). Moreover, cells consistently had a distinct rim around the pore plate (Fig. 3 J, K).

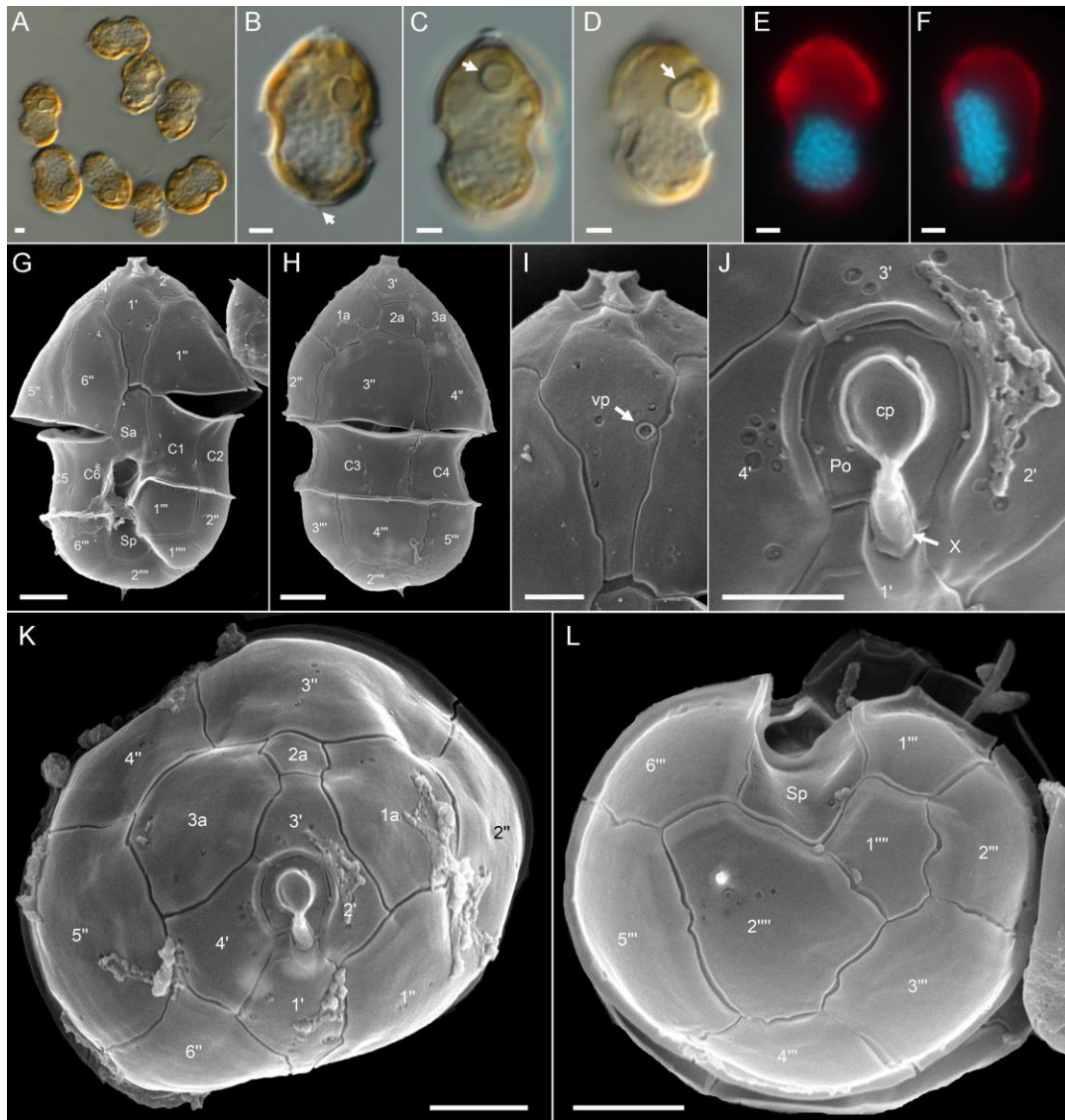


Figure 3: *Azadinium spinosum* ribotype A strains. (A–D) LM images of formalin fixed (A, B) or living (C, D) to indicate general size and shape. Note the antapical spine (arrow in B) and the distinct pyrenoid in the epicone (arrows in C, D). (G–L) SEM images of different thecae. (G) Ventral view. (H) Dorsal view. (I) First apical plate in ventral view. Note the position of the ventral pore (vp). (J) Detailed view of the apical pore complex (APC). (K) Apical view of epithecal plates. (L) Antapical view of hypothecal plates. Plate labels according to the Kofoidian system. Po = pore plate; cp = cover plate; X = X-plate or canal plate; vp = ventral pore. Abbreviation of sulcal plates: Sa = anterior sulcal plate; Sp = posterior sulcal plate. Scale bars = 2 μm (A–H, K, L) or 1 μm (I, J).

Ribotype B: All ribotype B strains were also similar in size, shape and general appearance (Fig. 4 for strain 5-F6, Figure plates for other ribotype B strains are Figs S2–S4 in the

supplementary material). With respect to most morphological features such as presence and location of a pyrenoid (Fig. 4 A), presence of the antapical spine (Fig. 4 B, G–I), the thecal plate pattern of epi- and hypotheca (Fig. 5) and location of the ventral pore (Figs 4 G, H; 5 A, C), ribotype B strains were not distinguishable from ribotype A strains. The nucleus was posterior in position and ellipsoid and elongated in most cases (Fig. 4 D–F). In contrast to ribotype A strains, for all seven strains identified as ribotype B, a distinct rim around the pore plate was missing (Fig. 4 A, E).

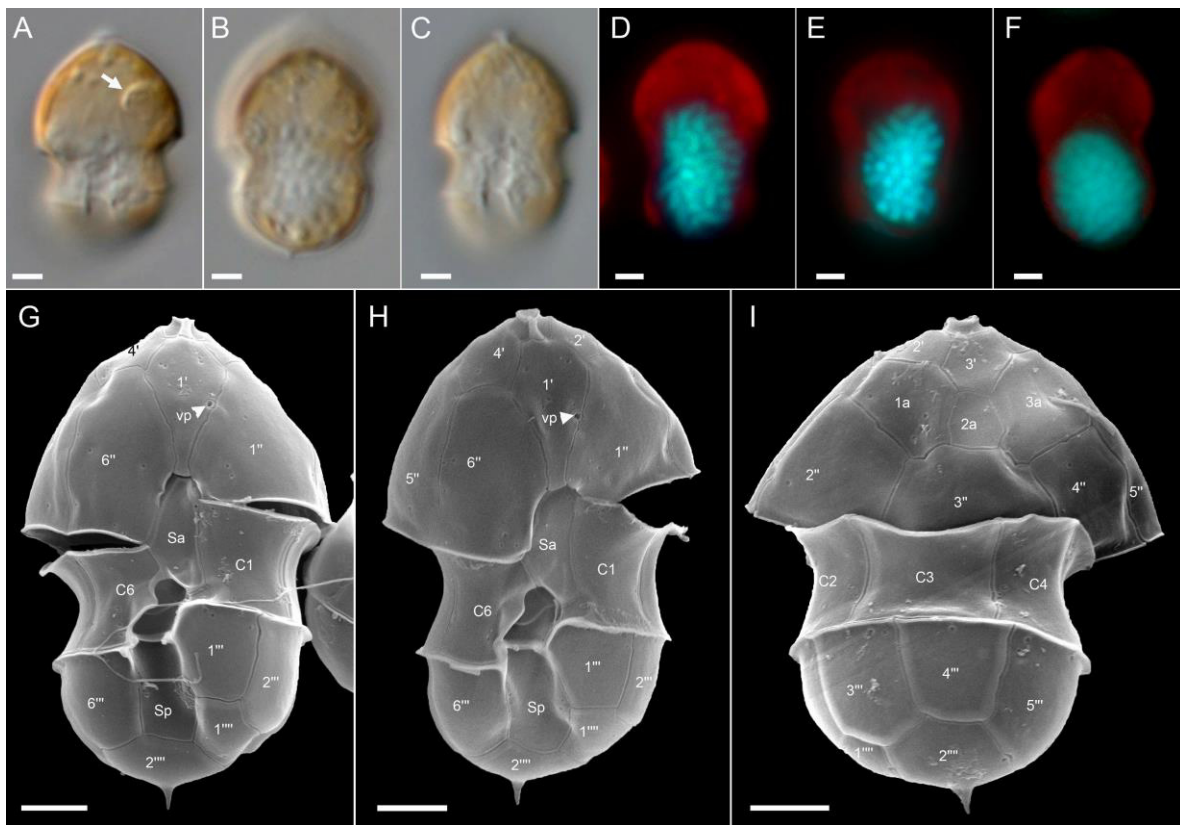


Figure 4: *Azadinium spinosum* ribotype B strain 5-F6. (A–F) LM images of living (A–C) cells to indicate general size and shape. Note the distinct pyrenoid in the epicone (arrow in A). (D–F) Formalin fixed and DAPI-stained cells viewed with UV excitation to indicate shape and position of the nucleus. (G–I) SEM images of different thecae in ventral (G, H) or dorsal (I) view. Note position of ventral pore (vp). Plate labels according the Kofoidian system. vp = ventral pore. Abbreviation of sulcal plates: Sa = anterior sulcal plate; Sp = posterior sulcal plate. Scale bars = 2 μ m.

Azadinium cf. spinosum: Morphology of the *Az. cf. spinosum* strains is compiled in Figs 6–7 for strain 5-B9 (Figure plates for other *Az. cf. spinosum* strains can be found in Figs S5–S7 in the

Supplementary Material). In terms of morphology, these strains shared the same morphological features described as distinctive for *Az. spinosum*, i.e. possession of one prominent pyrenoid in the episome (Fig. 6 A, F, G), an antapical spine (Fig. 6 E, F, K–M), a roundish posterior nucleus (Fig. 6 H, I) that can be elongated during cell division (Fig. 6 J), and a vp located on the left suture of plate 1' (Figs 6 K, L, 7 D–G). Plate pattern of epi- and hypotheca (Fig. 7 A, B) as well as of the cingulum and sulcus (Fig. 7 H–J) were indistinguishable from other *Az. spinosum* strains. Cells of all *Az. cf. spinosum* strains had a distinct rim around the pore plate (Fig. 7 A, C–G).

Amphidoma languida: All ten new *Am. languida* strains from the survey were obtained from the central North Sea station 71. They all shared an identical morphology as observed in LM (Fig. 8). In accordance with the species description, cells consistently had one large pyrenoid with a starch sheath (visible as a ring-like structure) located in the episome (Fig. 8 B, C). Detailed SEM (Fig. 8 D–M) performed for a selected number of strains (Tab. S5) revealed the Kofoidian plate pattern for the species (Po, cp, X, 6', 0a, 6", 6C, 5S, 6"', 2''') (Fig. 8 F, G, K, L), a vp located at the right side of plate 1' close to the pore plate (Fig. 8 F, I, J), and a large antapical pore located on the second antapical plate (Fig. 8 E, G, H). A number of, but not all, cells in the clonal cultures had a round ventral depression located at the anterior tip of the anterior sulcal plate (Fig. 8 M).

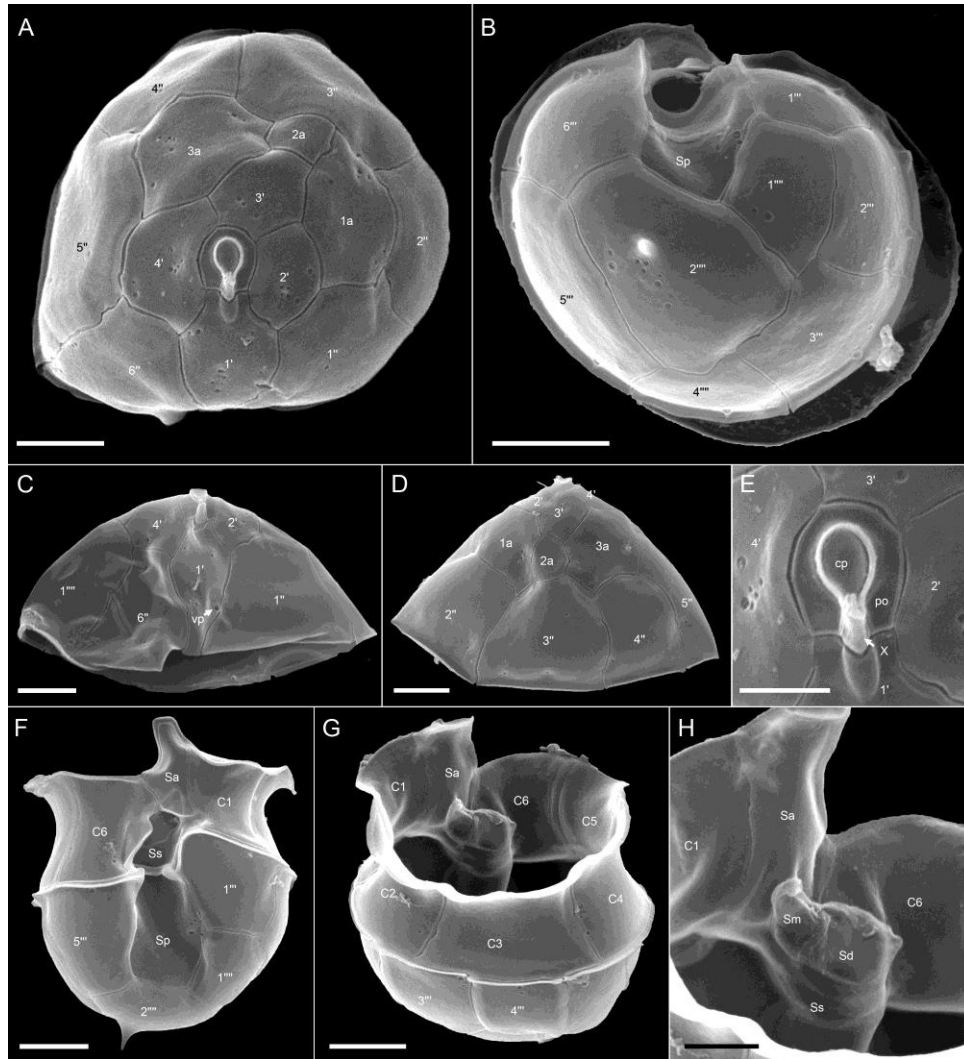


Figure 5: *Azadinium spinosum* ribotype B strain 5-F6. SEM images of different thecae. (A) Apical view of epithelial plates. (B) Antapical view of hypothecal plates. (C) Epitheca in ventral view. Note the position of the ventral pore (vp). (D) Epitheca in dorsal view. (E) Detailed view of the apical pore complex (APC). (F) Hypotheca in ventral view. (G) Hypothecal in apical/dorsal view. (H) Detailed internal view of the central sulcal plates. Plate labels according to the Kofoidian system. Po = pore plate; cp = cover plate; X = X-plate or canal plate; vp = ventral pore. Abbreviation of sulcal plates: Sa = anterior sulcal plate; Sp = posterior sulcal plate; Ss = left sulcal plate; Sm = median sulcal plate; Sd = right sulcal plate. Scale bars = 2 μm (A–D, F, G) or 1 μm (E, H).

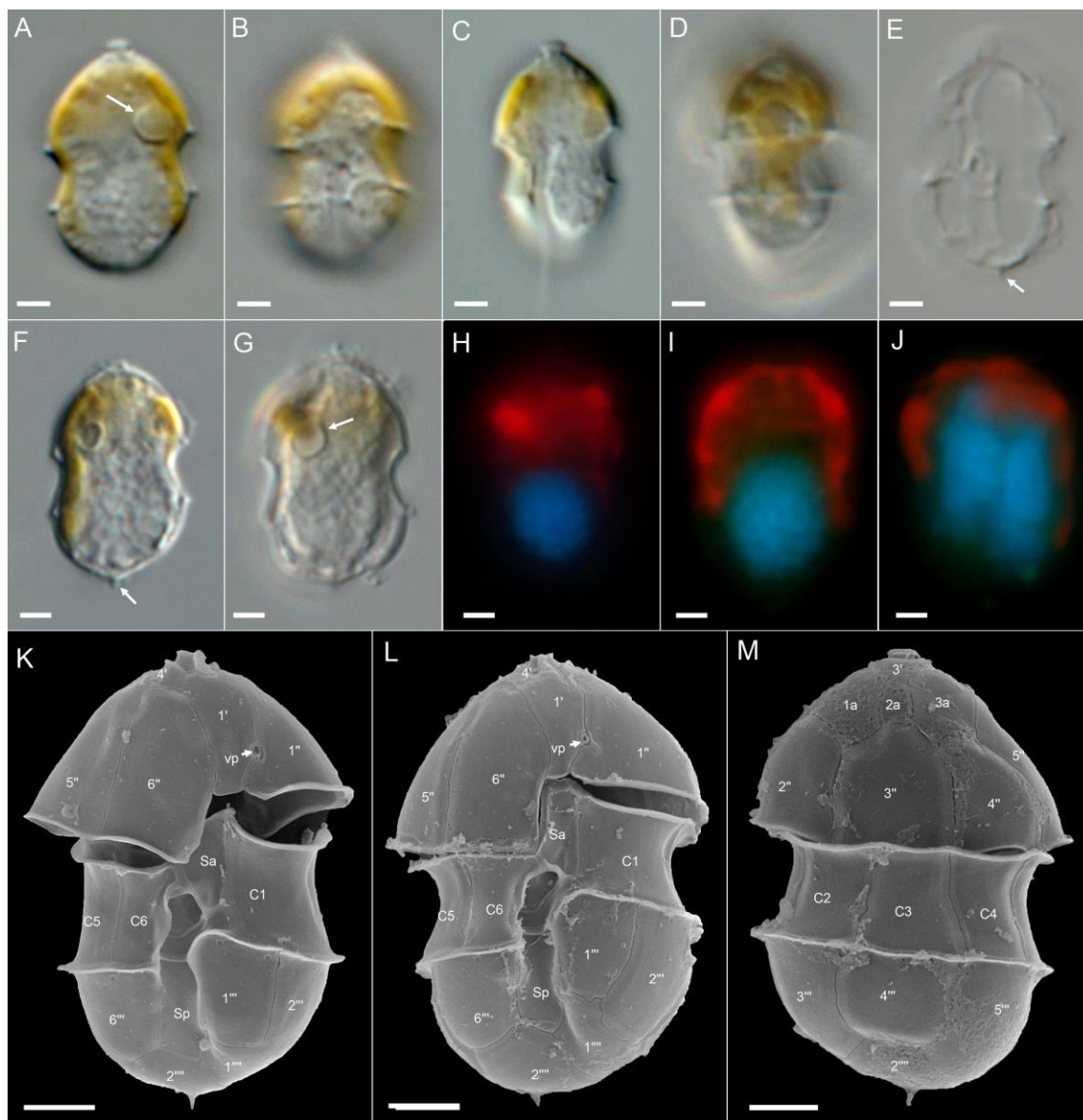


Figure 6: *Azadinium cf. spinosum* strain 5-B9. (A–G) LM images of living (A–D) or formalin fixed (E–G) cells to indicate general size and shape. Note the distinct pyrenoid in the epicone (arrow in A, G) and the antapical spine (arrow in E, F). (H–J) Formalin fixed and DAPI-stained cells viewed with UV excitation to indicate shape and position of the nucleus. (J) Late stage of nuclear division. Note the elongated shape of the nucleus. (K–M) SEM images of different thecae in ventral (G, H) or dorsal (I) view. Note position of ventral pore (vp). Plate labels according the Kofoidian system. Abbreviation of sulcal plates: Sa = anterior sulcal plate; Sp = posterior sulcal plate. Scale bars = 2 μm.

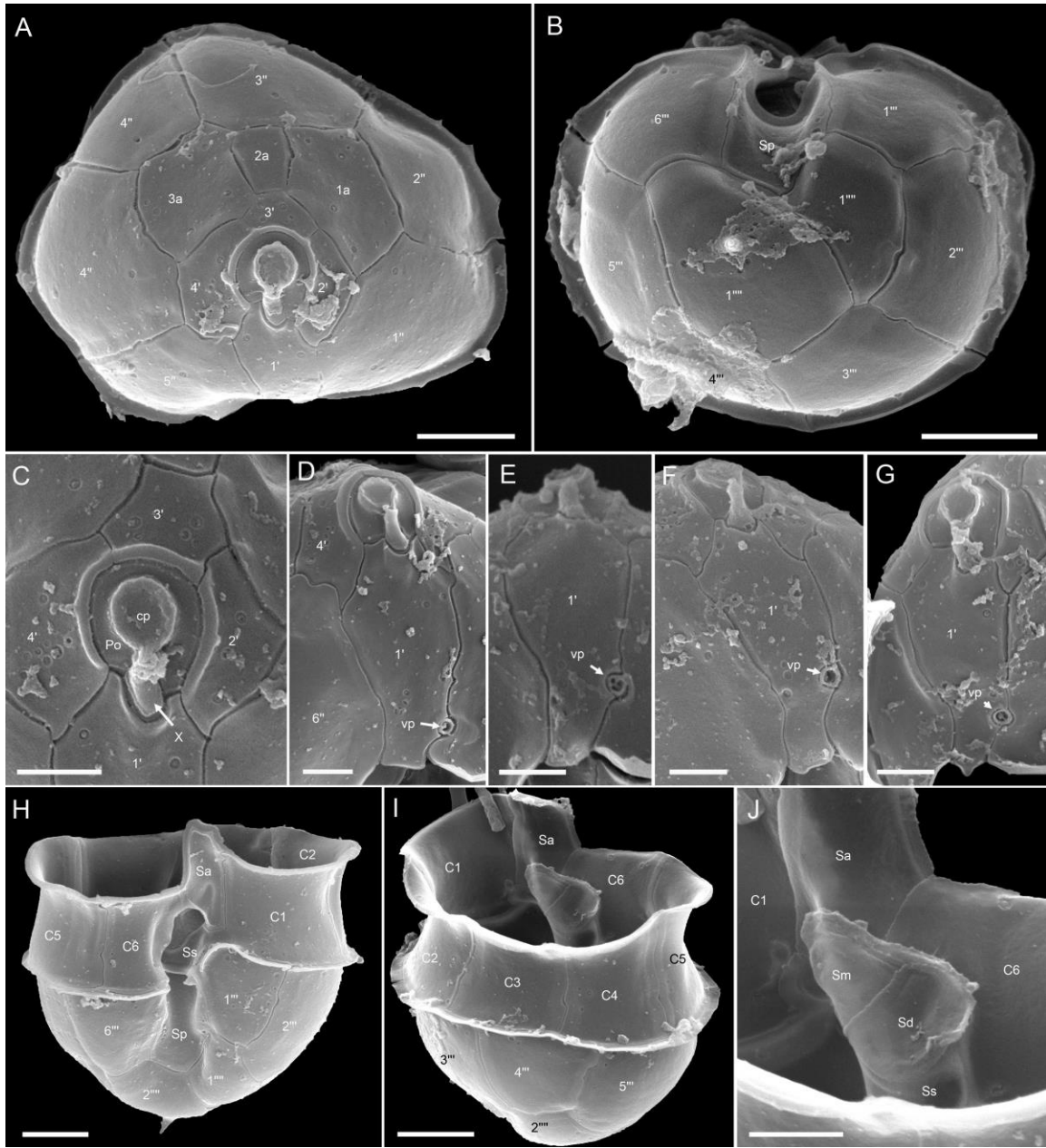


Figure 7: *Azadinium cf. spinosum* strain 5-B9. SEM images of different thecae. (A) Apical view of epithelial plates. (B) Antapical view of hypothecal plates. (C) Detailed view of the apical pore complex (APC) (D–G) First apical plate in ventral view. Note the position of the ventral pore (vp). (H) Hypotheca in ventral view. (I) Hypothecal in apical/dorsal view. (J) Detailed internal view of the central sulcal plates. Plate labels according the Kofoidian system. Po = pore plate; cp = cover plate; X = X-plate or canal plate; vp = ventral pore. Abbreviation of sulcal plates: Sa = anterior sulcal plate; Sp = posterior sulcal plate; Ss = left sulcal plate; Sm = median sulcal plate; Sd = right sulcal plate. Scale bars = 2 μm (A, B, H, I) or 1 μm (C–G, J).

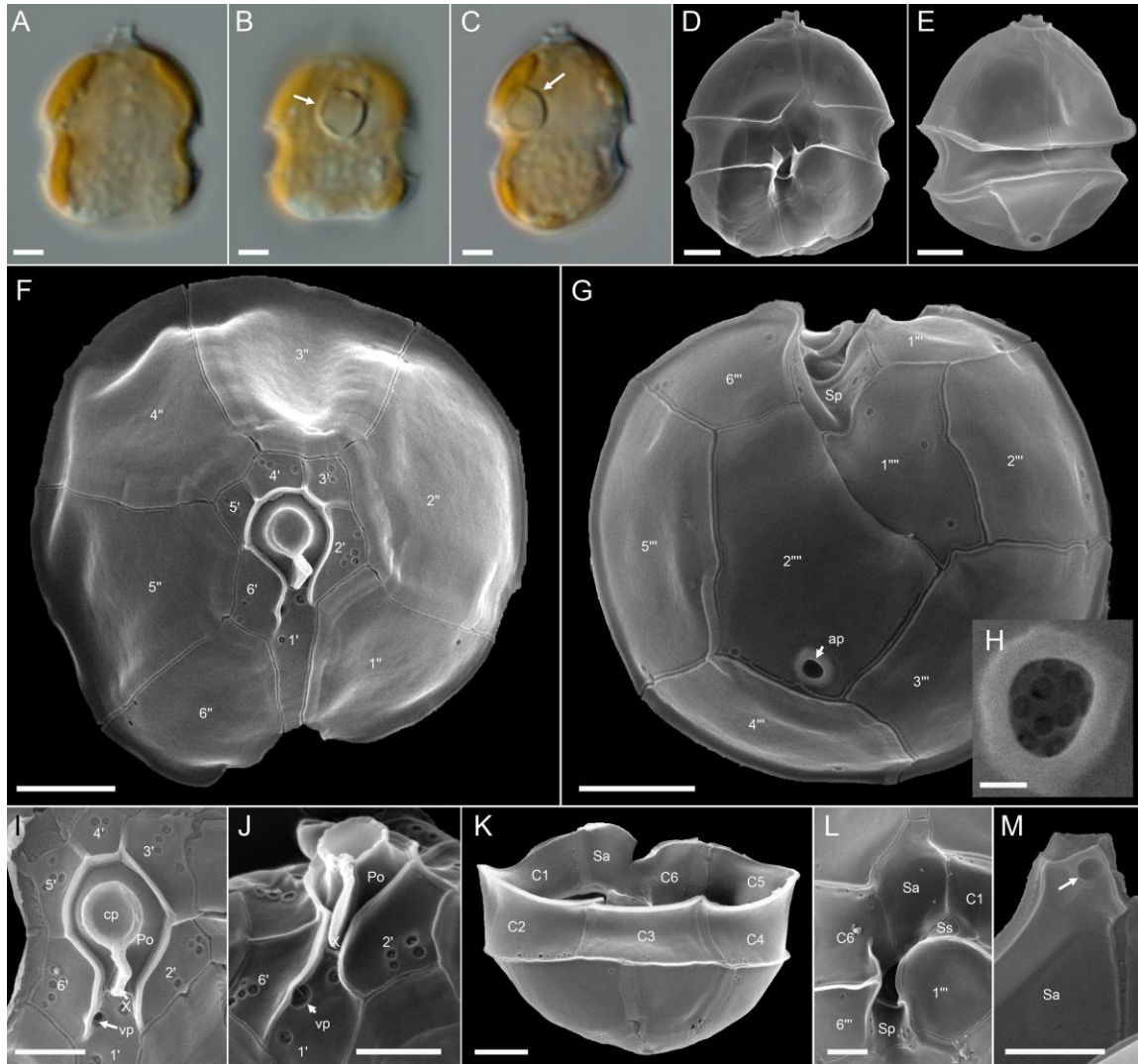


Figure 8: *Amphidoma languida* strains. (A–C) LM images of living cells to indicate general size and shape. Note the distinct pyrenoid in the episome (arrows in B, C). (D–M) SEM images of different thecae. (D) Ventral view. (E) Dorsal view. (F) Apical view of epithecal plates. (G) Antapical view of hypothecal plates. Note the antapical pore (ap). (H) Enlarged view of the antapical pore. (I) Detailed view of the apical pore complex (APC). (J) APC in ventral view, note the position of the ventral pore (vp). (K) Hypotheca in dorsal view. (L) Detailed view of sulcal plates. (M) Detailed view of the anterior sulcal plate. Note the anterior round ventral depression (arrow). Plate labels according to the Kofoidian system. Po = pore plate; cp = cover plate; X = X-plate or canal plate; vp = ventral pore; ap = antapical pore Abbreviation of sulcal plates: Sa = anterior sulcal plate; Sp = posterior sulcal plate; Ss = left sulcal plate; Sm = median sulcal plate; Sd = right sulcal plate. Scale bars = 2 μm (A–G, K) or 1 μm (I, J, L, M) or 0.2 μm (H).

3.3. Toxins

Azaspiracid profiles obtained for all strains initially referred to as *Az. spinosum* revealed the presence of three group of strains. The first group corresponding to ribotype A was characterised by the presence of AZA-1, -2, and -33, whereas the second group corresponding to all ribotype B strains was determined by the presence of AZA-11 and AZA-51. The third group consisted of all *Az. cf. spinosum* strains and lacked any AZA. The limit of detection for known AZA congeners and for yet unknown AZA (based on precursor experiments) were estimated for a number of selected strains of each group using high-biomass samples, and are reported in Tab. S2.

AZA profiles differed between strains of ribotype A. There were four different combinations of AZA-1, -2 and -33: (1) the majority (32 strains) had all three AZA congeners, (2) 10 strains contained only AZA-1, (3) 13 strains contained AZA-1 and -2 but lacked AZA-33, and (4) five strains contained only AZA-1 and -33 and lacked AZA-2. In contrast, no AZA profile variability was observed in group-2 (ribotype B) where all seven strains contained both AZA-11 and AZA-51.

As shown for a number of selected strains, all distinct toxin profiles (including absence of AZA of *Az. cf. spinosum* strains) were consistent and stable over time, as estimated for a period of up to 18 months (Tab. 4).

Table 4: *Az. spinosum* strains, stability of toxin profile. Data display the number of strains tested for toxin profile confirmation at different time points after isolation

Toxin profile	Toxin profile confirmation		
	ca. 2 months later	ca. 5 months later	> 1 year
AZA-1, -2, -33	12	11	4
AZA-1	5	2	1
AZA-1, -2	6	6	2
AZA-1, -33	2	2	1
AZA-11, 51	3	3	5
<i>cf. spinosum</i> (none)	5	4	3

In quantitative terms, however, AZA cell quotas were highly variable. Including all strains and all repeated analyses for single ribotype A strains, total AZA cell quota (sum of all detected AZA)

varied 53-fold and ranged from 1.2 to 63.1 fg cell⁻¹ (Fig. 9). Each single AZA compound showed high variability as well, with AZA-2 showing the highest fold-change of 330. Ratios of AZA compounds were also quite variable. The median ratio of AZA-1 to AZA-2 or AZA-33 was 2.2 and 5.0, respectively, but for single strains/single analysis ratios < 1 were also obtained, and the same was observed for AZA-2/AZA-33 ratios (Fig. 9). Cell quotas of all single AZA congeners and AZA-ratios were tested for significant differences between the four different toxin profile groups (Tab. 5, suppl. Tab. S8). Kruskal Wallis tests revealed significant differences for total AZA cell quotas (H=9.81, p = 0.020), whereas AZA-1, -2 and -33 were not significantly different between the four toxin-profile groups of ribotype A strains (p > 0.6). Whereas AZA-1/-2 ratio was just slightly below the 0.05 significance level (H = 3.68, p = 0.055) the AZA-1/-33 ratios were not significantly different (p = 0.865) (Tab. 5).

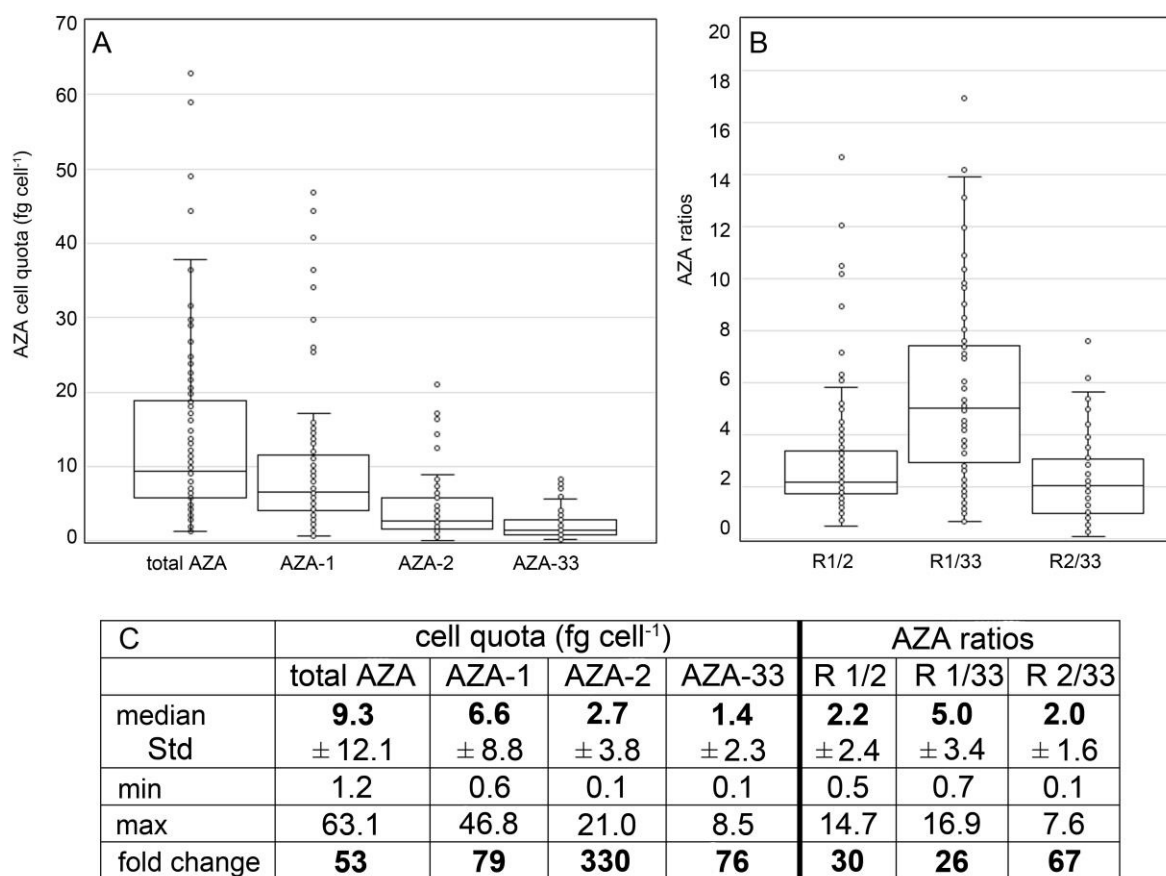


Figure 9: *Azadinium spinosum* ribotype A strains. Box-Whisker plots (A, B) and summary statistics (C) of all analyses (including repeated analyses of single strains) of AZA cell quota (A) and AZA ratios (B). Std = standard deviation.

Table 5: Summary statistics, ANOVA Kruskal Wallis test. Significance level < 0.05 are highlighted by grey shading.

ribotype A	Groups: toxin profile (1, 2, 3, 4)		
	DF, n	H	p
total AZA	3, n=125	9.81	0.0203
AZA-1	3, n=125	2.16	0.5417
AZA-2	1, n=94	1.05	0.3043
AZA-33	1, n=76	0.51	0.4740
R 1/2	1, n=94	3.68	0.0549
R 1/33	1, n=76	0.03	0.8652
	Groups: strains		
total AZA	21, n=79	26.37	0.1927
R 1/2	16, n=62	46.29	0.0001
R 1/33	13, n=51	35.82	0.0006
R 2/33	11, n=43	24.82	0.0097
ribotype B	Groups: strains		
	DF, n	H	p
total AZA	4, n=16	1.09	0.8956
AZA-11	4, n=16	2.91	0.5727
AZA-51	4, n=16	0.97	0.9157
R 11/51	4, n=16	8.60	0.0718

High variability in AZA cell quota was also obvious for those ribotype A strains for which multiple independent time-series analyses were available (Fig. 10, summary statistic tables are listed in the Supplementary Tables S8–S10). Total AZA within a single ribotype A strain varied up to 16-fold (strain 5-E4) but for other strains (e.g. 3-E6, 4-E11) cell quota was quite consistent. Fold-changes of multiple analyses of AZA-1/AZA-2 ratios were < 2 for many strains (Fig. 10, Tab. S8) but other strains showed high (up to 6.5-fold) changes of this ratio. Kruskal-Wallis ANOVA revealed that total AZA cell quota were not different between ribotype A strains ($H = 26.22$, $p = 0.198$). In contrast, for all AZA ratios (1/2, 1/33, 2/33) there were highly significant differences between strains ($p < 0.008$) (Tab. 5).

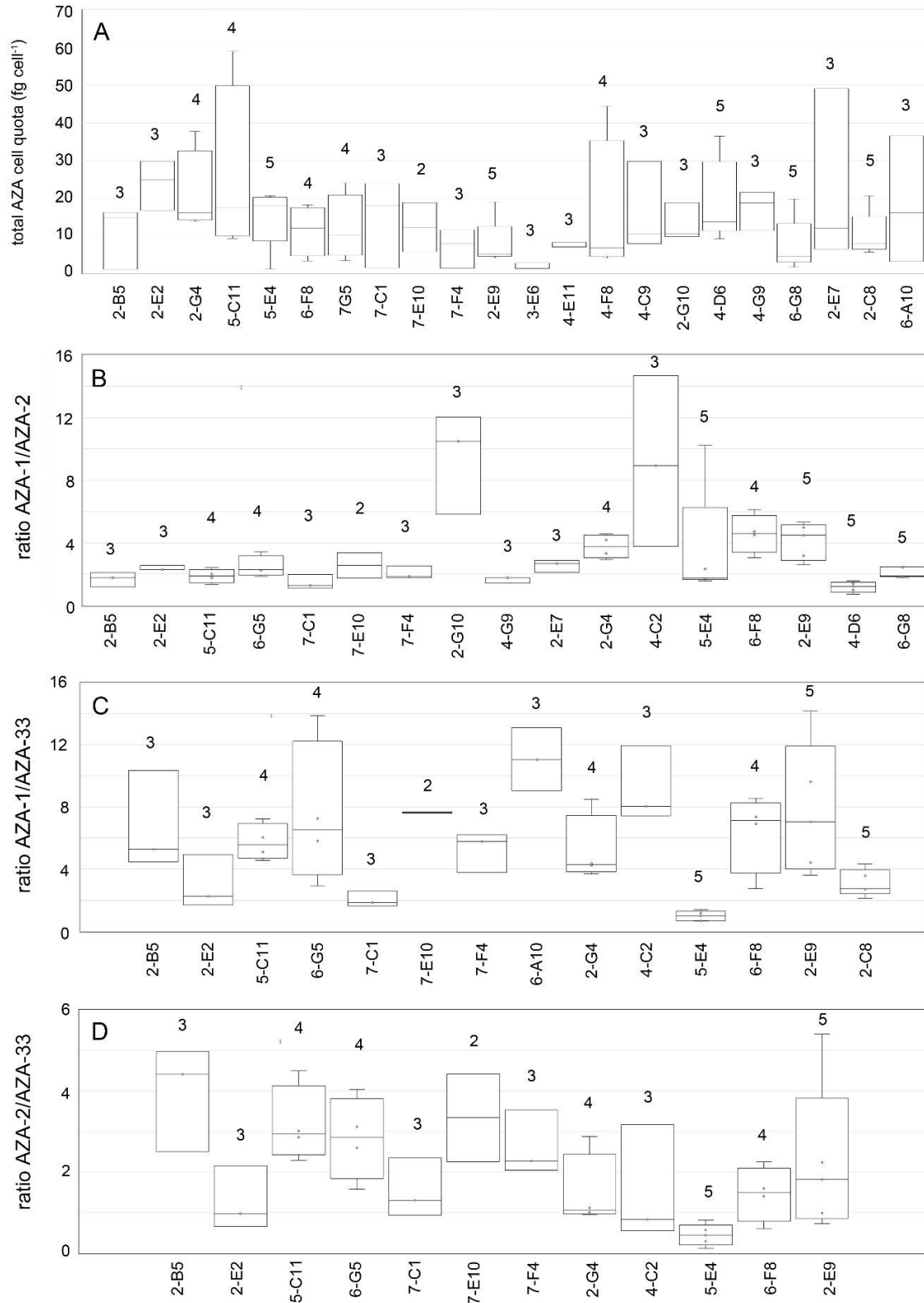
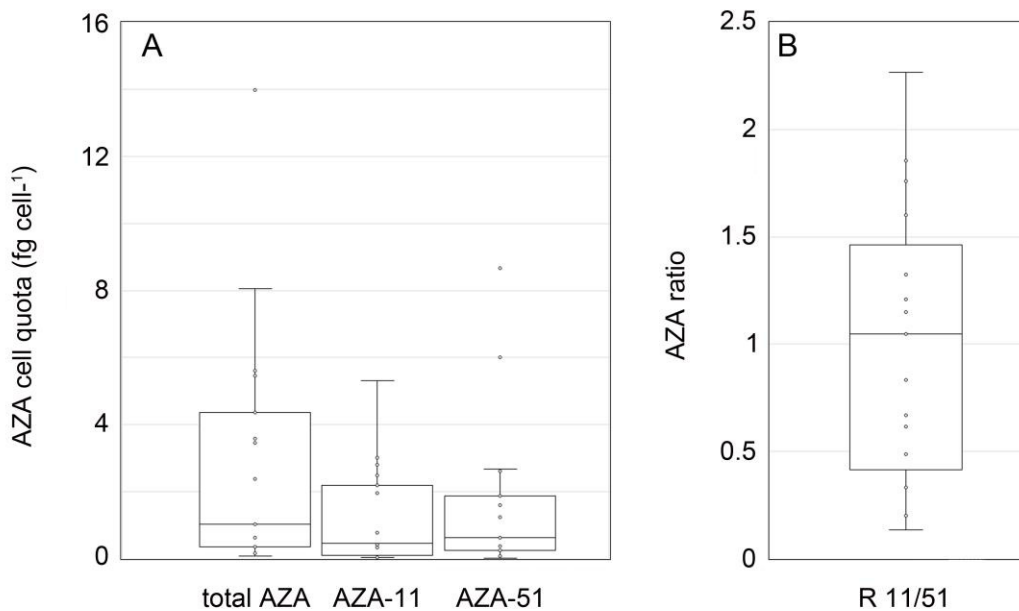


Figure 10: *Azadinium spinosum* ribotype A strains. Variability in total AZA cell quota (A) and AZA ratios (B–D) based on multiple analysis of single strains. Number above bars indicate number of analyses (n).

Toxin profile of *Az. spinosum* ribotype B strains consisted of AZA-11 and AZA-51 and was constant over time (Tab. 4). Total AZA cell quotas for ribotype-B strains ranged from < 0.1 to 14.0 fg cell⁻¹ (Fig. 11) While median cell quotas of all analyses were similar for AZA-11 and AZA-51, the AZA-11/51 ratio (with median value of 1.0) of individual analysis ranged from 0.1 to 2.3 (Fig. 11). Total AZA cell quota estimates of single strains were variable as well with fold changes of multiple estimates ranging up to 68-fold (Fig. 12, summary statistics are listed in the Supplementary Tables S11–S12). Ratio of AZA-11/51 within single strains also varied around 1.0 but was consistently < 1.0 or > 1.0 for two or one strain, respectively (Fig. 12). For none of the AZA parameters (total AZA cell quota, AZA-11, AZA-51, ratio 11/51) there were statistical differences between strains (Kruskal-Wallis ANOVA, $p > 0.07$) (Tab. 5).



C	cell quota (fg cell ⁻¹)			AZA ratio
	total AZA	AZA-11	AZA-51	R 11/51
median	1.0	0.5	0.6	1.0
±STD	± 3.6	± 1.5	± 2.3	± 0.6
min	0.09	0.04	0.03	0.14
max	14.0	5.3	8.7	2.3
fold change	159	133	321	17

Figure 11: *Azadinium spinosum* ribotype B strains. Box-Whisker plots (A, B) and summary statistics (C) of all analyses (including repeated analyses of single strains) of AZA cell quota (A) and AZA ratios (B). Std = standard deviation.

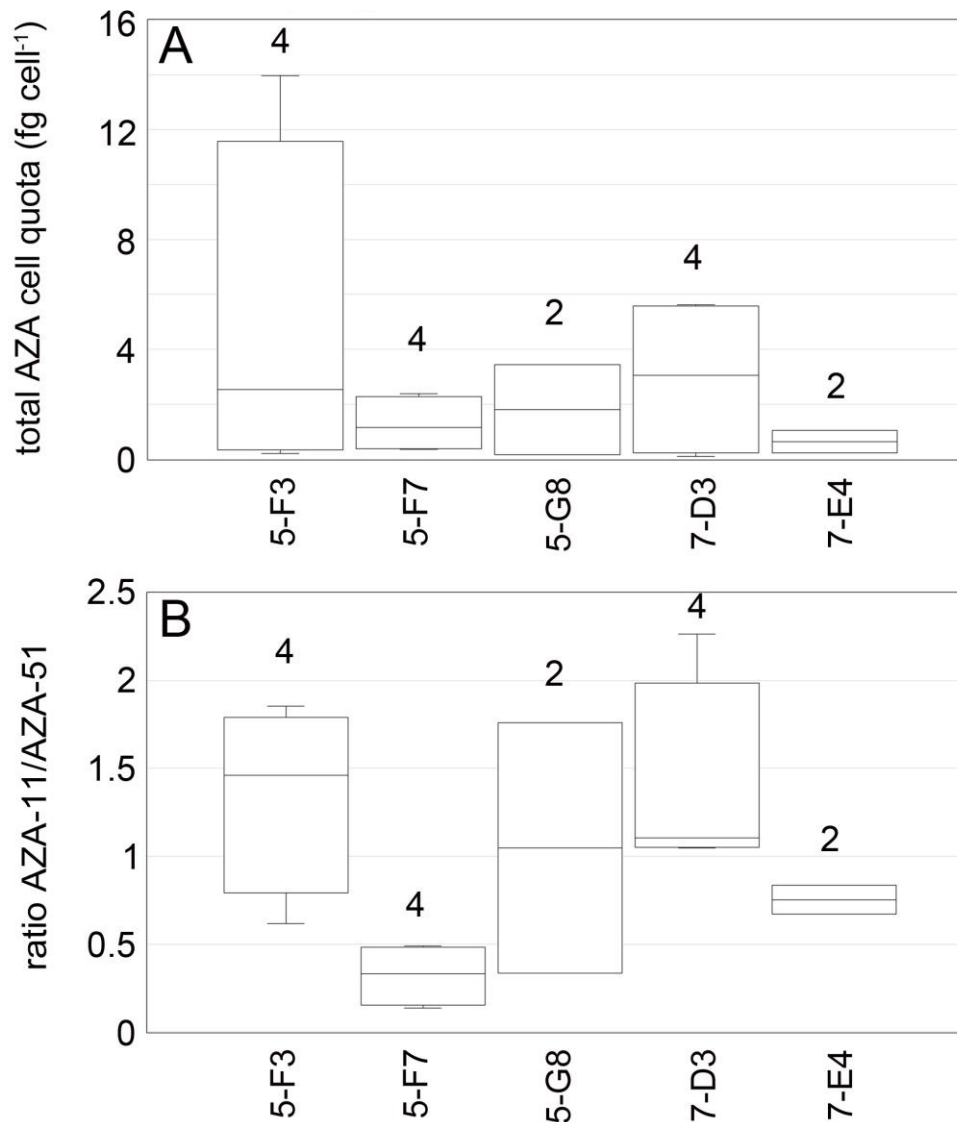
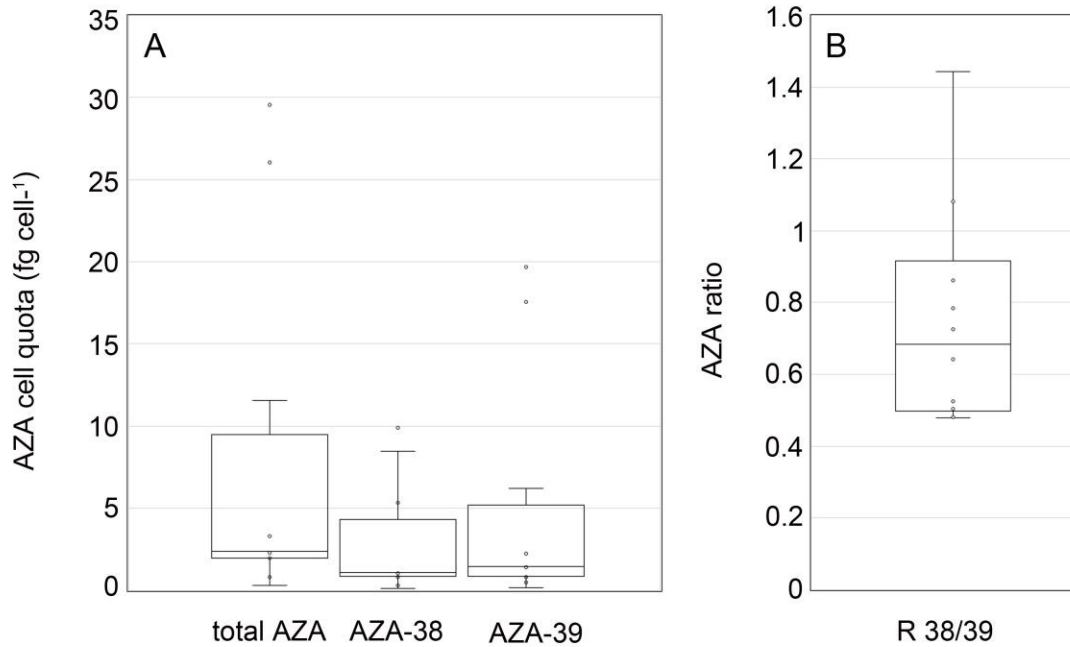


Figure 12: *Azadinium spinosum* ribotype B strains. Variability in total AZA cell quota (A) and AZA ratios (B) based on multiple analysis of single strains. Number above bars indicate number of analyses (n).

All strains of *Am. languida* produced AZA-38 and -39 (for LOD of other known and/or unknown AZA compounds see Supplementary Table S2). Total AZA cell quota ranged about 100-fold from 0.3 to 29.6 fg cell⁻¹ (Fig. 13). The mean ration of AZA-38/-39 was slightly below 1, but the ratio of single analyses varied between 0.5 and 1.4 (Fig. 13). There were no repeated analyses of single strains, so temporal stability and variability in cell quota for *Am. languida* could not be assessed.



C	cell quota (fg cell ⁻¹)			AZA ratio
	total AZA	AZA-38	AZA-39	R 38/39
median	2.4	1.1	1.5	0.7
± STD	± 10.4	± 3.4	± 7.0	± 0.3
min	0.3	0.1	0.2	0.5
max	29.6	9.9	19.7	1.4
fold change	96	73	114	3

Figure 13: *Amphidoma languida* strains. Box-Whisker plots (A, B) and summary statistics (C) of all analyses of AZA cell quota (A) and AZA ratios (B). Std = standard deviation.

4. Discussion

Isolation and characterisation of multiple amphidomatacean strains from Irish waters and the North Sea revealed a number of new insights into the diversity of this group of potentially toxic microalgae. At the taxonomic level we identified and described three new and non-toxicogenic *Azadinium* species presented in detail elsewhere (Publication V). In addition, we add a number of important facts about the diversity of the known toxigenic species *Az. spinosum* and *Am. languida* and thereby have added complementary information to the field data set on the abundance and distribution of toxigenic Amphidomataceae and their toxins to that which have been published previously (Wietkamp et al., 2020).

Azadinium spinosum, the first identified source organism of AZA, is regarded as the most important AZA producer in Irish waters (Salas et al., 2011; Tillmann et al., 2014c; Wietkamp et al., 2020). The first strains of this species isolated from Scotland (Tillmann et al., 2009), Denmark (Krock et al., 2013), the Shetland Islands (Tillmann et al., 2012b) and Ireland (Salas et al., 2011) all share the same sequence data and toxin profile consisting of AZA-1, -2, and -33, but subsequent multiple strain studies from Norway and Argentina revealed ribotype divergence and toxin profile diversity within *Az. spinosum* (Tillmann et al., 2018a; Tillmann et al., 2019). Ribotype B strains from Norway mainly have AZA-11 and -51, whereas a single ribotype B strain from Argentina only produce AZA-2. All ribotype B strains also differ morphologically from ribotype A strains by lacking a distinct bulged rim around the apical pore plate (Tillmann et al., 2018a; Tillmann et al., 2019). Moreover, there is morphological variability within ribotype B: The single AZA-2 producing strain from Argentina has striking slender shape and the first epithecal intercalary plate 1a has contact with the first apical plate, a character stage that is different from all other strains of *Az. spinosum*, irrespective of the ribotype (Tillmann et al., 2019). All ribotype C strains are morphologically indistinguishable from the type strain exhibiting ribotype A, but consistently lack any AZA. So far, in *Az. spinosum* there is thus found: (1) AZA strain profile variability among different ribotypes; (2) morphological differences within a distinct ribotype, and (3) minor but consistent morphological differentiation between different ribotypes. With the data presented here we can confirm these findings and also show that there is toxin profile variability within *Az. spinosum* ribotype A.

Azadinium spinosum ribotype A, and B

These results presented here thus confirm the presence of two different *Az. spinosum* ribotypes (A, and B) in the North Atlantic and their different AZA profiles (dominated by AZA-1, -2 and AZA-11, -51 respectively). From a chemical point of view, it has to be pointed out that AZA-11 and -51 of ribotype B are 3-hydroxylated, whereas AZA of ribotype A do not have any substituents at C3. Moreover, the major AZA of both ribotypes, i.e. AZA-1/2 of ribotype A and AZA-11/51 of ribotype B, consist of a methylated and unmethylated pair: AZA-2 is a methylated form of AZA-1 and AZA-11 is a methylated form of AZA-51. However, despite of this common feature, there is a difference between both ribotypes, which is the methylation site. AZA-1 of ribotype A is missing a methylation at C8, whereas AZA-51 of ribotype B is missing a methylation at C24 (Fig. 14). A similar pair of AZA congeners (3-hydroxylated or not) between different ribotypes can be seen within *Az. poporum*, where strains from Argentina (ribotype C2, see Tillmann et al. (2016)) have AZA-2 (lack of hydroxylation at C3) whereas *Az. poporum* ribotype A1 (see Tillmann et al. (2016)) strains from Chile solely having AZA-11 and -62 (3-hydroxylated) (Hall, 1999; Kilcoyne et al., 2014b; Kilcoyne et al., 2019).

Azadinium spinosum have been reported to contain several additional compounds next to the above mentioned major AZAs, such as AZA-33 (Tillmann et al., 2018a), AZA-2 methyl ester (Kilcoyne et al., 2014b), phosphorylated forms of AZA-1 and -2 (Kilcoyne et al., 2014b; Tillmann et al., 2018a), and AZA-34 and -35 (Krock et al., 2014). However, a number of minor AZA in *Az. spinosum* culture have been identified in dense stationary phase cultures only and thus are likely to be products of bacterial/chemical AZA degradation and not directly produced by the dinoflagellates (Gu et al., 2013). Minor azaspiracids identified in the present study in ribotype A strains also include methylated AZA-1 and -2 as well as phosphorylated forms of both AZA, and in some analyses of ribotype B strains phosphorylated AZA-11 and -51 were detected. All these minor compounds occurred always in low quantities ($< 1 \text{ fg cell}^{-1}$) and were not always detected, but this is likely because the limit of detection prevented detection of these minor compounds in low-biomass samples.

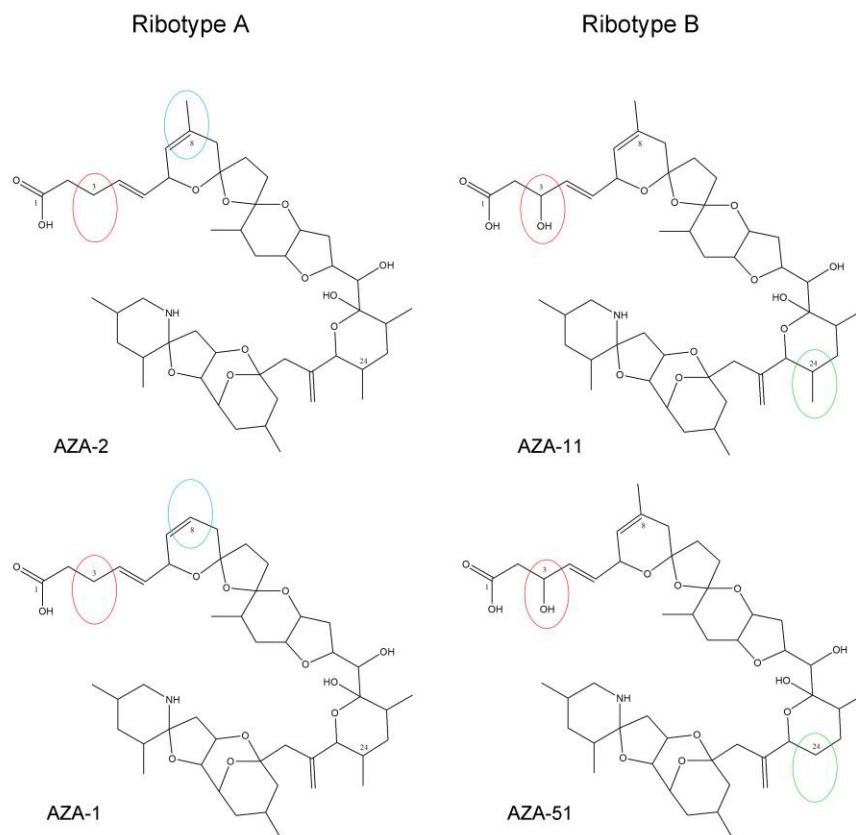


Figure 14: Planar structures of AZA-1, -2, -11 and -51. All AZA are closely related and can be regarded as variants of AZA-2: AZA of ribotype B are hydroxylated at C3 (red ovals), whereas ribotype A AZA are not. AZA profiles of both ribotypes consist of a base compound (AZA-2 and AZA-11, respectively) and a demethylated variant (AZA-1 and AZA-51, respectively). The demethylation site of ribotype A AZA is C8 and of ribotype B C24 (green ovals).

The multi-strain comparison of ribotype A and B strains show that ribotype B strains tend to generally have lower AZA cell quotas (median of all ribotype B strains: 1.0 fg cell⁻¹; compared to 9.3 fg cell⁻¹ for ribotype A strains). The same was found for A and B strains from the Norwegian coasts (median total AZA cell quota for ribotype B strains: 1.1 fg cell⁻¹; median total AZA cell quota for ribotype A strains: 4.5 fg cell⁻¹) (Tillmann et al., 2018a). It has to be kept in mind, however, that within ribotype A strains low AZA cell quota can also be found (Fig. 9), so it might be better to say that up to now no high cell quota (> 15 fg cell⁻¹) has been measured within B strains but are regularly registered within ribotype A strains. However, specific toxicity is not yet known for AZA-11 and AZA-51 and thus a direct conversion of cell quota to toxicity for a better

comparison with AZA-1 and -2 is not possible at the moment. One important finding related to *Az. spinosum* ribotypes A and B is that even with a large number of *Az. spinosum* strains isolated from Ireland (57 strains), no single ribotype B strain was obtained, whereas B strains were the majority (seven of ten) of strains isolated from the North Sea (Fig. 15). This relative dominance of B strains in the North Sea was not accompanied by detection of AZA-11 or AZA-51 in the North Sea (Wietkamp et al., 2020) showing that *Az. spinosum* ribotype B strain density in the North Sea is not at a critical level. Dominance of B-type *Az. spinosum* in the North Sea, together with the lower qPCR quantification efficiency of B compared to A strains (Tab. S7) may have contributed to the comparable lower total amphidomatacean density estimate based on qPCR in the North Sea compared to microscopy counts (Wietkamp et al., 2020). In any case, the snapshot in time obtained with the present survey does not allow to rule out the presence of B-type strains around Ireland, but our data at least indicate that current monitoring using the A-strain specific qPCR assay does not appear to be heavily biased.

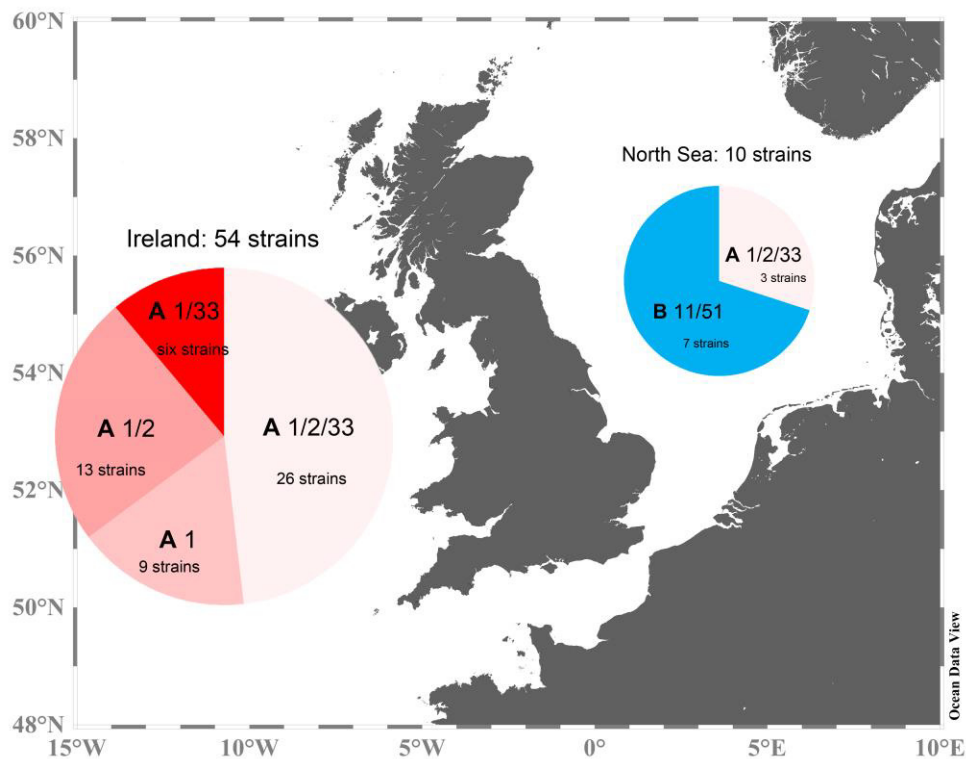


Figure 15: Summary of ribotype (A, B), toxin profile (1/2/33; 1/2; 1/33; 1; 11/51) and distribution of newly obtained *Az. spinosum* strains.

Toxin profile variability ribotype A

A new finding of the present study is that there is toxin profile variability within ribotype A. All ribotype A strains produce AZA-1 and toxin profile variability within ribotype A strain only refers to presence/absence of AZA-2 and/or AZA-33. Implication of this pattern in relation to AZA synthesis pathways, however, are not clear. Strains with AZA-1 but without AZA-33 indicate that the reduced molecule size of AZA-33 (molecular mass of 715 Da) cannot be considered a precursor for AZA-1. In contrast to the ribotype A, AZA profiles reported here, a single *Az. spinosum* ribotype B strain from Argentina lacks AZA-1 and only produces AZA-2 (Tillmann et al., 2019), and the production of solely AZA-2 is also known from *Azadinium poporum* (Kilcoyne et al., 2014b).

Structural variability of AZA profiles within a ribotype thus seems to be a common feature of toxic Amphidomataceae as it has also been seen in *Az. poporum* (Jauffrais et al., 2013b; Luo et al., 2018; Dai et al., 2019) and *Az. spinosum* ribotype B strains (Tillmann et al., 2019). In any case, the multiple strain approach clearly shows that within ribotype A strains there are consistent and stable (at least for one year) differences in presence/absence of AZA-1, -2 and/or -33. Implications of this, e.g. in terms of AZA synthesis pathways, are obscure at the moment but indicate that some AZA structural details may not be of vital importance for any physiological and/or ecological function. Ribotype A strains with deviating AZA profile all originate from Irish waters, and all three new *Az. spinosum* ribotype A strains from the North Sea had AZA-1, -2- and -33. However, among Irish strains, the presence of AZA-1, -2 and -33 clearly is the quantitatively dominant pattern (> 50 %; 32 of 60 strains), which may explain why this variability was not seen in previous Atlantic strains and also not in the new North Sea strains.

Notably, none of thirteen toxigenic strains tested after more than one year in culture completely lost AZA production potential. Moreover, our time series data provide no statistical support that toxin production may consistently diminish with time under cultivation. However, significant quantitative changes will be very difficult to be evaluated experimentally, considering that the underlying causes for the extraordinary large variability of AZA cell quota seen in the present study (Figs 9, 11, 13) are poorly understood.

Cell quota variability

A striking result of the multiple strain comparison is the enormous variability of AZA cell quota. Previous experimental studies show that cell quota of a given strain may change in response to environmental conditions like temperature (Jaufrais et al., 2013b; Dai et al., 2019; Kilcoyne et al., 2019) or nutrient conditions (Li et al., 2016). Here, however, we used the same growth conditions for all strains. Another factor affecting AZA cell quota is the growth stage; cells in stationary growth usually have higher cell quotas compared to exponential phase (Li et al., 2016; Dai et al., 2019; Kilcoyne et al., 2019), which might be explained by AZA accumulation when cell division stops. Growth phase of cultures used for toxin sampling in the present study was not fully controlled, so this may have contributed to the observed high fold differences among and within strains. Moreover, high variability (up to 20-fold differences in AZA-2 cell quota) is obvious in data presented by Li et al. (2016) for different sets of experiments (under the same conditions) with *Az. poporum*, and ~ 5-fold differences in cell quota of the same strain of *Az. spinosum* in different experiments performed at different time of the year are reported (Kilcoyne et al., 2019). Such a huge variability in toxin cell quota, even growing the same strain under identical environmental conditions, clearly indicates that there are other factors that are difficult, if not impossible, to control. In this respect, almost nothing is known about potential rhythmic or seasonal cycles in toxin production, or long-term changes in response to the artificial laboratory environment without competitive or food web interactions.

In conclusion, AZA cell quota estimates may vary considerably within a species (i.e. among strains) but also within a given strain and thus are of limited significance when simply extrapolating abundance data to evaluate toxic potential. However, the results presented here show that the qualitative toxin profile of a given strain is stable at least for one year in culture and thus likely to be genetically fixed. Nevertheless, long term loss of AZA production potential may occur as unpublished information indicate (Kilcoyne et al., 2019).

Non-toxigenic Az. cf. spinosum

Variability within *Az. spinosum* becomes even more complex considering the newly identified group of strains listed here as *Az. cf. spinosum*. This taxon conforms morphologically with *Az. spinosum*, but lacks AZA and groups in a phylogenetic cluster outside other *Az. spinosum*. A non-toxigenic *Az. spinosum* morphotype is present in Argentina, but these strains have been shown to cluster with other *Az. spinosum* forming a ribotype C clade. Due to the lack of

morphological differences between *Az. cf. spinosum* and other *Az. spinosum* ribotypes A and C, and despite their significant sequence differences and presence of CBCs between *Az. cf. spinosum* and all *Az. spinosum* ribotypes (Tab. 2), we currently refrain to finally conclude on the taxonomic level of these new strains, which we designate here as *Az. cf. spinosum*. All five strains of *Az. cf. spinosum* originate from the same station, but this does not necessarily indicate a limited distribution. In any case, this non-toxigenic taxon is of importance for monitoring, because with LM and even SEM it is impossible to differentiate between toxin-producing *Az. spinosum* and these non-toxigenic cells. It is thus important to point out that *Az. cf. spinosum* without AZA production differ significantly in the qPCR assay relevant sequence area and thus do not produce (false) positive signals in the *Az. spinosum* assay.

Amphidoma languida

In contrast to *Az. spinosum*, there was no toxin profile variability among the ten new *Am. languida* strains from the North Sea. However, it has to be kept in mind that all these strains were obtained from a fairly dense bloom population (Wietkamp et al., 2020) from the same station. Toxin profile variability within *Am. languida* is known from a Spanish Atlantic strain, which contains AZA-2 and -43 (Tillmann et al., 2017a). No new *Am. languida* strains were obtained from Irish waters, but the specific qPCR assay indicate that the species is widely present in the area (Wietkamp et al., 2019b; Wietkamp et al., 2020). Densities, however, seem to be lower compared to *Az. spinosum* which might explain the lack of new *Am. languida* strains from Irish coastal waters in this study. In terms of AZA cell quota, it is important to note that within *Am. languida* there is the same high intraspecific variability (Fig. 13) as reported in previous studies (Tillmann et al., 2018a; Wietkamp et al., 2019a) and as seen for AZA cell quotas in *Az. spinosum*.

5. Conclusions

The approach of multi-strain isolation and characterisation has enabled deeper insights into the molecular, morphological, and toxinological variability within Amphidomataceae, and has significantly added to our pre-existing knowledge of these species in Irish coastal waters and in the North Sea.

New details which have emerged from this study include: the magnitude of AZA cell quota variability observed, the previously unknown differences in AZA profile among *Az. spinosum* ribotype A strains, the presence and distribution of ribotype A and B in the area, and the identification of the non-toxicogenic *Az. cf. spinosum*. These details may altogether help to better understand the AZA toxin profile in these areas and to explain the differences that are often observed in the Irish biotoxin and phytoplankton monitoring programmes when trying to correlate AZA concentration in shellfish (via LC-MS/MS) with *Azadinium* cell abundances obtained with LM and/or qPCR.

Likewise, it is important to be aware that the current *Az. spinosum* qPCR assay is not addressing the diversity of strains/ribotypes in Irish and North Sea waters. New specific assay specifically targeting toxigenic ribotypes A or B, and also for the non-AZA ribotype C and/or the *Az. cf. spinosum* would help to more closely look at diversity and geographic distribution, and would also allow more focused alerts to the shellfish industry. This newly gathered information would also feed into predictive modelling and forecasting tools used by shellfish industries, monitoring agencies and regulatory authorities when ascertaining the risk or likelihood of AZA accumulation in shellfish, and also to provide further clarity on predicting the trends and patterns observed in the onset and during AZA events which can lead to prolonged closures of shellfish production areas.

Supplementary Materials: The following are available online at www.mdpi.com/xxx/s1, Figure S1: ITS secondary structure of *Az. spinosum* and *Az. cf. spinosum*, Figure S2: LM and SEM of *Az. spinosum* ribotype B, strain 5-F3, Figure S3: LM and SEM of *Az. spinosum* ribotype B, strain 5-F7, Figure S4: LM and SEM of *Az. spinosum* ribotype B, strain 7-E4, Figure S5: LM and SEM of *Az. cf. spinosum*, strain 6-A1, Figure S6: SEM of plate details of *Az. cf. spinosum* strain 6A1, Figure S7: LM and SEM of *Az. cf. spinosum*, strain 2-A3.

Table S1: SMR transitions for AZA analysis, Table S2: Limits of detection for AZA analyses, Table S3: GenBank accession numbers of new strains and strains used for the phylogenetic analyses, Table S4: Strain compilation *Az. spinosum*, Table S5: Strain compilation *Am. languida*; Table S6: ITS based genetic distances of selected *Azadinium* strains, Table S7: qPCR specificity tests of new strains, Table S8: Summary statistics *Az. spinosum* ribotype A, AZA cell quota of selected strains, Table S9: Summary statistics *Az. spinosum* ribotype A, AZA-1/AZA-2 ratios of selected strains, Table S10: Summary statistics *Az. spinosum* ribotype A, AZA-1/AZA-33 ratios of selected strains, Table S11: Summary statistics *Az. spinosum* ribotype B, AZA cell quota of selected strains, Table S12: Summary statistics *Az. spinosum* ribotype B, AZA-11/AZA-51 ratios of selected strains.

Author Contributions: Conceptualization, U.T.; methodology, U.T., S.W., B.K., H.G.; formal analysis, U.T., S.W., B.K., H.G.; investigation, U.T., S.W., B.K., H.G.; resources, U.T., R.S., D.C.; writing—original draft preparation, U.T., S.W., B.K.; writing—review and editing, U.T., S.W., B.K., H.G., R.S., D.C.; project administration, U.T.; funding acquisition, U.T., B.K. All authors have read and agreed to the published version of the manuscript.

Funding: This work was funded by the German Ministry for Education and Research (project RIPAZA, 03F0763A) and by the PACES II research program of the Alfred-Wegener-Institute as part of the Helmholtz Foundation initiative in Earth and Environment.

Acknowledgments: The authors thank Caroline Cusack, Paula Hynes and Joe Silke (Marine Institute, Galway, Ireland), as well as Luisa Hintze and Karina Krapf (AWI, Bremerhaven, Germany) for on-board technical support. Thomas Max and Anne Müller (both AWI Bremerhaven, Germany) are thanked for continued support in laboratory work and AZA analysis.

Conflicts of Interest: The authors declare no conflict of interest.

Supplementary material

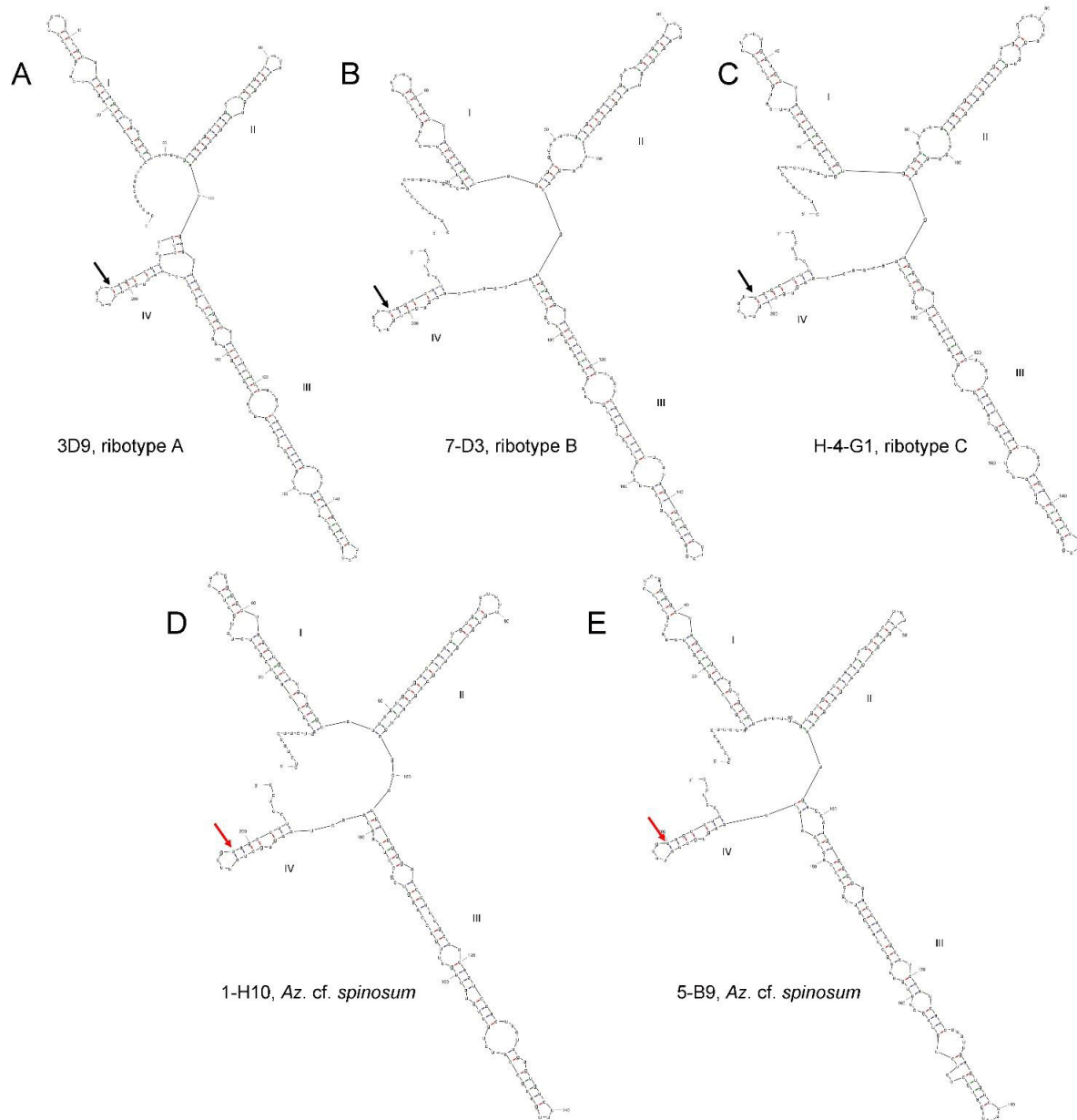


Figure S1. ITS2 secondary structure model of *Az. spinosum* strains 3D9 (A), 7-D3 (B), H-4-G1 (C) and *Az. cf. spinosum* strains 1-H10 (D), 5-B9 (E) showing four helices (I, II, III and IV) and a CBC in helix IV (arrows).

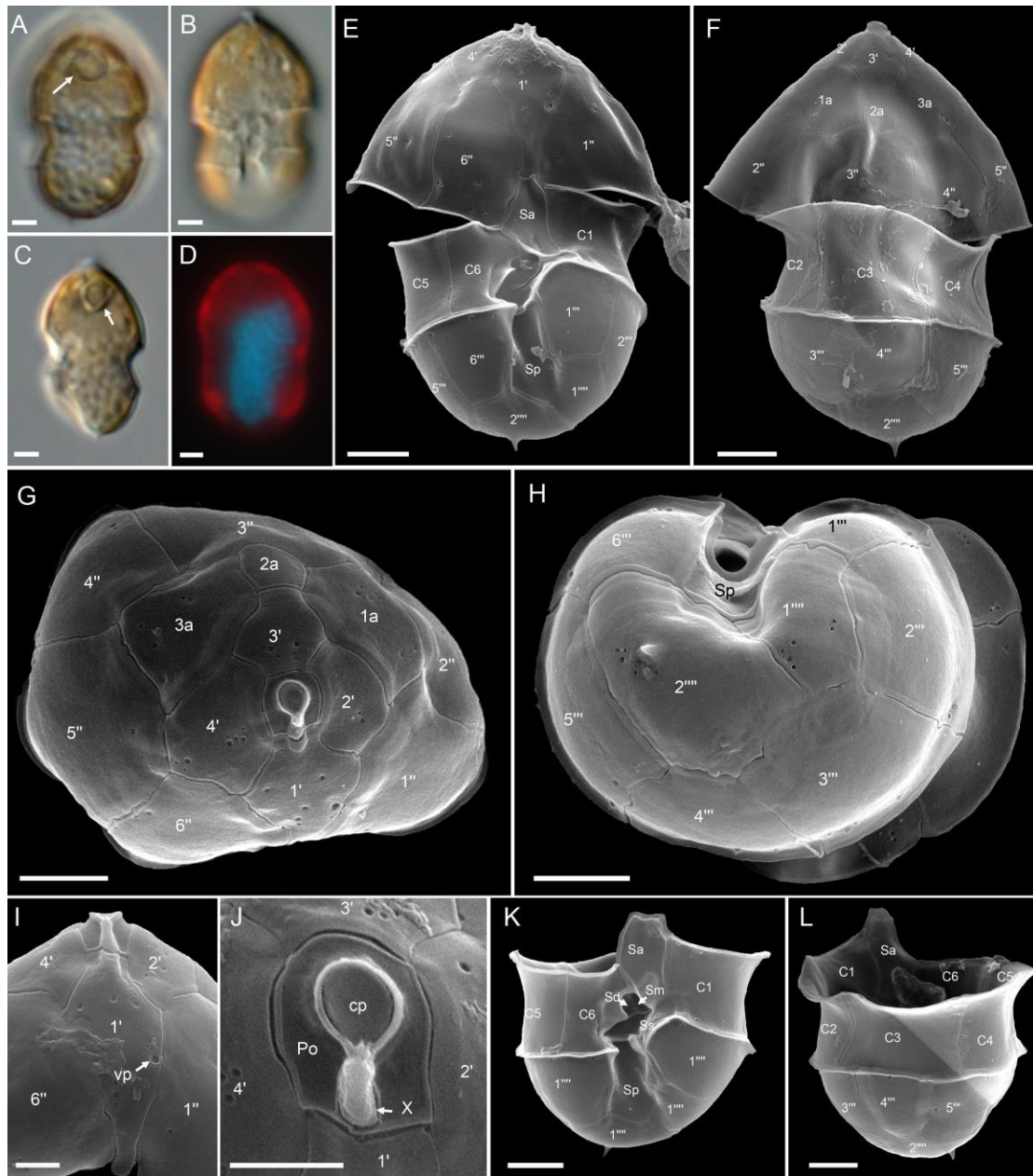


Figure S2. *Azadinium spinosum* ribotype B, strain 5-F3. (A–D) LM images to indicate general size and shape. Note the distinct pyrenoid in the episome (arrows in A, C). (D) Formalin fixed and DAPI-stained cells viewed with UV excitation to indicate shape and position of the nucleus. (E–L) SEM images of different thecae. (E) Ventral view. (F) Dorsal view. (G) Apical view of epithelial plates. (H) Antapical view of hypothecal plates. (I) Epitheca in ventral view, note the position of the ventral pore (vp). (J) Detailed view of the apical pore complex (APC). (K) Hypotheca and sulcal area in ventral view. (L) Hypotheca in dorsal view. Plate labels according to the Kofoidian system. Po = pore plate; cp = cover plate; X = X-plate or canal plate; vp = ventral pore. Abbreviation of sulcal plates: Sa = anterior sulcal plate; Sp = posterior sulcal plate; Ss = left sulcal plate; Sm = median sulcal plate; Sd = right sulcal plate. Scale bars = 2 μm (A–H, K, L) or 1 μm (I, J).

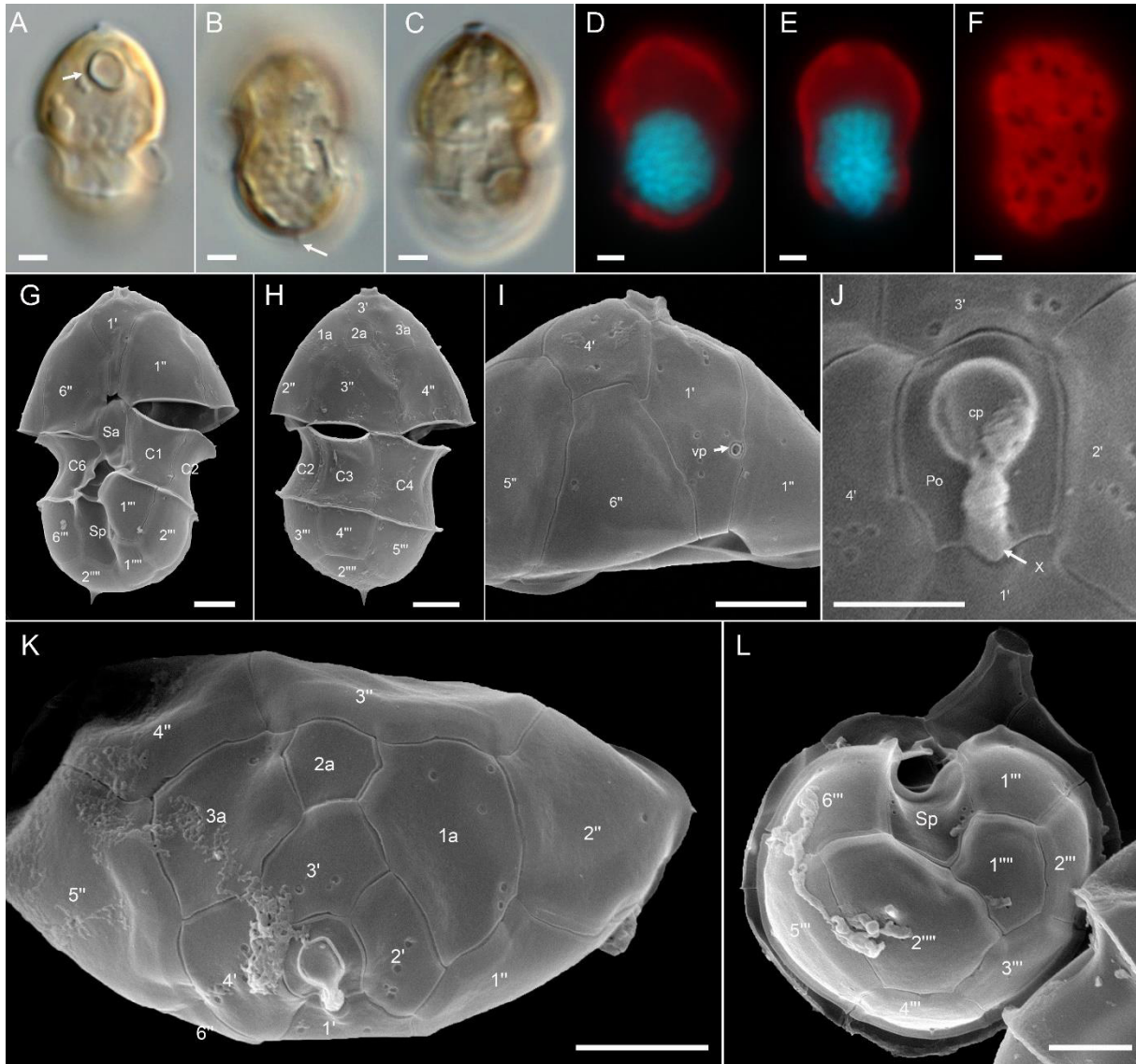


Figure S3. *Azadinium spinosum* ribotype B, strain 5-F7. (A–F) LM images to indicate general size and shape. Note the distinct pyrenoid in the episome (arrow in A) and the antapical spine (arrow in B). (D–F) Formalin fixed and DAPI-stained cells viewed with UV excitation to indicate shape and position of the nucleus (D, E) and of the chloroplast (F). (G–L) SEM images of different thecae. (G) Ventral view. (H) Dorsal view. (I) Epitheca in ventral view, note the position of the ventral pore (vp). (J) Detailed view of the apical pore complex (APC). (K) Apical view of epithecal plates. (L) Antapical view of hypothecal plates. Plate labels according the Kofoidian system. Po = pore plate; cp = cover plate; X = X-plate or canal plate; vp = ventral pore. Abbreviation of sulcal plates: Sa = anterior sulcal plate; Sp = posterior sulcal plate. Scale bars = 2 μm (A–I, K, L) or 1 μm (J).

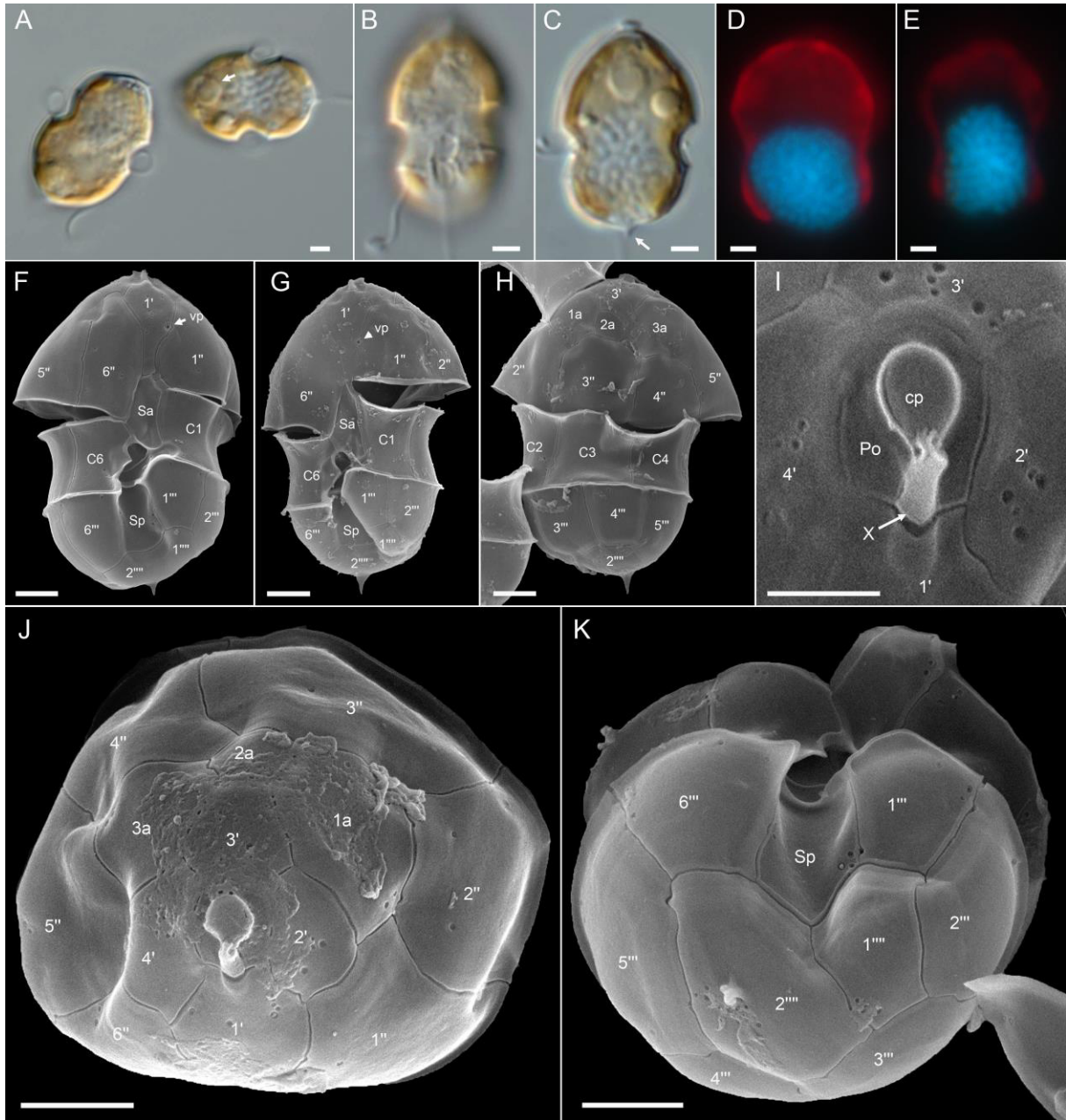


Figure S4. *Azadinium spinosum* ribotype B, strain 7-E4. (A–E) LM images to indicate general size and shape. Note the distinct pyrenoid in the episome (arrow in A) and the antapical spine (arrow in C). (D, E) Formalin fixed and DAPI-stained cells viewed with UV excitation to indicate shape and position of the nucleus. (F–K) SEM images of different thecae. (F, G) Ventral view. (H) Dorsal view. (I) Detailed view of the apical pore complex. (J) Apical view of epithelial plates. (K) Antapical view of hypothecal plates. Plate labels according the Kofoidian system. Po = pore plate; cp = cover plate; X = X-plate or canal plate; vp = ventral pore. Abbreviation of sulcal plates: Sa = anterior sulcal plate; Sp = posterior sulcal plate. Scale bars = 2 μm (A–H, J, K) or 1 μm (I).

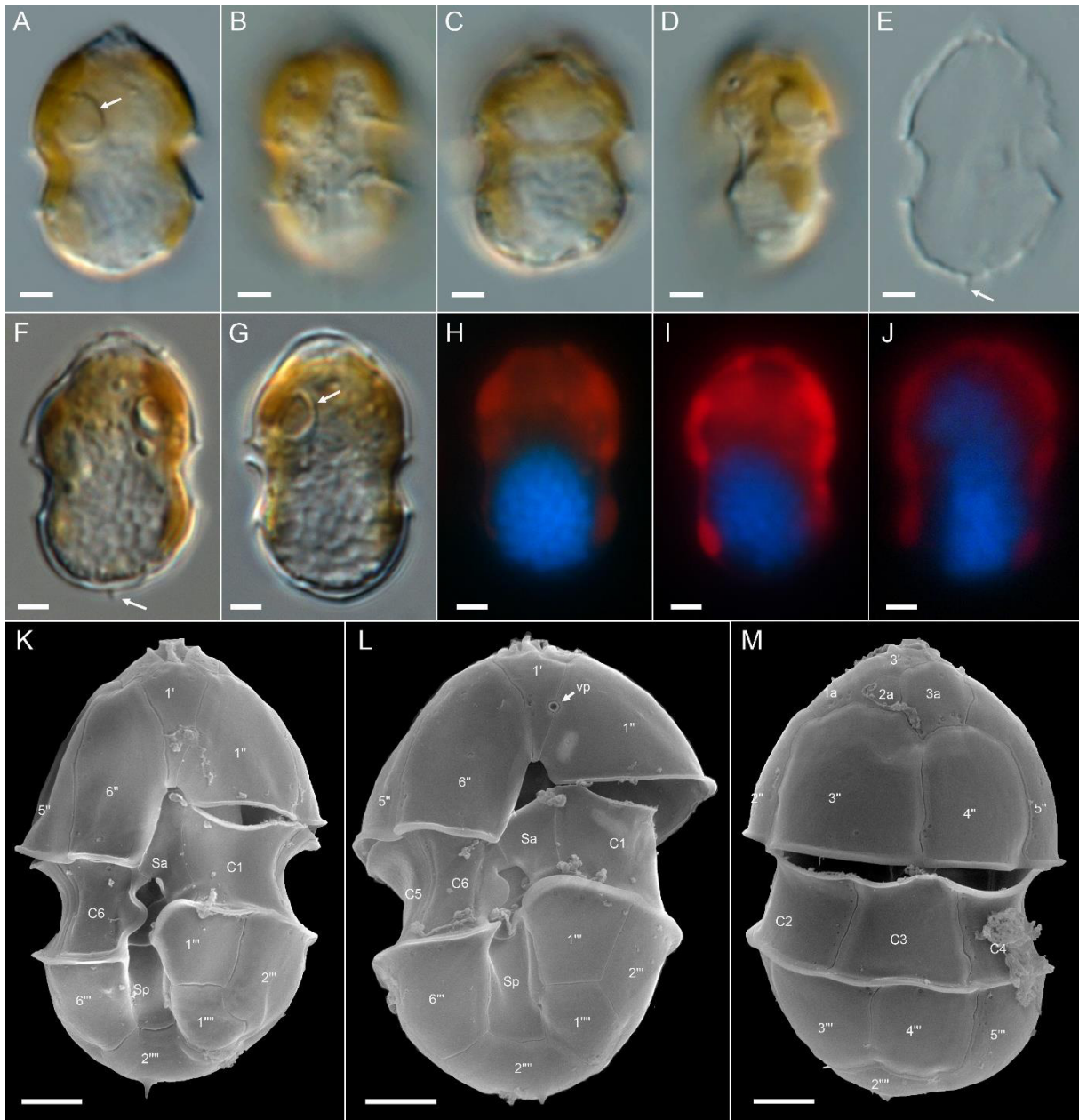


Figure S5. *Azadinium cf. spinosum* strain 6-A1. (A–J) LM images of living cells to indicate general size and shape. Note the distinct pyrenoid in the episome (arrows in A, G) and the antapical spine (arrow in E, F). (H–J) Formalin fixed and DAPI-stained cells viewed with UV excitation to indicate shape and position of the nucleus. (K–M) SEM images of different thecae. (K, L) Ventral view. (M) Dorsal view. Plate labels according to the Kofoidian system. vp = ventral pore. Abbreviation of sulcal plates: Sa = anterior sulcal plate; Sp = posterior sulcal plate. Scale bars = 2 μm.

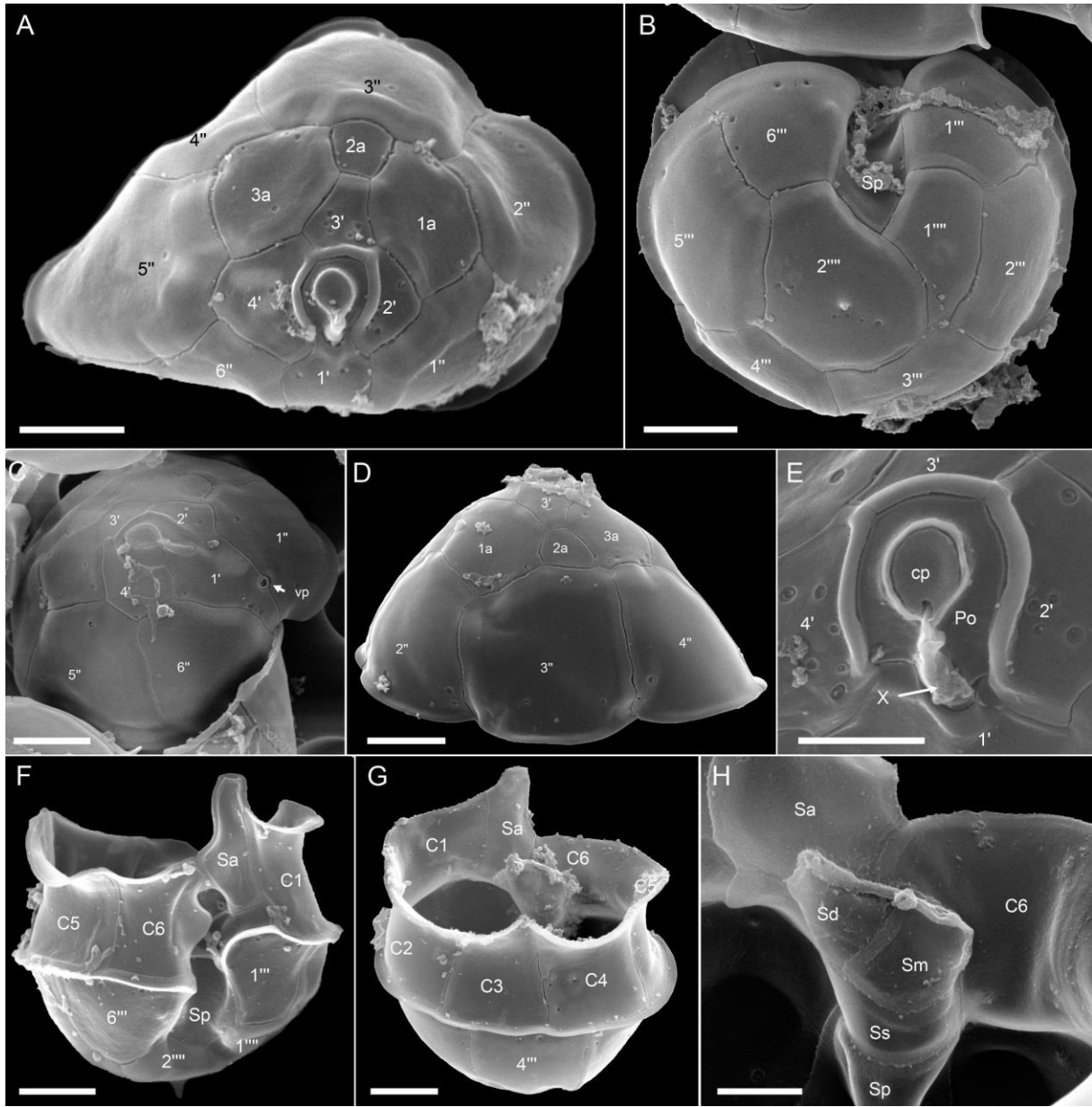


Figure S6. *Azadinium* cf. *spinosum*, strain 6-A1. SEM images of different cells. (A) Apical view of epithecal plates. (B) Antapical view of hypothecal plates. (C) Epitheca in apical/lateral view. (D) Epitheca in dorsal view. (E) Detailed view of the apical pore complex (APC). (F) Hypotheca and sulcal area in ventral view. (G) Hypotheca in dorsal view. (H) Internal view of sulcal plates. Plate labels according the Kofoidian system. Po = pore plate; cp = cover plate; X = X-plate or canal plate; vp = ventral pore. Abbreviation of sulcal plates: Sa = anterior sulcal plate; Sp = posterior sulcal plate; Ss = left sulcal plate; Sm = median sulcal plate; Sd = right sulcal plate. Scale bars = 2 μ m (A–D, F, G) or 1 μ m (E, H).

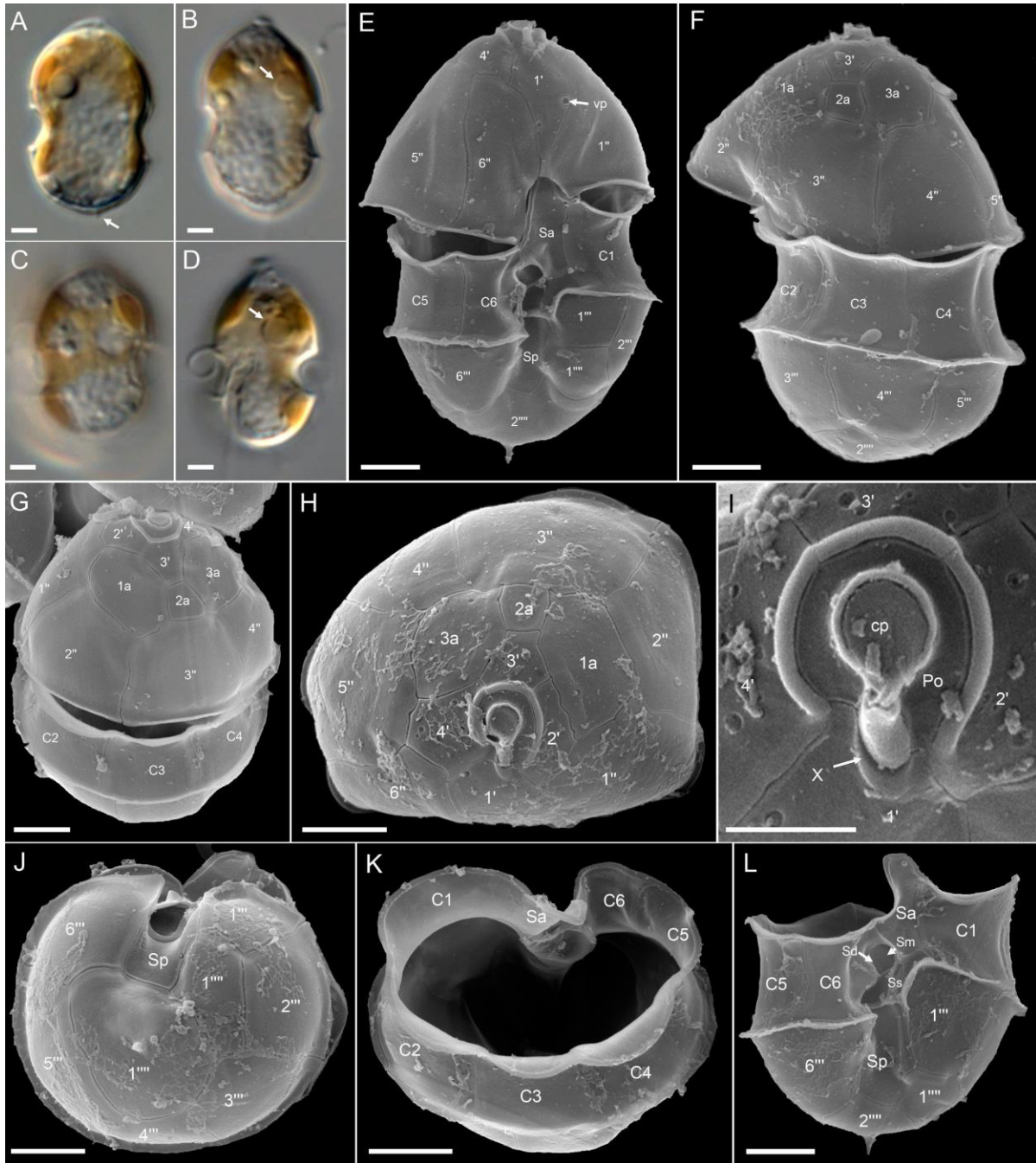


Figure S7. *Azadinium* cf. *spinosum*, strain 2-A3. (A–D) LM images to indicate general size and shape. Note the distinct pyrenoid in the episome (arrows in B, D) and the antapical spine (arrow in A). (E–L) SEM images of different thecae. (E) Ventral view. (F) Dorsal view. (G) Dorsal/apical view. (H) Apical view of epithecal plates. (I) Detailed view of the apical pore complex (APC). (J) Antapical view of hypothecal plates. (K) Hypotheca in apical/ dorsal view. (L) Hypotheca and sulcal area in ventral view. Plate labels according the Kofoidian system. Po = pore plate; cp = cover plate; X = X-plate or canal plate; vp = ventral pore. Abbreviation of sulcal plates: Sa = anterior sulcal plate; Sp = posterior sulcal plate; Ss = left sulcal plate; Sm = median sulcal plate; Sd = right sulcal plate. Scale bars = 2 μ m (A–H, J–L) or 1 μ m (I).

Suppl. Tables

Table S1: Selected reaction monitoring (SRM) transitions monitored for AZAs in the strains.

Mass transition	Toxin	Collision energy [V]
716>698	AZA-33	40
816>798	AZA-39, AZA-34	40
816>348	AZA-39	70
828>658	AZA-3, AZA-58	70
828>810	AZA-3, AZA-43	40
830>812	AZA-38, AZA-35	40
830>348	AZA-38	70
842>672	AZA-1	70
842>824	AZA-1, AZA-40	40
842>348	AZA-40	70
844>826	AZA-4, AZA-5, AZA-56	40
846>828	AZA-37	40
846>348	AZA-37	70
854>836	AZA-41	40
854>670	AZA-41	70
854>360	AZA-41	70
856>672	Me-AZA-1, AZA-2	70
856>838	AZA-2	40
858>840	AZA-7, AZA-8, AZA-9, AZA-10, AZA-36	40
858>348	AZA-36	70
860>842	AZA-59	40
868>850	AZA-55	40
868>362	AZA-55	70
870>852	Me-AZA-2, AZA-42, AZA-54, AZA-62	40
870>360	AZA-42	40
872>854	AZA-11, AZA-12	40
872>362	AZA-11, AZA-12	70
884>866	AZA-57	40
922>904	AZA-1 phosphate	40
936>918	AZA-2 phosphate	40
938>920	AZA-36 phosphate	40
940>842	AZA-59 phosphate	40
952>818	AZA-11 phosphate	40

Table S2: AZA analysis of “high biomass” samples of selected strains to calculate LOD for detecting known AZA (LOD SRM) and for detecting yet unknown AZA in precursor mode (LOD PREC).

Species	Strain	Profile	Pellet cells	LOD SRM known AZA (fg cell ⁻¹)	LOD PREC unknown AZA (fg cell ⁻¹)
<i>Az. spinosum</i>	5-C11	1, 2, 33	43,936,000	0.005	0.569
<i>Az. spinosum</i>	5-E4	1, 2, 33	46,559,000	0.001	0.054
<i>Az. spinosum</i>	6-G5	1, 2, 33	54,955,000	< 0.001	0.046
<i>Az. spinosum</i>	7-E10	1, 2, 33	22,899,250	0.002	0.076
<i>Az. spinosum</i>	7-F4	1, 2, 33	54,339,500	0.001	0.032
<i>Az. spinosum</i>	4-F8	1	46,056,000	0.001	0.054
<i>Az. spinosum</i>	6-G8	1, 2	33,134,100	0.001	0.098
<i>Az. spinosum</i>	2-C8	1, 33	90,041,000	< 0.001	0.028
<i>Az. spinosum</i>	5-F7	11, 51	3,571,000	0.012	0.488
<i>Az. spinosum</i>	7-D3	11, 51	6,980,250	0.002	0.358
<i>Az. spinosum</i>	8-B6	11, 51	7,672,250	0.002	0.326
<i>Az. spinosum</i>	5-F3	11, 51	2,880,300	0.015	0.606
<i>Az. cf. spinosum</i>	1-H10	-	35,917,200	0.001	0.049
<i>Az. cf. spinosum</i>	1-A3	-	90,713,000	< 0.001	0.019
<i>Az. cf. spinosum</i>	5-B9	-	25,535,400	0.002	0.068
<i>Az. cf. spinosum</i>	6-A1	-	27,979,800	0.002	0.062
<i>Am. languida</i>	5-F11	38, 39	1,122,150	0.024	2.230
<i>Am. languida</i>	8-D10	38, 39	5,967,720	0.007	0.292

Table S3. Species used for the molecular analyses based on SSU, ITS1–5.8S–ITS2 and LSU sequences, including strain designation, geographic origin and GenBank accession number. Only some selected new strains (marked with an asterisk (*)) were used to calculate the phylogenetic tree.

Species Name	Strain No.	Locality (Lat., Long)	GenBank No (SSU/ITS/LSU)	Ribotype	Reference
<i>Azadinium caudatum</i> var. <i>caudatum</i>	IFR1191 [IFR10-332]	North Atlantic, France (47°50'N, 03°57'W)	JQ247701 / JQ247700 / JQ247702		Nézan et al., 2012
	IFR10-330, [IFR11-033]	North Atlantic, UK–Scotland (58°38'N, 03°36'W)	- / JQ247705 / JQ247709		Nézan et al., 2012
<i>Azadinium caudatum</i> var. <i>margalefti</i>	AC1	North Atlantic, France (47°50'N, 03°57'W)	JQ247707 / JQ247704 / JQ247708		Nézan et al., 2012
<i>Azadinium concinnum</i>	IC6	North Atlantic, Irminger Sea, (62°14'N, 37°27'W)	- / KJ481829 / KJ481830		Tillmann et al., 2014
	3D6	North Atlantic, Iceland (65°27'N, 24°39'W)	KJ481822 / KJ481823 / KJ481824		Tillmann et al., 2014
<i>Azadinium curvatum</i>	963F5	North Atlantic, USA (47°49'N, 122°48'W)	- / KY404225 / KY404225		Kim et al., 2017
	AZCH02	East China Sea, China (39°15'N, 122°36'E)	KF543360 / KF543358 / KF543359		Luo et al., 2013
<i>Azadinium dalianense</i>	IFR-ADA-01C	North Atlantic, France (47°50'N, 3°57'W)	- / MF033117 / MF033126		Luo et al., 2017
	962B8	North Atlantic, USA (47°23'N, 122°58'W)	- / KY404222 (ITS+LSU)		Kim et al., 2017
<i>Azadinium dexteroporum</i>	N-38-03	North Atlantic, Norway (62°20'N, 03°22'E)	LS974153 (SSU+ITS+LSU)		Tillmann et al., 2018a
	H-2-G7	South Atlantic, Argentina (41°06'S, 57°43'W)	- / MK405513 (ITS+LSU)		Tillmann et al., 2019
<i>Azadinium dexteroporum</i>	n.inf.	Mediterranean Sea, Gulf of Naples (40°49'N, 14°15'W)	- / KJ179946 / KJ179945		Pescopo et al., 2013
	1-D12	North Atlantic, Irminger Sea (64°46'N, 29°57'W)	- / KR362889 / KR362887		Tillmann et al., 2015
<i>Azadinium gabwaense</i>	AZA-2-B1	Labrador Sea, Greenland (56°49'N, 52°13'W)	- / MK882968 / MK882952		Tillmann et al., 2020
	35-R6	North Atlantic, Ireland (52° 1' N, 10° 46'W)	MT644698 / MT644671 / MT644682		Salas et al., submitted
<i>Azadinium obesum</i>	35-R7	North Atlantic, Ireland (52° 1' N, 10° 46'W)	MT644699 / MT644672 / MT644683		Salas et al., submitted
	2E10	North Atlantic, UK–Scotland (57°04'N, 02°30'W)	GQ914935 / FJ766093 / GQ914936		Tillmann et al., 2010
<i>Azadinium perforatum</i>	LF-44-C03	North Atlantic, Denmark (54°33'N, 10°29'E)	- / MK612413 / MK613126		Wietkamp et al., 2019
	AZA-1G	Labrador Sea, Greenland (56°49'N, 52°13'W)	- / MK882967 / MK882951		Tillmann et al., 2020
<i>Azadinium perforatum</i>	N-41-01	North Atlantic, Norway (62°51'N, 06°24'E)	LS974154 / - / LS974155		Tillmann et al., 2018a
	AZA-2E	Labrador Sea, Greenland (56°49'N, 52°13'W)	MK883042 / MK882971 / MK882956		Tillmann et al., 2020
<i>Azadinium perforatum</i>	AZA-2H	Labrador Sea, Greenland (56°49'N, 52°13'W)	MK883043 / MK882974 / MK882959		Tillmann et al., 2020
	2-D1	North Atlantic, Ireland (52° 1' N, 10° 46'W)	MT644700 / MT644673 / MT644684		Salas et al., submitted
<i>Azadinium pseudohuanum</i>	5-B8	North Atlantic, Ireland (52° 1' N, 10° 46'W)	MT644701 / MT644674 / MT644685		Salas et al., submitted
	32-R1	North Atlantic, Ireland (51° 32'N, 10° 0'W)	- / MT644679 / MT644695		Salas et al., submitted
<i>Azadinium polongum</i>	SHE1B2	North Atlantic, Shetland Islands (60°13'N, 01°00'W)	JX559886 (SSU+ITS+LSU)		Tillmann et al., 2012b
	N-47-01	North Atlantic, Norway (63°58'N, 08°37'E)	- / LS974156 (ITS+LSU)		Tillmann et al., 2018a
<i>Azadinium poporum</i>	UTHC5	North Atlantic, Denmark (56°15'N, 07°28'E)	HQ324897 / HQ324889 / HQ324893	A	Tillmann et al., 2011
	TIO256	Mediterranean, France (42°08'N, 09°32'E)	MF033112 / MF033116 / MF033123	A	Luo et al., 2017
<i>Azadinium poporum</i>	AZFC15	South China Sea, China (21°30'N, 108°14'E)	- / KC286569 / KC286550	B	Gu et al., 2013
	GMD29	Gulf of Mexico, USA (29°19'50'N, 93°25'00'W)	- / KU686476 / KU686475	C	Luo et al., 2016
TIO431	Mediterranean Sea, Greece (39°30'N, 20°15'E)	- / MH685508 / MH685486	A	Luo et al., 2018	

Table S3. Continued.

Species Name	Strain No.	Locality (Lat., Long)	GenBank No (SSU/ITS/LSU)	Ribotype	Reference
<i>Azadinium spinosum</i>	3D9	North Atlantic, UK–Scotland (57°04'N, 02°30'W)	FJ217814 / FJ217816 / FJ217815	A	Tillmann et al., 2009
	SHEIF6	North Atlantic, Shetland Islands (60°13'N, 01°00'W)	JX559885 (SSU+ITS+LSU)	A	Tillmann et al., 2012b
	UTHE2	North Atlantic, Denmark (56°15'N, 07°28'E)	HQ324900 / HQ324892 / HQ324896	A	Tillmann et al., 2011
	N-04-02	North Atlantic, Norway (58°15'N, 06°24'E)	LS974160 (SSU+ITS+LSU)	A	Tillmann et al., 2018a
	2-B5	North Atlantic, Ireland (52°47'N, 09°41'W)	- / MT791452 / MT791416	A	this study
	2-C8	North Atlantic, Ireland (52°01'N, 10°46'W)	- / MT791453 / MT791417	A	this study
	2-E2	North Atlantic, Ireland (53°37'N, 09°54'W)	- / MT791454 / MT791418	A	this study
	2-G10	North Atlantic, Ireland (53°37'N, 09°54'W)	- / MT791456 / MT791420	A	this study
	2-G4	North Atlantic, Ireland (53°37'N, 09°54'W)	- / MT791455 / MT791419	A	this study
	3-B4*	North Atlantic, Ireland (53°37'N, 09°54'W)	- / MT791457 / MT791421	A	this study
	3-E6	North Atlantic, Ireland (52°01'N, 10°46'W)	- / MT791458 / MT791422	A	this study
	4-C2	North Atlantic, Ireland (53°37'N, 09°54'W)	- / MT791459 / MT791423	A	this study
	4-D6	North Atlantic, Ireland (53°37'N, 09°54'W)	- / MT791460 / MT791424	A	this study
	4-E11	North Atlantic, Ireland (53°37'N, 09°54'W)	- / MT791461 / MT791425	A	this study
	4-E12	North Atlantic, Ireland (53°37'N, 09°54'W)	- / MT791462 / MT791426	A	this study
	4-F8	North Atlantic, Ireland (53°37'N, 09°54'W)	- / MT791463 / MT791427	A	this study
	4-G9*	North Atlantic, Ireland (52°01'N, 10°46'W)	- / MT791464 / MT791428	A	this study
	5-C11*	North Atlantic, Ireland (53°37'N, 09°54'W)	- / MT791465 / MT791429	A	this study
	5-C12	North Atlantic, Ireland (53°37'N, 09°54'W)	- / MT791466 / MT791430	A	this study
	5-E4	North Atlantic, Ireland (53°37'N, 09°54'W)	- / MT791467 / MT791431	A	this study
	6-A10*	North Atlantic, Ireland (53°37'N, 09°54'W)	- / MT791468 / MT791432	A	this study
	6-F12	North Atlantic, Ireland (53°37'N, 09°54'W)	- / MT791470 / MT791434	A	this study
	6-F8	North Atlantic, Ireland (53°37'N, 09°54'W)	- / MT791469 / MT791433	A	this study
	6-G5	North Atlantic, Ireland (53°37'N, 09°54'W)	- / MT791471 / MT791435	A	this study
	6-G8	North Atlantic, Ireland (53°37'N, 09°54'W)	- / MT791472 / MT791436	A	this study
	7-C1	North Atlantic, North Sea (55°21'N, 04°39'E)	- / MT791473 / MT791437	A	this study
	7-E10	North Atlantic, North Sea (55°21'N, 04°39'E)	- / - / MT791438	A	this study
	7-F4	North Atlantic, North Sea (55°21'N, 04°39'E)	- / MT791474 / MT791439	A	this study
	N-05-01	North Atlantic, Norway (58°22'N, 05°57'E)	LS974163 (SSU+ITS+LSU)	B	Tillmann et al., 2018a
	N-16-02	North Atlantic, Norway (60°52'N, 04°34'E)	LS974168 (SSU+ITS+LSU)	B	Tillmann et al., 2018a
	N-04-04	North Atlantic, Norway (58°15'N, 06°24'E)	LS974162 / - / LS974161	B	Tillmann et al., 2018a
	H-1-D11	South Atlantic, Argentina (41°06'S, 57°43'W)	MK405493 (SSU+ITS+LSU)	B	Tillmann et al., 2019
5-F3	North Atlantic, North Sea (55°21'N, 04°39'E)	- / MT791475 / MT791440	B	this study	
5-F6	North Atlantic, North Sea (55°21'N, 04°39'E)	- / MT791476 / MT791441	B	this study	
5-F7	North Atlantic, North Sea (55°21'N, 04°39'E)	- / MT791477 / MT791442	B	this study	
5-G8*	North Atlantic, North Sea (55°21'N, 04°39'E)	- / MT791478 / MT791443	B	this study	
7-D3*	North Atlantic, North Sea (55°21'N, 04°39'E)	- / MT791479 / MT791444	B	this study	
7-E4	North Atlantic, North Sea (55°21'N, 04°39'E)	- / MT791480 / MT791445	B	this study	

Table S3. Continued.

Species Name	Strain No. <small>Accession</small>	Locality (Lat., Long)	GenBank No (SSU/ITS/LSU)	Ribotype	Reference
<i>Az. spinosum</i> continued	8-B8	North Atlantic, North Sea (55°21'N, 04°39'E)	- / MT791481 / MT791446	B	this study
	H-4-G1	South Atlantic, Argentina (41°06'S, 57°43'W)	- / MK405497 (ITS+LSU)	C	Tillmann et al., 2019
	H-2-D8	South Atlantic, Argentina (41°06'S, 57°43'W)	- / MK405500 (ITS+LSU)	C	Tillmann et al., 2019
	H-4-F9	South Atlantic, Argentina (41°06'S, 57°43'W)	- / MK405510 (ITS+LSU)	C	Tillmann et al., 2019
	H-4-G9	South Atlantic, Argentina (41°06'S, 57°43'W)	- / MK405512 (ITS+LSU)	C	Tillmann et al., 2019
	H-4-E9	South Atlantic, Argentina (41°06'S, 57°43'W)	- / MK405509 (ITS+LSU)	C	Tillmann et al., 2019
<i>Azadinium c.f. spinosum</i>	H-4-E6	South Atlantic, Argentina (41°06'S, 57°43'W)	- / MK405508 (ITS+LSU)	C	Tillmann et al., 2019
	1-H10*	North Atlantic, Ireland (52°01'N, 10°46'W)	MT791401 / MT791482 / MT791447		this study
	2-A3*	North Atlantic, Ireland (52°01'N, 10°46'W)	MT791402 / MT791483 / MT791448		this study
	5-B9*	North Atlantic, Ireland (52°01'N, 10°46'W)	MT791403 / MT791484 / MT791449		this study
	5-D3*	North Atlantic, Ireland (52°01'N, 10°46'W)	MT791404 / - / MT791450		this study
	6-A1*	North Atlantic, Ireland (52°01'N, 10°46'W)	MT791405 / MT791485 / MT791451		this study
<i>Azadinium trinitatum</i>	4A8	North Atlantic, Iceland (64°43'N, 24°02'W)	KJ481808 / KJ481809 / KJ481810		Tillmann et al., 2014
	A2D11	North Atlantic, Iceland (64°43'N, 24°02'W)	KJ481803 / KJ481806 / KJ481807		Tillmann et al., 2014
	N-39-04	North Atlantic, Norway (62°28'N, 05°46'E)	LS974170 (SSU+ITS+LSU)		Tillmann et al., 2018a
	AZA-2F	Labrador Sea, Greenland (56°49'N, 52°13'W)	- / MK882972 / MK882957		Tillmann et al., 2020
	AZA-Z-E10	Labrador Sea, Greenland (56°49'N, 52°13'W)	- / MK882979 / MK882964		Tillmann et al., 2020
	<i>Azadinium zhuanium</i>	TIO205	East China Sea, China (27°28'N, 121°03'E)	MF033110 / MF033114 / MF033120	
	TIO213	East China Sea, China (27°28'N, 121°03'E)	MF033111 / MF033115 / MF033121		Luo et al., 2017
<i>Amphidoma languida</i>	SM1	North Atlantic, Ireland (51°39'N, 09°35'E)	JN615412 / JQ247699 / JN615413		Tillmann et al., 2012a
	2A11	North Atlantic, Iceland (65°27'N, 24°39'W)	KR362880 / KR362882 / KR362885		Tillmann et al., 2015
	AND-A0920	eastern North Atlantic, Spain, (37°11'N, 07°02'W)	KX671042 / KX671038 / KX671043		Tillmann et al., 2017
	N-33-01	North Atlantic, Norway (61°07'N, 04°28'E)	LS974133 / - / LS974132		Tillmann et al., 2018a
	N-40-04	North Atlantic, Norway (62°43'N, 06°03'E)	LS974145 / - / LS974144		Tillmann et al., 2018a
	5-F10*	North Atlantic, North Sea (55°21'N, 04°39'E)	- / - / MT791406		this study
	5-F11	North Atlantic, North Sea (55°21'N, 04°39'E)	- / - / MT791407		this study
	6-D11*	North Atlantic, North Sea (55°21'N, 04°39'E)	- / - / MT791408		this study
	7-F8	North Atlantic, North Sea (55°21'N, 04°39'E)	- / - / MT791409		this study
	7-G4	North Atlantic, North Sea (55°21'N, 04°39'E)	- / - / MT791410		this study
	7-G6	North Atlantic, North Sea (55°21'N, 04°39'E)	- / - / MT791411		this study
	7-H4	North Atlantic, North Sea (55°21'N, 04°39'E)	- / - / MT791412		this study
	7-H5	North Atlantic, North Sea (55°21'N, 04°39'E)	- / - / MT791413		this study
	8-C4	North Atlantic, North Sea (55°21'N, 04°39'E)	- / - / MT791414		this study
8-D10	North Atlantic, North Sea (55°21'N, 04°39'E)	- / - / MT791415		this study	
<i>Amphidoma parvula</i>	H-1E9	Southwest Atlantic, Argentina (41°5.6'S, 37°43.2'W)	KY996792		Tillmann et al., 2018b

Table S4: Compilation of strains of *Az. spinosum* and *Az. cf. spinosum* obtained in this study.

Species	Strain	Origin station	Length (µm)	Width (µm)	l/w ratio	N	Morphological analysis	Sequence data	AZA profile
			Mean ± SD Min-max	Mean ± SD Min-max	Mean ± SD				
<i>Az. spinosum</i>	4-C2	45	14.3±1.1 12.0-16.8	9.6±0.8 7.8-11.2	1.50±0.07	55	LM SEM	LSU, ITS	1, 2, 33
<i>Az. spinosum</i>	2-E2	45	14.7±1.2 12.1-17.1	9.3±0.7 8.1-10.6	1.57±0.09	52	LM SEM	LSU, ITS	1, 2, 33
<i>Az. spinosum</i>	4-E12	45	15.5±1.1 13.3-17.6	10.1±0.8 8.4-11.8	1.54±0.08	50	LM SEM	LSU, ITS	1, 2, 33
<i>Az. spinosum</i>	5-C12	45	13.8±1.0 11.2-16.3	9.3±0.8 7.9-11.7	1.49±0.09	64	LM SEM	LSU, ITS	1, 2, 33
<i>Az. spinosum</i>	7-E10	71	15.0±1.2 11.8-18.2	9.4±0.8 8.2-11.3	1.61±0.09	54	LM SEM	LSU	1, 2, 33
<i>Az. spinosum</i>	2-G4	45	-	-	-	-	LM SEM	LSU, ITS	1, 2, 33
<i>Az. spinosum</i>	5-E4	45	-	-	-	-	LM SEM	LSU, ITS	1, 2, 33
<i>Az. spinosum</i>	7-C1	71	-	-	-	-	LM SEM	LSU, ITS	1, 2, 33
<i>Az. spinosum</i>	5-C11	45	-	-	-	-	LM SEM	LSU, ITS	1, 2, 33
<i>Az. spinosum</i>	7-F4	71	-	-	-	-	LM SEM	LSU, ITS	1, 2, 33
<i>Az. spinosum</i>	2-B5	38	-	-	-	-	LM	LSU, ITS	1, 2, 33
<i>Az. spinosum</i>	6-F8	45	-	-	-	-	LM	LSU, ITS	1, 2, 33
<i>Az. spinosum</i>	6-G5	45	-	-	-	-	LM	LSU, ITS	1, 2, 33
<i>Az. spinosum</i>	4-D3	45	14.5±0.6 13.4-16.0	9.3±0.5 8.3-10.9	1.56±0.07	52	LM SEM	-	1, 2, 33
<i>Az. spinosum</i>	35-R1	35	15.2±1.3 12.9-18.3	9.95±1.2 7.9-12.9	1.53±0.11	50	LM SEM	-	1, 2, 33
<i>Az. spinosum</i>	35-R5	35	15.2±1.3 12.9-18.3	9.95±1.2 7.9-12.9	1.53±0.11	50	LM SEM	-	1, 2, 33
<i>Az. spinosum</i>	2-E3	45	-	-	-	-	LM SEM	-	1, 2, 33
<i>Az. spinosum</i>	2-E9	45	-	-	-	-	LM SEM	-	1, 2, 33
<i>Az. spinosum</i>	2-E5	45	-	-	-	-	LM	-	1, 2, 33
<i>Az. spinosum</i>	2-C12	35	-	-	-	-	LM	-	1, 2, 33
<i>Az. spinosum</i>	4-F10	35	-	-	-	-	LM	-	1, 2, 33
<i>Az. spinosum</i>	4-G8	35	-	-	-	-	LM	-	1, 2, 33
<i>Az. spinosum</i>	4-H2	45	-	-	-	-	LM	-	1, 2, 33
<i>Az. spinosum</i>	6-B10	35	-	-	-	-	LM	-	1, 2, 33
<i>Az. spinosum</i>	3-E12	35	-	-	-	-	-	-	1, 2, 33
<i>Az. spinosum</i>	2-E4	45	-	-	-	-	-	-	1, 2, 33
<i>Az. spinosum</i>	2-G8	45	-	-	-	-	-	-	1, 2, 33
<i>Az. spinosum</i>	2-H7	45	-	-	-	-	-	-	1, 2, 33
<i>Az. spinosum</i>	5-D7	35	-	-	-	-	-	-	1, 2, 33
<i>Az. spinosum</i>	5-E10	45	-	-	-	-	-	-	1, 2, 33
<i>Az. spinosum</i>	6-C4	22	-	-	-	-	-	-	1, 2, 33
<i>Az. spinosum</i>	6-F9	45	-	-	-	-	-	-	1, 2, 33
<i>Az. spinosum</i>	4-E11	45	14.3±0.9 12.8-16.4	9.3±0.7 7.8-10.7	1.55±0.08	50	LM SEM	LSU, ITS	1
<i>Az. spinosum</i>	4-F8	45	15.6±1.1 13.6-17.6	10.0±0.9 8.2-11.9	1.56±0.07	51	LM SEM	LSU, ITS	1
<i>Az. spinosum</i>	3-E6	35	14.5±0.9 12.9-16.8	9.2±0.5 8.1-10.3	1.58±0.08	51	LM SEM	LSU, ITS	1
<i>Az. spinosum</i>	3-B4	45	14.7±1.0 12.5-16.7	9.5±0.7 7.8-11.3	1.54±0.08	51	LM SEM	LSU, ITS	1
<i>Az. spinosum</i>	4-C9	45	15.2±1.0 13.7-17.7	10.0±0.7 8.4-11.5	1.51±0.07	51	LM SEM	-	1

Species	Strain	Origin station	Length (µm)	Width (µm)	l/w ratio	N	Morphological analysis	Sequence data	AZA profile
			Mean ± SD Min-max	Mean ± SD Min-max	Mean ± SD				
<i>Az. spinosum</i>	2-E6	45	-	-	-	-	LM SEM	-	1
<i>Az. spinosum</i>	6-F3	45	-	-	-	-	LM	-	1
<i>Az. spinosum</i>	6-F5	45	-	-	-	-	LM	-	1
<i>Az. spinosum</i>	6-B3	45	-	-	-	-	-	-	1
<i>Az. spinosum</i>	6-G19	45	-	-	-	-	-	-	1
<i>Az. spinosum</i>	6-G8	45	15.1±1.2 12.2-18.7	9.9±0.8 8.0-11.8	1.53±0.07	49	LM SEM	LSU, ITS	1, 2
<i>Az. spinosum</i>	4-D6	45	14.8±0.8 12.8-16.2	9.7±0.8 8.4-11.4	1.52±0.07	50	LM SEM	LSU, ITS	1, 2
<i>Az. spinosum</i>	4-G9	35	14.0±1.0 12.1-16.7	9.2±0.6 7.9-10.6	1.52±0.08	50	LM SEM	LSU, ITS	1, 2
<i>Az. spinosum</i>	2-G10	45	14.1±0.9 12.8-16.6	9.1±0.7 8.1-11.0	1.55±0.05	53	LM SEM	LSU, ITS	1, 2
<i>Az. spinosum</i>	2-F7	45	14.5±0.9 11.9-16.1	9.6±0.8 7.9-11.1	1.51±0.09	50	LM SEM	-	1, 2
<i>Az. spinosum</i>	1-D10	35	-	-	-	-	LM	-	1, 2
<i>Az. spinosum</i>	6-G1	45	-	-	-	-	LM	-	1, 2
<i>Az. spinosum</i>	2-E7	45	-	-	-	-	LM	-	1, 2
<i>Az. spinosum</i>	2-G2	45	-	-	-	-	-	-	1, 2
<i>Az. spinosum</i>	3-E2	35	-	-	-	-	-	-	1, 2
<i>Az. spinosum</i>	4-F1	45	-	-	-	-	-	-	1, 2
<i>Az. spinosum</i>	5-D1	45	-	-	-	-	-	-	1, 2
<i>Az. spinosum</i>	6-A6	32	-	-	-	-	-	-	1, 2
<i>Az. spinosum</i>	2-C8	35	14.5±0.9 11.9-16.5	9.7±0.6 8.2-10.7	1.50±0.07	53	LM SEM	LSU, ITS	1, 33
<i>Az. spinosum</i>	6-A10	45	14.3±1.0 12.6-16.9	9.1±0.7 7.8-10.9	1.57±0.07	52	LM SEM	LSU, ITS	1, 33
<i>Az. spinosum</i>	6-F12	45	14.2±1.0 12.5-16.5	9.0±0.6 7.7-10.4	1.58±0.09	51	LM SEM	LSU, ITS	1, 33
<i>Az. spinosum</i>	5-E2	45	-	-	-	-	LM	-	1, 33
<i>Az. spinosum</i>	6-F1	45	-	-	-	-	LM	-	1, 33
<i>Az. spinosum</i>	8-B8	71	16.8±0.9 14.6-18.8	10.5±0.7 9.2-12.0	1.60±0.07	50	LM SEM	LSU, ITS	11, 51
<i>Az. spinosum</i>	7-D3	71	16.2±1.1 13.7-18.7	10.0±0.8 8.6-11.8	1.62±0.09	52	LM SEM	LSU, ITS	11, 51
<i>Az. spinosum</i>	5-F6	71	15.8±0.8 13.3-16.7	9.7±0.7 8.3-11.6	1.52±0.07	54	LM SEM	LSU, ITS	11, 51
<i>Az. spinosum</i>	5-F7	71	15.2±1.1 13.4-17.9	10.0±0.8 8.8-12.2	1.52±0.07	52	LM SEM	LSU, ITS	11, 51
<i>Az. spinosum</i>	5-G8	71	-	-	-	-	LM SEM	LSU, ITS	11, 51
<i>Az. spinosum</i>	7-E4	71	-	-	-	-	LM SEM	LSU, ITS	11, 51
<i>Az. spinosum</i>	5-F3	71	-	-	-	-	LM SEM	LSU, ITS	11, 51
<i>Az. cf. spinosum</i>	1-H10	35	15.0±0.9 13.4-17.6	9.5±0.5 8.3-10.6	1.58±0.08	31	LM SEM	SSU, LSU, ITS	no AZA
<i>Az. cf. spinosum</i>	2-A3	35	15.1±0.9 13.1-16.8	9.8±0.7 8.3-10.8	1.55±0.07	56	LM SEM	SSU, LSU, ITS	no AZA
<i>Az. cf. spinosum</i>	6-A1	35	16.6±0.9 14.9-18.7	10.7±0.8 9.5-12.9	1.56±0.08	54	LM SEM	SSU, LSU, ITS	no AZA
<i>Az. cf. spinosum</i>	5-B9	35	14.9±0.8 12.9-16.9	10.0±0.7 8.1-11.5	1.49±0.06	54	LM SEM	SSU, LSU, ITS	no AZA
<i>Az. cf. spinosum</i>	5-D3	35	-	-	-	-	LM SEM	SSU, LSU	no AZA

Table S5: Compilation of strains of *Am. languida* obtained in this study.

Species	Strain	Origin Station	Length (µm)	Width (µm)	l/w ratio	N	Morphological analysis	Sequence data
			Mean ± SD Min-max	Mean ± SD Min-max	Mean ± SD			
<i>Am. languida</i>	5-F11	71	12.6±1.2 7.4–14.9	9.4±0.7 7.7–11.7	1.35±0.10	54	LM SEM	LSU
<i>Am. languida</i>	6-D11	71	12.9±0.8 11.5–14.4	10.5±0.7 9.1–12.2	1.23±0.06	54	LM SEM	LSU
<i>Am. languida</i>	7-G6	71	14.4±1.1 12.3–16.6	11.8±1.0 9.8–14.5	1.23±0.06	51	LM SEM	LSU
<i>Am. languida</i>	7-H4	71	13.3±0.9 10.7–14.9	10.9±0.8 9.6–13.1	1.22±0.10	40	LM SEM	LSU
<i>Am. languida</i>	7-F8	71	13.3±0.7 11.6–14.9	10.9±0.9 9.1–14.4	1.22±0.09	51	LM	LSU
<i>Am. languida</i>	5-F10	71	13.4±1.3 10.7–15.8	10.0±1.0 7.5–12.5	1.34±0.10	51	LM	LSU
<i>Am. languida</i>	7-H5	71	13.6±1.1 10.4–16.0	10.9±1.0 8.8–13.3	1.25±0.08	51	LM	LSU
<i>Am. languida</i>	8-C4	71	-	-	-	-	LM SEM	LSU
<i>Am. languida</i>	8-D10	71	-	-	-	-	LM SEM	LSU
<i>Am. languida</i>	7-G4	71	-	-	-	-	LM	LSU

Table S6: Uncorrected p-distances of ITS sequence data between different *Az. spinosum* ribotypes, *Az. cf. spinosum*, and other closely related *Azadinium* species. Based on the threshold suggested by Litaker et al. (2007) of 0.04 to differentiate between dinophyte species the values are highlighted as green (< 0.04), yellow (= 0.04) or red (> 0.04).

	3-B4 <i>spinosum</i> A	3D9 <i>spinosum</i> A	7-D3 <i>spinosum</i> B	H-4-G1 <i>spinosum</i> C	5-B9 cf. <i>spinosum</i>	1-H10 cf. <i>spinoim</i>	A2D11 <i>triniatum</i>	3D6 <i>cuneatum</i>	UTHC8 <i>poporum</i>	2E10 <i>obesum</i>
3-B4 <i>Az. spinosum</i> A*										
3D9 <i>Az. spinosum</i> A	0.01									
7-D3 <i>Az. spinosum</i> B*	0.02	0.03								
H-4-G1 <i>Az. spinosum</i> C	0.03	0.03	0.03							
5-B9 <i>Az. cf. spinosum</i> *	0.06	0.07	0.06	0.07						
1-H10 <i>Az. cf. spinosum</i> *	0.05	0.06	0.05	0.06	0.02					
A2D11 <i>Az. triniatum</i>	0.06	0.06	0.06	0.07	0.06	0.05				
3D6 <i>Az. cuneatum</i>	0.11	0.11	0.10	0.11	0.09	0.09	0.08			
UTHC8 <i>Az. poporum</i>	0.08	0.08	0.08	0.09	0.07	0.06	0.08	0.08		
2E10 <i>Az. obesum</i>	0.06	0.06	0.06	0.07	0.04	0.03	0.05	0.08	0.05	
AZCH02 <i>Az. dalianense</i>	0.09	0.09	0.09	0.10	0.10	0.09	0.09	0.11	0.09	0.08

Table S7. Specificity test of the *Az. spinosum*, *Az. poporum* and *Am. languida* qPCR assays on normed DNA concentration (1 ng μL^{-1}) of pre-existing reference strains and newly gained strains from this study (in red) by comparisons of mean C_T values (technical replicates, n=3). Extended from Wietkamp et al. (2019b). n.a. = not assigned; ND = not detected.

Species	Strain	Toxin profile	Ribotype	Result of the <i>Az. spinosum</i> assay	Result of the <i>Az. poporum</i> assay	Result of the <i>Am. languida</i> assay	
<i>Az. spinosum</i>	3D9	AZA-1, -2, -33	A	$C_T = 19.3$	ND	ND	
	4-F8	AZA-1	A	$C_T = 18.4$	ND	ND	
	5-C11	AZA-1, -2, -33	A	$C_T = 18.4$	ND	ND	
	6-G8	AZA-1, -2	A	$C_T = 19.4$	ND	ND	
	N-04-01	AZA-1, -2, -33	A	$C_T = 19.4$	ND	ND	
	Shet-F6	AZA-1, -2, -33	A	$C_T = 19.2$	ND	ND	
	SM2	AZA-1, -2, -33	A	$C_T = 19.8$	ND	ND	
	UTH-E2	AZA-1, -2, -33	A	$C_T = 19.1$	ND	ND	
	5-F3	AZA-11, -51	B	$C_T = 25.6$	ND	ND	
	8-B8	AZA-11, -51	B	$C_T = 25.4$	ND	ND	
	H-1-D11	AZA-2	B	$C_T = 26.1$	ND	ND	
	N-04-04	AZA-11, -51	B	$C_T = 25.7$	ND	ND	
	N-05-01	AZA-11, -51	B	$C_T = 26.8$	ND	ND	
	N-16-02	AZA-11, -51	B	$C_T = 25.2$	ND	ND	
	H-4-A10	ND	C	ND	ND	ND	
	H-4-A1	ND	C	ND	ND	ND	
	H-4-C10	ND	C	ND	ND	ND	
	<i>Az. cf spinosum</i>	1-H10	ND	n.a.	ND	ND	ND
		2-A3	ND	n.a.	ND	ND	ND
5-B9		ND	n.a.	ND	ND	ND	
5-D3		ND	n.a.	ND	ND	ND	
6-A1		ND	n.a.	ND	ND	ND	
<i>Am. languida</i>	2-A11	AZA-38, -39	n.a.	ND	ND	$C_T = 20.5$	
	AND-A0920	AZA-2, -43	n.a.	ND	ND	$C_T = 20.4$	
	5-F11	AZA-38, -39	n.a.	ND	ND	$C_T = 20.7$	
	8-D10	AZA-38, -39	n.a.	ND	ND	$C_T = 20.4$	

Table S8: *Az. spinosum* ribotype A. Total AZA cell quota (fg cell⁻¹) single strains, summary statistics of multiple measurements. Toxin profile type: 1: AZA-1, -2, -33; 2: AZA-1; 3: AZA-1, -2; 4: AZA-1, -33. “period” indicates the time period (months) in which multiple measurements were performed.

strain	tox-type	median	SD	min	max	fold	n	period
2-G4	1	16.2	9.7	13.9	37.7	2.7	4	18
4-C2	1	31.6	22.8	7.4	63.1	8.5	3	16
5-E4	1	18.1	7.1	1.3	20.6	16.2	5	16
6-F8	1	12.2	5.7	3.7	18.3	4.9	4	18
2-E9	1	5.3	5.6	4.2	19.1	4.5	5	18
4-C9	2	18.9	10.9	8.0	29.8	3.7	2	16
4-D6	3	13.8	9.7	9.3	36.5	3.9	5	16
6-G8	3	4.7	6.3	1.8	19.7	11.1	5	16
2-C8	4	8.0	5.4	5.7	20.7	3.6	5	16
2-B5	1	14.8	6.8	1.2	16.2	13.6	3	8
2-E2	1	24.9	5.4	16.8	29.8	1.8	3	8
5-C11	1	17.6	19.7	9.3	58.9	6.3	4	9
6-G5	1	10.2	7.6	3.5	24.1	6.9	4	9
7-C1	1	18.1	9.4	1.6	23.9	15.0	3	9
7-E10	1	12.4	6.5	5.9	18.9	3.2	2	8
7-F4	1	8.1	4.2	1.5	11.7	8.0	3	8
3-E6	2	1.5	0.7	1.4	2.9	2.2	3	8
4-E11	2	7.3	0.6	7.1	8.3	1.2	3	8
4-F8	2	6.9	16.7	4.2	44.4	10.6	4	9
2-G10	3	10.7	4.0	9.9	18.8	1.9	3	8
4-G9	3	18.8	4.3	11.4	21.6	1.9	3	8
2-E7	3	12.1	18.9	6.6	49.1	7.5	3	8
6-A10	4	16.2	13.7	3.3	36.6	11.1	3	8

Table S9: *Az. spinosum* ribotype A. AZA-1/-2 ratio, variability single strains, multiple measurements. Toxin profile type: 1: AZA-1, -2, -33; 2: AZA-1; 3: AZA-1, -2; 4: AZA-1, -33. “period” indicates the time period (months) in which multiple measurements were performed.

strain	tox-type	median	SD	min	max	fold	n	period
2-G4	1	3.8	0.6	3.0	4.6	1.5	4	18
4-C2	1	8.9	4.5	3.8	14.7	3.9	3	16
5-E4	1	1.7	3.4	1.6	10.2	6.5	5	16
6-F8	1	4.6	1.1	3.1	6.1	2.0	4	18
2-E9	1	4.5	1.0	2.6	5.3	2.0	5	18
4-C9	2						3	16
4-D6	2	1.2	0.3	0.7	1.6	2.1	5	16
6-G8	2	1.9	0.3	1.8	2.5	1.4	5	16
2-C8	4						5	16
2-B5	1	1.8	0.4	1.2	2.1	1.7	3	8
2-E2	1	2.3	0.1	2.3	2.6	1.1	3	8
5-C11	1	1.9	0.4	1.3	2.4	1.8	4	9
6-G5	1	2.3	0.6	1.9	3.4	1.9	4	9
7-C1	1	1.3	0.4	1.1	2.0	1.8	3	9
7-E10	1	2.6	0.8	1.7	3.4	1.9	2	8
7-F4	1	1.9	0.3	1.8	2.5	1.4	3	8
3-E6	2						3	8
4-E11	2						3	8
4-F8	2						4	9
2-G10	3	10.5	2.6	5.8	12.0	2.1	3	8
4-G9	3	1.8	0.2	1.4	1.8	1.3	3	8
2-E7	3	2.7	0.3	2.1	2.9	1.4	3	8
6-A10	4						3	8

Table S10: *Az. spinosum* ribotype A. Ratio AZA-1/-33, variability single strains, multiple measurements. Toxin profile type: 1: AZA-1, -2, -33; 2: AZA-1; 3: AZA-1, -2; 4: AZA-1, -33. “period” indicates the time period (months) in which multiple measurements were performed.

strain	tox-type	median	SD	min	max	fold	n	period
2-G4	1	4.3	1.9	3.7	8.5	2.3	4	18
4-C2	1	8.0	2.0	7.4	11.9	1.6	3	16
5-E4	1	1.0	0.3	0.7	1.4	2.1	5	16
6-F8	1	7.1	2.2	2.7	8.6	3.1	4	18
2-E9	1	7.1	3.8	3.6	14.2	3.9	5	18
4-C9	2						3	16
4-D6	3						5	16
6-G8	3						5	16
2-C8	4	2.7	0.8	2.1	4.3	2.0	5	16
2-B5	1	5.3	2.6	4.5	10.4	2.3	3	8
2-E2	1	2.3	1.4	1.7	4.9	2.9	3	8
5-C11	1	5.6	1.0	4.6	7.2	1.6	4	9
6-G5	1	6.5	4.0	2.9	13.9	4.8	4	9
7-C1	1	1.8	0.4	1.6	2.6	1.6	3	9
7-E10	1	7.7	0.0	7.6	7.7	1.0	2	8
7-F4	1	5.8	1.1	3.8	6.2	1.6	3	8
3-E6	2						3	8
4-E11	2						3	8
4-F8	2						4	9
2-G10	3						3	8
4-G9	3						3	8
2-E7	3						3	8
6-A10	4	11.1	1.7	9.0	13.1	1.4	3	8

Table S11: *Az. spinosum* ribotype B. Total AZA cell quota (fg cell⁻¹) single strains, summary statistics of multiple measurements. Toxin profile type: AZA-11 and AZA-51. “period” indicates the time period (months) in which multiple measurements were performed.

strain	tox-type	median	SD	min	max	fold	n	period
5-F3	11-51	2.5	5.5	0.2	14.0	68.1	4	13
5-F7	11-51	1.2	0.8	0.4	2.4	6.6	4	13
5-G8	11-51	1.8	1.6	0.2	3.5	21.6	2	14
7-D3	11-51	3.1	2.6	0.1	5.6	63.7	4	13
7-E4	11-51	0.6	0.4	0.2	1.0	4.7	2	13

Table S12: *Az. spinosum* ribotype B. AZA-11/-51 ratio, variability single strains, multiple measurements. Toxin profile type: AZA-11 and AZA-51. “period” indicates the time period (months) in which multiple measurements were performed.

strain	tox-type	median	SD	min	max	fold	n	period
5-F3	11-51	1.4	0.5	0.6	1.9	2.6	4	13
5-F7	11-51	0.3	0.2	0.1	0.5	3.6	4	13
5-G8	11-51	1.1	0.7	0.3	1.8	5.3	2	14
7-D3	11-51	1.1	0.5	1.1	2.3	2.2	4	13
7-E4	11-51	0.8	0.1	0.7	0.8	1.2	2	13

Publication VIII: Temperature effect on toxigenic Amphidomataceae

The effect of temperature on growth and toxin production in three toxigenic amphidomatacean species.

Wietkamp, S., Bantle, A., Krock, B., Tillmann, U. (to be submitted)

Publication VIII will present the results of physiological studies on four selected toxigenic amphidomatacean strains from the three AZA-producing species known in the North Atlantic: *Az. spinosum*, *Az. poporum* and *Am. languida*. Experimental design aimed at the growth response and toxin production of the four strains in relation to different temperature regimes.

Previous studies revealed a relatively broad temperature tolerance and temperature dependent growth and toxin production. This could be confirmed here by a faster increase in population density at higher temperatures. In contrast, AZA cell quota were generally higher at lower temperatures. The calculation of a theoretical AZA production rate based on AZA cell quota and growth rate revealed that the generally higher growth rates at higher temperatures are able to compensate higher AZA cell quota in low temperature adapted cells, and leading to a similar potential AZP risk of cells growing at low and high temperatures per a defined water volume.

The study was designed by the candidate and conducted independently (80%) after consultation with the corresponding author. This included experimental set-up, daily growth observations, subsampling for AZA measurements and all related tasks (70%) with the help of A. Bantle. The results were evaluated (90%), graphically presented (90%), as well as scripted (100%) by the candidate. Further manuscript editing of the current preliminary version in close cooperation with the co-authors will be performed in the near future.

The effect of temperature on growth and toxin production in three toxigenic amphidomatacean species

Stephan Wietkamp¹, Alexis Bantle², Bernd Krock¹ and Urban Tillmann^{1*} (to be submitted)

¹ Alfred Wegener Institute, Helmholtz Center for Polar and Marine Research, Am Handelshafen 12, D-27570 Bremerhaven, Germany

² University of California, 9500 Gilman Drive, La Jolla, San Diego, California, USA

*Corresponding author: urban.tillmann@awi.de

Abstract

Azaspiracids (AZA) are a group of lipophilic biotoxins, which are produced by a few members of the marine dinoflagellate family Amphidomataceae. Temperature dependent growth and AZA-production were investigated in strains of all known AZA-producing species from the North Atlantic, i.e. *Azadinium spinosum* (2 strains), *Az. poporum* (1 strain) and *Amphidoma languida* (1 strain). All four amphidomatacean strains grew at a wide range of temperatures. Growth rates and AZA cell quota were temperature dependent. *Azadinium poporum* strain UTH-D4 (5 to 22.5 °C, optimum at 20 °C) and *Az. spinosum* strain 7-F4 grew at a wider range (10 to 27.5 °C, optimum at 20 and 25 °C) compared to *Az. spinosum* strain N-05-01 (10 to 20 °C, optimum at 20 °C) and *Am. languida* strain 8-D10 (10 to 20 °C, optimum at 20 °C). Growth rate and AZA cell quota were found to behave contrarily: While highest growth rates were observed at higher temperatures, AZA cell quota were highest at lower temperatures. However, the calculation of a theoretical AZA production rate based on AZA cell quota and growth rate revealed that the generally higher growth rates at higher temperatures compensated higher AZA cell quota in low temperature grown cells. This suggests a similar AZA intoxication risk by cells growing at low and high temperatures per a defined water volume. Intraspecific variability in AZA cell quotas for toxigenic amphidomataceans was confirmed here, but the responsible reasons remain unknown. Both, intra- and extracellular AZA was measured. In contrast to the three other strains, the *Az. spinosum* Ribotype B significantly contributed to particulate dissolved AZA in the supernatant.

Key Words: AZA, Amphidomataceae, culturing, temperature, AZP, toxin production

1. Introduction

Azaspiracids (AZA) are a group of lipophilic polyketides produced by some species of the marine dinophyte family Amphidomataceae. AZA officiate as biotoxins, as they can be accumulated in shellfish and lead to severe gastrointestinal symptoms in humans after consumption, the so-called Azaspiracid-Shellfish-Poisoning syndrome (AZP).

AZA contamination in shellfish (mussels, oysters, clams, scallops, cockles) and AZP incidents have been reported from various European countries like Ireland, Norway, Italy, France, Spain, Portugal (Ofuji et al., 1999; Braña Magdalena et al., 2003; Vale et al., 2008). However, AZA have also been confirmed in Africa, Chile, Argentina, China, the US and New Zealand, hypothesizing a global phenomenon (James et al., 2002; Taleb et al., 2006; Torgersen et al., 2008; Alvarez et al., 2010; Yao et al., 2010; Trainer et al., 2013; Turner and Goya, 2015; Smith et al., 2016). While AZA are known and investigated since the 90's, the producing organisms remained unknown until 2007, when Tillmann et al. (2009) described the new species *Azadinium spinosum* within the newly erected genus *Azadinium* as the first primary source of AZA. Since then, more than ten years of further research revealed existence of so far four AZA-producing amphidomatacean species and more than 62 AZA toxin isomers (Krock et al., 2019).

Already in 2001, the EU has set a regulatory limit for AZA contamination ($> 0.16 \mu\text{g g}^{-1}$) in shellfish flesh, based on a risk assessment by the Food Safety Authority of Ireland - FSAI (EU, 2001; FSAI, 2001). And in fact, toxigenic Amphidomataceae and AZA are a major threat to Irish mussel farmers (Salas et al., 2011), which has led to the implementation of frequent monitoring in Irish coastal waters and shellfish by the Marine Institute (Galway, Ireland). Albeit descriptive investigations on the biogeography and diversity of AZA and their producing species are demonstrated in a couple of field studies (Wietkamp et al., 2019a; Tillmann et al., 2020; Wietkamp et al., 2020), less is known about actual driving factors favoring amphidomatacean population growth and AZA production in the field.

Various studies have shown how abiotic parameters such as temperature, salinity, light and nutrients (nitrogen and phosphorus) can affect growth and toxin production in dinoflagellate species (Flynn et al., 1996; Maclean et al., 2003; Hu et al., 2006; Gedaria et al., 2007; Lartigue et al., 2009; Xu et al., 2010). However, the physiology of individual dinoflagellate species and the chemistry of biotoxin production varies significantly between species (Granéli and Turner, 2006) and it is thus difficult if not impossible to deduce the physiological response of yet unstudied species. With respect to Amphidomataceae, there are a few previous culture studies available.

Jauffrais et al. (2013b) conducted first laboratory experiments with *Azadinium spinosum* (strain 3D9) isolated from the North Sea and investigated the effect of several factors (salinity, temperature, photon flux density, aeration, culture media, nitrogen sources, phosphate source, and N/P ratios) on growth rates, maximum cell concentrations and AZA cell quota. Kilcoyne et al. (2019) also grew *Az. spinosum* strain 3D9 at different temperatures, media and photoperiodic regimes and observed growth rate, toxin production and AZA cell quota. The aim here was to maximize toxin yields, to assess changes in toxin profiles over different growth phases to identify potential new AZA and to obtain insights into factors which influence toxin cell quota. For another toxigenic amphidomatacean species, *Az. poporum*, Li et al. (2016) investigated the impact of different media on growth and toxin production in two strains (AZDY06 and AZFC22) from the South China Sea and Luo et al. (2018) subjected four newly isolated *Az. poporum* strains (TIO420, TIO424, TIO429 and TIO452) from the Mediterranean Sea to growth experiments under several temperature regimes. Growth and AZA cell quota in two *Az. poporum* strains (NWFSC1011 and NWFSC1018) from Puget Sound (Washington State) along temperature and salinity gradients were studied by Dai et al. (2019).

Despite these studies, relatively little is known about the physiology of toxigenic Amphidomataceae, especially under the perspective of relatively complex phylogeny, including several Ribotypes for *Az. spinosum* and *Az. poporum*. Although *Az. spinosum* has been studied by Jauffrais et al. (2013) and Kilcoyne et al. (2019), only the North Sea Ribotype A with the traditional toxin profile of AZA-1, -2 and -33 was investigated. In 2018 however, Tillmann et al. presented *Azadinium spinosum* Ribotype B strains, which differ with respect to morphology, DNA sequences and toxin profile (AZA-11, -51) from Ribotype A strains. Previous studies on *Az. poporum* included Ribotype A strains from the Mediterranean Sea and the US, but Ribotype A strains from the North Atlantic (the actual type locality of *Az. poporum* Ribotype A) have never been subjected to physiological studies.

Amphidoma languida, although confirmed to be a widely distributed AZA-producer (AZA-38, -39) in the eastern North Atlantic (Wietkamp et al., 2019 and 2020), have never been targeted in physiological studies.

The aim of this study was therefore to compare two toxigenic *Az. spinosum* strains (representing Ribotype A and Ribotype B), one *Az. poporum* strain (Ribotype A) and one *Am. languida* strain from the North Sea and adjacent areas in terms of growth and toxin production under different temperature regimes.

2. Materials & Methods

2.1 Toxigenic amphidomatacean strains

All four strains investigated in this study belong to the three AZA-producing species present in the North Sea and adjacent areas - *Azadinium spinosum* (Ribotype A and B), *Az. poporum* (Ribotype A) and *Amphidoma languida* (Table 1).

Table 1. The four toxigenic strains investigated in this study.

Species	Strain	Ribotype	Toxin Profile	Origin	Reference
<i>Azadinium spinosum</i>	7-F4	A	AZA-1, -2, -33	Central North Sea	Publication VII
<i>Azadinium spinosum</i>	N-05-01	B	AZA-11, -51	Norway	Tillmann et al. (2018)
<i>Azadinium poporum</i>	UTH-D4	A	AZA-37	Denmark	Tillmann et al. (2011), Krock et al. (2012)
<i>Amphidoma languida</i>	8-D10	n.a.	AZA-38, -39	Central North Sea	Publication VII

2.2 Stock cultures

2.2.1 Culture conditions

Clonal stock cultures of all strains were kept within 70 mL plastic culture flasks (TPP, Trasadingen, Switzerland) at 15 °C under a photon flux density of 50 $\mu\text{mol m}^{-2} \text{s}^{-1}$ on a 16:8 h light:dark photocycle. Cells were grown in a natural seawater medium prepared with sterile-filtered (0.2 μm VacuCap filters, Pall Life Sciences, Dreieich, Germany) Antarctic seawater (salinity: 34, pH adjusted to 8.0) and enriched with 1/10 strength K-medium (Keller et al. (1987); slightly modified by omitting addition of ammonium ions). Cell density (cells mL^{-1}) was determined by settling Lugol fixed samples and counting >400 cells under an inverted microscope (Axiovert 40C, Zeiss, Göttingen, Germany).

2.2.2 AZA analysis

For toxin analysis, subsamples (50 mL) of densely grown stock cultures (approx. 4.0×10^4 cells mL^{-1} for *Az. spinosum* and *Az. poporum*, 1.2×10^4 cells mL^{-1} for *Am. languida*) were harvested by centrifugation at $3,220 \times g$ at 10 °C for 15 min (5810 R, Eppendorf, Hamburg, Germany). The supernatant was discarded, the cell pellet was re-suspended within the remaining supernatant and

transferred to a 1.5 mL microtube for another centrifugation step with $16,000 \times g$ at $10\text{ }^{\circ}\text{C}$ for 10 min (5415 R, Eppendorf). The supernatant was discarded and the cell pellet was frozen at $-20\text{ }^{\circ}\text{C}$ until further processing.

Azaspiracids from cell pellets were extracted by adding 500 μL acetone and vortexing of the microtubes every 10 min for in total one hour at room temperature. Homogenates were centrifuged (Eppendorf 5810 R) at $15\text{ }^{\circ}\text{C}$ and $3,220 \times g$ for 15 min. The extracts were transferred to a 0.45 μm pore-size spin-filter (Millipore Ultrafree, Millipore, Burlington, USA) and centrifuged at $800 \times g$ for 30 s (Eppendorf 5415 R). Filtrates were then adjusted with acetone to a final volume of 0.5 mL and transferred into a liquid chromatography (LC) autosampler vial for LC-MS/MS analysis.

Liquid chromatography-tandem mass spectrometry (LC-MS/MS) in the SRM mode was used to screen the cell extracts for known AZA. The analytical system consisted of an Agilent model 1100 LC (Agilent, Waldbronn, Germany) coupled to an API 4000 Q-Trap, triple quadrupole mass spectrometer equipped with a TurboSpray interface (Sciex, Darmstadt, Germany). The measurements followed detailed descriptions presented in (Wietkamp et al., 2020).

The SRM experiments were carried out in the positive ion mode and screened transitions are presented in **Suppl. Table S1**. Quantitative measurements were calibrated against an external AZA-1 standard (certified reference material of the IMB-NRC, Halifax, Canada) and are expressed as AZA-1 equivalents. The limit of detection (LOD) was defined as a signal-to-noise ratio = 3 and evaluated for each strain. The LOD for *Az. spinosum* 7-F4 samples ranged from 0.008 to 0.145 fg cell⁻¹, for *Az. spinosum* N-05-01 from 0.001 to 0.063 fg cell⁻¹, for *Az. poporum* strain UTH-D4 from 0.001 to 0.045 fg cell⁻¹ and for *Am. languida* strain 8-D10 from 0.013 to 0.081 fg cell⁻¹.

2.3. Experimental cultures

2.3.1 Culture conditions and temperature adaptation

Subsamples from stock cultures (approx. 2×10^3 cells mL⁻¹) were adapted to several temperatures between 5 and $30\text{ }^{\circ}\text{C}$ within 50 mL flasks. Starting at $15\text{ }^{\circ}\text{C}$, acclimation was performed successively in $5\text{ }^{\circ}\text{C}$ steps within controlled environment growth chambers (MIR 252, Sanyo Biomedical, Wood Dale, USA), with an adaptation time of at least one week per temperature. Photon flux density in each chamber was adjusted to $150\text{ }\mu\text{mol m}^{-2}\text{ s}^{-1}$ (Econlux GmbH, Köln, Germany) using continuous recording HOBO Pendant Temperature/Light data loggers (Onset Computer Corporation, Bourne, Massachusetts, USA) and all cultures were kept at a 16:8 h

light:dark photo cycle. Culture growth was observed daily (for the 5 and 10 °C every 2 days) by counting 0.5 mL subsamples as described above. After the adaptation phase, final experimental cultures (starting concentration of approx. 10^3 cells mL⁻¹) were prepared in triplicate 270 mL sterile polystyrene flasks.

2.3.2 Cell counts and AZA collection

The cell density of each replicate was determined by microscopic counting as described above in order to calculate growth rates and toxin cell quota. For each experiment, the density of each replicate was observed daily for the first three days. Afterwards, the observation frequency was adjusted according to the respective growth rate and was performed between once a day (high growth rates) and once a week (low growth rates, usually the 5 °C samples).

Two times during the exponential growth phase and once during the stationary growth phase, 50 mL of each 270 mL flask were harvested for quantitative LC-MS/MS AZA analysis as described above. The flasks were subsequently refilled using fresh medium. Harvest followed the procedures described above, however the 50 mL supernatant gained after the first centrifugation step was not discarded but frozen at -20 °C for analyses of extracellular AZA. Cell growth was monitored until cell density did not increase compared to the two previous samplings, and then the third AZA-sample collection representing early stationary phase was performed. Temperatures, for which all three replicates did not show significant and sustained growth over the first seven days of the experiment were declared as either lower or upper growth limit.

2.4 Exponential growth rates

Exponential growth rates (μ d⁻¹) were determined for each culture flask and calculated for a defined period of exponential increase. To account for an initial lag-phase cell count data from day 3 until the first AZA-sampling point were used to calculate growth rate μ (d⁻¹) as exponent of an exponential regression fit using Microsoft Excel 2019.

2.5 AZA analysis of cell pellets and supernatants

AZA extraction from cell pellets and subsequent analyses followed descriptions in 2.2.2. To estimate AZA in the supernatants, Solid Phase Extraction (SPE) was performed. Therefore, 6 mL

Superclean LC-18 SPE cartridges (Supelco, Bellefonte, Pennsylvania, USA) were activated by 2.5 mL methanol and washed with 2.5 mL of H₂O (milli-Q). The sample was drop-wise loaded onto the cartridges, the sample container was rinsed with 5 mL of H₂O (milli-Q), the SPE cartridge was rinsed with 5 mL of H₂O (milli-Q) and subsequently eluted with 5 mL of methanol into a 15 mL falcon tube. The methanol was evaporated and the residual content was brought into solution by 0.2 mL of acetone, filtered through 0.45 µm pore-size spin-filters and transferred to an autosampler vial for LC-MS/MS analysis.

2.6 pH measurements

The culture medium was adjusted to pH of 8.0 before the experiment (2.2.1) by the addition of HCl and using an EcoScan pH5 (Eutech Instruments, Nijkerk, The Netherlands) pH-meter, and measured again in each culture flask after the cells have reached the late stationary growth phase.

2.7 Statistics

Statistical analyses were performed using the open source program “R”, version 3.4.3 (R-Core-Team, 2017). Differences between growth rates were evaluated by one-way Analysis of Variance (ANOVA) or Kruskal-Wallis tests after checking the respective assumptions for homogenic variances and normal distribution of the data. Post-hoc tests were performed by application of the “TukeyHSD()” function implemented in “R”.

3. Results

3.1 Maximum cell densities and growth rates

Azadinium spinosum 7-F4

Growth was observed at 10, 15, 20, 25 and 27.5 °C, but not at 5 and 30 °C (**Fig. 1**). Maximum cell densities at the stationary phase varied between temperatures (**Fig. 1 A**) and ranged from 0.6 to 7.9 x 10⁴ cells mL⁻¹ (**Table 2**). pH at stationary phase varied between 8.51 and 8.87 and was lowest at the lowest temperature (**Table 2**). Mean growth rates ranged from 0.086 day⁻¹ (10 °C) to 0.615 day⁻¹ (20 °C) (**Fig. 1 B**). Mean growth rates of 20 °C (0.615 ± 0.014 day⁻¹) and 25 °C (0.613 ± 0.010 day⁻¹) cultures were very similar (p = 0.999), but significantly higher compared to the 15 °C (0.428 ± 0.013 day⁻¹) and 27.5 °C (0.450 ± 0.011 day⁻¹) cultures (p < 0.001). The latter two did not differ significantly (p = 0.334). The mean growth rate of the 10 °C cultures (0.086 ± 0.003 day⁻¹) was significantly lower (p < 0.001) compared to the other groups.

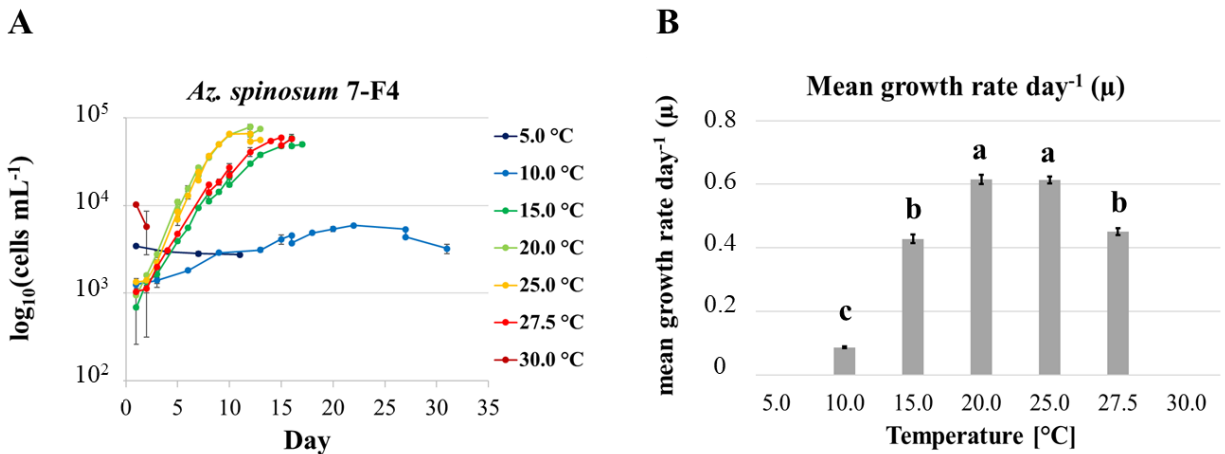


Fig. 1. Growth curves at log₁₀ scale (A) and mean growth rates per day (B) at different temperatures for *Azadinium spinosum* 7-F4. Cell collections are indicated by two data points on the same day in A. Bars represent mean growth rates day⁻¹ ± 1 SD (n=3). Letters above bars indicate statistically significant group differences (p < 0.05). No growth was observed at 5 and 30°C.

Table 2. Maximum cell densities ($\times 10^4$ cells mL⁻¹) and pH in the stationary growth phase per strain.

	7-F4		N-05-01		UTH-D4		8-D10	
Temp. [°C]	max density	pH	max density	pH	max density	pH	max density	pH
5.0	-	-	-	-	0.1 ± 0.0	8.31 ± 0.03	-	-
10.0	0.6 ± 0.0 A	8.51 ± 0.02	3.9 ± 0.5 A	8.45 ± 0.03	5.0 ± 0.6	8.63 ± 0.03	1.8 ± 0.0	8.44 ± 0.03
12.5			6.4 ± 0.6 B	8.85 ± 0.01	8.0 ± 0.2	8.76 ± 0.02		
15.0	5.9 ± 0.4 B	8.70 ± 0.02	3.5 ± 0.2 A	8.52 ± 0.02	7.3 ± 0.4	8.89 ± 0.01	1.3 ± 0.1	8.55 ± 0.02
20.0	7.9 ± 0.5 B	8.87 ± 0.02	3.4 ± 0.3 A	8.43 ± 0.02	7.8 ± 0.2	8.83 ± 0.03	1.5 ± 0.1	8.48 ± 0.01
22.5			-	-	7.2 ± 0.5	8.81 ± 0.02		
25.0	6.6 ± 0.4 B	8.84 ± 0.03			-	-	-	-
27.5	6.1 ± 0.5 B	8.68 ± 0.02						
30.0	-	-						

Azadinium spinosum N-05-01

Growth of strain N-05-01 was observed at 10, 12.5, 15 and 20 °C, whereas no growth could be observed at 5 and 22.5 °C (**Fig. 2**). Highest cell densities at stationary phase ranged from 3.4 to 6.4 $\times 10^4$ cells mL⁻¹ with no clear relation to temperature (**Table 2**). pH at stationary phase ranged from 8.43 to 8.85 (**Table 2**). Mean growth rates per day ranged from 0.147 day⁻¹ (10 °C) to 0.375 day⁻¹ (20 °C) (**Fig. 2 B**). The mean growth rate was highest at 20 °C (0.375 ± 0.020 day⁻¹) and significantly higher than for the other temperatures ($p < 0.05$). Culture grown at 12.5 °C (0.300 ± 0.004 day⁻¹) and 15 °C (0.287 ± 0.034 day⁻¹) had similar average growth rates ($p = 0.91$). Growth rates of the 10 °C cultures (0.147 ± 0.007 day⁻¹) were significantly lower compared to the other temperatures ($p < 0.001$).

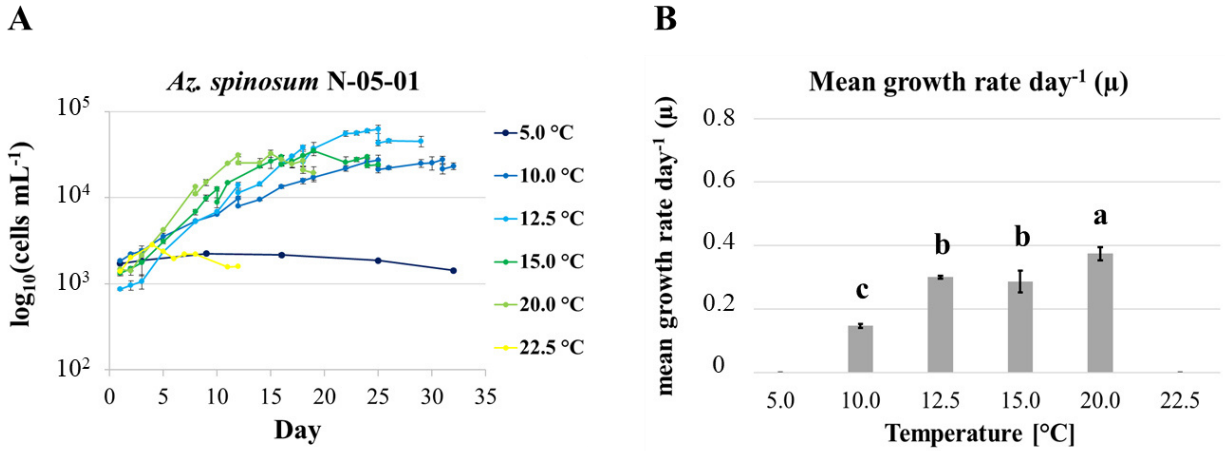


Fig. 2. Growth curves at log₁₀ scale (**A**) and mean growth rates per day (**B**) at different temperatures for *Azadinium spinosum* N-05-01. Cell collections are indicated by two data points on the same day in A. Bars represent mean growth rates day⁻¹ ± 1 SD (n=3). Letters above bars indicate statistically significant group differences (p < 0.05). No growth was observed at 5 and 22.5 °C.

Azadinium poporum UTH-D4

Strain UTH-D4 grew at 5, 10, 12.5, 15, 20 and 22.5 °C, whereas no growth was observed at 25 °C anymore. Maximum cell densities at stationary phase were exceptionally low (0.1 x 10⁴ cells mL⁻¹) at 5 °C and for other temperatures ranged from 5.0 to 8.0 x 10⁴ cells mL⁻¹ (**Table 2**). pH at stationary phase ranged from 8.31 (5 °C) to 8.89 (**Table 2**). Mean growth rate increased significantly (each p < 0.001) from 5 °C (0.035 ± 0.012 day⁻¹), 10 °C (0.116 ± 0.006 day⁻¹), 12.5 °C (0.215 ± 0.003 day⁻¹), 15 °C (0.287 ± 0.008 day⁻¹), 20 °C (0.399 ± 0.020 day⁻¹) to 22.5 °C (0.478 ± 0.006 day⁻¹) (**Fig. 3 B**).

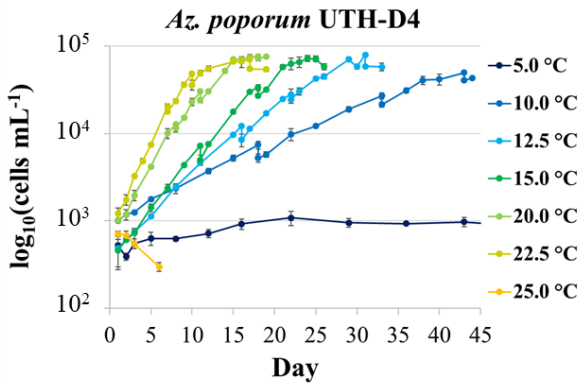
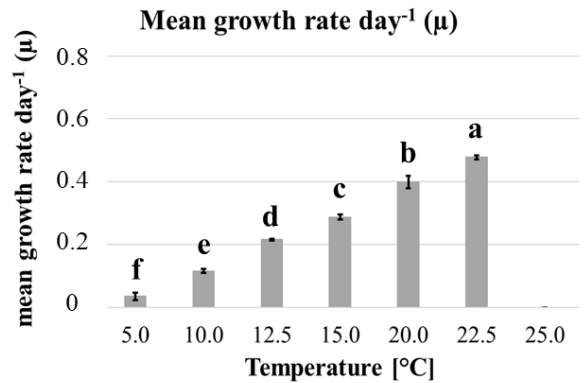
A**B**

Fig. 3. Growth curves at \log_{10} scale (**A**) and mean growth rates per day (**B**) at different temperatures for *Azadinium poporum* UTH-D4. Cell collections are indicated by two data points on the same day in A. Bars represent mean growth rates $\text{day}^{-1} \pm 1$ SD ($n=3$). Letters above bars indicate statistically significant group differences ($p < 0.05$). No growth was observed at 25°C.

Amphidoma languida 8-D10

Amphidoma languida 8-D10 grew at 10, 15, and 20 °C, but not at 5 °C and 25 °C (**Fig. 4**). Max cell densities at stationary phase ranged from 1.3 to 1.8×10^4 cells mL^{-1} (**Table 2**). pH at stationary phase for all three temperatures was quite similar around 8.5 (**Table 2**). Mean growth rate increased significantly (each $p < 0.01$) from 10 °C ($0.234 \pm 0.026 \text{ day}^{-1}$) over 15 °C ($0.333 \pm 0.003 \text{ day}^{-1}$) to 20 °C ($0.531 \pm 0.008 \text{ day}^{-1}$) (**Fig. 4 B**).

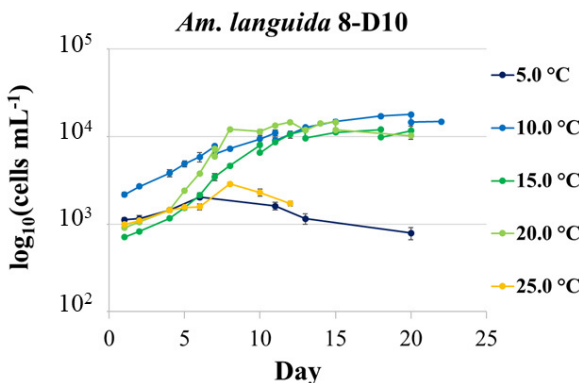
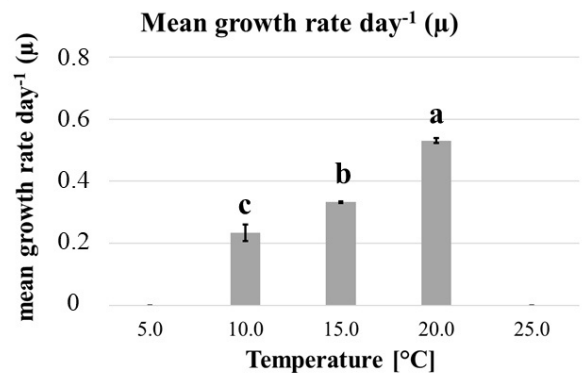
A**B**

Fig. 4. Growth curves at \log_{10} scale (**A**) and mean growth rates per day (**B**) at different temperatures for *Amphidoma languida* 8-D10. Cell collections are indicated by two data points on the same day in A. Bars represent mean growth rates $\text{day}^{-1} \pm 1$ SD ($n=3$). Letters above bars indicate statistically significant group differences ($p < 0.05$). No growth was observed at 5 and 25°C.

3.2 AZA cell quota and proportions

Azadinium spinosum 7-F4

Intracellular AZA measurements revealed the presence of AZA-1, -2 and -33 as major AZA compounds, as well as AZA-1-methyl, -1-phosphate, -2-methyl and -2-phosphate as minor AZA compounds in *Az. spinosum* 7-F4 (**Fig. 5**). For all replicates and all three collections, AZA-1 was the significantly dominant isomer, followed by intermediate AZA-2 and lower AZA-33 levels (**Fig. 5 A, D, G**).

Collection 1

Averaged sums of the major compounds AZA-1, -2 and -33 by temperature (**Fig. 5 A**) revealed significantly ($p < 0.05$) highest mean AZA cell quota at 10 °C ($33.2 \pm 6.9 \text{ fg cell}^{-1}$) followed by the 27.5 °C ($20.5 \pm 2.1 \text{ fg cell}^{-1}$), which was significantly higher ($p < 0.05$) than 15 °C ($8.9 \pm 1.5 \text{ fg cell}^{-1}$), 20 °C ($1.4 \pm 0.5 \text{ fg cell}^{-1}$) and 25 °C ($6.7 \pm 2.0 \text{ fg cell}^{-1}$). The 20 °C had the significantly ($p < 0.05$) lowest AZA cell quota.

Averaged sums of the minor compounds (**Fig. 5 B**) revealed significantly ($p < 0.05$) highest total cell quota in the 27.5 °C cultures (AZA-1-me, -1-ph, -2-ph: $0.45 \pm 0.05 \text{ fg cell}^{-1}$), intermediate cell quota at 10 °C (only AZA-1-me; $0.29 \pm 0.03 \text{ fg cell}^{-1}$) and lowest cell quota at 15 °C (only AZA-1-me; $0.10 \pm 0.02 \text{ fg cell}^{-1}$).

Mean total AZA isomer proportions per cell (**Fig. 5 C**) revealed AZA-1 being the dominant isomer inside the cells for all temperatures, ranging between $52.3 \pm 2.4 \%$ (25 °C) and $68.1 \pm 1.0 \%$ (15 °C). The 25 °C samples had a significantly lower AZA-1 proportion than the cells grown at 10 °C ($64.6 \pm 1.7 \%$; $p < 0.05$) and at 15 °C ($p < 0.01$), but were similar ($p > 0.05$) to those from 20 °C ($57.8 \pm 7.2 \%$) and 27.5 °C ($58.0 \pm 2.5 \%$). AZA-2 was the second most abundant isomer, ranging between $24.5 \pm 0.6 \%$ (15 °C) and $30.8 \pm 1.8 \%$ (25 °C), but no significant difference was observed between temperatures ($p > 0.05$). AZA-33 revealed relatively low but similar ($p = 0.98$) proportions at 10.0 °C ($6.3 \pm 2.1 \%$) and 15 °C ($6.2 \pm 1.5 \%$), whereas AZA-33 proportions measured in 25 °C ($16.9 \pm 4.1 \%$) and 27.5 °C ($12.2 \pm 1.2 \%$) cultures were significantly higher ($p < 0.05$) compared to the lower temperatures. Due to the relatively high standard deviation, AZA-33 content from 20 °C cultures ($14.7 \pm 8.8 \%$) did not differ significantly ($p > 0.05$) from all other temperatures. The minor component AZA-1-me was only detected in cells grown at 10 °C ($0.9 \pm 0.3 \%$), 15 °C (1.1

$\pm 0.1 \%$) and $27.5 \text{ }^\circ\text{C}$ ($0.9 \pm 0.1 \%$), and did not differ significantly ($p > 0.05$) between those temperatures. AZA-1-ph ($0.9 \pm 0.2 \%$) and AZA-2-ph ($0.4 \pm 0.1 \%$) were only observed in $27.5 \text{ }^\circ\text{C}$ cultures during collection 1.

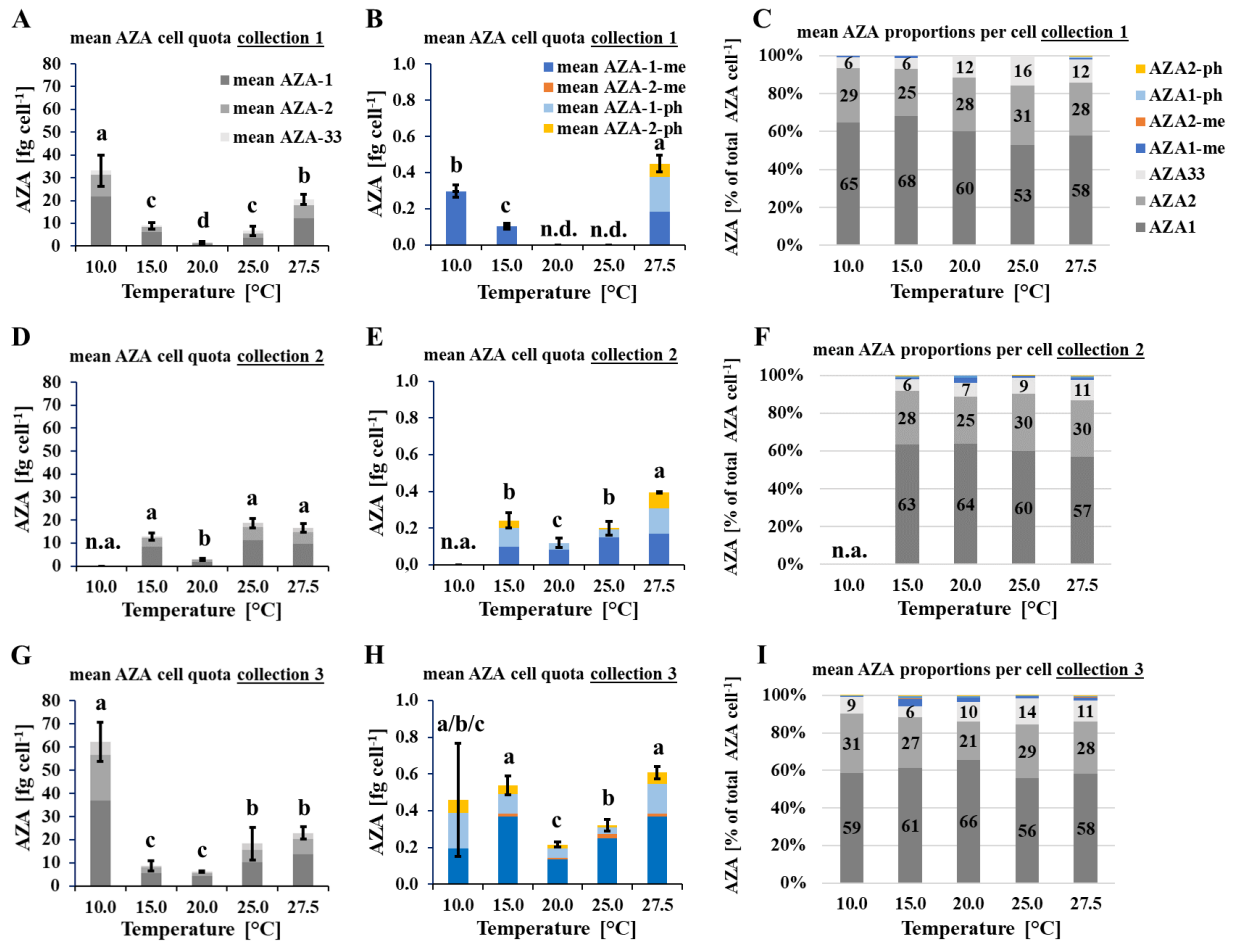


Fig. 5. Mean sums of AZA cell quota ± 1 SD (fg cell^{-1} , $n=3$) for major compounds (**A, D, G**), minor compounds (**B, E, H**) and the respective mean AZA proportions (% of intracellular AZA) cell⁻¹ (**C, F, I**) from collections 1-3 for *Azadinium spinosum* 7-F4. Letters above bars indicate statistically significant group differences ($p < 0.05$). n.a. = no data available. n.d. = not detected.

Collection 2

Averaged sums of the major compounds AZA-1, -2 and -33 (**Fig. 5 D**) revealed similar ($p = 0.58$) mean total AZA cell quota at $15 \text{ }^\circ\text{C}$ ($12.9 \pm 1.5 \text{ fg cell}^{-1}$), $25 \text{ }^\circ\text{C}$ ($18.7 \pm 1.9 \text{ fg cell}^{-1}$) and $27.5 \text{ }^\circ\text{C}$ ($16.6 \pm 1.8 \text{ fg cell}^{-1}$), whereas the $20 \text{ }^\circ\text{C}$ cultures ($2.8 \pm 0.5 \text{ fg cell}^{-1}$) had significantly ($p < 0.001$) lower cell quota. The cultures at $10 \text{ }^\circ\text{C}$ have not been sampled in the later exponential growth phase.

Averaged sums of the minor compounds (**Fig. 5 E**) revealed again significantly ($p < 0.05$) highest total cell quota in the 27.5 °C cultures (AZA-1-me, -1-ph, -2-ph: 0.40 ± 0.01 fg cell⁻¹), intermediate cell quota at 15 °C (AZA-1-me, -1-ph, -2-ph: 0.24 ± 0.04 fg cell⁻¹) and 25 °C (AZA-1-me, -1-ph, -2-ph: 0.20 ± 0.04 fg cell⁻¹) and significantly lowest ($p < 0.05$) cell quota at 20 °C (only AZA-1-me and -1-ph: 0.12 ± 0.03 fg cell⁻¹).

AZA-1 had highest proportions (**Fig. 5 F**), ranging between 57.0 ± 1.3 % (27.5 °C) and 63.7 ± 3.7 % (15 °C) and were not significantly different ($p > 0.05$) between temperatures. AZA-2 revealed similar proportions ($p > 0.05$) as well, ranging between 24.9 ± 2.0 % (20 °C) and 30.3 ± 2.2 % (25 °C). AZA-33 proportions ranged between 6.2 ± 0.8 % (15 °C) and 10.7 ± 0.3 % (27.5 °C) and revealed significantly ($p < 0.05$) lower values from 15 °C cultures compared to those grown at 25 °C (8.7 ± 0.4 %) and 27.5 °C. The 20 °C cultures (7.4 ± 1.0 %) did not differ from 15 °C and 25 °C cultures ($p > 0.05$), but were significantly lower ($p < 0.01$) than the 27.5 °C proportions for AZA-33. In contrast to collection 1, AZA-1-me was found in all cultures, i.e. 15 °C (0.8 ± 0.2 %), 20 °C (2.9 ± 0.5 %), 25 °C (0.8 ± 0.3 %) and 27.5 °C (1.0 ± 0.1 %), with proportions measured in the 20 °C cultures being significantly higher ($p < 0.05$) compared to all other temperatures, which were similar among themselves ($p > 0.05$). Also AZA-1-ph was detected in all cultures, with proportions between 0.2 ± 0.1 % (25 °C) and 1.9 ± 1.4 % (20 °C, only two of the three replicates had AZA-1-ph). Significantly lowest ($p < 0.05$) AZA-1-ph proportions were measured at 25 °C, followed by the similar ($p > 0.05$) 15 °C (0.8 ± 0.1 %) and 27.5 °C (0.8 ± 0.2 %) samples. High standard deviation in AZA-1-proportions of 20 °C cultures led to no significant differences to all other temperatures ($p > 0.05$).

Collection 3

In the stationary growth phase (**Fig. 5 G**), the 10 °C cultures revealed significantly ($p < 0.001$) highest major AZA cell quota (62.3 ± 8.9 fg cell⁻¹), followed by the similar ($p = 0.90$) 25 °C (18.3 ± 7.1 fg cell⁻¹) and 27.5 °C (22.9 ± 2.6 fg cell⁻¹) cultures. Significantly ($p < 0.05$) lowest cell quota were observed for the 15 °C (8.6 ± 2.1 fg cell⁻¹) and 20 °C (6.2 ± 0.3 fg cell⁻¹) samples.

Averaged sums of the minor compounds (**Fig. 5 H**) revealed significantly ($p < 0.05$) highest total cell quota in the 15 °C (AZA-1-me, -1-ph, -2-me, -2-ph: 0.54 ± 0.05 fg cell⁻¹) and 27.5 °C cultures (AZA-1-me, -1-ph, -2-me, -2-ph: 0.61 ± 0.03 fg cell⁻¹), intermediate cell quota at 25 °C (AZA-1-me, -1-ph, -2-me, -2-ph: 0.32 ± 0.03 fg cell⁻¹) and significantly lowest ($p < 0.05$) cell quota at 20 °C (AZA-1-me, -1-ph, -2-me, -2-ph: 0.22 ± 0.01 fg cell⁻¹). Data of the 10 °C replicates had a

relatively huge SD (AZA-1-me, -1-ph, -2-ph: 0.46 ± 0.31 fg cell⁻¹) and therefore did not differ significantly from all other temperatures. Notable, no AZA-2-me was detected in the 10 °C samples.

AZA-1 proportions (**Fig. 5 I**) ranged between 54.7 ± 3.1 % (25 °C) and 65.7 ± 1.2 % (20 °C). Cells from 10 °C (58.8 ± 1.9 %), 25 °C (54.7 ± 3.1 %) and 27.5 °C (57.9 ± 1.7 %) had lowest and not significantly different AZA-1 proportions ($p > 0.05$). The 20 °C samples differed significantly ($p < 0.05$) from those. The 15 °C samples revealed similar ($p > 0.05$) AZA-1 proportions (61.0 ± 1.6 %) to all but the 25 °C samples ($p < 0.05$). AZA-2 proportions were in the range of 20.7 ± 2.4 % (20 °C) to 31.3 ± 2.6 % (10 °C), which was the only statistically significant difference ($p < 0.05$) between all temperatures. AZA-33 proportions ranged between 6.1 ± 0.9 % (15 °C) to 16.2 ± 7.0 % (25 °C), but due to relatively high standard deviations, no significant difference ($p > 0.05$) between temperatures could be observed.

Proportions of AZA-1-me were between 0.3 ± 0.1 % (10 °C) to 4.1 ± 0.1 % (15 °C). The 10 °C samples had a significantly lower AZA-1-me proportion ($p < 0.01$) compared to all other temperatures, whereas the 15 °C were significantly highest ($p < 0.05$). Cells from 20 °C (2.1 ± 0.2 %), 25 °C (1.7 ± 0.9 %) and 27.5 °C (1.6 ± 0.1 %) were intermediate and did not differ from each other ($p > 0.05$). AZA-1-ph was also detected in samples from all temperatures and was in the range of 0.2 ± 0.1 % (25 °C) to 1.2 ± 0.2 % (15 °C). The proportions of the 25 °C cultures were significantly lower ($p < 0.05$) than the 15 °C, 20 °C (0.8 ± 0.1 %) and 27.5 °C (0.7 ± 0.1 %). AZA-2-ph was detected in cells grown at all temperatures, with 0.1 ± 0.0 % (25 °C) to 0.5 ± 0.1 % (15 °C). The 25 °C had significantly lower ($p < 0.05$) AZA-2-ph proportions than the other temperatures, which were of similar height ($p > 0.05$) among themselves. AZA-2-me was detected in cells from the all temperatures except for the 10 °C samples, but was represented by not more than 0.003 % of the total AZA per cell.

***Azadinium spinosum* N-05-01**

AZA-11 and -51 were detected in all samples of this strain. AZA-11 represented the major compound in all replicates and collections, with a usually more than two times higher AZA cell quota than AZA-51 (**Fig. 6**).

Collection 1

Averaged sums of AZA-11 and -51 by temperature (**Fig. 6 A**) revealed significantly ($p < 0.05$) highest mean AZA cell quota at 10 °C ($6.0 \pm 1.3 \text{ fg cell}^{-1}$), followed by AZA cell quota for 20 °C ($2.7 \pm 0.6 \text{ fg cell}^{-1}$), 15 °C ($1.3 \pm 0.2 \text{ fg cell}^{-1}$) and 12.5 °C ($0.8 \pm 0.2 \text{ fg cell}^{-1}$), which were all significantly different from each other ($p > 0.05$).

Mean AZA isomer proportions per cell (**Fig. 6 B**) revealed AZA-11 being the dominant isomer inside the cells for all temperatures, ranging between $70.9 \pm 1.2 \%$ (10 °C) and $78.5 \pm 1.7 \%$ (20 °C) and revealing the only significant difference ($p < 0.01$) between 10 °C and 20 °C. AZA-51 proportions vice versa were highest for the cells grown at 10 °C ($29.1 \pm 1.2 \%$) and lowest for those grown at 20 °C ($21.5 \pm 1.7 \%$).

Collection 2

After collection 2 (**Fig. 6 C**), the 10 °C cultures revealed again significantly ($p < 0.001$) highest total AZA-cell quota ($7.6 \pm 0.5 \text{ fg cell}^{-1}$) compared to the similar ($p > 0.05$) 12.5 °C ($1.8 \pm 0.2 \text{ fg cell}^{-1}$), 15 °C ($2.1 \pm 0.4 \text{ fg cell}^{-1}$) and 20 °C ($1.9 \pm 0.2 \text{ fg cell}^{-1}$) cultures.

AZA-11 proportions (**Fig. 6 D**) ranged between $63.3 \pm 4.1 \%$ (10 °C) and $83.0 \pm 2.5 \%$ (20 °C). 10 °C samples had a similar proportion compared to the 12.5 °C ($71.7 \pm 3.1 \%$) and the 15 °C ($73.3 \pm 2.9 \%$) samples ($p = 0.12$ and $p = 0.06$), but all those three were significantly lower ($p < 0.05$) compared to and 20 °C samples. Therefore, the AZA-51 proportion within the cells grown at 20 °C ($17.0 \pm 2.5 \%$) was significantly lower compared to the 10 °C ($36.7 \pm 4.1 \%$), 12.5 °C ($28.3 \pm 3.1 \%$) and 15 °C ($26.7 \pm 2.9 \%$) cultures.

Collection 3

In the stationary phase (**Fig. 6 E**), cells grown at 10 °C still had highest AZA cell quota ($7.0 \pm 0.3 \text{ fg cell}^{-1}$). The 12.5 °C ($2.1 \pm 0.2 \text{ fg cell}^{-1}$) and 15 °C ($1.5 \pm 0.4 \text{ fg cell}^{-1}$) samples had similar intermediate levels ($p = 0.20$). The 20 °C samples revealed the lowest AZA cell content ($0.5 \pm 0.2 \text{ fg cell}^{-1}$) compared to the other three temperatures ($p < 0.05$).

AZA-11 proportions (**Fig. 6 F**) ranged from $63.2 \pm 6.2 \%$ (10 °C) to $74.4 \pm 2.1 \%$ (20 °C), but no statistically significant difference was observed ($p > 0.05$). Equally, AZA-51 proportions ranged from $25.6 \pm 2.1 \%$ (20 °C) to $36.8 \pm 6.2 \%$ (20 °C) without significant differences between temperatures.

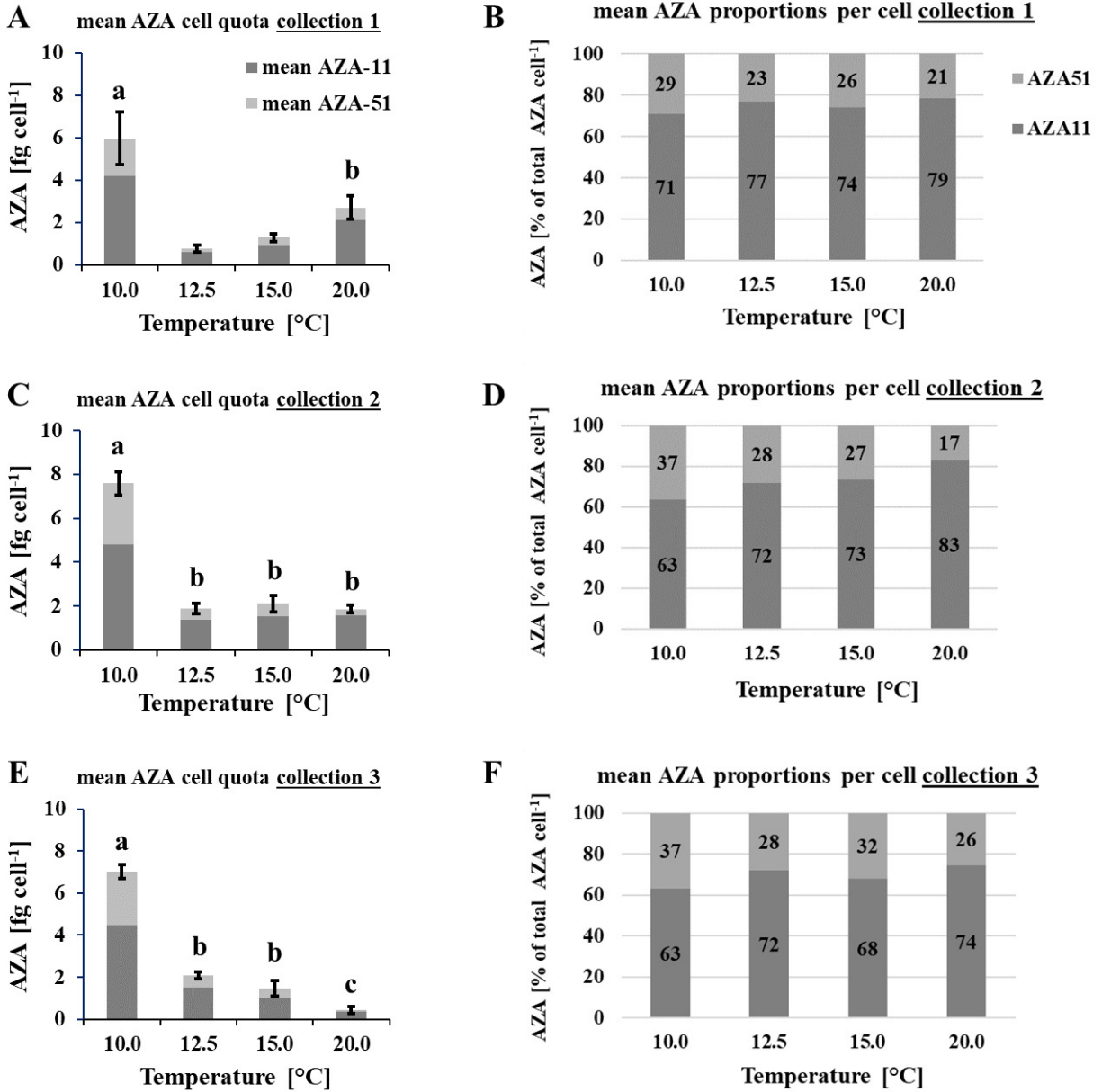


Fig. 6. Mean sums of AZA cell quota \pm 1SD (fg cell⁻¹, n=3) for AZA-11 and -51 (**A, C, E**) and the respective mean AZA proportions (% of intracellular AZA) cell⁻¹ (**B, D, F**) from collections 1-3 for *Azadinium spinosum* N-05-01. Letters above bars indicate statistically significant group differences ($p < 0.05$).

***Azadinium poporum* UTH-D4**

Only one AZA isomer, i.e. AZA-37, has been detected in *Azadinium poporum* UTH-D4 cells (**Fig. 7**).

Collection 1

Cells collected during the exponential growth phase revealed statistically significant differences ($p < 0.05$) between the cells grown at 10 °C ($4.3 \pm 1.3 \text{ fg cell}^{-1}$) and cells grown at 20 °C ($1.2 \pm 0.2 \text{ fg cell}^{-1}$) and 22.5 °C ($1.5 \pm 0.1 \text{ fg cell}^{-1}$) (**Fig. 7 A**). Cultures from the 12.5 °C ($3.6 \pm 0.2 \text{ fg cell}^{-1}$) and 15 °C ($1.8 \pm 1.4 \text{ fg cell}^{-1}$) chambers had no significantly different ($p > 0.05$) AZA cell quota compared to the 10 °C, 20 °C and 22.5 °C cultures.

Collection 2

Highest cell quota was reached by cells from the 10 °C ($8.5 \pm 0.6 \text{ fg cell}^{-1}$) cultures (**Fig. 7 B**). Cells grown at 12.5 °C ($4.7 \pm 0.6 \text{ fg cell}^{-1}$), 15 °C ($4.2 \pm 0.5 \text{ fg cell}^{-1}$) and 22.5 °C ($3.2 \pm 0.2 \text{ fg cell}^{-1}$) had significantly lower ($p < 0.001$) AZA cell quota, but were significantly higher ($p < 0.05$) than cells from the 20 °C ($2.3 \pm 0.4 \text{ fg cell}^{-1}$).

Collection 3

AZA cell quota for 10 °C ($8.8 \pm 1.3 \text{ fg cell}^{-1}$), 12.5 °C ($8.9 \pm 0.9 \text{ fg cell}^{-1}$) and 15 °C ($10.0 \pm 0.6 \text{ fg cell}^{-1}$) were highest and not significantly different ($p > 0.58$) from each other (**Fig. 7 C**). Samples taken from 20 °C ($6.6 \pm 0.7 \text{ fg cell}^{-1}$) had higher cell quota than the 22.5 °C ($5.2 \pm 0.3 \text{ fg cell}^{-1}$) ($p < 0.05$), but both were significantly lower ($p < 0.05$) compared to the other temperatures.

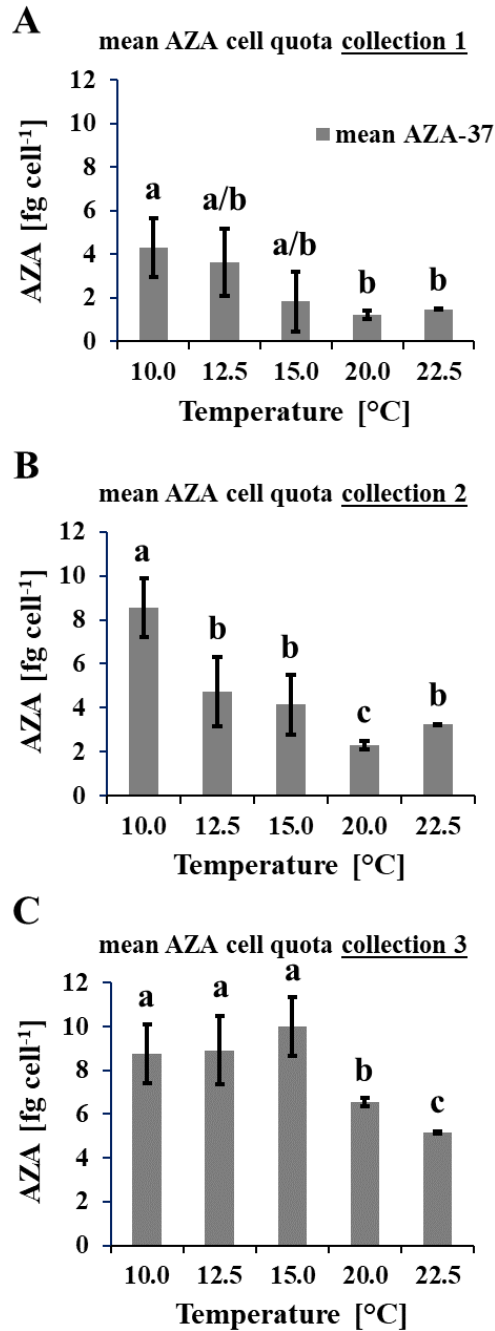


Fig. 7. Mean sums of AZA-37 cell quota \pm 1SD (fg cell⁻¹, n=3) from collections 1-3 (**A-C**) for *Azadinium poporum* UTH-D4. Letters above bars indicate statistically significant group differences ($p < 0.05$).

***Amphidoma languida* 8-D10**

Characteristic AZA isomers for *Am. languida* 8-D10 were AZA-38 and -39, for which the cell quota for AZA-39 were generally 1.5 to 1.8 times higher than for AZA-38 (**Fig. 8**).

Collection 1

Averaged sums of AZA-38 and -39 measured in cell pellets from the first harvest during the exponential growth phase did not reveal any statistical significant ($p \geq 0.65$) differences between 10 °C (8.0 ± 1.8 fg cell⁻¹), 15 °C (6.5 ± 1.1 fg cell⁻¹) and 20 °C (7.2 ± 1.8 fg cell⁻¹) (**Fig. 8 A**).

Mean AZA isomer proportions for AZA-38 ranged between 33.9 ± 4.6 % (20 °C) and 41.5 ± 9.7 % (15 °C) and no significant difference ($p > 0.05$) between temperatures was observed (**Fig. 8 B**). Likewise, AZA-39 proportions ranged between 58.5 ± 9.7 % (15 °C) and 66.1 ± 4.6 % (20 °C) and did not reveal any significant differences either.

Collection 2

Similar ($p \geq 0.63$) cell quota were measured for the 10 °C (6.5 ± 0.8 fg cell⁻¹), 15 °C (8.0 ± 2.0 fg cell⁻¹) and 20 °C (8.6 ± 3.0 fg cell⁻¹) cultures (**Fig. 8 C**).

AZA-38 proportion ranged between 41.4 ± 3.6 % (15 °C) and 43.0 ± 11.0 % (20 °C), and AZA-39 proportions were 57.0 ± 11.0 % (10 °C) and 58.6 ± 3.6 % (15 °C) (**Fig. 8 D**).

Collection 3

A significant difference ($p < 0.05$) in AZA cell quota was observed in the stationary growth phase between the relatively high 10 °C (13.5 ± 0.6 fg cell⁻¹), the intermediate 15 °C (16.9 ± 1.6 fg cell⁻¹) and the low-AZA 20 °C (2.7 ± 0.2 fg cell⁻¹) cultures (**Fig. 8 E**).

AZA-38 proportions ranged from 36.6 ± 7.4 % (20 °C) to 36.8 ± 7.5 % (10 and 15 °C), and no statistically significant difference ($p > 0.05$) was observed (**Fig. 8 F**). Equally, AZA-39 proportions ranged from 63.2 ± 7.5 % (10 °C) to 63.4 ± 7.4 % (20 °C) without significant differences between temperatures.

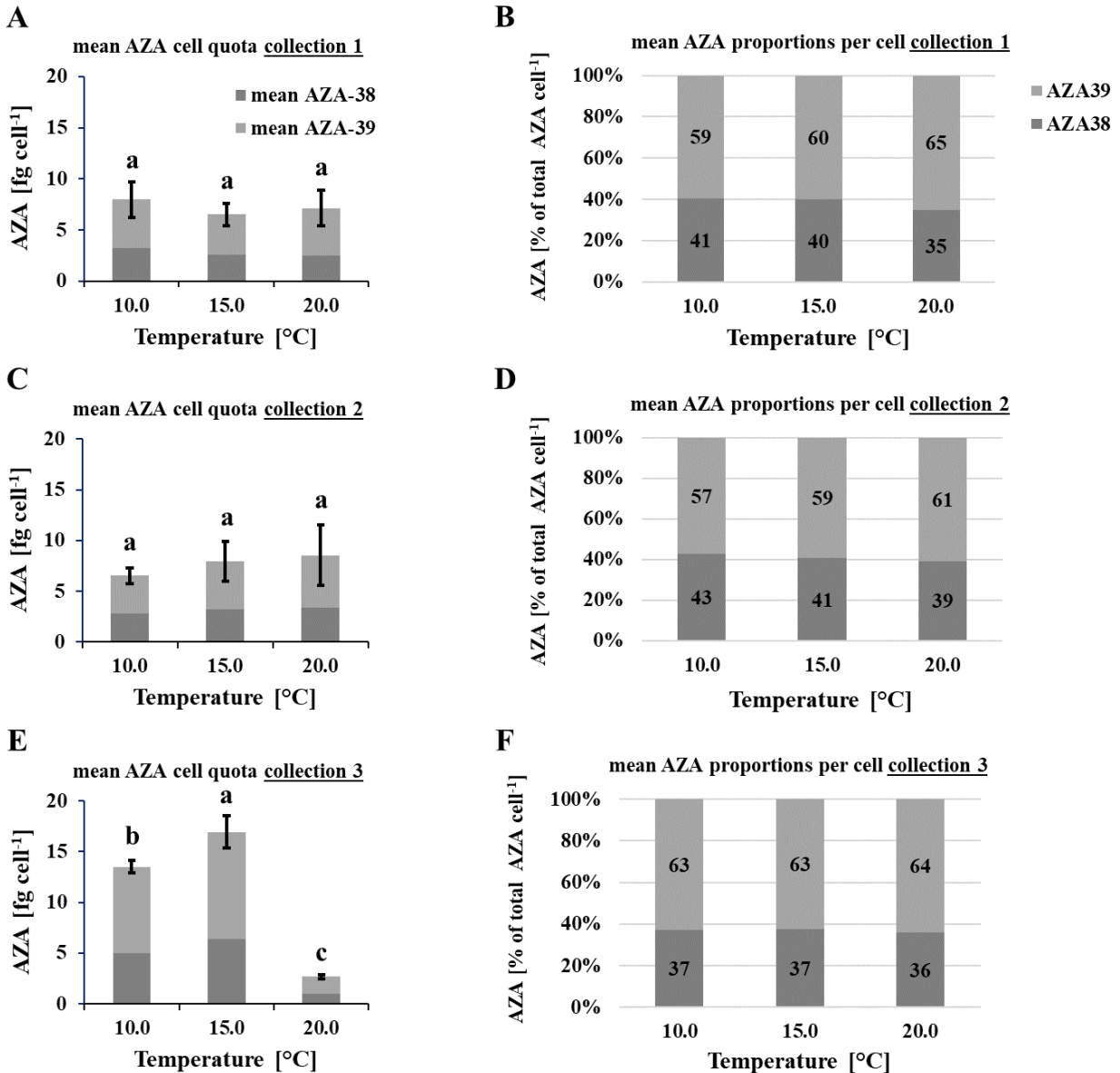


Fig. 8. Mean sums of AZA cell quota \pm 1SD (fg cell⁻¹, n=3) for AZA-38 and -39 (**A**, **C**, **E**) and the respective mean AZA proportions (% of intracellular AZA) cell⁻¹ (**B**, **D**, **F**) from collections 1-3 for *Amphidoma languida* 8-D10. Letters above bars indicate statistically significant group differences (p < 0.05).

3.3 Intracellular vs. extracellular AZA cell quota

From each centrifuged cell pellet for intracellular AZA analysis, the supernatant was kept and analyzed for released, extracellular AZA (fg cell⁻¹) as well. For all four investigated strains, extracellular AZA per cell was usually lower than AZA cell quota calculated from the cell pellets and are reported as proportion (%) of the respective intracellular cell quota. For *Az. spinosum* 7-

F4, the amount of extracellular AZA-1 was generally less than 5% compared the intracellular levels for all temperatures and collections (**Suppl. Fig. S1**). The 20 °C samples taken during the first collection (**Suppl. Fig. S1 A**) were exceptionally high ($0.18 \pm 0.07 \text{ fg cell}^{-1}$), representing $23.8 \pm 5.6\%$ of the respective intracellular AZA-1 ($0.84 \pm 0.36 \text{ fg cell}^{-1}$). The AZA-2 samples, which were generally below 5% of the intracellular AZA-2 cell quota, had also an exceptionally high proportion in the 20 °C cultures of collection 1 ($8.0 \pm 5.7\%$). Extracellular AZA-33 has only been detected in the supernatant one replicate grown at 25 °C after collection 3 (**Suppl. Fig. S1 C**) and revealed also a relatively low proportion of 6.5% compared to the intracellular cell quota.

Extracellular AZA-11 cell quota of *Az. spinosum* strain N-05-01 after collection 1 (**Suppl. Fig. S1 A**) ranged from $2.0 \pm 1.6\%$ (10 °C) to $19.2 \pm 4.8\%$ (12.5 °C). AZA-51 proportions ranged from $1.9 \pm 1.8\%$ (10 °C) to exceptionally high $56.1 \pm 7.7\%$ (12.5 °C). For collection 2 (**Suppl. Fig. S1 B**), both AZA-11 and AZA-51 proportions were up to $7.0 \pm 1.4\%$ (12.5 °C) and $16.3 \pm 3.6\%$ (20 °C), respectively. After the third collection (**Suppl. Fig. S1 C**), up to $21.5 \pm 19.2\%$ (20 °C) and $19.0 \pm 4.3\%$ (15 °C) were observed for AZA-11 and -51, respectively.

For *Az. poporum* UTH-D4, extracellular AZA-37 cell quota proportions were generally below 7% (**Suppl. Fig. S2**), with exceptional high proportions in the supernatant of the 12.5 °C cultures during collection 1 ($11.7 \pm 7.5\%$) and 2 ($15.7 \pm 5.0\%$). Notably, there was significantly less AZA-37 in the supernatant (in relation to the intracellular cell quota) at 10, 12.5 and 15 °C during collection 3 (**A**) than during collection 1 (**B**) and 2 (**C**).

Extracellular AZA-38 and -39 in *Am. languida* cultures were generally below 10% of the intracellular cell quota (**Suppl. Fig. S2**). In the supernatant of the 20 °C cultures, AZA-38 ($13.3 \pm 6.3\%$) and AZA-39 ($11.2 \pm 3.3\%$) proportions after collection 1 (**Suppl. Fig. S2 A**) were relatively high. Extracellular cell quotas in the 20 °C samples were exceptionally high during collection 3 (**Suppl. Fig. S2 C**), with values even surpassing the intracellular cell quota ($69.7 \pm 10.0\%$ for AZA-38; $127.1 \pm 30.5\%$ for AZA-39).

For *Az. spinosum* 7-F4 significantly higher (partly more than five times) extracellular levels of methyl-esters (AZA-1-me and AZA-2-me) were detected in the supernatant compared to the cell pellet measurements. For *Az. spinosum* strain N-05-01 AZA-51-me has only been detected in the supernatant. These results are not shown here, because it remains uncertain, if these methyl-esters were actually produced by the cells or the result of the Solid Phase Extraction of the supernatant samples using methanol.

3.4 AZA production rates

Based on all cell counts between both cell collections for AZA analysis during the exponential growth phase and the respective measured AZA quantities, mean total AZA production rates (relying on the assumption of a constant AZA production between both collections) were calculated for each strain (**Fig. 9**).

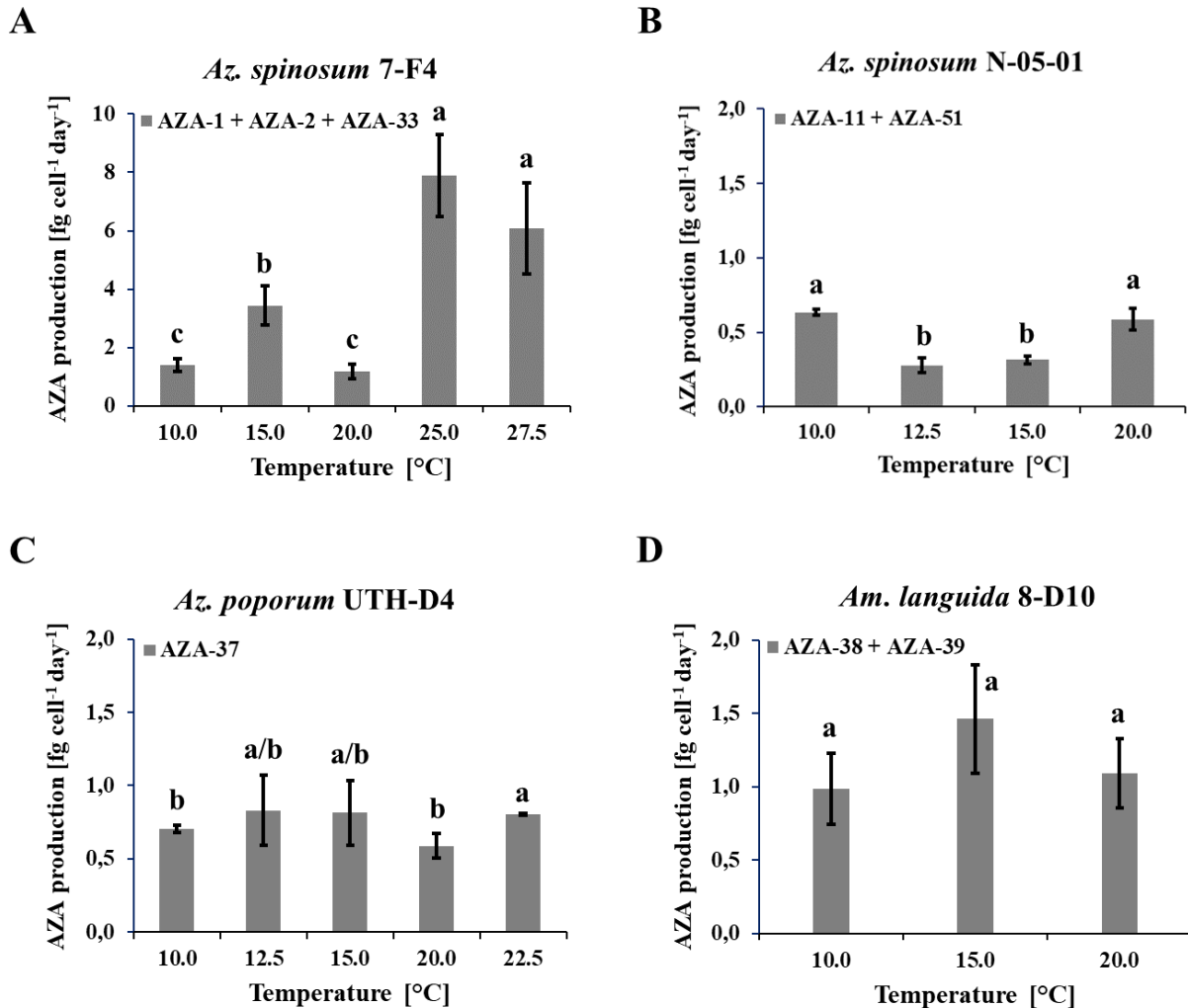


Fig. 9. Mean total AZA production rates (fg cell⁻¹ day⁻¹) per temperature for *Az. spinosum* strain 7-F4 (**A**), *Az. spinosum* strain N-05-01 (**B**), *Az. poporum* strain UTH-D4 (**C**) and *Am. languida* strain 8-D10 (**D**). Letters above bars indicate statistically significant different groups ($p < 0.05$).

For *Azadinium spinosum* 7-F4 (**Fig. 9 A**), highest AZA production (combined AZA-1, -2 and -33) was observed in cultures grown at 25 °C (7.9 ± 1.4 fg cell⁻¹ day⁻¹) and 27.5 °C (6.1 ± 1.6 fg cell⁻¹

day⁻¹), followed by cells grown at 15 °C (3.4 ± 0.7 fg cell⁻¹ day⁻¹). Significantly lowest AZA production was observed in the 10 °C (1.4 ± 0.2 fg cell⁻¹ day⁻¹) and 20 °C (1.2 ± 0.3 fg cell⁻¹ day⁻¹) cultures. *Azadinium spinosum* strain N-05-01 (**Fig. 9 B**) showed highest AZA production rates (combined AZA-11 and -51) at 10 °C (0.63 ± 0.02 fg cell⁻¹ day⁻¹) and 20 °C (0.59 ± 0.07 fg cell⁻¹ day⁻¹), whereas cultures from 12.5 °C (0.28 ± 0.05 fg cell⁻¹ day⁻¹) and 15 °C (0.32 ± 0.02 fg cell⁻¹ day⁻¹) produced significantly less AZA. Cells of *Azadinium poporum* strain UTH-D4 (**Fig. 9 C**) did not show huge differences in AZA-37 production between temperatures. The 10 °C (0.70 ± 0.03 fg cell⁻¹ day⁻¹) and 20 °C (0.59 ± 0.09 fg cell⁻¹ day⁻¹) produced significantly less AZA than the 22.5 °C cultures (0.80 ± 0.01 fg cell⁻¹ day⁻¹), but the 12.5 °C (0.83 ± 0.24 fg cell⁻¹ day⁻¹) and 15 °C (0.81 ± 0.22 fg cell⁻¹ day⁻¹) did not differ significantly from any other cultures. *Amphidoma languida* 8-D10 (**Fig. 9 D**) produced similar amounts of AZA (combined AZA-38 and -39) at 10 °C (0.99 ± 0.24 fg cell⁻¹ day⁻¹), 15 °C (1.46 ± 0.37 fg cell⁻¹ day⁻¹) and 20 °C (1.09 ± 0.24 fg cell⁻¹ day⁻¹).

4. Discussion

Azadinium spinosum

With up to 8.0×10^4 cells mL⁻¹, the North Sea *Az. spinosum* strain 7-F4 reached highest cell densities in this study compared to the other strains. It is difficult to evaluate in batch culture experiments, which factor actually limit growth at stationary phase and thus determine the maximum cell density. With reduced nutrient additions (1/10 of strength of regular K-medium) in the present experiments, nutrients may limit growth at stationary phase. With an relatively high ratio of nitrate to phosphate in the K-medium recipe, P-limitation seem to more likely, but testing for limiting factors (e.g. checking for resumed growth after addition of certain nutrients) was not the focus of the present work. Without bubbling or vigorous culture movement, carbon limitation may also be important to consider. In any case, it has been shown that pH, which continuously increases during batch culture growth, may set a physiological limit for growth of many microalgal species. In this respect, it is important to note that...limitation. Cell densities between 5×10^4 and

1×10^5 cells mL^{-1} are comparable to maximum cell densities reported by Jauffrais et al. (2013b) with another cultured *Az. spinosum* strain, namely 3D9. However, Kilcoyne et al. (2019) and Jauffrais et al. (2012c) were able to grow strain 3D9 to densities exceeding even 2.1×10^5 cells mL^{-1} (after another addition of nutrients) during mass culture optimization experiments.

Growth of strain 7-F4 was clearly temperature dependent, growing at a wide range of temperatures ($10 - 27.5^\circ\text{C}$), which confirms previous studies with strain 3D9 ($10 - 26^\circ\text{C}$) as well (Jauffrais et al., 2013b) and suggests a high physiological adaptation ability. As described by Jauffrais, also in this study growth rates were highest between 20 and 25°C , and much slower at 10°C .

The Ribotype A strain 7-F4 had significantly higher maximum cell numbers, higher growth rates and a wider temperature range compared to Norwegian Ribotype B strain N-05-01. That could be an indicator that Ribotype B strains might have a lower physiological tolerance towards higher temperatures. However, this was the first Ribotype B strain tested under different temperature regimes and further strains have to be investigated in the future to confirm this hypothesis.

Both *Az. spinosum* strains revealed a faster increase in population density at higher temperatures ($\geq 20^\circ\text{C}$), before a sudden stop of growth and death was observed, when the temperature being obviously too high. Contrary, AZA cell quota were generally higher at lower temperatures, probably because the cells had more time to accumulate AZA before cell division. Nevertheless, this confirms previous studies on toxigenic Amphidomataceae (Jauffrais et al., 2013b; Kilcoyne et al., 2019) suggesting that low temperatures might enhance the risk of AZA contamination in shellfish.

The AZA cell quotas in *Az. spinosum* 3D9 (Ribotype A) batch cultures reported from previous studies ranged from 0.1 to 100 fg cell^{-1} (exceptionally 220 fg cell^{-1}) (Krock et al., 2009; Salas et al., 2011; Jauffrais et al., 2013b; Tillmann et al., 2018a; Kilcoyne et al., 2019) and this could be confirmed here for strain 7-F4 (also Ribotype A). Multiple, recently established *Az. spinosum* strains from the North Sea confirmed high toxin quota variability (ranging from 1.2 to 63.1 fg cell^{-1}) in Ribotype A both, among different strains and also within single strains tested with several independent measurements.

In contrast, strain N-05-01 did not reveal total AZA cell quota (AZA-11 + AZA-51) higher than 10 fg cell^{-1} , which is also in accordance with previous analyses of this strain (Tillmann et al., 2018a). Total AZA cell quota for Ribotype-B strains isolated in the North Sea in 2018 ranged from < 0.1 to 14.0 fg cell^{-1} (Tillmann et al., 2020). These findings indicate that *Az. spinosum* Ribotype B might have generally lower total AZA cell quota compared to Ribotype A, but the high

variabilities do not allow a clear differentiation between both Ribotypes in terms of AZA cell quota. That AZA cell quotas increase significantly from the exponential to the stationary phase, i.e. 2 fold increases as it was shown by Kilcoyne et al. (2019) could not be confirmed for both *Az. spinosum* strains in this study. This was probably because the experiments here were terminated early in the stationary phase, whereas Kilcoyne et al. (2019) sampled during late stationary phase after more than 120 days.

In this study, AZA proportions per cell but not the ranking order (AZA-1 > AZA-2 > AZA-33) changed significantly with temperature and between the exponential and stationary growth phase. Recent strain establishment from North Sea survey revealed completely new insights, since four different toxin profile groups were identified in *Az. spinosum* Ribotype A strains (Tillmann et al., 2020): (1) most strains had all three AZA congeners, (2) some had only AZA-1, (3) some had AZA-1 and -2 but lacked AZA-33 (4) some had only AZA-1 and -33, but lacked AZA-2. The median ratio of AZA-1 to AZA-2 or AZA-33 was 2.2 and 5.0, respectively, but for single strains/single analysis ratios < 1 were also obtained, and the same was observed for AZA-2/AZA-33 ratios. Fold-changes of multiple analyses of AZA-1/AZA-2 ratios were < 2 for many strains, but other strains showed high (up to 6.5-fold) changes of this ratio. There were highly significant differences between strains for all AZA ratios (1/2, 1/33, 2/33). For Ribotype B strain N-05-01, AZA-11 was always the dominant isomer compared to AZA-51, which was usually, but not always the case in previous analyses of this strain (Tillmann et al., 2018a). Multiple, newly isolated Ribotype B strains from the North Sea showed also either AZA-11 or AZA-51 as the dominant compound, but both were always present in each strain and the AZA-11/-51 ratio varied around 1.0 (Tillmann et al., submitted). The dominance of one compound was stable over time within one strain. These findings imply a very complex picture of mechanisms that trigger AZA production. Supernatant analyses revealed for both *Az. spinosum* strains that extracellular AZA cell quotas are significantly lower compared to the intracellular AZA cell quotas. However, while total extracellular AZA made generally not more than 5% of the total intracellular AZA in strain 7-F4, total extracellular AZA in strain N-05-01 made generally 20 – 40% of the total intracellular AZA. This suggests that for Ribotype A strains the highest risk of AZP might be due to the intracellular AZA levels, whereas Ribotype B strains significantly contribute to particulate dissolved AZA in the water column, which should in turn not be underestimated in monitorings.

Minor AZA compounds with a 14 Da (methyl-esters) or 80 Da (phosphates) higher molecular mass as the respective free AZA forms were detected from the very beginning of the discovery of AZA-

producing species (Krock et al., 2009; Tillmann et al., 2009; Krock et al., 2012), but were as such documented just recently (Tillmann et al., 2016; Tillmann et al., 2017c). So far, they seem to be generally synthesized by AZA producing amphidomataceans (Tillmann et al., 2018a). In this study, minor compound proportions found in *Az. spinosum* 7-F4 did not display a significant fraction of the total AZA cell quota (neither intra- nor extracellular) and might be carefully disregarded in terms of AZP risk. The supernatants of *Az. spinosum* 7-F4 and N-05-01 samples revealed relatively high levels of methyl-esters AZA-1-me, AZA-2-me and AZA-51-me, respectively. If these isomers are produced by the *Azadinium* cells is not clear, because extraction with methanol from SPE cartridges may artificially lead to increased formation of methyl-esters (Jauffrais et al., 2012b).

Azadinium poporum

The North Sea *Az. poporum* strain UTH-D4 reached up to 8×10^4 cells mL⁻¹ which was together with *Az. spinosum* strain 7-F4 the highest maximum cell density observed in this study. Strain UTH-D4 has never been intensively investigate concerning growth. Dai et al. (2019) reported maximum cell densities for cultured *Az. poporum* strains from Puget Sound/USA of 6×10^4 to 10×10^4 cells mL⁻¹, which is to observations in this study. But these were also strains with a different toxin profile (AZA-59) and cell densities were observed indirectly by chlorophyll-a fluorescence measurements, making direct comparison less reliable.

However, cells in the study of Dai et al. (2019) grew at temperatures from 6.9 to 23.0°C (here from 5 to 22.5°C; Notably, strain UTH-D4 was the only strain surviving at 5°C in the study presented here), with increasing growth rates from low ($\sim 0.1 \mu \text{ d}^{-1}$) to higher temperatures ($\sim 0.4 \mu \text{ d}^{-1}$) and with a strong decline at temperatures $> 23.0^\circ\text{C}$ (here $> 22.5^\circ\text{C}$). These results indicate that strains from temperate areas despite their different geographical origin do share comparable physiological adaptation status.

Another study by Luo et al. (2018) investigated two newly isolates Ribotype A (TIO420 and TIO424) and two Ribotype C (TIO429 and TIO452) *Az. poporum* strains from the Mediterranean (with toxin profiles of AZA-2, -11, -40 and -59) on growth at different temperature regimes. While growth for Ribotype A strain UTH-D4 in this study was observed between 5 and 22.5°C, Ribotype A and C strains in the Mediterranean revealed a shifted growth window from 11 to 26 °C and from 11 to 32 °C, respectively. This might be an indicator for an adaption to higher water temperatures in the Mediterranean strains. Ribotype A and C strains revealed also higher growth rates (up to \sim

0.5 μ d⁻¹) at higher temperatures, a similar pattern to the study of Dai et al. (2019) and the study presented here. Ribotype A strain TIO420 however, had its growth rate peak (\sim 0.3 μ d⁻¹) at 14 °C and decreased towards lower and higher temperatures.

In *Az. poporum* UTH-D4, growth and AZA cell quota were temperature dependent and behaved contrarily. Lower temperatures revealed lower growth rates, but higher AZA cell quotas, confirming findings of Dai et al. (2019). Also, AZA cell quota increased from the exponential to the stationary phase, as it was shown for *Az. spinosum* strains investigated in previous studies. In terms of intracellular AZA levels, other Ribotype A strains (N-39-01, N-39-03, N-39-13) containing only AZA-37 were isolated from the Norwegian coast by Tillmann et al. (2018a) and revealed AZA cell quotas of 1.5 to 6.5 fg cell⁻¹ when grown at 15 °C. One replicate measurement of N-39-13 had exceptionally higher cell quota of 19.5 fg cell⁻¹. These results are in very good agreement with the findings of this paper.

Amphidoma languida

While both *Az. spinosum* strains and the *Az. poporum* strain reached between 6 x 10⁴ and 8 x 10⁴ cells mL⁻¹, maximum cell densities for *Am. languida* were significantly lower (up to 1.8 x 10⁴ cells mL⁻¹). Since intense culture experiments have not been performed with *Am. languida* so far, comparison to other studies is not possible. However, cell densities of the newly isolated strain 8-D10 from the central North Sea (Tillmann et al., in preparation) were in the same order of magnitude as previous cultured *Am. languida* strains (Tillmann et al., 2012a).

As it was observed for *Az. spinosum* and *Az. poporum* in this study, growth of *Am. languida* was clearly temperature dependent, with increasing growth rates at higher temperatures. Even if the strain has not been tested at 22.5°C, growth was limited to a rather narrow temperature range (10 – 20°C), as it was the case for *Az. spinosum* N-05-01 (10 – 20°C). AZA cell quotas in strain 8-D10 were generally in good agreement with previous measured cell quotas in *Am. languida*, however total AZA cell quotas for this species seem to be quite variable (1 – 100 fg cell⁻¹) as described previously for Norwegian or North Sea strains (Tillmann et al. (2018a); Wietkamp et al. (2019a); Tillmann et al., in preparation).

Whereas AZA cell quota in the other three strains of this study decreased with increasing temperature, AZA cell quota for *Am. languida* remained on the same level for 10, 15 and 20 °C. This is in contrast to previous studies on toxigenic Amphidomataceae and raises the question why

AZA cell quota should only be de-coupled from temperature especially in *Am. languida*. At least in samples from the stationary phase the cells grown at 15 °C had highest cell quota, whereas for the 20 °C samples much lower intracellular AZA levels were detected. That was interesting, because the 20 °C samples in the stationary phase showed the by far highest extracellular AZA levels (even higher than the intracellular cell quota), which were generally moderate (< 10% of the total AZA cell quota) in all other samples. It might be hypothesized that cell at 20 °C in the stationary phase have been stressed and released AZA into the surrounding medium. This finding highlights that AZA molecules released into the sea water could account for a significant proportion of total AZA in the water and therefore might increase the risk of AZA contamination in shellfish. In any case, the actual toxicity of AZA-38 and -39 has not been investigated yet, but these tests would be needed for a proper risk assessment, especially because *Am. languida* has been repeatedly detected in the North Sea and adjacent areas (e.g. Wietkamp et al., 2020; Tillmann et al., 2020). Multiple strain analysis by Tillmann et al. (2018), Wietkamp et al. (2019a) and Tillmann et al. (in preparation) revealed that the ratio of AZA-38 and -39 can be variable, indicating that there are no biosynthetic constraints determining and limiting the ratio of both compounds present in the cells. However, this study revealed stable AZA proportions, with AZA-39 being the dominant isomer. These contrary findings should be further addressed in the future.

5. Conclusion

In general, growth and toxin cell quota were clearly temperature dependent in all four investigated species. Thereby, growth rates and AZA cell quota behaved antagonistic (except for *Am. languida*). While highest growth rates were observed at higher temperatures around 20°C, toxin cell quota were highest at lower temperatures around 10°C. These findings confirm previous studies on other toxic dinoflagellates, as well (Ogata et al., 1987; Anderson et al., 1990; Navarro et al., 2006; Guerrini et al., 2007).

However, not only AZA cell quotas but also actual cell densities and the potential for population increase determine the potential danger of toxic amphidomatacean populations. Therefore, not only the AZA cell quota, but also the growth rate for each temperature has been taken into account to calculate AZA production rates. The data revealed that the generally higher growth rates at higher temperatures are able to compensate lower AZA cell quota at these high temperatures, leading to a similar potential AZP risk of cells growing at low and high temperatures per a defined water

volume. In the case of *Az. spinosum* strain 7-F4, high growth rates in higher temperatures even overcompensated the high AZA cell quotas in low temperature cultures, indicating an increasing AZP risk under potentially rising water temperatures in the future. Strain 7-F4 produced also the by far highest amount of AZA compared to the other three strains, confirming the need to frequently monitor *Az. spinosum* and its AZA in the North Sea.

In general, when comparing previous physiological studies, methodological differences, e.g. in terms of culture conditions may lead to differences between experiments. For example, aeration of the cultures increased AZA cell quota in *Az. spinosum* significantly (Jauffrais et al., 2013b), or phosphate limited media was shown to enhance AZA cell quota in *Az. poporum* (Li et al., 2016).

In any case, the studies conducted so far can only give limited insights into the whole physiology of AZA production. More experimental studies are needed, but will never fully reflect field conditions. There are only two previous studies quantifying AZA cell quota in the field, using microscopic and molecular (qPCR) cell counts together with chemical (LC-MS/MS) analyses (Wietkamp et al., 2019a; Wietkamp et al., 2020), and it has already been discussed that even AZA cell quota estimations directly in the field can be biased for example by methodology and AZA in small protistan grazers or detritus (Wietkamp et al., 2019a).

Apart from that, of all the AZA isomers that have been discovered the recent years, still only AZA-1, -2 and -3 are officially regulated and basically nothing is known about toxicity and metabolic pathways of other AZA in mollusks (Jauffrais et al., 2012d; Kilcoyne et al., 2014b; Krock et al., 2019). We therefore suggest to perform not only monitoring, but also more toxicity tests and biotransformation experiments at least for the prominent AZA of the North Sea (AZA-11, -37, -38, -39, -51) presented in this study.

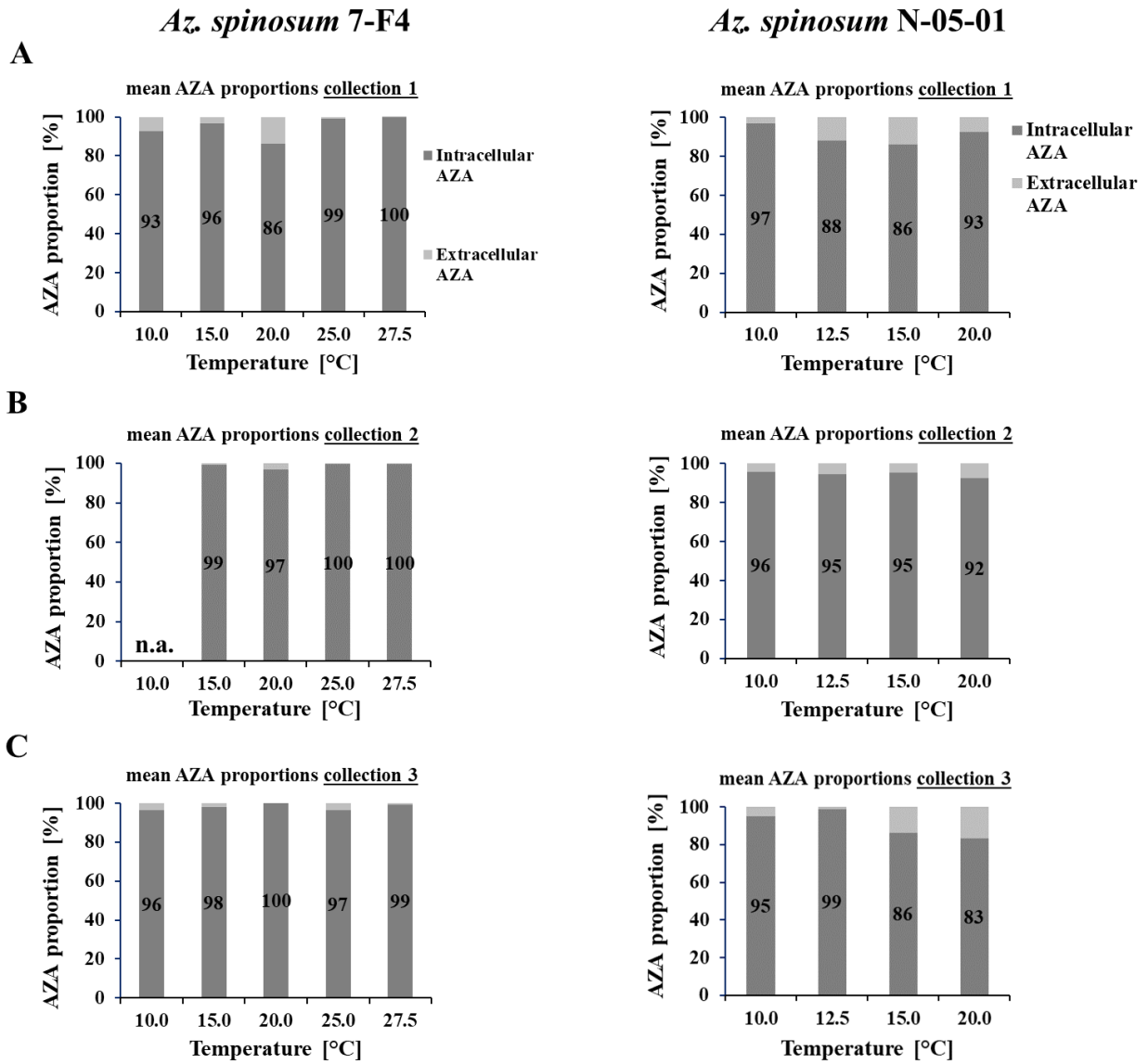
Acknowledgements

The authors thank especially Thomas Max, who carried out the preparation and measurements of the supernatants on AZA.

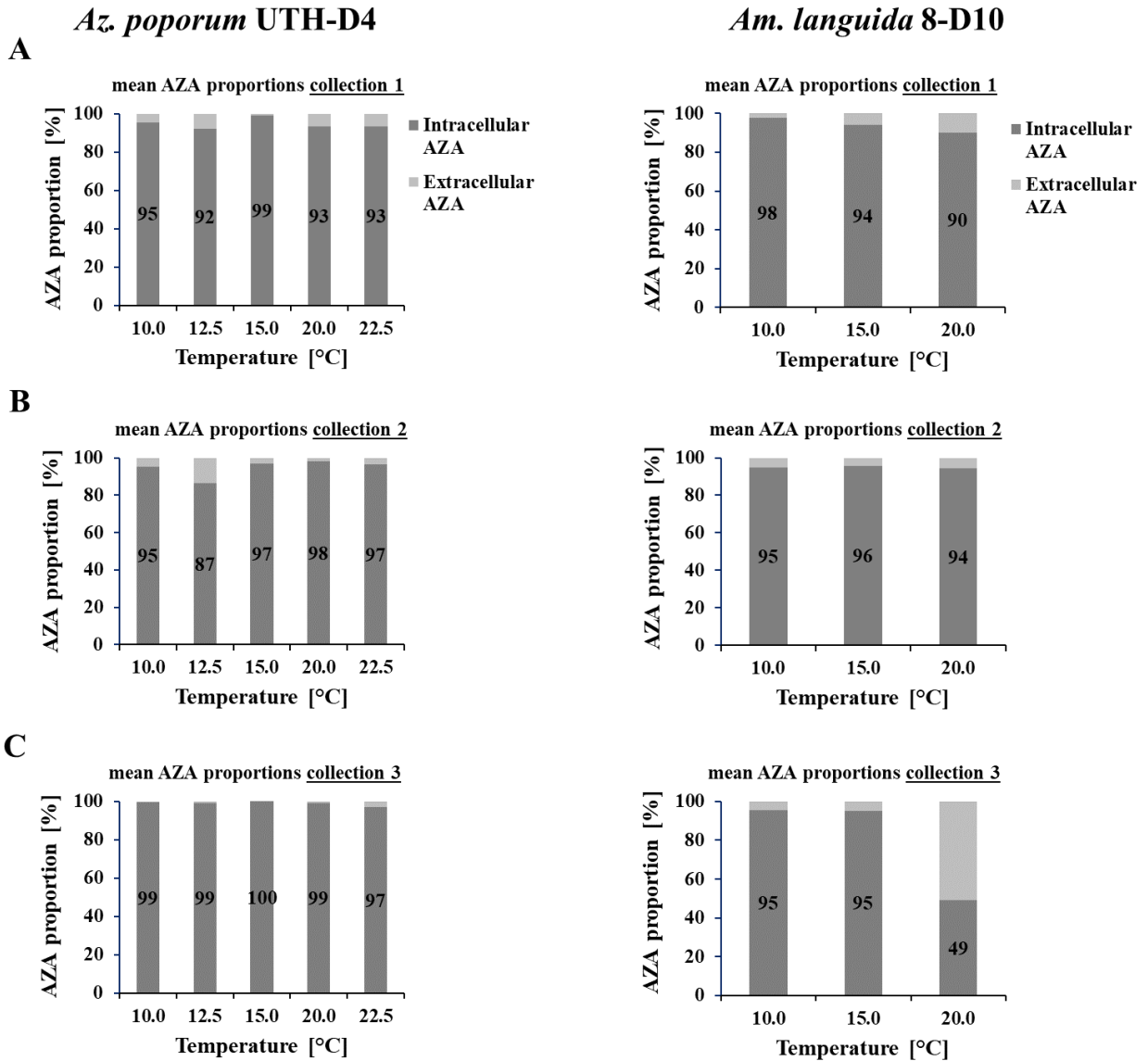
Supplementary Material

Suppl. Table S1: Mass transitions m/z (Q1>Q3 mass) and their respective AZA.

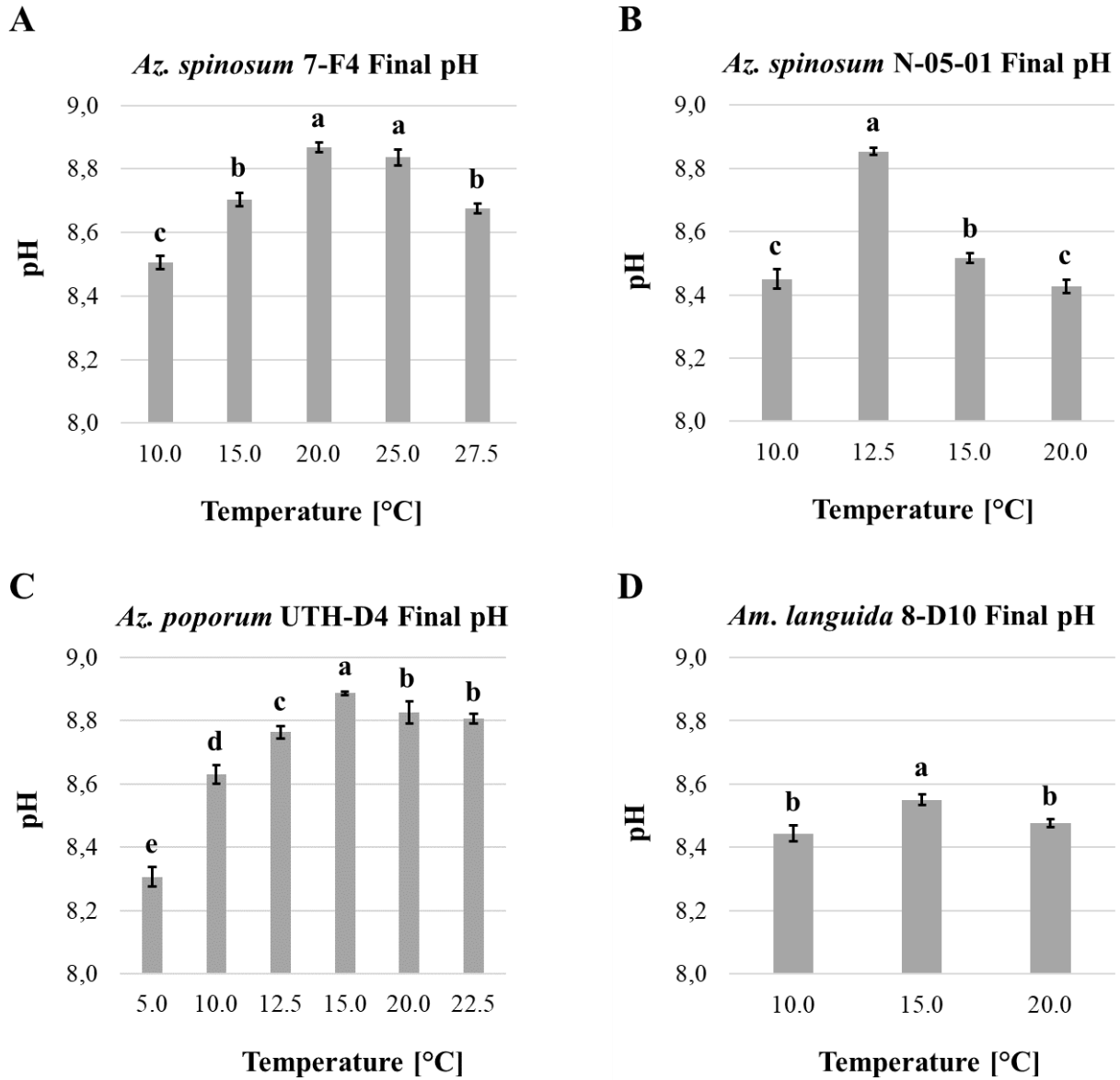
Mass transition	Toxin	Collision energy (CE) [V]
716>698	AZA-33	40
796>778	AZA-33 phosphate	40
816>798	AZA-34, AZA-39	40
816>348	AZA-39	70
828>658	AZA-3	70
828>810	AZA-3, AZA-43, AZA-58	40
830>812	AZA-38, AZA-52, AZA-53	40
830>348	AZA-38, AZA-52, AZA-53	70
842>672	AZA-1	70
842>824	AZA-1, AZA-40, AZA-50	40
842>348	AZA-40	70
844>826	AZA-4, AZA-5	40
846>828	AZA-37	40
846>348	AZA-37	70
854>836	AZA-41	40
854>670	AZA-41	70
854>360	AZA-41	70
856>672	AZA-2	70
856>838	AZA-2	40
858>840	AZA-7, AZA-8, AZA-9, AZA-10, AZA-36, AZA-51	40
858>348	AZA-36, AZA-51	70
860>842	AZA-59	40
868>362	AZA-55	70
870>852	Me-AZA-2, AZA-42, AZA-54	40
870>360	AZA-42	40
872>854	AZA-11, AZA-12	40
884>866	AZA-56	40
910>892	Undescribed	40
920>804	AZA-1 phosphate, AZA-40 phosphate	40
926>908	AZA-37 phosphate	40
936>918	AZA-2 phosphate	40
938>920	AZA-36 phosphate, AZA-51 phosphate	40
940>922	AZA-59 phosphate	40
952>938	AZA-11 phosphate	40



Suppl. Fig. S1. *Azadinium spinosum* strains 7-F4 and N-05-01: Mean intracellular and extracellular AZA cell quota as proportion of the total AZA cell quota (in %) per temperature for collection 1 (A), collection 2 (B) and collection 3 (C).



Suppl. Fig. S2. *Azadinium poporum* strain UTH-D4 and *Am. languida* strain 8-D10: Mean extracellular AZA cell quota as proportion of the intracellular AZA cell quota (in %) per temperature for collection 1 (A), collection 2 (B) and collection 3 (C). Letters above bars indicate statistically significant different groups ($p < 0.05$).



Suppl. Fig. S3. Mean pH (\pm 1SD) in the stationary growth phase of *Az. spinosum* 7-F4 (A), *Az. spinosum* N-05-01 (B), *Az. poporum* UTH-D4 (C) and *Am. languida* 8-D10 (D). Letters above bars indicate statistically significant different groups ($p < 0.05$).

References

1. Aasen, J., Torgersen, T., Dahl, E., Naustvoll, L., Aune, T. (2004) Confirmation of azaspiracids in mussels in Norwegian coastal areas, and full profile at one location, *Proceedings of the 5th International Conference on Molluscan Shellfish Safety, Galway, Ireland, June 14-18*, pp. 162-169.
2. Adams, N.G., Tillmann, U., Trainer, V.L. (2020) Temporal and spatial distribution of *Azadinium* species in the inland and coastal waters of the Pacific northwest in 2014–2018. *Harmful Algae* 98, 101874.
3. Akselman, R., Negri, R. (2010) *Azadinium spinosum* Elbrächter et Tillmann (Dinophyceae) is Present and also caused Blooms at the Southwestern Atlantic, *Abstract Book of the 14th International Conference Harmful Algae*, p. 132.
4. Akselman, R., Negri, R.M. (2012) Blooms of *Azadinium* cf. *spinosum* Elbrächter et Tillmann (Dinophyceae) in northern shelf waters of Argentina, Southwestern Atlantic. *Harmful Algae* 19, 30-38.
5. Alfonso, A., Vieytes, M.R., Ofuji, K., Satake, M., Nicolaou, K., Frederick, M.O., Botana, L. (2006) Azaspiracids modulate intracellular pH levels in human lymphocytes. *Biochem. Biophys. Res. Commun.* 346(3), 1091-1099.
6. Alvarez, G., Uribe, E., Avalos, P., Marino, C., Blanco, J. (2010) First identification of azaspiracid and spirolides in *Mesodesma donacium* and *Mulinia edulis* from Northern Chile. *Toxicon* 55(2-3), 638-641.
7. Amzil, Z., Sibat, M., Royer, F., Savar, V. (2008) First report on azaspiracid and yessotoxin groups detection in French shellfish. *Toxicon* 52(1), 39-48.
8. Andersen, P. (1996) Design and implementation of some harmful algal monitoring systems. *UNESCO: Conseil international pour l'exploration de la mer*, (44).
9. Anderson, D., Kulis, D., Sullivan, J., Hall, S., Lee, C. (1990) Dynamics and physiology of saxitoxin production by the dinoflagellates *Alexandrium* spp. *Mar. Biol.* 104(3), 511-524.
10. Anderson, D.M. (1989) Toxic algal blooms and red tides: a global perspective. *Red tides: biology, environmental science and toxicology*, 11-16.
11. Andree, K.B., Fernandez-Tejedor, M., Elandaloussi, L.M., Quijano-Scheggia, S., Sampedro, N., Garces, E., Camp, J., Diogene, J. (2011) Quantitative PCR coupled with melt curve analysis for detection of selected *Pseudo-nitzschia* spp. (Bacillariophyceae) from the Northwestern Mediterranean sea. *Appl. Environ. Microbiol.* 77(5), 1651-1659.
12. Anonymous (2004) Regulation (EC) No 854/2004 of the European Parliament and of the Council of 29 April 2004 laying down specific rules for the organisation of official controls on products of animal origin intended for human consumption. *J. Eur. Union L* 226, 83-127.
13. Backer, L.C., Manassaram-Baptiste, D., LePrell, R., Bolton, B. (2015) Cyanobacteria and algae blooms: review of health and environmental data from the harmful algal bloom-related illness surveillance system (HABISS) 2007–2011. *Toxins* 7(4), 1048-1064.

14. Balech, E. (1977) *Cachonina niei* Loeblich (Dinoflagellata) y sus variaciones. Buenos Aires Physis Sección A 36, 59-64.
15. Barra, L., Ruggiero, M.V., Sarno, D., Montresor, M., Kooistra, W.H. (2013) Strengths and weaknesses of microarray approaches to detect *Pseudo-nitzschia* species in the field. Environmental Science and Pollution Research 20(10), 6705-6718.
16. Boc, A., Diallo, A.B., Makarenkov, V. (2012) T-REX: a web server for inferring, validating and visualizing phylogenetic trees and networks. Nucleic Acids Res. 40(W1), W573-W579.
17. Bonk, F., Popp, D., Harms, H., Centler, F. (2018) PCR-based quantification of taxa-specific abundances in microbial communities: Quantifying and avoiding common pitfalls. J. Microbiol. Methods 153, 139-147.
18. Bowers, H.A., Tengs, T., Glasgow, H.B., Burkholder, J.M., Rublee, P.A., Oldach, D.W. (2000) Development of real-time PCR assays for rapid detection of *Pfiesteria piscicida* and related dinoflagellates. Appl. Environ. Microbiol. 66(11), 4641-4648.
19. Boxer, B., Salah, M. (2019) *Mediterranean Sea*. Encyclopædia Britannica.
20. Braña Magdalena, A., Lehane, M., Krys, S., Fernández, M.L., Furey, A., James, K.J. (2003) The first identification of azaspiracids in shellfish from France and Spain. Toxicon 42(1), 105-108.
21. Casabianca, S., Casabianca, A., Riobo, P., Franco, J.M., Vila, M., Penna, A. (2013) Quantification of the toxic dinoflagellate *Ostreopsis* spp. by qPCR assay in marine aerosol. Environ. Sci. Technol. 47(8), 3788-3795.
22. Cavalcante, K.P., Susini-Ribeiro, S.M.M., Tillmann, U. (2018) First detection of species of the potentially toxic genus *Azadinium* (Amphidomataceae, Dinophyceae) in tropical coastal waters of Brazil. Brazilian Journal of Botany 41(1), 209-218.
23. Cembella, A.D. (2003) Chemical ecology of eukaryotic microalgae in marine ecosystems. Phycologia 42(4), 420-447.
24. Charnock, H., Dyer, K., Huthnance, J., Liss, P., Simpson, B. (2012) *Understanding the North Sea System*. Springer Science & Business Media.
25. Cheung, V.G., Morley, M., Aguilar, F., Massimi, A., Kucherlapati, R., Childs, G. (1999) Making and reading microarrays. Nat. Genet. 21(1), 15-19.
26. Clarke, D. (2020) New insights and perspectives from 20 years of monitoring algal events in Irish coastal waters, In: D Clarke, M Gilmartin (Eds.), *Proceedings of the 11th Irish Shellfish Safety Workshop, Marine Environment and Health Series No. 41, Marine Institute, Galway (Ireland)*, in press.
27. Connolly, J.A., Oliver, M.J., Beaulieu, J.M., Knight, C.A., Tomanek, L., Moline, M.A. (2008) Correlated evolution of genome size and cell volume in diatoms (Bacillariophyceae) 1. J. Phycol. 44(1), 124-131.

28. Coyne, K.J., Hutchins, D.A., Hare, C.E., Cary, S.C. (2001) Assessing temporal and spatial variability in *Pfiesteria piscicida* distributions using molecular probing techniques. *Aquat. Microb. Ecol.* 24(3), 275-285.
29. Cushing, D. (1959) The seasonal variation in oceanic production as a problem in population dynamics. *ICES J. Mar. Sci.* 24(3), 455-464.
30. Dai, X., Bill, B.D., Adams, N.G., Tillmann, U., Sloan, C., Lu, D., Trainer, V.L. (2019) The effect of temperature and salinity on growth rate and azaspiracid cell quotas in two strains of *Azadinium poporum* (Dinophyceae) from Puget Sound, Washington State. *Harmful Algae* 89, 101665.
31. Dale, B., Yentsch, C.M. (1978) *Red Tide and Paralytic Shellfish Poisoning*. Oceanus.
32. Dhanji-Rapkova, M., O'Neill, A., Maskrey, B.H., Coates, L., Swan, S.C., Alves, M.T., Kelly, R.J., Hatfield, R.G., Rowland-Pilgrim, S.J., Lewis, A.M. (2019) Variability and profiles of lipophilic toxins in bivalves from Great Britain during five and a half years of monitoring: azaspiracids and yessotoxins. *Harmful Algae* 87, 101629.
33. Dodge, J., Hermes, H. (1981) A scanning electron microscopical study of the apical pores of marine dinoflagellates (Dinophyceae). *Phycologia* 20(4), 424-430.
34. Doležel, J., Greilhuber, J., Lucretti, S., Meister, A., Lysák, M., Nardi, L., Obermayer, R. (1998) Plant genome size estimation by flow cytometry: inter-laboratory comparison. *Ann. Bot.* 82(suppl_1), 17-26.
35. Dominguez, H.J., Paz, B., Daranas, A.H., Norte, M., Franco, J.M., Fernández, J.J. (2010) Dinoflagellate polyether within the yessotoxin, pectenotoxin and okadaic acid toxin groups: Characterization, analysis and human health implications. *Toxicon* 56(2), 191-217.
36. Ebenezer, V., Medlin, L.K., Ki, J.-S. (2012) Molecular detection, quantification, and diversity evaluation of microalgae. *Mar. Biotechnol.* 14(2), 129-142.
37. EC (2012) *Communication from the commission: "Blue growth," opportunities for marine and maritime sustainable growth*. European Commission.
38. EC (2013) *Strategic Guidelines for the sustainable development of EU aquaculture: Communication from the Commission to the European Parliament, the Council, the European Economic and Social Committee and the Committee of the Regions*. European Commission.
39. Eckford-Soper, L.K., Daugbjerg, N. (2015) Development of a multiplex real-time qPCR assay for simultaneous enumeration of up to four marine toxic bloom-forming microalgal species. *Harmful Algae* 48, 37-43.
40. Edvardsen, B., Dittami, S.M., Groben, R., Brubak, S., Escalera, L., Rodriguez, F., Reguera, B., Chen, J., Medlin, L.K. (2013) Molecular probes and microarrays for the detection of toxic algae in the genera *Dinophysis* and *Phalacroma* (Dinophyta). *Environ. Sci. Pollut. Res. Int.* 20(10), 6733-6750.

41. Elbrächter, M., Meyer, B. (2001) Plate pattern variability and plate overlap in a clonal culture of the freshwater dinoflagellate *Peridinium umbonatum* Stein species complex (Dinophyceae). *Neues Jahrbuch für Geologie und Paläontologie-Abhandlungen*, 221-227.
42. Emeis, K.-C., van Beusekom, J., Callies, U., Ebinghaus, R., Kannen, A., Kraus, G., Kröncke, I., Lenhart, H., Lorkowski, I., Matthias, V. (2015) The North Sea - A shelf sea in the Anthropocene. *J. Mar. Syst.* 141, 18-33.
43. Engesmo, A., Strand, D., Gran-Stadniczeñko, S., Edvardsen, B., Medlin, L.K., Eikrem, W. (2018) Development of a qPCR assay to detect and quantify ichthyotoxic flagellates along the Norwegian coast, and the first Norwegian record of *Fibrocapsa japonica* (Raphidophyceae). *Harmful Algae* 75, 105-117.
44. EU (2001) *Report of the meeting of the Working Wroup on Toxicology of DSP and AZP*. Report from CLR, 21-23 May 2001(Brussels).
45. EU (2011) *Commission Regulation (EU) No 15/2011 of 10 January 2011 amending Regulation (EC) No 2074/2005 as regards recognised testing methods for detecting marine biotoxins in live bivalve molluscs*. Official Journal of the European Union. Series L 6(3).
46. Fabro, E., Almandoz, G.O., Krock, B., Tillmann, U. (2020) Field observations of the dinoflagellate genus *Azadinium* and azaspiracid toxins in the south-west Atlantic Ocean. *Marine and Freshwater Research* 71(7), 832-843.
47. Farabegoli, F., Blanco, L., Rodríguez, L.P., Vieites, J.M., Cabado, A.G. (2018) Phycotoxins in marine shellfish: Origin, occurrence and effects on humans. *Mar. Drugs* 16(6), 188.
48. Flynn, K.J., Fynn, K., John, E.H., Reguera, B., Reyero, I., Franco, J.M. (1996) Changes in toxins, intracellular and dissolved free amino acids of the toxic dinoflagellate *Gymnodinium catenatum* in response to changes in inorganic nutrients and salinity. *J. Plankton Res.* 18(11), 2093-2111.
49. Frederick, M.O., Cole, K.P., Petrovic, G., Loizidou, E., Nicolaou, K. (2007) 16 Structural Assignment and Total Synthesis of Azaspiracid-1. *Phycotoxins*, 297.
50. FSAI (2001) *Food Safety Authority of Ireland: risk assessment of azaspiracids (AZAs) in shellfish, February 2001*. A Report of the Scientific Committee of the Food Safety Authority of Ireland (FSAI).
51. Furey, A., O'Doherty, S., O'Callaghan, K., Lehane, M., James, K.J. (2010) Azaspiracid poisoning (AZP) toxins in shellfish: toxicological and health considerations. *Toxicon* 56(2), 173-190.
52. Galluzzi, L., Bertozzini, E., Penna, A., Perini, F., Garcés, E., Magnani, M. (2010) Analysis of rRNA gene content in the Mediterranean dinoflagellate *Alexandrium catenella* and *Alexandrium taylori*: implications for the quantitative real-time PCR-based monitoring methods. *J. Appl. Phycol.* 22(1), 1-9.
53. Galluzzi, L., Penna, A., Bertozzini, E., Vila, M., Garcés, E., Magnani, M. (2004) Development of a Real-Time PCR Assay for Rapid Detection and Quantification of *Alexandrium minutum* (a Dinoflagellate). *Appl. Environ. Microbiol.* 70(2), 1199-1206.

54. Garneau, M.E., Schnetzer, A., Countway, P.D., Jones, A.C., Seubert, E.L., Caron, D.A. (2011) Examination of the seasonal dynamics of the toxic dinoflagellate *Alexandrium catenella* at Redondo Beach, California, by quantitative PCR. *Appl. Environ. Microbiol.* 77(21), 7669-7680.
55. Gedaria, A.I., Luckas, B., Reinhardt, K., Azanza, R.V. (2007) Growth response and toxin concentration of cultured *Pyrodinium bahamense* var. *compressum* to varying salinity and temperature conditions. *Toxicon* 50(4), 518-529.
56. Gobler, C.J. (2019) Climate Change and Harmful Algal Blooms: Insights and perspective. *Harmful Algae*, 101731.
57. Gobler, C.J., Doherty, O.M., Hattenrath-Lehmann, T.K., Griffith, A.W., Kang, Y., Litaker, R.W. (2017) Ocean warming since 1982 has expanded the niche of toxic algal blooms in the North Atlantic and North Pacific oceans. *Proc Natl Acad Sci* 114(19), 4975-4980.
58. Godhe, A., Asplund, M.E., Harnstrom, K., Saravanan, V., Tyagi, A., Karunasagar, I. (2008) Quantification of Diatom and Dinoflagellate Biomasses in Coastal Marine Seawater Samples by Real-Time PCR. *Appl. Environ. Microbiol.* 74(23), 7174-7182.
59. Godhe, A., Otta, S., Rehnstam-Holm, A.-S., Karunasagar, I., Karunasagar, I. (2001) Polymerase chain reaction in detection of *Gymnodinium mikimotoi* and *Alexandrium minutum* in field samples from southwest India. *Mar. Biotechnol.* 3(2), 152-162.
60. Gómez, F. (2012) A quantitative review of the lifestyle, habitat and trophic diversity of dinoflagellates (Dinoflagellata, Alveolata). *Syst. Biodivers.* 10(3), 267-275.
61. Granéli, E., Turner, J.T. (2006) *Ecology of harmful algae*. Springer.
62. Griffith, A.W., Doherty, O.M., Gobler, C.J. (2019) Ocean warming along temperate western boundaries of the Northern Hemisphere promotes an expansion of *Cochlodinium polykrikoides* blooms. *Proceedings of the Royal Society B* 286(1904), 20190340.
63. Gu, H., Luo, Z., Krock, B., Witt, M., Tillmann, U. (2013) Morphology, phylogeny and azaspiracid profile of *Azadinium poporum* (Dinophyceae) from the China Sea. *Harmful Algae* 21-22, 64-75.
64. Guerrini, F., Ciminiello, P., Dell'Aversano, C., Tartaglione, L., Fattorusso, E., Boni, L., Pistocchi, R. (2007) Influence of temperature, salinity and nutrient limitation on yessotoxin production and release by the dinoflagellate *Protoceratium reticulatum* in batch-cultures. *Harmful Algae* 6(5), 707-717.
65. Guillard, R.R. (1975) Culture of phytoplankton for feeding marine invertebrates, In: *Culture of marine invertebrate animals*. Springer, pp. 29-60.
66. Guillard, R.R., Ryther, J.H. (1962) Studies of marine planktonic diatoms: I. *Cyclotella nana* Hustedt, and *Detonula confervacea* (Cleve) Gran. *Canadian journal of microbiology* 8(2), 229-239.
67. Hall, T.A. (1999) BioEdit: a user-friendly biological sequence alignment editor and analysis program for Windows 95/98/NT, Nucleic acids symposium series. [London]: Information Retrieval Ltd., c1979-c2000., pp. 95-98.

68. Hallegraeff, G. (2003) Harmful algal blooms: a global overview. *Manual on harmful marine microalgae* 33, 1-22.
69. Hallegraeff, G., Dorantes-Aranda, J.J., Mardones, J., Seger, A. (2017) Review of progress in our understanding of fish-killing microalgae: implications for management and mitigation. *Marine and fresh-water harmful algae* 150.
70. Hallegraeff, G.M. (1993) A review of harmful algal blooms and their apparent global increase. *Phycologia* 32(2), 79-99.
71. Hallegraeff, G.M., Anderson, D.M., Cembella, A.D., Enevoldsen, H. (2004) *Manual on harmful marine microalgae*. Unesco.
72. Handy, S.M., Hutchins, D.A., Cary, S.C., Coyne, K.J. (2006) Simultaneous enumeration of multiple raphidophyte species by quantitative real-time PCR: capabilities and limitations. *Limnol. Oceanogr. Methods* 4(6), 193-204.
73. Hernández-Becerril, D.U., Barón-Campis, S.A., Escobar-Morales, S. (2012) A new record of *Azadinium spinosum* (Dinoflagellata) from the tropical Mexican Pacific. *Rev. Biol. Mar. Oceanogr.* 47(3), 553-557.
74. Hershkovitz, M.A., Lewis, L.A. (1996) Deep-level diagnostic value of the rDNA-ITS region. *Mol. Biol. Evol.* 13(9), 1276-1295.
75. Hess, P., McCarron, P., Krock, B., Kilcoyne, J., Miles, C.O. (2014) Azaspiracids: Chemistry, biosynthesis, metabolism, and detection. *Seafood and Freshwater Toxins: Pharmacology, Physiology, and Detection*, 799-821.
76. Hess, P., McMahon, T., Slattery, D., Swords, D., Dowling, G., McCarron, M., Clarke, D., Gobbons, W., Silke, J., O'Conneide, M. (2003) Use of LC-MS testing to identify lipophilic toxins, to establish local trends and interspecies differences and to test the comparability of LC-MS testing with the mouse bioassay: an example from the Irish biotoxin monitoring programme 2001. *Conselleria de Pesca e Asuntos Marítimos da Xunta de Galicia and Intergovernmental Oceanographic Commission of UNESCO*.
77. Hosoi-Tanabe, S., Sako, Y. (2005) Species-specific detection and quantification of toxic marine dinoflagellates *Alexandrium tamarense* and *A. catenella* by Real-time PCR assay. *Mar Biotechnol (NY)* 7(5), 506-514.
78. Hu, C., Barnes, B.B., Qi, L., Lembke, C., English, D. (2016) Vertical migration of *Karenia brevis* in the northeastern Gulf of Mexico observed from glider measurements. *Harmful Algae* 58, 59-65.
79. Hu, H., Chen, W., Shi, Y., Cong, W. (2006) Nitrate and phosphate supplementation to increase toxin production by the marine dinoflagellate *Alexandrium tamarense*. *Mar. Pollut. Bull.* 52(7), 756-760.
80. James, K., Furey, A., Satake, M., Yasumoto, T. (2000) Azaspiracid poisoning (AZP): A new shellfish toxic syndrome in Europe. *Harmful algal blooms*, 250-253.
81. James, K.J., Furey, A., Lehane, M., Ramstad, H., Aune, T., Hovgaard, P., Morris, S., Higman, W., Satake, M., Yasumoto, T. (2002) First evidence of an extensive northern European distribution of azaspiracid poisoning (AZP) toxins in shellfish. *Toxicon* 40(7), 909-915.

82. Jansen, H.M., Van Den Burg, S., Bolman, B., Jak, R.G., Kamermans, P., Poelman, M., Stuver, M. (2016) The feasibility of offshore aquaculture and its potential for multi-use in the North Sea. *Aquacult. Int.* 24(3), 735-756.
83. Jauffrais, T., Contreras, A., Herrenknecht, C., Truquet, P., Sechet, V., Tillmann, U., Hess, P. (2012a) Effect of *Azadinium spinosum* on the feeding behaviour and azaspiracid accumulation of *Mytilus edulis*. *Aquat. Toxicol.* 124-125, 179-187.
84. Jauffrais, T., Herrenknecht, C., Sechet, V., Sibat, M., Tillmann, U., Krock, B., Kilcoyne, J., Miles, C.O., McCarron, P., Amzil, Z., Hess, P. (2012b) Quantitative analysis of azaspiracids in *Azadinium spinosum* cultures. *Anal. Bioanal. Chem.* 403(3), 833-846.
85. Jauffrais, T., Kilcoyne, J., Herrenknecht, C., Truquet, P., Sechet, V., Miles, C.O., Hess, P. (2013a) Dissolved azaspiracids are absorbed and metabolized by blue mussels (*Mytilus edulis*). *Toxicon* 65, 81-89.
86. Jauffrais, T., Kilcoyne, J., Sechet, V., Herrenknecht, C., Truquet, P., Herve, F., Berard, J.B., Nulty, C., Taylor, S., Tillmann, U., Miles, C.O., Hess, P. (2012c) Production and isolation of azaspiracid-1 and -2 from *Azadinium spinosum* culture in pilot scale photobioreactors. *Mar. Drugs* 10(6), 1360-1382.
87. Jauffrais, T., Marcaillou, C., Herrenknecht, C., Truquet, P., Sechet, V., Nicolau, E., Tillmann, U., Hess, P. (2012d) Azaspiracid accumulation, detoxification and biotransformation in blue mussels (*Mytilus edulis*) experimentally fed *Azadinium spinosum*. *Toxicon* 60(4), 582-595.
88. Jauffrais, T., Séchet, V., Herrenknecht, C., Truquet, P., Savar, V., Tillmann, U., Hess, P. (2013b) Effect of environmental and nutritional factors on growth and azaspiracid production of the dinoflagellate *Azadinium spinosum*. *Harmful Algae* 27, 138-148.
89. Jeffrey, S.W., Wright, S.W., Zapata, M. (2011) Microalgal classes and their signature pigments, In: Llewellyn, C.A., Egeland, E.S., Johnsen, G., Roy, S. (Eds.), *Phytoplankton Pigments: Characterization, Chemotaxonomy and Applications in Oceanography*. Cambridge University Press, Cambridge, UK, pp. 3-77.
90. Jeong, H.J., Du Yoo, Y., Kim, J.S., Seong, K.A., Kang, N.S., Kim, T.H. (2010) Growth, feeding and ecological roles of the mixotrophic and heterotrophic dinoflagellates in marine planktonic food webs. *Ocean science journal* 45(2), 65-91.
91. Joint, I., Pomroy, A. (1993) Phytoplankton biomass and production in the southern North Sea. *Marine Ecology-Progress Series* 99, 169-169.
92. Kalaitzis, J.A., Chau, R., Kohli, G.S., Murray, S.A., Neilan, B.A. (2010) Biosynthesis of toxic naturally-occurring seafood contaminants. *Toxicon* 56(2), 244-258.
93. Katoh, K., Standley, D.M. (2013) MAFFT multiple sequence alignment software version 7: improvements in performance and usability. *Mol. Biol. Evol.* 30(4), 772-780.
94. Keller, M.D., Selvin, R.C., Claus, W., Guillard, R.R.L. (1987) Media for the culture of oceanic ultraphytoplankton. *J. Phycol.* 23(4), 633-638.

95. Kellmann, R., Schaffner, C.A., Grønset, T.A., Satake, M., Ziegler, M., Fladmark, K.E. (2009) Proteomic response of human neuroblastoma cells to azaspiracid-1. *Journal of proteomics* 72(4), 695-707.
96. Kilcoyne, J., Jauffrais, T., Twiner, M.J., Doucette, G.J., Aasen Bunes, J.A., Sosa, S., Krock, B., Séhet, V., Nulty, C., Salas, R. (2014a) *Azaspiracids—toxicological evaluation, test methods and identification of the source organisms (ASTOX II)*. Marine Institute, Galway, Ireland.
97. Kilcoyne, J., McCoy, A., Burrell, S., Krock, B., Tillmann, U. (2019) Effects of Temperature, Growth Media, and Photoperiod on Growth and Toxin Production of *Azadinium spinosum*. *Mar. Drugs* 17(9), 489.
98. Kilcoyne, J., Nulty, C., Jauffrais, T., McCarron, P., Herve, F., Foley, B., Rise, F., Crain, S., Wilkins, A.L., Twiner, M.J., Hess, P., Miles, C.O. (2014b) Isolation, Structure Elucidation, Relative LC-MS Response, and in Vitro Toxicity of Azaspiracids from the Dinoflagellate *Azadinium spinosum*. *J. Nat. Prod.* 77(11), 2465-2474.
99. Kim, J.H., Tillmann, U., Adams, N.G., Krock, B., Stutts, W.L., Deeds, J.R., Han, M.S., Trainer, V.L. (2017) Identification of *Azadinium* species and a new azaspiracid from *Azadinium poporum* in Puget Sound, Washington State, USA. *Harmful Algae* 68, 152-167.
100. Kraberg, A., Stern, R. (2017) *Phytoplankton: Diatoms*, *Marine Plankton: A practical guide to ecology, methodology, and taxonomy*, p. 151.
101. Krock, B., Tillmann, U., Alpermann, T.J., Voß, D., Zielinski, O., Cembella, A.D. (2013) Phycotoxin composition and distribution in plankton fractions from the German Bight and western Danish coast. *J. Plankton Res.* 35(5), 1093-1108.
102. Krock, B., Tillmann, U., John, U., Cembella, A.D. (2009) Characterization of azaspiracids in plankton size-fractions and isolation of an azaspiracid-producing dinoflagellate from the North Sea. *Harmful Algae* 8(2), 254-263.
103. Krock, B., Tillmann, U., Potvin, É., Jeong, H.J., Drebing, W., Kilcoyne, J., Al-Jorani, A., Twiner, M.J., Göthel, Q., Köck, M. (2015) Structure Elucidation and in Vitro Toxicity of New Azaspiracids Isolated from the Marine Dinoflagellate *Azadinium poporum*. *Mar. Drugs* 13(11), 6687-6702.
104. Krock, B., Tillmann, U., Tebben, J., Trefault, N., Gu, H. (2019) Two novel azaspiracids from *Azadinium poporum*, and a comprehensive compilation of azaspiracids produced by Amphidomataceae, (Dinophyceae). *Harmful Algae* 82, 1-8.
105. Krock, B., Tillmann, U., Voß, D., Koch, B.P., Salas, R., Witt, M., Potvin, E., Jeong, H.J. (2012) New azaspiracids in Amphidomataceae (Dinophyceae). *Toxicon* 60(5), 830-839.
106. Krock, B., Tillmann, U., Witt, M., Gu, H. (2014) Azaspiracid variability of *Azadinium poporum* (Dinophyceae) from the China Sea. *Harmful Algae* 36, 22-28.
107. Krock, B., Wisotzki, A. (2018) *Physical oceanography during HEINCKE cruise HE516*. Alfred Wegener Institute, Helmholtz Centre for Polar and Marine Research, Bremerhaven, PANGAEA.

108. Kumar, S., Stecher, G., Tamura, K. (2016) MEGA7: Molecular Evolutionary Genetics Analysis version 7.0. *Mol. Biol. Evol.* 33, 1870-1874.
109. Lartigue, J., Jester, E.L., Dickey, R.W., Villareal, T.A. (2009) Nitrogen source effects on the growth and toxicity of two strains of the ciguatera-causing dinoflagellate *Gambierdiscus toxicus*. *Harmful Algae* 8(5), 781-791.
110. Lassus, P. (1988) Plancton toxique et plancton d'eaux rouges sur les côtes européennes.
111. Lassus, P., Chomérat, N., Hess, P., Nézan, E. (2016) *Toxic and harmful microalgae of the World Ocean*. UNESCO.
112. Li, A.F., Jiang, B.Z., Chen, H.D., Gu, H.F. (2016) Growth and toxin production of *Azadinium poporum* strains in batch cultures under different nutrient conditions. *Ecotoxicol. Environ. Saf.* 127, 117-126.
113. Liao, J.C., Mastali, M., Li, Y., Gau, V., Suchard, M.A., Babbitt, J., Gornbein, J., Landaw, E.M., McCabe, E.R., Churchill, B.M. (2007) Development of an advanced electrochemical DNA biosensor for bacterial pathogen detection. *The Journal of Molecular Diagnostics* 9(2), 158-168.
114. Litaker, W.R., Vandersea, M.W., Kibler, S.R., Reece, K.S., Stokes, N.A., Lutzoni, F.M., Yonish, B.A., West, M.A., Black, M.N., Tester, P.A. (2007) Recognizing dinoflagellate species using ITS rDNA sequences 1. *J. Phycol.* 43(2), 344-355.
115. LoCicero, V.R. (1975) Proc. First Int. Conf. Toxic Dinoflagellate Blooms, *Boston, Massachusetts Science and Technology Foundation*, p. 541 pp.
116. Longhurst, A. (1995) Seasonal cycles of pelagic production and consumption. *Prog. Oceanogr.* 36(2), 77-167.
117. Lopes, V.M., Lopes, A.R., Costa, P., Rosa, R. (2013) Cephalopods as vectors of harmful algal bloom toxins in marine food webs. *Mar. Drugs* 11(9), 3381-3409.
118. López-Rivera, A., O'Callaghan, K., Moriarty, M., O'Driscoll, D., Hamilton, B., Lehane, M., James, K.J., Furey, A. (2010) First evidence of azaspiracids (AZAs): A family of lipophilic polyether marine toxins in scallops (*Argopecten purpuratus*) and mussels (*Mytilus chilensis*) collected in two regions of Chile. *Toxicon* 55(4), 692-701.
119. Luo, Z., Krock, B., Giannakourou, A., Venetsanopoulou, A., Pagou, K., Tillmann, U., Gu, H. (2018) Sympatric occurrence of two *Azadinium poporum* ribotypes in the Eastern Mediterranean Sea. *Harmful Algae* 78, 75-85.
120. Luo, Z., Yang, W., Leaw, C.P., Pospelova, V., Bilien, G., Liow, G.R., Lim, P.T., Gu, H. (2017a) Cryptic diversity within the harmful dinoflagellate *Akashiwo sanguinea* in coastal Chinese waters is related to differentiated ecological niches. *Harmful Algae* 66, 88-96.
121. Luo, Z.H., Krock, B., Mertens, K.N., Nézan, E., Chomérat, N., Billen, G., Tillmann, U., Gu, H. (2017b) Adding new pieces to the *Azadinium* (Dinophyceae) diversity and biogeography puzzle: Non-toxigenic *Azadinium zhuanum* sp. nov. from China, toxigenic *A. poporum* from the Mediterranean, and a non-toxigenic *A. dalianense* from the French Atlantic. *Harmful Algae* 66, 65-78.

122. Luo, Z.H., Krock, B., Mertens, K.N., Price, A.M., Turner, R.E., Rabalais, N.N., Gu, H.F. (2016) Morphology, molecular phylogeny and azaspiracid profile of *Azadinium poporum* (Dinophyceae) from the Gulf of Mexico. *Harmful Algae* 55, 56-65.
123. Macé, A., Kutalik, Z., Valsesia, A. (2018) Copy Number Variation. In: Evangelou E. (Ed) *Genetic Epidemiology*, Humana Press, New York, NY.
124. Maclean, C., Cembella, A.D., Quilliam, M.A. (2003) Effects of light, salinity and inorganic nitrogen on cell growth and spirolide production in the marine dinoflagellate *Alexandrium ostenfeldii* (Paulsen) Balech et Tangen. *Bot. Mar.* 46(5), 466-476.
125. Mardis, E.R. (2017) DNA sequencing technologies: 2006–2016. *Nature protocols* 12(2), 213.
126. McMahon, T. (1998) Re-occurrence of winter toxicity. *Harmful Algae News* 17, 12.
127. McMahon, T., Silke, J. (1996) Winter toxicity of unknown aetiology in mussels. *Harmful Algae News* 14(2), 1998.
128. Medhioub, W., Sechet, V., Truquet, P., Bardouil, M., Amzil, Z., Lassus, P., Soudant, P. (2011) *Alexandrium ostenfeldii* growth and spirolide production in batch culture and photobioreactor. *Harmful Algae* 10(6), 794-803.
129. Medina, M., Collins, A.G., Silberman, J.D., Sogin, M.L. (2001) Evaluating hypotheses of basal animal phylogeny using complete sequences of large and small subunit rRNA. *Proceedings of the National Academy of Sciences* 98(17), 9707-9712.
130. Medlin, L.K., Orozco, J. (2017) Molecular techniques for the detection of organisms in aquatic environments, with emphasis on harmful algal bloom species. *Sensors* 17(5), 1184.
131. Metfies, K., Huljic, S., Lange, M., Medlin, L.K. (2005) Electrochemical detection of the toxic dinoflagellate *Alexandrium ostenfeldii* with a DNA-biosensor. *Biosensors Bioelectron.* 20(7), 1349-1357.
132. Metfies, K., Medlin, L.K. (2004) DNA microchips for phytoplankton: the fluorescent wave of the future. *Nova Hedwigia* 79(1-2), 321-327.
133. Nagai, S., Suzuki, T., Nishikawa, T., Kamiyama, T. (2011) Differences in the production and excretion kinetics of okadaic acid, dinophysistoxin-1, and pectenotoxin-2 between cultures of *Dinophysis acuminata* and *Dinophysis fortii* isolated from western Japan. *J. Phycol.* 47(6), 1326-1337.
134. Navarro, J., Muñoz, M., Contreras, A. (2006) Temperature as a factor regulating growth and toxin content in the dinoflagellate *Alexandrium catenella*. *Harmful Algae* 5(6), 762-769.
135. Nézan, E., Tillmann, U., Bilien, G., Boulben, S., Cheze, K., Zentz, F., Salas, R., Chomerat, N. (2012) Taxonomic revision of the dinoflagellate *Amphidoma caudata*: Transfer to the genus *Azadinium* (Dinophyceae) and proposal of two varieties, based on morphological and molecular phylogenetic analyses. *J. Phycol.* 48(4), 925-939.

136. Nicolaou, K., Koftis, T.V., Vyskocil, S., Petrovic, G., Tang, W., Frederick, M.O., Chen, D.Y.-K., Li, Y., Ling, T., Yamada, Y.M. (2006) Total synthesis and structural elucidation of azaspiracid-1. Final assignment and total synthesis of the correct structure of azaspiracid-1. *J. Am. Chem. Soc.* 128(9), 2859-2872.
137. Nishimura, T., Hariganeya, N., Tawong, W., Sakanari, H., Yamaguchi, H., Adachi, M. (2016) Quantitative PCR assay for detection and enumeration of ciguatera-causing dinoflagellate *Gambierdiscus* spp.(Gonyaulacales) in coastal areas of Japan. *Harmful Algae* 52, 11-22.
138. Notomi, T., Okayama, H., Masubuchi, H., Yonekawa, T., Watanabe, K., Amino, N., Hase, T. (2000) Loop-mediated isothermal amplification of DNA. *Nucleic Acids Res.* 28(12), e63-e63.
139. O'Boyle, S., Raine, R. (2007) The influence of local and regional oceanographic processes on phytoplankton distribution in continental shelf waters off north-western Ireland, *Biology and Environment: Proceedings of the Royal Irish Academy*. JSTOR, pp. 95-109.
140. Ofuji, K., Satake, M., McMahon, T., Silke, J., James, K.J., Naoki, H., Oshima, Y., Yasumoto, T. (1999) Two analogs of azaspiracid isolated from mussels, *Mytilus edulis*, involved in human intoxication in Ireland. *Nat. Toxins* 7(3), 99-102.
141. Ogata, T., Ishimaru, T., Kodama, M. (1987) Effect of water temperature and light intensity on growth rate and toxicity change in *Protogonyaulax tamarensis*. *Mar. Biol.* 95(2), 217-220.
142. Olefeld, J.L., Majda, S., Albach, D.C., Marks, S., Boenigk, J. (2018) Genome size of chrysophytes varies with cell size and nutritional mode. *Organisms Diversity & Evolution* 18(2), 163-173.
143. Orozco, J., Villa, E., Manes, C.-L., Medlin, L.K., Guillebault, D. (2016) Electrochemical RNA genosensors for toxic algal species: enhancing selectivity and sensitivity. *Talanta* 161, 560-566.
144. OSPAR (2000) *Quality Status Report 2000: Region II: Greater North Sea*. OSPAR Commission for the Protection of the Marine Environment of the North-East Atlantic.
145. Park, T.G., de Salas, M.F., Bolch, C.J., Hallegraeff, G.M. (2007) Development of a real-time PCR probe for quantification of the heterotrophic dinoflagellate *Cryptoperidiniopsis brodyi* (Dinophyceae) in environmental samples. *Appl. Environ. Microbiol.* 73(8), 2552-2560.
146. Parkhill, J.-P., Cembella, A.D. (1999) Effects of salinity, light and inorganic nitrogen on growth and toxigenicity of the marine dinoflagellate *Alexandrium tamarense* from northeastern Canada. *J. Plankton Res.* 21(5).
147. Paterson, R.F. (2018) PhD Thesis: Investigating the distribution, seasonal dynamics and toxicity of *Azadinium spinosum* in Scottish waters using qPCR. University of Aberdeen.
148. Pelin, M., Kilcoyne, J., Florio, C., Hess, P., Tubaro, A., Sosa, S. (2019) Azaspiracids increase mitochondrial dehydrogenases activity in hepatocytes: Involvement of potassium and chloride ions. *Mar. Drugs* 17(5), 276.

149. Pelin, M., Kilcoyne, J., Nulty, C., Crain, S., Hess, P., Tubaro, A., Sosa, S. (2018) Toxic equivalency factors (TEFs) after acute oral exposure of azaspiracid 1,– 2 and– 3 in mice. *Toxicol. Lett.* 282, 136-146.
150. Penna, A., Galluzzi, L. (2013) The quantitative real-time PCR applications in the monitoring of marine harmful algal bloom (HAB) species. *Environ. Sci. Pollut. Res.* 20(10), 6851-6862.
151. Penna, A., Magnani, M. (1999) Identification of *Alexandrium* (Dinophyceae) species using PCR and rDNA-targeted probes. *J. Phycol.* 35(3), 615-621.
152. Percopo, I., Siano, R., Rossi, R., Soprano, V., Sarno, D., Zingone, A. (2013) A new potentially toxic *Azadinium* species (Dinophyceae) from the Mediterranean Sea, *A. dexteroporum* sp. nov. *J. Phycol.* 49(5), 950-966.
153. Perini, F., Casabianca, A., Battocchi, C., Accoroni, S., Totti, C., Penna, A. (2011) New Approach Using the Real-Time PCR Method for Estimation of the Toxic Marine Dinoflagellate *Ostreopsis* cf. *ovata* in Marine Environment. *PLOS ONE* 6(3), e17699.
154. Posada, D. (2008) jModelTest: phylogenetic model averaging. *Mol. Biol. Evol.* 25(7), 1253-1256.
155. Potvin, E., Hwang, Y.J., Yoo, Y.D., Kim, J.S., Jeong, H.J. (2013) Feeding by heterotrophic protists and copepods on the photosynthetic dinoflagellate *Azadinium* cf. *poporum* from western Korean waters. *Aquat. Microb. Ecol.* 68(2), 143-158.
156. Potvin, É., Jeong, H.J., Kang, N.S., Tillmann, U., Krock, B. (2012) First Report of the Photosynthetic Dinoflagellate Genus *Azadinium* in the Pacific Ocean: Morphology and Molecular Characterization of *Azadinium* cf. *poporum*. *J. Eukaryot. Microbiol.* 59(2), 145-156.
157. R-Core-Team (2017) R: A Language and Environment for Statistical Computing.
158. Rambaut, A., Drummond, A.J., Xie, D., Baele, G., Suchard, M.A. (2018) Posterior summarization in Bayesian phylogenetics using Tracer 1.7. *Syst. Biol.* 67(5), 901.
159. Ramsfjell, E. (1959) Two new phytoplankton species from the Norwegian Sea, the diatom *Coscinosira poroseriata*, and the dinoflagellate *Gonyaulax parva*. *Nytt Magasin for Botanikk* 7, 175-177.
160. Rehmann, N., Hess, P., Quilliam, M.A. (2008) Discovery of new analogs of the marine biotoxin azaspiracid in blue mussels (*Mytilus edulis*) by ultra-performance liquid chromatography/tandem mass spectrometry. *Rapid Communications in Mass Spectrometry: An International Journal Devoted to the Rapid Dissemination of Up-to-the-Minute Research in Mass Spectrometry* 22(4), 549-558.
161. Rick, H.J., Rick, S., Tillmann, U., Brockmann, U., Gärtner, U., Dürselen, C., Sündermann, J. (2006) Primary productivity in the German Bight (1994–1996). *Estuaries and Coasts* 29(1), 4-23.
162. Rick, W.Y., Wang, T., Bedzyk, L., Croker, K.M. (2001) Applications of DNA microarrays in microbial systems. *J. Microbiol. Methods* 47(3), 257-272.

163. Ritzman, J., Brodbeck, A., Brostrom, S., McGrew, S., Dreyer, S., Klinger, T., Moore, S.K. (2018) Economic and sociocultural impacts of fisheries closures in two fishing-dependent communities following the massive 2015 US West Coast harmful algal bloom. *Harmful Algae* 80, 35-45.
164. Rollo, F., Sassaroli, S., Boni, L., Marota, I. (1995) Molecular typing of the red-tide dinoflagellate *Gonyaulax polyedra* in phytoplankton suspensions. *Aquat. Microb. Ecol.* 9(1), 55-61.
165. Román, Y., Alfonso, A., Vieytes, M.R., Ofuji, K., Satake, M., Yasumoto, T., Botana, L.M. (2004) Effects of azaspiracids 2 and 3 on intracellular cAMP,[Ca²⁺], and pH. *Chem. Res. Toxicol.* 17(10), 1338-1349.
166. Ronquist, F., Huelsenbeck, J.P. (2003) MrBayes 3: Bayesian phylogenetic inference under mixed models. *Bioinformatics* 19(12), 1572-1574.
167. Rossi, R., Dell'Aversano, C., Krock, B., Ciminiello, P., Percopo, I., Tillmann, U., Soprano, V., Zingone, A. (2017) Mediterranean *Azadinium dexteroporum* (Dinophyceae) produces six novel azaspiracids and azaspiracid-35: a structural study by a multi-platform mass spectrometry approach. *Anal. Bioanal. Chem.* 409(4), 1121-1134.
168. Rossini, G.P. (2014) *Toxins and Biologically Active Compounds from Microalgae, Volume 2: Biological Effects and Risk Management*. CRC Press, Boca Raton, Florida, USA.
169. Ruvindy, R., Bolch, C.J., MacKenzie, L., Smith, K.F., Murray, S.A. (2018) qPCR assays for the detection and quantification of multiple Paralytic Shellfish Toxin-producing species of *Alexandrium*. *Frontiers in microbiology* 9.
170. Sabine, C.L., Feely, R.A. (2007) The oceanic sink for carbon dioxide. *Greenhouse gas sinks* 31.
171. Salas, R., Tillmann, U., John, U., Kilcoyne, J., Burson, A., Cantwell, C., Hess, P., Jauffrais, T., Silke, J. (2011) The role of *Azadinium spinosum* (Dinophyceae) in the production of azaspiracid shellfish poisoning in mussels. *Harmful Algae* 10(6), 774-783.
172. Salas, R., Tillmann, U., Kavanagh, S. (2014) Morphological and molecular characterization of the small armoured dinoflagellate *Heterocapsa minima* (Peridinales, Dinophyceae). *Eur. J. Phycol.* 49(4), 413-428.
173. Sanseverino, I., Conduto, D., Pozzoli, L., Dobricic, S., Lettieri, T. (2016) *Algal bloom and its economic impact*. European Commission, Joint Research Centre Institute for Environment and Sustainability.
174. Satake, M., Ofuji, K., James, K., Furey, A., Yasumoto, T. (1998a) New toxic event caused by Irish mussels. *Harmful Algae*, 468-469.
175. Satake, M., Ofuji, K., Naoki, H., James, K.J., Furey, A., McMahon, T., Silke, J., Yasumoto, T. (1998b) Azaspiracid, a new marine toxin having unique spiro ring assemblies, isolated from Irish mussels, *Mytilus edulis*. *J. Am. Chem. Soc.* 120(38), 9967-9968.
176. Sheehan, P.M., Berx, B., Gallego, A., Hall, R.A., Heywood, K.J., Queste, B.Y. (2020) Weekly variability of hydrography and transport of northwestern inflows into the northern North Sea. *J. Mar. Syst.* 204, 103288.

177. Shikata, T., Matsunaga, S., Nishide, H., Sakamoto, S., Onistuka, G., Yamaguchi, M. (2015) Diurnal vertical migration rhythms and their photoresponse in four phytoflagellates causing harmful algal blooms. *Limnol. Oceanogr.* 60(4), 1251-1264.
178. Shumway, S.E., Burkholder, J.M., Morton, S.L. (2018) *Harmful algal blooms: a compendium desk reference*. Wiley & Sons, New Jersey, USA.
179. Simbolo, M., Gottardi, M., Corbo, V., Fassan, M., Mafficini, A., Malpeli, G., Lawlor, R.T., Scarpa, A. (2013) DNA qualification workflow for next generation sequencing of histopathological samples. *PloS one* 8(6), e62692.
180. Smayda, T.J., Reynolds, C.S. (2003) Strategies of marine dinoflagellate survival and some rules of assembly. *J. Sea Res.* 49(2), 95-106.
181. Smith, K.F., Rhodes, L., Harwood, D.T., Adamson, J., Moisan, C., Munday, R., Tillmann, U. (2016) Detection of *Azadinium poporum* in New Zealand: the use of molecular tools to assist with species isolations. *J. Appl. Phycol.* 28(2), 1125-1132.
182. Sournia, A. (1984) Classification et nomenclature de divers dinoflagellés marins (Dinophyceae). *Phycologia* 23(3), 345-355.
183. Spector, D.L. (2012) *Dinoflagellates*. Academic Press, Cambridge, Massachusetts, USA.
184. Stamatakis, A. (2006) RAxML-VI-HPC: maximum likelihood-based phylogenetic analyses with thousands of taxa and mixed models. *Bioinformatics* 22(21), 2688-2690.
185. Streng, M. (2003) *Phylogenetic Aspects and Taxonomy of Calcareous Dinoflagellates*, Geosciences. University of Bremen, Berichte aus dem Fachbereich Geowissenschaften, p. 157.
186. Stryer, L. (1995) Genes for ribosomal RNAs are tandemly repeated several hundred times. *Biochemistry*, 4th ed. WH Freeman and Company, New York, USA, 992-993.
187. Sunesen, I., Rodríguez, F., Tardivo Kubis, J.A., Aguiar Juárez, D., Risso, A., Lavigne, A.S., Wietkamp, S., Tillmann, U., Sar, E.A. (2020) Morphological and molecular characterization of *Heterocapsa claromecoensis* sp. nov. (Peridinales, Dinophyceae) from Buenos Aires coastal waters (Argentina). *Eur. J. Phycol.*, 1-17.
188. Swofford, D.L. (2002) PAUP: phylogenetic analysis using parsimony, version 4.0 b10. Sinauer Associates, Sunderland, MA.
189. Taleb, H., Vale, P., Amanhir, R., Benhadouch, A., Sagou, R., Chafik, A. (2006) First detection of azaspiracids in mussels in north west Africa. *J. Shellfish Res.* 25(3), 1067-1070.
190. Taylor, F. (1979) The toxigenic gonyaulacoid dinoflagellates. *Toxic dinoflagellate blooms*, 47-56.

191. Te, S.H., Chen, E.Y., Gin, K.Y.-H. (2015) Comparison of quantitative PCR and droplet digital PCR multiplex assays for two genera of bloom-forming cyanobacteria, *Cylindrospermopsis* and *Microcystis*. *Appl. Environ. Microbiol.* 81(15), 5203-5211.
192. Tewhey, R., Warner, J.B., Nakano, M., Libby, B., Medkova, M., David, P.H., Kotsopoulos, S.K., Samuels, M.L., Hutchison, J.B., Larson, J.W. (2009) Microdroplet-based PCR enrichment for large-scale targeted sequencing. *Nat. Biotechnol.* 27(11), 1025-1031.
193. Tillmann, U. (2018) Amphidomataceae, In: Shumway, S.E., Burkholder, J.A., Morton, S.L. (Eds.), *Harmful Algae Blooms, a compendium desk reference*. Wiley, Hoboken, New Jersey, USA, pp. 575-582.
194. Tillmann, U., Akselman, R. (2016) Revisiting the 1991 algal bloom in shelf waters off Argentina: *Azadinium luciferelloides* sp. nov. (Amphidomataceae, Dinophyceae) as the causative species in a diverse community of other amphidomataceans. *Phycol. Res.* 64(3), 160-175.
195. Tillmann, U., Borel, C.M., Barrera, F., Lara, R., Krock, B., Almandoz, G.O., Witt, M., Trefault, N. (2016) *Azadinium poporum* from the Argentine Continental Shelf, Southwestern Atlantic, produces azaspiracid-2 and azaspiracid-2 phosphate. *Harmful Algae* 51, 40-55.
196. Tillmann, U., Edvardsen, B., Krock, B., Smith, K.F., Paterson, R.F., Voß, D. (2018a) Diversity, distribution, and azaspiracids of Amphidomataceae (Dinophyceae) along the Norwegian coast. *Harmful Algae* 80, 15-34.
197. Tillmann, U., Elbrächter, M., John, U., Krock, B. (2011) A new non-toxic species in the dinoflagellate genus *Azadinium*: *A. poporum* sp. nov. *Eur. J. Phycol.* 46(1), 74-87.
198. Tillmann, U., Elbrächter, M., John, U., Krock, B., Cembella, A. (2010) *Azadinium obesum* (Dinophyceae), a new nontoxic species in the genus that can produce azaspiracid toxins. *Phycologia* 49(2), 169-182.
199. Tillmann, U., Elbrächter, M., Krock, B., John, U., Cembella, A. (2009) *Azadinium spinosum* gen. et sp. nov. (Dinophyceae) identified as a primary producer of azaspiracid toxins. *Eur. J. Phycol.* 44(1), 63-79.
200. Tillmann, U., Gottschling, M., Guinder, V., Krock, B. (2018b) *Amphidoma parvula* (Amphidomataceae), a new planktonic dinophyte from the Argentine Sea. *Eur. J. Phycol.* 53(1), 14-28.
201. Tillmann, U., Gottschling, M., Krock, B., Smith, K.F., Guinder, V. (2019) High abundance of Amphidomataceae (Dinophyceae) during the 2015 spring bloom of the Argentinean Shelf and a new, non-toxic ribotype of *Azadinium spinosum*. *Harmful Algae* 84, 244-260.
202. Tillmann, U., Gottschling, M., Nézan, E., Krock, B. (2015) First records of *Amphidoma languida* and *Azadinium dexteroporum* (Amphidomataceae, Dinophyceae) from the Irminger Sea off Iceland. *Mar. Biodivers. Rec.* 8, 1-11.
203. Tillmann, U., Gottschling, M., Nezan, E., Krock, B., Bilien, G. (2014a) Morphological and molecular characterization of three new *Azadinium* species (Amphidomataceae, Dinophyceae) from the Irminger sea. *Protist* 165(4), 417-444.

204. Tillmann, U., Jaén, D., Fernández, L., Gottschling, M., Witt, M., Blanco, J., Krock, B. (2017a) *Amphidoma languida* (Amphidomataceae, Dinophyceae) with a novel azaspiracid toxin profile identified as the cause of molluscan contamination at the Atlantic coast of southern Spain. *Harmful Algae* 62, 113-126.
205. Tillmann, U., Krock, B., Taylor, B.B. (2014b) *Azadinium caudatum* var. *margalefii*, a poorly known member of the toxigenic genus *Azadinium* (Dinophyceae). *Mar. Biol. Res.* 10(10), 941-956.
206. Tillmann, U., Salas, R., Gottschling, M., Krock, B., O'Driscoll, D., Elbrächter, M. (2012a) *Amphidoma languida* sp. nov. (Dinophyceae) reveals a close relationship between *Amphidoma* and *Azadinium*. *Protist* 163(5), 701-719.
207. Tillmann, U., Salas, R., Jauffrais, T., Hess, P., Silke, J. (2014c) AZA - The producing organisms: Biology and trophic transfer., In: Botana, L.M. (Ed.), *Seafood and Freshwater Toxins*. CRC Press, Boca Raton, Florida, USA, pp. 773-798.
208. Tillmann, U., Sánchez-Ramírez, S., Krock, B., Bernales-Jiménez, A. (2017b) A bloom of *Azadinium polongum* in coastal waters off Peru. *Rev. Biol. Mar. Oceanogr.* 52(3), 591-610.
209. Tillmann, U., Soehner, S., Nézan, E., Krock, B. (2012b) First record of the genus *Azadinium* (Dinophyceae) from the Shetland Islands, including the description of *Azadinium polongum* sp. nov. *Harmful Algae* 20, 142-155.
210. Tillmann, U., Trefault, N., Krock, B., Parada-Pozo, G., De la Iglesia, R., Vasquez, M. (2017c) Identification of *Azadinium poporum* (Dinophyceae) in the Southeast Pacific: morphology, molecular phylogeny, and azaspiracid profile characterization. *J. Plankton Res.* 39(2), 350-367.
211. Tillmann, U., Wietkamp, S., Krock, B., Tillmann, A., Voss, D., Gu, H. (2020) Amphidomataceae (Dinophyceae) in the western Greenland area, including description of *Azadinium perforatum* sp. nov. *Phycologia* 59(1), 63-88.
212. Toebe, K., Joshi, A.R., Messtorff, P., Tillmann, U., Cembella, A., John, U. (2013) Molecular discrimination of taxa within the dinoflagellate genus *Azadinium*, the source of azaspiracid toxins. *J. Plankton Res.* 35(1), 225-230.
213. Toldrà, A., O'Sullivan, C.K., Diogène, J., Campàs, M. (2020) Detecting harmful algal blooms with nucleic acid amplification-based biotechnological tools. *Sci. Total Environ.*, 141605.
214. Torgersen, T., Bremnes, N.B., Rundberget, T., Aune, T. (2008) Structural confirmation and occurrence of azaspiracids in Scandinavian brown crabs (*Cancer pagurus*). *Toxicon* 51(1), 93-101.
215. Trainer, V.L., Moore, L., Bill, B.D., Adams, N.G., Harrington, N., Borchert, J., da Silva, D.A.M., Eberhart, B.T.L. (2013) Diarrhetic Shellfish Toxins and Other Lipophilic Toxins of Human Health Concern in Washington State. *Mar. Drugs* 11(6), 1815-1835.
216. Turner, A.D., Goya, A.B. (2015) Occurrence and profiles of lipophilic toxins in shellfish harvested from Argentina. *Toxicon* 102, 32-42.
217. Twiner, M.J., Hess, P., Doucette, G. (2014) Azaspiracids: Toxicology, Pharmacology, and Risk Assessment. *Seafood and Freshwater Toxins*, 823-855.

218. Twiner, M.J., Rehmann, N., Hess, P., Doucette, G.J. (2008) Azaspiracid shellfish poisoning: a review on the chemistry, ecology, and toxicology with an emphasis on human health impacts. *Mar. Drugs* 6(2), 39-72.
219. Ueoka, R., Ito, A., Izumikawa, M., Maeda, S., Takagi, M., Shin-Ya, K., Yoshida, M., van Soest, R.W.M., Matsunaga, S. (2009) Isolation of azaspiracid-2 from a marine sponge *Echinoclathria* sp. as a potent cytotoxin. *Toxicon* 53(6), 680-684.
220. Vale, P., Bire, R., Hess, P. (2008) Confirmation by LC-MS/MS of azaspiracids in shellfish from the Portuguese north-western coast. *Toxicon* 51(8), 1449-1456.
221. Van Dolah, F.M. (2000) Marine algal toxins: origins, health effects, and their increased occurrence. *Environ. Health Perspect.* 108(suppl 1), 133-141.
222. Wang, C., Zhang, T., Wang, Y., Katz, L.A., Gao, F., Song, W. (2017) Disentangling sources of variation in SSU rDNA sequences from single cell analyses of ciliates: impact of copy number variation and experimental error. *Proc. R. Soc. B* 284(1859), 20170425.
223. Wietkamp, S., Krock, B., Clarke, D., Voß, D., Salas, R., Kilcoyne, J., Tillmann, U. (2020) Distribution and abundance of azaspiracid-producing dinophyte species and their toxins in North Atlantic and North Sea waters in summer 2018. *PLoS ONE* 15(6), e0235015.
224. Wietkamp, S., Krock, B., Gu, H., Voß, D., Klemm, K., Tillmann, U. (2019a) Occurrence and distribution of Amphidomataceae (Dinophyceae) in Danish coastal waters of the North Sea, the Limfjord and the Kattegat/Belt area. *Harmful Algae* 88, 101637.
225. Wietkamp, S., Tillmann, U., Clarke, D., Toebe, K. (2019b) Molecular detection and quantification of the azaspiracid-producing dinoflagellate *Amphidoma languida* (Amphidomataceae, Dinophyceae). *J. Plankton Res.* 41(2), 101-113.
226. Wijsman, J., Troost, K., Fang, J., Roncarati, A. (2019) *Global production of marine bivalves. Trends and challenges*, In: Smaal A., Ferreira J., Grant J., Petersen J., Strand Ø. (Eds.) *Goods and services of marine bivalves*. Springer, Cham, pp. 7-26.
227. Xu, N., Duan, S., Li, A., Zhang, C., Cai, Z., Hu, Z. (2010) Effects of temperature, salinity and irradiance on the growth of the harmful dinoflagellate *Prorocentrum donghaiense* Lu. *Harmful Algae* 9(1), 13-17.
228. Yao, J., Tan, Z., Zhou, D., Guo, M., Xing, L., Yang, S. (2010) Determination of azaspiracid-1 in shellfishes by liquid chromatography with tandem mass spectrometry. *Chinese journal of chromatography* 28(4), 363-367.
229. Zamor, R.M., Glenn, K.L., Hambright, K.D. (2012) Incorporating molecular tools into routine HAB monitoring programs: Using qPCR to track invasive *Prymnesium*. *Harmful Algae* 15, 1-7.
230. Zuker, M. (2003) Mfold web server for nucleic acid folding and hybridization prediction. *Nucleic Acids Res.* 31(13), 3406-3415.

231. Zurhelle, C. (2019) Structural elucidation and quantification of novel toxins in marine microalgae by NMR- and molecular modelling-based techniques. University of Bremen, Bremen, Germany.

Supplementary material

Supplementary Method Information

Suppl. Method II. General DNA extraction, PCR amplification and Sanger Dideoxy Sequencing protocol used in this study. Divergent protocols are mentioned in the respective publications, which are attached to this thesis.

DNA extraction

DNA from microalgal cells was extracted by application of the NucleoSpin Soil DNA extraction kit (Macherey-Nagel, Düren, Germany) according to the manufacturer's instructions. Each sample was collected within a bead tube together with 500 μ L SL1 lysis buffer, both provided by the extraction kit. As a slight variation compared to the kit guidelines, the bead tubes were not vortexed but shaken in a cell disrupter (FastPrep FP120, Thermo-Savant-Ilkirch, France) for 45 sec and another 30 sec at a speed of 4 m s⁻¹. For final DNA elution, the elution step was performed twice with each 50 μ L of the provided elution buffer (to a final extraction volume of 100 μ L) for overall yield maximization. Until further processing, the DNA was stored at -20 °C.

PCR amplification

Prior to DNA sequencing, the respective rDNA regions, i.e. the SSU, ITS1-5.8S-ITS2 and LSU (D1/D2), were amplified by PCR with the primer sets summarized in the following table:

Primer sets used for Sanger Dideoxy Sequencing.

rDNA region	Primer name	Primer sequence (5'-3')
SSU	1F ^f	AAC CTG GTT GAT CCT GCC AGT
	1528R ^r	TGA TCC TTC TGC AGG TTC ACC TAC
ITS set 1	ITSa ^f	CCA AGC TTC TAG ATC GTA ACA AGG (ACT)TC CGT AGG T
	ITSb ^r	CCT GCA GTC GAC A(GT)A TGC TTA A(AG)T TCA GC(AG) GG
ITS set 2	ITS1 ^f	TCC GTA GGT GAA CCT GCG G
	ITS4 ^r	TCC TCC GCT TAT TGA TAT GC
LSU	DirF ^f	ACC CGC TGA ATT TAA GCA TA
	D2CR ^r	CCT TGG TCC GTG TTT CAA GA

^f Forward primer, ^r Reverse primer

Each PCR reaction contained 16.3 μL ultra-pure H_2O , 2.0 μL HotMaster Taq buffer (5Prime, Hamburg, Germany), 0.2 μL dNTPs (10 μM), 0.2 μL of each primer (10 μM), 0.1 μL of Taq Polymerase (Quantabio, Beverly, Massachusetts, USA) and 1.0 μL of extracted DNA template (10 $\text{ng } \mu\text{L}^{-1}$) to a final reaction volume of 20 μL . PCRs were conducted in a Nexus Gradient Mastercycler (Eppendorf, Hamburg, Germany) with conditions described in Tillmann et al. (2017c) and Tillmann et al. (2020):

For SSU amplifications, the following settings were used: initialisation at 94 $^{\circ}\text{C}$ for 5 min; 30 cycles of 94 $^{\circ}\text{C}$ for 2 min, 55 $^{\circ}\text{C}$ for 2 min, 68 $^{\circ}\text{C}$ for 3 min; a final extension at 68 $^{\circ}\text{C}$ for 10 min. PCR reaction conditions for ITS amplification: 4 min at 94 $^{\circ}\text{C}$, followed by 10 cycles of 50 sec at 94 $^{\circ}\text{C}$, 40 sec at 58 $^{\circ}\text{C}$, 1 min at 70 $^{\circ}\text{C}$, and then 30 cycles of 45 sec at 94 $^{\circ}\text{C}$, 45 sec at 50 $^{\circ}\text{C}$, 1 min at 70 $^{\circ}\text{C}$, and a final extension of 5 min at 70 $^{\circ}\text{C}$. For LSU amplification as follows: 2 min at 94 $^{\circ}\text{C}$, followed by 30 cycles of 30 sec at 94 $^{\circ}\text{C}$, 30 sec at 55 $^{\circ}\text{C}$, 2 min at 65 $^{\circ}\text{C}$, and a final extension of 10 min at 65 $^{\circ}\text{C}$. To verify the expected amplicon length, the PCR products were checked on a 1% agarose gel (in TE buffer, 70 mV, 30 min). The PCR amplicons were subsequently purified with the NucleoSpin Gel and PCR Clean-up Kit (Macherey-Nagel) according to the manufacturer's instructions.

Sequencing reaction

The PCR products were sequenced in both directions on an ABI PRISM 3730XL (Applied Biosystems by ThermoFisher Scientific). The sequencing reaction contained 1 μL of purified PCR product, 1.5 μL Big Dye Buffer (Life Technologies), 0.3 μL Big Dye, 1 μL of PCR primer (forward or reverse) and 7.2 μL of MilliQ H_2O (Tillmann et al., 2017c). Conditions for the sequencing reaction were: 1 min at 96 $^{\circ}\text{C}$, followed by 25 cycles of 10 sec at 96 $^{\circ}\text{C}$, 5 sec at 50 $^{\circ}\text{C}$ and 4 min at 60 $^{\circ}\text{C}$. Sequencing products were purified using the Agencourt CleanSEQ-Dye Terminator Removal kit (Beckman Coulter, Brea, California, USA) and sequenced in both directions. Raw sequence data were processed within the CLC Genomics Workbench 12 (Qiagen, Hilden, Germany).

Suppl. Method I2. Preparation of modified K medium (Keller et al., 1987).

Modified K medium (Keller et al., 1987) used for amphidomatacean cell cultivation. Prepared in 0.2 μm filtered, sterile North Sea water (salinity: 32, pH adjusted to 8.0 – 8.2). Quantities of ingredients are given as mL per liter of final medium.

Quantity (mL L ⁻¹)	Compound	Stock solution (g L ⁻¹ dH ₂ O)
0.10	NaNO ₃	75.0
0.10	NaH ₂ PO ₄ x H ₂ O	5.0
0.01	H ₂ SeO ₃	0.0125
0.10	TRIS-Base (pH 7.2)	121.1
0.10	K Trace Metal Solution	Recipe below
2.00	f/2 Vitamin Solution	Recipe below
ca. 0.2 to get pH 8.0 - 8.2	1M HCl	-

Recipe for one liter of K Trace Metal Solution.

Quantity	Compound	Stock solution (g L ⁻¹ dH ₂ O)
41.60 g	Na ₂ EDTA x 2H ₂ O	-
3.15 g	FeCl ₃ x 6H ₂ O	-
1.0 mL	Na ₂ MoO ₄ x 2H ₂ O	6.3
1.0 mL	ZnSO ₄ x 7H ₂ O	22.0
1.0 mL	CoCl ₂ x 6H ₂ O	10.0
1.0 mL	MnCl ₂ x 4H ₂ O	180.0
0.5 mL	CuSO ₄ x 5H ₂ O	9.8

Recipe for one liter of f/2 Vitamin Solution (Guillard and Ryther, 1962; Guillard, 1975). Solution prepared in 0.2 μm filtered, sterile dH₂O.

Quantity	Compound	Stock solution (g L ⁻¹ dH ₂ O)
10.0 mL	Vitamin B12 (Cyanocobalamin)	0.1
10.0 mL	Biotin	0.1
200 mg	Thiamine HCl	-

Suppl. Method I3. General protocol for the chemical analysis of azaspiracids by LC-MS/MS (texts taken or adjusted from Publications VI and VII). Divergent protocols are mentioned in the respective publications, which are attached to this thesis.

AZA extraction

A volume of 500 μL acetone was added to the cell pellets and were subsequently vortexed every 10 min during one hour at room temperature for extraction. Homogenates were then centrifuged (Eppendorf 5810 R, Eppendorf, Hamburg, Germany) at 15 $^{\circ}\text{C}$ and 3,220 $\times g$ for 15 min. Filtrates were then adjusted with acetone to a final volume of 500 μL . The supernatant was transferred to a 0.45 μm pore-size spin-filter (Millipore Ultrafree, Millipore, Burlington, USA) and centrifuged (Eppendorf 5415 R) at 800 $\times g$ for 30 sec, with the resulting filtrate transferred into a liquid chromatography (LC) autosampler vial for LC-MS/MS analysis.

AZA measurements

Extracts of strains were screened for known AZAs in the selected reaction monitoring (SRM) mode with an analytical system consisting of triple quadrupole mass spectrometer (API 4000 QTrap, Sciex, Darmstadt, Germany) equipped with a TurboSpray interface coupled to LC equipment (model LC 1100, Agilent, Waldbronn, Germany) that included a solvent reservoir, inline degasser (G1379A), binary pump (G1311A), refrigerated autosampler (G1329A/G1330B), and temperature-controlled column oven (G1316A). Separation of AZAs (5 μL sample injection volume) was performed by reverse-phase chromatography on a C8 phase. The analytical column (50 \times 2 mm) was packed with 3 μm Hypersil BDS 120 \AA (Phenomenex, Aschaffenburg, Germany) and maintained at 20 $^{\circ}\text{C}$. The flow rate was 0.2 mL min^{-1} , and gradient elution was performed with two eluents, where eluent A was water and eluent B was acetonitrile/water (95:5 v/v), both containing 2.0 mM ammonium formate and 50 mM formic acid. Initial conditions were 8-min column equilibration with 30% B, followed by a linear gradient to 100% B in 8 min and isocratic elution until 18 min with 100% B then returning to initial conditions until 21 min (total run time: 29 min). AZA profiles were determined in the SRM mode in one period (0-18) min with curtain gas: 10 psi, CAD: medium, ion spray voltage: 5,500 V, temperature: ambient, nebuliser gas: 10 psi, auxiliary gas: off, interface heater: on, declustering potential: 100 V, entrance potential: 10 V, exit potential: 30 V. SRM experiments were carried out in positive ion mode by selecting the transitions shown in the following table:

Mass transitions m/z (Q1>Q3 mass) and their respective AZAs screened by LC-MS/MS within the course of this PhD project.

Mass transition	Toxin	Collision energy (CE) [V]
716>698	AZA-33	40
796>778	AZA-33 phosphate	40
816>798	AZA-34, AZA-39	40
816>348	AZA-39	70
828>658	AZA-3	70
828>810	AZA-3, AZA-43, AZA-58	40
830>812	AZA-38, AZA-52, AZA-53	40
830>348	AZA-38, AZA-52, AZA-53	70
842>672	AZA-1	70
842>824	AZA-1, AZA-40, AZA-50	40
842>348	AZA-40	70
844>826	AZA-4, AZA-5	40
846>828	AZA-37	40
846>348	AZA-37	70
854>836	AZA-41	40
854>670	AZA-41	70
854>360	AZA-41	70
856>672	AZA-2	70
856>838	AZA-2	40
858>840	AZA-7, AZA-8, AZA-9, AZA-10, AZA-36, AZA-51	40
858>348	AZA-36, AZA-51	70
860>842	AZA-59	40
868>362	AZA-55	70
870>852	Me-AZA-2, AZA-42, AZA-54	40
870>360	AZA-42	40
872>854	AZA-11, AZA-12	40
884>866	AZA-56	40
910>892	Undescribed	40
920>804	AZA-1 phosphate, AZA-40 phosphate	40
926>908	AZA-37 phosphate	40
936>918	AZA-2 phosphate	40
938>920	AZA-36 phosphate, AZA-51 phosphate	40
940>922	AZA-59 phosphate	40
952>938	AZA-11 phosphate	40

In addition, precursor ion experiments were performed. Precursors of the characteristic AZA fragments m/z 348, m/z 350, m/z 360, m/z 362 and m/z 378 were scanned in the positive-ion mode from m/z 500 to 1,000 under the following conditions: curtain gas, 10 psi; CAD, medium; ion spray voltage, 5,500 V; temperature, ambient; nebuliser gas, 10 psi; auxiliary gas, off; interface heater, on; declustering potential, 100 V; entrance potential, 10 V; collision energy, 70 V; exit potential, 12 V. Collision induced dissociation (CID) spectra of the m/z values 716, 830, 842, 856, 858 and 872 were recorded in the Enhanced Product Ion (EPI) mode in the mass range from m/z 150 to 930. Positive ionization and unit resolution mode were used. The following parameters were applied: curtain gas: 10 psi, CAD: medium, ion spray voltage: 5,500 V, temperature: ambient, nebulizer gas: 10 psi, auxiliary gas: off, interface heater: on, declustering potential: 100 V, collision energy spread: 0, 10 V, collision energy: 70 V, exit potential, 12 V.

Supplementary Tables

Suppl. Table S1. Proposed derivatives of AZAs with the respective mass of the protonated ion ($[M+H]^+$) and origin, slightly modified after Krock et al. (2019) from review by Zurhelle (2019). Compounds confirmed by NMR are highlighted in grey; compounds highlighted in white have structures inferred by mass spectrometry only; # for R2: proposed with modification of the side chain and/or at ring A (C-1 to C-10); # for R6: with modification at ring H or ring I.

AZA derivative	R1	R2	R3	R4	R5	R6	$[M+H]^+$	Origin
AZA-1	H	H	H	CH ₃	H	CH ₃	842.5	<i>Az. spinosum</i>
AZA-2	H	CH ₃	H	CH ₃	H	CH ₃	856.5	<i>Az. spinosum</i> , <i>Az. poporum</i> , <i>Am. languida</i>
AZA-11	OH	CH ₃	H	CH ₃	H	CH ₃	872.5	<i>Az. spinosum</i> , <i>Az. poporum</i>
AZA-33	-	-	H	CH ₃	H	CH ₃	716.5	<i>Az. spinosum</i>
AZA-34	-	-	H	CH ₃	H	CH ₃	816.5	<i>Az. spinosum</i>
AZA-35	H	#	H	CH ₃	H	CH ₃	830.5	<i>Az. spinosum</i> , <i>Az. dexteroporum</i>
AZA-36	OH	CH ₃	H	CH ₃	H	H	858.5	<i>Az. poporum</i>
AZA-37	OH	H	H	CH ₃	H	H	846.5	<i>Az. poporum</i>
AZA-38	H	CH ₃	H	CH ₃	H	H	830.5	<i>Am. languida</i>
AZA-39	H	#	H	CH ₃	H	H	816.5	<i>Am. languida</i>
AZA-40	CH ₃	H	H	CH ₃	H	H	842.5	<i>Az. poporum</i>
AZA-41	H	H	H	CH ₃	H	#	854.5	<i>Az. poporum</i>
AZA-42	No proposed structure						870.5	<i>Az. poporum</i>
AZA-43	No proposed structure						828.5	<i>Am. languida</i>
AZA-50	H	CH ₃	H	CH ₃	H	CH ₃	842.5	<i>Az. spinosum</i>
AZA-51	OH	CH ₃	H	CH ₃	H	CH ₃	858.5	<i>Az. spinosum</i>
AZA-52	No proposed structure						830.5	<i>Am. languida</i>
AZA-53	No proposed structure						830.5	<i>Am. languida</i>
AZA-54	H	#	H	CH ₃	H	CH ₃	870.5	<i>Az. dexteroporum</i>
AZA-55	H	#	H	CH ₃	H	#	868.5	<i>Az. dexteroporum</i>
AZA-56	H	#	H	CH ₃	H	CH ₃	884.5	<i>Az. dexteroporum</i>
AZA-57	H	#	H	CH ₃	H	CH ₃	844.5	<i>Az. dexteroporum</i>
AZA-58	H	#	H	CH ₃	H	CH ₃	828.5	<i>Az. dexteroporum</i>
AZA-59	H	OH	H	CH ₃	H	CH ₃	860.5	<i>Az. poporum</i>
AZA-62	No proposed structure						870.5	<i>Az. poporum</i>
3-epi-AZA-7	One additional O atom between C1 and C9 compared to AZA-1 (Rossi et al., 2017)						858.5	<i>Az. dexteroporum</i>

Suppl. Table S2. Monitoring of AZAs in shellfish by European countries.

Country	Responsible organizations	AZA monitored in shellfish	Monitoring frequency	Monitoring methods
Belgium	<ul style="list-style-type: none"> Vlaams Instituut voor de Zee (VLIZ), Ostende Sciensano, Ixelles Royal Belgian Institute of Natural Sciences, Brussels Flanders Environment Agency, Aalst Wageningen University, Wageningen 	Yes (AZA-1,-2,-3)	weekly	LC-MS/MS
Denmark	<ul style="list-style-type: none"> NIRAS, Kopenhagen 	Yes (AZA-1,-2,-3)	weekly to monthly	LC-MS/MS
France	<ul style="list-style-type: none"> Institut français de recherche pour l'exploitation de la mer (IFREMER), Issy-les-Moulineaux 	Yes (AZA-1,-2,-3)	monthly	LC-MS/MS
Germany	<ul style="list-style-type: none"> Landesamt für Landwirtschaft, Umwelt und ländliche Räume (LLUR), Flintbek Landesamt für Verbraucherschutz und Lebensmittelsicherheit (LAVES), Wardenburg 	Yes (AZA-1,-2,-3)	Frequently all year long (not defined)	LC-MS/MS
Great Britain	<ul style="list-style-type: none"> Scottish Association for Marine Science (SAMS), Oban Centre for Environment, Fisheries and Aquaculture Science (CEFAS), Lowestoft 	Yes (AZA-1,-2,-3)	weekly to monthly	LC-MS/MS
Ireland	<ul style="list-style-type: none"> Marine Institute (MI), Galway 	Yes (AZA-1,-2,-3)	weekly	LC-MS/MS
Netherlands	<ul style="list-style-type: none"> Wageningen Food Safety Research, Wageningen National Institute for Public Health and the Environment (RIVM), Bilthoven 	Yes (AZA-1,-2,-3)	weekly	LC-MS/MS
Norway	<ul style="list-style-type: none"> The Norwegian Food Safety Authority (NFSA), Oslo 	Yes (AZA-1,-2,-3)	weekly	LC-MS/MS
Spain	<ul style="list-style-type: none"> Instituto Tecnológico para el Control del Medio Marino de Galicia (INTECMAR), Vilagarcía de Arousa 17 autonomous communities who have the exclusive responsibility for the implementation of control systems 	Yes (AZA-1,-2,-3,-4,-5)	weekly	LC-MS/MS
Sweden	<ul style="list-style-type: none"> Swedish National Food Agency, Uppsala 	Yes (AZA-1,-2,-3)	weekly to monthly	LC-MS/MS

Suppl. Table S3. Specificity tests of the *Az. spinosum*, *Az. poporum* and *Am. languida* qPCR assays on normed DNA concentration (1 ng μL^{-1}) of strains by comparisons of mean C_T values (n=3). Extended from Wietkamp et al. (2019b) and Wietkamp et al. (2020). n.a. = not assigned; n.d. = not detected.

Species	Strain	Toxin profile	Ribotype	Result of the <i>Az. spinosum</i> assay	Result of the <i>Az. poporum</i> assay	Result of the <i>Am. languida</i> assay
<i>Am. parvula</i>	H1-E9	n.d.	n.a.	n.d.	n.d.	n.d.
<i>Az. caudatum</i>	9-E13	n.d.	n.a.	n.d.	n.d.	n.d.
	AC-1	n.d.	n.a.	n.d.	n.d.	n.d.
<i>Az. concinnum</i>	1-C6	n.d.	n.a.	n.d.	n.d.	n.d.
<i>Az. cuneatum</i>	35-A2	n.d.	n.a.	n.d.	n.d.	n.d.
	35-C4	n.d.	n.a.	n.d.	n.d.	n.d.
	3-D6	n.d.	n.a.	n.d.	n.d.	n.d.
	96-5-F5	n.d.	n.a.	n.d.	n.d.	n.d.
<i>Az. dalianense</i>	121-F6	n.d.	D	n.d.	n.d.	n.d.
	48-1-F8	n.d.	C	n.d.	n.d.	n.d.
	H-2-G7	n.d.	E	n.d.	n.d.	n.d.
	LF-14-F7	n.d.	E	n.d.	n.d.	n.d.
	N-12-04	n.d.	B	n.d.	n.d.	n.d.
	N-12-09	n.d.	B	n.d.	n.d.	n.d.
	N-38-02	n.d.	A	n.d.	n.d.	n.d.
N-38-03	n.d.	D	n.d.	n.d.	n.d.	
<i>Az. dexteroporum</i>	1-D12	n.d.	n.a.	n.d.	n.d.	n.d.
	AZA-2B1	n.d.	n.a.	n.d.	n.d.	n.d.
<i>Az. galwayense</i>	35-R7	n.d.	n.a.	n.d.	n.d.	n.d.
<i>Az. obesum</i>	2-E10	n.d.	n.a.	n.d.	n.d.	n.d.
	48-1-F2	n.d.	n.a.	n.d.	n.d.	n.d.
	AZA-2D	n.d.	n.a.	n.d.	n.d.	n.d.
	AZA-Z-E11	n.d.	n.a.	n.d.	n.d.	n.d.
	LF-12-A12	n.d.	n.a.	n.d.	n.d.	n.d.
	LF-44-C3	n.d.	n.a.	n.d.	n.d.	n.d.
	N-41-01	n.d.	n.a.	n.d.	n.d.	n.d.
<i>Az. perforatum</i>	AZA-2C	n.d.	n.a.	n.d.	n.d.	n.d.
	AZA-2E	n.d.	n.a.	n.d.	n.d.	n.d.
	AZA-2H	n.d.	n.a.	n.d.	n.d.	n.d.
<i>Az. perfusorium</i>	2-D1	n.d.	n.a.	n.d.	n.d.	n.d.
	5-B8	n.d.	n.a.	n.d.	n.d.	n.d.
	6-B4	n.d.	n.a.	n.d.	n.d.	n.d.
<i>Az. polongum</i>	N-47-01	n.d.	n.a.	n.d.	n.d.	n.d.
	Shet-B2	n.d.	n.a.	n.d.	n.d.	n.d.
<i>Az. trinitatum</i>	A2-D11	n.d.	n.a.	n.d.	n.d.	n.d.
	AZA-2F	n.d.	n.a.	n.d.	n.d.	n.d.
	AZA-ZE10	n.d.	n.a.	n.d.	n.d.	n.d.
	N-39-04	n.d.	n.a.	n.d.	n.d.	n.d.
<i>Az. zhuanum</i>	TIO213	n.d.	n.a.	n.d.	n.d.	n.d.
<i>Az. pseudozhuanum</i>	32-R1	n.d.	n.a.	n.d.	n.d.	n.d.

<i>Am. languida</i>	2-A11	AZA-38, -39	n.a.	n.d.	n.d.	20.5
	5-F11	AZA-38, -39	n.a.	n.d.	n.d.	20.7
	8-D10	AZA-38, -39	n.a.	n.d.	n.d.	20.4
	AND-A0920	AZA-2, -43	n.a.	n.d.	n.d.	20.4
	LF-14-E7	AZA-38, -39	n.a.	n.d.	n.d.	20.3
	LF-14-F2	AZA-38, -39	n.a.	n.d.	n.d.	20.5
	LF-14-G7	AZA-38, -39	n.a.	n.d.	n.d.	20.7
	LF-9-C4	AZA-38, -39	n.a.	n.d.	n.d.	20.5
	LF-9-C9	AZA-38, -39	n.a.	n.d.	n.d.	20.4
	N-01-01	AZA-38, -39	n.a.	n.d.	n.d.	20.5
	N-01-02	AZA-38, -39	n.a.	n.d.	n.d.	20.3
	N-12-01	AZA-38, -39	n.a.	n.d.	n.d.	20.3
	N-39-12	AZA-38, -39	n.a.	n.d.	n.d.	20.4
	N-40-03	AZA-39, -52	n.a.	n.d.	n.d.	20.3
	N-40-06	AZA-39, -53	n.a.	n.d.	n.d.	20.5
<i>Az. poporum</i>	AZ-BH-03	AZA-40, -41	B	n.d.	C _T = 18.9	n.d.
	18-A1	AZA-2	C	n.d.	n.d.	n.d.
	1-D5	AZA-11	A	n.d.	C _T = 19.9	n.d.
	LF-14-E12	n.d.	A	n.d.	C _T = 19.4	n.d.
	N-39-03	AZA-37	A	n.d.	C _T = 19.5	n.d.
	N-39-13	AZA-37	A	n.d.	C _T = 19.6	n.d.
	UTH-C5	AZA-37	A	n.d.	C _T = 18.8	n.d.
	UTH-C8	AZA-37	A	n.d.	C _T = 19.9	n.d.
UTH-D4	AZA-37	A	n.d.	C _T = 19.3	n.d.	
<i>Az. spinosum</i>	3D9	AZA-1, -2, -33	A	C _T = 19.3	n.d.	n.d.
	4-F8	AZA-1	A	C _T = 18.4	n.d.	n.d.
	5-C11	AZA-1, -2, -33	A	C _T = 18.4	n.d.	n.d.
	6-G8	AZA-1, -2	A	C _T = 19.4	n.d.	n.d.
	N-04-01	AZA-1, -2, -33	A	C _T = 19.4	n.d.	n.d.
	Shet-F6	AZA-1, -2, -33	A	C _T = 19.2	n.d.	n.d.
	SM2	AZA-1, -2, -33	A	C _T = 19.8	n.d.	n.d.
	UTH-E2	AZA-1, -2, -33	A	C _T = 19.1	n.d.	n.d.
	5-F3	AZA-11, -51	B	C _T = 25.6	n.d.	n.d.
	8-B8	AZA-11, -51	B	C _T = 25.4	n.d.	n.d.
	H-1-D11	AZA-2	B	C _T = 26.1	n.d.	n.d.
	N-04-04	AZA-11, -51	B	C _T = 25.7	n.d.	n.d.
	N-05-01	AZA-11, -51	B	C _T = 26.8	n.d.	n.d.
	N-16-02	AZA-11, -51	B	C _T = 25.2	n.d.	n.d.
	H-4-A10	n.d.	C	n.d.	n.d.	n.d.
	H-4-A1	n.d.	C	n.d.	n.d.	n.d.
	H-4-C10	n.d.	C	n.d.	n.d.	n.d.
	<i>Az. cf. spinosum</i>	1-H10	n.d.	n.a.	n.d.	n.d.
2-A3		n.d.	n.a.	n.d.	n.d.	n.d.
5-B9		n.d.	n.a.	n.d.	n.d.	n.d.
5-D3		n.d.	n.a.	n.d.	n.d.	n.d.
6-A1		n.d.	n.a.	n.d.	n.d.	n.d.

Suppl. Table S4. Mean DNA and rDNA copy cell quota for several strains (representing different ribotypes) of the three toxigenic amphidomatacean species *Az. spinosum*, *Az. poporum* and *Am. languida*, including the new non-toxicogenic *Az. cf. spinosum*. n.a. = not assigned.

Species	Strain	Ribotype	Origin	mean		mean	
				DNA cell ⁻¹ (pg) ± 1SD	n	copies cell ⁻¹ ± 1SD	n
<i>Az. cf. spinosum</i>	1-H10	n.a.	Ireland	0.62 ± 0.29	6	n.a.	n.a.
<i>Az. cf. spinosum</i>	5-B9	n.a.	Ireland	0.92 ± 0.29	6	n.a.	n.a.
<i>Az. spinosum</i>	3D9	A	Scotland	2.89 ± 0.62	20	1,276 ± 184	6
<i>Az. spinosum</i>	7-F4	A	North Sea	2.49 ± 0.15	6	n.a.	n.a.
<i>Az. spinosum</i>	N-04-01	A	Norway	3.63 ± 0.36	6	n.a.	n.a.
<i>Az. spinosum</i>	UTH-E2	A	Denmark	2.56 ± 0.11	8	1,212 ± 185	6
<i>Az. spinosum</i>	5-F3	B	North Sea	4.03 ± 0.20	6	n.a.	n.a.
<i>Az. spinosum</i>	5-F6	B	North Sea	7.74 ± 0.38	6	n.a.	n.a.
<i>Az. spinosum</i>	7-E4	B	North Sea	7.59 ± 0.98	6	n.a.	n.a.
<i>Az. spinosum</i>	H-1-D11	B	Argentina	1.43 ± 0.73	6	n.a.	n.a.
<i>Az. spinosum</i>	N-04-04	B	Norway	3.68 ± 0.32	6	1,057 ± 89	6
<i>Az. spinosum</i>	N-16-02	B	Norway	1.52 ± 0.12	6	1,151 ± 188	6
<i>Az. spinosum</i>	N-39-02	B	Norway	3.95 ± 0.19	6	n.a.	n.a.
<i>Az. spinosum</i>	H-1-D4	C	Argentina	5.72 ± 0.63	6	n.a.	n.a.
<i>Az. spinosum</i>	H-4-C10	C	Argentina	4.31 ± 0.14	6	n.a.	n.a.
<i>Az. poporum</i>	1-D5	A	Chile	4.09 ± 0.27	6	1,196 ± 136	6
<i>Az. poporum</i>	2-B9	A	Chile	3.26 ± 0.27	6	1,212 ± 202	6
<i>Az. poporum</i>	N-39-01	A	Norway	1.82 ± 0.35	4	n.a.	n.a.
<i>Az. poporum</i>	N-39-01	A	Norway	2.05 ± 0.44	6	874 ± 107	6
<i>Az. poporum</i>	N-39-03	A	Norway	2.85 ± 0.24	6	n.a.	n.a.
<i>Az. poporum</i>	N-39-13	A	Norway	3.21 ± 0.15	6	n.a.	n.a.
<i>Az. poporum</i>	UTH-D4	A	Denmark	3.02 ± 0.46	18	888 ± 130	6
<i>Az. poporum</i>	LF-14-E12	A	Denmark	0.64 ± 0.23	6	n.a.	n.a.
<i>Az. poporum</i>	AZ-BH-03	B	China	3.02 ± 0.19	6	n.a.	n.a.
<i>Am. languida</i>	2A11	n.a.	Irminger Sea	2.73 ± 0.18	6	719 ± 48	6
<i>Am. languida</i>	8-D10	n.a.	North Sea	3.04 ± 0.14	6	n.a.	n.a.
<i>Am. languida</i>	AND-A0920	n.a.	Spain	2.95 ± 0.15	6	777 ± 38	6
<i>Am. languida</i>	N-12-01	n.a.	Norway	3.15 ± 0.35	6	830 ± 93	6
<i>Am. languida</i>	LF-9-C9	n.a.	Denmark	3.15 ± 0.41	6	829 ± 107	6

Suppl. Table S5. Mean DNA cell quotas (pg cell⁻¹) for various non-toxigenic amphidomataceans.

Species	Strain	Origin	mean DNA cell ⁻¹ (pg)	SD	n
<i>Amphidoma parvula</i>	H1-E9	Argentina	3.81	0.61	5
<i>Azadinium caudatum</i>	AC-1	Scotland	19.03	4.07	4
<i>Azadinium caudatum</i>	9-E13	Ireland	16.81	1.10	5
<i>Azadinium concinnum</i>	1-C6	Irminger Sea	0.52	0.02	6
<i>Azadinium cuneatum</i>	3-D6	Irminger Sea	1.55	0.03	6
<i>Azadinium dalianense</i>	121-F6	Seattle	2.47	0.17	6
<i>Azadinium dalianense</i>	48-1-F8	Seattle	2.79	0.23	6
<i>Azadinium dalianense</i>	N-12-04	Norway	3.75	0.07	6
<i>Azadinium galwayense</i>	35-R6	Ireland	1.29	0.15	6
<i>Azadinium galwayense</i>	35-R7	Ireland	1.43	0.30	6
<i>Azadinium obesum</i>	2-E10	Scotland	4.21	0.41	6
<i>Azadinium obesum</i>	48-1-F2	Seattle	5.90	0.37	5
<i>Azadinium obesum</i>	N-41-01	Norway	5.03	0.12	6
<i>Azadinium obesum</i>	LF-12-A12	Denmark	6.58	0.61	6
<i>Azadinium perforatum</i>	AZA-2H	Labrador Sea	5.33	0.14	5
<i>Azadinium polongum</i>	Shet-B2	Shetland Islands	1.42	0.08	6
<i>Azadinium trinitatum</i>	A2-D11	Irminger Sea	3.58	0.15	6
<i>Azadinium perfusorium</i>	5-B8	North Sea	2.56	0.22	6
<i>Azadinium pseudozhuanum</i>	32-R1	Ireland	4.55	0.42	5

Suppl. Table S6. Field samples of several expeditions with species counts (cells L⁻¹) of *Az. spinosum*, *Az. poporum* and *Am. languida* based on qPCR analysis (Cell number calculation based on mean C_T value of three technical replicates). n.d. = not detected. LOD = 1 to 3 cells L⁻¹.

Expedition*	Sampling Date	Latitude [°N]	Longitude [°E]	<i>Az. spinosum</i> [cells L ⁻¹]	<i>Az. poporum</i> [cells L ⁻¹]	<i>Am. languida</i> [cells L ⁻¹]	Sum [cells L ⁻¹]	Reference
HE-516	18.07.2018	53.765	6.239	n.d.	n.d.	n.d.	n.d.	Wietkamp et al. 2020
HE-516	18.07.2018	53.119	4.332	n.d.	n.d.	n.d.	n.d.	Wietkamp et al. 2020
HE-516	19.07.2018	52.668	2.246	n.d.	n.d.	n.d.	n.d.	Wietkamp et al. 2020
HE-516	19.07.2018	51.509	2.680	n.d.	n.d.	n.d.	n.d.	Wietkamp et al. 2020
HE-516	20.07.2018	50.807	0.955	n.d.	19	n.d.	19	Wietkamp et al. 2020
HE-516	20.07.2018	50.239	-0.948	n.d.	n.d.	n.d.	n.d.	Wietkamp et al. 2020
HE-516	21.07.2018	49.772	-2.833	n.d.	57	n.d.	57	Wietkamp et al. 2020
HE-516	21.07.2018	48.913	-4.899	n.d.	1	312	313	Wietkamp et al. 2020
HE-516	22.07.2018	50.047	-5.967	509	n.d.	314	823	Wietkamp et al. 2020
HE-516	22.07.2018	50.341	-6.069	1,860	1	82	1,943	Wietkamp et al. 2020
HE-516	22.07.2018	50.636	-6.172	692	n.d.	931	1,623	Wietkamp et al. 2020
HE-516	22.07.2018	50.926	-6.266	2,375	n.d.	n.d.	2,375	Wietkamp et al. 2020
HE-516	23.07.2018	51.220	-6.364	785	24	700	1,509	Wietkamp et al. 2020
HE-516	23.07.2018	51.515	-6.480	59	7	3	69	Wietkamp et al. 2020
HE-516	23.07.2018	51.804	-6.582	151	34	10	195	Wietkamp et al. 2020
HE-516	24.07.2018	52.099	-6.709	n.d.	2	4	6	Wietkamp et al. 2020
HE-516	24.07.2018	51.908	-7.452	88	29	n.d.	117	Wietkamp et al. 2020
HE-516	24.07.2018	51.708	-8.233	n.d.	n.d.	15	15	Wietkamp et al. 2020
HE-516	25.07.2018	50.520	-9.070	n.d.	n.d.	7	7	Wietkamp et al. 2020
HE-516	25.07.2018	50.683	-9.071	n.d.	n.d.	7	7	Wietkamp et al. 2020
HE-516	25.07.2018	50.850	-9.066	1,119	7	956	2,082	Wietkamp et al. 2020
HE-516	26.07.2018	51.021	-9.068	1,354	n.d.	10	1,364	Wietkamp et al. 2020
HE-516	26.07.2018	51.185	-9.069	7	5	18	30	Wietkamp et al. 2020
HE-516	26.07.2018	51.349	-9.060	n.d.	n.d.	1	1	Wietkamp et al. 2020
HE-516	27.07.2018	51.517	-9.071	668	n.d.	188	856	Wietkamp et al. 2020
HE-516	27.07.2018	51.388	-9.318	n.d.	n.d.	1,489	1,489	Wietkamp et al. 2020
HE-516	27.07.2018	51.381	-9.696	178	14	7	199	Wietkamp et al. 2020
HE-516	28.07.2018	51.132	-11.150	n.d.	1	4	5	Wietkamp et al. 2020
HE-516	28.07.2018	51.235	-10.884	n.d.	n.d.	5	5	Wietkamp et al. 2020
HE-516	28.07.2018	51.334	-10.574	2,953	n.d.	n.d.	2,953	Wietkamp et al. 2020
HE-516	29.07.2018	51.639	-9.715	34,273	n.d.	58	34,331	Wietkamp et al. 2020
HE-516	29.07.2018	51.542	-10.010	3,889	4	409	4,302	Wietkamp et al. 2020
HE-516	29.07.2018	51.437	-10.288	1,660	n.d.	123	1,783	Wietkamp et al. 2020
HE-516	30.07.2018	51.737	-10.519	13,710	1	291	14,002	Wietkamp et al. 2020
HE-516	30.07.2018	52.029	-10.777	6,061	n.d.	1,486	7,547	Wietkamp et al. 2020
HE-516	30.07.2018	52.289	-10.410	10,904	n.d.	33	10,937	Wietkamp et al. 2020
HE-516	02.08.2018	53.080	-9.414	7,815	n.d.	1	7,816	Wietkamp et al. 2020
HE-516	02.08.2018	52.793	-9.688	3,818	n.d.	n.d.	3,818	Wietkamp et al. 2020
HE-516	02.08.2018	52.541	-10.049	9,491	n.d.	n.d.	9,491	Wietkamp et al. 2020
HE-516	03.08.2018	53.777	-11.556	n.d.	n.d.	n.d.	n.d.	Wietkamp et al. 2020
HE-516	03.08.2018	53.746	-11.221	n.d.	n.d.	3	3	Wietkamp et al. 2020
HE-516	03.08.2018	53.715	-10.891	3,630	n.d.	106	3,736	Wietkamp et al. 2020
HE-516	04.08.2018	53.684	-10.561	6,907	n.d.	53	6,960	Wietkamp et al. 2020
HE-516	04.08.2018	53.656	-10.224	5,689	n.d.	n.d.	5,689	Wietkamp et al. 2020
HE-516	04.08.2018	53.629	-9.906	83,059	n.d.	n.d.	83,059	Wietkamp et al. 2020
HE-516	05.08.2018	53.935	-10.342	5,612	n.d.	n.d.	5,612	Wietkamp et al. 2020
HE-516	05.08.2018	54.336	-10.114	26,301	n.d.	n.d.	26,301	Wietkamp et al. 2020
HE-516	05.08.2018	54.357	-9.397	4,063	n.d.	57	4,120	Wietkamp et al. 2020
HE-516	06.08.2018	55.405	-10.773	n.d.	n.d.	n.d.	n.d.	Wietkamp et al. 2020
HE-516	06.08.2018	55.214	-10.288	n.d.	n.d.	n.d.	n.d.	Wietkamp et al. 2020
HE-516	06.08.2018	55.028	-9.811	n.d.	n.d.	n.d.	n.d.	Wietkamp et al. 2020

HE-516	07.08.2018	54.557	-8.300	n.d.	n.d.	n.d.	n.d.	Wietkamp et al. 2020
HE-516	07.08.2018	54.645	-8.874	16,429	n.d.	3	16,432	Wietkamp et al. 2020
HE-516	07.08.2018	54.839	-9.324	10,245	n.d.	2	10,247	Wietkamp et al. 2020
HE-516	08.08.2018	56.107	-8.594	4	n.d.	n.d.	4	Wietkamp et al. 2020
HE-516	08.08.2018	56.510	-8.399	n.d.	n.d.	14	14	Wietkamp et al. 2020
HE-516	08.08.2018	56.916	-8.245	n.d.	n.d.	n.d.	n.d.	Wietkamp et al. 2020
HE-516	09.08.2018	57.751	-8.201	n.d.	n.d.	n.d.	n.d.	Wietkamp et al. 2020
HE-516	09.08.2018	58.141	-7.948	n.d.	n.d.	1	1	Wietkamp et al. 2020
HE-516	09.08.2018	58.475	-7.470	n.d.	n.d.	n.d.	n.d.	Wietkamp et al. 2020
HE-516	10.08.2018	58.737	-4.336	n.d.	n.d.	n.d.	n.d.	Wietkamp et al. 2020
HE-516	10.08.2018	58.729	-3.394	n.d.	n.d.	n.d.	n.d.	Wietkamp et al. 2020
HE-516	10.08.2018	58.495	-2.529	n.d.	n.d.	6	6	Wietkamp et al. 2020
HE-516	11.08.2018	57.992	-1.275	n.d.	1	n.d.	1	Wietkamp et al. 2020
HE-516	11.08.2018	57.690	-0.530	n.d.	1	n.d.	1	Wietkamp et al. 2020
HE-516	11.08.2018	57.384	0.214	n.d.	n.d.	n.d.	n.d.	Wietkamp et al. 2020
HE-516	12.08.2018	56.890	1.436	5	n.d.	n.d.	5	Wietkamp et al. 2020
HE-516	12.08.2018	56.590	2.167	19	n.d.	276	295	Wietkamp et al. 2020
HE-516	12.08.2018	56.288	2.880	102	5	n.d.	107	Wietkamp et al. 2020
HE-516	13.08.2018	55.739	4.009	1,074	n.d.	n.d.	1,074	Wietkamp et al. 2020
HE-516	13.08.2018	55.360	4.651	6,198	n.d.	122,810	129,008	Wietkamp et al. 2020
HE-516	13.08.2018	55.176	5.470	n.d.	n.d.	802	802	Wietkamp et al. 2020
HE-516	14.08.2018	54.673	6.621	n.d.	n.d.	656	656	Wietkamp et al. 2020
HE-516	14.08.2018	54.369	7.311	n.d.	n.d.	5,592	5,592	Wietkamp et al. 2020
HE-516	14.08.2018	54.069	7.990	n.d.	n.d.	69	69	Wietkamp et al. 2020
HE-517	19.08.2018	54.145	7.861	n.d.	n.d.	n.d.	n.d.	This study
HE-517	22.08.2018	59.030	-7.460	n.d.	n.d.	n.d.	n.d.	This study
HE-517	22.08.2018	59.113	-7.601	n.d.	n.d.	2	2	This study
HE-517	23.08.2018	59.892	-4.355	n.d.	n.d.	n.d.	n.d.	This study
HE-517	23.08.2018	59.960	-4.804	n.d.	n.d.	n.d.	n.d.	This study
HE-517	23.08.2018	59.998	-5.098	n.d.	n.d.	1	1	This study
HE-517	23.08.2018	60.091	-5.808	n.d.	n.d.	n.d.	n.d.	This study
HE-517	24.08.2018	60.080	-2.693	n.d.	n.d.	1	1	This study
HE-517	24.08.2018	60.342	-3.115	n.d.	n.d.	n.d.	n.d.	This study
HE-517	24.08.2018	60.607	-3.543	n.d.	n.d.	n.d.	n.d.	This study
HE-517	24.08.2018	60.821	-3.889	n.d.	n.d.	n.d.	n.d.	This study
HE-517	25.08.2018	61.054	-0.665	n.d.	n.d.	n.d.	n.d.	This study
HE-517	25.08.2018	61.191	-1.062	n.d.	n.d.	42	42	This study
HE-517	25.08.2018	61.393	-2.253	n.d.	n.d.	17	17	This study
HE-517	26.08.2018	61.675	0.001	n.d.	n.d.	14	14	This study
HE-517	26.08.2018	62.405	-0.058	n.d.	n.d.	1	1	This study
HE-517	27.08.2018	60.321	0.000	48	2	26	75	This study
HE-517	27.08.2018	60.684	0.007	n.d.	n.d.	12	12	This study
HE-517	27.08.2018	61.072	0.001	n.d.	n.d.	10	10	This study
HE-517	29.08.2018	59.809	0.155	n.d.	2	19	21	This study
HE-517	30.08.2018	58.578	0.147	86	n.d.	n.d.	86	This study
HE-517	31.08.2018	58.955	2.611	851	n.d.	1	852	This study
HE-517	31.08.2018	59.084	3.210	1	n.d.	n.d.	1	This study
HE-534	17.06.2019	53.913	6.269	n.d.	n.d.	n.d.	n.d.	This study
HE-534	17.06.2019	54.933	6.103	n.d.	n.d.	n.d.	n.d.	This study
HE-534	18.06.2019	54.899	7.322	n.d.	n.d.	2	2	This study
HE-534	19.06.2019	54.300	7.530	n.d.	n.d.	1	1	This study
HE-534	20.06.2019	54.317	7.844	n.d.	n.d.	2	2	This study
HE-534	20.06.2019	54.536	7.074	1	n.d.	7	8	This study
HE-534	21.06.2019	54.166	7.722	n.d.	n.d.	1	1	This study
HE-534	21.06.2019	54.226	7.757	n.d.	n.d.	3	3	This study
HE-534	22.06.2019	54.320	7.836	n.d.	n.d.	7	7	This study
HE-534	23.06.2019	54.164	7.728	n.d.	n.d.	12	12	This study
HE-534	24.06.2019	54.718	7.738	n.d.	n.d.	9	9	This study

HE-534	25.06.2019	53.957	8.116	n.d.	n.d.	3	3	This study
HE-534	26.06.2019	54.869	7.145	n.d.	n.d.	5	5	This study
HE-541	20.09.2019	54.446	7.419	n.d.	n.d.	11	11	This study
HE-541	22.09.2019	54.438	7.920	n.d.	n.d.	n.d.	n.d.	This study
HE-541	24.09.2019	53.985	6.651	n.d.	n.d.	134	134	This study
HE-541	26.09.2019	54.009	6.870	n.d.	n.d.	13	13	This study
PS-92	20.05.2015	58.080	4.532	n.d.	n.d.	n.d.	n.d.	This study
PS-92	21.05.2015	60.359	3.299	n.d.	n.d.	1,692	1,692	This study
PS-92	21.05.2015	62.383	3.583	n.d.	n.d.	98	98	This study
PS-92	22.05.2015	64.520	3.550	n.d.	n.d.	2,225	2,225	This study
PS-92	22.05.2015	64.940	3.589	n.d.	n.d.	114	114	This study
PS-92	22.05.2015	65.903	3.643	n.d.	n.d.	n.d.	n.d.	This study
PS-92	22.05.2015	66.358	3.727	n.d.	n.d.	n.d.	n.d.	This study
PS-92	22.05.2015	67.300	4.283	n.d.	n.d.	1,195	1,195	This study
PS-92	23.05.2015	67.733	4.400	n.d.	n.d.	n.d.	n.d.	This study
PS-92	23.05.2015	67.899	3.886	n.d.	n.d.	n.d.	n.d.	This study
PS-92	23.05.2015	68.331	3.916	n.d.	n.d.	n.d.	n.d.	This study
PS-92	23.05.2015	68.685	3.971	n.d.	n.d.	326	326	This study
PS-92	23.05.2015	69.289	4.013	n.d.	n.d.	n.d.	n.d.	This study
PS-92	23.05.2015	69.496	4.016	n.d.	n.d.	755	755	This study
PS-92	24.05.2015	70.000	10.000	n.d.	n.d.	117	117	This study
PS-92	24.05.2015	70.227	13.149	n.d.	n.d.	n.d.	n.d.	This study
PS-92	25.05.2015	73.250	12.250	n.d.	n.d.	n.d.	n.d.	This study
PS-92	25.05.2015	74.130	11.692	n.d.	n.d.	37	37	This study
PS-92	25.05.2015	74.843	11.208	n.d.	n.d.	68	68	This study
PS-92	26.05.2015	75.518	10.729	n.d.	n.d.	223	223	This study
PS-92	26.05.2015	77.167	9.867	n.d.	n.d.	433	433	This study
PS-92	26.05.2015	77.280	9.351	n.d.	n.d.	589	589	This study
PS-92	27.05.2015	80.871	18.448	n.d.	n.d.	n.d.	n.d.	This study
PS-92	27.05.2015	81.000	19.844	n.d.	n.d.	n.d.	n.d.	This study
PS-92	28.05.2015	81.183	19.100	n.d.	n.d.	n.d.	n.d.	This study
PS-92	28.05.2015	81.183	19.100	n.d.	n.d.	n.d.	n.d.	This study
PS-92	29.05.2015	81.230	18.550	n.d.	n.d.	n.d.	n.d.	This study
PS-92	29.05.2015	81.232	18.759	n.d.	n.d.	n.d.	n.d.	This study
PS-92	29.05.2015	81.232	18.759	n.d.	n.d.	n.d.	n.d.	This study
PS-92	30.05.2015	81.072	18.926	n.d.	n.d.	n.d.	n.d.	This study
PS-92	30.05.2015	81.232	18.926	n.d.	n.d.	n.d.	n.d.	This study
PS-92	31.05.2015	81.383	17.117	n.d.	n.d.	n.d.	n.d.	This study
PS-92	01.06.2015	81.317	17.300	n.d.	n.d.	n.d.	n.d.	This study
PS-92	02.06.2015	81.750	19.167	n.d.	n.d.	n.d.	n.d.	This study
PS-92	03.06.2015	81.550	19.517	n.d.	n.d.	n.d.	n.d.	This study
PS-92	04.06.2015	81.517	18.367	n.d.	n.d.	n.d.	n.d.	This study
PS-92	07.06.2015	81.217	19.417	n.d.	n.d.	n.d.	n.d.	This study
PS-92	11.06.2015	81.900	13.400	n.d.	n.d.	n.d.	n.d.	This study
PS-92	11.06.2015	81.900	13.400	n.d.	n.d.	n.d.	n.d.	This study
PS-92	15.06.2015	82.200	7.383	n.d.	n.d.	n.d.	n.d.	This study
UTH-16	13.06.2016	54.135	7.953	n.d.	9	1	10	Wietkamp et al., 2019
UTH-16	14.06.2016	54.277	7.827	n.d.	18	15	33	Wietkamp et al., 2019
UTH-16	14.06.2016	54.540	7.562	n.d.	4	1	5	Wietkamp et al., 2019
UTH-16	14.06.2016	54.732	7.537	n.d.	n.d.	n.d.	n.d.	Wietkamp et al., 2019
UTH-16	14.06.2016	55.011	7.595	n.d.	9	1	10	Wietkamp et al., 2019
UTH-16	15.06.2016	55.272	7.586	n.d.	21	27	48	Wietkamp et al., 2019
UTH-16	15.06.2016	55.535	7.480	n.d.	72	102	174	Wietkamp et al., 2019
UTH-16	15.06.2016	55.780	7.288	n.d.	9	24	33	Wietkamp et al., 2019
UTH-16	15.06.2016	56.127	7.470	1	9	1,023	1,033	Wietkamp et al., 2019
UTH-16	15.06.2016	56.633	6.715	31	n.d.	n.d.	31	Wietkamp et al., 2019
UTH-16	16.06.2016	56.562	8.522	n.d.	n.d.	107	107	Wietkamp et al., 2019
UTH-16	16.06.2016	56.625	8.350	n.d.	20	3,023	3,043	Wietkamp et al., 2019

UTH-16	16.06.2016	56.633	7.115	4	10	433	447	Wietkamp et al., 2019
UTH-16	16.06.2016	56.693	7.686	8	75	2,528	2,611	Wietkamp et al., 2019
UTH-16	16.06.2016	56.712	8.161	n.d.	13	1,227	1,240	Wietkamp et al., 2019
UTH-16	17.06.2016	56.630	8.670	n.d.	n.d.	n.d.	n.d.	Wietkamp et al., 2019
UTH-16	18.06.2016	56.621	9.301	n.d.	n.d.	n.d.	n.d.	Wietkamp et al., 2019
UTH-16	18.06.2016	56.633	9.104	n.d.	n.d.	n.d.	n.d.	Wietkamp et al., 2019
UTH-16	18.06.2016	56.675	9.143	n.d.	n.d.	n.d.	n.d.	Wietkamp et al., 2019
UTH-16	19.06.2016	56.681	8.761	n.d.	n.d.	n.d.	n.d.	Wietkamp et al., 2019
UTH-16	19.06.2016	56.770	8.861	n.d.	n.d.	n.d.	n.d.	Wietkamp et al., 2019
UTH-16	19.06.2016	56.957	9.112	n.d.	n.d.	n.d.	n.d.	Wietkamp et al., 2019
UTH-16	20.06.2016	56.793	8.528	n.d.	n.d.	n.d.	n.d.	Wietkamp et al., 2019
UTH-16	20.06.2016	56.928	8.738	n.d.	n.d.	n.d.	n.d.	Wietkamp et al., 2019
UTH-16	20.06.2016	56.982	8.980	n.d.	n.d.	n.d.	n.d.	Wietkamp et al., 2019
UTH-16	21.06.2016	56.745	9.211	n.d.	n.d.	n.d.	n.d.	Wietkamp et al., 2019
UTH-16	21.06.2016	56.809	9.053	n.d.	n.d.	n.d.	n.d.	Wietkamp et al., 2019
UTH-16	21.06.2016	56.888	9.138	n.d.	n.d.	n.d.	n.d.	Wietkamp et al., 2019
UTH-16	24.06.2016	56.960	10.546	n.d.	n.d.	n.d.	n.d.	Wietkamp et al., 2019
UTH-16	25.06.2016	57.227	10.693	n.d.	n.d.	3	3	Wietkamp et al., 2019
UTH-16	25.06.2016	57.463	11.277	n.d.	3	387	390	Wietkamp et al., 2019
UTH-16	25.06.2016	57.490	10.779	n.d.	n.d.	298	298	Wietkamp et al., 2019
UTH-16	25.06.2016	57.676	10.828	n.d.	n.d.	n.d.	n.d.	Wietkamp et al., 2019
UTH-16	26.06.2016	56.185	11.359	n.d.	n.d.	n.d.	n.d.	Wietkamp et al., 2019
UTH-16	26.06.2016	56.443	11.169	n.d.	n.d.	1	1	Wietkamp et al., 2019
UTH-16	26.06.2016	56.704	11.266	n.d.	n.d.	n.d.	n.d.	Wietkamp et al., 2019
UTH-16	26.06.2016	56.966	11.367	n.d.	n.d.	n.d.	n.d.	Wietkamp et al., 2019
UTH-16	27.06.2016	55.216	11.003	n.d.	n.d.	n.d.	n.d.	Wietkamp et al., 2019
UTH-16	27.06.2016	55.465	10.876	n.d.	n.d.	n.d.	n.d.	Wietkamp et al., 2019
UTH-16	27.06.2016	55.691	10.734	n.d.	n.d.	n.d.	n.d.	Wietkamp et al., 2019
UTH-16	27.06.2016	55.948	10.961	n.d.	n.d.	n.d.	n.d.	Wietkamp et al., 2019
UTH-16	28.06.2016	54.468	10.893	n.d.	n.d.	n.d.	n.d.	Wietkamp et al., 2019
UTH-16	28.06.2016	54.557	10.475	n.d.	n.d.	n.d.	n.d.	Wietkamp et al., 2019
UTH-16	28.06.2016	54.685	10.738	n.d.	n.d.	n.d.	n.d.	Wietkamp et al., 2019

* HE-516: July/August 2018, North Atlantic, Celtic Sea/Irish coastal waters/Scottish coastal waters/North Sea

HE-517: August 2018, North Atlantic, North Sea, northern part

HE-534: June 2019, North Atlantic, North Sea, German Bight

HE-541: September 2019, North Atlantic, German Bight

PS-92: May/June 2015, North Atlantic, Arctic

UTH-16: June 2016, North Atlantic, North Sea, German Bight/Kattegat/Belt

Suppl. Table S7. Species counts (cells L⁻¹) of *Az. spinosum*, *Az. poporum* and *Am. languida* based on qPCR analysis of samples from routine sampling at several locations (Cell number calculation based on mean C_T value of three technical replicates). n.d. = not detected. LOD = 1 to 3 cells L⁻¹.

Location	Year	Date	<i>Az. spinosum</i> [cells L ⁻¹]	<i>Az. poporum</i> [cells L ⁻¹]	<i>Am. languida</i> [cells L ⁻¹]
Scapa Flow, Scotland	2016	10-Apr	n.d.	n.d.	n.d.
Scapa Flow, Scotland	2016	16-Apr	n.d.	n.d.	n.d.
Scapa Flow, Scotland	2016	20-Apr	n.d.	n.d.	n.d.
Scapa Flow, Scotland	2016	23-Apr	n.d.	n.d.	n.d.
Scapa Flow, Scotland	2016	26-Apr	n.d.	n.d.	n.d.
Scapa Flow, Scotland	2016	29-Apr	n.d.	n.d.	n.d.
Scapa Flow, Scotland	2016	3-May	n.d.	n.d.	n.d.
Scapa Flow, Scotland	2016	6-May	n.d.	n.d.	n.d.
Scapa Flow, Scotland	2016	9-May	n.d.	n.d.	n.d.
Scapa Flow, Scotland	2016	12-May	n.d.	n.d.	n.d.
Scapa Flow, Scotland	2016	15-May	n.d.	n.d.	n.d.
Scapa Flow, Scotland	2016	18-May	n.d.	n.d.	n.d.
Scapa Flow, Scotland	2016	23-May	n.d.	n.d.	n.d.
Scapa Flow, Scotland	2016	26-May	n.d.	924	n.d.
Scapa Flow, Scotland	2016	29-May	n.d.	n.d.	n.d.
Scapa Flow, Scotland	2016	1-Jun	n.d.	n.d.	n.d.
Scapa Flow, Scotland	2016	5-Jun	n.d.	n.d.	n.d.
Scapa Flow, Scotland	2016	18-Jun	n.d.	n.d.	n.d.
Scapa Flow, Scotland	2016	21-Jun	n.d.	n.d.	n.d.
Scapa Flow, Scotland	2016	25-Jun	n.d.	2,920	n.d.
Scapa Flow, Scotland	2016	30-Jun	n.d.	n.d.	n.d.
Scapa Flow, Scotland	2016	3-Jul	n.d.	n.d.	n.d.
Scapa Flow, Scotland	2016	7-Jul	n.d.	n.d.	n.d.
Scapa Flow, Scotland	2016	10-Jul	n.d.	n.d.	n.d.
Scapa Flow, Scotland	2016	12-Jul	1,269	n.d.	n.d.
Scapa Flow, Scotland	2016	17-Jul	2,982	343	n.d.
Scapa Flow, Scotland	2016	20-Jul	n.d.	n.d.	n.d.
Scapa Flow, Scotland	2016	24-Jul	17,618	n.d.	140
Scapa Flow, Scotland	2016	27-Jul	n.d.	n.d.	n.d.
Scapa Flow, Scotland	2016	31-Jul	40,316	326	180
Scapa Flow, Scotland	2016	3-Aug	n.d.	n.d.	n.d.
Scapa Flow, Scotland	2016	7-Aug	9,105	n.d.	225
Scapa Flow, Scotland	2016	14-Aug	3,847	440	122
Scapa Flow, Scotland	2016	23-Aug	6,153	616	162
Scapa Flow, Scotland	2016	28-Aug	4,607	n.d.	20
Scapa Flow, Scotland	2016	4-Sep	925	n.d.	n.d.
Scapa Flow, Scotland	2016	11-Sep	4,988	n.d.	n.d.
Scapa Flow, Scotland	2016	14-Sep	n.d.	n.d.	n.d.
Scapa Flow, Scotland	2016	19-Sep	17,042	n.d.	69
Scapa Flow, Scotland	2016	23-Sep	1,046	n.d.	19
Scapa Flow, Scotland	2016	2-Oct	47,134	n.d.	n.d.
Scapa Flow, Scotland	2016	19-Oct	1,990	n.d.	n.d.
Cuxhaven, Germany	2016	10-Mar	n.d.	n.d.	n.d.
Cuxhaven, Germany	2016	17-Mar	n.d.	n.d.	n.d.
Cuxhaven, Germany	2016	22-Mar	n.d.	n.d.	n.d.

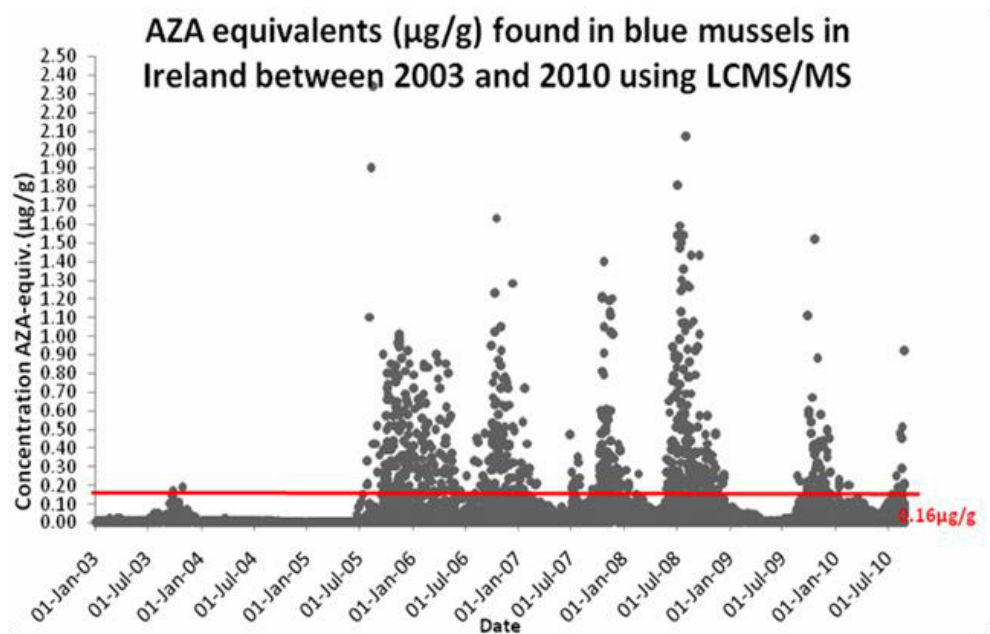
Cuxhaven, Germany	2016	29-Mar	n.d.	n.d.	n.d.
Cuxhaven, Germany	2016	7-Apr	n.d.	n.d.	n.d.
Cuxhaven, Germany	2016	14-Apr	n.d.	n.d.	n.d.
Cuxhaven, Germany	2016	21-Apr	n.d.	n.d.	n.d.
Cuxhaven, Germany	2016	28-Apr	n.d.	n.d.	n.d.
Cuxhaven, Germany	2016	3-May	n.d.	n.d.	n.d.
Cuxhaven, Germany	2016	12-May	n.d.	n.d.	n.d.
Cuxhaven, Germany	2016	19-May	n.d.	n.d.	n.d.
Cuxhaven, Germany	2016	26-May	n.d.	n.d.	n.d.
Cuxhaven, Germany	2016	2-Jun	n.d.	n.d.	n.d.
Cuxhaven, Germany	2016	8-Jun	n.d.	n.d.	n.d.
Cuxhaven, Germany	2016	16-Jun	n.d.	n.d.	n.d.
Cuxhaven, Germany	2016	23-Jun	n.d.	n.d.	n.d.
Cuxhaven, Germany	2016	30-Jun	n.d.	n.d.	n.d.
Cuxhaven, Germany	2016	7-Jul	n.d.	n.d.	n.d.
Cuxhaven, Germany	2016	14-Jul	n.d.	n.d.	n.d.
Cuxhaven, Germany	2016	21-Jul	n.d.	n.d.	n.d.
Cuxhaven, Germany	2016	27-Jul	n.d.	n.d.	n.d.
Cuxhaven, Germany	2016	9-Aug	n.d.	n.d.	n.d.
Cuxhaven, Germany	2016	18-Aug	n.d.	n.d.	n.d.
Cuxhaven, Germany	2016	24-Aug	136	n.d.	n.d.
Cuxhaven, Germany	2016	1-Sep	n.d.	n.d.	n.d.
Cuxhaven, Germany	2016	9-Sep	n.d.	n.d.	n.d.
Cuxhaven, Germany	2016	15-Sep	n.d.	n.d.	n.d.
Cuxhaven, Germany	2016	22-Sep	n.d.	n.d.	n.d.
Cuxhaven, Germany	2016	29-Sep	n.d.	n.d.	n.d.
Cuxhaven, Germany	2016	6-Oct	n.d.	n.d.	n.d.
Cuxhaven, Germany	2016	13-Oct	n.d.	n.d.	n.d.
Cuxhaven, Germany	2016	20-Oct	n.d.	n.d.	n.d.
Cuxhaven, Germany	2016	27-Oct	n.d.	n.d.	n.d.
Helgoland, Germany	2016	15-Jun	13	n.d.	n.d.
Helgoland, Germany	2016	29-Jun	n.d.	6	n.d.
Helgoland, Germany	2016	20-Jul	n.d.	n.d.	16
Helgoland, Germany	2016	10-Aug	n.d.	21	50
Helgoland, Germany	2016	25-Aug	n.d.	n.d.	3
Helgoland, Germany	2016	12-Oct	n.d.	n.d.	2,548
Wilhelmshaven, Germany	2016	20-Apr	n.d.	n.d.	n.d.
Wilhelmshaven, Germany	2016	17-May	n.d.	n.d.	n.d.
Wilhelmshaven, Germany	2016	1-Jun	n.d.	n.d.	n.d.
Wilhelmshaven, Germany	2016	15-Jun	n.d.	n.d.	n.d.
Wilhelmshaven, Germany	2016	29-Jun	n.d.	n.d.	n.d.
Wilhelmshaven, Germany	2016	13-Jul	n.d.	n.d.	n.d.
Wilhelmshaven, Germany	2016	28-Jul	n.d.	n.d.	n.d.
Wilhelmshaven, Germany	2016	25-Aug	n.d.	n.d.	n.d.
Wilhelmshaven, Germany	2016	12-Sep	n.d.	n.d.	n.d.
Wilhelmshaven, Germany	2016	26-Sep	n.d.	n.d.	n.d.
Wilhelmshaven, Germany	2016	14-Oct	n.d.	n.d.	n.d.
Wilhelmshaven, Germany	2016	25-Oct	n.d.	n.d.	n.d.
Helgoland, Germany	2018	6-Feb	n.d.	n.d.	n.d.
Helgoland, Germany	2018	20-Feb	n.d.	n.d.	n.d.
Helgoland, Germany	2018	27-Feb	n.d.	n.d.	n.d.

Helgoland, Germany	2018	6-Mar	n.d.	n.d.	n.d.
Helgoland, Germany	2018	13-Mar	n.d.	n.d.	n.d.
Helgoland, Germany	2018	20-Mar	n.d.	n.d.	n.d.
Helgoland, Germany	2018	27-Mar	n.d.	n.d.	n.d.
Helgoland, Germany	2018	3-Apr	n.d.	n.d.	n.d.
Helgoland, Germany	2018	10-Apr	n.d.	n.d.	n.d.
Helgoland, Germany	2018	17-Apr	n.d.	n.d.	n.d.
Helgoland, Germany	2018	24-Apr	n.d.	n.d.	n.d.
Helgoland, Germany	2018	8-May	n.d.	n.d.	n.d.
Helgoland, Germany	2018	15-May	n.d.	n.d.	n.d.
Helgoland, Germany	2018	22-May	n.d.	n.d.	n.d.
Helgoland, Germany	2018	29-May	n.d.	n.d.	n.d.
Helgoland, Germany	2018	5-Jun	n.d.	n.d.	n.d.
Helgoland, Germany	2018	12-Jun	n.d.	n.d.	n.d.
Helgoland, Germany	2018	19-Jun	n.d.	n.d.	n.d.
Helgoland, Germany	2018	26-Jun	n.d.	n.d.	n.d.
Helgoland, Germany	2018	3-Jul	n.d.	n.d.	n.d.
Helgoland, Germany	2018	10-Jul	n.d.	n.d.	n.d.
Helgoland, Germany	2018	17-Jul	n.d.	n.d.	15
Helgoland, Germany	2018	24-Jul	n.d.	n.d.	n.d.
Helgoland, Germany	2018	31-Jul	n.d.	n.d.	n.d.
Helgoland, Germany	2018	7-Aug	n.d.	n.d.	n.d.
Helgoland, Germany	2018	14-Aug	n.d.	n.d.	3
Helgoland, Germany	2018	21-Aug	n.d.	n.d.	13
Helgoland, Germany	2018	28-Aug	n.d.	n.d.	10
Helgoland, Germany	2018	4-Sep	n.d.	n.d.	31
Helgoland, Germany	2018	11-Sep	n.d.	n.d.	118
Helgoland, Germany	2018	18-Sep	n.d.	n.d.	100
Helgoland, Germany	2018	25-Sep	n.d.	n.d.	6
Helgoland, Germany	2018	2-Oct	n.d.	n.d.	44
Helgoland, Germany	2018	9-Oct	n.d.	n.d.	n.d.
Helgoland, Germany	2018	6-Nov	n.d.	n.d.	n.d.
Helgoland, Germany	2019	21-Jan	n.d.	n.d.	n.d.
Helgoland, Germany	2019	25-Feb	n.d.	n.d.	n.d.
Helgoland, Germany	2019	3-Mar	n.d.	n.d.	n.d.
Helgoland, Germany	2019	9-Apr	n.d.	n.d.	n.d.
Helgoland, Germany	2019	16-Apr	n.d.	n.d.	n.d.
Helgoland, Germany	2019	25-Apr	n.d.	n.d.	n.d.
Helgoland, Germany	2019	30-Apr	n.d.	n.d.	n.d.
Helgoland, Germany	2019	7-May	n.d.	n.d.	n.d.
Helgoland, Germany	2019	14-May	n.d.	n.d.	n.d.
Helgoland, Germany	2019	28-May	n.d.	n.d.	n.d.
Helgoland, Germany	2019	28-May	n.d.	n.d.	n.d.
Helgoland, Germany	2019	4-Jun	n.d.	n.d.	n.d.
Helgoland, Germany	2019	11-Jun	n.d.	n.d.	n.d.
Helgoland, Germany	2019	18-Jun	n.d.	n.d.	n.d.
Helgoland, Germany	2019	25-Jun	n.d.	n.d.	n.d.
Helgoland, Germany	2019	2-Jul	n.d.	n.d.	27
Helgoland, Germany	2019	9-Jul	n.d.	n.d.	n.d.
Helgoland, Germany	2019	16-Jul	n.d.	n.d.	n.d.
Helgoland, Germany	2019	23-Jul	n.d.	n.d.	n.d.

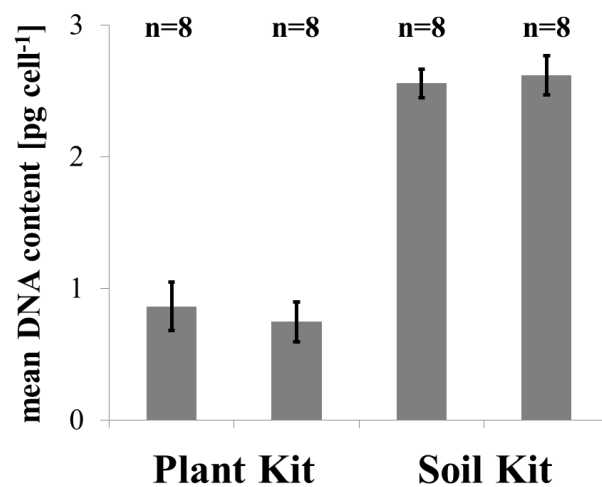
Helgoland, Germany	2019	30-Jul	n.d.	n.d.	n.d.
Helgoland, Germany	2019	6-Aug	n.d.	n.d.	n.d.
Helgoland, Germany	2019	13-Aug	n.d.	n.d.	n.d.
Helgoland, Germany	2019	20-Aug	n.d.	n.d.	n.d.
Helgoland, Germany	2019	27-Aug	n.d.	n.d.	n.d.
Helgoland, Germany	2019	10-Sep	n.d.	n.d.	n.d.
Helgoland, Germany	2019	17-Sep	n.d.	n.d.	n.d.
Helgoland, Germany	2019	24-Sep	n.d.	n.d.	n.d.
Helgoland, Germany	2019	1-Oct	n.d.	n.d.	42
Helgoland, Germany	2019	8-Oct	n.d.	n.d.	42
Helgoland, Germany	2019	15-Oct	n.d.	n.d.	26
Helgoland, Germany	2019	22-Oct	n.d.	n.d.	45
Helgoland, Germany	2019	3-Dec	n.d.	n.d.	45
Helgoland, Germany	2019	17-Dec	n.d.	n.d.	n.d.
Sylt, Germany	2018	18-Apr	n.d.	n.d.	n.d.
Sylt, Germany	2018	25-Apr	n.d.	n.d.	n.d.
Sylt, Germany	2018	2-May	n.d.	n.d.	n.d.
Sylt, Germany	2018	9-May	n.d.	n.d.	n.d.
Sylt, Germany	2018	14-May	n.d.	n.d.	n.d.
Sylt, Germany	2018	16-May	n.d.	n.d.	n.d.
Sylt, Germany	2018	23-May	4	n.d.	n.d.
Sylt, Germany	2018	30-May	n.d.	n.d.	n.d.
Sylt, Germany	2018	6-Jun	n.d.	n.d.	n.d.
Sylt, Germany	2018	20-Jun	n.d.	n.d.	n.d.
Sylt, Germany	2018	27-Jun	n.d.	n.d.	n.d.
Sylt, Germany	2018	4-Jul	n.d.	n.d.	n.d.
Sylt, Germany	2018	11-Jul	n.d.	n.d.	n.d.
Sylt, Germany	2018	18-Jul	n.d.	n.d.	n.d.
Sylt, Germany	2018	25-Jul	n.d.	n.d.	n.d.
Sylt, Germany	2018	1-Aug	n.d.	n.d.	n.d.
Sylt, Germany	2018	8-Aug	15	n.d.	n.d.
Sylt, Germany	2018	15-Aug	n.d.	n.d.	n.d.
Sylt, Germany	2018	22-Aug	9	n.d.	n.d.
Sylt, Germany	2018	29-Aug	n.d.	n.d.	n.d.
Sylt, Germany	2018	5-Sep	n.d.	n.d.	n.d.
Sylt, Germany	2018	12-Sep	n.d.	n.d.	n.d.
Sylt, Germany	2018	20-Sep	n.d.	n.d.	n.d.
Sylt, Germany	2018	26-Sep	n.d.	n.d.	n.d.
Sylt, Germany	2018	4-Oct	171	n.d.	n.d.
Sylt, Germany	2018	11-Oct	n.d.	n.d.	n.d.
Sylt, Germany	2018	25-Oct	n.d.	n.d.	n.d.
Sylt, Germany	2018	8-Nov	n.d.	n.d.	n.d.
Sylt, Germany	2018	15-Nov	n.d.	n.d.	n.d.
Sylt, Germany	2018	22-Nov	n.d.	n.d.	n.d.
Sylt, Germany	2018	29-Nov	n.d.	n.d.	n.d.
Sylt, Germany	2018	6-Dec	n.d.	n.d.	n.d.
Sylt, Germany	2018	13-Dec	n.d.	n.d.	n.d.
Sylt, Germany	2018	20-Dec	n.d.	n.d.	n.d.
Sylt, Germany	2019	3-Jan	n.d.	n.d.	n.d.
Sylt, Germany	2019	10-Jan	n.d.	n.d.	n.d.
Sylt, Germany	2019	17-Jan	n.d.	n.d.	n.d.

Sylt, Germany	2019	31-Jan	n.d.	n.d.	n.d.
Sylt, Germany	2019	6-Feb	n.d.	n.d.	n.d.
Sylt, Germany	2019	14-Feb	n.d.	n.d.	n.d.
Sylt, Germany	2019	21-Feb	n.d.	n.d.	n.d.
Sylt, Germany	2019	28-Feb	n.d.	n.d.	n.d.
Sylt, Germany	2019	5-Mar	n.d.	n.d.	n.d.
Sylt, Germany	2019	14-Mar	n.d.	n.d.	n.d.
Sylt, Germany	2019	25-Mar	n.d.	n.d.	n.d.
Sylt, Germany	2019	28-Mar	n.d.	n.d.	n.d.
Sylt, Germany	2019	4-Apr	n.d.	n.d.	n.d.
Sylt, Germany	2019	11-Apr	n.d.	n.d.	n.d.
Sylt, Germany	2019	18-Apr	n.d.	n.d.	n.d.
Sylt, Germany	2019	25-Apr	n.d.	n.d.	n.d.
Sylt, Germany	2019	2-May	n.d.	n.d.	n.d.
Sylt, Germany	2019	9-May	n.d.	n.d.	n.d.
Sylt, Germany	2019	16-May	n.d.	n.d.	n.d.
Sylt, Germany	2019	23-May	n.d.	n.d.	n.d.
Sylt, Germany	2019	28-May	n.d.	n.d.	n.d.
Sylt, Germany	2019	6-Jun	n.d.	n.d.	n.d.
Sylt, Germany	2019	12-Jun	n.d.	n.d.	n.d.
Sylt, Germany	2019	19-Jun	n.d.	n.d.	n.d.
Sylt, Germany	2019	27-Jun	n.d.	n.d.	n.d.
Sylt, Germany	2019	1-Jul	n.d.	n.d.	n.d.
Sylt, Germany	2019	11-Jul	n.d.	n.d.	n.d.
Sylt, Germany	2019	18-Jul	n.d.	n.d.	n.d.
Sylt, Germany	2019	25-Jul	n.d.	n.d.	537
Sylt, Germany	2019	1-Aug	n.d.	n.d.	n.d.
Sylt, Germany	2019	8-Aug	n.d.	n.d.	681
Sylt, Germany	2019	15-Aug	n.d.	n.d.	n.d.
Sylt, Germany	2019	22-Aug	n.d.	n.d.	319
Sylt, Germany	2019	29-Aug	n.d.	n.d.	1,841
Sylt, Germany	2019	5-Sep	n.d.	n.d.	180
Sylt, Germany	2019	12-Sep	n.d.	n.d.	53
Sylt, Germany	2019	19-Sep	n.d.	n.d.	n.d.
Sylt, Germany	2019	26-Sep	n.d.	n.d.	n.d.
Sylt, Germany	2019	2-Oct	n.d.	n.d.	n.d.
Sylt, Germany	2019	9-Oct	n.d.	n.d.	n.d.
Sylt, Germany	2019	17-Oct	n.d.	n.d.	n.d.
Sylt, Germany	2019	24-Oct	n.d.	n.d.	57
Sylt, Germany	2019	30-Oct	n.d.	n.d.	n.d.
Sylt, Germany	2019	7-Nov	n.d.	n.d.	n.d.
Sylt, Germany	2019	14-Nov	n.d.	n.d.	n.d.
Sylt, Germany	2019	21-Nov	n.d.	n.d.	n.d.
Sylt, Germany	2019	28-Nov	n.d.	n.d.	n.d.
Sylt, Germany	2019	5-Dec	n.d.	n.d.	n.d.
Sylt, Germany	2019	12-Dec	n.d.	n.d.	n.d.
Sylt, Germany	2019	20-Dec	n.d.	n.d.	n.d.

Supplementary Figures



Suppl. Fig. S1. AZA equivalents ($\mu\text{g g}^{-1}$) found in Irish blue mussels between 2003 and 2010 by LC-MS/MS. Adapted from Salas et al. (2011).



Suppl. Fig. S2: DNA cell quota of *Az. spinosum* (strain UTH-E2) of the NucleoSpin Plant Kit and the NucleoSpin Soil Kit (both Macherey Nagel, Düren, Germany) after two individual extraction processes with eight replicates each.

